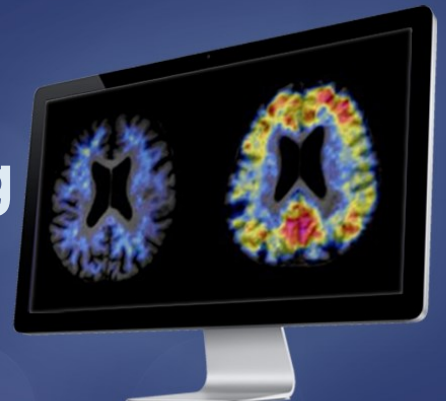# 13th Human Amyloid Imaging

January 16-18, 2019
Miami, Florida

Co-Organizers:
Keith A. Johnson, MD ● William J. Jagust, MD ● William E. Klunk, MD, PhD ● Chester A. Mathis, PhD

Conference Program and Abstracts

TABLE OF CONTENTS

HAI 2019 PROGRAM AT-A-GLANCE

Wednesday, January 16, 2019			Page
11:45	Welcome Notes	**Keith Johnson**, Massachusetts General Hospital, Boston, MA, US	
12:00pm	**SESSION 1:** Tracer properties	CHAIRS: **Roger Gunn**, Invicro, Boston, MA, US/ICL, London, UK **Bradley Christian**, Univ. of Wisconsin-Madison, Madison, WI, US	36
2:00	**POSTER SESSION 1** and Coffee Break		52
3:30	**SESSION 2:** Methods	CHAIRS: **Robert Koeppe**, Univ. of Michigan Med School, Ann Arbor, MI, US **Mark Lubberink**, Uppsala University, Uppsala, Sweden	158
5:45	**Keynote Lecture**	**Richard Carson**, Yale University, New Haven, CT, US	180
6:30-8:30	Welcome Reception		
Thursday, January 17, 2019			
7:30am	Check-in (Grande Promenade Foyer) and Breakfast (Starlight Ballrooom - 18th Floor)		
8:30	**SESSION 3:** **Neuropathological validation of amyloid and tau tracers**	CHAIRS: **Laetitia Lemoine**, Karolinska Institute, Stockholm, Sweden **Rik Vandenberghe**, KU Leuven, Leuven, Belgium	182
10:15	**POSTER SESSION 2A** and Coffee Break		188
11:00	**SESSION 4:** **In vivo-postmortem correlates of flortaucipir PET**	CHAIRS: **Teresa Gomez-Isla**, Massachusetts General Hospital, Boston, MA, US **David Wolk**, University of Pennsylvania, Philadelphia, PA, US	295
12:30	**Keynote Lecture**	**Michel Goedert**, MRC Lab of Molecular Biology, Cambridge, UK	306
1:15	Lunch		
2:45	**SESSION 5:** **Modeling amyloid & tau relationships and spread**	CHAIRS: **Elizabeth Mormino**, Stanford University, Palo Alto, CA, US **Michel Grothe**, DZNE, Rostock, Germany	307
4:45	**POSTER SESSION 2B** and Coffee Break		
5:30-7:30	Networking Reception		
Friday, January 18, 2019			
7:30am	Check-in (Grande Promenade Foyer) and Breakfast (Starlight Ballroom - 18th Floor)		
8:30	**SESSION 6:** **PET and fluid biomarkers**	CHAIRS: **Oskar Hansson**, Lund University, Lund, Sweden **Susan Landau**, University of California, Berkeley, Berkeley, CA, US	332
10:00	**POSTER SESSION 3A** and Coffee Break		341
10:45	**SESSION 7:** **Multi-modality: cognitively normal**	CHAIRS: **William Jagust**, University of California, Berkeley, Berkeley, CA, US **Tobey Betthauser**, Univ. of Wisconsin-Madison, Madison, WI, US	444
12:30	**Keynote Lecture**	**John Trojanowski**, University of Pennsylvania, Philadelphia, PA, US	462
1:15	Lunch		
2:30	**SESSION 8:** **Multi-modality: patient populations**	CHAIRS: **Ann Cohen**, University of Pittsburgh, Pittsburgh, PA, US **Keith Johnson**, Massachusetts General Hospital, Boston, MA, US	463
4:15	**POSTER SESSION 3B** and Coffee Break		
5:00	Awards Ceremony		
5:05	**SESSION 9:** **Clinical applications**	CHAIRS: **Pedro Rosa-Neto**, McGill University, Montreal, QC, Canada **Gil Rabinovici**, University of California, San Francisco, CA, US	482

HAI 2019 PROGRAM

	Wednesday, January 16, 2019	
10:30am	Check-in (Grande Promenade Foyer)	
11:45	Welcome Notes	**Keith Johnson**, Massachusetts General Hospital, Boston, MA, US
12:00pm	**SESSION 1: Tracer properties**	CHAIRS: **Roger Gunn**, Invicro, Boston, MA, US/ Imperial College London, London, UK **Bradley Christian**, University of Wisconsin-Madison, Madison, WI, US
12:00	Head-to-head in vivo comparison of tau positron emission tomography ligands [18F]Flortaucipir (AV1451) and [18]RO948	**Michael Schöll**, University of Gothenburg, Gothenburg, Sweden
12:15	Retrospective comparison of [F-18]MK-6240, [F-18]THK5351 and [F-18]THK-5317 ((S)-THK-5117) in subjects scanned with all three PET tracers	**Tobey Betthauser**, University of Wisconsin-Madison School of Medicine and Public Health, Madison, WI, US
12:30	Head-to-Head Comparison of neurofibrillary tangles imaging in Alzheimer's disease	**Pedro Rosa-Neto**, McGill University, Montreal, QC, Canada
12:45	Assessment of longitudinal change of tau pathology in Alzheimer's disease using [18F]GTP1 (Genentech tau probe 1) PET imaging	**Sandra Sanabria Bohorquez**, Genentech, Inc., South San Francisco, CA, US
1:00	Evaluation of 18F-PI-2620, a novel selective tau tracer for the assessment of Alzheimer's and non-Alzheimer's tauopathies	**Victor Villemagne**, Austin Health/The University of Melbourne, Melbourne, Australia
1:15	Evidence of differential in vitro and in vivo binding of APN-1607 in progressive supranuclear palsy and Alzheimer's disease	**Cristian Salinas**, Biogen, Cambridge, MA, US
1:30	Discussion Session 1	
2:00	**POSTER SESSION 1** and Coffee Break	
3:30	**SESSION 2: Methods**	CHAIRS: **Robert Koeppe**, University of Michigan Medical School, Ann Arbor, MI, US **Mark Lubberink**, Uppsala University, Uppsala, Sweden
3:30	Variability of uptake in potential reference regions for longitudinal flortaucipir-PET analysis	**Jungho Cha**, University of California, San Francisco, San Francisco, CA, US
3:45	Test-retest repeatability of [18F]Flortaucipir PET in Alzheimer's disease and controls	**Tessa Timmers**, Amsterdam UMC, Amsterdam, The Netherlands
4:00	AmyloidIQ demonstrates increased power in longitudinal Amyloid PET studies	**Alexander Whittington**, Invicro, Boston, MA, US/Imperial College London, London, UK
4:15	Regionalized spatial association between PiB and FTP PET assessed via variography	**Tobias Estime**, Massachusetts General Hospital, Boston, MA, US
4:30	Evaluation of the Centiloid scale for use in multi-amyloid PET tracer, multi-center trials	**Jacob Hesterman**, Invicro, Boston, MA, US
4:45	A comparison of partial volume correction techniques for measuring change in Serial AV-1451 Tau PET SUVR	**Christopher Schwarz**, Mayo Clinic, Rochester, MN, US
5:00	Detecting the earlier stages of amyloid deposition	**Tengfei Guo**, University of California, Berkeley, CA, US
5:15	Discussion Session 2	
5:45	**Keynote Lecture:** Quantitative brain PET: is SUVR the best we can do? *(This lecture will be recorded)*	**Richard Carson**, Yale University, New Haven, CT, US
6:15	Keynote Discussion	
6:30-8:30	Welcome Reception	

Thursday, January 17, 2019

7:30am	Check-in (Grande Promenade Foyer) and Breakfast (Starlight Ballroom - 18th Floor)	
8:30	**SESSION 3: Neuropathological validation of amyloid and tau tracers**	CHAIRS: **Laetitia Lemoine**, Karolinska Institute, Stockholm, Sweden **Rik Vandenberghe**, KU Leuven, Leuven, Belgium
8:30	Neuropathologic correlates of [11C]PiB PET and [11C]altropane dopamine transporter PET in the Lewy body diseases	**Stephen Gomperts**, Massachusetts General Hospital, Boston, MA, US
8:45	Postmortem analyses of PiB and Flutemetamol integrated density measures in diffuse and neuritic plaques in Alzheimer's disease	**Milos Ikonomovic**, University of Pittsburgh, Pittsburgh, PA, US
9:00	In vitro characterisation of 3H-MK6240 in human autopsy brain tissue in comparison to the first generation tau PET tracers	**Mona-Lisa Malarte**, Karolinska Institute, Stockholm, Sweden
9:15	Postmortem binding study of 18F-AV1451 in semantic variant primary progressive aphasia	**Rik Vandenberghe**, University Hospitals Leuven/KU Leuven, Leuven, Belgium
9:30	Neuropathologic maturity of neurofibrillary tangles: implications for tau PET imaging	**Melissa Murray**, Mayo Clinic Jacksonville, Jacksonville, FL, US
9:45	Discussion Session 3	
10:15	**POSTER SESSION 2A** and Coffee Break	
11:00	**SESSION 4: In vivo-postmortem correlates of flortaucipir PET**	CHAIRS: **Teresa Gomez-Isla**, Massachusetts General Hospital, Boston, MA, US **David Wolk**, University of Pennsylvania, Philadelphia, PA, US
11:00	Pathologic correlations of in vivo [18F]-AV-1451 imaging in autopsy-confirmed Alzheimer's disease, Frontotemporal lobar degeneration with TDP-43 inclusions and control cases	**Cinthya Aguero**, MassGeneral Institute for Neurodegenerative Disease, Charlestown, MA, US
11:15	[18F]Flortaucipir PET and pathology correlations in Alzheimer's disease, non-Alzheimer's tauopathies, and other neurodegenerative diseases	**David Soleimani-Meigooni**, University of California, San Francisco, San Francisco, CA, US
11:30	Tau PET imaging correlates with neuropathology	**Val Lowe**, Mayo Clinic, Rochester, MN, US
11:45	Relationships between Flortaucipir PET signal and tau neurofibrillary tangle pathology at autopsy	**Mark Mintun**, Avid Radiopharmaceuticals, Philadelphia, PA, US
12:00pm	Discussion Session 4	
12:30	**Keynote Lecture**: Conformers of assembled Tau *(This lecture will be recorded)*	**Michel Goedert**, MRC Laboratory of Molecular Biology, Cambridge, UK
1:00	Keynote Discussion	
1:15	Lunch	
2:45	**SESSION 5: Modeling amyloid & tau relationships and spread**	CHAIRS: **Elizabeth Mormino**, Stanford University, Palo Alto, CA, US **Michel Grothe**, German Center for Neurodegenerative Diseases, Rostock, Germany
2:45	Data-driven characterization of cross-sectional and longitudinal molecular imaging in aging and Alzheimer's disease	**Hugo Botha**, Mayo Clinic, Rochester, MN, US
3:00	The cortical site of origin and initial spread of medial temporal tauopathy assessed with positron emission tomography	**Justin Sanchez**, Massachusetts General Hospital, Boston, MA, US
3:15	Amyloid and tau pathology are related to functional signal homogeneity and isolation of the hippocampus in cognitively healthy older adults	**Theresa Harrison**, University of California Berkeley, Berkeley, CA, US

3:30	Cross-method identification of earliest regions to display amyloid burden	**Isadora Lopes Alves**, VU University Medical Center, Amsterdam, The Netherlands
3:45	Tau organization precedes Aβ deposition across the brain cortex	**Tharick Pascoal**, McGill University, Montreal, QC, Canada
4:00	Increased task activation and amyloid independently explain advanced tau pathology in older adults	**Anne Maass**, German Center for Neurodegenerative Diseases, Magdeburg, Germany
4:15	Discussion Session 5	
4:45	**POSTER SESSION 2B** and Coffee Break	
5:30 - 7:30	Networking Reception	

Friday, January 18, 2019

7:30am	Check-in (Grande Promenade Foyer) and Breakfast (Starlight Ballrooom - 18th Floor)	
8:30	**SESSION 6: PET and fluid biomarkers**	CHAIRS: **Oskar Hansson**, Lund University, Lund, Sweden **Susan Landau**, University of California, Berkeley, Berkeley, CA, US
8:30	Longitudinal investigation of concordant vs. discordant amyloid CSF/PET biomarkers	**Arianna Sala**, Karolinska Institute, Stockholm, Sweden
8:45	CSF and PET tau measures in different stages of Alzheimer's disea	**Niklas Mattsson**, Lund University, Lund, Sweden
9:00	Predicting brain amyloidosis using peripheral blood-based gene expression and early stage neurodegeneration biomarkers	**Apoorva Bharthur Sanjay**, Indiana University School of Medicine, Indianapolis, IN, US
9:15	Friend or foe? Regional dependent roles of neuroinflammation in Alzheimer's disease pathophysiology	**Min Su Kang**, McGill Centre for Studying in Aging, Verdun, QC, Canada
9:30	Discussion Session 6	
10:00	**POSTER SESSION 3A** and Coffee Break	
10:45	**SESSION 7: Multi-modality: cognitively normal**	CHAIRS: **William Jagust**, University of California, **Berkeley, Berkeley, CA, US** **Tobey Betthauser**, University of Wisconsin-Madison School of Medicine a Public Health, Madison, WI, US
10:45	Protective effect of physical activity on prospective cognitive decline and longitudinal neurodegeneration in clinically normal older adults with elevated β-amyloid burden	**Jennifer Rabin**, Massachusetts General Hospital, Boston, MA, US
11:00	MRI measures of neurodegeneration and vascular injury, but not smyloid status predict cognitive decline in normal individuals followed for more than 9 Years	**Charles DeCarli**, University of California at Davis, Sacramento, CA, US
11:15	Fluorodeoxyglucose and Flortaucipir PET independently predict subsequent cognitive decline in clinically normal adults with elevated amyloid	**Bernard Hanseeuw**, Massachusetts General Hospital, Boston, MA, US
11:30	MK-6240 and PIB PET are associated with retrospective cognitive trajectories in late-middle aged persons clinically unimpaired at baseline	**Sterling Johnson**, University of Wisconsin-Madison School of Medicine and Public Health, Madison, WI, US
11:45	Individual variations in sleep architecture are associated with tau PET, cognition, and functional network architecture: preliminary findings from the Harvard Aging Brain Study	**Jasmeer Chhatwal**, Massachusetts General Hospital, Boston, MA, US
12:00	Discussion Session 7	

12:30	**Keynote Lecture:** Tau strains and spreading in pure tauopathies and Alzheimer's disease *(This lecture will be recorded)*	**John Trojanowski**, University of Pennsylvania, Philadelphia, PA, US
1:00	Keynote Discussion	
1:15	Lunch	
2:30	**SESSION 8: Multi-modality: patient populations**	CHAIRS: **Ann Cohen**, University of Pittsburgh, Pittsburgh, PA, US **Keith Johnson**, Massachusetts General Hospital, Boston, MA, US
2:30	Tau imaging with [18F]Flortaucipir predicts the severity and the topography of subsequent cortical atrophy in patients with Alzheimer's disease	**Renaud La Joie**, University of California, San Francisco, San Francisco, CA, US
2:45	Epidemic spreading of tau through human functional brain connections	**Jacob Vogel**, Montreal Neurological Institute, McGill University, Montreal, QC, Canada
3:00	Spatial extent and topographical relationships between pathology accumulation and neurodegeneration in Alzheimer's disease	**Leonardo Iaccarino**, University of California San Francisco, San Francisco, CA, US
3:15	Functional connectivity associated with tau levels in aging, Alzheimer's, and small-vessel disease	**Nicolai Franzmeier**, Ludwig-Maximilians-Universität LMU, Munich, Germany
3:30	Associations between longitudinal Aβ and cross-sectional tau in adults with Down syndrome	**Dana Tudorascu**, University of Pittsburgh, Pittsburgh, PA, US
3:45	Discussion Session 8	
4:15	**POSTER SESSION 3B** and Coffee Break	
5:00	Awards Ceremony	
5:05	**SESSION 9: Clinical applications**	CHAIRS: **Pedro Rosa-Neto**, McGill University, Montreal, QC, Canada **Gil Rabinovici**, University of California, San Francisco, CA, US
5:05	Tau PET imaging with 18F-PI2620 in aging and neurodegenerative diseases	**Elizabeth Mormino**, Stanford University, Palo Alto, CA, US
5:20	In vivo distribution pattern of 18F-PM-PBB3 (18F-APN-1607) and its relationship with clinical features in diverse 4-repeat tauopathies	**Hitoshi Shimada**, National Institute of Radiological Sciences/National Institutes for Quantum and Radiological Science and Technology, Chiba, Japan
5:35	Tau imaging with 18F-MK6240 in Alzheimer's disease and in past traumatic brain injury	**Christopher Rowe**, Austin Health/The University of Melbourne, Melbourne, Australia
5:50	[18F]-AV-1451 binding profile in early and late-onset Alzheimer's disease and suspected non-Alzheimer pathophysiology	**Eddie Stage**, Indiana University School of Medicine, Indianapolis, IN, US
6:05	Towards a topographic imaging biomarker of TDP-43 pathology in amnestic dementia: patient stratification based on FDG-PET patterns in autopsy-confirmed cases	**Michel Grothe**, German Center for Neurodegenerative Diseases, Rostock, Germany
6:20	Discussion Session 9	

POSTER INDEX (by board number)

WEDNESDAY

Board #	Poster Title	Authors	Presenter
01	Novel PET radioligands show that COX-1 is constitutively expressed and COX-2 is upregulated by inflammation	Kim | Shrestha | Eldridge | Singh | Cortes | Hong | Morse | Gladding | Henry | Gallagher | Frankland | Tye | Liow | Zoghbi | Fujita | Pike | Innis	**Kim, Min-Jeong**
02	Regression-based predictive features for clinical brain images	Clark | Del Gaizo | Goukasian | Hwang | Apostolova	**Apostolova, Liana**
03	Subcortical amyloid load is associated with volume and shape in cognitively normal individuals	Rahayel | Bocti | Sévigny Dupont | Joannette | Lavallée | Nikelski | Chertkow | Joubert	**Rahayel, Shady**
04	Subcortical amyloid relates to cortical surface area in cognitively normal individuals	Rahayel | Bocti | Sévigny Dupont | Joannette | Lavallée | Nikelski | Chertkow | Joubert	**Rahayel, Shady**
05	Global cortical network organization analysis of amyloid and tau across AD clinical spectrum	Qureshi | Pascoal | Mathotaarachchi | Benedet | Rosa-Neto	**Qureshi, Muhammad Naveed Iqbal**
06	Abnormal AV1451 signal in popular reference regions	Schwarz | Kantarci | Murray | Przybelski | Min | Lowe | Nedelska | Vemuri | Senjem | Gunter | Petersen | Knopman | Jack	**Schwarz, Christopher**
07	X-ray method for estimating amyloid load in the brain	Badano | Dahal	**Badano, Aldo**
08	Impact of different image analysis methods on baseline 18F-Florbetapir PET measurements in the API ADAD Colombia trial	Ghisays | Chen | Protas | Goradia | Thiyyagura | Langbaum | Sink | Hu | Guthrie | Smith | Cho | Clayton | Thomas | Toga | Boker | Alvarez | Quiroz | Rios-Romenets | Chen | Su | Tariot | Lopera | Reiman	**Ghisays, Valentina**
09	Sub-threshold regional amyloid levels mediates parahippocampal thinning associated with reduced cerebral blood flow.	Sisley | Sanchez | Domoto-Reilly | Grabowski | Rane	**Rane, Swati**
10	[18F]GTP1 (Genentech tau probe 1) SUVR has a very little dependence on changes in regional or global cerebral blood flow	Sanabria | Baker | Marik | de Crespigny | Weimer	**Sanabria, Sandra**
11	Multimodal magnetic resonance imaging predicts regional cerebral amyloid burden	Alathur Rangarajan | Wu | Joseph | Karim | Laymon | Tudorascu | Snitz | Cohen | Mathis | Klunk | Aizenstein	**Alathur Rangarajan, Anusha**
12	Evaluation of [18F]APN-1607 to image tau protein in patients with Alzheimer's disease and test-retest studies	Sandiego | Barret | Carroll | Gouasmat | Madonia | Marek | Margolin | Tempest | Jang	**Sandiego, Christine**
13	Discovery of [18F]SMBT-1: a novel selective MAO-B PET tracer for imaging astrogliosis	Harada | Ezura | Iwata | Arai | Yanai | Furumoto | Kudo | Okamura	**Harada, Ryuichi**
14	Effect of point spread function specification error on GTM partial volume correction in PiB imaging	Laymon | Minhas | Kolibash | Aizenstein | Cohen | Lopresti | Mathis | Snitz | Tudorascu | Klunk	**Laymon, Charles**
15	11C-ER176 has superior quality than 11C-PBR28 to image brain inflammation with positron emission tomography	Zanotti Fregonara | Pascual | Yu | Beers | Appel | Masdeu	**Zanotti Fregonara, Paolo**
16	Subject-specific site of maximum uptake is most sensitive to longitudinal change in 18F-AV1451 PET data	Scott | Adamczuk | Gorman | Runkle | Suhy	**Scott, David**
17	Functional connectivity of the entorhinal cortex predicts tau deposition in aging	Adams | Maass | Harrison | Jagust	**Adams, Jenna**
18	A fully automatic technique for precise localization and quantification of Amyloid-β PET scans	Tahmi | Bou Zeid | Razlighi	**Razlighi, Qolamreza**
19	Network-based modeling of tau spread and seeding using PET and DTI	Yang | Chowdhury | Jacobs | Johnson | Dutta	**Jacobs, Heidi**

Board #	Poster Title	Authors	Presenter
20	Establishment of a simplified method to quantify [18F]PM-PBB3 ([18F]APN-1607) binding in the brains of living human subjects	Seki | Tagai | Shimada | Kitamura | Kimura | Ichise | Ono | Takahata | Kubota | Takado | Shinotoh | Okada | Kikuchi | Zhang | Suhara | Higuchi	Seki, Chie
21	PET and CSF amyloid status are differently predicted by patient features	Reimand | de Wilde | Teunissen | Zwan | Windhorst | Boellaard | van der Flier | Scheltens | van Berckel | Ossenkoppele | Bouwman	Reimand, Juhan
22	TauIQ – an algorithm to quantify global and local Tau accumulation	Whittington | Seibyl | Hesterman | Gunn	Gunn, Roger
23	AmyloidIQ – an automated algorithm for classifying amyloid-β PET scans	Whittington | Seibyl | Eichenlaub | Stephens | Hesterman | Gunn	Whittington, Alex
24	Reconsidering in-vivo models of regional amyloid pathology progression: region-specific thresholds and longitudinal data	Jelistratova | Bugla | Teipel | Grothe	Jelistratova, Irina
25	Sensitivity of the Standard Centiloid to Track Longitudinal Amyloid-Beta Changes Using 18F-Florbetaben PET	Bullich | Villemange | Koglin | Jovalekic | Perrotin | Doré | Stephens | Rowe | De Santi	De Santi, Susan
26	Increased tau aggregation in young traumatic brain injury and post-concussion syndrome patients	Lubberink | Wall | Vedung | Fahlström | Weis | Haller | Larsson | Antoni | Marklund	Lubberink, Mark
27	Effect of blood flow changes on quantification of [18F]flutemetamol studies	Heeman | Yaqub | Lopes Alves | Heurling | Gispert | Foley | Boellaard | Lammertsma	Heeman, Fiona
28	Longitudinal [18F]Flortaucipir in the BioFINDER 1 Cohort	Smith | Strandberg | Stomrud | Hansson	Smith, Ruben
29	Preclinical characterization of two new promising tau PET tracers in vitro and in vivo	Skaddan | Mugnaini | Guo | Wooten | Wilcox | Reuter | Voorbach | Montavon | Reed | Relo | Mezler | Haupt | Geneste | Erhard | Pohlki | Tovcimak | Finnema | Martarello | Comley	Guo, Qi
30	Study on tissue-based and histogram-based reference regions for semi-quantitation of 18F-APN-1607 Tau PET Imaging	Hsiao | Huang | Chen | Lin | Huang	Hsiao, Ing-Tsung
31	Predicting amyloid accumulation in dominantly inherited Alzheimer's disease	Luckett | McCullough | McCarthy | Hassenstab | Fagan | Schindler | McDade | Bateman | Benzinger | Ances	Luckett, Patrick
32	Modeling the nonlinear effect of amyloid on cognitive impairment mediated by neurodegeneration in Alzheimer's disease using path analysis	Kim | Shin | Seong	Kim, Sung-Woo
33	Identification and characterization of selective and high affinity small molecules for PET imaging of pathological alpha-synuclein	Capotosti | Tsika | Molette | Ravache | Vokali | Rodriguez | Darmency | Piorkowska | Purohit | Paterson | Evans | Martarello | Salinas | Poli | Kroth | Stoehr | Lowe | Pfeifer | Muhs	Capotosti, Francesca
34	APOE genotype is associated with specific regional patterns of amyloid accumulation	Katz | Hanseeuw | Farrell | Moody | Sanchez | Mayblyum | Estime | Jacobs | Vannini | Sepulcre | Jiang | Schultz | Price | Sperling | Johnson	Katz, Samantha
35	Association of reported sleep-wake disturbances with tau pathology in mild cognitive impairment and normal cognitive aging	Shokouhi | Conley | Gwirtsman | Newhouse	Shokouhi, Sepideh
36	Defining the lowest threshold for baseline amyloid-PET to predict future cognitive decline and amyloid accumulation in clinically normal adults	Farrell | Jiang | Schultz | Properzi | Rentz | Papp | Mormino | Betensky | Johnson | Sperling | Buckley	Farrell, Michelle
37	Mild behavioral impairment is associated with β-amyloid and tau in cognitively intact elderly individuals	Lussier | Pascoal | Chamoun | Therriault | Tissot | Savard | Kang | Mathotaarachchi | Benedet | Thomas | Parsons | Ismail | Rosa-Neto | Gauthier	Lussier, Firoza
38	Evaluation of a visual read method for flortaucipir PET scans	Arora | Pontecorvo | Mintun | Fleisher | Devous | Lu | Galante | Stevenson | Flitter | Beach | Montine | Serrano | Sue | Intorcia | Curtis | Salloway | Thein |	Arora, Anupa K.

Board #	Poster Title	Authors	Presenter
		Wellman | Perrin | Lowe | Grossman | Irwin | Ikonomovic | Seeley | Rabinovici | Masdeu	
39	An MRI-free, template-based method for quantifying cortical florbetapir uptake in vivo	Korman | Landau | Jagust	**Korman, Deniz**
40	Early increase in tau-PET signal is associated with changes in amyloid, CSF p-tau and cognition	McSweeney | Pichet Binette | Meyer | Gonneaud | Bedetti | Ozlen | Daoust | Labonté | Rosa-Neto | Breitner | Poirier | Villeneuve	**McSweeney, Melissa**
41	Mental and physical activity during the 80-minute uptake time affects off-target binding in tau PET scans (18F-AV-1451)	Apgar | Min | Maltais | Scott | Lecy | Lundt | Albertson | Schwarz | Botha | Jones | Kantarci | Vemuri | Knopman | Petersen | Jack | Lowe	**Min, Hoon-Ki**
42	Functional network changes occur prior to symptomatic conversion in AD	Wisch | Roe | Babulal | Benzinger | Morris | Ances	**Wisch, Julie**
43	Enhancing tau signal of PET imaging using a convolutional autoencoder	Mathotaarachchi | Pascoal | Benedet | Chamoun | Savard | Kang | Therriault | Fonov | Gauthier | Rosa-Neto	**Mathotaarachchi, Sulantha**
44	Co-evolving patterns of functional connectivity with amyloid and tau deposition in Alzheimer's disease progression	Svaldi | Goñi | Amico | Risacher | Stage | West | Saykin | Apostolova	**Svaldi, Diana**
45	Joint reconstruction method for longitudinal Tau-PET imaging	Tiss | Petibon | Ouyang | Ihsani | Kas | Habert | Johnson | El Fakhri	**El Fakhri, Georges**
46	Associations between quantitative susceptibility mapping and measures of amyloid and tau in patients with Alzheimer's disease	Baker | La Joie | Liu | Cobigo | Bourakova | Harrison | Rabinovici | Jagust	**Baker, Suzanne**
47	The relationship between Aβ-related hippocampal activity and metabolism in impaired individuals	Scott | Hanseeuw | Huijbers | Hampton | Manning | Chhatwal | Buckley | Johnson | Sperling | Schultz	**Scott, Matthew**
48	Centiloid scale in practice: effect of different SUVR reference regions and comparison of Centiloid cut-offs	Adamczuk | Sampat | Runkle | Gorman | Suhy | Scott	**Adamczuk, Kate**
49	Amyloid-beta imaging in glial cells	Jethava | Prakash | Chopra	**Jethava, Krupal**
50	Preliminary longitudinal evaluation of the novel tau tracer [18F]MK-6240	Pascoal | Chamoun | Kang | Mathotaarachchi | Benedet | Therriault | Souvy | Gauthier | Rosa-Neto	**Pascoal, Tharick**
51	NODDI modeling reveals neurite orientation and dispersion differences in white matter tracts of beta-amyloid positive individuals	Hunt | Vogt | Dean, III | Betthauser | Christian | Johnson | Alexander | Bendlin	**Hunt, Jack**

THURSDAY

Board #	Poster Title	Authors	Presenter
60	18F-Florbetaben and 18F-Flutemetamol PET beta-amyloid binding expressed in centiloids	Cho | Choe | Kim | Kim | Kim | Jang | Kim | Jung | Na | Park | Seo	**Cho, Soo Hyun**
61	Modelling tau pathology progression in Alzheimer's disease: Preliminary results and parameters required at a minimum to inform the model	Soucy | Hortelan | Benali	**Soucy, Jean-Paul**
62	Determination of FTD candidates in an MCI-SNAP cohort by PET amyloid and MRI structural analysis	Buckley | Esteban | Wilkens | Wolk	**Buckley, Christopher**
63	Striatal amyloid load predicts conversion from aMCI to pAD	Buckley | Chedumbarum-Pillay | Jenkinson | Smith | Beach | Thal | Wolk	**Buckley, Christopher**
64	Evaluation of [18F]GTP1 (Genentech tau probe 1) Extent and Load for assessing tau burden in Alzheimer's disease	Sanabria Bohorquez | Baker | Manser | Toth | Marik | Weimer	**Sanabria Bohorquez, Sandra**
65	Novel tau PET ligand compound series for detecting 4-repeat tau lesions	Koga | Svensson | Sohn | Dickson	**Koga, Shunsuke**

Board #	Poster Title	Authors	Presenter
66	Comparable associations between memory impairment and hippocampal [18F]flortaucipir signal after optimization	Wolters | Ossenkoppele | Golla | Verfaillie | Timmers | Visser | Tuncel | Coomans | Scheltens | Windhorst | van der Flier | Boellaard | van Berckel	**Wolters, Emma E**
67	Vascular medical treatment influences the association between vascular burden and amyloid pathology in middle-to-late-aged cognitively healthy individuals at risk for Alzheimer's disease	Köbe | Gonneaud | Pichet Binette | Meyer | McSweeney | Rosa-Neto | Breitner | Poirier | Villeneuve | (PREVENT-AD) Research Group	**Köbe, Theresa**
68	Amyloid deposition and hippocampal atrophy in non-demented elderly subjects over 85 years	Treyer | Meyer | Buchmann | Crameri | Studer | Saake | Gruber | Unschuld | Nitsch | Hock | Gietl	**Gietl, Anton**
69	Association between elevated brain tau pathology and subsequent cognitive decline among non-demented PSEN1 E280A mutation carriers: Preliminary findings from the COLBOS project	Quiroz | Sperling | Guzman-Velez | Hanseeuw | Pardilla-Delgado | Bocanegra | Vila-Castelar | Baena | Artola | Sanchez | Hampton | Fuller | Ramirez-Gomez | Gatchel | Schultz | Arboleda-Velasquez | Lopera | Reiman | Johnson	**Quiroz, Yakeel**
70	[18F]AV1451 deposition pattern across the Alzheimer's disease spectrum – characterization at the individual level	Pichet Binette | Gonneaud | Villeneuve | Neuroimaging Initiative	**Pichet Binette, Alexa**
71	BLAzER: A versatile and efficient workflow for analyzing PET neuroimaging data in Alzheimer's disease	Raman | Grandhi | Murchison | Kennedy | Landau | Roberson | McConathy	**Raman, Fabio**
72	Longitudinal 18F-APN-1607 (18F-PM-PBB3) PET in the rTg4510 mouse model of tauopathy	Hsiao | Huang | Lin | Yang	**Hsiao, Ing-Tsung**
73	Healthy brain structural connectome predicts regional tau accumulation in amyloid-positive mild cognitive impairment patients	Lee | Shin | Na | Seo | Seong	**Lee, Wha Jin**
74	Pearls and pitfalls of using centiloids in interventional anti-amyloid studies – an examination of amyloid reductions in the gantenerumab open label extension studies	Klein | Delmar | Abi-Saab | Andjelkovic | Ristic | Voyle | Hesterman | Seibyl | Marek | Baudler | Fontoura | Doody	**Klein, Gregory**
75	AV1451 and THK5351 PET with pathology correlations in a patient with Sporadic Creutzfeldt-Jakob Disease	Kim | Cho | Park | Jang | Ryu | Choi | Moon | Oh | Oh | Na | Lyoo | Kim | Choi | Seo	**Kim, Hee Jin**
76	Associations among amyloid, tau, cerebrovascular disease, and neurodegeneration across cognitive stages in the Alzheimer's continuum	Lao | Kreisl | Brickman	**Lao, Patrick**
77	Association between neuroinflammation (level) and cognitive performance	Thomas | Chamoun | Pascoal | Savard | Nazar | Sbeiti | Olmand | Mathotaarachchi | Kang | Therriault | Gauthier | Rosa-Neto	**Thomas, Emilie**
78	Relationship of amyloid-beta and neurofibrillary tau deposition in Down syndrome using [11C]PiB and [18F]AV-1451 PET	Zammit | Tudorascu | Cody | Laymon | Cohen | Minhas | Ellison | Sabbagh | Zaman | Johnson | Mathis | Klunk | Handen | Christian	**Zammit, Matt**
79	Amyloid accumulation in the striatum is more rapid than in the cortex early in Down syndrome and can serve as a marker for early intervention	Zammit | Cody | Betthauser | Tudorascu | Lao | Laymon | Cohen | Murali | Minhas | Zaman | Johnson | Mathis | Klunk | Handen | Christian	**Zammit, Matt**
80	Cross-sectional associations between temporal tau and cortical thickness across the lifespan	Moody | Jacobs | Sidwell | Hanseeuw | Katz | Sanchez | Mayblyum | Estime | Sepulcre | Satizabal | Pase | Beiser | Demissie | Daniluk | Schaefer | Peets | Price | Sperling | DeCarli | Seshadri | Johnson	**Moody, Kirsten**
81	Amyloid-dependent and –independent effects of Tau on clinical function in Alzheimer's disease	Therriault | Pascoal | Sefranek | Mathotaarachchi | Savard | Benedet | Chamoun | Kang | Gauthier | Rosa-Neto	**Therriault, Joseph**
82	Voxel-wise receiver operating characteristic analysis reveals clinically relevant sites of amyloid-beta deposition	Therriault | Pascoal | Leuzy | Collij | Lessa Benedet | Mathotaarachchi | Kang | Alves | Massarweh | Soucy | Gauthier | Rosa-Neto	**Therriault, Joseph**

Board #	Poster Title	Authors	Presenter
83	In-vivo tau burden correlates with subregional atrophy in medial temporal lobe in amyloid negative individuals	Das | Xie | Wisse | Cui | Ittyerah | Yushkevich | Wolk	**Das, Sandhitsu**
84	Distinct tau PET patterns in atrophy-defined subtypes of Alzheimer's disease	Ossenkoppele | Lyoo | Rabinovici | Hansson	**Ossenkoppele, Rik**
85	Item-level analysis of the Cognitive Function Index by screening amyloid PET in the A4 Study	Amariglio | Sikkes | Marshall | Buckley | Gatchel | Johnson | Rentz | Donohue | Raman | Sun | Yaari | Holdridge | Grill | Aisen | Sperling	**Amariglio, Rebecca**
86	Cross-sectional and longitudinal effects of asymmetric amyloid deposition on memory in Baltimore Longitudinal Study of Aging (BLSA) participants	Brinson | Bilgel | An | Huang | Wong | Resnick	**Brinson, Zabecca**
87	Regional sex-differences in tau pathology in asymptomatic individuals with elevated amyloid	Jacobs | Buckley | Mormino | Schultz | Raman | Donohue | Sun | Marek | Seibyl | Mintun | Shcherbinin | Pontecorvo | Rowe | VanDyck | Salloway | Jack | Yaari | Holdridge | Aisen | Sperling | Johnson	**Jacobs, Heidi**
88	CSF tau biomarkers correlate with [18F]MK6240 SUVR in Alzheimer's disease related areas	Chamoun | Kang | Pascoal | Benedet | Mathotaarachchi | Therriault | Savard | Thomas | Bouhachi | Hsiao | Massarweh | Soucy | Gauthier | Rosa-Neto	**Chamoun, Mira**
89	Diagnostic accuracy of [18F]RO948 PET for differentiating Alzheimer's disease from other neurodegenerative disorders	Hansson | Stomrud | Borroni | Klein | Strandberg | Smith	**Hansson, Oskar**
90	Amyloid burden and hippocampal function	Beason-Held | Shafer | Bilgel | Wong | Resnick	**Beason-Held, Lori**
91	Ante-post mortem binding of THK5317 and its vitro comparability with MK-6240 in a case of FTLD	Lemoine | Chiotis | Leuzy | Graff | Nennesmo | Nordberg	**Lemoine, Laetitia**
92	Tau and amyloid protein accumulation affect distinct white matter fiber tracts in Alzheimer's disease	Savard | Kang | Pascoal | Mathotaarachchi | Therriault | Chamoun | Lessa Benedet | M. Thomas | Parsons | Tissot | Lussier | Gauthier | Rosa-Neto	**Savard, Melissa**
93	Plasma neurofilament light chain concentrations in relation to [18F]florbetapir and [18F]flortaucipir PET in Alzheimer's disease	Lessa Benedet | Leuzy | A. Pascoal | Mathotaarachchi | Savard | Therriault | Kang | Chamoun | Schöll | J. Ashton | Gauthier | Zetterberg | Rosa-Neto | Blennow | for the Alzheimer's Disease Neuroimaging Initiative	**Savard, Melissa**
94	APOEε4 potentiates the relationship between amyloid-β and tau pathologies in a dose-dependent manner	Parsons | Therriault | Benedet | Pascoal | Mathotaarachchi | Savard | Kang | Chamoun | Soucy | Massarweh | Saha-Chaudhuri | Poirier | Gauthier | Rosa-Neto	**Therriault, Joseph**
95	Quantitative gradient recalled echo (qGRE) MRI identifies significant neuronal loss in the hippocampal subfields related to cognitive impairment in mild Alzheimer's disease	Kothapalli | Benzinger | Hassenstab | Goyal | Morris | Yablonskiy	**Kothapalli, Satya**
96	Predictors for β-amyloid positivity in cognitively impaired patients. Data from the Imaging Dementia—Evidence for Amyloid Scanning (IDEAS) Study	Lesman-Segev | Hanna | La Joie | Iaccarino | Siegel | Hillner | Whitmer | Carrillo | Edwards | Chaudhary | Gatsonis | Rabinovici	**Lesman-Segev, Orit**
97	Regional tau and atrophy: domain-specific relationships with cognition	Digma | Reas | Brewer | Banks	**Banks, Sarah**
98	Inferior temporal tau is associated with greater prospective cortical thinning in clinically-normal older adults	Hampton | Scott | Buckley | Chhatwal | Jacobs | Hanseeuw | Johnson | Sperling | Schultz	**Hampton, Olivia**
99	Lower left ventricular ejection fraction relates to increased cerebrospinal fluid biomarker evidence of neurodegeneration in older adults	Kresge | Liu | Gupta | Osborn | Acosta | Bell | Pechman | Gifford | Mendes | Wang | Blennow | Zetterberg | Hohman | Jefferson	**Kresge, Hailey**

Board #	Poster Title	Authors	Presenter
100	ApoE4 as a moderating factor between mild traumatic brain injury and tau deposition in the temporal cortex	Munro | Chen | Rundle | Cullum | Rodrigue | Park	**Munro, Catherine**
101	A longitudinal examination of amyloid burden and myelin content in major white matter tracts	Yang | Dean III | Vogt | Jonaitis | Hunt | Merluzzi | Kohli | Christian | Oh | Betthauser | Asthana | Johnson | Alexander | Bendlin	**Yang, Kao Lee**
102	Initial clinical evaluation of [18F] PI-2620 as a potent PET radiotracer imaging tau protein	Oh | Oh | Lee | Oh | Roh | Chung | Lee | Lee | Kim	**Oh, Minyoung**
103	Asymmetric tau and focal amyloid PET in an autopsy-confirmed case of Alzheimer's disease presenting as primary progressive aphasia	Martersteck | Sridhar | Coventry | Mesulam | Rogalski	**Martersteck, Adam**
104	Sex-specific effects of APOE-e4 genotype on amyloid burden and cognitive function	Isenberg | Aslanyan | Pa	**Isenberg, Lisette**
105	Amyloid-β and cortical atrophy in adults with Down Syndrome	Cody | Tudorascu | Lao | Cohen | Zaman | Laymon | Johnson | Klunk | Handen | Christian	**Cody, Karly**
106	Relationship between intracranial blood flow and beta-amyloid assessed with PiB PET	Cody | Betthauser | Koscik | Rivera-Rivera | Berman | Cary | Hoffman | Clark | Chin | Barnhart | Bendlin | Johnson | Wieben | Christian | Johnson	**Cody, Karly**
107	Personalizing the use of the ATN framework in clinical research: integrating the clinical phenotype and biomarkers in a case series across the MCI/dementia spectrum	Dickerson | McGinnis | Quimby | Hochberg | Brickhouse | Collins | Putcha | Eldaief | Wong | Frosch | Das | McMillan | Yuschkevich | de Flores | Wisse | Xie | Wolk	**Dickerson, Brad**
108	The ATN framework in ADNI: How do different A,T, and N biomarkers influence the definition of AD pathology and cognitive trajectories?	Landau | Korman | Shaw | Trojanowski | Jagust	**Landau, Susan**
109	Neuropsychiatric symptoms are correlated with tau deposition in the Alzheimer's disease spectrum	Tissot | Pascoal | Therriault | Chamoun | Lussier | Savard | Mathotaarachchi | Lessa Benedet | Thomas | Parsons | Rosa-Neto | Gauthier	**Tissot, Cécile**
110	Amyloid-sex interaction effect on cognitive decline: Differential effects on memory versus executive functioning are not mediated by temporal lobe atrophy	Gavett | Fletcher | Mungas | DeCarli	**DeCarli, Charles**
111	Molecular imaging discordance with CSF AD biomarkers in atypical Alzheimer's disease	Townley	**Townley, Ryan**

FRIDAY

Board #	Poster Title	Authors	Presenter
120	Longitudinal [18F]AV-1451 PET imaging in primary progressive apraxia of speech	Utianski | Martin | Schwarz | Hugo | Duffy | Petersen | Clark | Machulda | Butts | Jack, Jr. | Lowe | Whitwell | Josephs	**Utianski, Rene**
121	Disease progression modeling from preclinical stages of Alzheimer's disease (AD) to AD dementia	Cho | Woo | Kim | Kim | Kim | Kim | Jang | Kim | Kim | Jung | Kim | Lockhart | Ossenkoppele | Landau | Jagust | Weiner | Na | Seo	**Cho, Soo Hyun**
122	Metabolism mediates the effect of tau on cognition in mild cognitive impairment and dementia	Rodriguez-Vieitez | Mazrina | Chiotis | Colato | Nordberg	**Rodriguez-Vieitez, Elena**
123	Patterns of cerebral tau deposition across Alzheimer's disease stages: A study comparing 18F-THK5317 and 18F-AV-1451 PET tracers	Rodriguez-Vieitez | Colato | Chiotis | Mazrina | Nordberg	**Rodriguez-Vieitez, Elena**
124	Association of subjective cognitive decline and gait slowing with Aβ deposition in cognitively normal individuals	Nadkarni | Perera | Snitz | Mathis | DeKosky | Klunk | Lopez	**Nadkarni, Neelesh**

Board #	Poster Title	Authors	Presenter
125	Cerebrospinal fluid synaptic vesicle glycoprotein 2A in Alzheimer's disease	Ashton	Höglund	Leuzy	Heurling	Hansson	Schöll	Zetterberg	Blennow	**Ashton, Nicholas**
126	Longitudinal evaluation of [18F]MK-6240 in Alzheimer's disease and cognitively normal adults: preliminary results at 6 and 12 months	Salinas	Purohit	Lohith	Struyk	Martarello	Beaver	**Salinas, Cristian**
127	Subicular volume as a surrogate marker of beta-amyloid associated episodic memory variation at high age	Schroeder	Van Bergen	Schreiner	Meyer	Kagerer	Vionnet	Gietl	Treyer	Buck	Kaufmann	Nitsch	Pruessmann	Hock	Unschuld	**Unschuld, Paul**
128	Clinical significance of amyloid β positivity in patients with probable cerebral amyloid angiopathy markers	Jang.	Jang	Kim	Werring	Lee	Choe	Park	Lee	Kim	Kim	Cho	Kim	Kim	Charidimou	Na	Seo	**Jang, Young Kyoung**
129	Tau deposition in amyloid negative subjects: the application of the AT(N) model in the Geneva Memory Center experience	Dodich	Frisoni	Andryszak	Scheffler	Mendes	Assal	Schibli	Schwarz	Rakotomiaramanana	Gold	Zekry	Lovblad	Chicherio	Boccardi	Unschuld	Garibotto	**Dodich, Alessandra**
130	Characterizing the spatial distribution of cross-sectional [18F]GTP1 (Genentech tau probe 1) SUVR using multivariate statistical analysis and machine learning	Manser	Sanabria Bohorquez	Baker	Toth	Teng	Marik	Weimer	**Manser, Paul**
131	Spatially compact components of non-negative matrix factorization applied to AV-1451 PET images reveal distinct demographic associations	Bilgel	Ziontz	Shafer	Wong	Resnick	**Bilgel, Murat**
132	Independent contributions of hippocampal activity, amyloid burden, and retrospective decline to Subjective Cognitive Decline	Chen	Jingting	Farrell	Park	**Chen, Xi**
133	Amyloid and tau accumulate across distinct spatial networks and are differentially associated with brain connectivity	Pereira	Ossenkoppele	Palmqvist	Strandberg	Smith	Westman	Hansson	**Pereira, Joana**
134	Influence of apolipoprotein-E (APOE) genotype on amyloid trajectories in a longitudinal subject cohort	Lopresti	Campbell	Yu	Snitz	Anderson	Aizenstein	Minhas	Kolibash	Cohen	Mathis	Klunk	Lopez	Tudorascu	**Lopresti, Brian**
135	A follow-up report on the prevalence and magnitude of amyloid positivity between cognitively normal elderly Japanese and Americans	Yu	Lopresti	Ihara	Cui	Aizenstein	Higashiyama	Fukuda	Koizumi	Minhas	Lopez	Klunk	Mathis	Miyamoto	Kuller	Sekikawa	**Lopresti, Brian**
136	Association of in vivo [F-18]AV-1451 with [C-11]PiB, [F-18]FDG hypometabolism, and cortical atrophy in chronic TBI subjects	Minhas	Mountz	Laymon	Lopresti	Beers	Sharpless	Puccio	Edelman	Mathis	Okonkwo	**Minhas, Davneet**
137	Staging cortical amyloid deposition using PET imaging	Collij	Heeman	Salvadó	Altomare	de Wilde	Konijnenberg	van Buchem	Yaqub	Markiewicz	Golla	Wottschel	Wink	Visser	Lammertsma	Scheltens	van der Flier	Boellaard	van Berckel	Gispert	Schmidt	Barkhof	Lopes Alves	AMYPAD consortium	**Collij, Lyduine**
138	PET analysis of verubecestat effect on amyloid load in mild-to-moderate Alzheimer's disease patients (EPOCH trial)	Sur	Adamczuk	Sampat	Kost	Scott	Suhy	Egan	**Sur, Cyrille**
139	Effect of verubecestat on amyloid load in prodromal Alzheimer's disease patients: Results from the PhIII APECS trial	Sur	Kost	Adamczuk	Scott	Suhy	Egan	**Sur, Cyrille**
140	AV1451 retention is associated with hippocampal volume and memory declines in cognitively normal older adults	Ziontz	Bilgel	Shafer	June	Wong	Resnick	**Ziontz, Jacob**
141	[11C]PIB PET is associated with the brain biopsy amyloid β load and CSF amyloid β levels in subjects with normal pressure hydrocephalus	Rinne	Suotunen	Rummukainen	Herukka	Nerg	Koivisto	Rauramaa	Nagren	Hiltunen	Alzfuzoff	Rinne	Jääskeläinen	Soininen	Leinonen	**Rinne, Juha**

Board #	Poster Title	Authors	Presenter
142	The BIN1 rs744373 SNP is associated with increased tau-PET levels and worse memory independent of amyloid	Franzmeier | Neitzel | Rubinski | Ewers	**Franzmeier, Nicolai**
143	Optimal scanning time for the novel tau PET Tracer 18F-APN-1607	Huang | Hsiao | Lin | Lian | Hsu | Huang	**Huang, Chin-Chang**
144	Associations between behavioral factors and Alzheimer's pathology: Findings from cognitively normal older adults at risk of AD and presymptomatic ADAD mutation carriers	Pichet Binette | Gonneaud | Ozlen | Bedetti | Morris | Bateman | Benzinger | Poirier | Breitner | Villeneuve | Research Group | Study Group	**Pichet Binette, Alexa**
145	Early localized network dysfunction in APOE ε4 carriers without biomarker evidence of Alzheimer's disease	Butt | Strain | Wisch | Schindler | Fagan | Curchaga | Benzinger | Ances	**Butt, Omar**
146	Association between retinal thickness and brain β-amyloid accumulation in individuals with Subjective Cognitive Decline: data from the FACEHBI study	Marquié | Monté-Rubio | Rodríguez-Gómez | Sanabria | Castilla-Martí | Martínez | Alegret | Pérez-Cordón | Lomeña | Pavia | Gismondi | Bullich | Vivas-Larruy | Tejero | Gómez-Chiari | Orellana | Valero | Ruiz | Tárraga | Boada	**Marquié, Marta**
147	Image features and clinical associations of the novel tau PET tracer 18F-APN-1607 in Alzheimer's disease	Hsu | Lin | Hsiao | Lian | Huang | Huang | Yen	**Hsu, Jung-Lung**
148	Safety, biodistribution and radiation dosimetry for the tau PET Tracer 18F-APN-1607 in healthy human subjects	Lin | Hsiao | Lian | Huang | Hsu | Huang | Yen	**Lin, Kun-Ju**
149	Longitudinal associations between Aβ and glucose metabolism in a normal elderly population	Tudorascu | Yu | Anderson | Snitz | Minhas | Laymon | Lopresti | Mathis | Aizenstein | Klunk | Cohen	**Cohen, Ann**
150	Associations between Aβ, tau, and cerebrovascular reactivity in a non-demented elderly population	Cohen | Huppert | Tudorascu | Snitz | Laymon | Lopresti | Mathis | Nadkarni | Lopez | Aizenstein | Klunk | Reis	**Cohen, Ann**
151	Comparing amyloid PET tracers and interpretation strategies: A multicenter study	Bischof | Bartenstein | Barthel | van Berckel | Doré | van Eimeren | Forster | Hammes | Lammertsma | Minoshima | Rowe | Sabri | Seibyl | van Laere | Vandenberghe | Villemagne | Yakushev | Drzezga	**Bischof, Gérard**
152	Amyloid and memory impairment have additive effects on microglial activation but not tau pathology	Kreisl | Tao | Zou | Johnson | Tomljanovic | Razlighi | Brickman | Lee | Stern	**Kreisl, William**
153	A preliminary analysis of the association between cerebral blood flow and amyloid and tau PET binding in older adults	Albrecht | Isenberg | Stradford | Monreal | Jann | Pa	**Albrecht, Daniel**
154	Random forests of amyloid PET may pinpoint key brain regions predictive of MoCA score	Zukotynski | Gaudet | Kuo | Adamo | Goubran | Scott | Bocti | Borrie | Chertkow | Frayne | Hsiung | Laforce | Noseworthy | Prato | Sahlas | Smith | Sossi | Thiel | Soucy | Tardif | Black	**Black, Sandra**
155	Comparison of objective and self-reported sleep, tau, and Aβ in healthy older adults	Winer | Fenton | Harrison | Maass | Baker | Jagust	**Winer, Joseph**
156	Relation of cardiovascular risk factors to markers of pathology and memory in autosomal-dominant Alzheimer's disease	Martínez | Guzmán-Vélez | Padilla-Delgado | Vila-Castelar | Fuller | Artola | Sperling | Quiroz	**Guzmán-Vélez, Edmarie**
157	Beta-amyloid accumulation in non-demented elderly individuals correlates with baseline beta-amyloid load, ApoE genotype and age	Gietl | Treyer | Buchmann | Meyer | Saake | Gruber | Mu | Unschuld | Buck | Nitsch | Hock	**Gietl, Anton**
158	Identification of rapid amyloid accumulators: A longitudinal PET amyloid study	Koychev | Vaci | Bilgel | An | Albert | Resnick	**Koychev, Ivan**
159	Age-of-onset dependent associations between [18F]Flortaucipir PET and cognitive impairment in Alzheimer's disease	Visser | Wolters | Verfaillie | Ossenkoppele | Timmers | Tuncel | Golla | Boellaard | Windhorst | Scheltens | van der Flier | van Berckel	**Visser, Denise**

Board #	Poster Title	Authors	Presenter
160	Derivation of amyloid PET centiloid cut-offs using core AD CSF biomarkers including the whole Alzheimer's continuum: a joint analysis in ALFA and ADNI	Salvadó | Brugulat-Serrat | Falcon | Pavia | Niñerola | Perissinotti | Lomeña | Zetterberg | Blennow | Molinuevo | Gispert | ADNI, TRIBEKA Consortium and ALFA study	**Salvadó, Gemma**
161	SSRI reduces CSF Ab42 in healthy older adults and transgenic mice: dose, duration and baseline amyloid effects	Sheline | Snider | Lee | Linn | Fagan | Yan | Aselcioglu | Waligorska | Korecka | Morris | Shaw | Cirrito	**Sheline, Yvette**
162	Determination of the optimal scanning time point for the assessment of tau deposition in Alzheimer's disease using [18F]PI-2620 PET	Bullich | Mueller | Barret | Berndt | Madonia | Seibyl | Marek | Stephens	**Stephens, Andrew**
163	Prediction of brain age using resting-state functional connectivity suggests accelerated aging in the preclinical phase of autosomal dominant Alzheimer's disease, irrespectively of amyloid pathology	Gonneaud | Vachon-Presseau | Baria | Pichet Binette | Benzinger | Morris | Bateman | Breitner | Poirier | Villeneuve | Study Group | Research Group	**Gonneaud, Julie**
164	Vascular risk factors and multimodal neuroimaging biomarkers: Preliminary analyses from a biracial older adult cohort	Lockhart | Craft | Sachs | Rapp | Jung | Whitlow | Hayden | Hughes	**Lockhart, Samuel**
165	Chronic low-grade inflammation associates with lower TSPO binding in elderly individuals without dementia	Ekblad | Toppala | Tuisku | Helin | Marjamäki | Laine | Jula | Viitanen | Rinne	**Ekblad, Laura**
166	Cognitive trajectory of subcortical vascular cognitive impairment	Kim | Woo | Jang | Cho | Kim | Lee | Kim | Kim | Lee | Kim | Seo	**Kim, Hee Jin**
167	F18-PI2620 Tau PET in three memory clinic patients with uncertain CSF biomarker profiles	Frolov | Sha | Fredericks | Nadiadwala | Azevedo | Hall | Toueg | Castillo | Deutsch | Greicius | Davidzon | Zaharchuk | Chin | Mormino	**Frolov, Alexander**
168	Differential associations of cortisol plasma level with glucose metabolism, hippocampal atrophy, and amyloid deposition across Alzheimer's disease stages	Oh | Leung | Canli | Slifstein	**Oh, Hwamee**
169	Cerebral small vessel disease is associated with medial temporal lobe hyperconnectivity in pre-clinical AD	Wu | Tudorascu | Mathis | Lopresti | Cohen | Snitz | Klunk | Aizenstein	**Wu, Minjie**
170	Modeling PiB PET trajectory groups identifies a subgroup with PiB beta-amyloid accumulation near age 50 and predicts MK-6240 SUVR	Koscik | Betthauser | Jonaitis | Clark | Allison | Mueller | Hermann | Poetter | Sanson | Shouel | Chin | Christian | Johnson	**Koscik, Rebecca**
171	Application of amyloid and tau classification system in subcortical vascular cognitive impairment patients	Jang | Kim | Park | Park | Choe | Cho | Lyoo | Lee | Kim | Cho | Kim | Kim | Jung | Ryu | Choi | Moon | Seong | DeCarli | Weiner | Lockhart | Na | Seo	**Jang, Hyemin**

POSTER INDEX (by presenter's last name)

WEDNESDAY

Board #	Poster Title	Authors	Presenter
48	Centiloid scale in practice: effect of different SUVR reference regions and comparison of Centiloid cut-offs	Adamczuk | Sampat | Runkle | Gorman | Suhy | Scott	**Adamczuk, Kate**
17	Functional connectivity of the entorhinal cortex predicts tau deposition in aging	Adams | Maass | Harrison | Jagust	**Adams, Jenna**
11	Multimodal magnetic resonance imaging predicts regional cerebral amyloid burden	Alathur Rangarajan | Wu | Joseph | Karim | Laymon | Tudorascu | Snitz | Cohen | Mathis | Klunk | Aizenstein	**Alathur Rangarajan, Anusha**
02	Regression-based predictive features for clinical brain images	Clark | Del Gaizo | Goukasian | Hwang | Apostolova	**Apostolova, Liana**
38	Evaluation of a visual read method for flortaucipir PET scans	Arora | Pontecorvo | Mintun | Fleisher | Devous | Lu | Galante | Stevenson | Flitter | Beach | Montine | Serrano | Sue | Intorcia | Curtis | Salloway | Thein | Wellman | Perrin | Lowe | Grossman | Irwin | Ikonomovic | Seeley | Rabinovici | Masdeu	**Arora, Anupa K.**
07	X-ray method for estimating amyloid load in the brain	Badano | Dahal	**Badano, Aldo**
46	Associations between quantitative susceptibility mapping and measures of amyloid and tau in patients with Alzheimer's disease	Baker | La Joie | Liu | Cobigo | Bourakova | Harrison | Rabinovici | Jagust	**Baker, Suzanne**
33	Identification and characterization of selective and high affinity small molecules for PET imaging of pathological alpha-synuclein	Capotosti | Tsika | Molette | Ravache | Vokali | Rodriguez | Darmency | Piorkowska | Purohit | Paterson | Evans | Martarello | Salinas | Poli | Kroth | Stoehr | Lowe | Pfeifer | Muhs	**Capotosti, Francesca**
25	Sensitivity of the Standard Centiloid to Track Longitudinal Amyloid-Beta Changes Using 18F-Florbetaben PET	Bullich | Villemange | Koglin | Jovalekic | Perrotin | Doré | Stephens | Rowe | De Santi	**De Santi, Susan**
45	Joint reconstruction method for longitudinal Tau-PET imaging	Tiss | Petibon | Ouyang | Ihsani | Kas | Habert | Johnson | El Fakhri	**El Fakhri, Georges**
36	Defining the lowest threshold for baseline amyloid-PET to predict future cognitive decline and amyloid accumulation in clinically normal adults	Farrell | Jiang | Schultz | Properzi | Rentz | Papp | Mormino | Betensky | Johnson | Sperling | Buckley	**Farrell, Michelle**
08	Impact of different image analysis methods on baseline 18F-Florbetapir PET measurements in the API ADAD Colombia trial	Ghisays | Chen | Protas | Goradia | Thiyyagura | Langbaum | Sink | Hu | Guthrie | Smith | Cho | Clayton | Thomas | Toga | Boker | Alvarez | Quiroz | Rios-Romenets | Chen | Su | Tariot | Lopera | Reiman	**Ghisays, Valentina**
22	TauIQ – an algorithm to quantify global and local Tau accumulation	Whittington | Seibyl | Hesterman | Gunn	**Gunn, Roger**
29	Preclinical characterization of two new promising tau PET tracers in vitro and in vivo	Skaddan | Mugnaini | Guo | Wooten | Wilcox | Reuter | Voorbach | Montavon | Reed | Relo | Mezler | Haupt | Geneste | Erhard | Pohlki | Tovcimak | Finnema | Martarello | Comley	**Guo, Qi**
13	Discovery of [18F]SMBT-1: a novel selective MAO-B PET tracer for imaging astrogliosis	Harada | Ezura | Iwata | Arai | Yanai | Furumoto | Kudo | Okamura	**Harada, Ryuichi**
27	Effect of blood flow changes on quantification of [18F]flutemetamol studies	Heeman | Yaqub | Lopes Alves | Heurling | Gispert | Foley | Boellaard | Lammertsma	**Heeman, Fiona**
30	Study on tissue-based and histogram-based reference regions for semi-quantitation of 18F-APN-1607 Tau PET Imaging	Hsiao | Huang | Chen | Lin | Huang	**Hsiao, Ing-Tsung**

Board #	Poster Title	Authors	Presenter
51	NODDI modeling reveals neurite orientation and dispersion differences in white matter tracts of beta-amyloid positive individuals	Hunt | Vogt | Dean, III | Betthauser | Christian | Johnson | Alexander | Bendlin	**Hunt, Jack**
19	Network-based modeling of tau spread and seeding using PET and DTI	Yang | Chowdhury | Jacobs | Johnson | Dutta	**Jacobs, Heidi**
24	Reconsidering in-vivo models of regional amyloid pathology progression: region-specific thresholds and longitudinal data	Jelistratova | Bugla | Teipel | Grothe	**Jelistratova, Irina**
49	Amyloid-beta imaging in glial cells	Jethava | Prakash | Chopra	**Jethava, Krupal**
34	APOE genotype is associated with specific regional patterns of amyloid accumulation	Katz | Hanseeuw | Farrell | Moody | Sanchez | Mayblyum | Estime | Jacobs | Vannini | Sepulcre | Jiang | Schultz | Price | Sperling | Johnson	**Katz, Samantha**
01	Novel PET radioligands show that COX-1 is constitutively expressed and COX-2 is upregulated by inflammation	Kim | Shrestha | Eldridge | Singh | Cortes | Hong | Morse | Gladding | Henry | Gallagher | Frankland | Tye | Liow | Zoghbi | Fujita | Pike | Innis	**Kim, Min-Jeong**
32	Modeling the nonlinear effect of amyloid on cognitive impairment mediated by neurodegeneration in Alzheimer's disease using path analysis	Kim | Shin | Seong	**Kim, Sung-Woo**
39	An MRI-free, template-based method for quantifying cortical florbetapir uptake in vivo	Korman | Landau | Jagust	**Korman, Deniz**
14	Effect of point spread function specification error on GTM partial volume correction in PiB imaging	Laymon | Minhas | Kolibash | Aizenstein | Cohen | Lopresti | Mathis | Snitz | Tudorascu | Klunk	**Laymon, Charles**
26	Increased tau aggregation in young traumatic brain injury and post-concussion syndrome patients	Lubberink | Wall | Vedung | Fahlström | Weis | Haller | Larsson | Antoni | Marklund	**Lubberink, Mark**
31	Predicting amyloid accumulation in dominantly inherited Alzheimer's disease	Luckett | McCullough | McCarthy | Hassenstab | Fagan | Schindler | McDade | Bateman | Benzinger | Ances	**Luckett, Patrick**
37	Mild behavioral impairment is associated with β-amyloid and tau in cognitively intact elderly individuals	Lussier | Pascoal | Chamoun | Therriault | Tissot | Savard | Kang | Mathotaarachchi | Benedet | Thomas | Parsons | Ismail | Rosa-Neto | Gauthier	**Lussier, Firoza**
43	Enhancing tau signal of PET imaging using a convolutional autoencoder	Mathotaarachchi | Pascoal | Benedet | Chamoun | Savard | Kang | Therriault | Fonov | Gauthier | Rosa-Neto	**Mathotaarachchi, Sulantha**
40	Early increase in tau-PET signal is associated with changes in amyloid, CSF p-tau and cognition	McSweeney | Pichet Binette | Meyer | Gonneaud | Bedetti | Ozlen | Daoust | Labonté | Rosa-Neto | Breitner | Poirier | Villeneuve	**McSweeney, Melissa**
41	Mental and physical activity during the 80-minute uptake time affects off-target binding in tau PET scans (18F-AV-1451)	Apgar | Min | Maltais | Scott | Lecy | Lundt | Albertson | Schwarz | Botha | Jones | Kantarci | Vemuri | Knopman | Petersen | Jack | Lowe	**Min, Hoon-Ki**
50	Preliminary longitudinal evaluation of the novel tau tracer [18F]MK-6240	Pascoal | Chamoun | Kang | Mathotaarachchi | Benedet | Therriault | Souvy | Gauthier | Rosa-Neto	**Pascoal, Tharick**
05	Global cortical network organization analysis of amyloid and tau across AD clinical spectrum	Qureshi | Pascoal | Mathotaarachchi | Benedet | Rosa-Neto	**Qureshi, Muhammad Naveed Iqbal**
03	Subcortical amyloid load is associated with volume and shape in cognitively normal individuals	Rahayel | Bocti | Sévigny Dupont | Joannette | Lavallée | Nikelski | Chertkow | Joubert	**Rahayel, Shady**
04	Subcortical amyloid relates to cortical surface area in cognitively normal individuals	Rahayel | Bocti | Sévigny Dupont | Joannette | Lavallée | Nikelski | Chertkow | Joubert	**Rahayel, Shady**
09	Sub-threshold regional amyloid levels mediates parahippocampal thinning associated with reduced cerebral blood flow.	Sisley | Sanchez | Domoto-Reilly | Grabowski | Rane	**Rane, Swati**

Board #	Poster Title	Authors	Presenter
18	A fully automatic technique for precise localization and quantification of Amyloid-β PET scans	Tahmi | Bou Zeid | Razlighi	**Razlighi, Qolamreza**
21	PET and CSF amyloid status are differently predicted by patient features	Reimand | de Wilde | Teunissen | Zwan | Windhorst | Boellaard | van der Flier | Scheltens | van Berckel | Ossenkoppele | Bouwman	**Reimand, Juhan**
10	[18F]GTP1 (Genentech tau probe 1) SUVR has a very little dependence on changes in regional or global cerebral blood flow	Sanabria | Baker | Marik | de Crespigny | Weimer	**Sanabria, Sandra**
12	Evaluation of [18F]APN-1607 to image tau protein in patients with Alzheimer's disease and test-retest studies	Sandiego | Barret | Carroll | Gouasmat | Madonia | Marek | Margolin | Tempest | Jang	**Sandiego, Christine**
06	Abnormal AV1451 signal in popular reference regions	Schwarz | Kantarci | Murray | Przybelski | Min | Lowe | Nedelska | Vemuri | Senjem | Gunter | Petersen | Knopman | Jack	**Schwarz, Christopher**
16	Subject-specific site of maximum uptake is most sensitive to longitudinal change in 18F-AV1451 PET data	Scott | Adamczuk | Gorman | Runkle | Suhy	**Scott, David**
47	The relationship between Aβ-related hippocampal activity and metabolism in impaired individuals	Scott | Hanseeuw | Huijbers | Hampton | Manning | Chhatwal | Buckley | Johnson | Sperling | Schultz	**Scott, Matthew**
20	Establishment of a simplified method to quantify [18F]PM-PBB3 ([18F]APN-1607) binding in the brains of living human subjects	Seki | Tagai | Shimada | Kitamura | Kimura | Ichise | Ono | Takahata | Kubota | Takado | Shinotoh | Okada | Kikuchi | Zhang | Suhara | Higuchi	**Seki, Chie**
35	Association of reported sleep-wake disturbances with tau pathology in mild cognitive impairment and normal cognitive aging	Shokouhi | Conley | Gwirtsman | Newhouse	**Shokouhi, Sepideh**
28	Longitudinal [18F]Flortaucipir in the BioFINDER 1 Cohort	Smith | Strandberg | Stomrud | Hansson	**Smith, Ruben**
44	Co-evolving patterns of functional connectivity with amyloid and tau deposition in Alzheimer's disease progression	Svaldi | Goñi | Amico | Risacher | Stage | West | Saykin | Apostolova	**Svaldi, Diana**
23	AmyloidIQ – an automated algorithm for classifying amyloid-β PET scans	Whittington | Seibyl | Eichenlaub | Stephens | Hesterman | Gunn	**Whittington, Alex**
42	Functional network changes occur prior to symptomatic conversion in AD	Wisch | Roe | Babulal | Benzinger | Morris | Ances	**Wisch, Julie**
15	11C-ER176 has superior quality than 11C-PBR28 to image brain inflammation with positron emission tomography	Zanotti Fregonara | Pascual | Yu | Beers | Appel | Masdeu	**Zanotti Fregonara, Paolo**

THURSDAY

Board #	Poster Title	Authors	Presenter
85	Item-level analysis of the Cognitive Function Index by screening amyloid PET in the A4 Study	Amariglio | Sikkes | Marshall | Buckley | Gatchel | Johnson | Rentz | Donohue | Raman | Sun | Yaari | Holdridge | Grill | Aisen | Sperling	**Amariglio, Rebecca**
97	Regional tau and atrophy: domain-specific relationships with cognition	Digma | Reas | Brewer | Banks	**Banks, Sarah**
90	Amyloid burden and hippocampal function	Beason-Held | Shafer | Bilgel | Wong | Resnick	**Beason-Held, Lori**
86	Cross-sectional and longitudinal effects of asymmetric amyloid deposition on memory in Baltimore Longitudinal Study of Aging (BLSA) participants	Brinson | Bilgel | An | Huang | Wong | Resnick	**Brinson, Zabecca**
62	Determination of FTD candidates in an MCI-SNAP cohort by PET amyloid and MRI structural analysis	Buckley | Esteban | Wilkens | Wolk	**Buckley, Christopher**

Board #	Poster Title	Authors	Presenter
63	Striatal amyloid load predicts conversion from aMCI to pAD	Buckley | Chedumbarum-Pillay | Jenkinson | Smith | Beach | Thal | Wolk	**Buckley, Christopher**
88	CSF tau biomarkers correlate with [18F]MK6240 SUVR in Alzheimer's disease related areas	Chamoun | Kang | Pascoal | Benedet | Mathotaarachchi | Therriault | Savard | Thomas | Bouhachi | Hsiao | Massarweh | Soucy | Gauthier | Rosa-Neto	**Chamoun, Mira**
60	18F-Florbetaben and 18F-Flutemetamol PET beta-amyloid binding expressed in centiloids	Cho | Choe | Kim | Kim | Kim | Jang | Kim | Jung | Na | Park | Seo	**Cho, Soo Hyun**
105	Amyloid-β and cortical atrophy in adults with Down Syndrome	Cody | Tudorascu | Lao | Cohen | Zaman | Laymon | Johnson | Klunk | Handen | Christian	**Cody, Karly**
106	Relationship between intracranial blood flow and beta-amyloid assessed with PiB PET	Cody | Betthauser | Koscik | Rivera-Rivera | Berman | Cary | Hoffman | Clark | Chin | Barnhart | Bendlin | Johnson | Wieben | Christian | Johnson	**Cody, Karly**
83	In-vivo tau burden correlates with subregional atrophy in medial temporal lobe in amyloid negative individuals	Das | Xie | Wisse | Cui | Ittyerah | Yushkevich | Wolk	**Das, Sandhitsu**
110	Amyloid-sex interaction effect on cognitive decline: Differential effects on memory versus executive functioning are not mediated by temporal lobe atrophy	Gavett | Fletcher | Mungas | DeCarli	**DeCarli, Charles**
107	Personalizing the use of the ATN framework in clinical research: integrating the clinical phenotype and biomarkers in a case series across the MCI/dementia spectrum	Dickerson | McGinnis | Quimby | Hochberg | Brickhouse | Collins | Putcha | Eldaief | Wong | Frosch | Das | McMillan | Yuschkevich | de Flores | Wisse | Xie | Wolk	**Dickerson, Brad**
68	Amyloid deposition and hippocampal atrophy in non-demented elderly subjects over 85 years	Treyer | Meyer | Buchmann | Crameri | Studer | Saake | Gruber | Unschuld | Nitsch | Hock | Gietl	**Gietl, Anton**
98	Inferior temporal tau is associated with greater prospective cortical thinning in clinically-normal older adults	Hampton | Scott | Buckley | Chhatwal | Jacobs | Hanseeuw | Johnson | Sperling | Schultz	**Hampton, Olivia**
89	Diagnostic accuracy of [18F]RO948 PET for differentiating Alzheimer's disease from other neurodegenerative disorders	Hansson | Stomrud | Borroni | Klein | Strandberg | Smith	**Hansson, Oskar**
72	Longitudinal 18F-APN-1607 (18F-PM-PBB3) PET in the rTg4510 mouse model of tauopathy	Hsiao | Huang | Lin | Yang	**Hsiao, Ing-Tsung**
104	Sex-specific effects of APOE-e4 genotype on amyloid burden and cognitive function	Isenberg | Aslanyan | Pa	**Isenberg, Lisette**
87	Regional sex-differences in tau pathology in asymptomatic individuals with elevated amyloid	Jacobs | Buckley | Mormino | Schultz | Raman | Donohue | Sun | Marek | Seibyl | Mintun | Shcherbinin | Pontecorvo | Rowe | VanDyck | Salloway | Jack | Yaari | Holdridge | Aisen | Sperling | Johnson	**Jacobs, Heidi**
75	AV1451 and THK5351 PET with pathology correlations in a patient with Sporadic Creutzfeldt-Jakob Disease	Kim | Cho | Park | Jang | Ryu | Choi | Moon | Oh | Oh | Na | Lyoo | Kim | Choi | Seo	**Kim, Hee Jin**
74	Pearls and pitfalls of using centiloids in interventional anti-amyloid studies – an examination of amyloid reductions in the gantenerumab open label extension studies	Klein | Delmar | Abi-Saab | Andjelkovic | Ristic | Voyle | Hesterman | Seibyl | Marek | Baudler | Fontoura | Doody	**Klein, Gregory**
67	Vascular medical treatment influences the association between vascular burden and amyloid pathology in middle-to-late-aged cognitively healthy individuals at risk for Alzheimer's disease	Köbe | Gonneaud | Pichet Binette | Meyer | McSweeney | Rosa-Neto | Breitner | Poirier | Villeneuve | (PREVENT-AD) Research Group	**Köbe, Theresa**
65	Novel tau PET ligand compound series for detecting 4-repeat tau lesions	Koga | Svensson | Sohn | Dickson	**Koga, Shunsuke**

Board #	Poster Title	Authors	Presenter
95	Quantitative gradient recalled echo (qGRE) MRI identifies significant neuronal loss in the hippocampal subfields related to cognitive impairment in mild Alzheimer's disease	Kothapalli | Benzinger | Hassenstab | Goyal | Morris | Yablonskiy	**Kothapalli, Satya**
99	Lower left ventricular ejection fraction relates to increased cerebrospinal fluid biomarker evidence of neurodegeneration in older adults	Kresge | Liu | Gupta | Osborn | Acosta | Bell | Pechman | Gifford | Mendes | Wang | Blennow | Zetterberg | Hohman | Jefferson	**Kresge, Hailey**
108	The ATN framework in ADNI: How do different A,T, and N biomarkers influence the definition of AD pathology and cognitive trajectories?	Landau | Korman | Shaw | Trojanowski | Jagust	**Landau, Susan**
76	Associations among amyloid, tau, cerebrovascular disease, and neurodegeneration across cognitive stages in the Alzheimer's continuum	Lao | Kreisl | Brickman	**Lao, Patrick**
73	Healthy brain structural connectome predicts regional tau accumulation in amyloid-positive mild cognitive impairment patients	Lee | Shin | Na | Seo | Seong	**Lee, Wha Jin**
91	Ante-post mortem binding of THK5317 and its vitro comparability with MK-6240 in a case of FTLD	Lemoine | Chiotis | Leuzy | Graff | Nennesmo | Nordberg	**Lemoine, Laetitia**
96	Predictors for β-amyloid positivity in cognitively impaired patients. Data from the Imaging Dementia—Evidence for Amyloid Scanning (IDEAS) Study	Lesman-Segev | Hanna | La Joie | Iaccarino | Siegel | Hillner | Whitmer | Carrillo | Edwards | Chaudhary | Gatsonis | Rabinovici	**Lesman-Segev, Orit**
103	Asymmetric tau and focal amyloid PET in an autopsy-confirmed case of Alzheimer's disease presenting as primary progressive aphasia	Martersteck | Sridhar | Coventry | Mesulam | Rogalski	**Martersteck, Adam**
80	Cross-sectional associations between temporal tau and cortical thickness across the lifespan	Moody | Jacobs | Sidwell | Hanseeuw | Katz | Sanchez | Mayblyum | Estime | Sepulcre | Satizabal | Pase | Beiser | Demissie | Daniluk | Schaefer | Peets | Price | Sperling | DeCarli | Seshadri | Johnson	**Moody, Kirsten**
100	ApoE4 as a moderating factor between mild traumatic brain injury and tau deposition in the temporal cortex	Munro | Chen | Rundle | Cullum | Rodrigue | Park	**Munro, Catherine**
102	Initial clinical evaluation of [18F] PI-2620 as a potent PET radiotracer imaging tau protein	Oh | Oh | Lee | Oh | Roh | Chung | Lee | Lee | Kim	**Oh, Minyoung**
84	Distinct tau PET patterns in atrophy-defined subtypes of Alzheimer's disease	Ossenkoppele | Lyoo | Rabinovici | Hansson	**Ossenkoppele, Rik**
70	[18F]AV1451 deposition pattern across the Alzheimer's disease spectrum – characterization at the individual level	Pichet Binette | Gonneaud | Villeneuve | Neuroimaging Initiative	**Pichet Binette, Alexa**
69	Association between elevated brain tau pathology and subsequent cognitive decline among non-demented PSEN1 E280A mutation carriers: Preliminary findings from the COLBOS project	Quiroz | Sperling | Guzman-Velez | Hanseeuw | Pardilla-Delgado | Bocanegra | Vila-Castelar | Baena | Artola | Sanchez | Hampton | Fuller | Ramirez-Gomez | Gatchel | Schultz | Arboleda-Velasquez | Lopera | Reiman | Johnson	**Quiroz, Yakeel**
71	BLAzER: A versatile and efficient workflow for analyzing PET neuroimaging data in Alzheimer's disease	Raman | Grandhi | Murchison | Kennedy | Landau | Roberson | McConathy	**Raman, Fabio**
64	Evaluation of [18F]GTP1 (Genentech tau probe 1) Extent and Load for assessing tau burden in Alzheimer's disease	Sanabria Bohorquez | Baker | Manser | Toth | Marik | Weimer	**Sanabria Bohorquez, Sandra**
92	Tau and amyloid protein accumulation affect distinct white matter fiber tracts in Alzheimer's disease	Savard | Kang | Pascoal | Mathotaarachchi | Therriault | Chamoun | Lessa Benedet | M. Thomas | Parsons | Tissot | Lussier | Gauthier | Rosa-Neto	**Savard, Melissa**

Board #	Poster Title	Authors	Presenter
93	Plasma neurofilament light chain concentrations in relation to [18F]florbetapir and [18F]flortaucipir PET in Alzheimer's disease	Lessa Benedet | Leuzy | A. Pascoal | Mathotaarachchi | Savard | Therriault | Kang | Chamoun | Schöll | J. Ashton | Gauthier | Zetterberg | Rosa-Neto | Blennow | for the Alzheimer's Disease Neuroimaging Initiative	**Savard, Melissa**
61	Modelling tau pathology progression in Alzheimer's disease: Preliminary results and parameters required at a minimum to inform the model	Soucy | Hortelan | Benali	**Soucy, Jean-Paul**
81	Amyloid-dependent and –independent effects of Tau on clinical function in Alzheimer's disease	Therriault | Pascoal | Sefranek | Mathotaarachchi | Savard | Benedet | Chamoun | Kang | Gauthier | Rosa-Neto	**Therriault, Joseph**
82	Voxel-wise receiver operating characteristic analysis reveals clinically relevant sites of amyloid-beta deposition	Therriault | Pascoal | Leuzy | Collij | Lessa Benedet | Mathotaarachchi | Kang | Alves | Massarweh | Soucy | Gauthier | Rosa-Neto	**Therriault, Joseph**
94	APOEε4 potentiates the relationship between amyloid-β and tau pathologies in a dose-dependent manner	Parsons | Therriault | Benedet | Pascoal | Mathotaarachchi | Savard | Kang | Chamoun | Soucy | Massarweh | Saha-Chaudhuri | Poirier | Gauthier | Rosa-Neto	**Therriault, Joseph**
77	Association between neuroinflammation (level) and cognitive performance	Thomas | Chamoun | Pascoal | Savard | Nazar | Sbeiti | Olmand | Mathotaarachchi | Kang | Therriault | Gauthier | Rosa-Neto	**Thomas, Emilie**
109	Neuropsychiatric symptoms are correlated with tau deposition in the Alzheimer's disease spectrum	Tissot | Pascoal | Therriault | Chamoun | Lussier | Savard | Mathotaarachchi | Lessa Benedet | Thomas | Parsons | Rosa-Neto | Gauthier	**Tissot, Cécile**
111	Molecular imaging discordance with CSF AD biomarkers in atypical Alzheimer's disease	Townley	**Townley, Ryan**
66	Comparable associations between memory impairment and hippocampal [18F]flortaucipir signal after optimization	Wolters | Ossenkoppele | Golla | Verfaillie | Timmers | Visser | Tuncel | Coomans | Scheltens | Windhorst | van der Flier | Boellaard | van Berckel	**Wolters, Emma E**
101	A longitudinal examination of amyloid burden and myelin content in major white matter tracts	Yang | Dean III | Vogt | Jonaitis | Hunt | Merluzzi | Kohli | Christian | Oh | Betthauser | Asthana | Johnson | Alexander | Bendlin	**Yang, Kao Lee**
78	Relationship of amyloid-beta and neurofibrillary tau deposition in Down syndrome using [11C]PiB and [18F]AV-1451 PET	Zammit | Tudorascu | Cody | Laymon | Cohen | Minhas | Ellison | Sabbagh | Zaman | Johnson | Mathis | Klunk | Handen | Christian	**Zammit, Matt**
79	Amyloid accumulation in the striatum is more rapid than in the cortex early in Down syndrome and can serve as a marker for early intervention	Zammit | Cody | Betthauser | Tudorascu | Lao | Laymon | Cohen | Murali | Minhas | Zaman | Johnson | Mathis | Klunk | Handen | Christian	**Zammit, Matt**

FRIDAY

Board #	Poster Title	Authors	Presenter
153	A preliminary analysis of the association between cerebral blood flow and amyloid and tau PET binding in older adults	Albrecht | Isenberg | Stradford | Monreal | Jann | Pa	**Albrecht, Daniel**
125	Cerebrospinal fluid synaptic vesicle glycoprotein 2A in Alzheimer's disease	Ashton | Höglund | Leuzy | Heurling | Hansson | Schöll | Zetterberg | Blennow	**Ashton, Nicholas**
131	Spatially compact components of non-negative matrix factorization applied to AV-1451 PET images reveal distinct demographic associations	Bilgel | Ziontz | Shafer | Wong | Resnick	**Bilgel, Murat**
151	Comparing amyloid PET tracers and interpretation strategies: A multicenter study	Bischof | Bartenstein | Barthel | van Berckel | Doré | van Eimeren | Forster | Hammes | Lammertsma | Minoshima | Rowe | Sabri | Seibyl | van Laere | Vandenberghe | Villemagne | Yakushev | Drzezga	**Bischof, Gérard**

Board #	Poster Title	Authors	Presenter
154	Random forests of amyloid PET may pinpoint key brain regions predictive of MoCA score	Zukotynski | Gaudet | Kuo | Adamo | Goubran | Scott | Bocti | Borrie | Chertkow | Frayne | Hsiung | Laforce | Noseworthy | Prato | Sahlas | Smith | Sossi | Thiel | Soucy | Tardif | Black	**Black, Sandra**
145	Early localized network dysfunction in APOE ε4 carriers without biomarker evidence of Alzheimer's disease	Butt | Strain | Wisch | Schindler | Fagan | Curchaga | Benzinger | Ances	**Butt, Omar**
132	Independent contributions of hippocampal activity, amyloid burden, and retrospective decline to Subjective Cognitive Decline	Chen | Jingting | Farrell | Park	**Chen, Xi**
121	Disease progression modeling from preclinical stages of Alzheimer's disease (AD) to AD dementia	Cho | Woo | Kim | Kim | Kim | Kim | Jang | Kim | Kim | Jung | Kim | Lockhart | Ossenkoppele | Landau | Jagust | Weiner | Na | Seo	**Cho, Soo Hyun**
149	Longitudinal associations between Aβ and glucose metabolism in a normal elderly population	Tudorascu | Yu | Anderson | Snitz | Minhas | Laymon | Lopresti | Mathis | Aizenstein | Klunk | Cohen	**Cohen, Ann**
150	Associations between Aβ, tau, and cerebrovascular reactivity in a non-demented elderly population	Cohen | Huppert | Tudorascu | Snitz | Laymon | Lopresti | Mathis | Nadkarni | Lopez | Aizenstein | Klunk | Reis	**Cohen, Ann**
137	Staging cortical amyloid deposition using PET imaging	Collij | Heeman | Salvadó | Altomare | de Wilde | Konijnenberg | van Buchem | Yaqub | Markiewicz | Golla | Wottschel | Wink | Visser | Lammertsma | Scheltens | van der Flier | Boellaard | van Berckel | Gispert | Schmidt | Barkhof | Lopes Alves | AMYPAD consortium	**Collij, Lyduine**
129	Tau deposition in amyloid negative subjects: the application of the AT(N) model in the Geneva Memory Center experience	Dodich | Frisoni | Andryszak | Scheffler | Mendes | Assal | Schibli | Schwarz | Rakotomiaramanana | Gold | Zekry | Lovblad | Chicherio | Boccardi | Unschuld | Garibotto	**Dodich, Alessandra**
165	Chronic low-grade inflammation associates with lower TSPO binding in elderly individuals without dementia	Ekblad | Toppala | Tuisku | Helin | Marjamäki | Laine | Jula | Viitanen | Rinne	**Ekblad, Laura**
142	The BIN1 rs744373 SNP is associated with increased tau-PET levels and worse memory independent of amyloid	Franzmeier | Neitzel | Rubinski | Ewers	**Franzmeier, Nicolai**
167	F18-PI2620 Tau PET in three memory clinic patients with uncertain CSF biomarker profiles	Frolov | Sha | Fredericks | Nadiadwala | Azevedo | Hall | Toueg | Castillo | Deutsch | Greicius | Davidzon | Zaharchuk | Chin | Mormino	**Frolov, Alexander**
157	Beta-amyloid accumulation in non-demented elderly individuals correlates with baseline beta-amyloid load, ApoE genotype and age	Gietl | Treyer | Buchmann | Meyer | Saake | Gruber | Mu | Unschuld | Buck | Nitsch | Hock	**Gietl, Anton**
163	Prediction of brain age using resting-state functional connectivity suggests accelerated aging in the preclinical phase of autosomal dominant Alzheimer's disease, irrespectively of amyloid pathology	Gonneaud | Vachon-Presseau | Baria | Pichet Binette | Benzinger | Morris | Bateman | Breitner | Poirier | Villeneuve | Study Group | Research Group	**Gonneaud, Julie**
156	Relation of cardiovascular risk factors to markers of pathology and memory in autosomal-dominant Alzheimer's disease	Martínez | Guzmán-Vélez | Padilla-Delgado | Vila-Castelar | Fuller | Artola | Sperling | Quiroz	**Guzmán-Vélez, Edmarie**
147	Image features and clinical associations of the novel tau PET tracer 18F-APN-1607 in Alzheimer's disease	Hsu | Lin | Hsiao | Lian | Huang | Huang | Yen	**Hsu, Jung-Lung**
143	Optimal scanning time for the novel tau PET Tracer 18F-APN-1607	Huang | Hsiao | Lin | Lian | Hsu | Huang	**Huang, Chin-Chang**
171	Application of amyloid and tau classification system in subcortical vascular cognitive impairment patients	Jang | Kim | Park | Park | Choe | Cho | Lyoo | Lee | Kim | Cho | Kim | Kim | Jung | Ryu | Choi | Moon | Seong | DeCarli | Weiner | Lockhart | Na | Seo	**Jang, Hyemin**

Board #	Poster Title	Authors	Presenter
128	Clinical significance of amyloid β positivity in patients with probable cerebral amyloid angiopathy markers	Jang. | Jang | Kim | Werring | Lee | Choe | Park | Lee | Kim | Kim | Cho | Kim | Kim | Charidimou | Na | Seo	Jang, Young Kyoung
166	Cognitive trajectory of subcortical vascular cognitive impairment	Kim | Woo | Jang | Cho | Kim | Lee | Kim | Kim | Lee | Kim | Seo	Kim, Hee Jin
170	Modeling PiB PET trajectory groups identifies a subgroup with PiB beta-amyloid accumulation near age 50 and predicts MK-6240 SUVR	Koscik | Betthauser | Jonaitis | Clark | Allison | Mueller | Hermann | Poetter | Sanson | Shouel | Chin | Christian | Johnson	Koscik, Rebecca
158	Identification of rapid amyloid accumulators: A longitudinal PET amyloid study	Koychev | Vaci | Bilgel | An | Albert | Resnick	Koychev, Ivan
152	Amyloid and memory impairment have additive effects on microglial activation but not tau pathology	Kreisl | Tao | Zou | Johnson | Tomljanovic | Razlighi | Brickman | Lee | Stern	Kreisl, William
148	Safety, biodistribution and radiation dosimetry for the tau PET Tracer 18F-APN-1607 in healthy human subjects	Lin | Hsiao | Lian | Huang | Hsu | Huang | Yen	Lin, Kun-Ju
164	Vascular risk factors and multimodal neuroimaging biomarkers: Preliminary analyses from a biracial older adult cohort	Lockhart | Craft | Sachs | Rapp | Jung | Whitlow | Hayden | Hughes	Lockhart, Samuel
134	Influence of apolipoprotein-E (APOE) genotype on amyloid trajectories in a longitudinal subject cohort	Lopresti | Campbell | Yu | Snitz | Anderson | Aizenstein | Minhas | Kolibash | Cohen | Mathis | Klunk | Lopez | Tudorascu	Lopresti, Brian
135	A follow-up report on the prevalence and magnitude of amyloid positivity between cognitively normal elderly Japanese and Americans	Yu | Lopresti | Ihara | Cui | Aizenstein | Higashiyama | Fukuda | Koizumi | Minhas | Lopez | Klunk | Mathis | Miyamoto | Kuller | Sekikawa	Lopresti, Brian
130	Characterizing the spatial distribution of cross-sectional [18F]GTP1 (Genentech tau probe 1) SUVR using multivariate statistical analysis and machine learning	Manser | Sanabria Bohorquez | Baker | Toth | Teng | Marik | Weimer	Manser, Paul
146	Association between retinal thickness and brain β-amyloid accumulation in individuals with Subjective Cognitive Decline: data from the FACEHBI study	Marquié | Monté-Rubio | Rodríguez-Gómez | Sanabria | Castilla-Martí | Martínez | Alegret | Pérez-Cordón | Lomeña | Pavia | Gismondi | Bullich | Vivas-Larruy | Tejero | Gómez-Chiari | Orellana | Valero | Ruiz | Tárraga | Boada	Marquié, Marta
136	Association of in vivo [F-18]AV-1451 with [C-11]PiB, [F-18]FDG hypometabolism, and cortical atrophy in chronic TBI subjects	Minhas | Mountz | Laymon | Lopresti | Beers | Sharpless | Puccio | Edelman | Mathis | Okonkwo	Minhas, Davneet
124	Association of subjective cognitive decline and gait slowing with Aβ deposition in cognitively normal individuals	Nadkarni | Perera | Snitz | Mathis | DeKosky | Klunk | Lopez	Nadkarni, Neelesh
168	Differential associations of cortisol plasma level with glucose metabolism, hippocampal atrophy, and amyloid deposition across Alzheimer's disease stages	Oh | Leung | Canli | Slifstein	Oh, Hwamee
133	Amyloid and tau accumulate across distinct spatial networks and are differentially associated with brain connectivity	Pereira | Ossenkoppele | Palmqvist | Strandberg | Smith | Westman | Hansson	Pereira, Joana
144	Associations between behavioral factors and Alzheimer's pathology: Findings from cognitively normal older adults at risk of AD and presymptomatic ADAD mutation carriers	Pichet Binette | Gonneaud | Ozlen | Bedetti | Morris | Bateman | Benzinger | Poirier | Breitner | Villeneuve | Research Group | Study Group	Pichet Binette, Alexa
141	[11C]PIB PET is associated with the brain biopsy amyloid β load and CSF amyloid β levels in subjects with normal pressure hydrocephalus	Rinne | Suotunen | Rummukainen | Herukka | Nerg | Koivisto | Rauramaa | Nagren | Hiltunen | Alzfuzoff | Rinne | Jääskeläinen | Soininen | Leinonen	Rinne, Juha

Board #	Poster Title	Authors	Presenter
122	Metabolism mediates the effect of tau on cognition in mild cognitive impairment and dementia	Rodriguez-Vieitez | Mazrina | Chiotis | Colato | Nordberg	**Rodriguez-Vieitez, Elena**
123	Patterns of cerebral tau deposition across Alzheimer's disease stages: A study comparing 18F-THK5317 and 18F-AV-1451 PET tracers	Rodriguez-Vieitez | Colato | Chiotis | Mazrina | Nordberg	**Rodriguez-Vieitez, Elena**
126	Longitudinal evaluation of [18F]MK-6240 in Alzheimer's disease and cognitively normal adults: preliminary results at 6 and 12 months	Salinas | Purohit | Lohith | Struyk | Martarello | Beaver	**Salinas, Cristian**
160	Derivation of amyloid PET centiloid cut-offs using core AD CSF biomarkers including the whole Alzheimer's continuum: a joint analysis in ALFA and ADNI	Salvadó | Brugulat-Serrat | Falcon | Pavia | Niñerola | Perissinotti | Lomeña | Zetterberg | Blennow | Molinuevo | Gispert | ADNI, TRIBEKA Consortium and ALFA study	**Salvadó, Gemma**
161	SSRI reduces CSF Ab42 in healthy older adults and transgenic mice: dose, duration and baseline amyloid effects	Sheline | Snider | Lee | Linn | Fagan | Yan | Aselcioglu | Waligorska | Korecka | Morris | Shaw | Cirrito	**Sheline, Yvette**
162	Determination of the optimal scanning time point for the assessment of tau deposition in Alzheimer's disease using [18F]PI-2620 PET	Bullich | Mueller | Barret | Berndt | Madonia | Seibyl | Marek | Stephens	**Stephens, Andrew**
138	PET analysis of verubecestat effect on amyloid load in mild-to-moderate Alzheimer's disease patients (EPOCH trial)	Sur | Adamczuk | Sampat | Kost | Scott | Suhy | Egan	**Sur, Cyrille**
139	Effect of verubecestat on amyloid load in prodromal Alzheimer's disease patients: Results from the PhIII APECS trial	Sur | Kost | Adamczuk | Scott | Suhy | Egan	**Sur, Cyrille**
127	Subicular volume as a surrogate marker of beta-amyloid associated episodic memory variation at high age	Schroeder | Van Bergen | Schreiner | Meyer | Kagerer | Vionnet | Gietl | Treyer | Buck | Kaufmann | Nitsch | Pruessmann | Hock | Unschuld	**Unschuld, Paul**
120	Longitudinal [18F]AV-1451 PET imaging in primary progressive apraxia of speech	Utianski | Martin | Schwarz | Hugo | Duffy | Petersen | Clark | Machulda | Butts | Jack, Jr. | Lowe | Whitwell | Josephs	**Utianski, Rene**
159	Age-of-onset dependent associations between [18F]Flortaucipir PET and cognitive impairment in Alzheimer's disease	Visser | Wolters | Verfaillie | Ossenkoppele | Timmers | Tuncel | Golla | Boellaard | Windhorst | Scheltens | van der Flier | van Berckel	**Visser, Denise**
155	Comparison of objective and self-reported sleep, tau, and Aβ in healthy older adults	Winer | Fenton | Harrison | Maass | Baker | Jagust	**Winer, Joseph**
169	Cerebral small vessel disease is associated with medial temporal lobe hyperconnectivity in pre-clinical AD	Wu | Tudorascu | Mathis | Lopresti | Cohen | Snitz | Klunk | Aizenstein	**Wu, Minjie**
140	AV1451 retention is associated with hippocampal volume and memory declines in cognitively normal older adults	Ziontz | Bilgel | Shafer | June | Wong | Resnick	**Ziontz, Jacob**

PODIUM and POSTER PRESENTER INDEX

WEDNESDAY, January 16, 2019

Wednesday, January 16, 2019			Page
11:45 am	**Welcome Notes**	**Keith Johnson**, Massachusetts General Hospital, Boston, MA, US	
12:00 pm	**SESSION 1: Tracer properties**	CHAIRS: **Roger Gunn**, Invicro, Boston, MA, US/ICL, London, UK **Bradley Christian**, University of Wisconsin-Madison, Madison, WI, US	36
2:00	**POSTER SESSION 1** and Coffee Break		52
3:30	**SESSION 2: Methods**	CHAIRS: **Robert Koeppe**, Univ. of Michigan Med School, Ann Arbor, MI, US **Mark Lubberink**, Uppsala University, Uppsala, Sweden	158
5:45	**Keynote Lecture**	**Richard Carson**, Yale University, New Haven, CT, US	180
6:30-8:30	Welcome Reception		

Wednesday, January 16, 2019 - 12:00 pm - 01:30 pm

Podium Session

Session 1: Tracer Properties

CHAIRS: Bradley Christian, Roger Gunn

12:00 pm - 01:30 pm	Session 1: Tracer Properties	CHAIRS: Roger Gunn, Invicro, Boston, MA, US/ICL, London, UK Bradley Christian, University of Wisconsin-Madison, Madison, WI, US	Page
12:00	Head-to-head in vivo comparison of tau positron emission tomography ligands [18F]Flortaucipir (AV1451) and [18]RO948	**Michael Schöll**, University of Gothenburg, Gothenburg, Sweden	37
12:15	Retrospective comparison of [F-18]MK-6240, [F-18]THK5351 and [F-18]THK-5317 ((S)-THK-5117) in subjects scanned with all three PET tracers	**Tobey Betthauser**, University of Wisconsin-Madison School of Medicine and Public Health, Madison, WI, US	41
12:30	Head-to-Head comparison of neurofibrillary tangles imaging in Alzheimer's disease	**Pedro Rosa-Neto**, McGill University, Montreal, QC, Canada	44
12:45	Assessment of longitudinal change of tau pathology in Alzheimer's disease using [18F]GTP1 (Genentech tau probe 1) PET imaging	**Sandra Sanabria Bohorquez**, Genentech, Inc., South San Francicso, CA, US	46
1:00	Evaluation of 18F-PI-2620, a novel selective tau tracer for the assessment of Alzheimer's and non-Alzheimer's tauopathies	**Victor L Villemagne**, Austin Health, Melbourne, Australia	48
1:15	Evidence of differential in vitro and in vivo binding of APN-1607 in progressive supranuclear palsy and Alzheimer's disease	**Cristian Salinas**, Imaging Biomarkers, Biogen, Cambridge, MA, US	50
01:30-02:00	Discussion		

Head-to-head in vivo comparison of tau positron emission tomography ligands [18F]Flortaucipir (AV1451) and [18]RO948

Michael Schöll[1,2,3], Ruben Smith[2,4], Tomas Ohlsson[5], Olof Strandberg[2], Oskar Hansson[2,4]

[1]*Wallenberg Centre for Molecular and Translational Medicine and the Department for Psychiatry and Neurochemistry, University of Gothenburg, Gothenburg, Sweden*
[2]*Clinical Memory Research Unit, Department of Clinical Sciences, Lund University, Malmö, Sweden*
[3]*Dementia Research Centre, Department of Neurodegenerative Disease, University College London, London, UK*
[4]*Department of Neurology, Skåne University Hospital, Lund, Sweden*
[5]*Department of Radiation Physics, Skåne University Hospital, Lund, Sweden*

Introduction: [18F]Flortaucipir (FTP) is the most widely used PET ligand for the **in vivo** assessment of tau pathology. It binds to paired-helical filament tau and has been shown to be useful in the diagnosis of AD. However, off-target binding e.g. in the choroid plexus and the basal ganglia hamper accurate quantification of FTP in these and adjacent regions. Recently, several other tau PET ligands have been developed. Here, we compare [18F]FTP with the novel tau ligand [18]RO948 head-to-head **in vivo**.

Methods: Within this study, 24 individuals will undergo [18F]FTP PET at 80-100 min and [18F]RO948 at 70-90 min post ligand injection, a subsample will undergo dynamic scanning for up to 100 min. To date, 15 patients (mean age 73.3 ± 7.8 y; 13 AD (Aβ positive), one MCI (Aβ negative), one DLB (Aβ negative)) have been enrolled (average time between PET scans 33 ± 43 days). Standardized uptake value ratios (SUVR) were created using an identically derived inferior cerebellar reference region.

Results: On visual inspection, [18]RO948 uptake was substantially lower in the basal ganglia, the thalamus, and the choroid plexus, but not in the substantia nigra compared to [18F]FTP uptake. However, some cases exhibited strong [18]RO948 signal in the skull or the meninges, which was not observed for [18F]FTP.

Statistical comparison confirmed significantly lower [18]RO948 uptake in the choroid plexus and the basal ganglia, but also higher uptake in the entorhinal cortex.

Figure 1: Selection of [18F]Flortaucipir and [18F]RO948 scans of the same individuals
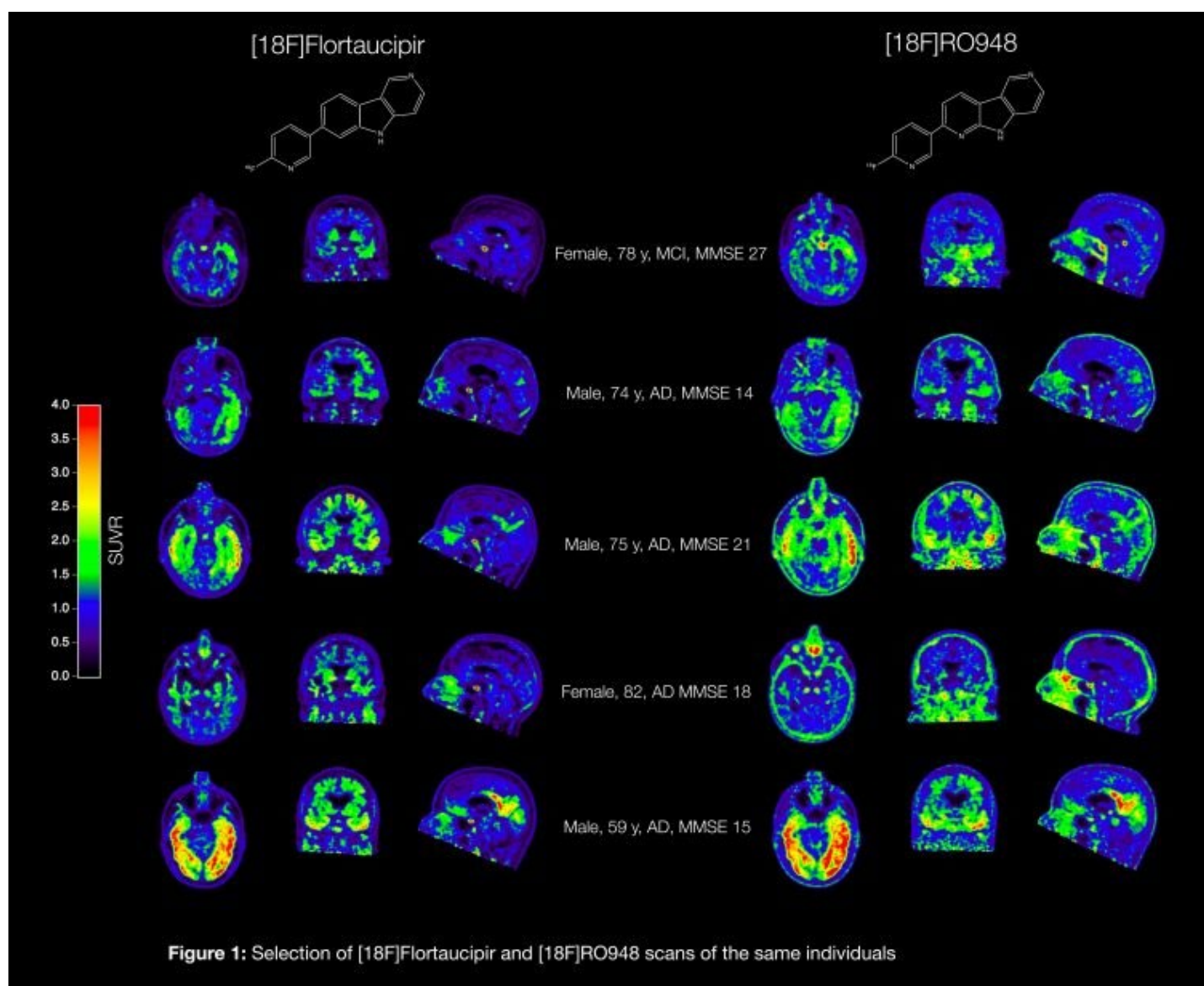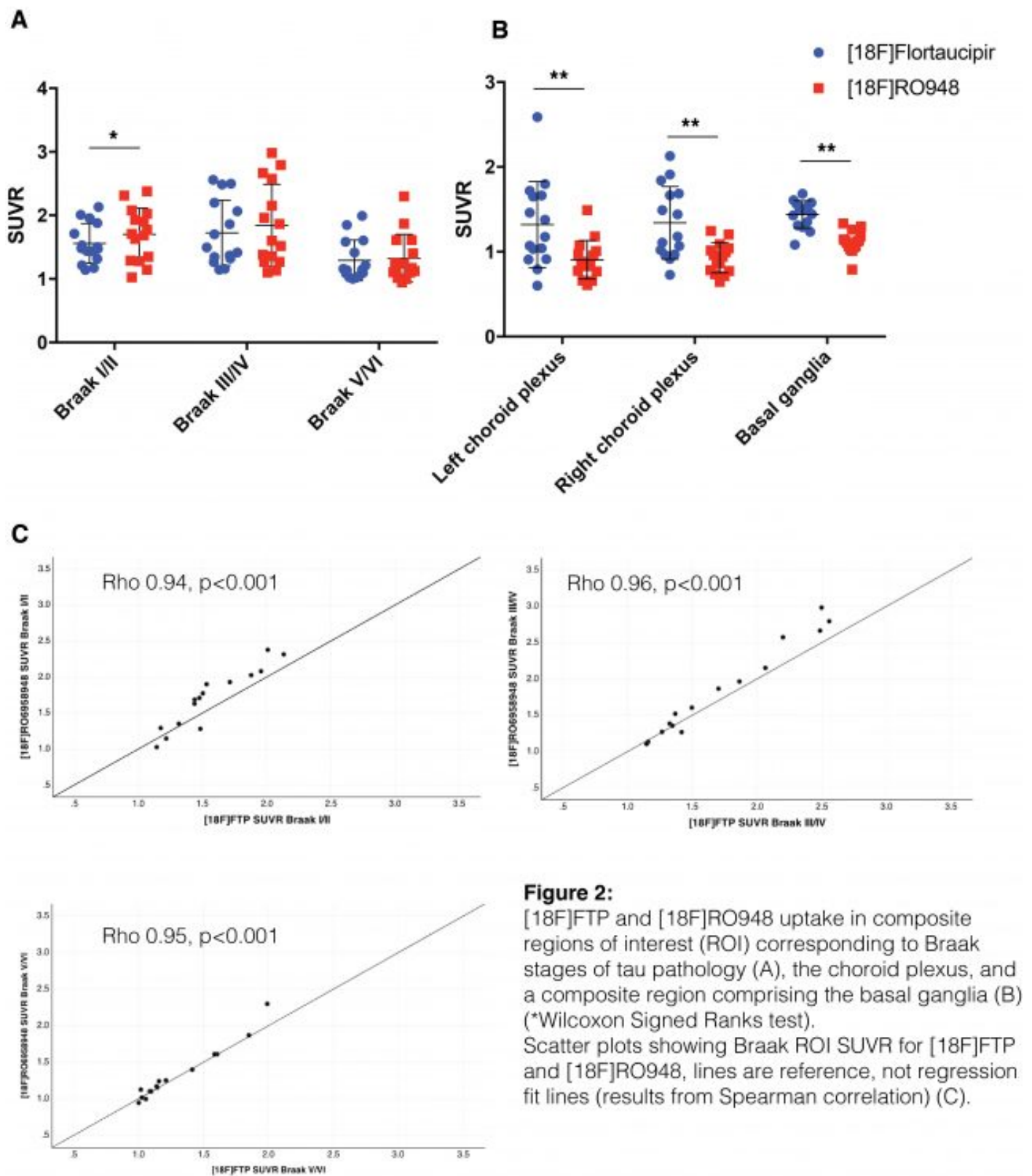
Figure 2:
[18F]FTP and [18F]RO948 uptake in composite regions of interest (ROI) corresponding to Braak stages of tau pathology (A), the choroid plexus, and a composite region comprising the basal ganglia (B) (*Wilcoxon Signed Ranks test).
Scatter plots showing Braak ROI SUVR for [18F]FTP and [18F]RO948, lines are reference, not regression fit lines (results from Spearman correlation) (C).

Voxelwise comparison of uptake patterns on a group level yielded significantly higher [18F]FTP uptake predominantly in the basal ganglia and the thalamus whereas the reverse contrast did not result in statistical significance.

Figure 3: Voxelwise t-test showing voxels with higher [18F]FTP uptake compared to [18F]RO948 in the same subjects (p<0.001 uncorrected, reverse contrast did not yield statistical significance at this threshold).
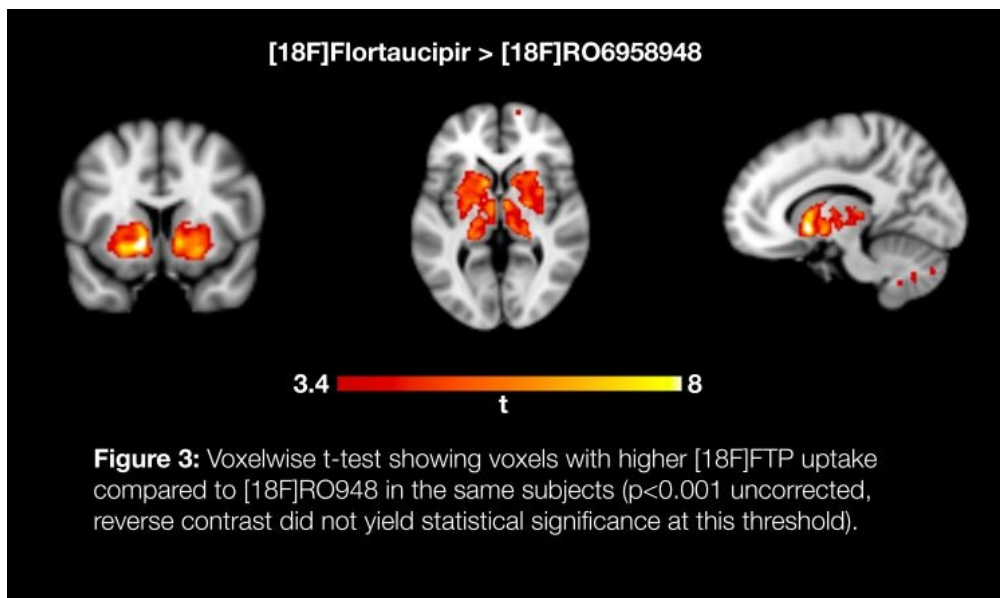
Conclusion: Our preliminary results suggest that [18]RO948 shows lower off-target binding in the choroid plexus and the basal ganglia compared to [18F]FTP, but demonstrates high uptake in regions surrounding the brain in a subset of cases.

Keywords: *PET, tau, [18F]AV1451, [18F]Flortaucipir, [18F]RO948*

Retrospective comparison of [F-18]MK-6240, [F-18]THK5351 and [F-18]THK-5317 ((S)-THK-5117) in subjects scanned with all three PET tracers

Tobey Betthauser[1], Alexander Converse[1], Dhanabalan Murali[1], Todd Barnhart[1], Charles Stone[1], Sterling Johnson[1], Bradley Christian[1]

[1]*University of Wisconsin-Madison School of Medicine and Public Health, Madison, WI, US*

Objectives: Previous studies have demonstrated that THK-5351 binds to MAO-B with high affinity, and that MK-6240 has a high affinity and selectivity for neurofibrillary tangles. The goal of this study was to investigate the likelihood that THK-5317 binds to MAO-B in vivo by retrospectively comparing the spatial distributions of THK-5317, THK-5351 and MK-6240 in individuals scanned with all three tracers over a three year period.

Methods: Individuals (n=8) were recruited from the Wisconsin Registry for Alzheimer's disease Prevention (WRAP) for [F-18]MK-6240, [F-18]THK-5351, [F-18]THK-5317 and [C-11]PiB PET and T1-weighted MR imaging as part of separate studies with an average of 1.5 ± 0.7 years between scans (THK-5317 first, THK-5351 second, MK-6240 last, Table 1). Cognitive status was determined based on consensus review of longitudinal cognitive assessments. PiB(+/-) status was determined based on a global DVR threshold (DVR$\geq$1.19, Logan graphical analysis, cerebellum GM reference region). PET data were registered to a longitudinally derived subject-specific T1w MRI template. SUVR estimates (MK-6240 70-90 min, THK 50-70 min, inferior cerebellum GM reference region) were compared by linear regression in cortical regions associated with NFT pathophysiology (i.e. neocortical Braak regions) and regions associated with high MOA-B density (caudate, putamen, pallidum, cingulate).

Results: Binding estimates of THK compounds were highly correlated with similar slopes in regions associated with cortical NFTs and high MAO-B (Figure1). MK-6240 SUVR indicated minimal correlation with either THK compound. Visual comparisons of parametric images were consistent with the ROI-level analysis (Figure2).

Conclusions: Agreement between THK-5317 and THK-5351 SUVR in regions expected to have differential ratios of MAO-B to NFTs suggests that THK-5317 may bind to MAO-B with a similar relative affinity to NFTs as THK-5351. The lack of agreement between THK and MK-6240 suggests that THK-5317 and THK-5351 have minimal use for detecting NFT pathophysiology, particularly when using reference tissue quantification strategies.

Subject No	1	2	3	4	5	6	7	8	Total
Sex	F	M	F	F	F	F	F	M	6F, 2M
APOE-ε4 Alleles	+	-	+	-	+	+	-	-	4+, 4-
Family History	+	-	+	+	-	+	+	+	6+, 2-
PiB Status	+	-	+	+	+	+	-	+	6+, 2-
Cognitive Status	MCI	Unimpaired	MCI	Unimpaired	Unimpaired	Unimpaired	Unimpaired	Unimpaired	2 MCI, 6 Unimpaired
CDR	0.5	0	0	0	0	0	0	0	
MMSE	28	30	30	29	30	29	30	29	29.4 ± 0.7
Δt(THK5351-THK5317) (yrs)	0.77	0.72	1.05	0.7	0.94	1.02	0.83	0.9	0.9 ± 0.1
Δt(MK6240-THK5351) (yrs)	1.97	2.54	2.01	2.5	1.7	1.63	2.01	2.73	2.1 ± 0.4
Age at MK-6240 (yrs)	78	77	72	77	64	67	60	76	71 ± 6
Braak Equivalent MK-6240 Stage	1+	0	5	5	0	5	0	1	

Table1: Participant demographics and time intervals between THK-5317, THK-5351, and MK-6240 PET scans. PiB and cognitive statues, CDR and MMSE were determined at the time of the MK-6240 PET scan.
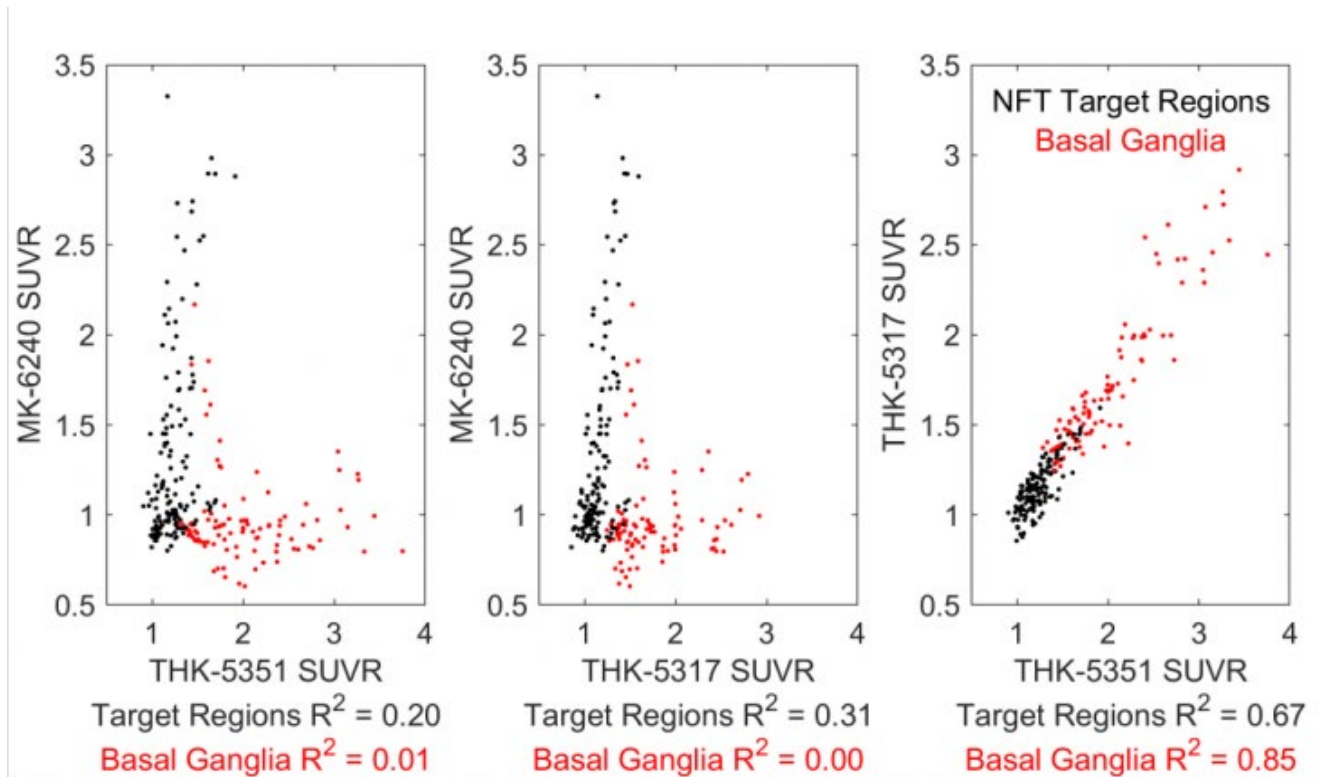
Figure 1: Comparisons of MK-6240, THK-5317, and THK-5351 SUVR estimates indicated minimal to no agreement between MK-6240 and the THK compounds, particularly in regions known to have high MAO-B density (e.g. basal ganglia). THK compounds were highly correlated in regions associated with NFTs and MAO-B. Agreement between THK compounds in both target and basal ganglia regions suggests similar relative affinities to MAO-B and NFTs. (Black points: 8 subjects by 18 unilateral ROIs consisting of inferior, middle and superior temporal gyri, anterior and posterior supramarginal gyri, angular gyrus, superior and middle frontal gyrus, and lateral occipital cortex; Red points: 8 subjects by 12 unilateral ROIs consisting of paracingulate, posterior and anterior cingulate gyri, caudate, putamen, and pallidum. ROIs from GM restricted Harvard-Oxford Atlas)
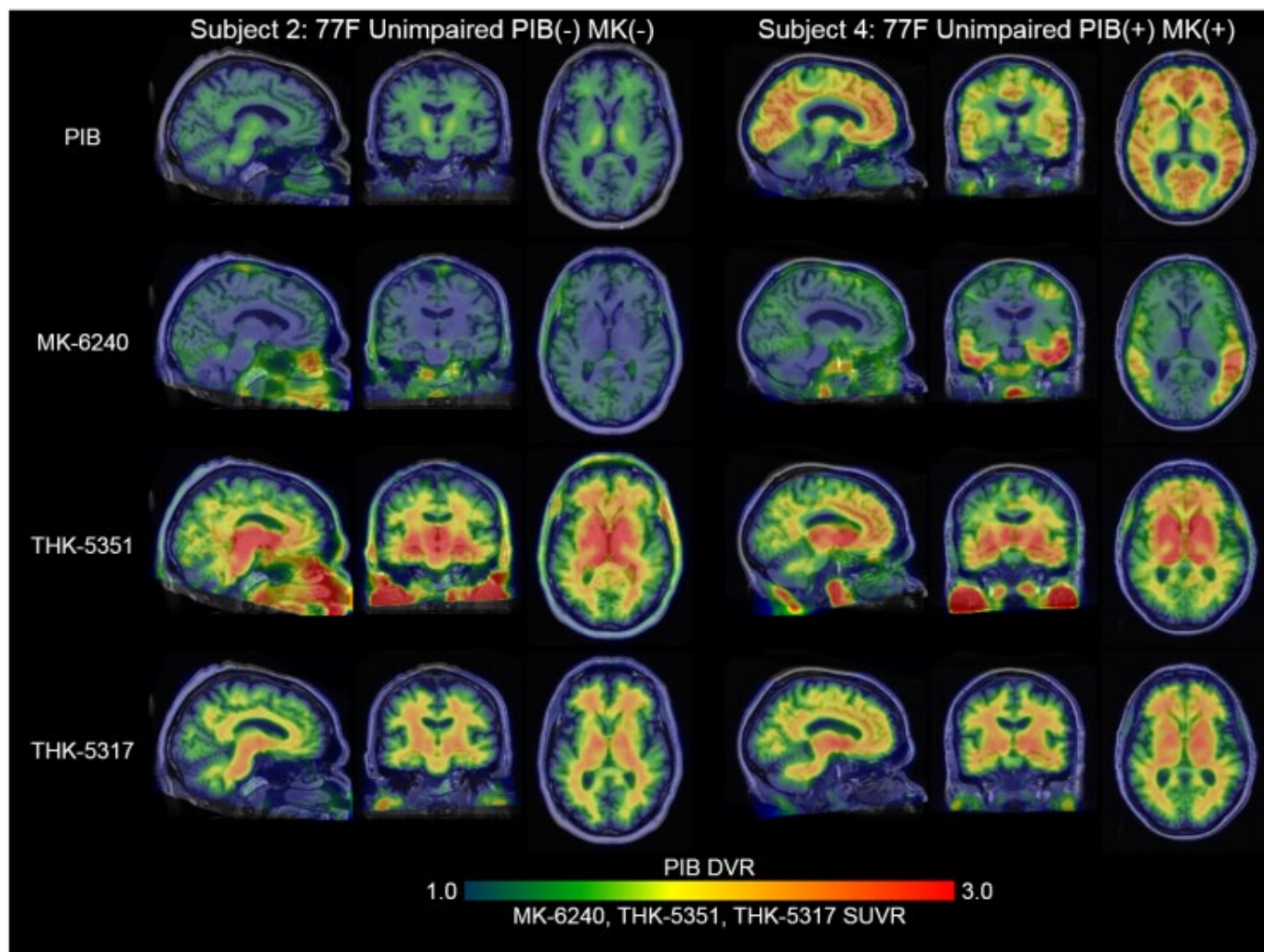
Figure 2: Comparison of parametric MK-6240, THK-5351 and THK-5317 SUVR images in age- and sex-matched individuals devoid of MK-6240 binding in the brain (left) and with high MK-6240 binding (right) in regions associated with NFT pathology. MK-6240 showed no elevated binding in regions associated with MAO-B (e.g. basal caudate, putamen, cingulate, etc.), whereas the THK compounds had moderate to high binding in these regions. MK-6240 and THK SUVR images were visually dissimilar across all individuals in the study. Taken together with the expected specificity of MK-6240 for NFTs, this suggests that THK compounds are not suitable for imaging NFT pathophysiology when using reference tissue quantification methods.

Head-to-head comparison of neurofibrillary tangles imaging in Alzheimer's disease

Tharick Pascoal[1], Mira Chamoin[1], Min Su Kang[1], Sulantha Mathotaarachchi[1], Andréa Benedet[1], Melissa Savard[1], Marlee Parsons[1], Joseph Therriault[1], Jean-Paul Soucy[1], Serge Gauthier[1], Pedro Rosa-Neto[1]

[1]McGill University, Montreal, QC, Canada

Objective: To compare the brain uptake of the neurofibrillary tangles tracer [^{18}F]MK-6240 and [^{18}F]AV-1451 in the same individuals.

Methods: 4 individuals from autosomal dominant Alzheimer's disease (AD) families (2 AD dementia, 1 male, mean age = 52.8 (8.2)) underwent positron emission tomography (PET) [^{18}F]AZD4694, [^{18}F]MK-6240, and [^{18}F]AV-1451. [^{18}F]MK-6240, and [^{18}F]AV-1451 standardized uptake value ratios (SUVRs) used the inferior cerebellum grey matter as the reference region and were calculated between 90 to 110 min and 80 to 100 min post-injection, respectively.

Results: The radiotracers showed distinct dynamic ranges of cortical uptake showing SUVRs values up to 8.94 and 4.53 for [^{18}F]MK-6240 and [^{18}F]AV-1451, respectively. In AD dementia individuals, both tau tracers showed the highest cortical uptake in the precuneus and posterior cingulate cortices followed by the temporal and medial prefrontal regions. A representative AD dementia individual is presented in figure 1.

| [¹⁸F]MK-6240 | [¹⁸F]AV-1451 | MRI |
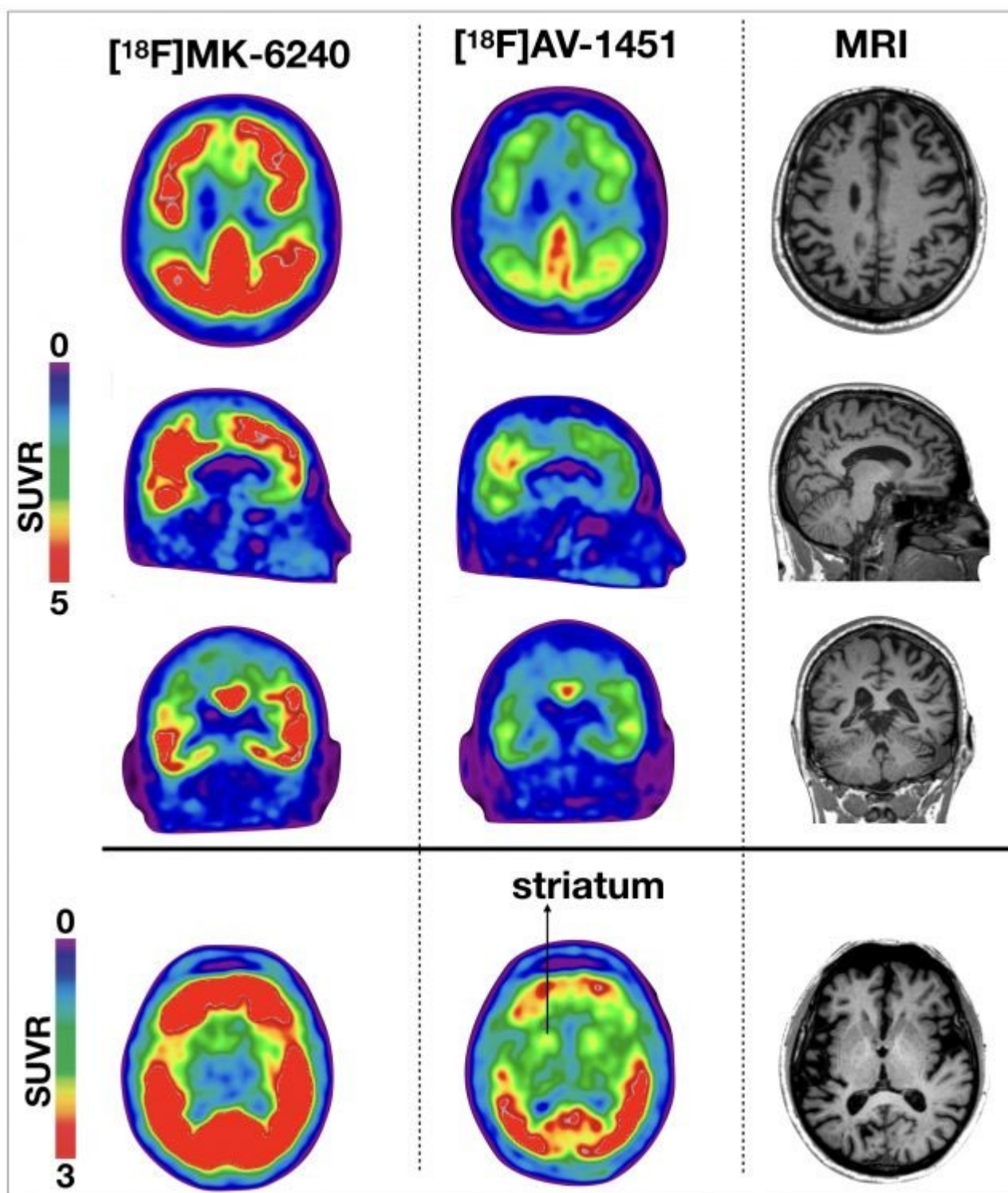
Conclusions: In this preliminary analysis, we found that although the two studied tau tracers showed substantial differences in the dynamical range of cortical SUVR, they showed uptake patterns similar to those reported in early tau histopathological observations.

Assessment of longitudinal change of tau pathology in Alzheimer's disease using [18F]GTP1 (Genentech tau probe 1) PET imaging

Sandra Sanabria Bohorquez[1], Suzanne Baker[1,2], Paul Manser[1], Balazs Toth[1], Edmond Teng[1], Jan Marik[1], Robby Weimer[1]

[1]*Genentech, Inc., South San Francicso, CA, US*
[2]*Molecular Biophysics and Integrated Bioimaging, Lawrence Berkeley National Lab., Berkeley, CA, US*

Objective: To quantify the longitudinal change of [^{18}F]GTP1 PET measurements in Alzheimer's disease (AD).

Methods: [^{18}F]GTP1 PET scans were performed at baseline and 12 months in amyloid negative and positive healthy volunteers (HV; n=2 and 7, respectively), and amyloid positive prodromal (Prod; n=18; MMSE 24-30, CDR = 0.5) and mild/moderate (MM; n=27; MMSE 22-30, CDR = 0.5-2) AD patients. Quantification was performed using the cerebellum gray as reference to calculate SUVR. Extent was defined as the percent voxels in an ROI above a SUVR threshold (Weimer et al. HAI 2017), the threshold is defined as the mean SUVR plus 2 standard deviations within the cerebellar gray. Measurements were made within a whole cortical gray matter (WCG) ROI or within **in vivo** Braak ROIs (Schöll et al., Neuron 2016).

Results: Baseline [^{18}F]GTP1 measures were, on average, higher in mild/moderate patients relative to prodromal or healthy volunteer (Figure 1). At 12 months, increases in [^{18}F]GTP1 measures were observed in the WCG and Braak ROIs in the prodromal and mild/moderate patients but not in healthy volunteers (Figure 2). In the prodromal patients, larger increases were observed in the Braak 1/2 ROI relative to the Braak 3/4 and 5/6 ROIs, whereas in mild/moderate patients larger increases were observed in Braak 3/4 and 5/6 ROIs. The variance of the change over 12 months was lower for Extent than for SUVR measures.

Conclusion: In the cohort of Alzheimer's disease patients in this study, tau pathology detected by [^{18}F]GTP1 PET imaging increased on average over a 12 month period. The magnitude and regionality of change appear to be disease stage-related. For example, larger increases were observed in 'early' Braak regions (i.e. 1/2) in prodromal patients relative to mild/moderate, consistent with the reported spatial relationship of tau pathology and disease severity (Braak and Braak et al.)

Figure 1. Boxplots of [^{18}F]GTP1 SUVR and extent in GM and Braak ROIs. MM: red circles; Prod: blue circles; HV: black circles.
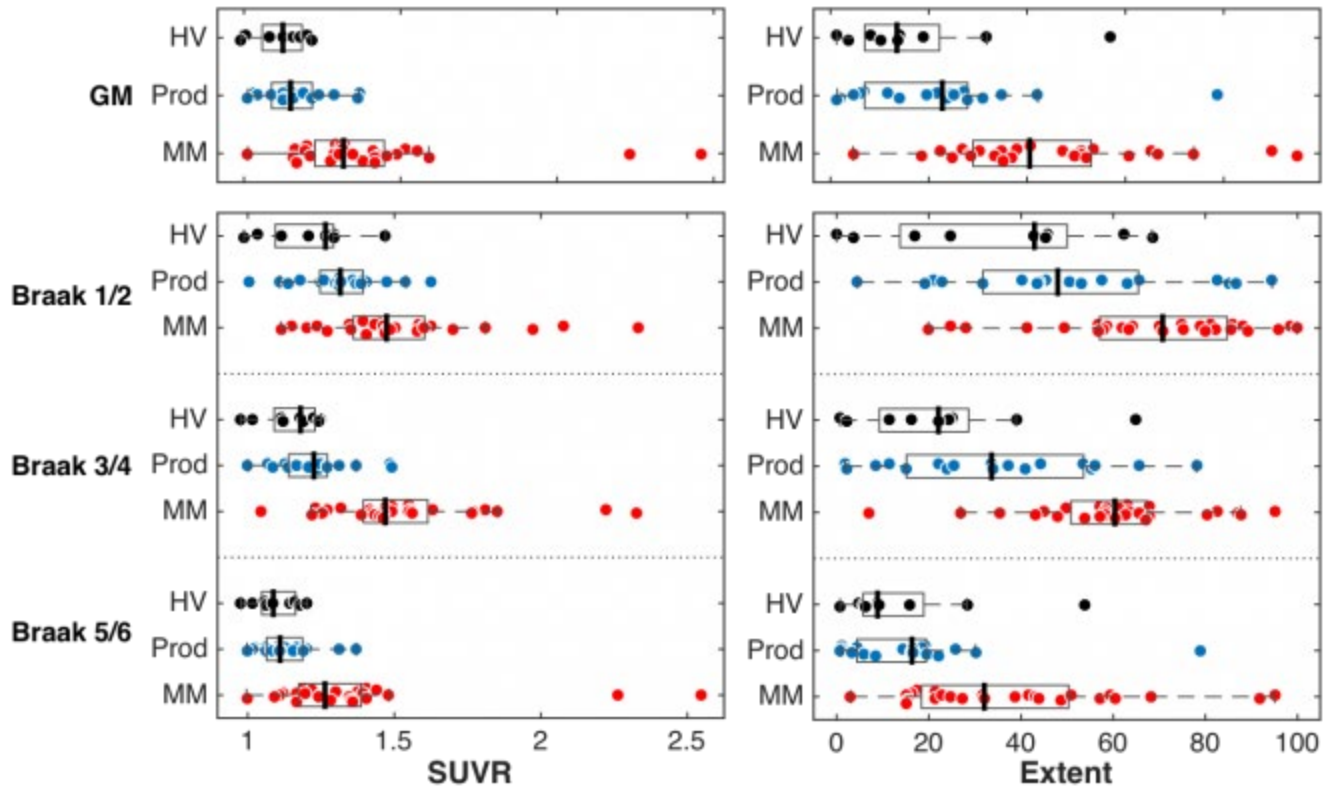
Figure 2. Measured average changes in SUVR and Extent and their corresponding confidence intervals in GM and Braak ROIs. MM: red circles; Prod: blue circles; HV: black circles.
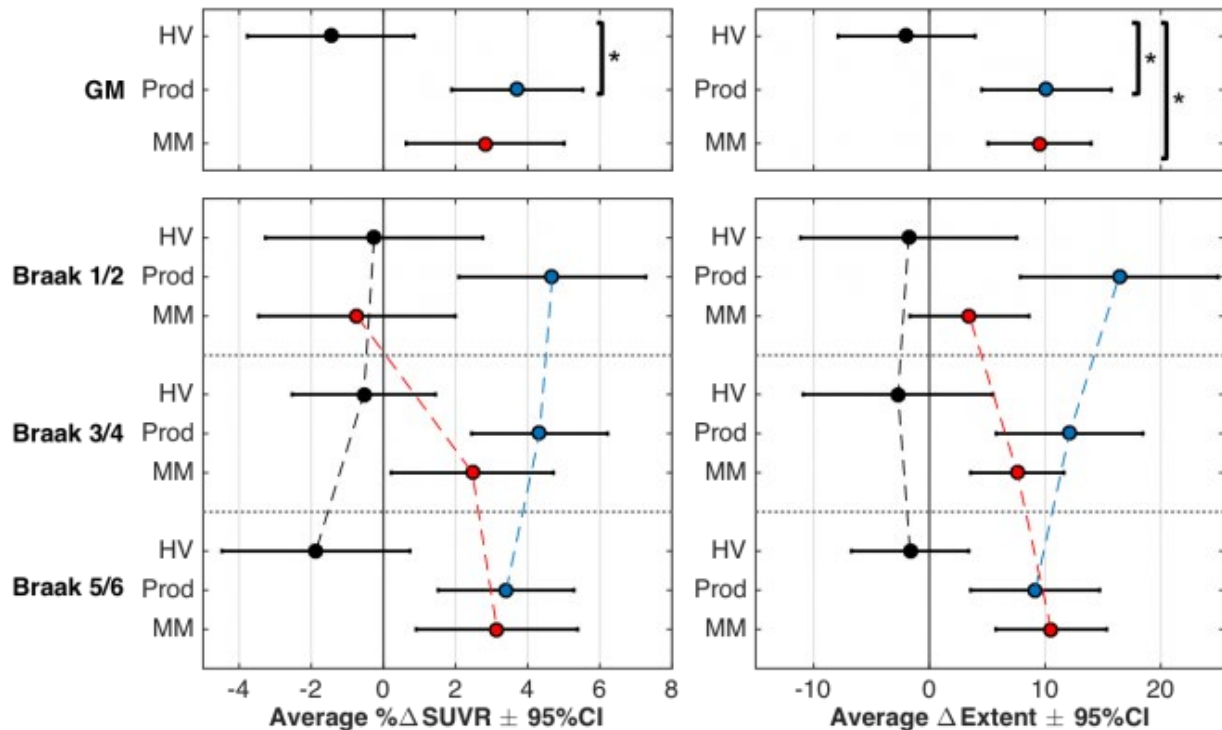
Evaluation of 18F-PI-2620, a novel selective tau tracer for the assessment of Alzheimer's and non-Alzheimer's tauopathies

Victor Villemagne[1,2,4], Vincent Doré[1,3], Rachel Mulligan[1], Regan Tyrrell[1], Fiona Lamb[1], Pierrick Bourgeat[3], Jurgen Fripp[3], Colin Masters[4], Christopher Rowe[1,2,4]

[1]Department of Molecular Imaging & Therapy, Austin Health, Melbourne, Australia
[2]Department of Medicine, The University of Melbourne, Melbourne, Australia
[3]CSIRO e-Health Research Centre, Brisbane, Australia
[4]The Florey Institute of Neuroscience and Mental Health, The University of Melbourne, Melbourne, Australia

Objectives: The purpose of the study was to assess the ability of ^{18}F-PI-2620 to measure global and regional tau burden in the brain in healthy older controls, AD, non-AD tauopathies such as Progressive Supranuclear Palsy (PSP) and other dementias such as Frontotemporal Lobar Degeneration (FTLD).

Methods: Participants with clinical diagnosis of probable AD (n=10, 1 Aβ-/9 Aβ+), PSP (n=6, 5 Aβ-/1 Aβ+), FTLD (n=3 Aβ-) as well as 10 healthy age-matched controls (HC, 7 Aβ-/3 Aβ+) and 3 participants classified as suffering mild cognitive impairment (MCI, 2 Aβ-/1 Aβ+), underwent a 50-70 min static scan with ^{18}F-NAV4694 to establish Aβ-status, and 0-120 min dynamic tau imaging with ^{18}F-PI-2620. Global and regional ^{18}F-PI-2620 binding was assessed using Distribution Volume Ratios (DVR), and with standardized uptake value ratios (SUVR), calculated using the cerebellar cortex as reference region.

Results: ^{18}F-PI-2620 displayed reversible kinetics and was rapidly metabolized with ~15% parent compound at 30 min. No "off-target" binding in choroid plexus or basal ganglia was observed in any of the participants scanned, although different degrees of tracer retention were observed along the longitudinal sinuses and the scalp (Fig 1). No significant tracer retention was observed in Aβ-HC, PSP or FTLD (Fig 1). In Aβ+AD patients, ^{18}F-PI-2620 binding was significantly higher than in Aβ-HC (temporoparietal: 2.46±0.99 vs. 0.99±0.12, *p=0.002,* Cohen's **d**=2.1), with the highest tracer retention in temporoparietal and posterior cingulate areas. While not reaching significance Aβ+HC had higher cortical tracer retention than Aβ-HC (Fig 1). Tau burden was inversely associated with FDG and cognitive performance. Identical classification into tau-/tau+ resulted from semiquantitative measures and visual inspection of the images.

Conclusions: Results indicate ^{18}F-PI-2620, is a sensitive tool to detect tau deposits in AD. Furthermore, our studies show ^{18}F-PI-2620 is not affected by potentially confounding "off-target" binding.
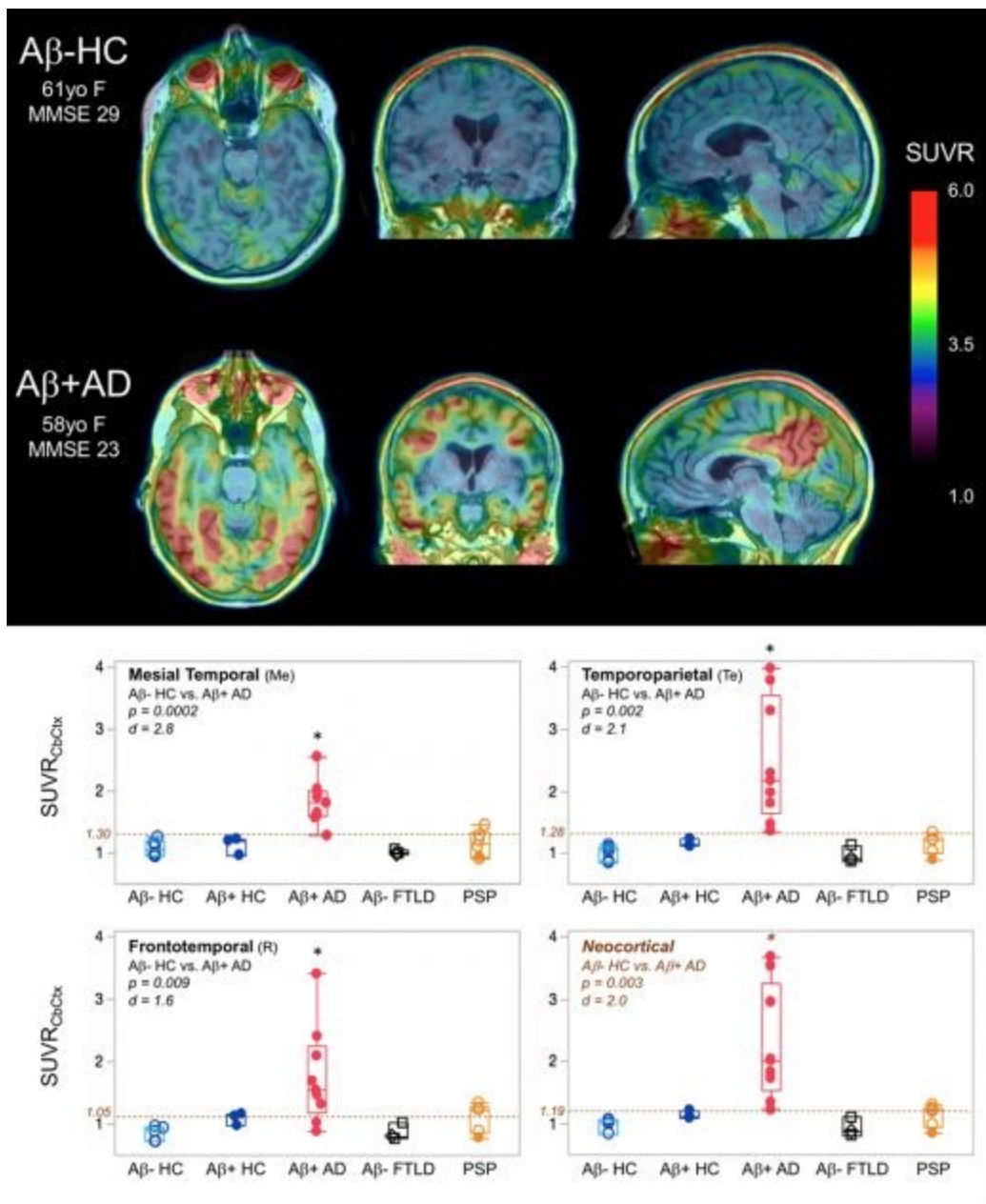
Figure 1. Tau imaging with 18F-PI2620

Top. Representative transaxial, coronal, and sagittal 18F-PI2620 min images in a Aβ- healthy control (Aβ-HC, 61 yo female, MMSE 29) and an Aβ+ Alzheimer's disease (Aβ+AD, 58yo female, MMSE 23) patient, showing significantly higher temporoparietal and post cingulate/precuneus tracer retention in the AD patient.

No 'off-target' binding in choroid plexus or basal ganglia was observed.

Bottom. Scatterplots for the mesial temporal (Me) temporoparietal (Te) and frontotemporal regions (R), as well as a global cortical measure of 18F-PI2620 retention in the brain, showing significantly higher global and regional cortical retention in AD compared to Aβ-HC, FTLD and PSP.

Keywords: *Tau imaging, Amyloid imaging, Alzheimer's disease, Progressive Supranuclear Palsy, Frontotemporal Lobar Degeneration*

Evidence of differential in vitro and in vivo binding of APN-1607 in progressive supranuclear palsy and Alzheimer's disease

Cristian Salinas[1], Sara Girmay[1], Paul Tempest[2], Richard Margolin[2], Kun-Ju Lin[3], Ajay Purohit[1], David Paterson[1], John Beaver[1], Ming-Kuei Jang[2], Laurent Martarello[1]

[1]Imaging Biomarkers, Biogen, Cambridge, MA, US
[2]Aprinoia Therapeutics, Taipei, Taiwan
[3]Linkou Chang Gung Memorial Hospital, Taoyuan, Taiwan

Introduction: [^{18}F]APN-1607 (previously [^{18}F]PM-PBB3) is a radiotracer being investigated for detection and longitudinal monitoring of aggregated tau in AD and non-AD tauopathies, e.g., progressive supranuclear palsy (PSP). Here we present results from tissue section autoradiographic (ARG) experiments and in vivo PET scanning of PSP, AD, and CN. ARG demonstrated [^{3}H]APN-1607 distribution patterns consistent with postmortem immunohistochemistry (IHC) findings in PSP. The regional uptake of [^{18}F]APN-1607 differentiated PSP subjects from AD and cognitively normal (CN) subjects.

Methods: ARG assays were conducted by incubating fresh frozen PSP, AD, and CN sections with [^{3}H]APN-1607 at K_D and under low specific activity conditions to calculate specific binding. to assess hyperphosphorylated tau (p-tau). Three PSP, 19 AD and 12 CN subjects were scanned dynamically with [^{18}F]APN-1607. Binding potentials for select regions were calculated using cerebellar grey matter as reference.

Results: Postmortem studies showed a specific binding distribution pattern consistent with the localization of p-tau by IHC. Additionally, specific binding in both AD and PSP was higher than control samples (Figure 1(A)). PET studies showed that [^{18}F]APN-1607 distributed differently among the three populations studied: high cortical uptake in AD, high binding in brain stem structures and basal ganglia (but low cortical uptake) in PSP, and low cortical, basal ganglia and brain stem structure binding in CN subjects (Figure 1(B)). Data analysis also showed that uptake in PSP was consistent with the known distribution of tau pathology in this disease (Figure 1(C)).

Conclusion: These in vitro and in vivo data suggest that [^{18}F]APN-1607 recognizes tau aggregates in AD and PSP with a topological distribution that is consistent with the pathology of the diseases.
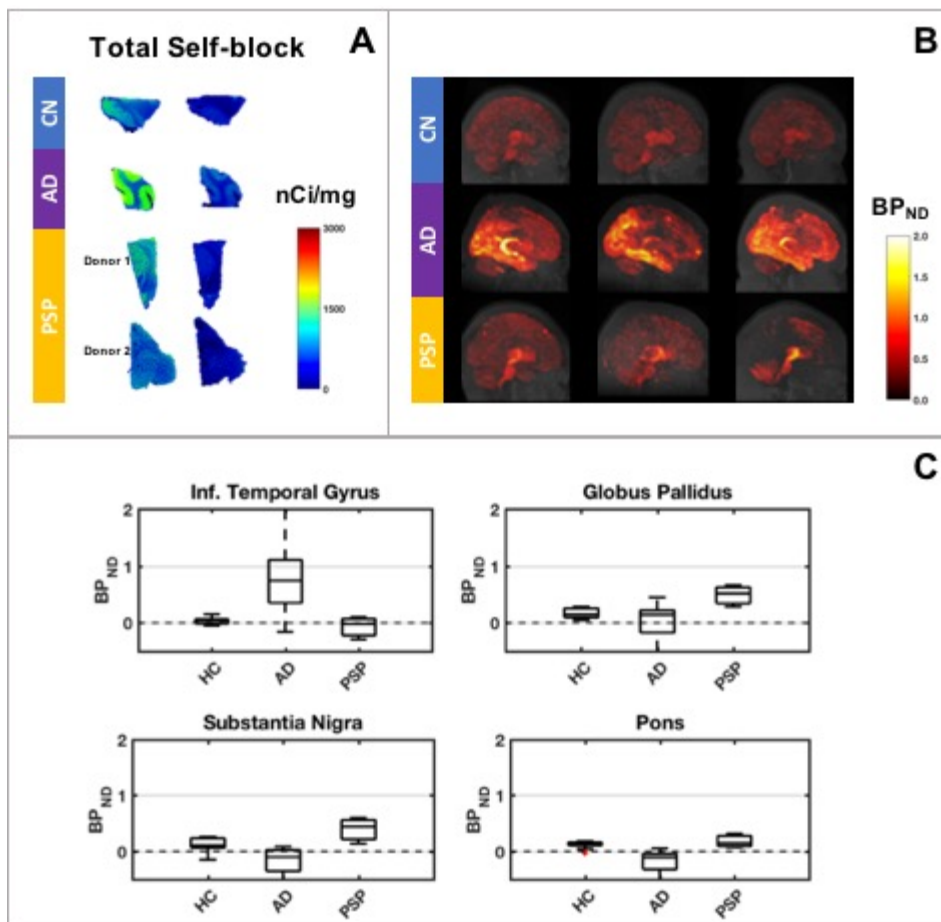
Figure 1: (A) Total and self-bock [18F]APN-1607 binding in human tissue samples (B) Maximum intensity projection BPND parametric images. (C) Differential uptake of [18F]APN-1607 across different populations.

Keywords: *APN-1607, tau PET, Alzheimer's disease, Progressive Supranuclear Palsy*

Wednesday, January 16, 2019 - 02:00 pm - 03:30 pm

Poster Session 1

Board #	Poster Title	Authors	Presenter	Page
	Wednesday, January 16, 2019			
48	Centiloid scale in practice: effect of different SUVR reference regions and comparison of Centiloid cut-offs	Adamczuk | Sampat | Runkle | Gorman | Suhy | Scott	**Adamczuk, Kate**	150
17	Functional connectivity of the entorhinal cortex predicts tau deposition in aging	Adams | Maass | Harrison | Jagust	**Adams, Jenna**	80
11	Multimodal magnetic resonance imaging predicts regional cerebral amyloid burden	Alathur Rangarajan | Wu | Joseph | Karim | Laymon | Tudorascu | Snitz | Cohen | Mathis | Klunk | Aizenstein	**Alathur Rangarajan, Anusha**	70
02	Regression-based predictive features for clinical brain images	Clark | Del Gaizo | Goukasian | Hwang | Apostolova	**Apostolova, Liana**	56
38	Evaluation of a visual read method for flortaucipir PET scans	Arora | Pontecorvo | Mintun | Fleisher | Devous | Lu | Galante | Stevenson | Flitter | Beach | Montine | Serrano | Sue | Intorcia | Curtis | Salloway | Thein | Wellman | Perrin | Lowe | Grossman | Irwin | Ikonomovic | Seeley | Rabinovici | Masdeu	**Arora, Anupa**	129
07	X-ray method for estimating amyloid load in the brain	Badano | Dahal	**Badano, Aldo**	64
46	Associations between quantitative susceptibility mapping and measures of amyloid and tau in patients with Alzheimer's disease	Baker | La Joie | Liu | Cobigo | Bourakova | Harrison | Rabinovici | Jagust	**Baker, Suzanne**	146
33	Identification and characterization of selective and high affinity small molecules for PET imaging of pathological alpha-synuclein	Capotosti | Tsika | Molette | Ravache | Vokali | Rodriguez | Darmency | Piorkowska | Purohit | Paterson | Evans | Martarello | Salinas | Poli | Kroth | Stoehr | Lowe | Pfeifer | Muhs	**Capotosti, Francesca**	119
25	Sensitivity of the Standard Centiloid to Track Longitudinal Amyloid-Beta Changes Using 18F-Florbetaben PET	Bullich | Villemange | Koglin | Jovalekic | Perrotin | Doré | Stephens | Rowe | De Santi	**De Santi, Susan**	102
45	Joint reconstruction method for longitudinal Tau-PET imaging	Tiss | Petibon | Ouyang | Ihsani | Kas | Habert | Johnson | El Fakhri	**El Fakhri, Georges**	145
36	Defining the lowest threshold for baseline amyloid-PET to predict future cognitive decline and amyloid accumulation in clinically normal adults	Farrell | Jiang | Schultz | Properzi | Rentz | Papp | Mormino | Betensky | Johnson | Sperling | Buckley	**Farrell, Michelle**	125
08	Impact of different image analysis methods on baseline 18F-Florbetapir PET measurements in the API ADAD Colombia trial	Ghisays | Chen | Protas | Goradia | Thiyyagura | Langbaum | Sink | Hu | Guthrie | Smith | Cho | Clayton | Thomas | Toga | Boker | Alvarez | Quiroz | Rios-Romenets | Chen | Su | Tariot | Lopera | Reiman	**Ghisays, Valentina**	65
22	TauIQ – an algorithm to quantify global and local Tau accumulation	Whittington | Seibyl | Hesterman | Gunn	**Gunn, Roger**	94
29	Preclinical characterization of two new promising tau PET tracers in vitro and in vivo	Skaddan | Mugnaini | Guo | Wooten | Wilcox | Reuter | Voorbach | Montavon | Reed | Relo | Mezler | Haupt | Geneste | Erhard | Pohlki | Tovcimak | Finnema | Martarello | Comley	**Guo, Qi**	110
13	Discovery of [18F]SMBT-1: a novel selective MAO-B PET tracer for imaging astrogliosis	Harada | Ezura | Iwata | Arai | Yanai | Furumoto | Kudo | Okamura	**Harada, Ryuichi**	75
27	Effect of blood flow changes on quantification of [18F]flutemetamol studies	Heeman | Yaqub | Lopes Alves | Heurling | Gispert | Foley | Boellaard | Lammertsma	**Heeman, Fiona**	105

Board #	Poster Title	Authors	Presenter	Page
30	Study on tissue-based and histogram-based reference regions for semi-quantitation of 18F-APN-1607 Tau PET Imaging	Hsiao | Huang | Chen | Lin | Huang	**Hsiao, Ing-Tsung**	112
50	NODDI modeling reveals neurite orientation and dispersion differences in white matter tracts of beta-amyloid positive individuals	Hunt | Vogt | Dean, III | Betthauser | Christian | Johnson | Alexander | Bendlin	**Hunt, Jack**	154
19	Network-based modeling of tau spread and seeding using PET and DTI	Yang | Chowdhury | Jacobs | Johnson | Dutta	**Jacobs, Heidi**	87
24	Reconsidering in-vivo models of regional amyloid pathology progression: region-specific thresholds and longitudinal data	Jelistratova | Bugla | Teipel | Grothe	**Jelistratova, Irina**	99
49	Amyloid-beta imaging in glial cells	Jethava | Prakash | Chopra	**Jethava, Krupal**	151
34	APOE genotype is associated with specific regional patterns of amyloid accumulation	Katz | Hanseeuw | Farrell | Moody | Sanchez | Mayblyum | Estime | Jacobs | Vannini | Sepulcre | Jiang | Schultz | Price | Sperling | Johnson	**Katz, Samantha**	120
01	Novel PET radioligands show that COX-1 is constitutively expressed and COX-2 is upregulated by inflammation	Kim | Shrestha | Eldridge | Singh | Cortes | Hong | Morse | Gladding | Henry | Gallagher | Frankland | Tye | Liow | Zoghbi | Fujita | Pike | Innis	**Kim, Min-Jeong**	55
32	Modeling the nonlinear effect of amyloid on cognitive impairment mediated by neurodegeneration in Alzheimer's disease using path analysis	Kim | Shin | Seong	**Kim, Sung-Woo**	116
39	An MRI-free, template-based method for quantifying cortical florbetapir uptake in vivo	Korman | Landau | Jagust	**Korman, Deniz**	130
14	Effect of point spread function specification error on GTM partial volume correction in PiB imaging	Laymon | Minhas | Kolibash | Aizenstein | Cohen | Lopresti | Mathis | Snitz | Tudorascu | Klunk	**Laymon, Charles**	76
26	Increased tau aggregation in young traumatic brain injury and post-concussion syndrome patients	Lubberink | Wall | Vedung | Fahlström | Weis | Haller | Larsson | Antoni | Marklund	**Lubberink, Mark**	103
31	Predicting amyloid accumulation in dominantly inherited Alzheimer's disease	Luckett | McCullough | McCarthy | Hassenstab | Fagan | Schindler | McDade | Bateman | Benzinger | Ances	**Luckett, Patrick**	114
37	Mild behavioral impairment is associated with β-amyloid and tau in cognitively intact elderly individuals	Lussier | Pascoal | Chamoun | Therriault | Tissot | Savard | Kang | Mathotaarachchi | Benedet | Thomas | Parsons | Ismail | Rosa-Neto | Gauthier	**Lussier, Firoza**	127
43	Enhancing tau signal of PET imaging using a convolutional autoencoder	Mathotaarachchi | Pascoal | Benedet | Chamoun | Savard | Kang | Therriault | Fonov | Gauthier | Rosa-Neto	**Mathotaarachchi, Sulantha**	141
40	Early increase in tau-PET signal is associated with changes in amyloid, CSF p-tau and cognition	McSweeney | Pichet Binette | Meyer | Gonneaud | Bedetti | Ozlen | Daoust | Labonté | Rosa-Neto | Breitner | Poirier | Villeneuve	**McSweeney, Melissa**	133
41	Mental and physical activity during the 80-minute uptake time affects off-target binding in tau PET scans (18F-AV-1451)	Apgar | Min | Maltais | Scott | Lecy | Lundt | Albertson | Schwarz | Botha | Jones | Kantarci | Vemuri | Knopman | Petersen | Jack | Lowe	**Min, Hoon-Ki**	137
51	Preliminary longitudinal evaluation of the novel tau tracer [18F]MK-6240	Pascoal | Chamoun | Kang | Mathotaarachchi | Benedet | Therriault | Souvy | Gauthier | Rosa-Neto	**Pascoal, Tharick**	152
05	Global cortical network organization analysis of amyloid and tau across AD clinical spectrum	Qureshi | Pascoal | Mathotaarachchi | Benedet | Rosa-Neto	**Qureshi, Muhammad Naveed Iqbal**	59

Wednesday, January 16, 2019

Board #	Poster Title	Authors	Presenter	Page
03	Subcortical amyloid load is associated with volume and shape in cognitively normal individuals	Rahayel | Bocti | Sévigny Dupont | Joannette | Lavallée | Nikelski | Chertkow | Joubert	**Rahayel, Shady**	57
04	Subcortical amyloid relates to cortical surface area in cognitively normal individuals	Rahayel | Bocti | Sévigny Dupont | Joannette | Lavallée | Nikelski | Chertkow | Joubert	**Rahayel, Shady**	58
09	Sub-threshold regional amyloid levels mediates parahippocampal thinning associated with reduced cerebral blood flow.	Sisley | Sanchez | Domoto-Reilly | Grabowski | Rane	**Rane, Swati**	66
18	A fully automatic technique for precise localization and quantification of Amyloid-β PET scans	Tahmi | Bou Zeid | Razlighi	**Razlighi, Qolamreza**	83
21	PET and CSF amyloid status are differently predicted by patient features	Reimand | de Wilde | Teunissen | Zwan | Windhorst | Boellaard | van der Flier | Scheltens | van Berckel | Ossenkoppele | Bouwman	**Reimand, Juhan**	90
10	[18F]GTP1 (Genentech tau probe 1) SUVR has a very little dependence on changes in regional or global cerebral blood flow	Sanabria | Baker | Marik | de Crespigny | Weimer	**Sanabria, Sandra**	68
12	Evaluation of [18F]APN-1607 to image tau protein in patients with Alzheimer's disease and test-retest studies	Sandiego | Barret | Carroll | Gouasmat | Madonia | Marek | Margolin | Tempest | Jang	**Sandiego, Christine**	74
06	Abnormal AV1451 signal in popular reference regions	Schwarz | Kantarci | Murray | Przybelski | Min | Lowe | Nedelska | Vemuri | Senjem | Gunter | Petersen | Knopman | Jack	**Schwarz, Christopher**	61
16	Subject-specific site of maximum uptake is most sensitive to longitudinal change in 18F-AV1451 PET data	Scott | Adamczuk | Gorman | Runkle | Suhy	**Scott, David**	79
47	The relationship between Aβ-related hippocampal activity and metabolism in impaired individuals	Scott | Hanseeuw | Huijbers | Hampton | Manning | Chhatwal | Buckley | Johnson | Sperling | Schultz	**Scott, Matthew**	148
20	Establishment of a simplified method to quantify [18F]PM-PBB3 ([18F]APN-1607) binding in the brains of living human subjects	Seki | Tagai | Shimada | Kitamura | Kimura | Ichise | Ono | Takahata | Kubota | Takado | Shinotoh | Okada | Kikuchi | Zhang | Suhara | Higuchi	**Seki, Chie**	89
35	Association of reported sleep-wake disturbances with tau pathology in mild cognitive impairment and normal cognitive aging	Shokouhi | Conley | Gwirtsman | Newhouse	**Shokouhi, Sepideh**	124
28	Longitudinal [18F]Flortaucipir in the BioFINDER 1 Cohort	Smith | Strandberg | Stomrud | Hansson	**Smith, Ruben**	107
44	Co-evolving patterns of functional connectivity with amyloid and tau deposition in Alzheimer's disease progression	Svaldi | Goñi | Amico | Risacher | Stage | West | Saykin | Apostolova	**Svaldi, Diana**	142
23	AmyloidIQ – an automated algorithm for classifying amyloid-β PET scans	Whittington | Seibyl | Eichenlaub | Stephens | Hesterman | Gunn	**Whittington, Alex**	96
42	Functional network changes occur prior to symptomatic conversion in AD	Wisch | Roe | Babulal | Benzinger | Morris | Ances	**Wisch, Julie**	138
15	11C-ER176 has superior quality than 11C-PBR28 to image brain inflammation with positron emission tomography	Zanotti Fregonara | Pascual | Yu | Beers | Appel | Masdeu	**Zanotti Fregonara, Paolo**	78

P01: Novel PET radioligands show that COX-1 is constitutively expressed and COX-2 is upregulated by inflammation

<u>Min-Jeong Kim</u>[1], Stal Shrestha[1], Mark Eldridge[2], Prachi Singh[1], Michelle Cortes[1], Jinsoo Hong[1], Cheryl Morse[1], Robert Gladding[1], Katharine Henry[1], Evan Gallagher[1], Michael Frankland[1], George Tye[1], Jeih-San Liow[1], Sami Zoghbi[1], Masahiro Fujita[1], Victor Pike[1], Robert Innis[1]

[1]*Molecular Imaging Branch, National Institute of Mental Health, National Institutes of Health, Bethesda, MD, US*
[2]*Laboratory of Neuropsychology, National Institute of Mental Health, National Institutes of Health, Bethesda, MD, US*

Introduction: The cyclooxygenase (COX) system comprises two isoforms—COX-1 and COX-2—that are important targets for neuroinflammatory biomarkers. We developed two PET radioligands: [^{11}C]PS13 for COX-1 and [^{11}C]MC1 for COX-2. Using these radioligands, this study sought: 1) to assess the distribution of uptake and in vivo selectivity of these radioligands, and 2) to determine whether COX-1 and COX-2 are upregulated by neuroinflammation.

Methods: Intravenous injection of either radioligand was followed by dynamic PET scans. For [^{11}C]PS13, eight brain and 11 whole-body scans were obtained in human subjects, and 16 whole-body scans were obtained in monkeys. For [^{11}C]MC1, eight whole-body scans were obtained in monkeys. To measure in vivo selectivity, scans were also performed pretreated with non-radioactive drugs preferential for COX-1 or COX-2. To induce transient neuroinflammation, lipopolysaccharide (LPS) was injected into the right putamen of four monkeys, and brain PET scans were obtained on post-injection Days 1, 3, and 8.

Results: In both humans and monkeys under baseline conditions, [^{11}C]PS13 showed specific uptake in most major organs including the spleen, gastrointestinal tract, kidneys, and brain. [^{11}C]PS13 uptake in these organs was blocked by COX-1 inhibitors, but not by COX-2 inhibitors. In human brain, [^{11}C]PS13 showed prominent uptake in the hippocampus and occipital cortex, consistently with the known expression of the COX-1 gene. In contrast, under baseline conditions, specific uptake of [^{11}C]MC1 was only observed in the ovaries in monkeys. In addition, specific binding of [^{11}C]MC1 was markedly increased after LPS injection in monkey brain.

Conclusions: Our results suggest that COX-1 is constitutively expressed in major organs while COX-2 is upregulated with inflammation. The in vivo selectivity of [^{11}C]PS13 and [^{11}C]MC1 was also well demonstrated by pharmacological blockade. These radioligands are potential probes for measuring neuroinflammation in brain disorders, as well as for measuring target engagement by therapeutic drugs.

Keywords: *cyclooxygenase-1; cyclooxygenase-2; positron-emission tomography; inflammation; nonsteroidal antiinflammatory agents*

P02: Regression-based predictive features for clinical brain images

David Clark[1], John Del Gaizo[2], Naira Goukasian[3], Kristy Hwang[4], Liana Apostolova[1]

[1]*Indiana University, Indianapolis, IN, US*
[2]*Medical University of South Carolina, Charleston, SC, US*
[3]*University of Vermont, Burlington, VT, US*
[4]*Emory University, Atlanta, GA, US*

Objective: To develop straightforward scoring methods for brain images and assess their predictive power.

Background: Brain images constitute a rich source of information for clinical machine learning applications. In previous work, a predictive feature derived through regression-based image comparison (**Rs** score) was shown to have value for discerning between individuals with mild cognitive impairment (MCI) who do or do not develop dementia during follow up. In the current work, we address a potential weakness in the previous analysis by developing a set of new regression-based predictive features and demonstrating their relative and complementary value for predicting clinical outcomes.

Methods: One hundred fifty-eight individuals (107 with MCI and 51 cognitively normal controls) were recruited into a longitudinal study of aging and genetics. All participants underwent structural MRI scans. Seventy participants also underwent flutemetamol amyloid PET scans. Structural MRI scans were processed using previously described methods to derive a representation of the cortical surface. We assessed the value of eight regression-based features derived from cortical surfaces for predicting two outcomes of interest: conversion from MCI to dementia and amyloid positivity. As there were only eight predictive features, we performed an exhaustive evaluation including every possible combination (255 support vector regression models per outcome).

Results: The best performing model for predicting amyloid status had an AUC score of 0.93 and incorporated the **Rs** score along with four chronological features, while the highest performing model with regard to conversion had an AUC of 0.87 with four chronological features and did not include **Rs**.

Conclusion: Our results suggest that the **Rs** score has more potential for prediction of amyloid status than conversion, while the remaining features are useful for predicting both outcomes. Regression-based methods may have general value for generating predictive features from images.

Keywords: *PET, Alzheimer's disease, imaging, machine learning, MRI*

P03: Subcortical amyloid load is associated with volume and shape in cognitively normal individuals

Shady Rahayel[1,2], Christian Bocti[3], Pénélope Sévigny Dupont[1,2], Maude Joannette[1,2], Marie Maxime Lavallée[1,2], Jim Nikelski[4], Howard Chertkow[4,5], Sven Joubert[1,2]

[1]*Department of Psychology, Université de Montréal, Montreal, QC, Canada*
[2]*Research Centre, Institut universitaire de gériatrie de Montréal, Montreal, QC, Canada*
[3]*Department of Neurology, Université de Sherbrooke, Sherbrooke, QC, Canada*
[4]*Lady Davis Institute for Medical Research, Jewish General Hospital, McGill University, Montreal, QC, Canada*
[5]*Department of Neurology and Neurosurgery, McGill University, Montreal, QC, Canada*

Aβ is frequent in cognitively normal individuals and associated with structural changes in subcortical structures, especially in the hippocampus. We investigated whether Aβ burden in the cortex and in subcortical structures differentially affected subcortical volume and surface in cognitively normal individuals.

We recruited 104 cognitively normal individuals who underwent neuropsychological assessment, PiB-PET imaging, and acquisition of T1-weighted MRI scan. PiB retention values were derived for the cortex and subcortical structures (hippocampus, amygdala, putamen, caudate, pallidum, thalamus). Subcortical volume and surface were computed for each structure, including volumes of the hippocampal subfields. We investigated the associations of PiB retention values with volume (partial correlations) and surface (vertex-wise GLM) of subcortical structures. Surface-based analysis were performed in two ways: without scaling for surface changes due to volume/shape and with scaling for surface changes due to shape only.

We found that cortical PiB retention was not associated with subcortical morphology. In contrast, PiB retention in the hippocampus was associated with increased volume of the hippocampus, specifically in the CA1 subfield, subiculum, and molecular layer (uncorrected). PiB retention in the hippocampus, thalamus, and pallidum was also associated with changes in subcortical surface. Specifically, outward surface displacement in the hippocampus and most of the thalamus was due to local volume only, medial and dorsal surface displacement in the thalamus and displacement in the pallidum were due to local shape only.

In summary, subcortical Aβ is associated with subcortical surface changes in cognitively normal individuals. Whereas hippocampal surface changes were due to increased volume, surface changes in the thalamus were due to both volume and shape and changes in the pallidum to shape only. Subcortical Aβ in the hippocampus was also marginally associated with hippocampal volume. This underlines the importance of investigating the effect of subcortical Aβ on subcortical morphology in cognitively normal individuals.

Keywords: *surface, subcortical, volume, shape, hippocampus*

P04: Subcortical amyloid relates to cortical surface area in cognitively normal individuals

Shady Rahayel[1,2], Christian Bocti[3], Pénélope Sévigny Dupont[1,2], Maude Joannette[1,2], Marie Maxime Lavallée[1,2], Jim Nikelski[4], Howard Chertkow[4,5], Sven Joubert[1,2]

[1]*Department of Psychology, Université de Montréal, Montreal, QC, Canada*
[2]*Research Centre, Institut universitaire de gériatrie de Montréal, Montreal, QC, Canada*
[3]*Department of Neurology, Université de Sherbrooke, Sherbrooke, QC, Canada*
[4]*Lady Davis Institute for Medical Research, Jewish General Hospital, McGill University, Montreal, QC, Canada*
[5]*Department of Neurology and Neurosurgery, McGill University, Montreal, QC, Canada*

Aβ has been associated with cortical changes in cognitively normal individuals. However, the relative contribution of cortical thickness and surface area to volume changes remains unknown.

We recruited 104 cognitively normal individuals who underwent neuropsychological assessment, PiB-PET imaging, and acquisition of T1-weighted MRI scan. PiB retention values were derived for the cortex and subcortical structures (hippocampus, amygdala, putamen, caudate, pallidum, thalamus). Whole-brain vertex-wise surface-based cortical analyses were performed to investigate the associations between cortical and subcortical PiB retention values and local cortical volume, surface area, and thickness. Mediation analyses were then performed on the clusters showing significant association with cortical volume to investigate the relative contribution of cortical surface area and thickness to Aβ-associated cortical volume changes.

We found that Aβ in the hippocampus, amygdala, and pallidum revealed decreased cortical volume in the medial frontal cortex. Volume changes were primarily driven by reductions in cortical surface area, except for the amygdala, which revealed a concomitant effect of cortical thinning on volume. We also found that Aβ in the thalamus was associated with increased cortical volume in the posterior portion of the lateral temporal cortex, which was also driven by increased surface area; the effect of cortical thickening on increased volume was borderline.

In summary, in contrast to cortical Aβ, subcortical Aβ was associated with changes in cortical morphology, in terms of volume, surface area, and thickness, in cognitively normal individuals. This highlights the importance of investigating subcortical Aβ burden and cortical surface area in cognitively normal individuals.

Keywords: *amyloid, cortical, volume, thickness, surface*

P05: Global cortical network organization analysis of amyloid and tau across AD clinical spectrum

Muhammad Naveed Iqbal Qureshi[1], Tharick Ali Pascoal[1], Sulantha Mathotaarachchi[1], Andréa Lessa Benedet[1], Pedro Rosa-Neto[1]

[1]*McGill Center for Studies in Aging, McGill University, Montreal, QC, Canada*

Introduction: This study examines the progression of Tau and Amyloid protein aggregates deposition networks in Alzheimer's disease (AD).

Method: We studied CN (n=90), mild cognitive impairment MCI (n=22), and AD (n=36) subjects of our in-house study cohort (TRIAD). We hypothesized that the protein aggregates deposition in the control normal should be minimum and gradually increase in the MCI and AD groups i.e., AD > MCI > CN. A global (whole brain gray matter voxels) correlation technique is used to measure the associations between protein deposition across brain voxels. All the images from each study group were processed in the following steps. For T1 structural MRI images, we applied N4 bias correction, brain masking (extraction), tissue segmentation, and template registration. For PET images, we applied smoothing by c3d, T1 registration, template registration, and created SUVR images by ImageMath function of ANTs tool. Later these SUVR image volumes were concatenated in a time-series fashion to obtain the global connectivity maps. An AFNI program 3dTcorrMap was used for this purpose. It computes the voxel-wise correlation from each non-zero voxel as a seed to all the non-zero voxels in the brain and creates the connectivity maps. Later these maps were z-transformed, then all these connectivity maps were averaged together to create a global average connectivity map. Finally, we created subtraction images from the final global correlation images to visualize the difference between each sub-group for the same protein aggregates.

Result and Conclusion: We found significant differences in same groups for the deposition of two protein aggregates. In addition, a significant difference was found between the groups for the same protein aggregates. We may regard these differences as the protein aggregates deposition progression patterns. These results indicate that the strength of amyloid connectivity is higher than tau.

Individual Group Protein Deposition and Progression

Figure 1. The connectivity networks of each protein aggregate in each study sub-group

Group Differences
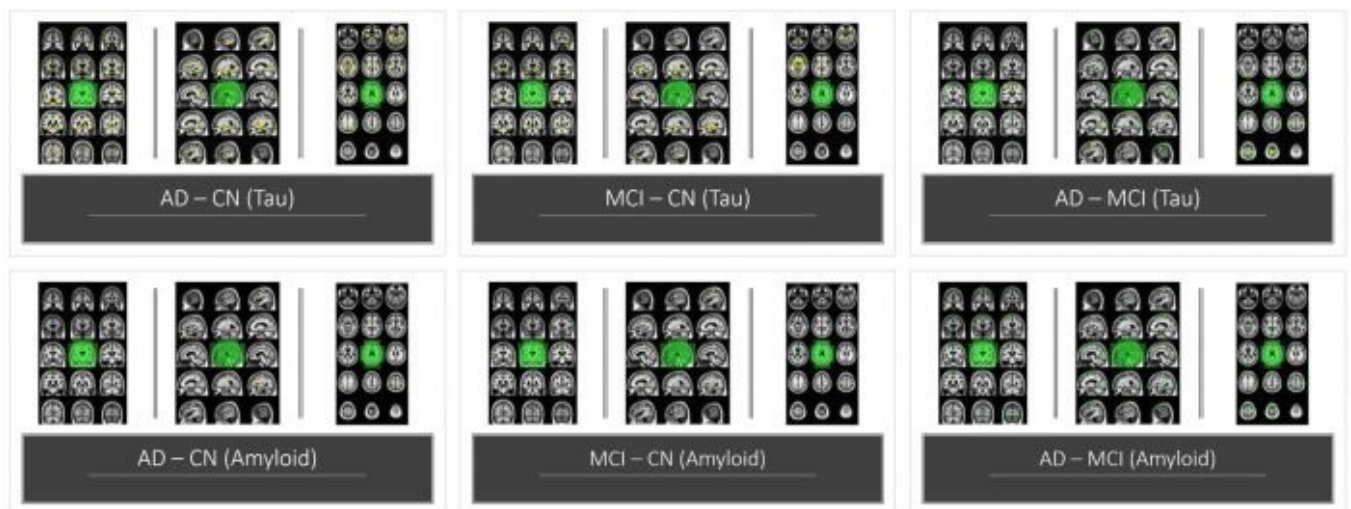
Figure 2. The group differences between the sub-groups for the same protein aggregates

P06: Abnormal AV1451 signal in popular reference regions

Christopher Schwarz[1], Kejal Kantarci[1], Melissa Murray[1], Scott Przybelski[1], Hoon-Ki Min[1], Val Lowe[1], Zuzana Nedelska[1], Prashanthi Vemuri[1], Matthew Senjem[1], Jeffrey Gunter[1], Ronald Petersen[1], David Knopman[1], Clifford Jack[1]

[1]*Mayo Clinic, Rochester, MN, US*

Background: Cerebellar crus and eroded supratentorial white matter (SWM) are each popular choices of AV-1451 SUVR reference regions. In our large population-based sample from the Mayo Clinic Study of Aging (n=911 participants), we found that for both choices a small subset of scans contain prominent binding in the reference region.

Methods: PET scans were aligned to corresponding MRI and regions were localized using SPM12 with MCALT and ANTs. We measured mean signal in the cerebellar crus (bilateral crus1+crus2) and SWM eroded by 5mm (defined in template space). We analyzed the ratio of crus/SWM across our cohort.

Results: 80.5% of scans had crus/SWM < 1.0 (overall mean=0.93). To examine extreme outliers, we empirically chose thresholds of crus/SWM<0.75 for high SWM signal (n=25 scans, 2.74%), and crus/SWM>1.2 for high crus signal (n=21 scans, 2.31%). Age among high-SWM participants ranged from 32-94 (mean=57.7, SD=19.5), and 22/25 were cognitively unimpaired. Age among high-crus participants ranged from 32-87 (mean=64.2, SD=18.2) and 18/21 were cognitively unimpaired. One high-crus-signal participant (age 67, M, crus/SWM=1.2) underwent autopsy, which found diffuse Lewy body disease and medial-temporal tau pathology (Braak 3). His crus-normalized medial temporal lobe SUVR was only 0.83, demonstrating that the high crus signal likely contributed to the unexpectedly low SUVR. Follow-up scans were available for 3 high-SWM participants and 7 high-crus participants. Crus/SWM differed across time by <15% for 9/10 (mean=8.7%, range=1.0-23.5%).

Discussion: Across the population, cerebellar crus had less average signal than eroded SWM, but both reference regions had rare, problematic signal in some scans. A crus/SWM ratio may help identify scans unsuitable to quantify using each region. In both regions, participants with the largest signals spanned a wide age range, and were mostly unimpaired. Crus/SWM ratios were fairly stable over time, suggesting an unknown underlying biology requiring further investigation.
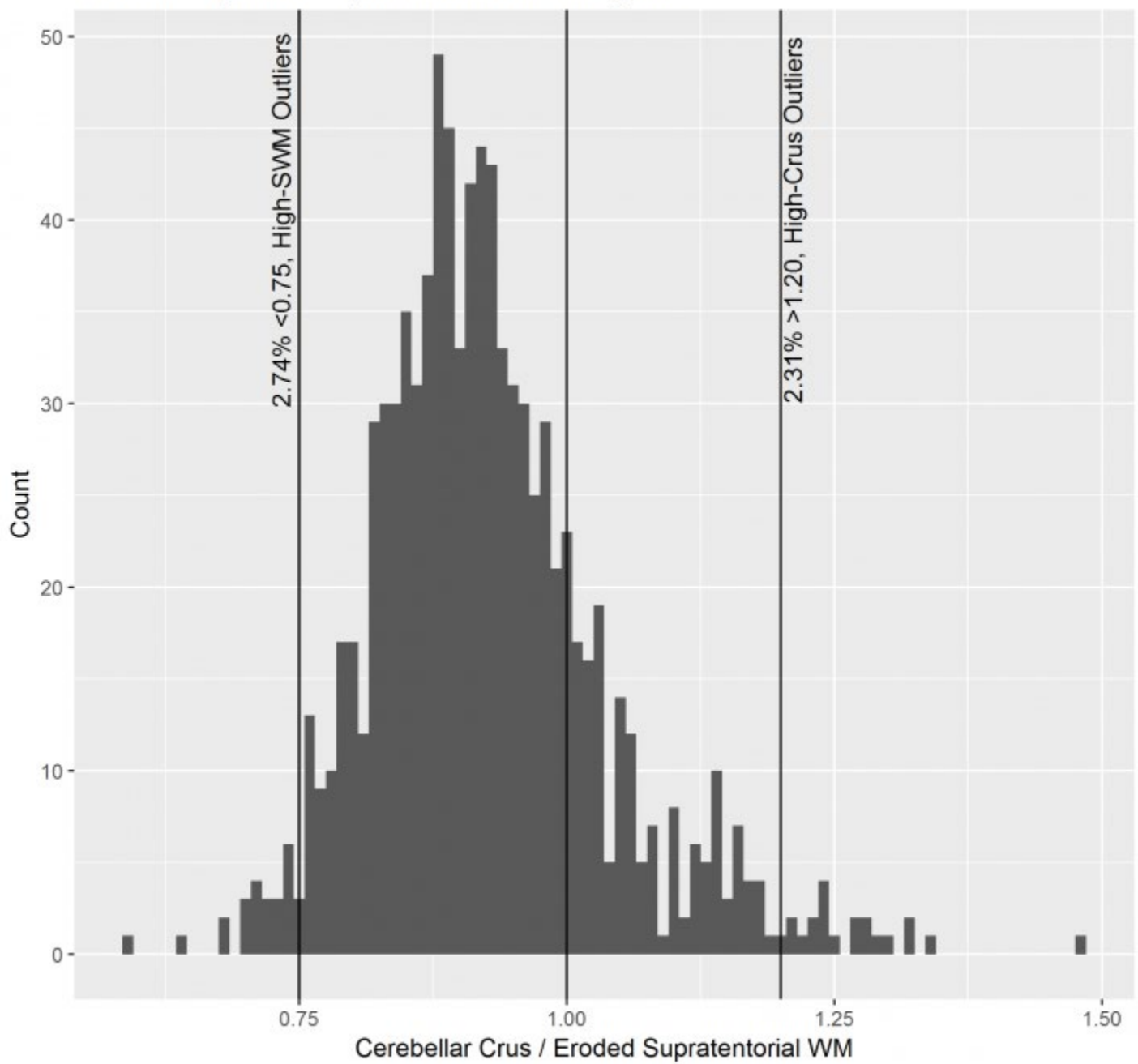
Figure 1: Histogram of AV1415 signal in a ratio of cerebellar crus / eroded supratentorial WM, across a large n=911 population sample.

Figure 2: AV1451 PET SUVR (eroded SWM reference) of a 67 year old man clinically diagnosed with probable DLB. Abnormal signal is visible in the cerebellar crus (mask overlaid in white). At autopsy, he had Braak Stage 3 NFT-tau pathology and diffuse/neocortical Lewy body disease. Crus-normalized SUVR in the medial temporal lobe was only 0.83, inconsistent with the Braak Stage 3 NFT-tau pathology. Likely, this was caused at least partially by the abnormal crus signal (crus/SWM=1.2).

Figure 3: AV1451 PET SUVR (cerebellar crus reference) of a 54 year old cognitively unimpaired man. Abnormal signal (crus/SWM= 0.64) is visible in the eroded supratentorial WM (mask overlaid in white).

P07: X-ray method for estimating amyloid load in the brain

Aldo Badano[1], Eshan Dahal[1]

[1]*US FDA, Silver Spring, MD, US*

We describe a novel technique for estimating amyloid load in the brain using small-angle x-ray scattering (SAXS). The characteristic SAXS signal of the plaque beta-sheet structure is best captured using mono-energetic x-ray beams and energy discriminating detectors. However, for a practical clinical implementation of the approach, we studied the use of poly-energetic conventional x-ray sources and energy discriminating spectral detectors in a computed tomography configuration. In previous work, we have used a laboratory SAXS set-up for planar imaging of Alzheimer's disease model, and control mouse brains slices to detect regions with high density of amyloid plaques validated with histology. We experimentally confirmed these predictions by placing a surrogate amyloid fibril target made from bovine serum albumin on a wild-type mouse brain slice imaged using planar SAXS. Using Monte Carlo techniques, we simulated a SAXS experiment through a human head model with detailed anatomy. To decrease radiation dose, we describe a weighted-sum, energy-scaled image visualization approach that allows a radiation dose reduction by a factor of more than 10. Our findings suggest that an optimally designed, dedicated computed tomography add-on system holds promise for noninvasive, tracer-less, amyloid plaque estimation. An experimental prototype system using medical x-ray tubes and spectroscopic x-ray detectors is being built in the laboratory and will be used in conjunction with physical head phantoms to validate the computational predictions and demonstrate the feasibility of this approach.
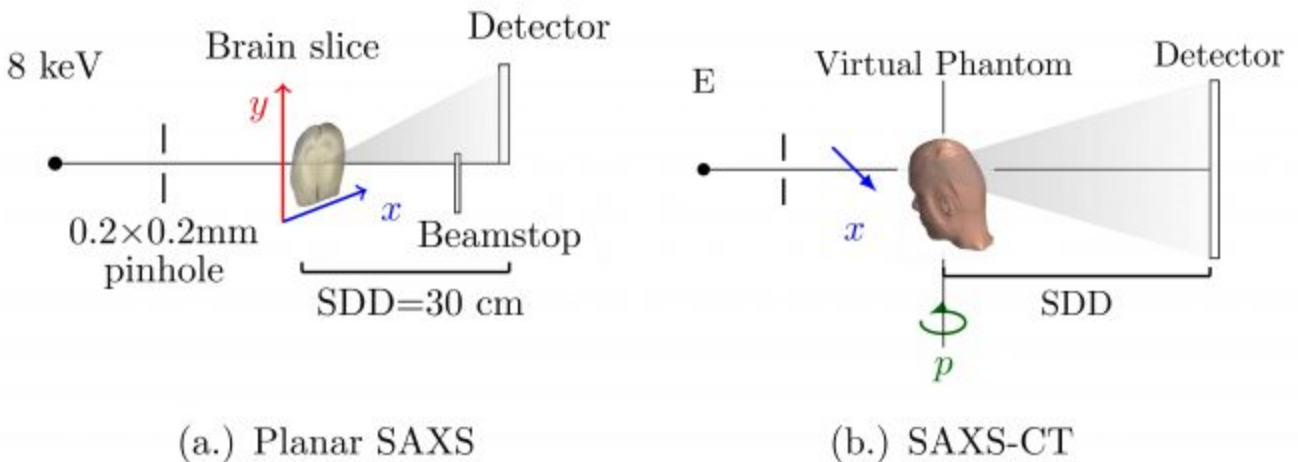
Schematic of (a.) Planar SAXS and (b.) CT preliminary experimental setups for the technique.

Keywords: *SAXS, amyloid load, CT, x-ray, coherent scatter*

P08: Impact of different image analysis methods on baseline 18F-Florbetapir PET measurements in the API ADAD Colombia trial

Valentina Ghisays[1,2], Yinghua Chen[1,2], Hillary Protas[1,2], Dhruman Goradia[1,2], Pradeep Thiyyagura[1,2], Jessica Langbaum[1,2], Kaycee Sink[9], Nan Hu[9], Heather Guthrie[9], Jillian Smith[9], William Cho[9], David Clayton[9], Ronald Thomas[11], Arthur W. Toga[12], Connie Boker[1], Sergio Alvarez[8], Yakeel T. Quiroz[7,8], Silvia Rios-Romenets[6], Kewei Chen[1,2,3,5], Yi Su[1,2], Pierre Tariot[1,2], Francisco Lopera[6], Eric Reiman[1,2,3,4,5]

[1]*Banner Alzheimer's Institute, Phoenix, AR, US*
[2]*Arizona Alzheimer's Consortium, Phoenix, AR, US*
[3]*University of Arizona, Tucson, AR, US*
[4]*Translational Genomics Research Institute, Phoenix, AR, US*
[5]*Arizona State University, Tempe, AR, US*
[6]*Grupo de Neurociencias, Universidad de Antioquia, Medellin, CO*
[7]*Harvard Medical School and Massachusetts General Hospital, Boston, MA, US*
[8]*Hospital Pablo Tobón Uribe, Medellin, CO*
[9]*Genentech Inc., South San Francisco, CA, US*
[10]*Roche Products Ltd., Welwyn Garden City, UK*
[11]*University of California, San Diego, CA, US*
[12]*University of Southern California, Los Angeles, CA, US*

Background: PET measurements of fibrillar amyloid-β(Aβ) deposition depend on the radiotracer, imaging protocol, and image analysis methods. We compare the impact of two different image analysis platforms, three different reference regions, and use of partial-volume correction on florbetapir-PET standard-uptake value ratios(SUVRs) in Presenilin-1 **(PSEN1)** E280A mutation carriers and non-carriers from the largest autosomal dominant Alzheimer's disease (ADAD) kindred.

Methods: Template-based (SPM12) and FreeSurfer6-based regions-of-interest definitions were compared in combination with three different reference regions (whole-cerebellum, pons, and cerebral white-matter), and a regional spread function method for partial-volume correction(PVC) (Su et.al.,2015;2016) on the ability to distinguish florbetapir SUVRs from PSEN1 E280A mutation carriers and non-carriers and characterize their associations with age. The study capitalized on baseline florbetapir PET images from 167cognitively unimpaired mutation carriers and 75 non-carriers, ages 30-53, enrolled in the API ADAD Colombia Trial(NCT01998841).

Results: Using either SPM12 or FreeSurfer6, the pontine and white-matter reference regions were significantly better than the cerebellar reference region in distinguishing florbetapir SUVRs in carriers and non-carriers (Cohen's d effect-size comparison, $p<.05$), partly due to increased cerebellar Aβ deposition at older ages in this ADAD kindred. Freesurfer6-based PVC was associated with significantly greater ability to distinguish cerebral-to-pontine and cerebral-to-cerebellum florbetapir SUVRs, in the carrier and non-carrier groups (Cohen's d effect-size comparison, $p<.05$).

Conclusion: This study supports the potential of FreeSurfer6, a pontine or white-matter reference region and, in some instances, PVCs to characterize cross-sectional measurements of fibrillar-Aβ deposition in preclinical ADAD with increased statistical power. A cerebellar reference region may be confounded by Aβ burden in ADAD's latter preclinical and clinical stages. Additional studies are needed to characterize the optimal image analysis techniques that can aid in identifying individuals at preclinical stages, extend our findings to multi-center studies, and better inform future clinical trials involving different PET ligands and persons with other ADAD mutations.

P09: Sub-threshold regional amyloid levels mediates parahippocampal thinning associated with reduced cerebral blood flow.

Austin Sisley[1], Victor Sanchez[1], Kimiko Domoto-Reilly[1], Thomas Grabowski[1], Swati Rane[1]

[1]*University of Washington Medical Center, Seattle, WA, US*

Increased amyloid plaque density and vascular insufficiency are both observed in Alzheimer's disease (AD) prior to cortical atrophy. Whether the relationship of amyloid accumulation and vascular pathology to atrophy is causal and/or additive is under active investigation. Vascular contributions are a hypothesized cause of AD-like symptoms in MCI individuals without high amyloid. Our goal was to apply mediation analysis to determine whether (i) reduced cerebral blood flow (CBF) mediated atrophy (i.e., cortical thinning) in amyloid-positive (Aβ+ regions indicating abnormal accumulation), and (ii) sub-threshold amyloid (S_{Ab} regions) mediated atrophy in areas of reduced CBF. We calculated amyloid accumulation using ^{18}F-AV45 PET and CBF using ASL in 119 older adults from ADNI (26 controls [NC], total 55 APOE-ε4 with 9 NC ε4 carriers).

T1 cortical segmentation was performed using FreeSurfer. Individual PET and CBF images were registered to the T1 and partial-volume-corrected using Mueller-Gartner Method. PET SUVRs per region were calculated using the composite brainstem as reference in PetSurfer. Aβ+ regions were SUVR ^{3} 0.79 and $S_{Aβ}$ regions were 0<SUVR<0.79. Bootstrapped mediation was performed using the 'mediation' package in R. Significance was at p<0.05 (Figure 1).

Aβ+ regions: No significant mediation by CBF was observed. Amyloid levels were directly associated with atrophy in anterior cingulate (n=58, 5 NC) and frontal pole (n=56, 5 NC). **$S_{Aβ}$ regions:** Sub-threshold amyloid partially mediated the association between CBF and atrophy in fusiform (n=90, 26 NC) and parahippocampal gyri (n=101, 26 NC, Figure 2). CBF was directly associated with atrophy in the inferior temporal gyrus (n=68, 5 NC). Results matched with CSF-Aβ status and known regional vulnerability for early AD symptoms (Figure 3).

Amyloid pathology contributes independently and in a CBF-dependent manner to atrophy. Validation of these findings and further investigation of the role of CBF and localized sub-threshold amyloid especially in MCI is warranted.

A. Model for testing Aβ+ regions
How does high amyloid accumulation drive atrophy?

B. Model for testing $S_{Aβ}$ regions
How does low CBF drive atrophy?
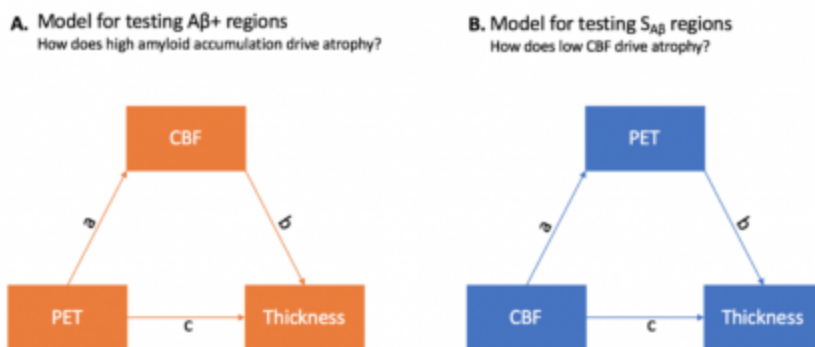
Figure 1: Mediation models (Type 4). *Hypothesis:* For the Aβ+ regions, we tested whether high amyloid was related to low CBF and indirectly contributed to atrophy in addition to the direct effects of amyloid toxicity. In the $S_{Aβ}$ regions, we tested whether low CBF was related to higher sub-threshold amyloid and indirectly contributed to atrophy.
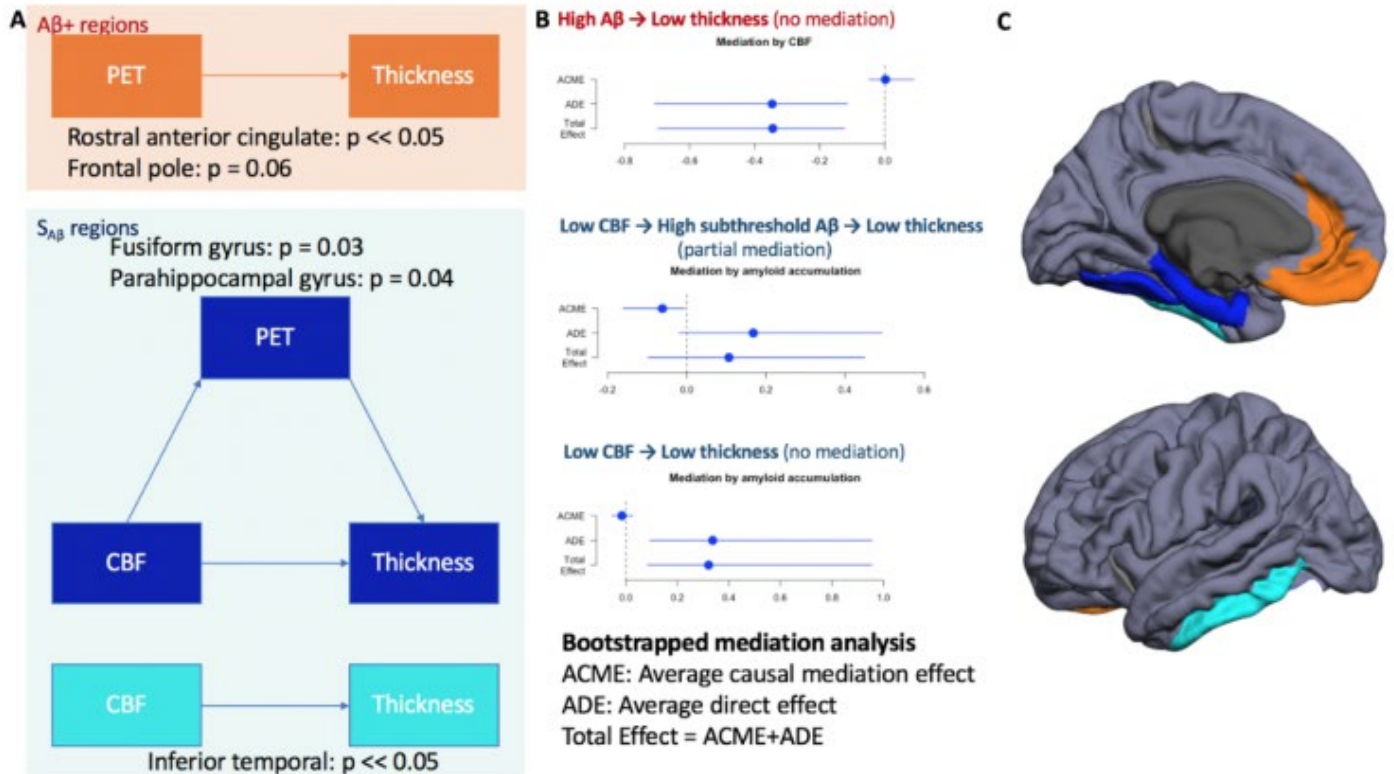
Figure 2: Amyloid positivity in anterior cingulate and frontal regions is directly associated with cortical atrophy with no mediation by CBF. Sub-threshold parahippocampal and fusiform regions are associated with cortical atrophy with significant partial mediation by sub-threshold amyloid. Additionally, the inferior temporal region is directly associated with cortical atrophy with no mediation by amyloid. Panel A and B shows models that survived (no mediation or partial mediation). Panel C shows the brain regions with significant associations between amyloid accumulation (orange) and atrophy as well as between CBF (blue) and atrophy (with and without mediation).
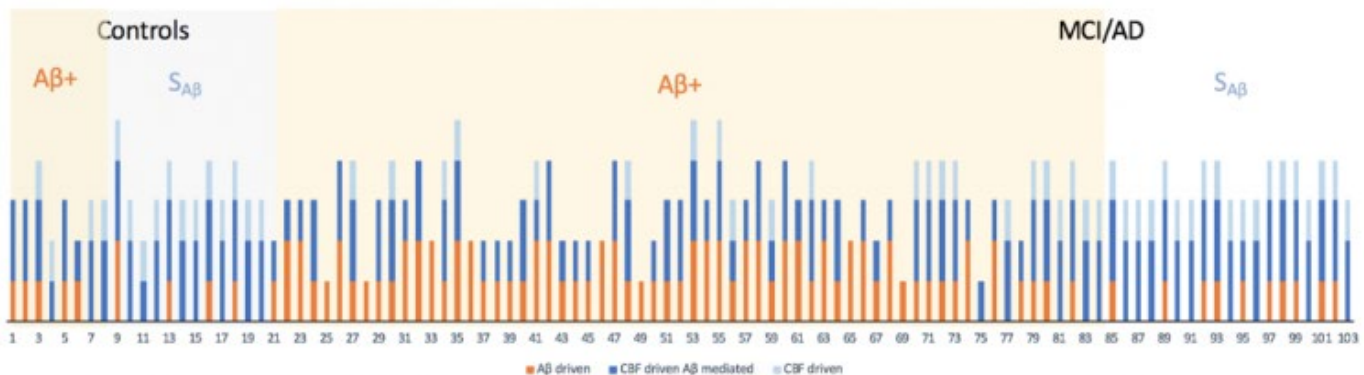
Figure 3: Of the 119 individuals, CSF amyloid levels were available on 103 individuals. The yellow and light gray rectangles in the background show amyloid positivity based on CSF. The bar graphs in the foreground reflect the amyloid driven (orange), CBF driven-amyloid mediated (blue), and CBF driven (light blue) processes within each of the 103 individuals. Amyloid status based on CSF corresponds well with the regional PET amyloid positivity.

P10: [18F]GTP1 (Genentech tau probe 1) SUVR has a very little dependence on changes in regional or global cerebral blood flow

Sandra Sanabria[1], Suzanne Baker[1,2], Jan Marik[1], Alex de Crespigny[1], Robby Weimer[1]

[1]Genentech, Inc., South San Francicso, CA, US
[2]Molecular Biophysics and Integrated Bioimaging, Lawrence Berkeley National Lab., Berkeley, CA, US

Objective: Here we evaluate the potential impact of changes in cerebral blood flow (CBF) and [^{18}F]GTP1 metabolism on SUVR and discuss the implications on longitudinal assessments.

Methods: [^{18}F]GTP1 imaging with arterial input function was performed in 5 AD subjects. Noise-free time-activity curves for cerebellum and four cortical regions with increasing levels of tau burden were constructed using the population average parameters. CBF changes were simulated using the Renkin–Crone model to establish the relationship between K_1, k_2 and flow. Baseline flow values of 0.35, 0.5 and 0.75 mL cm^{-3} min^{-1} were considered and large CBF changes were simulated: -50% (e.g.: -35 to -25% due to caffeine consumption) to +70% (e.g. transient +65% following visual stimulation). Metabolism changes were simulated using the observed **slow** and **fast** [^{18}F]GTP1 fractions (f_P). SUVR was calculated using the 60-90 min interval with the cerebellum as a reference.

Results: The average K_1 values in cerebellum and cortex were 0.13 and 0.11-0.12 mL cm^{-3} min^{-1}, respectively. Calculated PS values were between 0.11 and 0.15 ml/g/min across brain regions. A 70% CBF increase resulted in 6% K_1 increase and a 50% CBF decrease in a 12% K_1 decrease. The SUVR changes were below 3.5% due to regional or global CBF changes alone or when combining with f_P changes for the three baseline flow values considered. Figure 1 (E-F) shows the histogram of the %SUVR change at the follow up relative to baseline.

Conclusions: A small bias (3.5% or less) was introduced in the [^{18}F]GTP1 SUVR estimation across a large range of regional or global CBF changes with or without changes in [^{18}F]GTP1 metabolism. For the longitudinal flow changes reported due to disease progression in AD (up to -10% over two years, Hanaoka et al. **GeriatrGerontolInt** 2016) we would predict a negligible impact (<1%) on [^{18}F]GTP1 SUVR measurements.

Figure 1. (A) Measured [^{18}F]GTP1 plasma fractions, (B) simulated TACs using the *slow* and *fast* (dashed) parent tracer fraction and (C) the corresponding SUVRs. (D) Relationship between the K_1 %change and the CBF %change assuming a baseline value of 0.5 mL cm^{-3} min^{-1}; the dashed box shows the relevant CBF and K_1 changes range. Histogram of the respective percentage SUVR changes relative to baseline assuming (E) the same f_P or (F) different f_P at baseline and follow up scans.
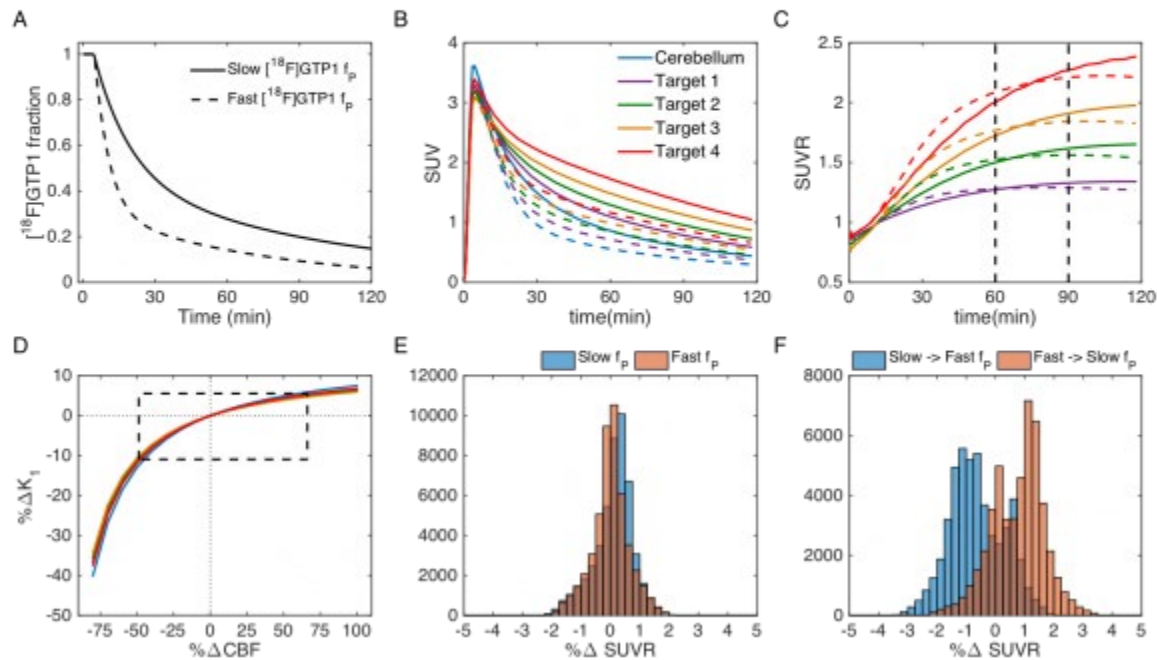
Keywords: *[18F]GTP1, Tau PET imaging, CBF, quantification*

P11: Multimodal magnetic resonance imaging predicts regional cerebral amyloid burden

Anusha Alathur Rangarajan[1], Minjie Wu[2], Naomi Joseph[3], Helmet Karim[2], Charles Laymon[1,4], Dana Tudorascu[2,5,6], Beth Snitz[7], Annie Cohen[2], Chester Mathis[4], William Klunk[2,7], Howard Aizenstein[1,2]

[1]*Department of Bioengineering, Swanson School of Engineering, University of Pittsburgh, Pittsburgh, PA, US*
[2]*Department of Psychiatry, University of Pittsburgh, Pittsburgh, PA, US*
[3]*Department of Chemical Engineering, Swanson School of Engineering, University of Pittsburgh, Pittsburgh, PA, US*
[4]*Department of Radiology, University of Pittsburgh, Pittsburgh, PA, US*
[5]*Department of Biostatistics, School of Public Health, University of Pittsburgh, Pittsburgh, PA, US*
[6]*Department of Medicine, University of Pittsburgh School of Medicine, Pittsburgh, PA, US*
[7]*Department of Neurology, University of Pittsburgh School of Medicine, Pittsburgh, PA, US*

Introduction: Alzheimer's disease (AD) is the most common cause of dementia and monitoring its early biomarkers is important for development of prevention and treatment strategies. Amyloid deposition is a defining pathological marker of AD and is typically quantified using positron emission tomography (PET). However, PET is expensive and exposes subjects to ionizing radiation. Thus, using machine learning, we developed an approach to predicting brain amyloid from multimodal magnetic resonance (MR) imaging.

Methods: We used a LASSO regression model to learn the voxel-wise relationship between imaging features extracted from multiple MR modalities (T1-weighted, T2-weighted, T2 fluid attenuated inversion recovery [FLAIR], susceptibility weighted imaging, and proton density) and amyloid from PiB PET (ground truth) from a group of cognitively normal participants (N=36, Aβ-: 27, Aβ+: 9). Imaging features (intensities, gradient magnitude, gabor filters, local binary patterns) were obtained from each modality. For longitudinal amyloid change prediction, we used models learnt within each participant baseline data to predict the participant's longitudinal amyloid (N=14). For cross-sectional amyloid status classification, we generalized the models across participants using participant features (age, gender, race, weight, normalized gray matter and white matter, hippocampal volume and white matter hyper-intensities).

Results: Learning voxel-wise MR-amyloid relationship performed better than using participant-level features alone to classify the amyloid status. T1-weighted imaging predicted the status best when compared to other modalities in classification of cross-sectional amyloid status [F-score (Mean(SD)) (20 subsets) = 67.82 (10.92)%]. T2-weighted imaging performed the best in change detection across longitudinal time points [F-score (Mean(SD)) (50 subsets) = 71.15 (3.78)%].

Conclusion: The results show feasibility of voxel-wise amyloid prediction, classification of amyloid status and its potential use as an amyloid image-screening tool.

Figure 1: Overview of methods
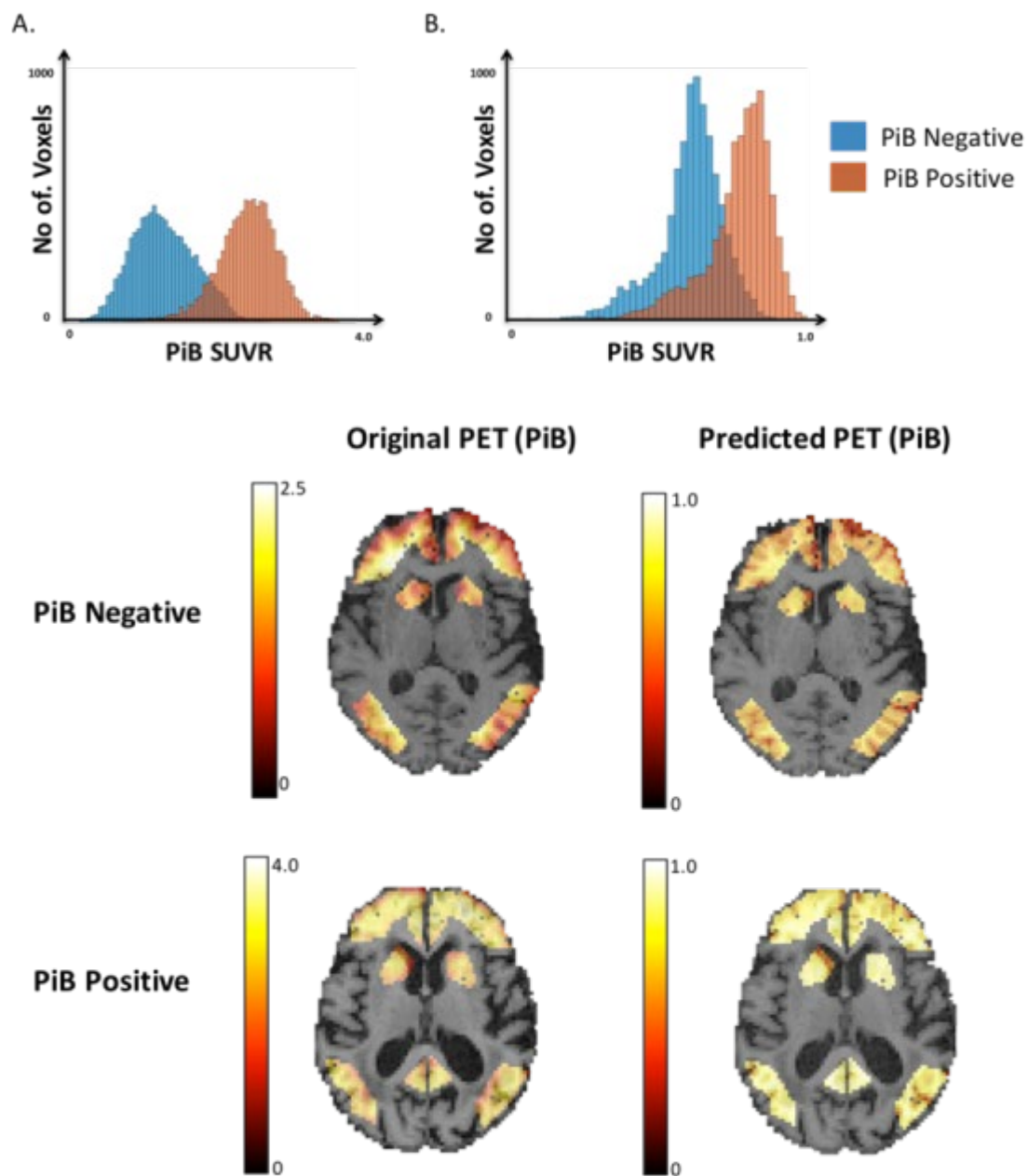
Figure 2. Cross sectional amyloid prediction (PiB voxels) A. Histogram of original PET (PiB) image B. Histogram of predicted PET (PiB) image
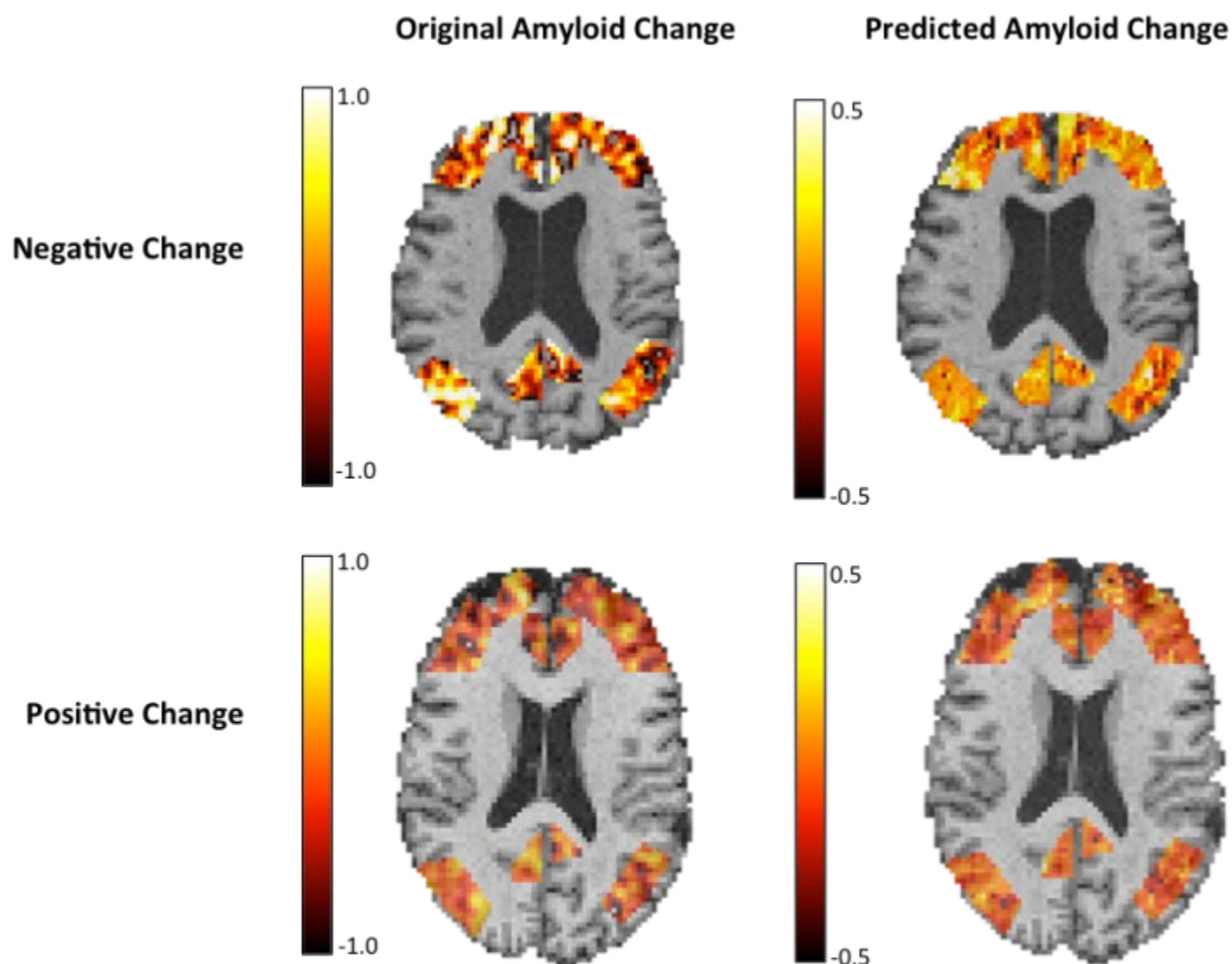
Figure 3: Original and Predicted Amyloid change in longitudinal data

---

P12: Evaluation of [18F]APN-1607 to image tau protein in patients with Alzheimer's disease and test-retest studies

Christine Sandiego[1], Olivier Barret[1], Vincent Carroll[1], Alexandra Gouasmat[1], Jennifer Madonia[1], Ken Marek[1], Richard Margolin[2,3], Paul Tempest[2], Ming-Kuei Jang[2]

[1]*Invicro, a Konica Minolta Company, New Haven, CT, US*
[2]*Aprinoia Therapeutics, Taipei, Taiwan*
[3]*CNS Research Solutions, LLC, Cambridge, MA, US*

Objective: [^{18}F]APN-1607 (previously [^{18}F]PM-PBB3) is a novel PET tracer being developed for imaging fibrillar tau, a key characteristic of several neurodegenerative diseases known as tauopathies. These conditions include Alzheimer's disease (AD) and progressive supranuclear palsy. The present study aimed to assess [^{18}F]APN-1607 binding in patients with AD and healthy adult volunteers (HV) and to evaluate test-retest variability (TRTV) of important imaging measures.

Methods: [^{18}F]APN-1607 PET was conducted over 180 min in seven AD and five HV subjects; 4 AD and 2 HV subjects returned for a retest scan. In subjects that completed test and retest scans, arterial blood samples were collected throughout the imaging sessions, as required for quantitative analysis. Distribution volume ratio (DVR) was estimated with invasive (blood-based) and non-invasive (reference region-based) Logan graphical analysis (LGA). SUVr was averaged between 60-90 and 120-150 min, using the cerebellar cortex as reference region. TRTV of DVR and SUVr were evaluated across temporal, parietal and frontal lobes, and cingulum, putamen, pallidum, and hippocampus. DVR(invasive) was considered the gold standard and was compared via linear regression analysis with DVR(non-invasive) and SUVr in AD subjects. SUVr was compared between AD and HV subjects.

Results: TRTV of [^{18}F]APN-1607 in HV and AD subjects was less than 10% for DVR and SUVr, averaged across regions. Compared with invasive DVR, SUVr(120-150 min) was in best agreement (R^2=0.95, slope=0.98), compared with non-invasive DVR(R^2=0.95, slope=0.82) and SUVr(60-90 min)(R^2=0.82, slope=0.80). Averaged across regions SUVr(120-150 min) range was 1.2-2.1 in AD (n=7) and 1.1-1.4 in HV (n=5) subjects. Mean SUVr in the temporal cortex was 1.9 (max 3.1) in AD and 1.0 (max 1.3) in HV subjects.

Conclusions: [^{18}F]APN-1607 is a suitable PET radioligand for imaging tau in neurodegenerative disease and showed excellent test-retest across outcome measures.

Keywords: *Alzheimer's disease, PET imaging, tauopathy, test-retest, analysis*

P13: Discovery of [18F]SMBT-1: a novel selective MAO-B PET tracer for imaging astrogliosis

Ryuichi Harada[1,2], Michinori Ezura[3], Ren Iwata[4], Hiroyuki Arai[2], Kazuhiko Yanai[1,4], Shozo Furumoto[4], Yukitsuka Kudo[2], Nobuyuki Okamura[4,5]

[1]*Department of Pharmacology, Tohoku University School of Medicine, chennai, IN*
[2]*Institute of Development, Aging and Cancer, Tohoku University, Sendai, Japan*
[3]*Department of Neurology, Tohoku University Hospital, Sendai, Japan*
[4]*Cyclotron and Radioisotope Center, Tohoku University, Sendai, Japan*
[5]*Division of Pharmacology, Faculty of Medicine, Tohoku Medical and Pharmaceutical University, Sendai, Japan*

Objectives: Reactive astrocytes are considered to play an important role in the pathogenesis of various neurodegenerative diseases. Monoamine oxidase-B (MAO-B) is known as a promising target for molecular imaging of astrogliosis. We have developed a novel compound for MAO-B imaging in the human brain. The aim of this study was to characterize the binding and pharmacokinetic properties of ^{18}F-SMBT-1, a candidate for MAO-B PET tracer.

Methods: In vitro competitive binding assays against recombinant MAO-A and MAO-B were performed using ^{18}F-fluoroethyl harmine and ^{3}H-THK5351, respectively. **In vitro** autoradiography on frozen human brain tissues was performed using ^{18}F-SMBT-1 and compared with MAO-B selective tracer, ^{125}I-Ro 43-0463. Pharmacokinetics were assessed in normal mice after intravenous injection of ^{18}F-SMBT-1.

Results: SMBT-1 was highly selective to MAO-B over MAO-A and showed higher binding affinity for MAO-B than THK5351 and Ro 43-0463. Higher amount of ^{18}F-SMBT-1 binding was observed in AD brain samples than in control brains. These binding was completely displaced with lazabemide, indicating that ^{18}F-SMBT-1 selectively binds to MAO-B. The spatial distribution of ^{18}F-SMBT-1 binding was quite similar to that of ^{125}I-Ro 43-0463. ^{18}F-SMBT-1 showed high initial brain uptake and rapid washout from normal mouse brain. The radiolabeled metabolites did not penetrate the blood-brain barrier in mice.

Conclusions: ^{18}F-SMBT-1 is a promising candidate for selective MAO-B PET tracer, which will enable the quantitative monitoring of astrogliosis in the human brain.

Keywords: *Novel tracers, Monoamine oxidase-B, Alzheimer's disease, autoradiography*

P14: Effect of point spread function specification error on GTM partial volume correction in PiB imaging

Charles Laymon[1], Davneet Minhas[1], Sarah Kolibash[1], Howard Aizenstein[1], Ann Cohen[1], Brian Lopresti[1], Chester Mathis[1], Beth Snitz[1], Dana Tudorascu[1], William Klunk[1]

[1]*University of Pittsburgh, Pittsburgh, PA, US*

Background: An important source of error in quantifying amyloid-beta (Ab) PET is the partial volume effect (PVE) resulting from the poor spatial resolution of PET relative to MRI. A commonly employed procedure for PVE compensation (PVC) is the Geometric Transfer Matrix (GTM) method, which requires an estimate of the scanner point spread function (PSF). However, there are errors associated with the PSF measurement. Furthermore, in the context of GTM, the PSF is usually simplistically parameterized as spatially invariant. The goal of this work was to determine the effect of PSF specification error on GTM-corrected PiB outcome measures.

Methods: Sixteen PiB-PET (8 PiB+) scans acquired (Siemens mCT) over 50-70 minutes post-injection and corresponding T1 MPRAGE MR images were analyzed. FreeSurfer 5.3 (FS) was employed to parcellate the MPRAGE images into regions-of-interest (ROIs) that were used for sampling the PET and generating GTM corrections. Values were normalized by FS-determined cerebellar gray matter to generate standardized uptake value ratios (SUVRs). A standard parameterization for the PET scanner PSF [Gaussian, 5mm x 5mm x 4.8mm (axial) FWHM] was used in the GTM procedure, in addition to two misspecified PSFs: 1mm larger (3D) and 1mm smaller than standard. Fractional change in GTM-corrected SUVR due to a ±1mm change in PSF [%f=(ΔSUVR/SUVR)×100] was tabulated for a global ROI.

Results: For the 1mm larger PSF, **%f** is positive at SUVR > 1.2 and increases with increasing SUVR, reaching %f≈5% at a global GTM-corrected SUVR of about 2.6. Below 1.2 GTM-corrected SUVR, %f becomes negative and falls rapidly with SUVR. For the 1mm smaller PSF, the opposite is observed, with GTM-corrected SUVR > 1.2 being underestimated and GTM-corrected SUVR < 1.2 being overestimated (Figure 1).

Conclusion: There is a moderate PiB-uptake dependent bias associated with PSF misspecification in GTM PVC that should be considered when planning analysis strategies.
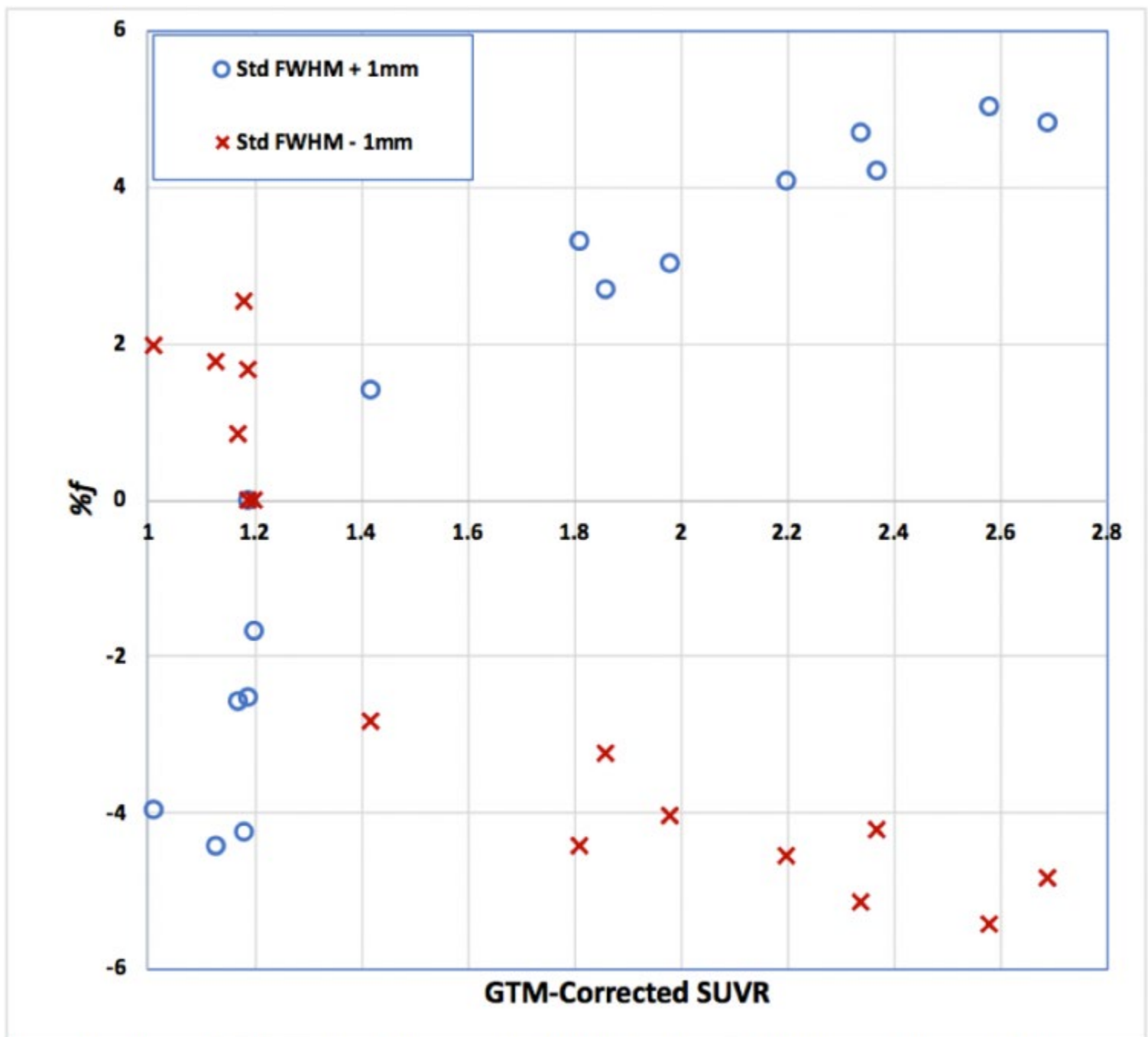
Figure 1 – Plot of % change in GTM-corrected SUVR for 1 mm of PSF kernel change (%*f*) vs. GTM-corrected Global SUVR for 16 subjects.

Keywords: *PET, Image Processing*

P15: 11C-ER176 has superior quality than 11C-PBR28 to image brain inflammation with positron emission tomography

Paolo Zanotti Fregonara[1], Belen Pascual[1], Meixiang Yu[1], David Beers[1], Stanley Appel[1], Joseph Masdeu[1]

[1]Houston Methodist Neurological Institute and Weill Cornell Medicine, Houston, TX, US

Frontotemporal dementia is associated with increased brain inflammation, which can be quantified with positron emission tomography (PET). ^{11}C-PBR28 is perhaps the most widely used PET tracer for inflammation. The aim of this study was to compare ^{11}C-PBR28 with a new inflammation tracer, ^{11}C-ER176, by scanning healthy volunteers with both tracers during the same day. Five subjects underwent a 90-minute PET scan with ^{11}C-PBR28 in the morning and ^{11}C-ER176 in the afternoon. In each subject, we drew serial blood samples from the radial artery for both tracers, and measured the percentage of parent compound in plasma by liquid chromatography. Using MR images for anatomical landmarks, we segmented the PET brain images using the Hammers' probabilistic atlas, and quantified the binding of the tracer in terms of total volume of distribution (V_T) with a two-tissue compartmental model.

[11]C-ER176 was more stable in arterial blood than ^{11}C-PBR28 (the percentages of unmetabolized parent in plasma at 30 minutes were $54.7 \pm 11.6\%$ and $22.5 \pm 10.0\%$, and at 90 minutes were $30.2 \pm 9.8\%$ and $8.6 \pm 3.6\%$, respectively). Greater concentrations of parent are associated with more reliable measurements, and indeed the coefficient of variation (%COV) of the area under the parent curve (in SUV) was higher for ^{11}C-PBR28 than for ^{11}C-ER176 (37.5% vs 21.3%). Similarly, the %COV of the area under the brain curve was higher with ^{11}C-PBR28 (16.5% vs. 9.0%). The brain time-activity curves for both tracers were well fitted by the two-tissue model, but ^{11}C-ER176 had higher V_T values (6.1 ± 1.6 vs. 4.6 ± 2.6 mL/cm^3), which suggests a higher specific binding.

In summary, ^{11}C-ER176 displays a smaller variability in the measurements in both plasma and brain and has a higher V_T. Thanks to these characteristics, clinical studies performed with ^{11}C-ER176 are expected to have higher statistical power.

Keywords: *Brain, Inflammation, PBR28, ER176, PET*

P16: Subject-specific site of maximum uptake is most sensitive to longitudinal change in 18F-AV1451 PET data

David Scott[1], Katarzyna Adamczuk[1], Beth Gorman[1], Maureen Runkle[1], Joyce Suhy[1]

[1]*Bioclinica, Oakland, CA, US*
[2]*Bioclinica, Philadelphia, PA, US*

Background: 18F-AV1451 PET allows in vivo visualization of tau pathology, the accumulation of which contributes to a neurodegenerative cascade toward Alzheimer's Disease. Interindividual differences in 18F-AV1451 uptake patterns complicate the application of group-level cortical composites to index SUVR as typical in analysis of amyloid and FDG-PET. We compared the longitudinal sensitivity of Braak-stage composites against a subject-specific search region.

Methods: 38 NL, 32 MCI and 6 AD subjects with multiple AV1451 PET exams in the ADNI database (http://adni.loni.ucla.edu) were selected for longitudinal analysis (average between exams 480 days ± 140). ADNI PET core PVC values were used to index cerebellar-cortex SUVR across the entire FreeSurfer parcellation. Composite SUVR for each exam was computed within Braak-stages, lateral and middle temporal cortex, and lateral and medial parietal cortex through volume-weighted combination of appropriate subregions; we also computed longitudinal change in the subregion with highest uptake at baseline for each subject. Longitudinal sensitivity was assessed as mean within-subject change from baseline and effect size for each patient group.

Results & Conclusion: Longitudinal effect sizes were modest across all composites (Cohen's d around 0.4), reflecting interindividual heterogeneity in spatiotemporal distribution of AV1451. The site of highest uptake at baseline yielded the highest increase in SUVR among normal and MCI groups, though AD patients showed decreasing SUVR. Among composites, Braak stage 1, limbic and temporal subregions showed the largest increase in SUVR in normal and MCI subjects, with apparent reduction in SUVR for AD patient group. Later Braak stages and frontal subregions do not reliably capture change in SUVR at the group level. Clinical trials seeking to use change in SUVR as an endpoint may find group-level composite ROIs inadequate to demonstrate therapeutic efficacy.
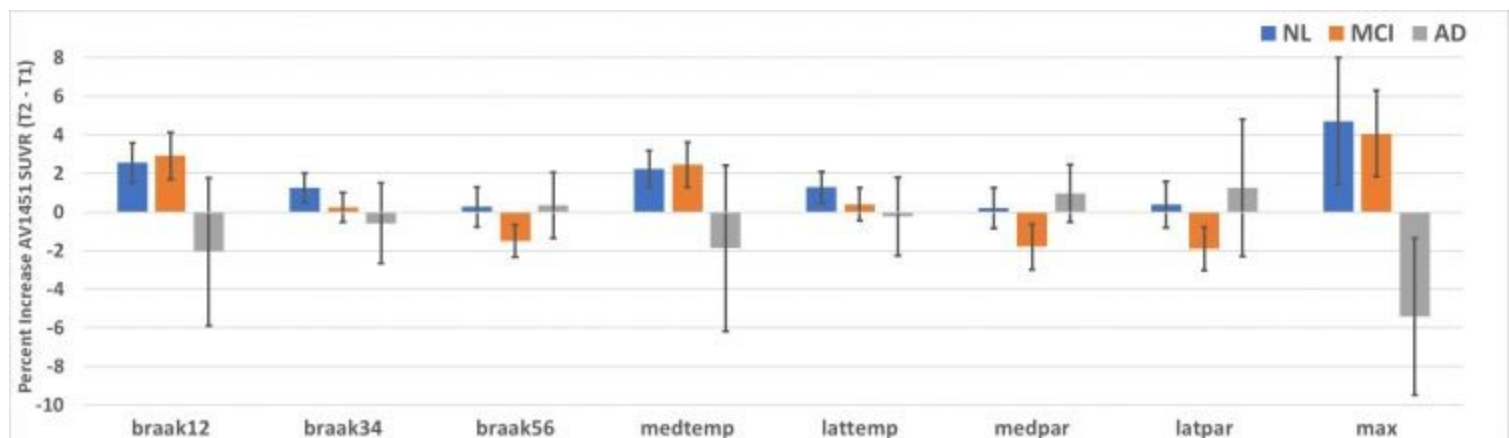
Keywords: *tau, PET, AV1451, SUVR, analysis*

P17: Functional connectivity of the entorhinal cortex predicts tau deposition in aging

Jenna N. Adams[1], Anne Maass[1,2], Theresa M. Harrison[1], William J. Jagust[1,3]

[1]*Helen Wills Neuroscience Institute, UC Berkeley, Berkeley, CA, US*
[2]*German Center for Neurodegenerative Disease, Magdeburg, Germany*
[3]*Lawrence Berkeley National Laboratory, Berkeley, CA, US*

Background: In aging and Alzheimer's disease, tau initially deposits in the lateral portion of the entorhinal cortex (EC) before spreading to downstream regions. We investigated whether functional connectivity (FC) patterns of the EC derived from a young adult (YA) sample predict tau deposition in cognitively normal older adults (OA). Further, we tested whether anterolateral EC (alEC) FC better predicted tau deposition than posteromedial EC (pmEC).

Methods: Resting-state fMRI was performed on 25 YA (27±4 years, 10F). Seed-to-voxel FC analyses were performed in MNI space for the total EC, alEC, and pmEC seeds. Regions of significant within-hemisphere FC (**p**<0.005 uncorrected) were extracted. Tau was quantified in 112 OA (76±6 years, 67F) using FTP-PET. OA subjects were classified into Braak-like Stages (0, **n**=23; I/II, **n**=72; III/IV, **n**=17) based on FTP SUVR in Braak ROIs. FTP SUVR images were warped to MNI space for voxelwise analyses.

Results: Distinct patterns of FC were found for the EC, alEC, and pmEC seeds (Fig-1). OA had a higher percentage of suprathreshold FTP voxels (>1.4 SUVR) within regions of EC FC than in cortical regions outside the mask (Fig-2A), and more suprathreshold voxels within alEC FC than pmEC FC or outside regions (Fig-2B) (repeated measures ANCOVAs, **p**s<0.001). Within the EC and alEC masks, but not pmEC, mean FC strength in a voxel was positively associated with the OA group mean FTP SUVR in that voxel, increasing with Braak Stage (voxelwise linear regression, **p**s<0.001; Fig-3A). Stronger EC and alEC FC also predicted greater FTP accumulation in progression from Braak I/II to III/IV (voxelwise correlation, **p**s<0.001; Fig-3B).

Conclusions: FC of the EC and alEC, but not pmEC, predicted the spatial location and amount of tau deposition in aging. These results suggest that tau pathology spreads from a lateral EC site of origin via activity-driven mechanisms to functionally connected cortex.
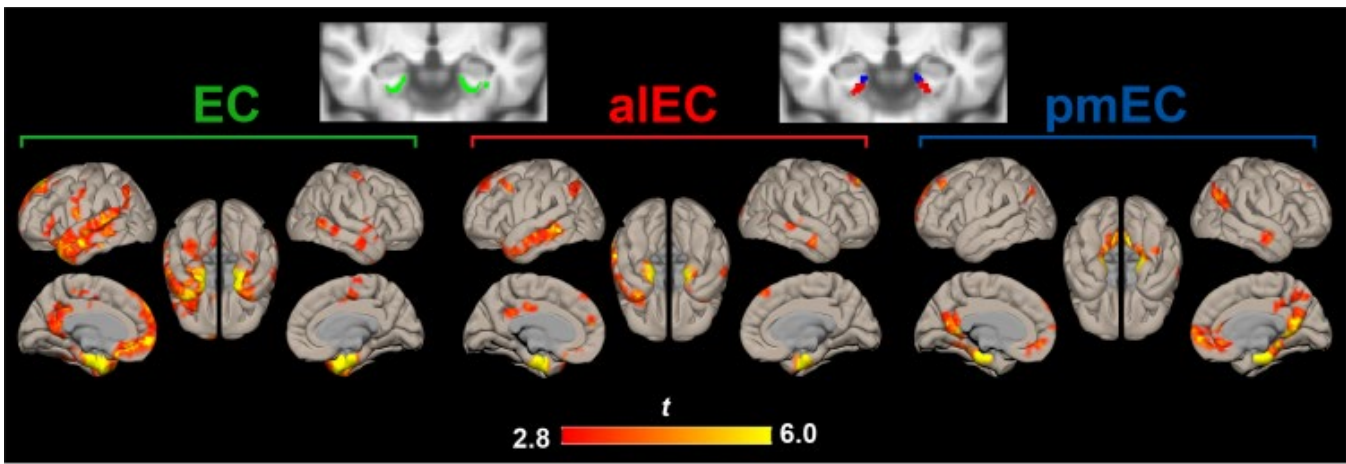
Figure 1. Entorhinal cortex resting-state functional connectivity (FC) in young adults. Seed-to-voxel FC analysis was peformed for each seed region (entorhinal cortex, EC, green; anterolateral EC, alEC, red; posteromedial EC, pmEC, blue; seeds depicted on a coronal slice) within each hemisphere using semi-partial correlations. One sample t-tests were perfomed across all subjects, with age and sex included as covariates of no interest. FC maps were considered significant at a voxelwise threshold of $p<0.005$ and cluster threshold of $p<0.05$ FDR corrected. Seed regions were removed from the masks for all subsequent analyses.
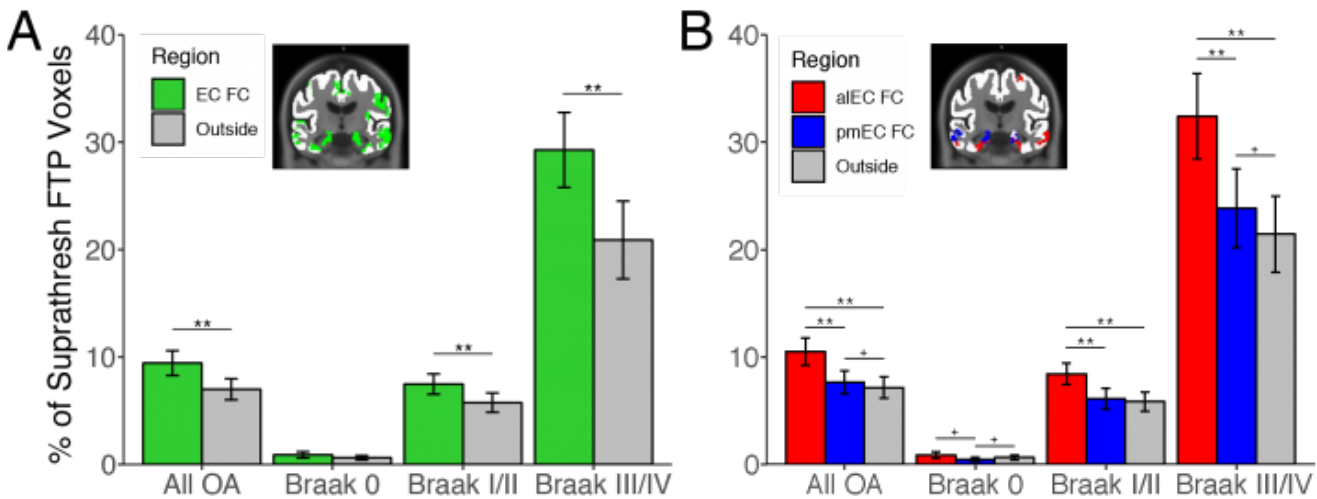
Figure 2. Comparison of FTP within versus outside regions of functional connectivity. Functional connectivity (FC) maps were binarized and "outside" masks were created by subtracting the FC mask from a cortical gray mask (seed regions removed from all masks). The percentage of suprathreshold FTP voxels (SUVR >1.4) was calculated for both FC masks and outside masks. Repeated measures ANCOVAs found significant main effects of region ($ps<0.001$) and region by Braak Stage interactions ($ps<0.001$) for both **A)** EC vs. outside and **B)** alEC vs. pmEC vs. outside models. Post-hoc paired-samples t-tests confirmed a higher percentage of suprathreshold FTP voxels in EC compared to outside and alEC compared to outside, and this difference increased with Braak Stage. **p<0.01, *p<0.05, + p<0.10
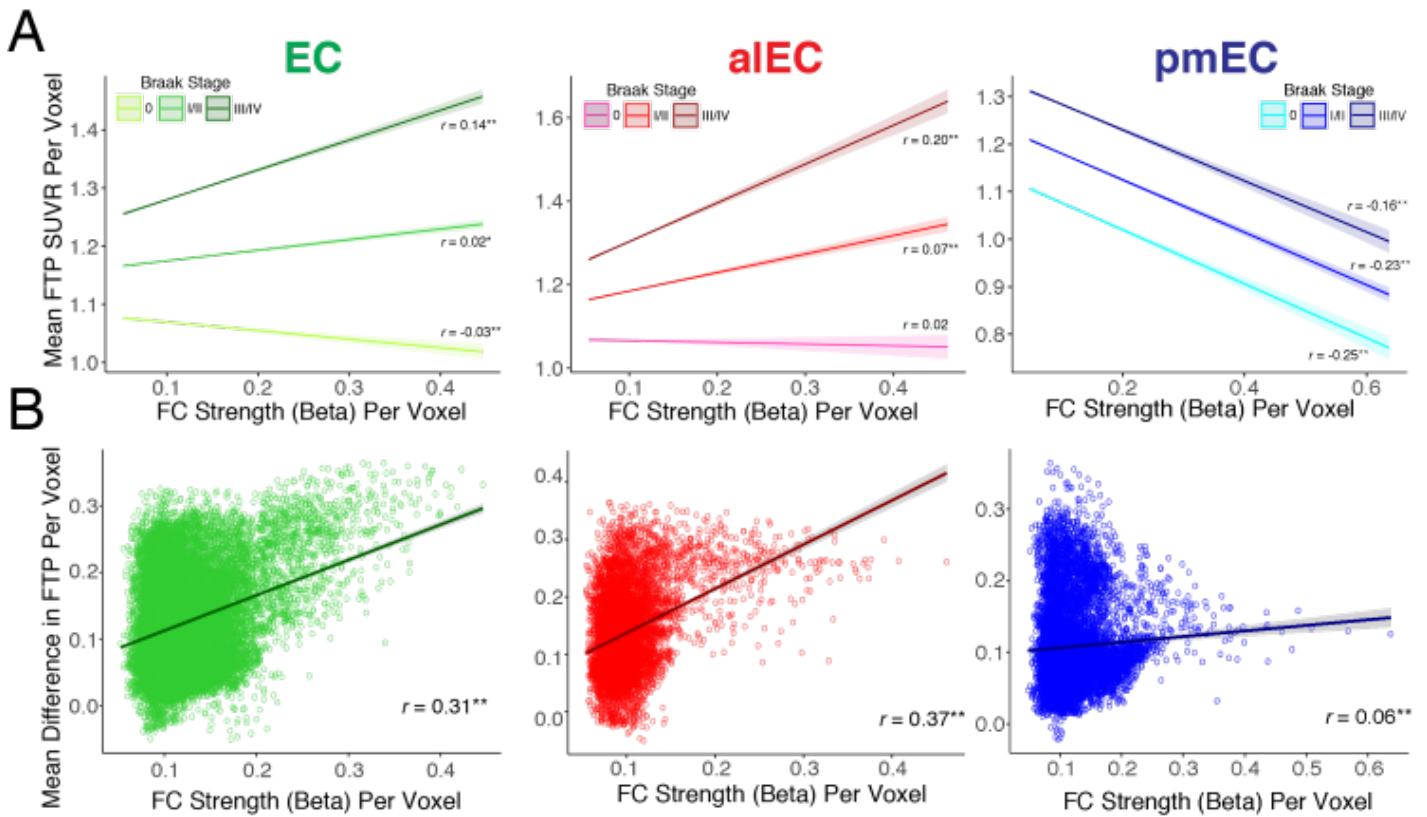
Figure 3. Voxelwise associations between functional connectivity (FC) strength and group mean FTP. For subjects within each Braak Stage, group mean FTP images were created controlling for age and sex. Results are shown for each seed region separately (EC: green, left; alEC: red, middle; pmEC: blue, right). **A)** Voxelwise linear regressions within the FC masks predicting to mean FTP found significant FC strength by Braak Stage interactions for EC and alEC. Increased FC strength to a voxel predicted higher mean FTP in that voxel, and this association increased by Braak Stage ($ps<0.001$). **B)** An FTP accumulation map was created by subtracting the mean Braak I/II image from the Braak III/IV image. Voxelwise correlations within the FC masks found significant positive correlations between FC strength to a voxel and FTP accumulation in that voxel ($ps<0.001$), which were strongest for EC and alEC. **$p<0.01$ *$p<0.05$

Keywords: *tau, entorhinal cortex, aging, functional connectivity, fMRI*

P18: A fully automatic technique for precise localization and quantification of Amyloid-β PET scans

Mouna Tahmi[1], Wassim Bou Zeid[1], Qolamreza Razlighi[1]

[1]Columbia University Medical Center, New York, NY, US

Background: Spatial heterogeneity in the accumulated Amyloid-β plaques throughout the brain during asymptomatic as well as clinical stage of the Alzheimer's diseases calls for precise localization and quantification of this protein in PET imaging studies. To address this need, we have developed and evaluated a technique that quantifies the Amyloid-β PET scans on a millimeter-by-millimeter scale in the brain with an unprecedented precision.

Method: Figure 1 illustrates the flowchart of our proposed technique. An inter-modal, and intra-subject registration with information theoretic cost function has been utilized to transform all FreeSurfer's neuroanatomical labels into PET images which subsequently used to quantify the accumulation of the Amyloid-β plaques at every point in the brain by dividing its uptake to the reference region. We have evaluated our developed technique using the post-mortem histopathological data from 53 old participants which all clinically diagnosed with Alzheimer's disease. Regional SUVRs were computed in seven ROIs where the histopathological examination has also been performed. Two-way ANOVA and post-hoc slope difference test has been used to assess whether our technique improved the relationship between the PET image quantification results and the histopathological assessment.

Results: As seen in Figure 2 and Table I, our method resulted in consistently and significantly higher SUVR in comparison to the conventional method in almost all ROIs ($P < 0.01$). In addition, two-way ANOVA test resulted in a significant main effect of method ($p < 0.0001$) as well as significant interaction effect of method ($p < 0.01$) on the relationship between quantified SUVR and histopathological assessment data. Post-hoc slope difference test showed that our technique significantly outperformed existing conventional method.

Conclusion: Our developed technique can quantify Amyloid-β PET scans on an almost millimeter-by-millimeter scale with significantly higher precision which nowadays is an absolute necessity in any PET imaging studies that takes into account regional heterogeneity of the Amyloid-β plaque accumulation.
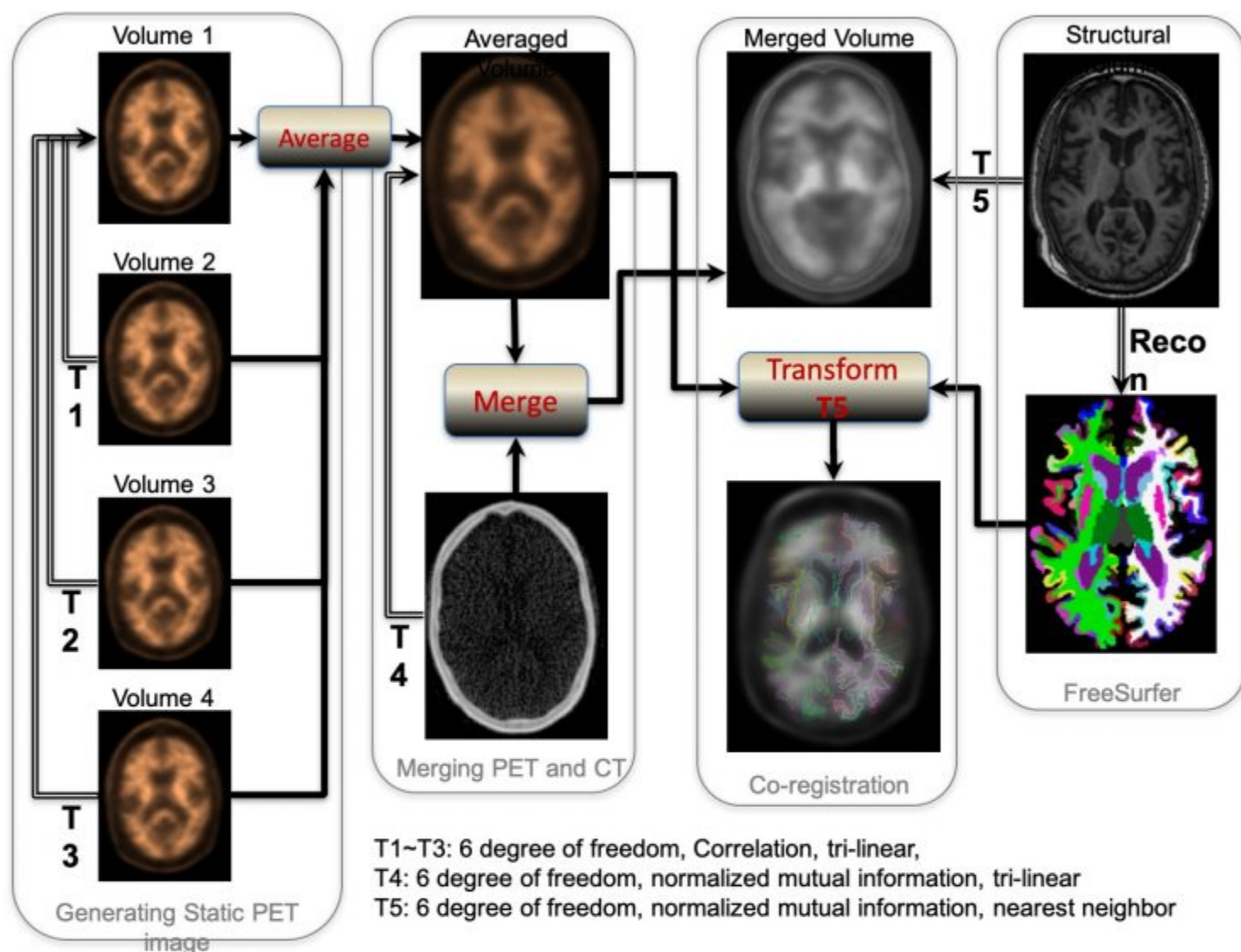
Figure 1. Flowchart of our developed PET image reconstruction technique. Each subject's structural MRI scan is reconstructed with FreeSurfer to obtain neuroanatomical labeling at every point in the brain. The dynamic PET scans will be registered to each other and merged with the CT image to generate a fused image that contains both skull and tissue. An inter-modal, and intra-subject registration with information theoretic cost function has been utilized to transform all FreeSufer's labels into PET images which subsequently can be used to quantify the regional accumulation of the Amyloid-β plaques at every point in the brain.
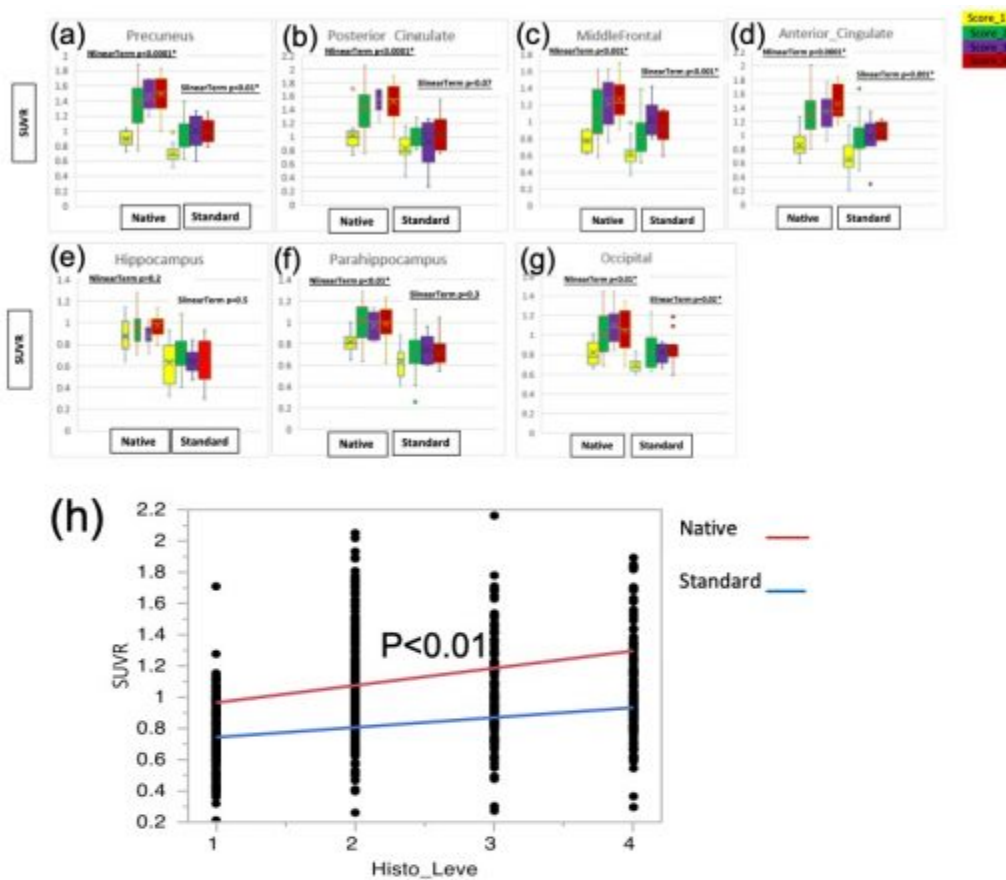
Figure 2. Depicts the distribution of regional uptakes obtained from our technique (Native) as well as the conventional method (Standard) for every level of histopathological staining for each of the seven selected ROIs in a separate plot (a to g). Table I shows that almost for every histopathological staining level our technique gives significantly higher SUVR in comparison to conventional method in all seven regions. (h) Depicts the significant slope difference between the two methods highlighting the superiority of our developed method in comparison to the conventional method.

Table 2. Regional mean and SD of SUVRs for Native and Standard methods based on histopathological staining levels and t-test results comparing the two methods.

ROI	Histo Score	Native SUVR	Standard SUVR	P
Middle frontal	1 (n= 12)	0.77±0.12	0.62±0.17	<0.05*
	2 (n=17)	1.11±0.32	0.83±0.24	<0.01*
	3 (n=13)	1.22±0.29	1.03±0.20	0.06
	4 (n=10)	1.27±0.26	0.93±0.19	<0.01*
Ant Cingulate	1 (n=14)	0.86±0.18	0.65±0.23	0.01*
	2 (n=21)	1.33±0.33	1.01±0.30	<0.01*
	3 (n=10)	1.34±0.26	0.97±0.28	<0.01*
	4 (n=6)	1.45±0.27	1.08±0.13	0.01*
Post Cingulate	1 (n=16)	1.02±0.22	0.83±0.19	0.01*
	2 (n=18)	1.42±0.34	1.01±0.14	<0.001*
	3 (n=8)	1.56±0.29	0.93±0.35	0.001*
	4 (n=9)	1.53±0.29	1.04±0.28	<0.01*
precuneus	1 (n=14)	0.89± 0.1	0.7±0.11	<0.001*
	2 (n=14)	1.37±0.30	0.95±0.2	<0.001*
	3 (n=7)	1.46±0.2	1.00±0.24	<0.01*
	4 (n=9)	1.49±0.27	0.99±0.16	<0.001*
Hippocampus	1 (n=17)	0.88±0.15	0.63±0.19	<0.001*
	2 (n=14)	0.95±0.15	0.73±0.19	<0.01*
	3 (n=12)	0.88±0.09	0.64±0.11	<0.001*
	4 (n=9)	0.97±0.11	0.68±0.22	<0.01*
Parahippocampus	1 (n=17)	0.81±0.1	0.63±0.14	<0.001*
	2 (n=14)	1.01±0.18	0.71±0.21	<0.001*
	3 (n=7)	0.97±0.13	0.75±0.13	<0.01*
	4 (n=11)	0.99±0.17	0.72±0.13	<0.001*
Occipital	1 (n=13)	0.82±0.12	0.69±0.07	<0.01*
	2 (n=14)	1.01±0.23	0.84±0.19	0.056
	3 (n=10)	1.1±0.21	0.82±0.1	0.001*
	4	1.04±0.22	0.86±0.15	0.01*

P19: Network-based modeling of tau spread and seeding using PET and DTI

Fan Yang[1,2], Samadrita Roy Chowdhury[1], <u>Heidi Jacobs</u>[2], Keith Johnson[2], Joyita Dutta[1,2]

[1]*University of Massachusetts Lowell, Lowell, MA, US*
[2]*Massachusetts General Hospital, Boston, MA, US*

Objective: Several recent studies have investigated the trans-synaptic spread of tau neurofibrillary tangle pathology in aging and Alzheimer's disease using mouse models. Here we investigate the relative roles of tau buildup via localized generation (seeding) vs. propagation (spread) along the structural network of the brain through a spread model using diffusion tensor imaging (DTI) and longitudinal positron emission tomography (PET) using the 18F-Flortaucipir radiotracer.

Method: We built a linear predictive model for two-time-point tau PET data using structural connectivity information captured by graph Laplacian matrices computed from DTI scans. The model contains a network-dependent term that represents tau propagation along fiber tracts at a given time-point. It also accommodates a network-independent "source" term that captures spatially-localized tau generation patterns that are constrained to be spatially sparse. We applied the model to 62 subjects (75.85 ± 6.18 years, 37 females) from the Harvard Aging Brain Study with two-time-point Flortaucipir-PET scans for tau, DTI scans for structural connectivity, and Pittsburgh-compound-B (PIB) PET scans for amyloid.

Results: Model fitting was performed separately on high- and low-amyloid cohorts (41 PIB+ and 21 PIB- subjects). FreeSurfer parcellation was used for region-of-interest (ROI) analysis. Figure 1 shows the differential aggregation of tau across the two time points averaged over each group split into propagative and generative components. Whereas the groups showed similar levels of propagative buildup for most ROIs, the PIB+ subjects showed more substantial generative buildup in several cortical and striatal ROIs.

Conclusion: Combination of DTI and PET can offer a macroscopic perspective on tau propagation along neural pathways. Our model, which predicts tau PET SUVRs at a given time from tau PET SUVRs at a previous time using structural network information and sparse source localization, identified distinct patterns of network-based

spread vs. seeding in PIB+ and PIB- subjects.
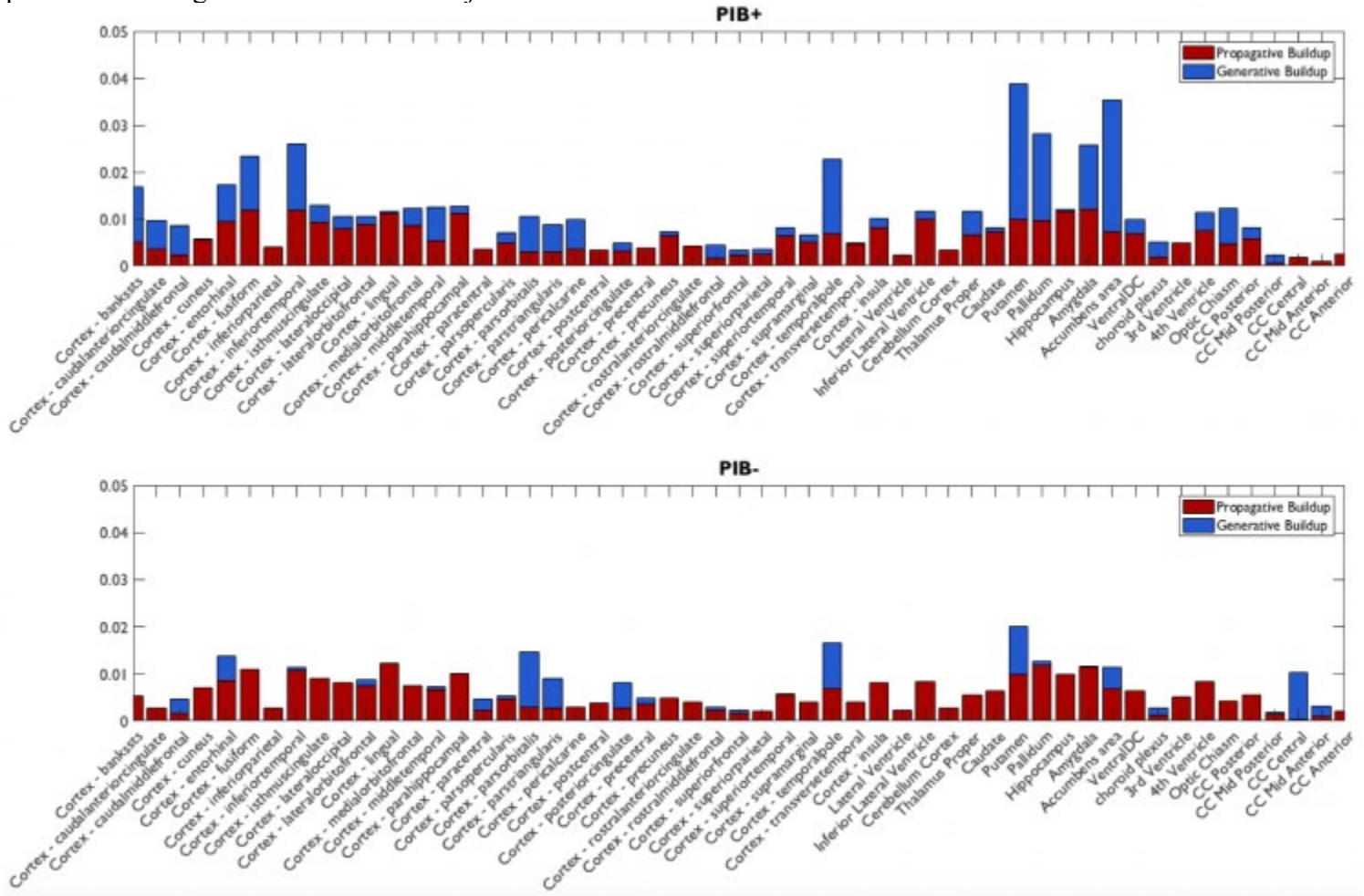
Figure 1: Relative extents of tau buildup via propagation along neural fiber tracts (spread) and localized generation (seeding) in high-amyloid (PIB+) and low-amyloid (PIB-) groups. These results indicate a more pronounced role of tau seeding over tau spread in the high-amyloid subjects vs. the low-amyloid subjects.

Keywords: *PET, DTI, tau spread, tau seeding, Alzheimer's disease*

P20: Establishment of a simplified method to quantify [18F]PM-PBB3 ([18F]APN-1607) binding in the brains of living human subjects

<u>Chie Seki</u>[1], Kenji Tagai[1,2], Hitoshi Shimada[1,3], Soichiro Kitamura[1], Yasuyuki Kimura[1], Masanori Ichise[1], Maiko Ono[1], Keisuke Takahata[1], Manabu Kubota[1], Yuhei Takado[1], Hitoshi Shinotoh[1,4], Maki Okada[5], Tatsuya Kikuchi[5], Ming-Ring Zhang[5], Tetsuya Suhara[1], Makoto Higuchi[1]

[1]*Department of Functional Brain Imaging Research, National Institute of Radiological Sciences, National Institutes for Quantum and Radiological Science and Technology, Chiba, Japan*
[2]*Department of Psychiatry, Jikei University School of Medicine, Tokyo, Japan*
[3]*Department of Neurology, Graduate School of Medicine, Chiba University, Chiba, Japan*
[4]*Neurology Clinic Chiba, Chiba, Japan*
[5]*Department of Radiopharmaceutics Development, National Institute of Radiological Sciences, National Institutes for Quantum and Radiological Science and Technology, Chiba, Japan*

Aim: PET imaging with [^{18}F]PM-PBB3 ([^{18}F]APN-1607) has demonstrated the capability of this radioligand for high-contrast visualization of tau deposits in the brains of Alzheimer's disease (AD) and diverse other neurodegenerative disorders. This study was aimed at determining an optimal time frame of a PET scan to obtain a reliable target-to-reference ratio of radioligand concentrations in comparison with analytical models with an arterial input function.

Methods: Ten subjects consisting of 5 healthy controls (HCs) and 3 AD and 2 progressive supranuclear palsy (PSP) patients underwent dynamic PET scans over 150 or 180 minutes after intravenous injection of [^{18}F]PM-PBB3. Serial arterial blood samples were withdrawn during the scan to determine a metabolite-corrected plasma input function. Regional time-activity curves were analyzed with 1- and 2-tissue compartment models (TCMs) and Logan's graphical analysis (LGA). Time-stability of total distribution (V_T) values was examined to estimate scan duration sufficient for determination of V_T. Non-displaceable biding potential (BP_{ND}) of [^{18}F]PM-PBB3 was calculated using V_T obtained with LGA, and SUVR in a 20-minute frame beginning at different time points after radioligand injection was calculated. SUVR-1 values were then compared with BP_{ND} to determine an optimal scan frame.

Results: A peak [^{18}F]PM-PBB3 SUV in the brain approximated 2.5 at < 5 minutes, followed by rapid radioactivity washout. Radioligand retentions in the lateral temporal cortex of AD patients and midbrain of PSP patients were characteristically increased relative to HCs. Two-TCM better described the radioligand kinetics in target regions than 1-TCM. V_T values obtained with LGA presented the highest time-stability, and SUVR-1 values at 90-110 min showed the highest correlation with BP_{ND} among different frames.

Conclusions: [^{18}F]PM-PBB3 kinetics showed reversible binding and could be described without radiometabolite compartments in the brain. Estimation of SUVR at 90-110 min can be employed as a simplified means to quantify radioligand retention with sufficient robustness.

Keywords: *Tau, PET, [18F]PM-PBB3, quantification, SUVR*

P21: PET and CSF amyloid status are differently predicted by patient features

Juhan Reimand[1,2,3], Arno de Wilde[1], Charlotte Teunissen[4], Marissa Zwan[1], Albert Windhorst[5], Ronald Boellaard[5], Wiesje van der Flier[1,6], Philip Scheltens[1], Bart NM van Berckel[5], Rik Ossenkoppele[1,7], Femke Bouwman[1]

[1]*Department of Neurology & Alzheimer Center, Amsterdam Neuroscience, VU University Medical Center, Amsterdam UMC, Amsterdam, The Netherlands*
[2]*Department of Health Technologies, Tallinn University of Technology, Tallinn, EE*
[3]*Center of Radiology, North Estonia Medical Centre, Tallinn, EE*
[4]*Neurochemistry Laboratory, Department of Clinical Chemistry, Amsterdam Neuroscience, VU University Medical Center, Amsterdam UMC, Amsterdam, The Netherlands*
[5]*Department of Radiology & Nuclear Medicine, Amsterdam Neuroscience, VU University Medical Center, Amsterdam UMC, Amsterdam, The Netherlands*
[6]*Department of Epidemiology & Biostatistics, Amsterdam Neuroscience, VU University Medical Center, Amsterdam UMC, Amsterdam, The Netherlands*
[7]*Lund University, Clinical Memory Research Unit, Lund University, Malmö, Sweden*

Amyloid PET and CSF Aβ42 have been shown to yield discordant results in 10-20% of patients, possibly providing unique information. Although the predictive power of various demographic, clinical, genetic and imaging features for amyloid-positivity has previously been investigated it is currently unknown whether these features differentially predict amyloid status based on PET or CSF.

We included 768 Amsterdam Dementia Cohort-patients (SCD (n=194), MCI (n=127), dementia (n=447, AD and non-AD) with amyloid PET and CSF Aβ42 measurement within one year (Table-1). We performed two random forest models predicting separately PET and CSF status using 17 patient features (including demographics, APOE4 positivity, CSF (p)tau, cognitive performance, MRI visual ratings) in both the total group and separately per syndrome diagnosis. Thereafter, we selected the features with the highest variable importance measure (VIM) as input for logistic regression models, where amyloid status on either PET or CSF was predicted by the selected patient feature and the status of the other amyloid modality.

APOE4, CSF tau and p-tau had highest VIM for amyloid positivity in all groups (Figure-1). P-tau was a significant predictor for PET in SCD (OR=1.02[1.01-1.04], $p_{fdr}<0.05$), MCI (OR=1.05[1.02-1.07], $p_{fdr}<0.01$) and dementia (OR=1.04[1.02-1.05], $p_{fdr}<0.001$), but not for CSF (Table-2). APOE4 (OR=3.07[1.33-7.07], $p_{unc}<0.01$) and MMSE (OR=1.21[1.03-1.41], $p_{unc}<0.05$) were significant for predicting only CSF amyloid status in SCD, and memory (OR=1.17[1.04-1.30], $p_{fdr}<0.05$) for only predicting PET amyloid status in dementia.

Amyloid status based on PET and CSF was predicted by a different pattern of patient features and this varied by disease stage, indicating that PET-CSF discordance contains important information. The higher importance of APOE4 and memory for predicting CSF-amyloid in SCD supports previous findings that CSF-amyloid might be more sensitive early in the disease course. CSF p-tau being more predictive for PET suggests that PET is a more specific modality for amyloid pathology.

	PET-CSF-	PET+CSF-	PET-CSF+	PET+CSF+
DEMOGRAPHICS:				
N (%)	315 (41)	32 (4)	66 (9)	355 (46)
Sex, male (%)	211 (67)^D	17 (53)	42 (64)	191 (54)^A
Age, years (mean (SD))	62.8 (7.7)	65.0 (7.7)	62.3 (9.0)	63.7 (7.3)
Education (median [IQR])	5 [4, 6]	5 [4, 6]	5 [4, 6]	5[4, 6]
SYNDROME DIAGNOSIS (%):				
SCD	136 (43)	10 (31)	20 (30)	28 (8)
MCI	55 (18)	8 (25)	9 (14)	55 (16)
Alzheimer's disease (AD) dementia	28 (9)	11 (34)	18 (27)	252 (71)
non-AD dementia	96 (31)	3 (9)	19 (29)	20 (6)
BIOMARKERS:				
CSF-PET difference, days (mean (SD))	61 (75)	54 (70)	73 (84)	58 (67)
CSF Abeta42 (median [IQR])	1134 [989, 1275]^{BCD}	875 [832, 959]^{ACD}	674 [626, 741]^{ABD}	615 [537, 688]^{ABC}
CSF tau (median [IQR])	277 [207, 375]^{BD}	468 [324, 716]^{AC}	295 [175, 505]^{BD}	607 [402, 845]^{AC}
CSF p-tau (median [IQR])	44 [35, 54]^{BD}	67 [50, 90]^{AC}	42 [28, 64]^{BD}	82 [58, 103]^{AC}
APOE E4 positivity (%)	84 (28)^{BCD}	18 (60)^A	33 (53)^A	237 (70)^A
COGNITION:				
MMSE (mean (SD))	26 (3)^{BCD}	24 (5)^A	25 (4)^A	23 (4)^A
Memory z-score (mean (SD))	-1.39 (2.27)^{BD}	-3.14 (2.73)^A	-2.25 (2.97)^D	-3.33 (2.76)^{AC}
Language z-score (mean (SD))	-0.65 (1.29)^{CD}	-0.95 (1.48)	-1.43 (2.26)^A	-1.03 (1.84)^A
Attention z-score (mean (SD))	-0.69 (1.09)^D	-0.82 (1.08)	-1.00 (1.02)	-1.10 (1.21)^A
Executive z-score (mean (SD))	-1.01 (1.38)^D	-1.39 (1.55)	-1.29 (1.32)	-1.53 (1.40)^A
Visuospatial z-score (mean (SD))	-0.34 (1.18)^D	-1.04 (1.90)	-1.01 (1.90)	-1.34 (2.38)^A
MRI:				
MRI-amyloid difference, days (mean (SD))	16 (50)^C	35 (60)	43 (78)^{AD}	14 (46)^C
MTA (median [IQR])	0.5 [0.0, 1.0]^D	0.5 [0.0, 1.0]	0.5 [0.0, 1.6]	1.0 [0.5, 1.5]^A
PCA (median [IQR])	1.0 [0.0, 1.1]^D	1.0 [1.0, 1.0]	1.0 [0.0, 1.3]^D	1.0 [1.0, 2.0]^{AC}
Fazekas (median [IQR])	1.0 [0.0,1.0]	1.0 [0.8, 1.0]	1.0 [0.0, 2.0]	1.0 [0.0, 1.0]
Lacune positivity (%)	14 (6)	0 (0)	7 (11)	17 (7)
Microbleed positivity (%)	31 (13)	4 (15)	4 (7)	54 (21)

Table 1. Patient groups by PET/CSF amyloid status

Education is staged by Verhage classification (1-7). Lacune and microbleed positivity indicates that at least one is present. MTA - medial temporal lobe atrophy scale. PCA - posterior cortical atrophy scale. Bonferroni correction was performed for multiple comparisons.

A, B, C, D show significant difference ($p < 0.05$) from other groups:

    A - difference from PET-CSF-
    B - difference from PET+CSF-
    C - difference from PET-CSF+
    D - difference from PET+CSF+
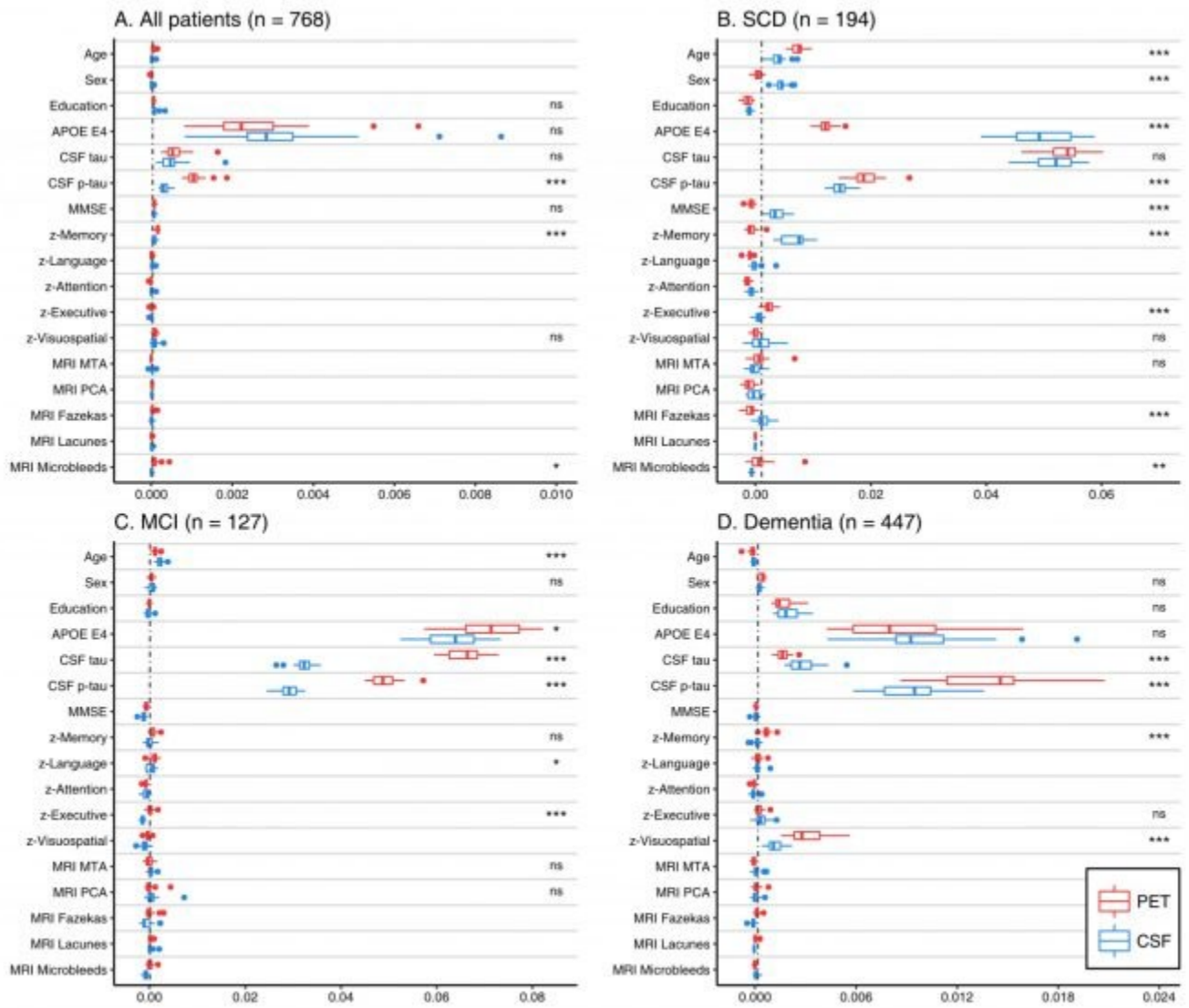
Figure 1. Average variable importance of patient features from random forest models predicting PET and CSF positivity

P-values (*** - p<0.001, ** - p<0.01, * - p<0.05, ns - non-significant) indicate the bootstrapped difference of Area under the curve (AUC) based variable importance between models predicting PET and CSF status. False discovery rate (FDR) correction was performed for multiple comparisons.

		TOTAL			SCD			MCI			DEMENTIA		
Predictor	Outcome	Odds ratio	p raw	p corr	Odds ratio	p raw	p corr	Odds ratio	p raw	p corr	Odds ratio	p raw	p corr
Age	PET				1.04 (0.99,1.10)			0.97 (0.91,1.04)					
	CSF				1.02 (0.97,1.07)			0.98 (0.92,1.04)					
Sex, F	PET				1.17 (0.49,2.77)			2.27 (0.75,6.90)			1.99 (1.07,3.69)	*	
	CSF				1.76 (0.80,3.90)			1.11 (0.37,3.35)			0.82 (0.43,1.55)		
Education	PET	1.05 (0.88,1.26)									1.14 (0.89,1.46)		
	CSF	1.00 (0.84,1.19)									1.17 (0.90,1.52)		
APOE E4	PET	2.52 (1.61,3.93)	***	***	1.54 (0.62,3.78)			9.44 (2.93,30.39)	***	**	2.12 (1.16,3.89)	*	*
	CSF	2.34 (1.50,3.67)	***	***	3.07 (1.33,7.07)	**		1.85 (0.58,5.92)			2.07 (1.10,3.90)	*	
CSF tau	PET	1.003 (1.003,1.004)	***	***	1.003 (1.001,1.005)	**	*	1.008 (1.004,1.012)	***	***	1.003 (1.001,1.004)	***	***
	CSF	1.001 (1.000,1.002)	**	**	1.002 (1.000,1.003)			0.999 (0.997,1.001)			1.001 (1.000,1.002)	*	
CSF p-tau	PET	1.04 (1.03,1.05)	***	***	1.02 (1.01,1.04)	**	*	1.05 (1.02,1.07)	***	**	1.04 (1.02,1.05)	***	***
	CSF	1.01 (1.00,1.02)	*	*	1.01 (1.00,1.03)			0.99 (0.98,1.01)			1.01 (1.00,1.02)		
MMSE	PET	1.10 (1.04,1.17)	***	**	0.93 (0.80,1.10)								
	CSF	1.10 (1.04,1.17)	**	**	1.21 (1.03,1.41)	*							
Memory	PET	1.21 (1.11,1.33)	***	***	0.99 (0.69,1.42)			1.25 (0.96,1.64)			1.17 (1.04,1.30)	**	*
	CSF	1.10 (1.01,1.19)	*	*	1.23 (0.87,1.75)			0.96 (0.71,1.30)			1.00 (0.90,1.12)		
Language	PET							0.23 (0.08,0.68)	**	*			
	CSF							1.59 (0.77,3.27)					
Executive	PET				0.99 (0.67,1.48)			0.61 (0.33,1.12)			1.10 (0.87,1.39)		
	CSF				1.05 (0.71,1.55)			1.18 (0.64,2.17)			0.81 (0.64,1.03)		
Visuospatial	PET	1.15 (1.00,1.31)	*		0.77 (0.49,1.22)						1.25 (1.05,1.48)	*	*
	CSF	1.22 (1.06,1.41)	**	*	1.53 (0.99,2.38)						1.03 (0.87,1.21)		
MRI MTA	PET				1.68 (0.77,3.68)			0.55 (0.28,1.05)					
	CSF				1.15 (0.53,2.51)			1.78 (0.87,3.63)					
MRI PCA	PET							1.09 (0.48,2.46)					
	CSF							0.69 (0.30,1.58)					
MRI Fazekas	PET				0.76 (0.36,1.62)								
	CSF				1.56 (0.83,2.96)								
MRI microbleeds	PET	2.11 (1.09,4.08)	*	*	2.15 (0.60,7.67)								
	CSF	0.88 (0.45,1.71)			1.01 (0.29,3.57)								

Table 2. Predictive value of patient features for amyloid status based on PET or CSF while adjusting for the amyloid status of the other amyloid modality

P-values show the significance of the patient feature in the model (*** - p<0.001, ** - p<0.01, * - p<0.05). Raw p-values and corrected p-values are reported per model. False discovery rate (FDR) correction was performed for multiple comparisons. Cognitive scores have been multiplied by -1, therefore lower scores usually indicate higher odds ratios for amyloid positivity.

P22: TauIQ – an algorithm to quantify global and local tau accumulation

Alex Whittington[1,2], John Seibyl[1], Jacob Hesterman[1], Roger Gunn[1,2]

[1]*Invicro, Boston, MA, US*
[2]*Imperial College London, London, UK*

Introduction: Tau PET scans are potentially valuable biomarkers in clinical trials of novel AD drugs. To date, data have been quantified using SUVR but this does not adequately account for the complex distribution of tau or harness the power of canonical image based quantification approaches recently introduced for amyloid (Amyloid[IQ]). We introduce the Tau[IQ] algorithm that is able to decompose the tau signal into global (stereotypical pattern expected at a certain disease stage) and local (distinct additional local tau deposits) outcome measures.

Methods: Data from 234 subjects (88 healthy controls (HC), 40 significant memory concern, 58 early mild cognitive impairment [MCI], 16 MCI and 30 late MCI) each with [18F]Flortaucipir, [18F]Florbetapir and T1-MRI scans were downloaded from ADNI. First, canonical images for the tau carrying capacity (K), and non-specific binding (NS) were calculated - amyloid scans were analysed using Amyloid[IQ] to derive a subject-specific time in the disease trajectory allowing spatiotemporal modelling of the associated tau data with a regression model (Figure 1). Tau[IQ] then uses these canonical images (Figure 2) within an image based regression framework to estimate global (Tau_L) and local tau metrics (Figure 3). Tau-/Tau+ classification was determined from the distribution of Tau_L in amyloid negative HC.

Results: The [18F]Flortaucipir canonical images successfully partitioned background (NS: non-specific and off-target binding) and tau (K: stereotypical tau distribution in AD) signals. Only 22% of subjects had local tau signal (median extent: 506mm^3, range: 3-29220mm^3). Tau_L was 30%(+/-19%) in HC rising to 50%(+/-54%) in late MCI subjects. The percentage of Tau+ scans in amyloid negative healthy controls was 5% (by design) rising to 26% in late MCI subjects.

Conclusions: Tau[IQ] quantifies both global and local tau deposition from a static tau PET scan and can provide important metrics for quantitative biomarker studies in AD.
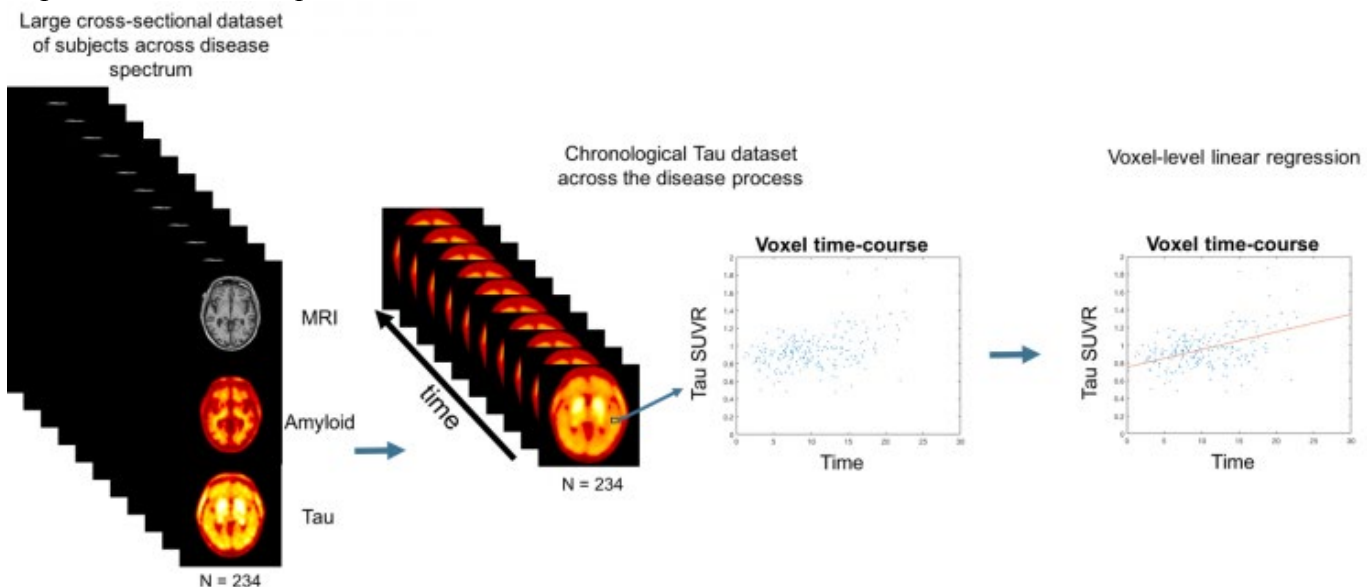
Figure 1
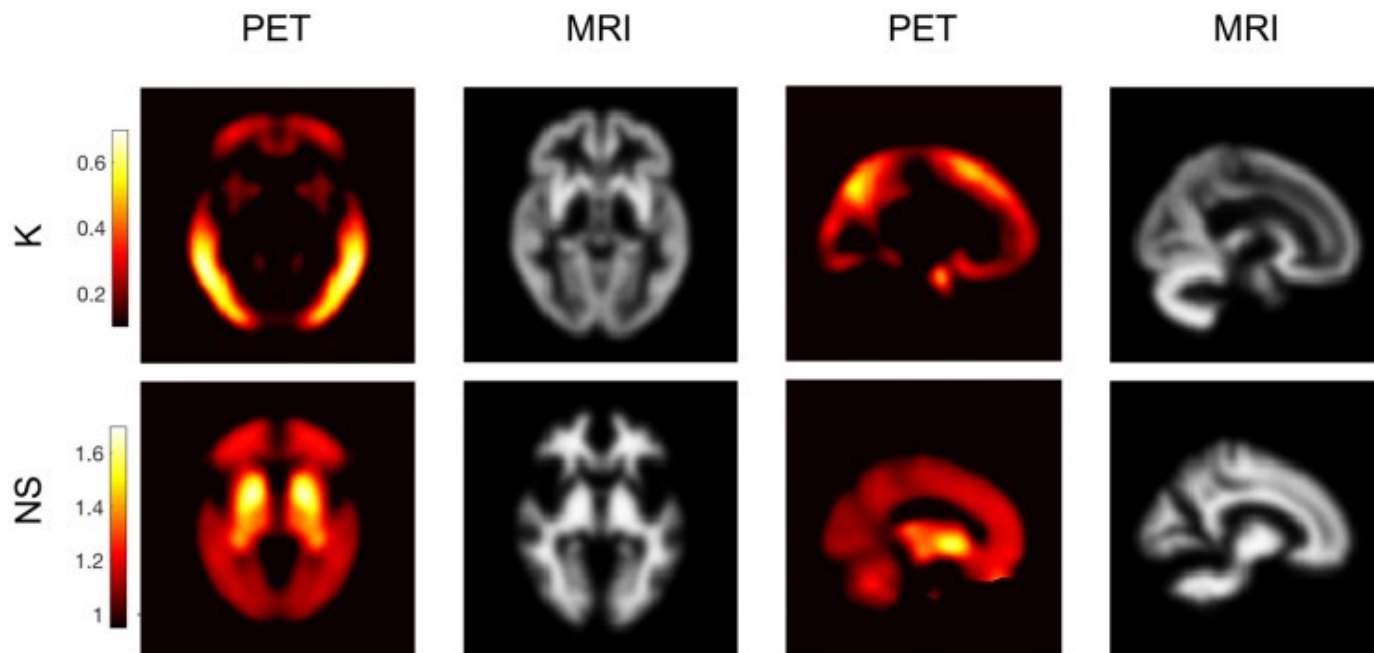
Figure 2

$$SUVR = ns\ \mathbf{NS} + Tau_L\ \mathbf{K} + \mathbf{Local\_Tau}$$

Figure 3
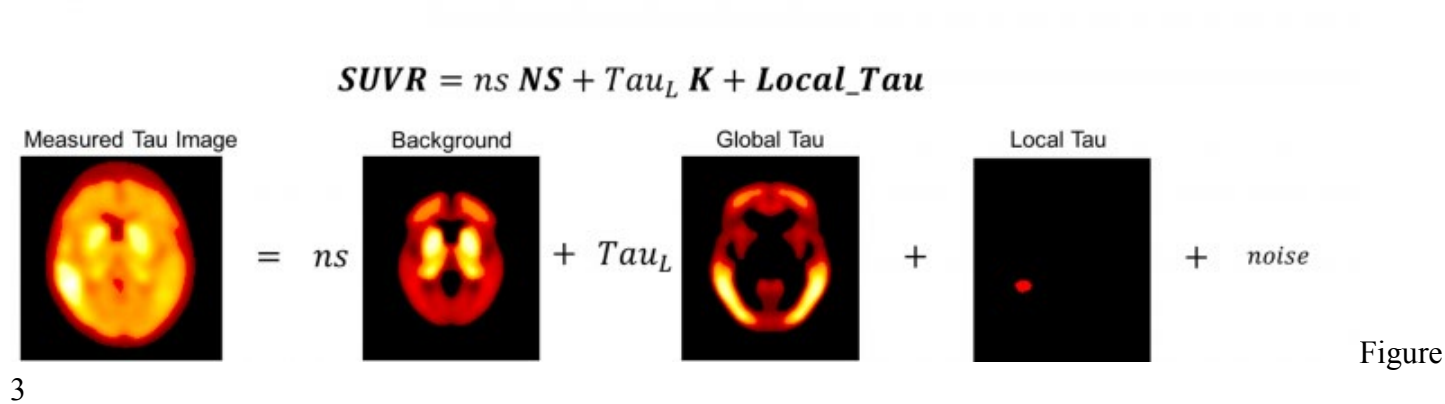
P23: AmyloidIQ – an automated algorithm for classifying amyloid-β PET scans

Alex Whittington[1,2], John Seibyl[1], Udo Eichenlaub[3], Andrew Stephens[4], Jacob Hesterman[1], Roger Gunn[1,2]

[1]*Invicro, Boston, MA, US*
[2]*Imperial College London, London, UK*
[3]*Roche Diagnostics GmbH, Penzberg, Germany*
[4]*Life Molecular Imaging GmbH, Berlin, Germany*

Introduction: Classification of amyloid-β (Aβ) PET scans as Aβ-positive or Aβ-negative is important in both clinical practice and clinical research for determining enrolment eligibility. Visual reads currently provide the gold standard for classifying scans but they require multiple trained readers often operating under time constraints and are not as cost-efficient as automated quantitative assessments. SUVR has been proposed as a fully automated outcome measure however the agreement with visual assessment has not been good enough to gain widespread adoption. In this work, we assess whether the novel outcome measure as calculated with Amyloid[IQ] can provide a specific and sensitive approach to automatically classify Aβ scans.

Methods: For the data outlined in Table 1 we computed Amyloid Load (Aβ$_L$) using the Amyloid[IQ] algorithm (Figure 1) and a composite SUVR for [18F]Flobetapir, [18F]Florbetaben and [18F]Flutametamol. ROC curves were calculated for Aβ$_L$ and SUVR under the assumption that visual reads provided the ground truth. PET-MR and PET only pipelines were also compared.

Tracer	n	PET	MR	Visual Read
[18F]Florbetapir	672	Yes	Yes	Yes
[18F]Florbetaben	268	Yes	Yes	Yes
[18F]Flutametamol	120	Yes	No	Yes

Results: Spatially normalised amyloid PET images from the three different tracers were effectively modelled using a linear combination of previously derived canonical images using Amyloid[IQ] (Figure 2). For both [18F]Flobetapir and [18F]Florbetaben, there was a good agreement between the PET-only and PET-MR pipelines (r^2=0.93 and r^2=0.96 respectively). For all three radiotracers, the ROC AUC for Aβ$_L$ was higher than SUVR (Figure 3). The accuracy of the pipeline for each of the radiotracers at the optimum threshold was [18F]Florbetapir = 93%,[18F]Florbetaben = 95% and[18F]Flutametamol = 93%.

Conclusions: Amyloid[IQ] is an automated algorithm that can accurately classify amyloid PET scans.

Figure 1
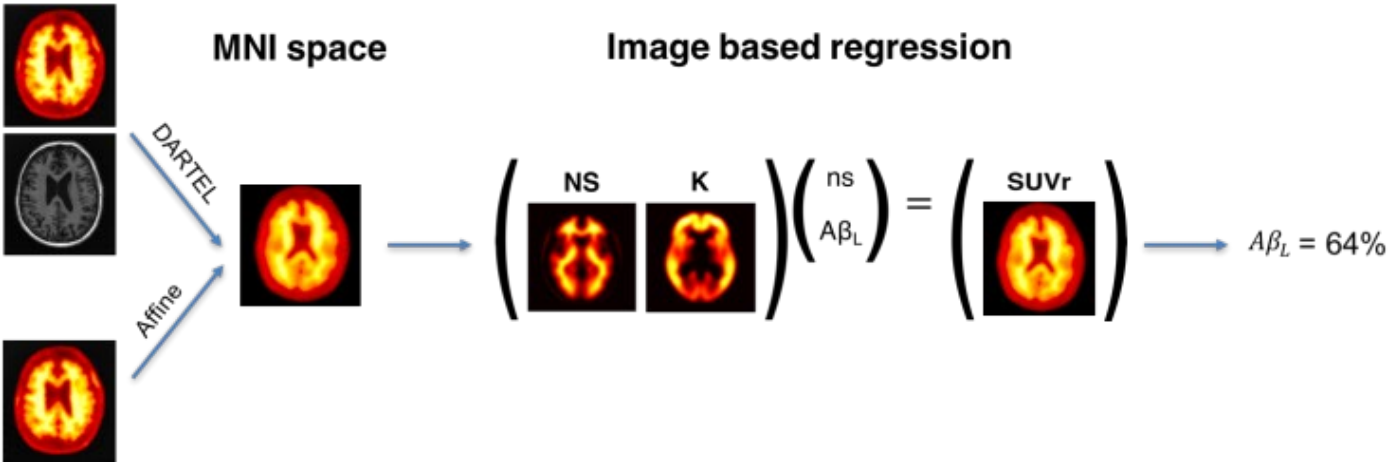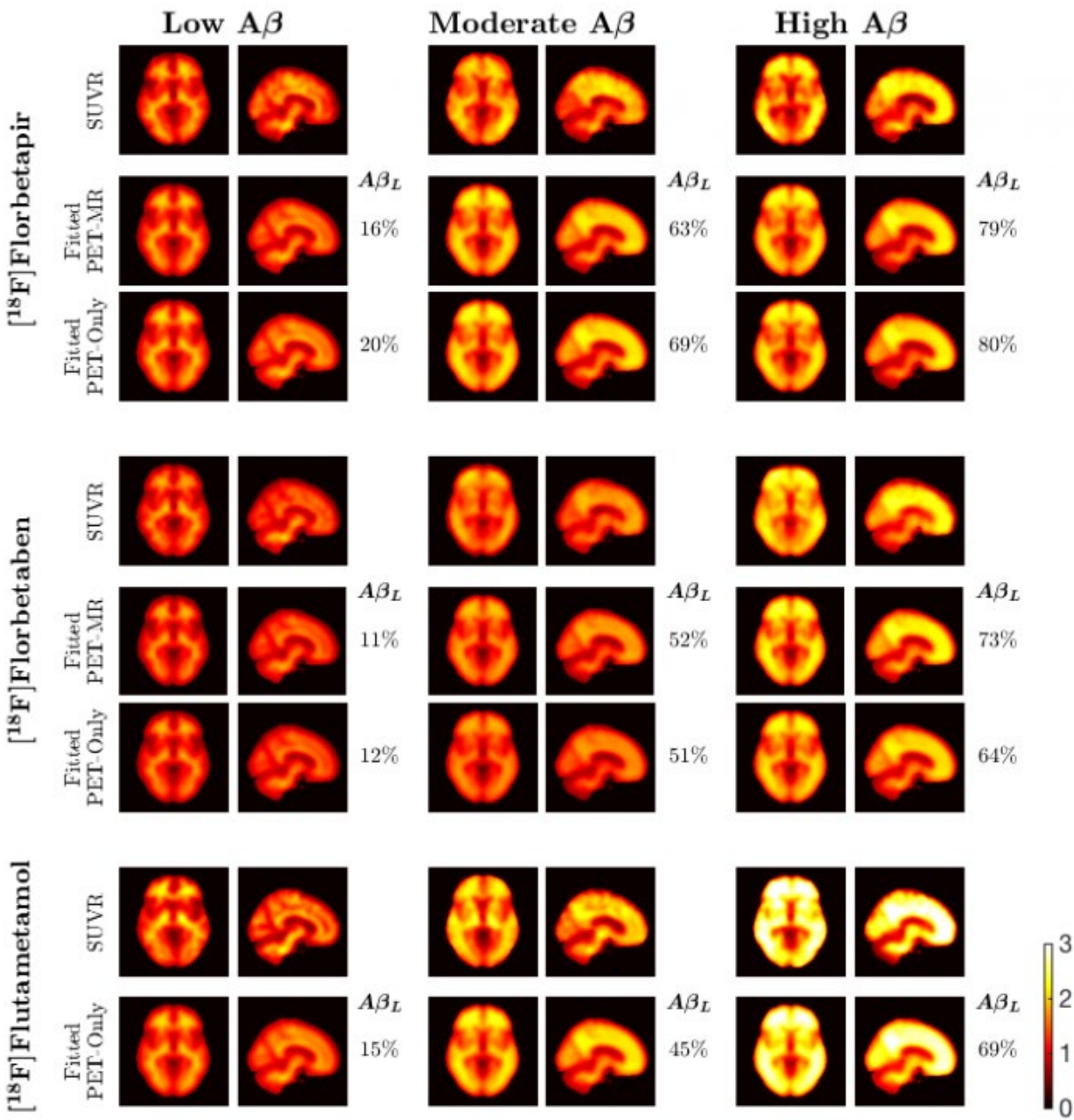
Figure 2

[¹⁸F]Florbetapir
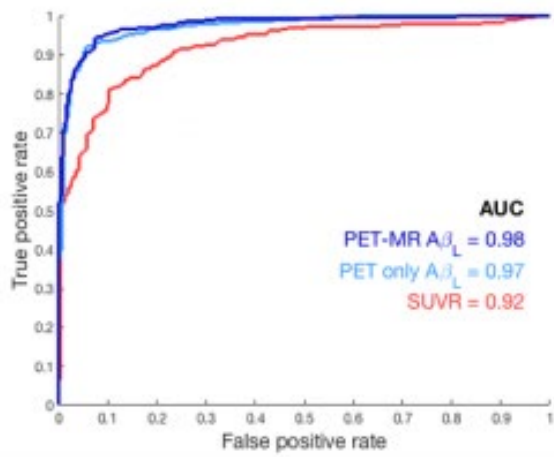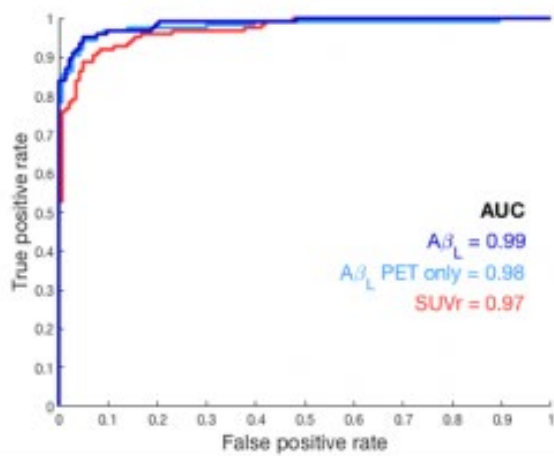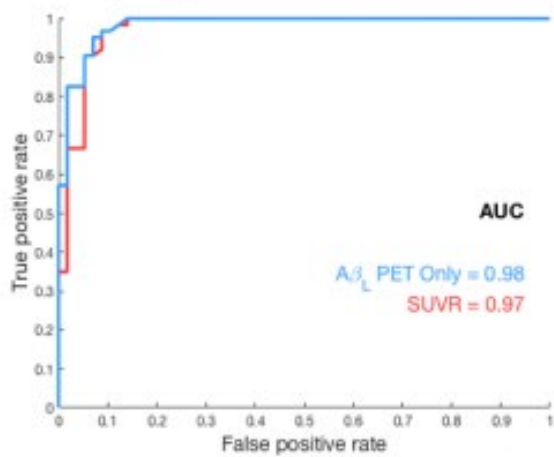
AUC
PET-MR Aβ_L = 0.98
PET only Aβ_L = 0.97
SUVR = 0.92

[¹⁸F]Florbetaben

AUC
Aβ_L = 0.99
Aβ_L PET only = 0.98
SUVr = 0.97

[¹⁸F]Flutametamol

AUC
Aβ_L PET Only = 0.98
SUVR = 0.97

Figure 3

P24: Reconsidering in-vivo models of regional amyloid pathology progression: region-specific thresholds and longitudinal data

Irina Jelistratova[1], Keanu Bugla[1,2], Stefan Teipel[1,2], Michel Grothe[1]

[1]*German Center for Neurodegenerative Diseases (DZNE), Rostock, Germany*
[2]*Department of Psychosomatic Medicine, University of Rostock, Rostock, Germany*

Background: We previously developed an in-vivo model of regional amyloid progression based on the frequency of regional amyloid-positivity across cross-sectional Florbetapir-PET scans of older individuals. Here we reassess this progression model by using methodology that accounts for regionally varying noise levels when estimating amyloid-positivity and further incorporates longitudinal data in model estimation.

Methods: We estimated region-specific thresholds of amyloid-positivity based on the signal measured in Florbetapir-PET data of 13 young controls (age≤45y) available from the Centiloid project. We then applied these thresholds to the Florbetapir-PET data of 179 cognitively normal (CN) older ADNI participants to reassess our previously estimated frequency-based model. We further used serial Florbetapir-PET scans with 2-year follow-up from a larger sample of 436 ADNI participants to develop a longitudinal trajectory model. The probabilistic model starts with the longitudinal detection of earliest amyloid accumulation in cases that are amyloid-negative at baseline, and then iteratively searches for individuals at increasing amyloid progression phases in the baseline data to record their regional progression over follow-up.

Results: Using region-specific thresholds, amyloid-positivity in CN individuals was most frequently observed in the anterior temporal lobe, followed by the remaining associative neocortex, and then primary sensory-motor areas. No evidence of amyloidosis was detected in hippocampus, amygdala, or striatum (Fig.1). This progression pattern was replicated and further refined by the longitudinal model, showing first amyloid accumulation in anterior temporal areas, followed by increasing probability of the precuneus and anterior cingulate to become amyloid-positive (Fig.2). Probability for primary sensory-motor and medial temporal areas to become amyloid-positive only increased at advanced phases of amyloidosis, at which probability for subcortical amyloid accumulation still remained low.

Conclusions: A consistent pattern of amyloid spreading from associative cortex over primary sensory-motor areas to subcortical structures is supported across methods, but the relative involvement of different association areas requires further study.
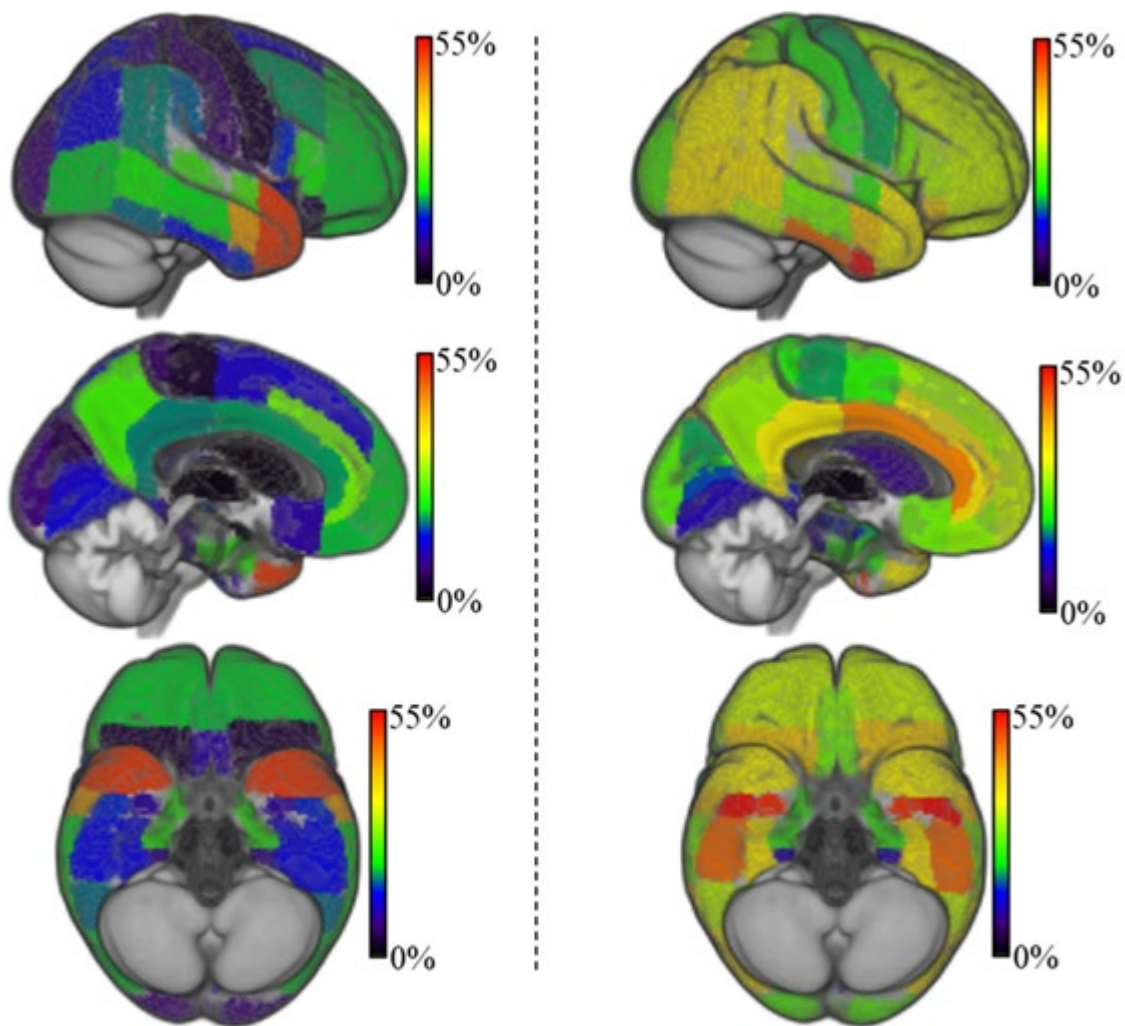
Figure 1: Frequency-based model of amyloid progression using region-specific thresholds (left) in comparison to our previously estimated model using a constant regional threshold (right).
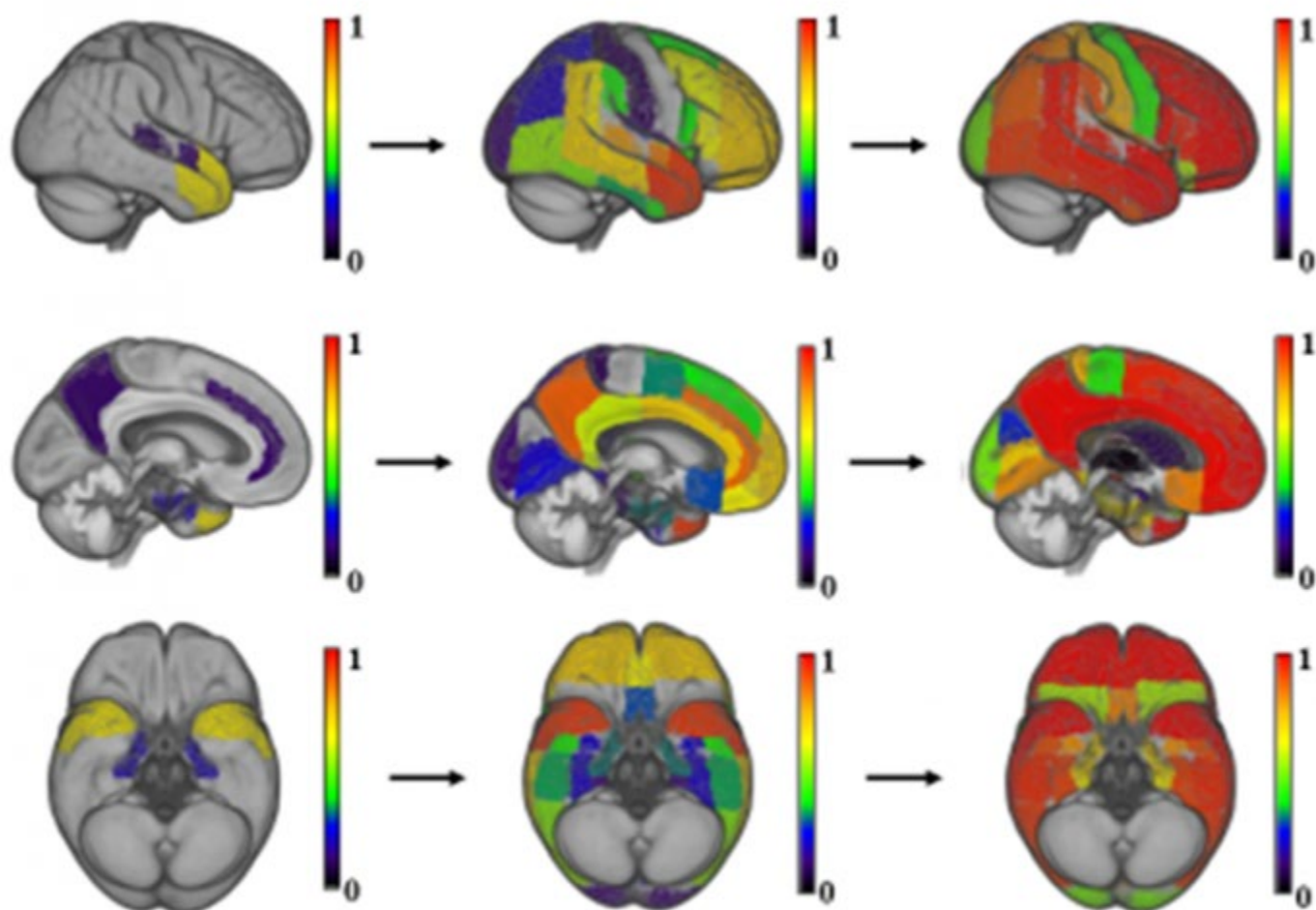
Figure 2: The probabilistic longitudinal trajectory model. Warmer colours denote higher probability of a region to become amyloid-positive in earliest amyloid accumulation (left), moderate (middle) and advanced (right) phases of amyloidosis.

P25: Sensitivity of the Standard Centiloid to Track Longitudinal Amyloid-Beta Changes Using 18F-Florbetaben PET

Santiago Bullich[1], Victor L Villemange[2,4], Norman Koglin[1], Aleksandar Jovalekic[1], Audrey Perrotin[1], Vincent Doré[2,3], Andrew W. Stephens[1], Christopher C. Rowe[2,4], <u>Susan De Santi</u>[5]

[1]*Life Molecular Imaging GmbH, Berlin, Germany*
[2]*Dept of Molecular Imaging & Therapy, Austin Health, Melbourne, Australia*
[3]*CSIRO Health and Biosecurity Flagship: The Australian e-Health Research Centre, Brisbane, Australia*
[4]*Dept of Medicine, Austin Health, The University of Melbourne, Melbourne, Australia*
[5]*Life Molecular Imaging Inc, Boston, MA, US*

Introduction: The Centiloid (CL) project is intended to set a common quantitative scale for reporting amyloid-PET. The objective of this work was to analyze the sensitivity of the standard CL analysis to detect subtle longitudinal Aβ changes using ^{18}F-Florbetaben PET.

Methods: Forty-five MCI patients (29 men/16 women; 72.69±6.54 years) underwent ^{18}F-Florbetaben PET and MRI scans at baseline (n=45), 1 year (n=41), and 2 years (n=36). Images were assessed using the standard CL analysis and using individualized MRI-based ROIs. SUVR was measured using cerebellar gray matter (CG) and whole cerebellum (WC) as reference regions (RR). CL values were derived from WC SUVRs ($CL=153.4\times SUVR_{WC}-154.9$). Baseline scans were visually classified as high (Aβ+) or low (Aβ-) amyloid. SUVR increase from baseline to 1 year and 2 years, and percentage Aβ deposition per year were assessed across Aβ+ and Aβ- groups.

Results: The SUVR increase over time in Aβ+ scans compared with baseline was significantly larger than in Aβ- scans using WC as RR at 1 year (P=0.048) and 2 years (P=0.011). Significant SUVR changes were detected only at 2 years when using the CG (P=0.063 (1 year), P=0.036 (2 years)) as the RR. Percentage Aβ deposition per year (mean±SD) derived from standard CL analysis was 1.48±1.85% (Aβ+) and 0.31±1.66% (Aβ-) (P=0.02) for WC and 1.65±2.37% (Aβ+) and 0.26±2.30% (Aβ-) (P=0.033) for CG. The annual CL change was 3.36±4.40 CL (Aβ+) and 0.51±2.71 CL (Aβ-). Percentage Aβ deposition per year (Aβdep) derived from standard CL analysis and individualized MRI-based ROIs correlated strongly (WC: Aβdep(CL)=0.18+1.00×Aβdep(MRI-based), R^2=0.94). However, MRI-based ROIs were slightly more sensitive to detect subtle SUVR longitudinal changes at 1- and 2-year follow-up (WC: P=0.039 (1 year), P=0.011 (2 years); CG: P=0.048 (1 year), P=0.023 (2 years)).

Conclusions: Standard CL analysis is robust and sensitive to detect subtle longitudinal Aβ changes in ^{18}F-Florbetaben PET.

Keywords: *centiloid, florbetaben, longitudinal*

P26: Increased tau aggregation in young traumatic brain injury and post-concussion syndrome patients

Mark Lubberink[1], Anders Wall[1], Fredrik Vedung[1], Markus Fahlström[1], Jan Weis[1], Sven Haller[1], Elna-Marie Larsson[1], Gunnar Antoni[1], Niklas Marklund[1]

[1]*Uppsala University, Uppsala, Sweden*

Introduction: Traumatic brain injury (TBI) and post-concussion syndrome (PCS) due to repeated sports-related injury have been suggested to be associated with aggregation of neurofibrillary tangles (tau). The aim of the present work was to simultaneously study structural brain damage and both tau aggregation and neuroinflammation (TSPO) in TBI and PCS patients in-vivo using PET-MRI.

Methods: 29 subjects (6 TBI and 12 PCS in chronic phase, 11 age-matched HC) underwent 60-min dynamic PET-MRI scans after bolus injection of ^{18}F-THK5317 and ^{11}C-PK11195. Simultaneous MRI consisted of T1, T2, SWI, ASL, DTI, MRS and resting state fMRI. Parametric images of ^{18}F-THK5317 DVR-1 and ^{11}C-PK11195 BP_{ND} were made using the reference Logan method and SRTM2, with cerebellar gray matter (tau) and a supervised clustering based region (TSPO) as reference tissue. All images were spatially normalised to MNI space using SPM12, and differences between groups were assessed using t-tests at the voxel level and using a volume of interest template.

Results: Diffuse axonal injury and microhemorrhages were seen on MRI in TBI, whereas no structural abnormalities were found for PCS. In TBI, voxel clusters with significantly increased ^{18}F-THK5317 and ^{11}C-PK11195 binding were seen mainly in thalamus, temporal lobe white matter and midbrain (tau only). In PCS, ^{18}F-THK5317 binding was increased in corpus callosum, whereas ^{11}C-PK11195 binding was increased in hippocampus. ASL showed decreased overall grey matter CBF in both TBI and PCS by about 20%.

Conclusion: The results suggest co-localised tau aggregation and neuroinflammation in thalamus and temporal lobe white matter, as well as tau aggregation in midbrain, in TBI, and tau aggregation in corpus callosum and neuroinflammation in hippocampus in PCS. Individual variations within TBI and PCS groups need to be further studied.
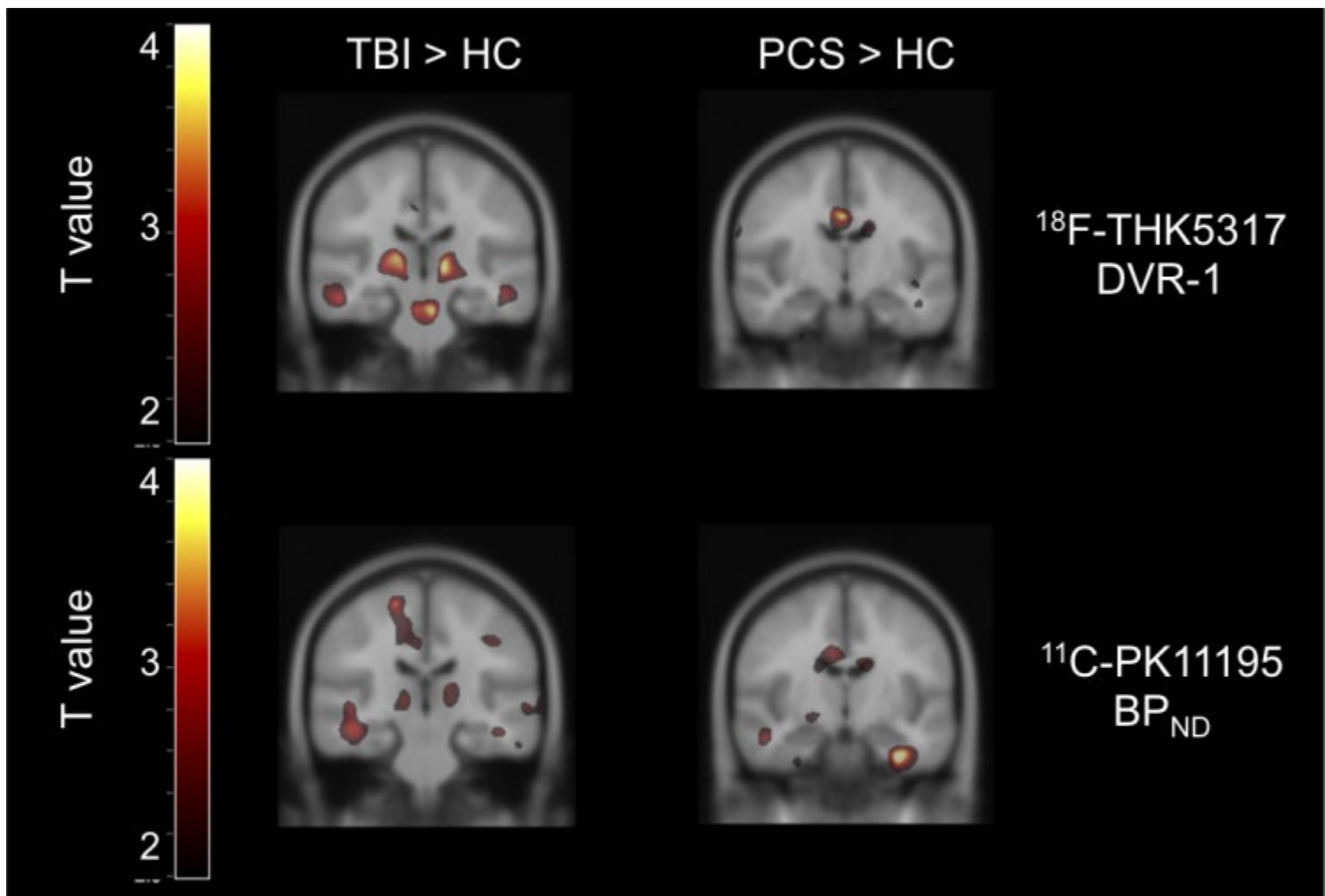
T score images of 18F-THK5317 DVR-1 (top) and 11C-PK11195 BPnd (bottom), for TBI>HC (left) and PCS>HC (right).

Keywords: *tau, TSPO, PET-MRI, traumatic brain injury, post-concussion syndrome*

P27: Effect of blood flow changes on quantification of [18F]flutemetamol studies

Fiona Heeman[1], Maqsood Yaqub[1], Isadora Lopes Alves[1], Kerstin Heurling[2], Juan Domingo Gispert[3], Christopher Foley[4], Ronald Boellaard[1], Adriaan Lammertsma[1]

[1]*Amsterdam UMC, Vrije Universiteit Amsterdam, Radiology and Nuclear Medicine, Amsterdam Neuroscience, De Boelelaan 1117, Amsterdam, The Netherlands*
[2]*Wallenberg Centre for Molecular and Translational Medicine and the Department of Psychiatry and Neurochemistry, University of Gothenburg, Gothenburg, Sweden*
[3]*Barcelonaβeta Brain Research Centre, Pasqual Maragall Foundation, Barcelona, Spain*
[4]*GE Healthcare, Amersham, UK*

Introduction: Cerebral blood flow (CBF) declines with increasing age[1]. Additional reductions have been reported in individuals with elevated levels of amyloid in the brain and in patients suffering from Alzheimer's dementia (AD)[2,3]. This may compromise longitudinal assessments of amyloid load, as bias may be sensitive to changes in CBF[4]. The purpose of this study was to assess the effect of CBF changes on quantification of [^{18}F]flutemetamol scans.

Methods: Cortical and cerebellar grey matter time-activity curves (TACs) of 110 minutes were simulated using a two tissue compartment model together with a metabolite corrected plasma input function and kinetic parameters established previously[5]. Subsequently, both global and local CBF reductions were simulated by reducing the tracer delivery (K_1) (0 to - 25%, while keeping the K_1/k_2 ratio constant) in both cortical and cerebellar regions (global changes), or by reducing K_1 in the cortical region only (local changes). Next, amyloid load was quantified using both SUVr (90-110 minutes post injection) and DVR (=BP_{ND}+1), the latter obtained using the simplified reference tissue mode, and compared to the simulated level of amyloid load (DVR).

Results: Even large global K_1 reductions resulted in only a small bias in DVR (<3%), for all simulated amyloid levels. Bias in SUVr was larger (4-16%) and affected by the level of amyloid load (Fig.1a+b). A local decline in K_1 resulted in relatively stable bias in SUVr, however strongly affected by level of amyloid load (Fig.1c+d).

Conclusion: Changes in derived amyloid load may be affected by reductions in CBF when using SUVr. Hence, for more accurate amyloid load estimates, especially in a longitudinal setting, dynamic scans should be used.
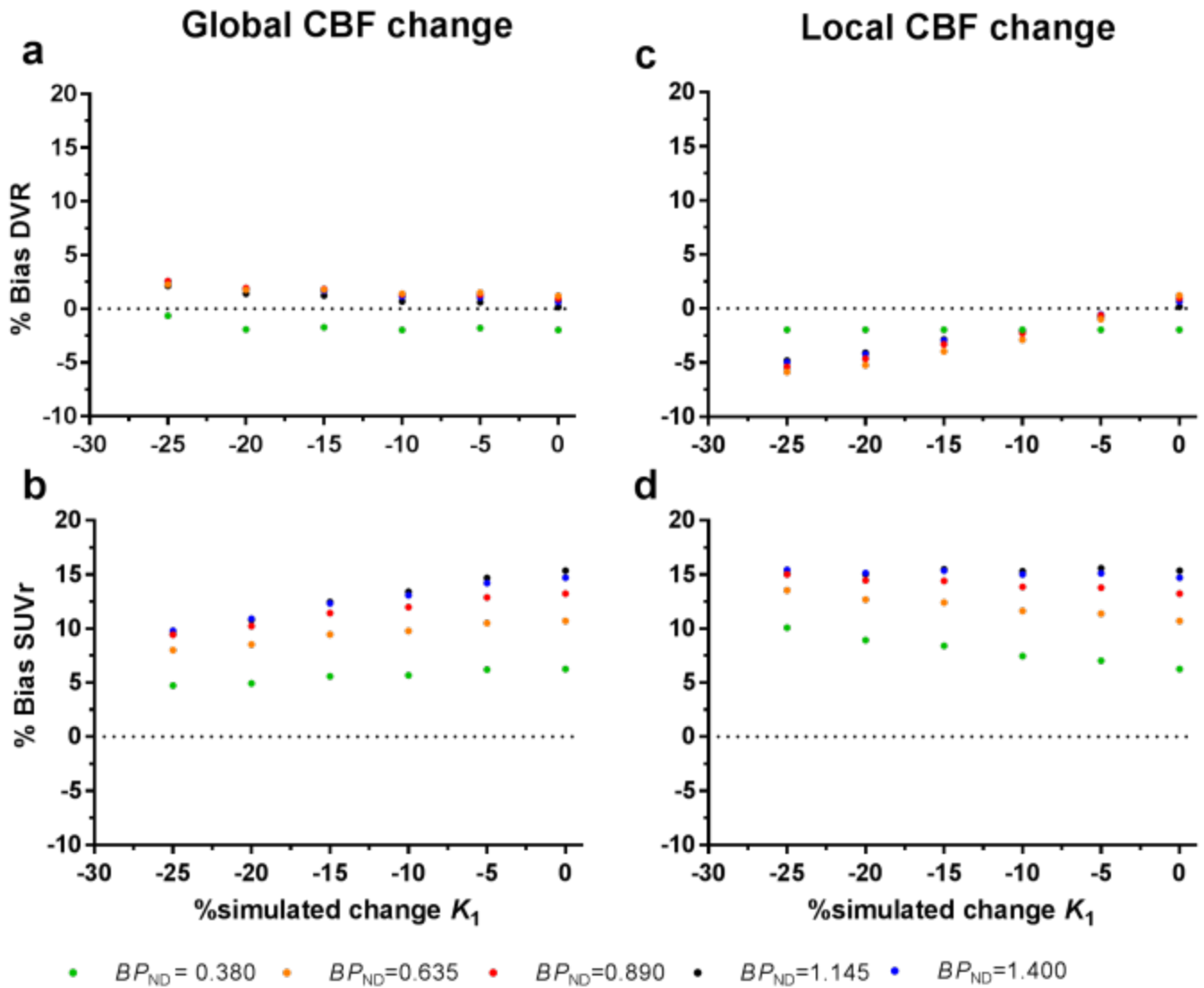
Figure 1. Percentage bias, for various simulated levels of amyloid load (BP_{ND}), in **a)** DVR (distribution volume ratio) and **b)** SUVr (standardized uptake value ratio), as a result of global changes in CBF (K_1) and **c)** DVR and **d)** SUVr, as a result of local changes in CBF(K_1). Cerebellar grey matter BP_{ND}=0.35.

P28: Longitudinal [18F]Flortaucipir in the BioFINDER 1 Cohort

Ruben Smith[1], Olof Strandberg[1], Erik Stomrud[1], Oskar Hansson[1]

[1]*Clinical Memory Research Unit, Lund University, Lund, Sweden*

Aim: We assessed longitudinal change in [^{18}F]Flortaucipir PET retention in subjects with Alzheimer's Disease (AD), Mild cognitive impairment (MCI) and in healthy controls.

Methods: Participants were scanned longitudinally using [^{18}F]Flortaucipir, with a mean[±SD] interscan interval of 1.93[±0.38] years. The study included 24 controls (13 Amyloid-β(Aβ)+, 11 Aβ-), five with Aβ+ MCI, and 22 AD dementia patients. Results were analyzed using three different reference regions (inferior cerebellar grey matter, whole cerebellum, and eroded white matter), using both partial volume error correction(PVEC) as well as non-PVEC-data. [^{18}F]Flortaucipir uptake was assessed in Braak imaging stages I-IV, III-IV, and V-VI as defined by Cho et al (Annals Neurol 2016;80(2):247-58) (Figure 1).

Results: The variability of the results was least using the eroded white matter reference, and PVEC did not alter results. We found increased [^{18}F]Flortaucipir retentions of 2.5%[±3.9], 2.6%[±3.9], and 1.8%[±4.0] per year in MCI/AD in the three regions (Figure 2C). In controls the yearly increases were 0.5-1.2% [± 1.1-1.7]. The longitudinal SUVRs in MCI/AD were variable, and the variability persisted irrespective of reference region and PVEC. The yearly change in MCI/AD SUVR was correlated to the baseline cortical thickness, indicating that subjects decreasing in signal had a more pronounced atrophy (Figure 2D). Splitting the MCI/AD group in two based on yearly SUVR change showed that the half with a lower increase in [^{18}F]Flortaucipir retention had higher [^{18}F]Flutemetamol retention, longer disease duration and thinner cortex at baseline. Our results indicate that Flortaucipir retention reaches a plateau in AD and that longitudinal retention even decreases in advanced stages of disease.

Conclusion: Longitudinal [^{18}F]Flortaucipir PET showed significant increases of ~2.5 percent per year in MCI/AD as compared to ~1 percent in controls. Some subjects with MCI/AD showed a reduction in longitudinal [^{18}F]Flortaucipir retention, that was associated with more pronounced atrophy, longer disease duration and higher Aβ-load.
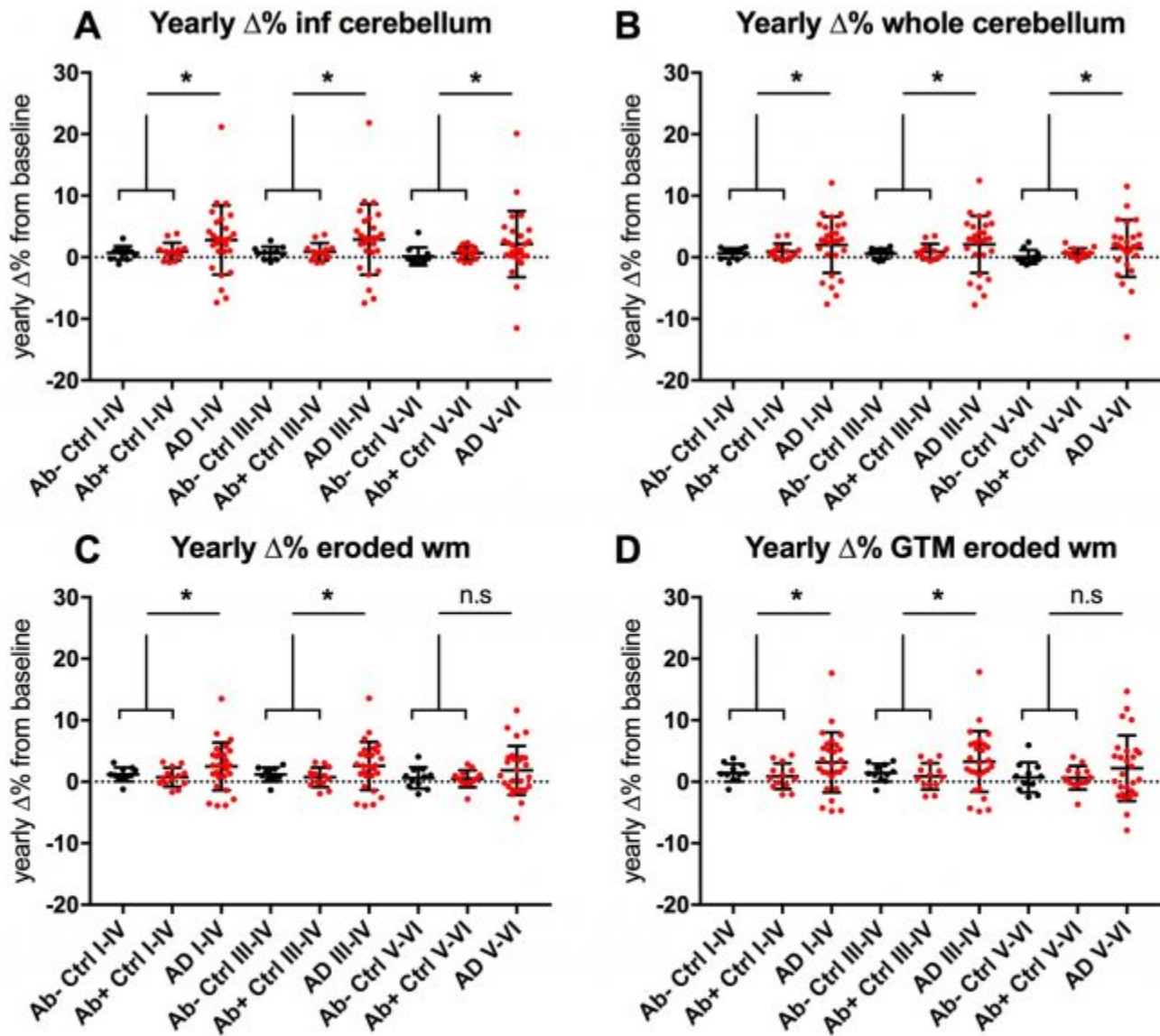
Figure 1. Longitudinal yearly change of ^{18}F-Flortaucipir retention expressed as percent of baseline. Changes are plotted using different reference regions: A) inferior cerebellar grey matter; B) whole cerebellum; C) eroded white matter. Panel D) depicts the results using partial volume corrected data (GTM) with an eroded white matter reference region. Controls (Ctrl) are separated according to amyloid status into beta-amyloid negative (Ab-) and positive (Ab+). Stages correspond to imaging Braak stages defined by Cho et al (Cho, Ann Neurol 2016 Aug;80(2):247-58). * p < 0.05.
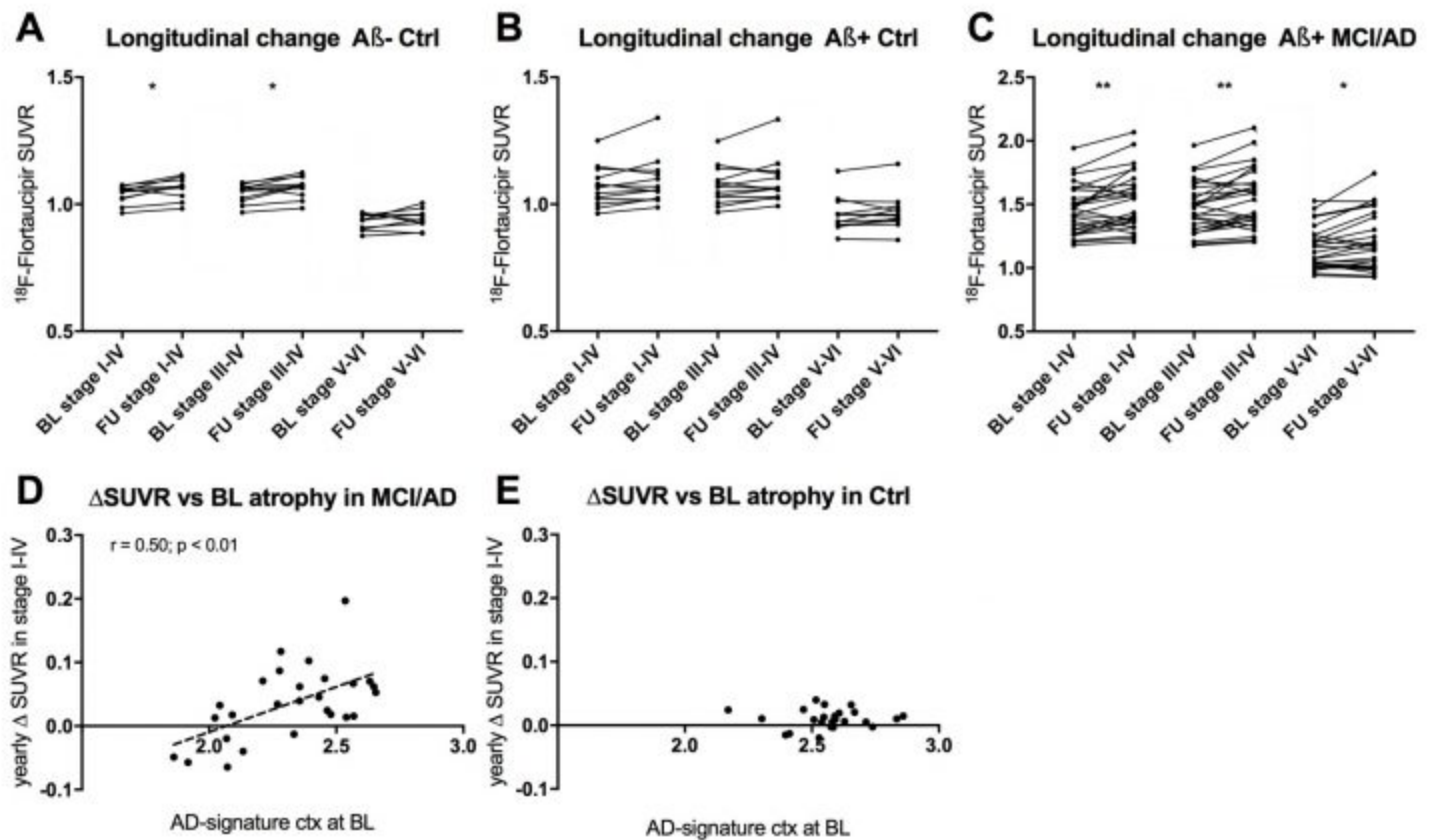
Figure 2. Comparison of Baseline (BL) and Follow-up (FU) ^{18}F-Flortaucipir scans in A) Aß- and B) Aß+ controls (Ctrl) and in C) MCI/AD patients. D and E) Yearly changes in ^{18}F-Flortaucipir SUVR in stage I-IV plotted against baseline cortical thickness in "AD-signature" cortex (bilateral entorhinal, fusiform, inferior and middle temporal gyri) in D) MCI/AD patients and E) healthy controls.

Stages correspond to imaging Braak stages defined by Cho et al (Cho, Ann Neurol 2016 Aug;80(2): 247-58). * p < 0.05; ** p < 0.01.

P29: Preclinical characterization of two new promising tau PET tracers in vitro and in vivo

Marc Skaddan[1], Manolo Mugnaini[2], Qi Guo[1], Dustin Wooten[1], Kyle Wilcox[1], David Reuter[1], Martin Voorbach[1], Timothy Montavon[1], Aimee Reed[1], Ana Relo[2], Mario Mezler[2], Andreas Haupt[2], Herve Geneste[2], Thomas Erhard[2], Frauke Pohlki[2], Ann Tovcimak[1], Sjoerd Finnema[1], Laurent Martarello[3], Robert Comley[1]

[1]AbbVie Inc, North Chicago, IL, US
[2]AbbVie Deutschland GmbH & Co. KG, Ludwigshafen, Germany
[3]Former AbbVie employee, Cambridge, MA, US

Objectives: Tau plays a defining role in the pathogenesis and characterization of Alzheimer's disease (AD). In this study we evaluated two candidate tau PET tracers in vitro using human tissue and in vivo in nonhuman primates (NHPs).

Methods: Tau and Ab binding were assessed using AD brain tissue homogenates, with [^{3}H]MK-c6 and [^{3}H]PIB, respectively. Selectivity against MAO-A and MAO-B was evaluated using rat brain homogenates, with [^{3}H]harmine and [^{3}H]selegiline, respectively. Autoradiography was performed using tritiated or F-18 labeled compounds 1 and 2 on human AD and non-AD brain sections. The degree of non-displaceable binding was determined by co-incubation with 1 or 2, T808, RO-6958948, and MK-6240. Baseline and self-block PET studies were performed in cynomologus monkeys and included arterial blood sampling. Regional volumes of distribution (V_T) were estimated using compartment modeling.

Results: Compounds 1 and 2 were identified to bind with high affinity (K_i<1 nM) and selectivity (9-10 uM vs. Ab, >800x vs. MAO-A, >600x vs. MAO-B) to tau. Autoradiography demonstrated high displaceable binding for both compounds in AD brains, regardless of the blocking compound, while studies in control brains showed no/very low displaceable binding. For PET studies, both radiotracers were prepared to high radiochemical yield and specific activity by nucleophilic displacement of the chloroheteroarene precursor with [^{18}F]KF/K222. Both radioligands in NHPs showed high brain penetration, homogeneous distribution across regions (V_T=2.29±0.25 for ^{18}F-1, V_T=5.06±0.46 for ^{18}F-2 at baseline) and rapid washout kinetics. Self-block studies did not indicate specific binding in vivo in the absence of tau pathology in NHPs.

Conclusions: Compounds 1 and 2 possess **in vitro** and **in vivo** properties consistent with their being suitable PET tracers to quantify tau aggregates in the human AD brain.
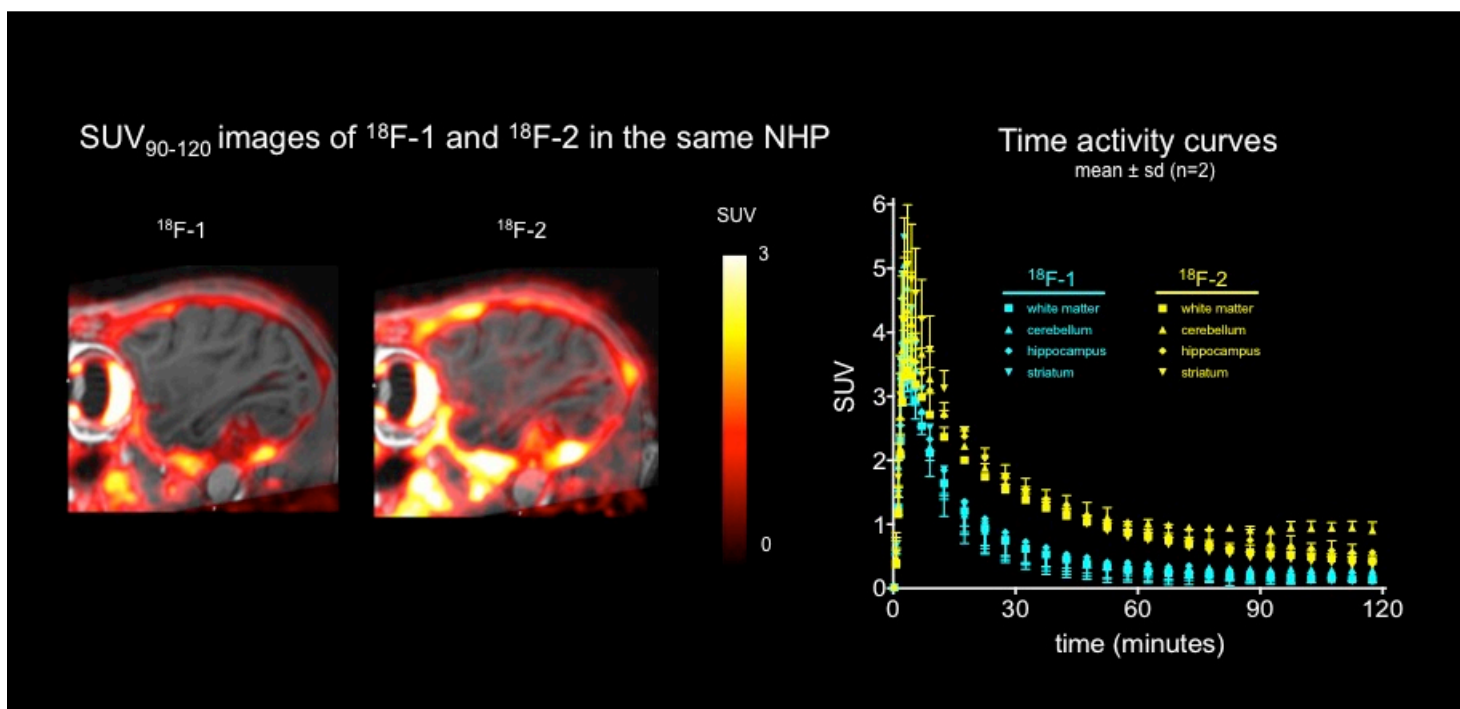
Evaluation of [^{18}F]1 and [^{18}F]2 in nonhuman primates

P30: Study on tissue-based and histogram-based reference regions for semi-quantitation of 18F-APN-1607 Tau PET Imaging

Ing-Tsung Hsiao[1,2], Kuo-Lun Huang[3], Po-Yen Chen[1], Kun-Ju Lin[1,2], Chin-Chang Huang[3]

[1]*Department of Medical Imaging and Radiological Sciences & Healthy Aging Center, Chang Gung University, Taoyuan, Taiwan*
[2]*Department of Nuclear Medicine, Chang Gung Memorial Hospital, Taoyuan, Taiwan*
[3]*Department of Neurology, Chang Gung Memorial Hospital, Taoyuan, Taiwan*

Background: A novel tau PET tracer ^{18}F-PMPBB3 was developed for imaging the in-vivo tau aggregates in Alzheimer's disease (AD) and non-AD tauopathies. The semi-quantitation SUVR is usually calculated using the tissue-based reference regions. Recently, the histogram-based reference region methods were proposed to alleviate the contamination of off-target uptake in the reference regions due to partial volume effect. This study was to compare histogram-based and tissue-based reference regions in tau PET semi-quantitation.

Methods: ^{18}F-PM-PBB3 PET images of 12 normal control (NC), 10 AD, 3 familiar MCI (fMCI) and 4 PSP were included. Tissue-based reference regions of whole cerebellum and cerebellar cortex were used for calculating SUVR. Two histogram-based methods including PERSI (parametric estimate of reference signal intensity) and SUVM (SUV mode from the intensity histogram of the whole brain) were also applied to estimate the SUVR. The reference SUV, regional SUVR and effect size were evaluated between three disease groups and NC.

Results: For NC, all four methods are with similar reference SUV. For AD, the reference SUVs from four methods are similar but with less variation from PERSI. For fMCI, the histogram-based reference SUV is in the same level as AD, and much smaller than the tissue-based reference SUV. The estimated SUVRs for fMCI from the tissue-based methods are smaller than those of NC, while the histogram-based methods lead to much higher SUVR than NC and AD. For PSP, the reference SUVs from all methods are also in the similar range. For differential power between the diseased groups and NC, the effect size within the target regions from histogram-based methods is higher than that from tissue-based methods.

Conclusion: As compared with the conventional tissue-based methods, the histogram-based methods may generate more stable and compatible semi-quantitation results as well as higher differential power for ^{18}F-APN1607 PET imaging of various tauopathies.
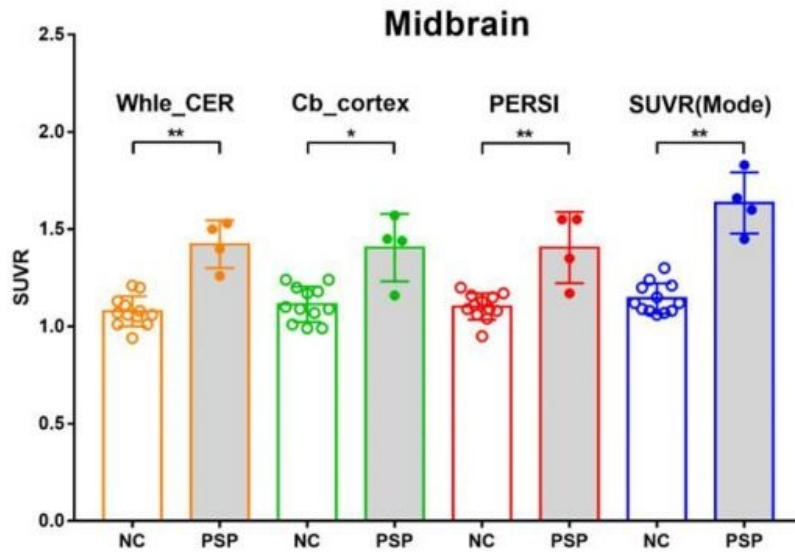
Figure 1: This illustrates the regional SUVR plots in midbrain for both NC and PSP from four reference regions of whole cerebellum, cerebellar cortex, PERSI and SUVM.
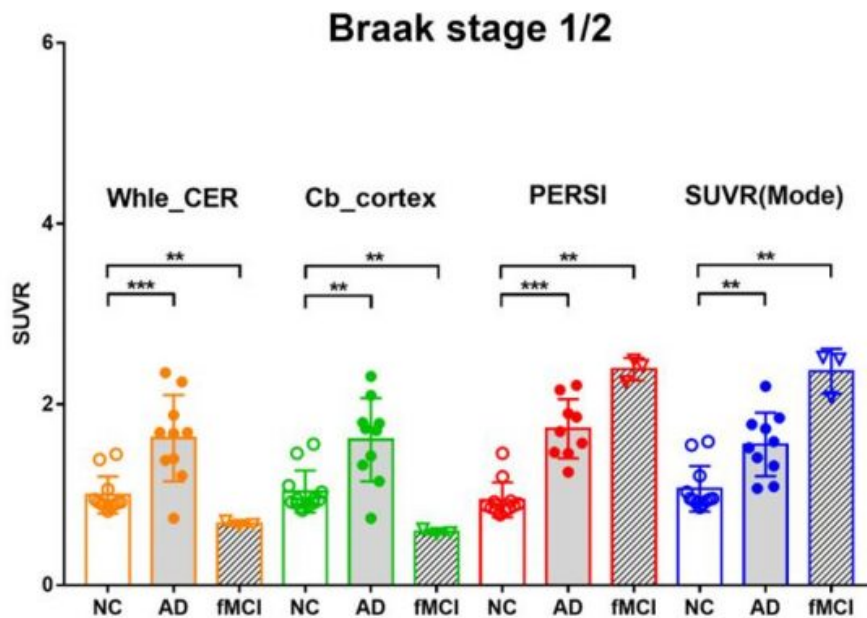
Figure 2: This illustrates the regional SUVR plots in the Braak stage I/II for NC, AD and fMCI from four reference regions of whole cerebellum, cerebellar cortex, PERSI and SUVM.

P31: Predicting amyloid accumulation in dominantly inherited Alzheimer's disease

Patrick Luckett[1], Austin McCullough[1], John McCarthy[2], Jason Hassenstab[1], Anne Fagan[1], Suzanne Schindler[1], Eric McDade[1], Randy Bateman[1], Tammie Benzinger[1], Beau Ances[1]

[1]*Washington University School of Medicine, St Louis, MO, US*
[2]*Washington University, St Louis, MO, US*

Introduction: Predicting the accumulation of beta-amyloid in specific brain regions could allow for more accurate evaluation of targeted therapies for individuals with Alzheimer's disease (AD). We propose an ensemble deep learning approach to predict beta-amyloid accumulation in autosomal dominant (mutations in APP, PSEN1, PSEN2) AD which utilizes multimodal imaging, demographics, and genetic information.

Methods: 131 mutation positive (M+) participants and 74 mutation negative (M-) controls with at least 2 separate imaging sessions were modeled. Structural MRI, amyloid PET (PIB), and metabolic activity (FDG) was acquired for each participant at each time point and analyzed for 236 Freesurfer brain regions of interest (ROI). The imaging data was combined with genetic information, familial year of symptom onset, and demographic variables as features for training. For each cortical and subcortical region, a deep feed forward artificial neural network was trained to predict changes in amyloid in that region over time. 70% of the data was used for training with the remaining used for testing. The mean squared error (MSE) was calculated for each ROI in each test case matrix and averaged across all the test cases to evaluate the overall model performance.

Results: The average MSE was .006 (+/- .01), indicating the model performed well over all ROIs. Figure 1 depicts 3 examples of the difference in the actual amyloid values and the values the algorithm predicted for 2 M+ participants, one M- participant, and the combined values. Most errors were clustered around zero, indicating a negligible difference in the actual and predicted values.

Conclusion: Machine learning algorithms can provide decision support and predictive analytics in medicine. Our model is highly accurate and capable of forecasting amyloid accumulation and illustrates the feasibility of applying machine learning algorithms for targeted patient care in people with Alzheimer's disease.

	Mutation +	Mutation -	P Values
N	131	74	
Age	39.2 years +/- 10.6	39.3 years +/- 10.2	.95
Education	14.3 years +/-2.7	15.1 years +/-2.6	.06
Gender (% Male)	40%	35%	.45
Average Time Between Scans	2.6 years (+/- 1.4)		

Table 1: Demographics

Figure 1: Predicted Versus Actual Error Histograms
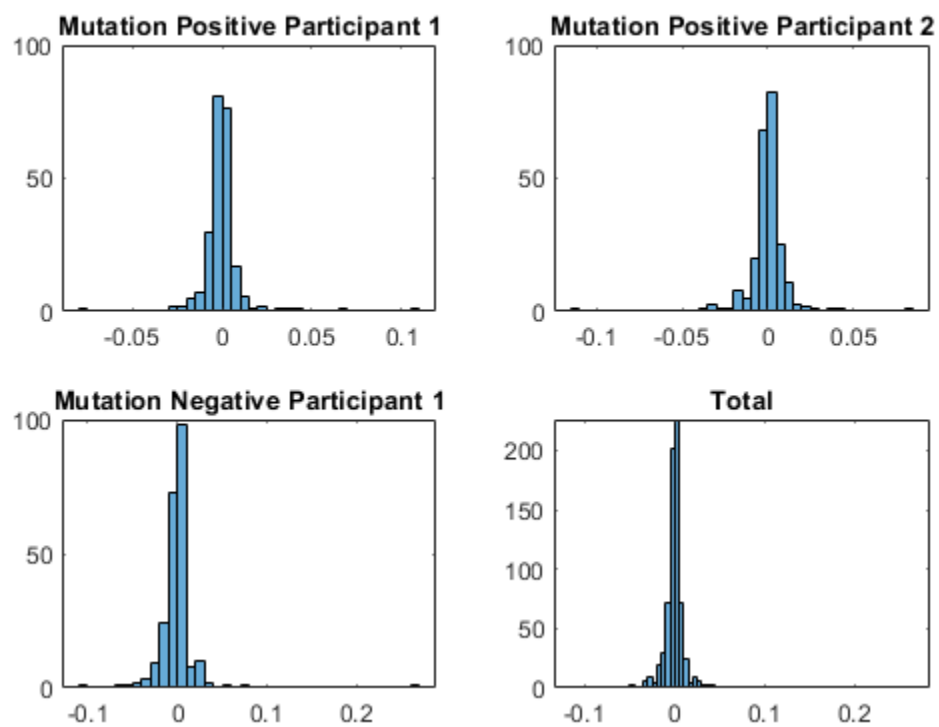
Keywords: *Machine learning, Alzheimer's disease*

P32: Modeling the nonlinear effect of amyloid on cognitive impairment mediated by neurodegeneration in Alzheimer's disease using path analysis

Sung-Woo Kim[1,2], Jeong-Hyun Shin[1,2], Joon-Kyung Seong[1]

[1]*School of Biomedical Engineering, Korea University, Seoul, Korea*
[2]*Department of Bio-convergence Engineering, Korea University, Seoul, Korea*

Objective: Focusing local relationships explaining statistical dependencies among amyloid, neurodegeneration, and cognitive impairment may lead biased interpretations in Alzheimer's disease (AD) spectrum. We therefore sought to model the unified causal relationship among them considering effects of both continuous and discrete behaviors of amyloid on AD progression.

Methods: ^{18}F-AV45, ^{18}F-FDG PET, and T1-weighted MR images were downloaded for 501 patients in AD spectrum from ADNI database (Table). For each patient, overall neurodegeneration score was computed using FDG SUVR and cortical thickness with latent variable model approach. Amyloid positivity was decided using AV45 SUVR. We constructed and assessed several models that explain causal relationships among amyloid, neurodegeneration, and cognition impairment (MMSE) using both single and multiple group path analyses after controlling effects of age, sex, education, and intracranial volume (ICV). comparative fit index (CFI) and standardized root mean square residual (SRMR) were used for model fit evaluation, and Akaike information criterion (AIC), Bayesian information criterion (BIC) and sample-size adjusted BIC (aBIC) were used for model comparison. Significance tests for path coefficients and mediation effects were performed using bootstrap method with 10,000 replicates.

Table 1. Demographic and clinical characteristics.

	Amyloid negative	Amyloid positive [§]
Sample size, N.	192	309
Age, year	70.19±8.20	73.16±7.12
Female Sex, N. (%)	88 (45.8)	153 (49.5)
Education, year	16.23±2.51	16.04±2.71
ICV, cm^3 [*]	1466.33±200.39	1477.04±204.02
AV45 SUVR [†]	1.01±0.06	1.39±0.17
Neurodegeneration [‡]	-0.29±0.84	0.18±1.05
MMSE	28.15±2.30	26.01±3.34

ICV, intracranial volume; SUVR, standardized uptake value ratio; MMSE, Mini-Mental State Examination.

[*] ICV was computed using FreeSurfer v.5.1.0

[†] AV45 SUVR was computed as average AV45 SVUR of frontal, anterior cingulate, precuneus, and parietal cortex relative to the cerebellum at a baseline (ADNI merge).

[‡] Neurodegeneration was computed a common factor of ^{18}F-FDG SUVR and cortical thickness using latent variable model.

[§] Amyloid positive was decided if AV45 SUVR was greater than 1.11.

Results: Amyloid affected cognitive impairment through neurodegeneration (mediation) and changes the association between neurodegeneration and cognitive impairment (moderation). For a single group, the model using continuous accumulation of amyloid was better than that using dichotomous (discrete) stage. For amyloid positive and negative groups, the model with mediation of continuous amyloid accumulation and moderation of dichotomous amyloid stage showed better fit than others (Figure). As a result, the whole effect of amyloid on cognitive impairment occurs nonlinearly as well as continuously, showing the synergistic effect between amyloid and neurodegeneration on cognitive impairment.
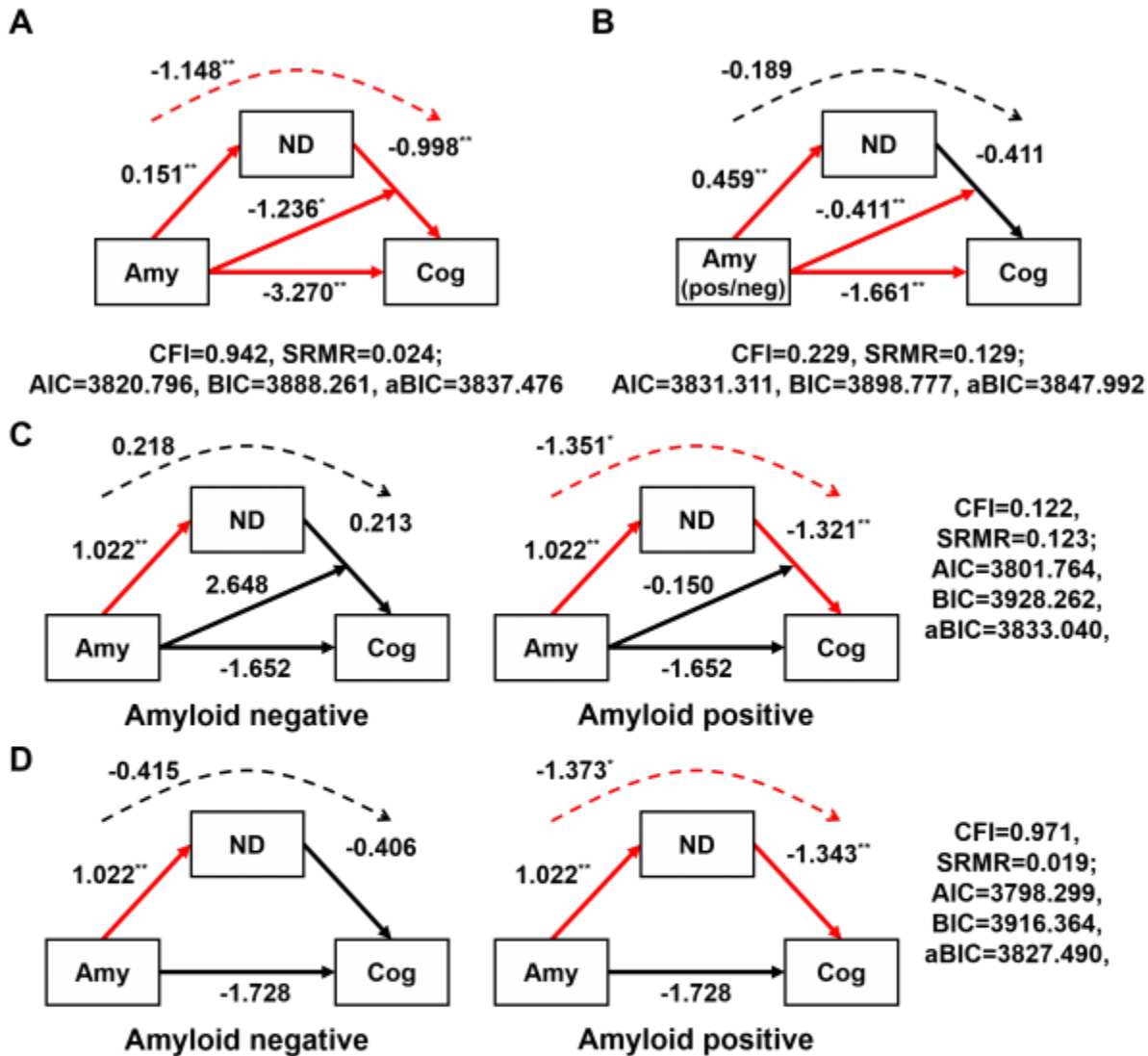
Figure 1. Unstandardized path coefficients (solid lines) and mediation effects (dashed lines) of several hypothetical models among amyloid (amy), neurodegeneration (ND), and cognition (Cog). In each model, path coefficients were estimated using a single group (A-B) and multiple group (C-D) path analyses with maximum likelihood estimation after controlling the effects of covariates. For single group approach, amyloid was measured as continuous accumulation of AV45 SUVR (A) and dichotomous stage representing amyloid positive and negative (B), respectively. Red lines represent significant path coefficients or mediation effects. CFI, comparative fit index; SRMR, standardized root mean squared residual; AIC, Akaike information criterion; BIC, Bayesian information criterion; aBIC, sample size adjusted BIC. * $p<0.05$, ** $p<0.01$.

Conclusions: Amyloid behaves continuously on the mediation of amyloid on cognitive impairment by neurodegeneration and discretely on the moderation of amyloid on the association between neurodegeneration and cognitive impairment.

Keywords: *Alzheimer's disease, neurodegeneration, cognitive impairment, amyloid, path analysis*

P33: Identification and characterization of selective and high affinity small molecules for PET imaging of pathological alpha-synuclein

Francesca Capotosti[1], Elpida Tsika[1], Jerome Molette[1], Myriam Ravache[1], Efthymia Vokali[1], Patrick Rodriguez[1], Vincent Darmency[1], Kasia Piorkowska[1], Ajay Purohit[2], David Paterson[2], Karleyton Evans[2], Laurent Martarello[2], Cristian Salinas[2], Sonia Poli[1], Heiko Kroth[1], Jan Stoehr[1], David Lowe[1], Andrea Pfeifer[1], Andreas Muhs[1]

[1]AC Immune SA, Lausanne, Switzerland
[2]Biogen, Cambridge, MA, US

Objectives: The progressive accumulation of aggregated alpha-synuclein (aSyn) in form of Lewy bodies and neurites is the pathognomonic hallmark of Parkinson's disease (PD). The link between aSyn inclusions and disease severity warrants the development of PET tracers as tools to study the distribution and longitudinal changes of the aggregated protein in the human living brain. Due to the low density of aSyn pathology and the frequency of co-existing proteinopathies in PD (e.g., β-amyloid, tau), an aSyn PET tracer must display high binding affinity to aSyn aggregates, high selectivity over other proteinaceous deposits, as well as minimal non-specific binding.

Methods: We screened our proprietary Morphomer^{TM} library of small molecules for suitable aSyn PET tracer candidates. Affinity to aggregated aSyn and selectivity over other proteinopathies were measured on post-mortem PD and Alzheimer's disease (AD) samples. Several compounds were ^{18}F radiolabeled, and assessed for brain penetration and pharmacokinetic (PK) profile in rodent and non-human primate (NHP).

Results: Compounds derived from several chemical series showed binding to isolated Lewy bodies and neurites (e.g. by high resolution autoradiography) in PD brain sections with single-digit nanomolar affinities. These compounds were selective for aSyn aggregates over β-amyloid and tau aggregates. Furthermore, studies with fluorine-18 labeled candidates demonstrated favorable tissue kinetics in the NHP brains.

Conclusions: We identified compounds with high affinity to aSyn deposits and selectivity over the most common co- existing proteinopathies. Current lead candidate shows optimized CNS-PET profile with minimal non-specific binding in NHP and further in-vitro characterization is underway.

Keywords: *Parkinson's disease, a-synuclein, synucleinopathies, PET, new tracer*

P34: APOE genotype is associated with specific regional patterns of amyloid accumulation

Samantha Katz[1], Bernard Hanseeuw[1,2], Michelle Farrell[1], Kirsten Moody[1], Justin Sanchez[1], Danielle Mayblyum[1], Tobias Estime[1], Heidi Jacobs[4], Patrizia Vannini[1,3], Jorge Sepulcre[1], Shu Jiang[1], Aaron Schultz[1], Julie Price[1], Reisa Sperling[1,3], Keith Johnson[1]

[1]*Massachusetts General Hospital, Boston, MA, US*
[2]*Cliniques Universitaires Saint-Luc, Brussels, Belgium*
[3]*Brigham and Women Hospital, Boston, MA, US*
[4]*Maastricht University, Maastricht, The Netherlands*

Background: Autopsy and cross-sectional PET studies suggest that amyloidosis progresses from neocortex to medial temporal lobe to subcortex. We sought to determine whether the regional pattern of accumulation was different across APOE genotypes.

Methods: We analyzed PiB-PET data from 569 clinically normal older adults (age=46-90), including 224 with follow-up (2-6 time-points, median=3). PiB-PET data were expressed as the distribution-volume-ratio (DVR, 40-60min) with cerebellar grey as reference tissue. Regional thresholds were defined as +2SD above the average of 54 young adults (age=20-45). The proportion of older individuals positive in each region was used to infer regional patterns of amyloid accumulation. These patterns were compared between ε2 (n=58), ε3ε3 (n=318), and ε4 (n=113) carriers, excluding ε2ε4. We also compared voxel-wise DVR-maps. We confirmed cross-sectional findings by computing regional amyloid accumulation slopes using linear-mixed-models.

Results: Age and sex did not significantly differ across genotypes. ε4 carriers had higher global PiB signal (+0.26DVR) and ε2 had lower signal (-0.05DVR) than ε3ε3 (Fig.1). The regional pattern analysis (Fig.2) indicated that, beyond the global DVR difference, ε4 carriers were more frequently positive than ε3ε3 carriers in the precuneus, inferior-parietal, middle-temporal, rostral-anterior-cingulate, and rostral-middle-frontal regions. Similarly, ε2 carriers were more frequently positive than ε3ε3 carriers in the hippocampus. Longitudinal analyses demonstrated PiB decrease in ε3ε3 and PiB increase in ε4 carriers, specifically in the precuneus, inferior-parietal, middle-temporal, rostral-anterior-cingulate, and rostral-middle-frontal regions. ε2 carriers accumulated amyloid in the hippocampus and amygdala, while ε3ε3 and ε4 carriers did not (Fig.3). Genotype differences remained significant after accounting for baseline PiB and age.

Conclusions: The regional pattern of amyloid accumulation is genotype-dependent. ε4 carriers are more frequently positive and demonstrate higher amyloid accumulation rates in the frontal, lateral temporo-parietal, and retrosplenial regions. In contrast, ε2 carriers are more frequently positive and demonstrate higher amyloid accumulation rates in the medial temporal lobe.

Figure 1: Global average and difference maps of the PiB PET DVR across APOE genotypes, at the level of the precuneus and middle-temporal regions:

E2: 1.17 Global Average DVR   E33: 1.22 Global Average DVR   E4: 1.48 Global Average DVR

E2 vs E3 - .05 Global DVR Difference   E3 vs E4 .26 Global DVR Difference
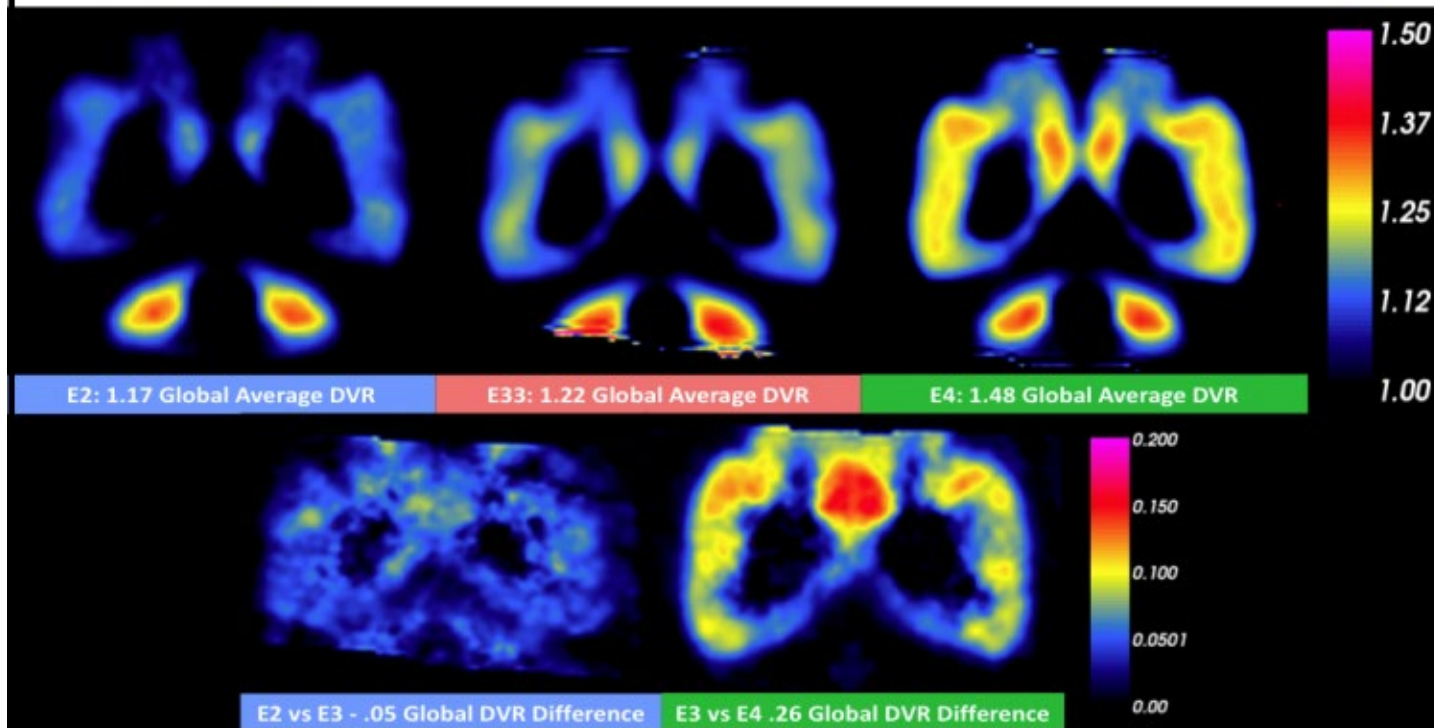
Figure 2: Brain regions ordered by the percentage of ε3ε3 individuals with greater PiB signal than threshold across APOE genotypes
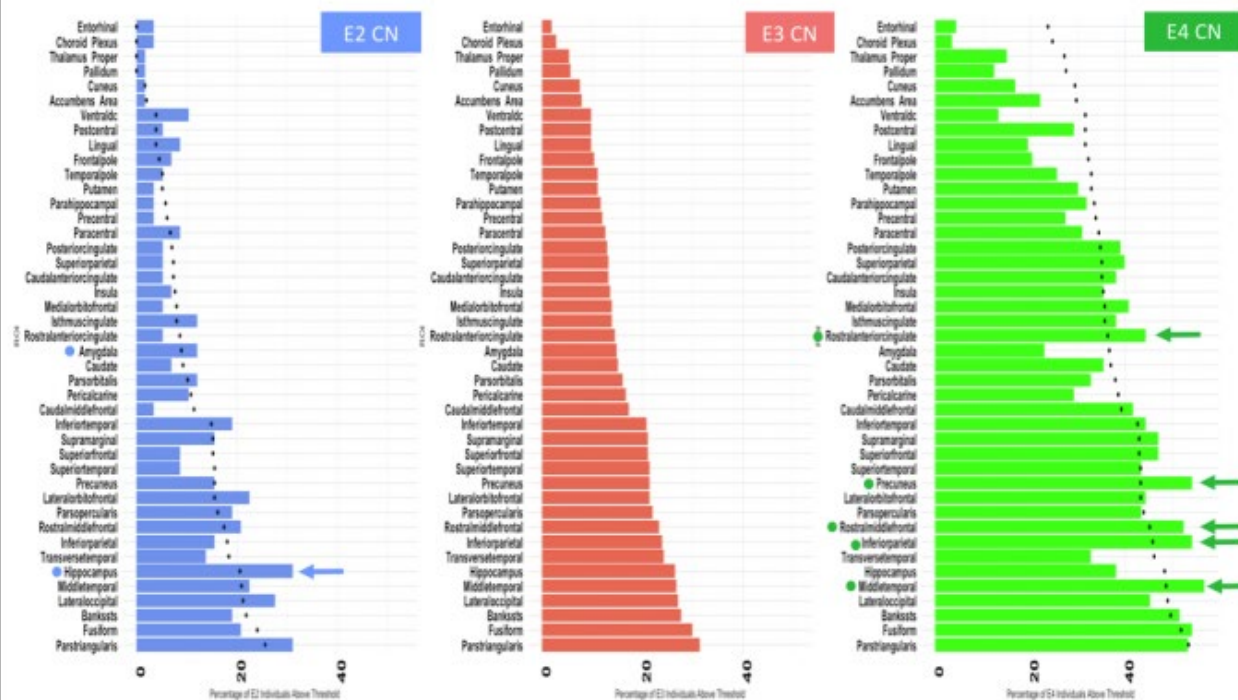
Brain regions with higher percentage are suggestive of earlier amyloid accumulation. Brain regions are ordered by the percentage of ε3ε3 individuals with greater PiB signal than threshold(young adult mean + 2SD) for all genotypes. Black circle landmarks indicate the predicted percentage of carriers based on average global differences between ε2 and ε3ε3 individuals (-5.8%) and ε4 and ε3ε3 individuals (+21.8%). Arrows indicate regions with percentages higher than the predicted percentage, suggesting specific regional patterns distinct to either ε2 or ε4 genotypes.

Figure 3: Brain regions ordered by the magnitude of change in PiB signal over time across APOE genotypes
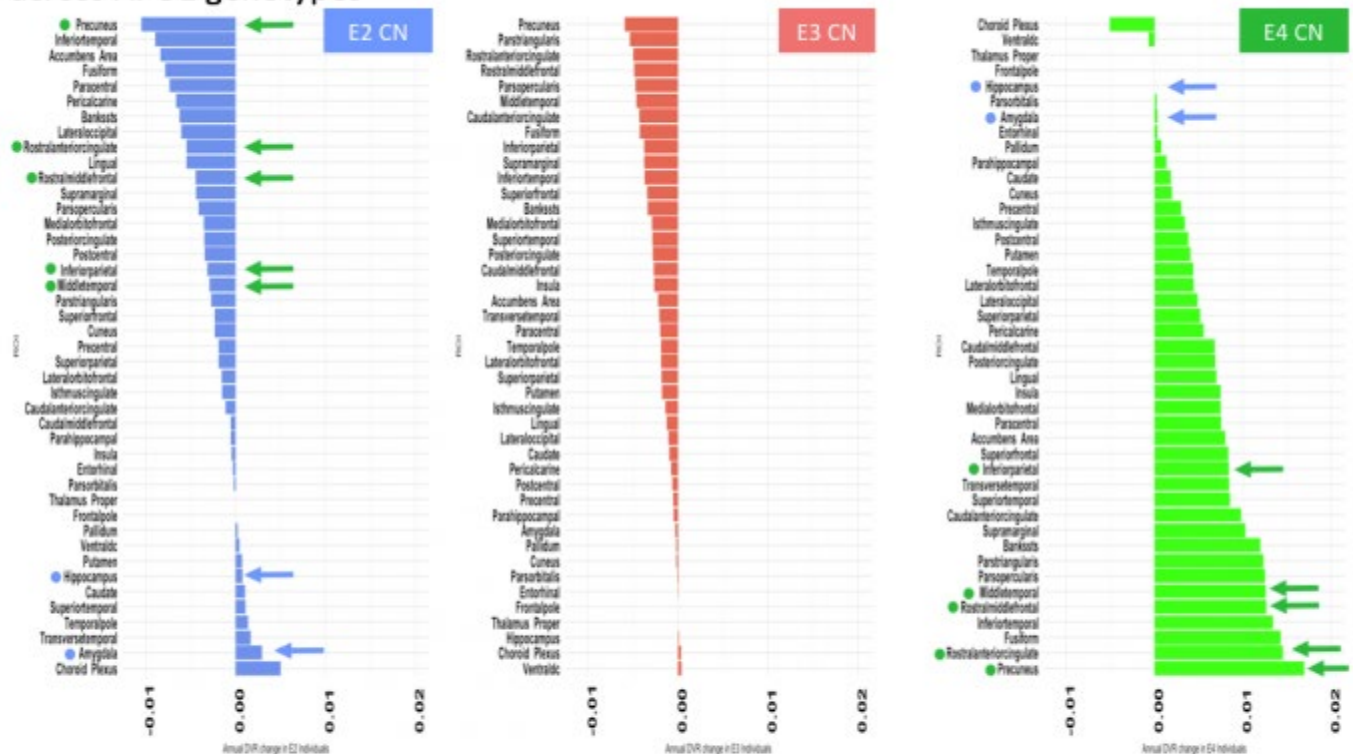
Regions with higher than expected percentages observed at the cross section (Fig.2), are highlighted with arrows. These regions demonstrate longitudinal accumulation in the ε2 and the ε4 genotypes respectively confirming the cross-sectional findings.

P35: Association of reported sleep-wake disturbances with tau pathology in mild cognitive impairment and normal cognitive aging

Sepideh Shokouhi[1], Alexander Conley[1], Harry Gwirtsman[1,2], Paul Newhouse[1,2]

[1]*Center for Cognitive Medicine, Department of Psychiatry and Behavioral Sciences, Vanderbilt University Medical Center, Nashville, TN, US*
[2]*Geriatric Research, Education, and Clinical Center, Tennessee Valley Veterans Affairs Medical Center, Nashville, TN, US*

Significance: Sleep-wake disturbances have been described in preclinical AD where associations of Aβ accumulation with nighttime sleep fragmentation and excessive daytime napping were reported. There is little known about the role of sleep-wake patterns in AD beyond Aβ. The influence of tau pathology is likely important to the sleep-wake disturbances observed in AD but has not heretofore been explored in a rigorous way to clarify the biological basis of sleep dysfunction.

Methods: All imaging and neurobehavioral data were downloaded from ADNI. We identified 35 normal and 36 MCI subjects (age: 75 ± 7) who had completed flortaucipir and florbetapir PET scans and Neuropsychiatric Inventory (NPI) examinations (addressed to informed caregiver) at time points within close proximity of each other. The NPI sleep questionnaire, which tracks recent changes in sleep behavior, was separated in two categories based on the nature of dysfunction. Questions related to reduced nighttime sleep duration, fragmentation, and latency were grouped together as "sleep deficiency". Questions related to abnormal nocturnal behavior (wandering, pacing, or other inappropriate activities) and excessive daytime napping were grouped together as "napping & abnormal nighttime behavior". The severity of each category was determined by the number of positive answers to associated questions. Linear regression analyses determined their influence on regional tau PET SUVRs after accounting for covariates (age, sex, global Aβ).

Results: We found positive association between entorhinal tau and napping & abnormal nighttime behavior (p = 0.02, [0.021, 0.214], R^2 = 0.51) in normal group, which diminished in MCI. We found negative association between isocortical tau and sleep deficiency (p = 0.005, [-0.14,-0.03], R^2 = 0.34) in MCI only. We found no significant association between tau and the total score from both NPI sleep categories.

Conclusion: Different sleep-wake and behavioral disturbances are not equally associated with tau burden and may have disparate biological bases.

Keywords: *sleep-wake disturbance, tauopathy, mild cognitive impairment, normal aging, Neuropsychiatric Inventory*

P36: Defining the lowest threshold for baseline amyloid-PET to predict future cognitive decline and amyloid accumulation in clinically normal adults

Michelle Farrell[1], Shu Jiang[1,2], Aaron Schultz[1], Michael Properzi[1], Dorene Rentz[1,3], Kathryn Papp[1,3], Elizabeth Mormino[6], Rebecca Betensky[2,4], Keith Johnson[1,3,5], Reisa Sperling[1,3], Rachel Buckley[1,3,7,8]

[1]*Department of Neurology, Massachusetts General Hospital, Harvard Medical School, Boston, MA, US*
[2]*Department of Biostatistics, Harvard T.H. Chan School of Public Health, Boston, MA, US*
[3]*Center for Alzheimer Research and Treatment, Brigham and Women's Hospital, Boston, MA, US*
[4]*Department of Biostatistics, New York University, New York, NY, US*
[5]*Department of Radiology, Massachusetts General Hospital, Harvard Medical School, Boston, MA, US*
[6]*Department of Neuroscience, Stanford University, Palo Alto, CA, US*
[7]*Florey institute of Neuroscience and Mental Health, Melbourne, Australia*
[8]*Melbourne School of Psychological Sciences, University of Melbourne, Melbourne, Australia*

Objective: Current standards for defining beta-amyloid (Aβ) positivity are based on selecting cutoffs that maximize the likelihood of substantial Aβ burden in cross-sectional Aβ-PET. The aim of the present study was to redefine the positivity cut-off using longitudinal cognitive and PET data to identify the lowest point in the Aβ-PET distribution that predicts both future cognitive decline and Aβ accumulation.

Methods: 351 clinically normal participants (CDR=0; Age=51-90yrs) were included from the Harvard Aging Brain Study; 212 with longitudinal PIB-PET, mean follow-up$_{cog}$=2.5(2.14)yrs, median follow-up$_{PIB}$=3.52(1.18)yrs. To measure baseline Aβ, DVR was computed with a neocortical aggregate and a cerebellar gray reference region (predefined cut-off=1.2 DVR from GMM). For longitudinal Aβ, a composite reference region of whole cerebellum/eroded cortical white matter was used. Cognition was measured with the Preclinical Alzheimer Cognitive Composite (PACC-5). We implemented a series of two-level linear mixed regression models for longitudinal PACC-5 using iterative cutoffs for amyloid positivity (1.0-1.8 by 0.01DVR). An optimal Aβ cutoff was chosen in a model with the lowest Akaike/Bayesion information criterion (AIC/BIC). A similar mixed effects approach was conducted to predict PIB accumulation using iterative DVR cutoffs.

Results: A 1.14 DVR cutoff provided optimal model fit to predict future PACC-5 decline (Figure 1). Based on the AIC/BIC criterion for model fit, PIB accumulation was predicted similarly well by a range of DVR cutoffs from 0.87-1.02 (equivalent to 1.14-1.31 with cross-sectional pipeline; Figure 2A). We then examined the β$_{Standarized}$ estimates within this range, and found that the lowest cutoff (0.87, equivalent to 1.14) exhibited the greatest effect size.

Conclusion: Independently deriving optimal cross-sectional Aβ cutoffs to best predict future cognitive decline and future Aβ accumulation converged on the same DVR cutoff of 1.14. Out-of-sample validation studies will be necessary to determine the reliability of this cut-off to optimize selection of individuals for early-intervention trials.
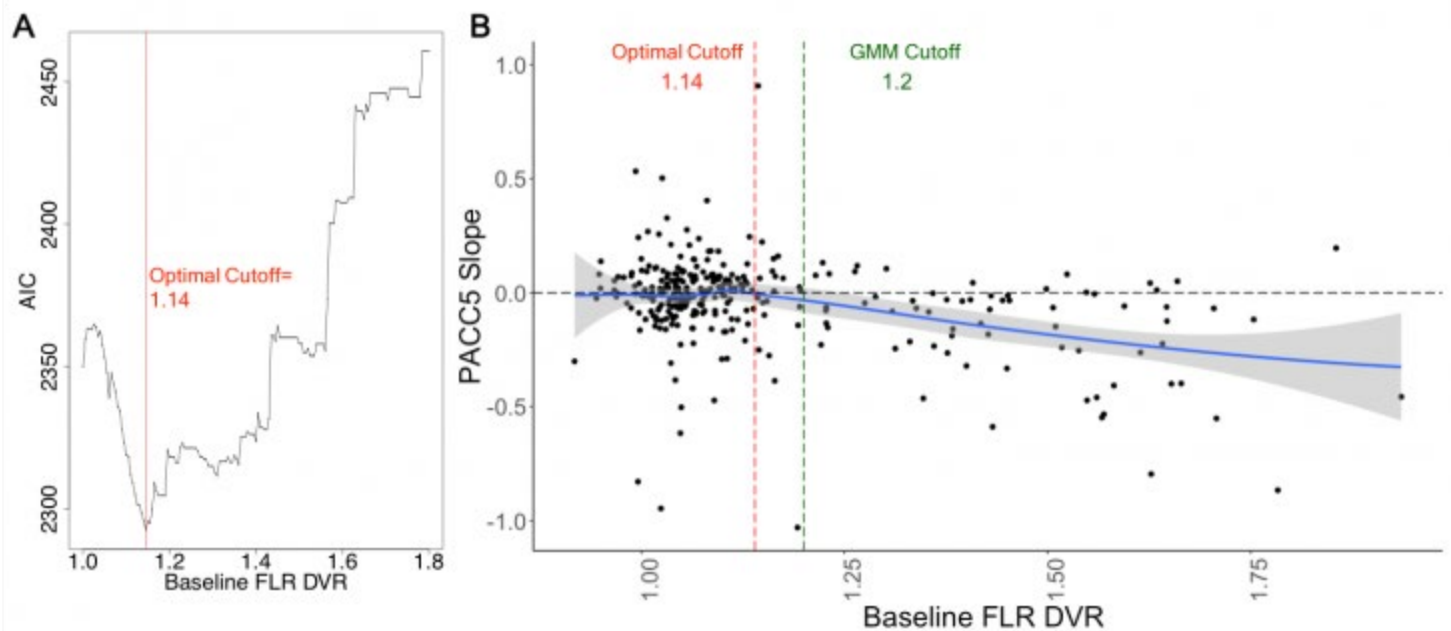
Figure 1. PACC decline identifies an optimal DVR cutoff of 1.14. A) The optimal DVR cutoff was selected based on iterative modeling of various DVR cutoffs to best model PACC decline. The best fitting model (defined by the lowest AIC/BIC) was found at the 1.14 DVR cutoff, indicating the estimate with least information loss. B) PACC slopes are plotted as a function of baseline DVR with a loess fit line. The optimal 1.14 DVR cutoff appears to represent an inflection point in the Aβ continuum at which the PACC first starts exhibiting subtle decline. This cutoff sits lower in the Aβ continuum than the study-specific predefined cutoff based on GMM (which is honed for maximizing the highest probability of Aβ + individuals).
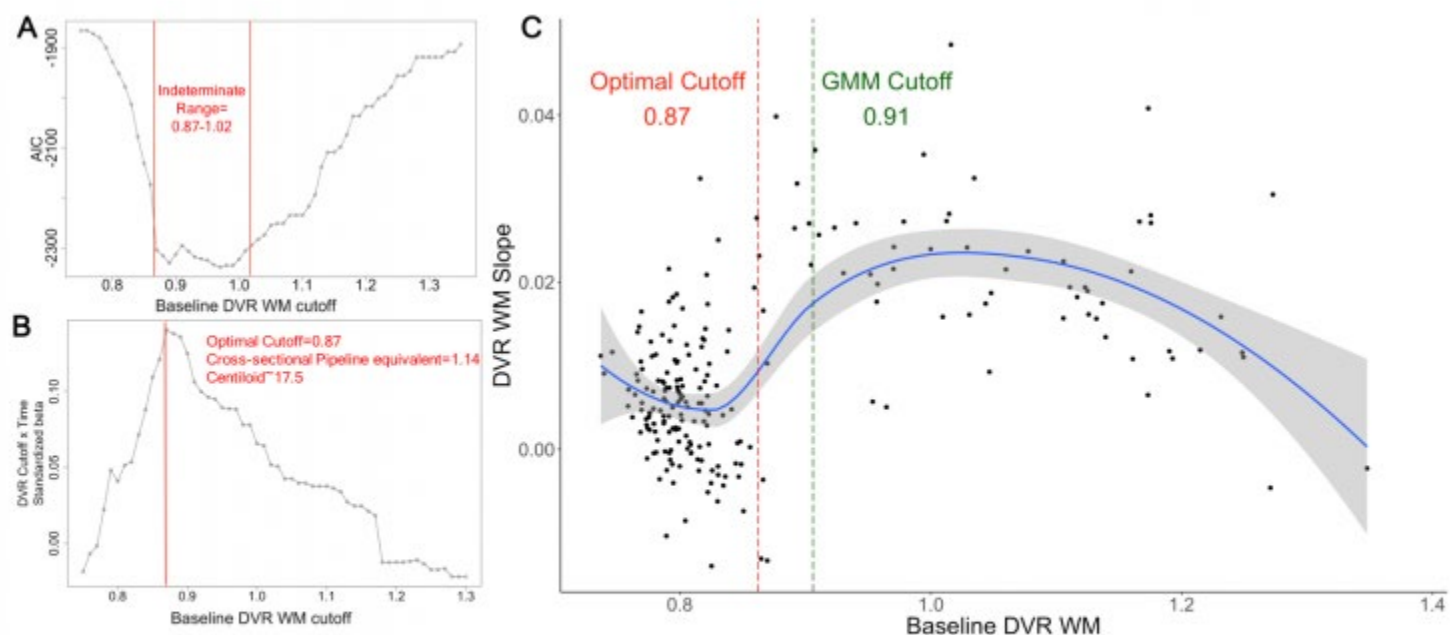
Figure 2. PIB DVR accumulation identifies an equivalent optimal baseline cutoff sitting within an indeterminate range of good AIC values [0.87-1.02]. DVR was modified for optimal longitudinal Aβ measurement with a revised reference region that includes eroded cortical WM. A) Iterative models of the prediction of DVR over time using different baseline cutoffs were conducted, but an the optimal cutoff was indeterminate using AIC/BIC, as a range of values from 0.87-1.02 exhibited similarly good model fit. B) To further hone in on the optimal cutoff in this indeterminate range, we selected the DVR cutoff that provided the maximum standardized beta for the DVR Cutoff*Time interaction. The baseline DVR cutoff with the highest beta (0.87) equated to a cross-sectional pipeline cutoff of 1.14 (derived from both linear regression and an Empirical Cumulative Distribution Function analysis). This cutoff was identical to the optimal cutoff independently derived from the PACC decline models. B) Evaluation of the relationship between baseline DVR and DVR slope demonstrates a clear shift at the optimal cutoff from random fluctuations in noise towards larger increases likely to denote high Aβ accumulation, while the predefined GMM cutoff misses some individuals with high rates of Aβ accumulation.

P37: Mild behavioral impairment is associated with β-amyloid and tau in cognitively intact elderly individuals

Firoza Lussier[1,2], Tharick A. Pascoal[1,2], Mira Chamoun[1,2], Joseph Therriault[1,2], Cecile Tissot[1,2], Melissa Savard[1,2], Min Su Kang[1,2], Sulantha Mathotaarachchi[1,2], Andrea Lessa Benedet[1,2], Emilie Thomas[1], Marlee Parsons[1,2], Zahinoor Ismail[4], Pedro Rosa-Neto[1,2], Serge Gauthier[1,3]

[1]*McGill University Research Centre for Studies in Aging, Verdun, QC, Canada*
[2]*Translational Neuroimaging Laboratory, McGill University, Verdun, QC, Canada*
[3]*Douglas Hospital Research Centre, Verdun, QC, Canada*
[4]*Hotchkiss Brain Institute, University of Calgary, Calgary, AB, CA*

Background: Mild behavioral impairment (MBI) is a neurobehavioral syndrome characterized by the emergence of sustained non-cognitive neuropsychiatric symptoms in elderly persons. MBI therefore represents an at-risk state for dementia. While studies have revealed correlations between certain neuropsychiatric symptoms and Alzheimer's disease (AD) biomarkers, little is known about the association of MBI with brain β-amyloid and tau proteins in pre-dementia populations.

Objective: To test whether MBI depends on brain deposition of β-amyloid and tau proteins in cognitively normal elderly persons.

Methods: Sixty-one cognitively healthy individuals aged from 56 to 86 years old underwent [^{18}F]-AZD4694 β-amyloid and [^{18}F]-MK6240 tau PET. [^{18}F]AZD4694 and [^{18}F]MK-6240 standardized uptake value ratios (SUVRs) used the cerebellum grey matter as the reference region and were calculated between 40 to 70 min and 90 to 110 min post-injection, respectively. MBI was assessed using the MBI Checklist (MBI-C) which is composed of 5 domains: decreased motivation, emotional dysregulation, impulse dyscontrol, social inappropriateness, and abnormal perception. Voxel-based regressions were used to evaluate the relationship between [^{18}F]-AZ4694, [^{18}F]-MK6240, adjusting for age, gender, and education.

Results: A significant positive correlation was found between total MBI-C score and [^{18}F]-AZD4694 retention in the frontal lobe, precuneus, posterior cingulate cortex, and putamen. The MBI domains of abnormal perception and emotional dysregulation were highly correlated with β-amyloid deposition in the right and left orbitofrontal cortex respectively. Higher total MBI-C scores were significantly correlated with increased [^{18}F]-MK6240 retention bilaterally in the superior temporal lobe.

Conclusions: This study is the first to reveal an association between brain deposition of β-amyloid and tau and mild behavioral impairment in a cognitively intact population. This supports a conceptual framework in which MBI may constitute an early clinical manifestation of AD pathophysiology and may be used in clinical trials to select cognitively normal individuals with a higher probability of presenting with AD pathophysiology.

Figure 1: Parametric maps show significant correlation between mild behavioral impairment checklist (MBI-C) total score and [18F]-AZD4694 and [18F]-MK6240 retention.

Figure 2: Parametric maps show significant correlation between domain MBI-C scores and [18F]-AZD4694 retention.
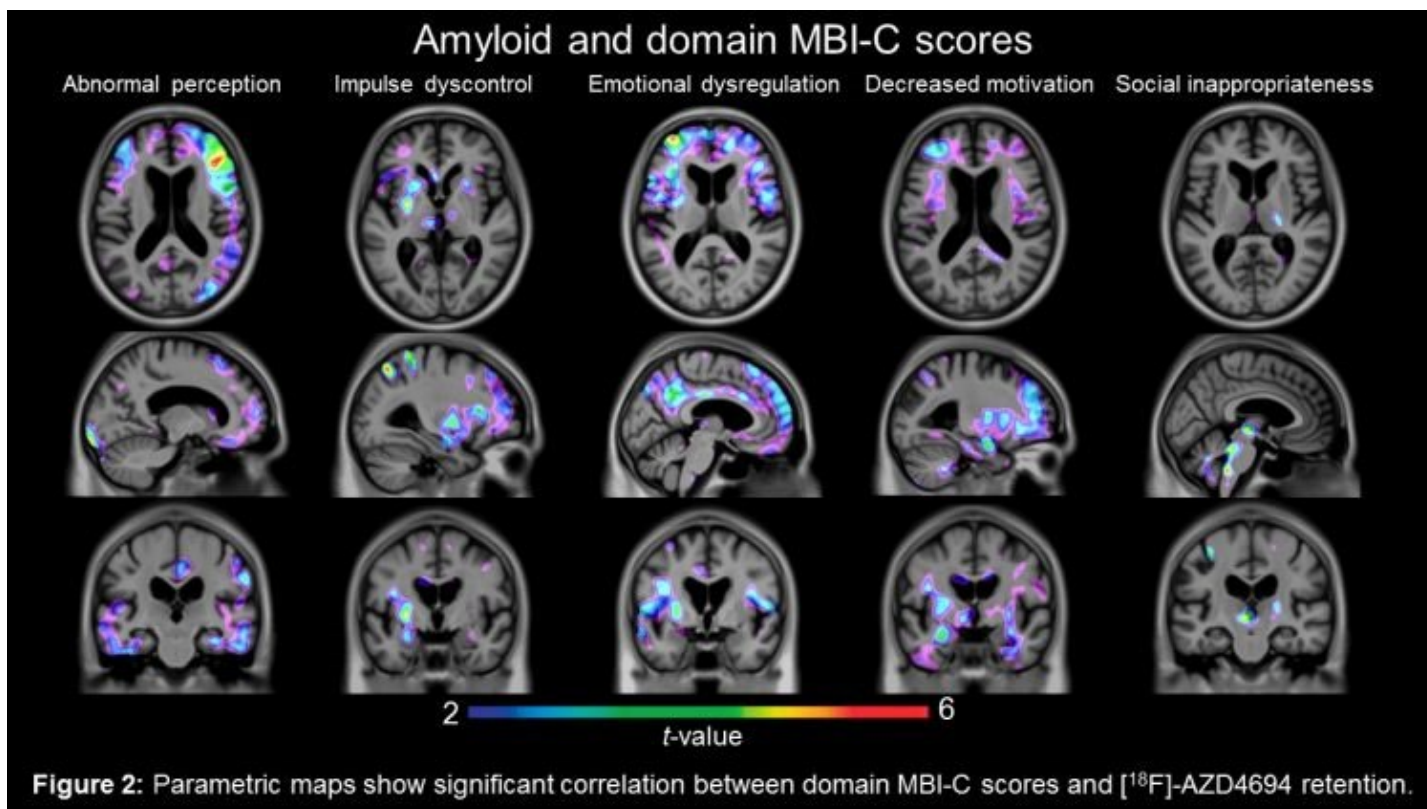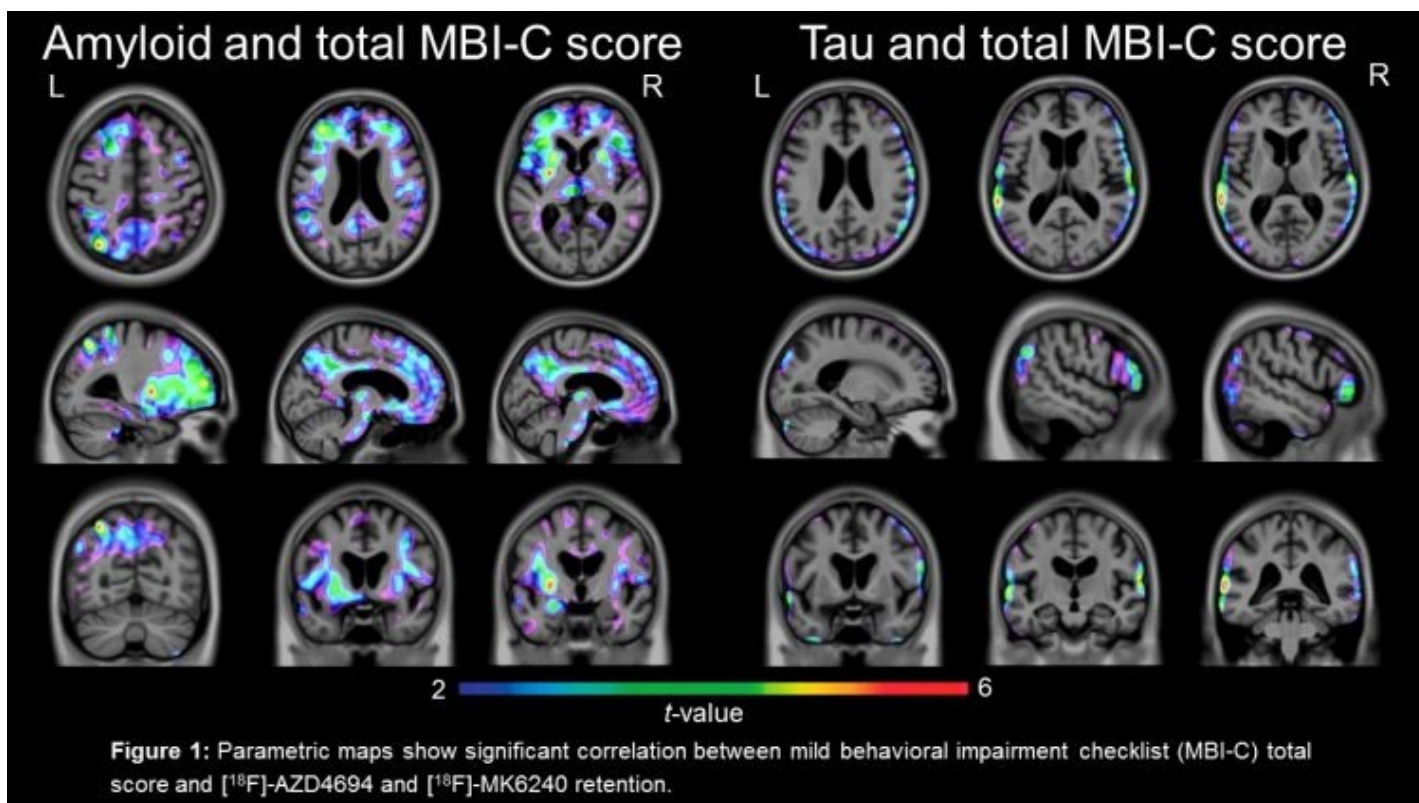
Keywords: *Alzheimer's disease, mild behavioral impairment, amyloid, tau*

P38: Evaluation of a visual read method for flortaucipir PET scans

Anupa Arora[1], Michael Pontecorvo[1], Mark Mintun[1], Adam Fleisher[1], Michael Devous[1], Ming Lu[1], Nicholas Galante[1], Patricia Stevenson[1], Matthew Flitter[1], Thomas Beach[2], Thomas Montine[8], Geidy Serrano[2], Lucia Sue[2], Anthony Intorcia[2], Craig Curtis[9], Stephen Salloway[11], Stephen Thein[12], Charles Wellman[13], Allison Perrin[10], Val Lowe[3], Murray Grossman[4], David Irwin[4], Milos Ikonomovic[5], William Seeley[6], Gil Rabinovici[6], Joseph Masdeu[7]

[1]*Avid Radiopharmaceuticals, West Chester, PA, US*
[2]*Banner Sun Health Research Institute, Sun City, AZ, US*
[3]*Mayo Clinic Rochester, Rochester, MN, US*
[4]*Hospital of the University of Pennsylvania, Philadelphia, PA, US*
[5]*University of Pittsburgh, Pittsburgh, PA, US*
[6]*University of California, San Francisco, San Francisco, CA, US*
[7]*Houston Methodist Neurological Institute, Houston, TX, US*
[8]*Stanford University, Stanford, CA, US*
[9]*Compass Research, Orlando, FL, US*
[10]*Banner Alzheimer's Institute, Phoenix, AZ, US*
[11]*Butler Hospital, Providence, RI, US*
[12]*Pacific Research Network, Inc., San Diego, CA, US*
[13]*Hospice of the Western Reserve, Cleveland, OH, US*

Objective: To evaluate a clinically applicable visual read method for flortaucipir PET scans

Methods: Five imaging physicians were trained in-person using a predefined read methodology to visually interpret flortaucipir PET scans. After scaling images to cerebellum, they were instructed to evaluate regions of the neocortex (the posterolateral temporal (PLT), occipital, parietal and frontal regions) for increased tracer uptake, and interpret scans as either not consistent (tAD-) or consistent with an AD pattern (tAD+ or tAD++) using the following criteria:

tAD-: no increased activity or increased activity isolated to the mesial temporal, anterior lateral temporal, and/or frontal region(s)
tAD+: increased activity in the PLT or occipital region(s)
tAD++: increased activity in the parietal/precuneus region(s) or frontal region with PLT, occipital, or parietal region(s)

Read categories were derived from studies A05 and LZAX, where increased neocortical uptake in the PLT was associated with amyloid positivity, and activity beyond the PLT/occipital regions was associated with greater cognitive decline. After training on demonstration and practice cases, all readers independently read 105 scans from subjects enrolled in a Phase 3 clinical trial (study A16) plus 17 scans from a supplemental academic cohort (total n=122). The primary objectives tested the relationship between scan results and neuropathology of AD at autopsy.

Results: 82 cases came to autopsy and had evaluable scans. Median sensitivity and specificity for identifying Braak V/VI pathology were 89.1% and 83.3%, respectively. The median sensitivity and specificity for identifying high AD neuropathic change were 95.1% and 80.5%, respectively. Interrater reliability as measured by Fleiss' kappa for all interpreted scans (n=122) was 0.80 and overall agreement was 90.3%.

Conclusions: There was substantial agreement among readers. Using the proposed read method, readers were able to distinguish between scans consistent and not consistent with an AD pattern.

Keywords: *tau, flortaucipir, pathology*

P39: An MRI-free, template-based method for quantifying cortical florbetapir uptake in vivo

Deniz Korman[1,2], Susan Landau[1,2], William Jagust[1,2]

[1]*Helen Wills Neuroscience Institute, University of California, Berkeley, Berkeley, CA, US*
[2]*Lawrence Berkeley National Laboratory, Berkeley, CA, US*

Objectives: Missing structural MRI scans complicate implementation of MRI-dependent Aβ-PET pipelines. To determine whether predictive information is lost when quantifying Aβ-PET without an MRI for defining regions of interest, we developed an MRI-free template-based quantification method for calculating cortical florbetapir uptake and compared it to our default MRI-based pipeline.

Methods: We calculated two sets of florbetapir cortical summary SUVRs (MRI-based and MRI-free) for 1214 ADNI participants (Normal:461, MCI:552, AD:201). For the MRI-based pipeline, SUVRs were calculated using Freesurfer 5.3 defined cortical regions relative to the whole cerebellum. For the MRI-free pipeline, florbetapir images were warped to a group template and cortical SUVRs were calculated using custom analogous cortical and whole cerebellum ROIs. We examined (1) MRI-based and MRI-free florbetapir cortical summary SUVRs' agreement with CSF $A\beta_{1-42}$ (Roche Elecsys) and (2) each pipeline's association with subsequent memory decline and MCI to AD conversion. We used an MRI-based autopsy-validated threshold of 1.11 and an MRI-free threshold of 1.17 based on a linear transformation of the MRI-based threshold.

Results: MRI-based and MRI-free SUVRs were highly correlated (R^2=0.93), and had high +/- status agreement (93.3%; Fig1). Agreement between CSF $A\beta_{1-42}$ and florbetapir +/- status was similar (58.7% agreement with the MRI-based +/- status, 57.8% agreement with the MRI-free +/- status).

In regression models predicting memory decline based on continuous florbetapir SUVRs, age, sex, education, diagnosis, and APOE4 status, the predictive value of the model with MRI-based SUVRs (β_{SUVR}=-0.252, $p<7.2*10^{-11}$) did not differ from the model with MRI-free SUVRs (β_{SUVR}= -0.236, $p<1.7*10^{-10}$; Vuong's test p>0.33). Finally, in Cox proportional hazards analyses predicting MCI to AD conversion, the predictive value of continuous florbetapir SUVRs also did not differ between MRI-based (β_{SUVR}=3.65, $p<2*10^{-15}$) MRI-free SUVRs (β_{SUVR}=3.34, $p<1.2*10^{-16}$; Fig2).

Conclusion: Our MRI-free quantification scheme closely follows our MRI-based results, calling into question the value of MRI-dependent florbetapir quantification.
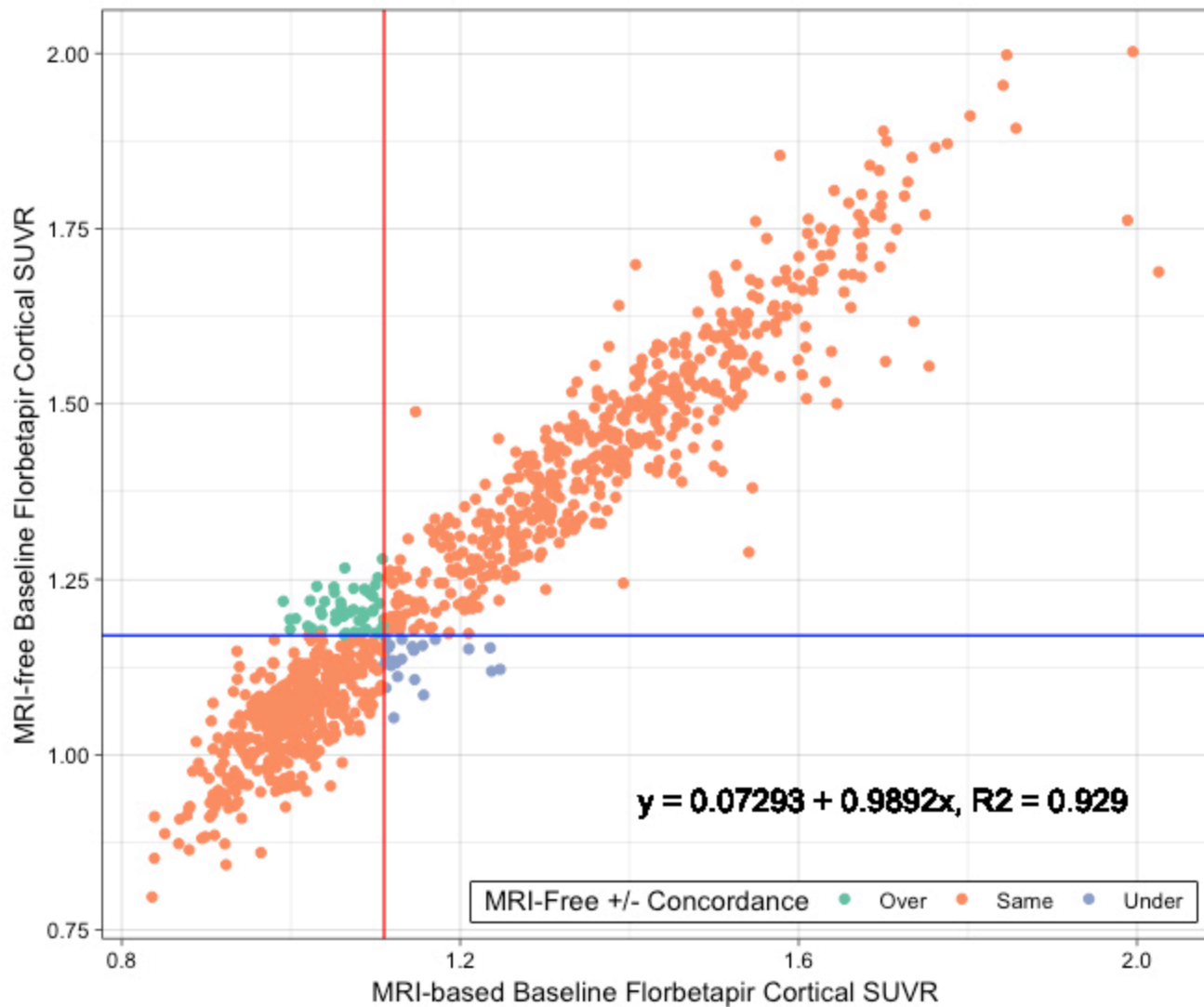
Figure 1: Relationship between MRI-based and MRI-free cortical SUVRs.
The +/- status agreements (*4.44% Over, 93.3% Same, 2.22% Under*) between the pipelines is shown in color. The results from the two pipelines match one another closely with low variation, indicating that MRI-free quantification can provide comparable levels of information about cortical Aβ as MRI-based methods.

MCI to AD Conversion Probabilities
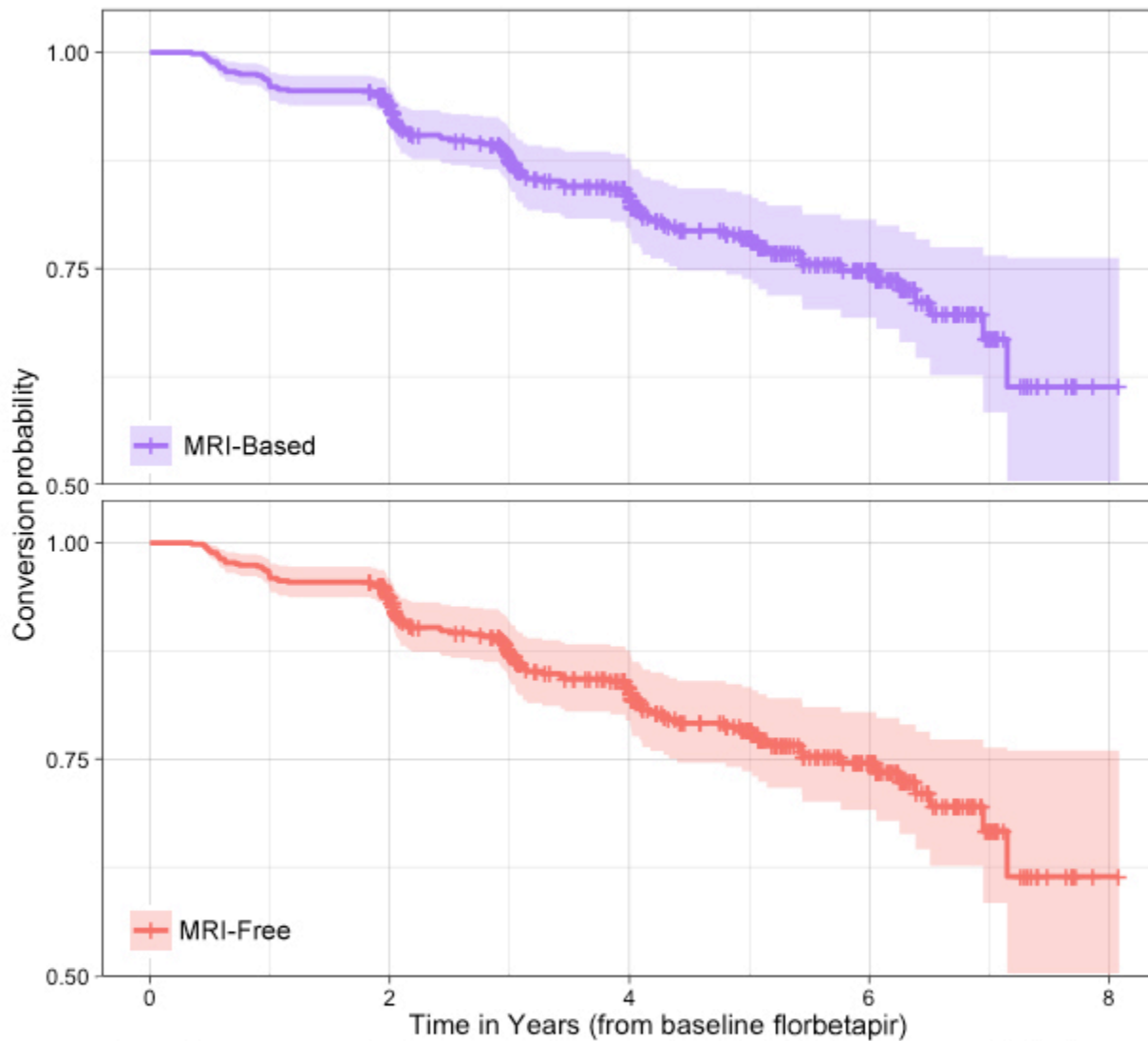
Figure 2: MCI to AD Conversion Curves for the MRI-based and MRI-free pipelines. The curves are based on Cox proportional hazards models with continuous florbetapir SUVRs, age, sex, education, and APOE4 as predictors. The absence of notable differences between the two curves highlight the similarity of the two pipeline's predictive powers, and the viability of MRI-free quantification.

P40: Early increase in tau-PET signal is associated with changes in amyloid, CSF p-tau and cognition

Melissa McSweeney[1,2], Alexa Pichet Binette[1,2], Pierre-François Meyer[1,2], Julie Gonneaud[1,2], Christophe Bedetti[2], Hazal Ozlen[1,2], Leslie-Ann Daoust[2], Anne Labonté[1,2], Pedro Rosa-Neto[1,2], John Breitner[1,2], Judes Poirier[1,2], Sylvia Villeneuve[1,2]

[1]*McGill University, Montreal, QC, Canada*
[2]*Douglas Mental Health Research Institute, Montreal, QC, Canada*

Objective: To investigate relationships between tau PET binding and other established Alzheimer's disease (AD) markers in cognitively normal late-middle-aged and older adults at increased risk of sporadic AD.

Methods: One-hundred-nineteen cognitively normal older adults with a family history of sporadic AD (PREVENT-AD cohort, mean age=67±5) underwent tau PET ([^{18}F]AV1451), β-amyloid (Aβ) PET ([^{18}F]NAV4694), and cognitive assessment. A subsample of 59 participants also had CSF phosphorylated (p)-tau data available. We investigated regional tau SUVR differences between Aβ-positive and Aβ-negative individuals using general linear models adjusted for age and sex. In regions showing significantly higher [^{18}F]AV1451 binding in Aβ-positive individuals, we then assessed whether [^{18}F]AV1451 SUVRs were related to CSF p-tau and cognitive performance. Finally, we repeated these analyses while iteratively removing individuals with higher entorhinal [^{18}F]AV1451 binding to detect thresholds at which associations with Aβ-PET, CSF p-tau and cognition were lost.

Results: Aβ-positive individuals had higher [^{18}F]AV1451 SUVRs than Aβ-negative ones in predominantly limbic, temporal, occipital, and inferior parietal regions (Fig.1). Increased tau SUVRs in a subset of limbic and temporal regions were also associated with increased CSF p-tau and worse cognitive performance (Fig.2). The association between [^{18}F]AV1451 in the entorhinal cortex and CSF p-tau, Aβ, and cognition were lost when removing individuals above SUVRs of 1.15, 1.23 and 1.44, respectively (Fig.3).

Conclusions: Even in cognitively normal late-middle-aged and older adults, [^{18}F]AV1451 binding in AD-typical regions is associated with established AD markers. Except for the association with cognition, these findings were not driven by individuals that would be classified as tau-positive using a conventional entorhinal SUVR threshold of ~1.3, supporting the idea that very early or "subthreshold" elevation in [^{18}F]AV1451 signal is clinically meaningful.
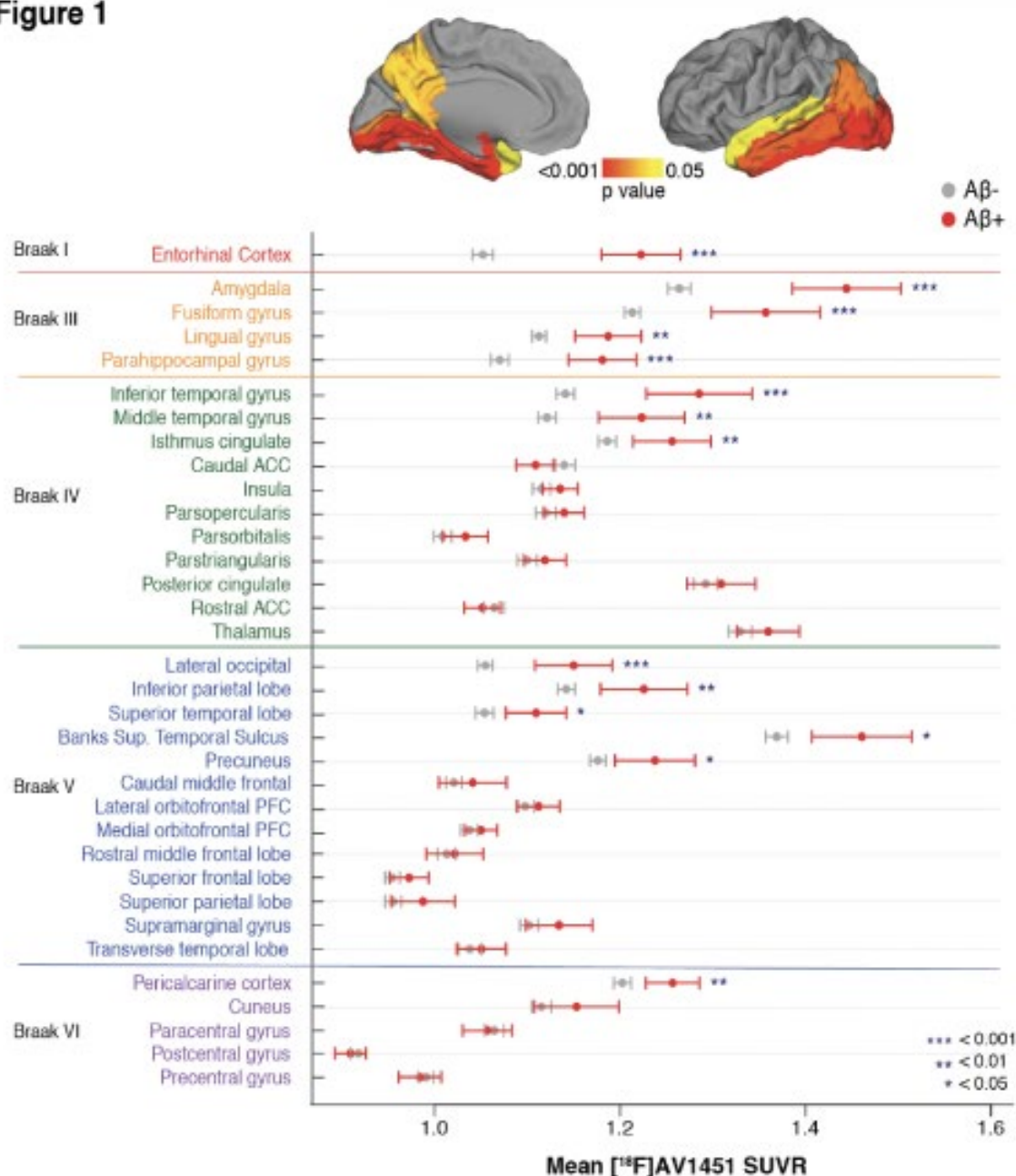
Figure 1: There is higher [¹⁸F]AV1451 binding in AD-typical regions in Aβ-positive individuals.
Mean [¹⁸F]AV1451 SUVRs across all FreeSurfer Desikan regions, organized by Braak stages, in Aβ-positive (red) and Aβ-negative (gray) groups. (Aβ-positivity was established at a data-driven and literature-confirmed SUVR threshold of 1.42.) Asterisks indicate the 14 regions in which the [¹⁸F]AV1451 SUVR is different between the Aβ + and Aβ- groups. P-values of the significant regions are projected onto the brain template above the graph.

Figure 2
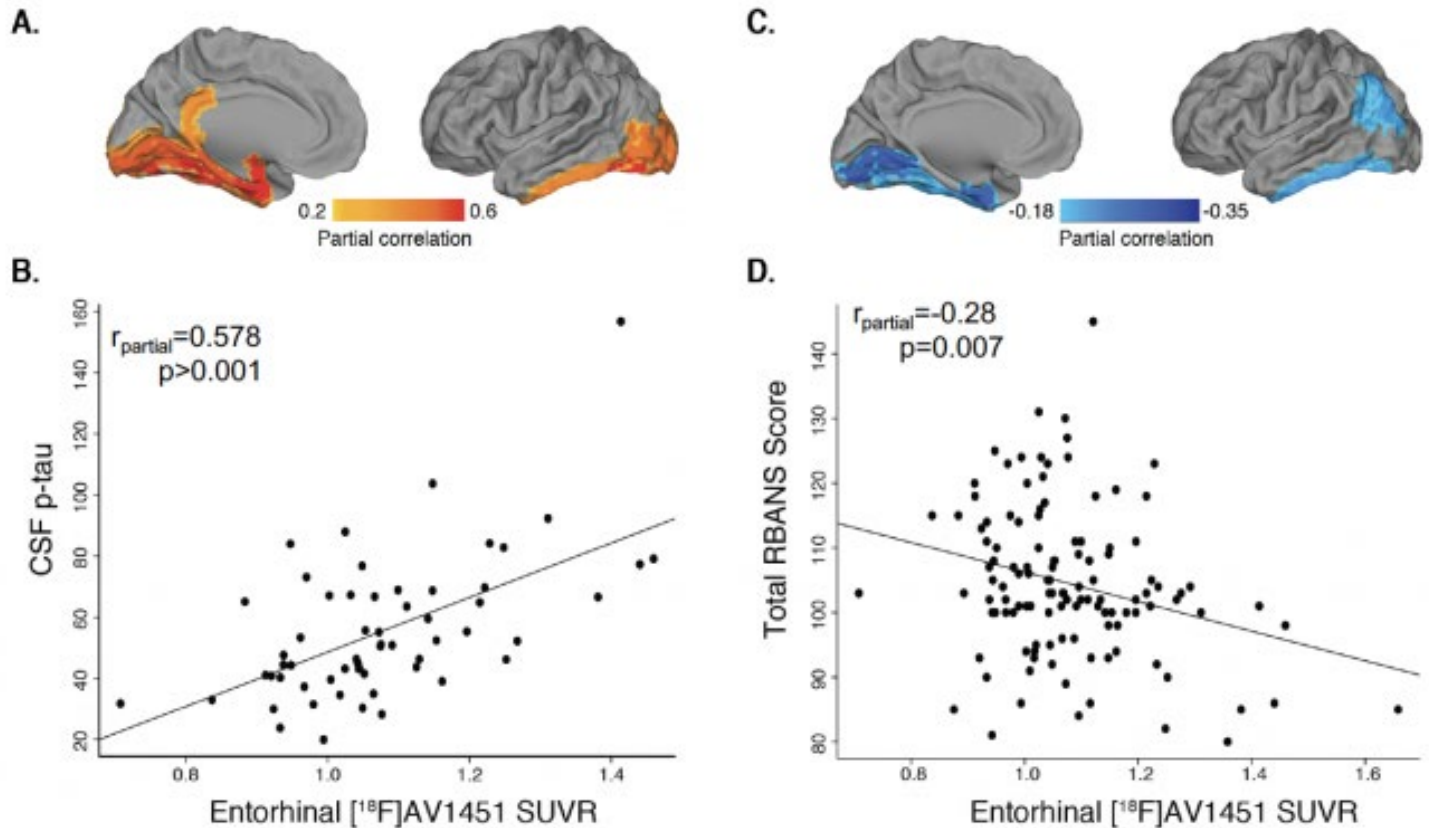
Figure 2: Higher [18F]AV1451 binding in AD-typical regions is associated with greater levels of CSF p-tau and worse cognition.

2A) Partial correlation coefficients, adjusted for age and sex, of the regions associated with CSF p-tau projected onto a brain template. Only the regions that showed higher [18F]AV1451 binding in the Aβ-positive individuals in the previous analysis were included in the current analyses.

2B) Positive correlation between entorhinal tau SUVR and CSF p-tau. Entorhinal [18F]AV1451 binding had one of the strongest associations with CSF p-tau among the 14 ROIs in this analysis.

2C) Partial correlation coefficients, adjusted for age and sex, of the regions associated with lower overall performance on the Repeatable Battery for the Assessment of Neuropsychological Status (RBANS) projected onto a brain template.

2D) Negative correlation between entorhinal tau SUVR and RBANS Total Index Score. Entorhinal [18F]AV1451 binding had the strongest association with overall RBANS performance out of the 14 ROIs in this analysis.

Figure 3
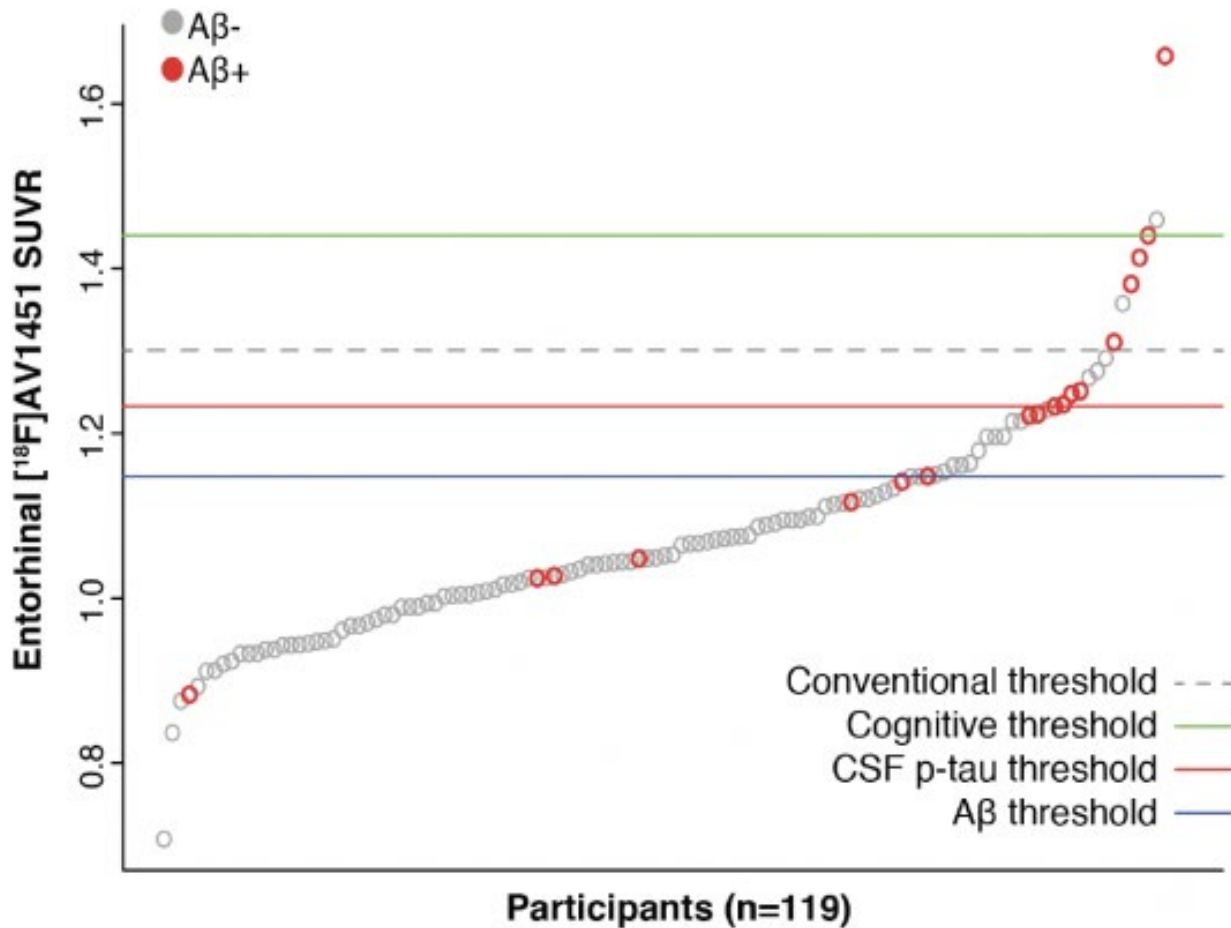
Figure 3: Subthreshold entorhinal [18F]AV1451 binding is associated with CSF p-tau and Aβ PET binding.

Individual participants are ranked in order of entorhinal [18F]AV1451 binding. Aβ-positive individuals are indicated in red, and Aβ-negative individuals are in gray. The horizontal lines indicate at which entorhinal [18F]AV1451 SUVR values the associations between continuous Aβ (red), CSF p-tau (blue), and RBANS (green) are lost, as compared to a conventional literature-based threshold of 1.3 (dashed line). These values were obtained by iteratively running linear regressions (with 1000 permutations) and removing the subject with the highest entorhinal [18F]AV1451 SUVR for each iteration. The indicated values are the lowest entorhinal SUVRs at which the association between entorhinal [18F]AV1451 binding and the variable of interest are still significant.

P41: Mental and physical activity during the 80-minute uptake time affects off-target binding in tau PET scans (18F-AV-1451)

Christopher Apgar[1], <u>Hoon-Ki Min</u>[1], Daniela Maltais[1], Nancy Scott[1], Emily Lecy[1], Emily Lundt[1], Sabrina Albertson[1], Christopher Schwarz[1], Hugo Botha[1], David Jones[1], Kejal Kantarci[1], Prashanthi Vemuri[1], David Knopman[1], Ronald Petersen[1], Clifford Jack[1], Val Lowe[1]

[1]*Mayo Clinic, Rochester, MN, US*

Background: With the application of longitudinal tau PET studies to track disease progress, identifying the factors that cause variability in tau PET scans is critical. Many have observed off-target uptake with tau PET in regions outside of the brain but close enough for bleed-in effects, including in the meninges, cortical bone, and jaw muscles. During the uptake period for [^{18}F]AV-1451 tau PET scans, no standard participant activity recommendations are given, and participants are free to engage in various activities prior to PET scan acquisition. In this study, we assessed whether mental and physical activity during the 80-minute uptake time correlated with off-target tau PET uptake.

Methods: We conducted a post-scan survey about the mental and physical activity of participants (n=149) during the 80-minute uptake time. The survey questions identified activities that had the potential to affect perfusion of the body and brain, including conversation, reading, listening to music, watching videos, internet use, sleeping, walking, and food/liquid intake. Predetermined off-target regions of interest (ROI) outside of the brain including, retina, ocular muscle, sinus, jaw muscles (masseter, pterygoid, temporalis), pituitary gland, and cortical bone/dura (superior, inferior-anterior, inferior-posterior positions) were measured with standardized uptake values (SUV) by two independent scan readers. Pearson's correlation coefficients were used to evaluate potential associations between SUV and prior activity.

Results: Intra-class correlation of the two readers' SUV values was 0.98. Several behaviors correlated with off-target [^{18}F]AV-1451 SUV, among them sleeping and walking, each of which were significant ($p < 0.001$, uncorrected). While sleep had a positive correlation with off-target tau SUV, walking had a negative correlation.

Discussion: Our findings show that certain behaviors during the 80-minute uptake period were correlated with off-target tau PET uptake. In the future, activity restriction protocols in preparation for [^{18}F]AV-1451 scans may need to be considered to reduce variability in brain-adjacent off-target binding.

Keywords: *Tau, PET, [18F]AV-1451, Off-target*

P42: Functional network changes occur prior to symptomatic conversion in AD

Julie Wisch[1], Catherine Roe[1], Ganesh Babulal[1], Tammie Benzinger[1], John Morris[1], Beau Ances[1]

[1]*Washington University, St. Louis, MO, US*

Background: The goal of this project was to consider longitudinal changes in positron emission tomography (PET) amyloid, PET tau, flurodeoxyglucose (FDG) and their relationships to blood oxygen level dependent resting state functional connectivity (rs-fc) in participants who remained cognitively normal (clinical dementia rating (CDR) 0) compared to participants who converted from CDR 0 to symptomatic Alzheimer disease (AD) (CDR > 0).

Methods: We obtained rs-fc (n=419), PET amyloid (n=346), PET tau (n=152), and FDG (n=78). Participants aged 42 to 90 (77 ± 9.4) were followed for up to 19 years (8.0 ± 3.4 years). Of these, 70 (17%) participants developed CDR > 0. We assigned a year of onset (EYO) based on CDR conversion date for individuals who transitioned to AD, and randomly generated for those who remained CDR 0 throughout follow-up. Network changes over time were considered via MANOVA, one-way ANOVA, and post hoc Tukey's HSD. Changes in PET imaging as a function of rs-fc were assessed using maximum likelihood tests.

Results: There was a difference in rs-fc by CDR conversion (p = 7.27e-08). Trajectories over time were different for converters vs. non-converters for the following network connections: lateral somatomotor (SM lat) intranetwork connection, SM lat x visual attention network (VAN), cingulo-opercular intranetwork connection (CO x CO), and the fronto-parietal (FP) x salience (SAL) network (Fig 1).

Converters had higher amyloid level throughout, as well as different tau accumulation trajectory (Fig. 2). In each of the four networks, converters possessed higher levels of amyloid and tau at given levels of connectivity (Fig. 3).

Conclusions: Connectivity changes occurred years prior to CDR conversion in some intra-network connections. Nearly all individuals who had elevated tau and/or amyloid as well as high network connectivity in the FP x SAL network were converters. Further study is required to understand this relationship.
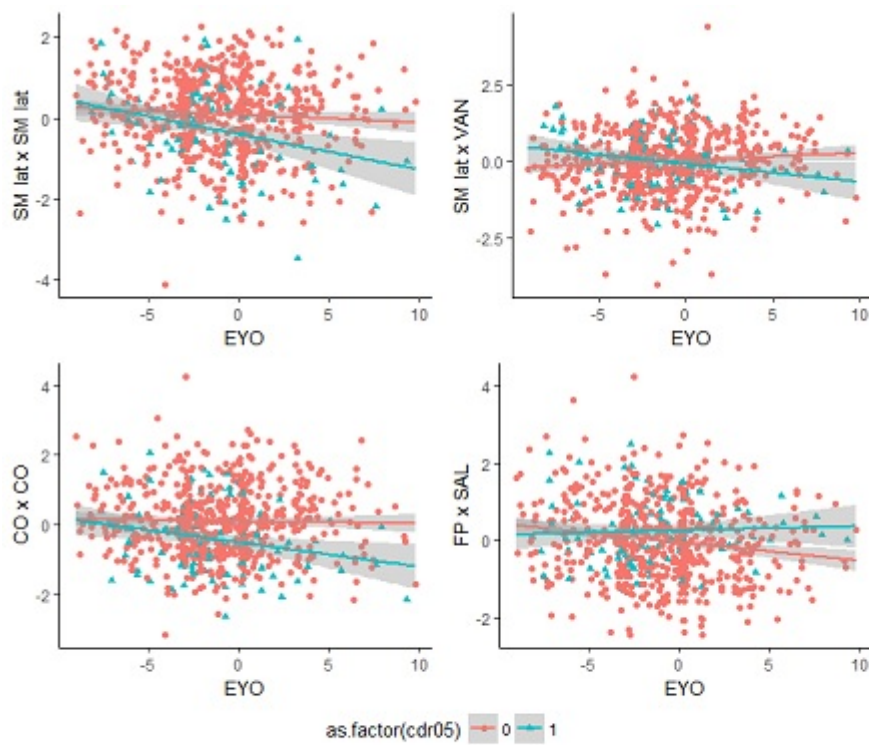
Figure 1. Functional network trajectories with significant differences between converters and non converters
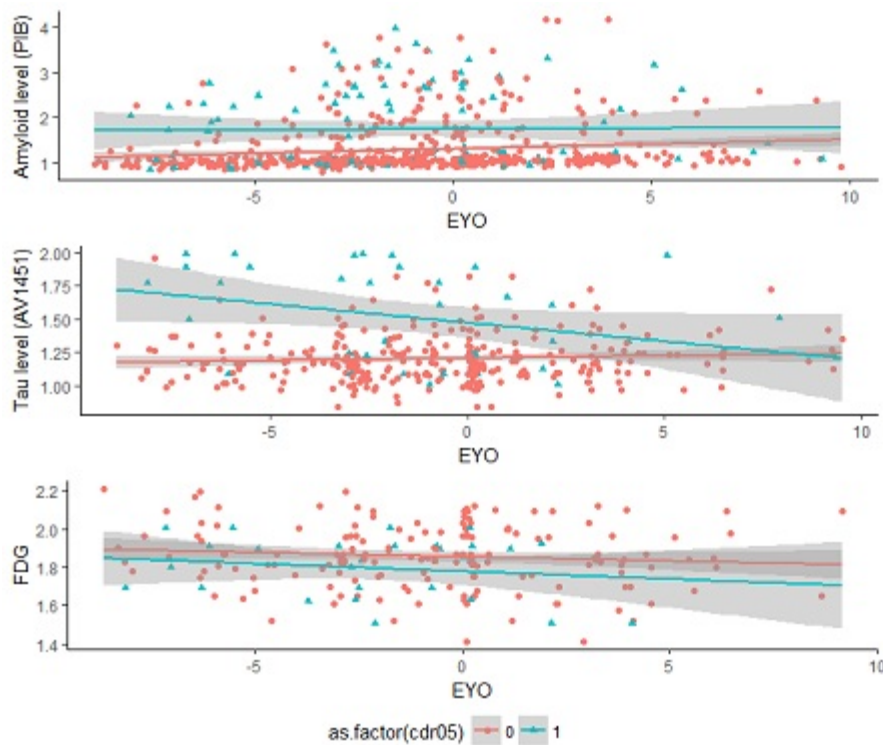
Figure 2. PET Imaging markers as a function of years to CDR Conversion
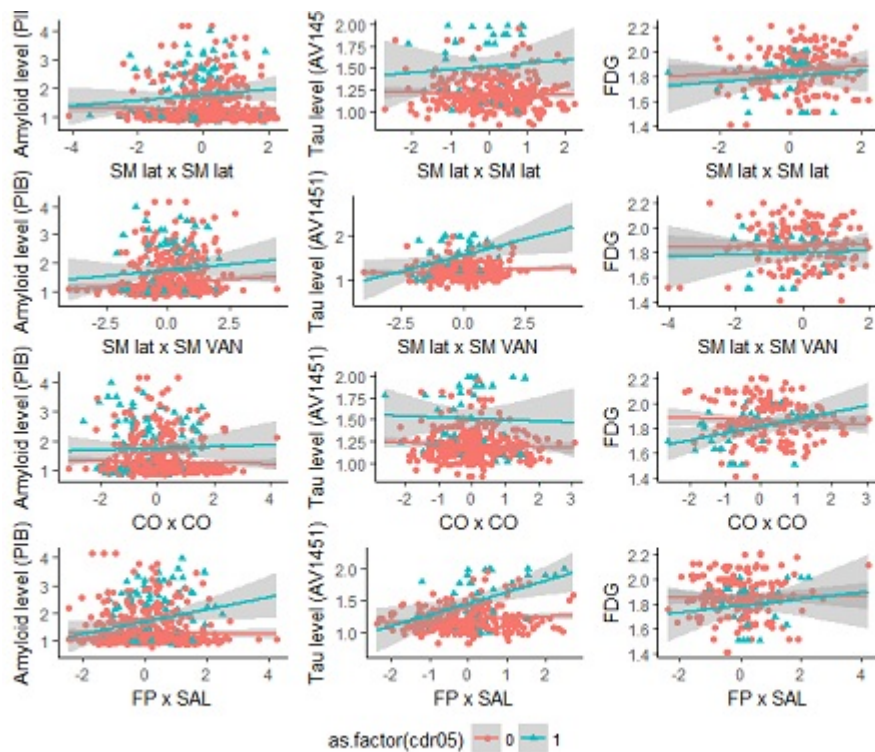
Figure 3: PET Imaging markers as a function of network connectivity

P43: Enhancing tau signal of PET imaging using a convolutional autoencoder

Sulantha Mathotaarachchi[1], Tharick A. Pascoal[1], Andréa L. Benedet[1], Mira Chamoun[1], Mélissa Savard[1], Min Su Kang[1], Joseph Therriault[1], Vladimir S. Fonov[1], Serge Gauthier[1], Pedro Rosa-Neto[1]

[1]*McGill University Research Center for Studies in Aging, Montreal, QC, Canada*

Introduction: [^{18}F]MK-6240 is a new generation tau tracer with sub-nanomolar affinity and high selectivity for neurofibrillary tangles that showed excellent pharmacokinetic properties in a preclinical observation. However, PET images are susceptible to noise particularly in brain regions with reduced tau concentrations, typically observed in early disease stages. We propose an automatic denoising technique to enhance tau PET signal based on convolutional auto-encoders which have been proven successful in other image denoising tasks.

Methods: A 3D convolutional autoencoder was trained with 14,272 input neuroimages consisting of Amyloid ([^{18}F] Florbetapir PET), Glucose Metabolism ([^{18}F] FDG PET), and T1 based Voxel-Based Morphometric images acquired from the ADNI database. 175, [^{18}F]MK-6240 images acquired at the McGill University Research Center for Studies for Aging (MCSA) TRIAD cohort was used in the analysis. All images were first registered to the MNI152 template space prior to model training or analysis. To investigate the reduction of noise, the standard deviation and the inverse of the coefficient of variance for cognitively normal individuals was calculated. To investigate the effect of the reduction of noise on the image statistics, we calculated the association between voxel-wise tau load and MMSE measure (adjusted for age, gender) in corrected and uncorrected images within a population of individuals containing cognitively normal and MCI individuals.

Results: The standard deviation images (Figure 1. A) show a substantial reduction of deviation within cognitively normal subjects between the uncorrected and corrected images. This is further supported by the increase in the inverse of the coefficient of variance (Figure 1. B). In the analysis of the association between MMSE and tau uptake, the corrected images indicate a stronger association (Figure 1. C).

Discussion: Our results indicate that the denoising technique using an autoencoder was able to recover a higher amount of PET signal compared to an uncorrected image.
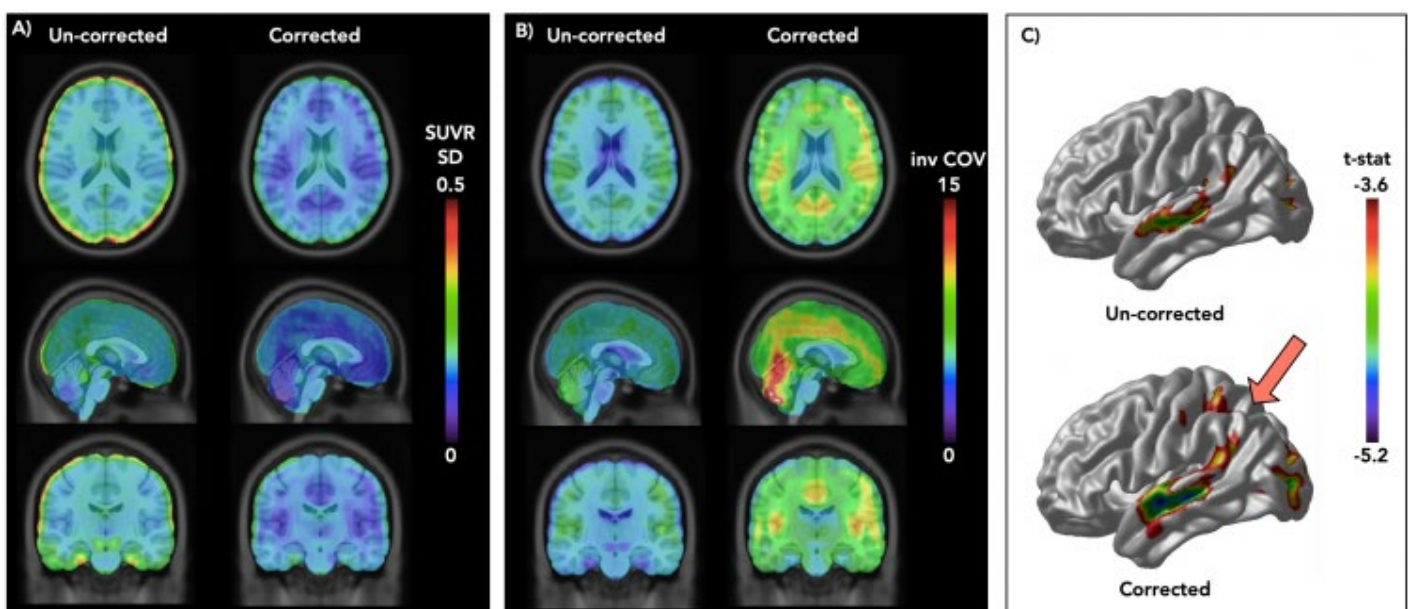
P44: Co-evolving patterns of functional connectivity with amyloid and tau deposition in Alzheimer's disease progression

Diana Svaldi[1], Joaquín Goñi[2], Enrico Amico[2], Shannon Risacher[1], Eddie Stage[1], John West[1], Andrew Saykin[1], Liana Apostolova[1]

[1]*Indiana University School of Medicine, Indianapolis, IN, US*
[2]*Purdue University College of Engineering, West Lafayette, IN, US*

Objective: Alzheimer's Disease pathology results in dysfunctional signaling that aids in further propagation of pathology. We use multi-modal connectivity independent component analysis (hybrid-connICA) to identify joint components integrating functional connectivity (FC), amyloid deposition, and tau deposition information to characterize Alzheimer's progression.

Methods: We assessed resting-state-fMRI, F18-Flortaucipir, and F18-Florbetapir PET scans from 33 ADNI3 subjects (Table1). Average Florbetapir cortical-SUVR and average Flortaucipir medial-temporal-lobe (MTL) SUVR were determined using Freesurfer-ROIs. Whole-brain FC matrices in each subject were estimated using a functional parcellation (286 cortical-ROIs). This parcellation was applied to Florbetapir and Flortaucipir data, generating 286 mean SUVR vectors, normalized by the maximum ROI-SUVR across subjects.

FC and Florbetapir/Flortaucipir vectors were merged to create FC-PET hybrid vectors (FC-Florbetapir, FC-Flortaucipir). connICA was performed on a matrix containing hybrid vectors from all subjects (5 ICs), resulting in hybrid-ICs containing a FC-pattern and a PET-pattern. ICs were determined to be disease relevant if corresponding weights correlated (**p**<0.01) with Florbetapir cortical SUVR or Flortaucipir MTL SUVR (as appropriate) or if corresponding weights exhibited a significant diagnostic-group effect (ANOVA,**p**<0.01). ICs were also required to exhibit significant spatial correlation (**p**<0.05) between the PET and FC-patterns.

Results: One FC-Florbetapir (Figure1) and one FC-Flortaucipir IC (Figure2) met required criteria. FC-Florbetapir IC weight and FC-Flortaucipir IC weights were positively correlated with cortical SUVR (correlation coefficient; Corr=0.78) and MTL SUVR (Corr=0.33), respectively. The FC-patterns of the ICs correlated 0.76, while the PET-patterns of the ICs correlated 0.48. Both FC-patterns resembled canonical resting-state networks (Yeo cortical networks plus subcortical and cerebellar networks).

Conclusions: Amyloid and tau deposition exhibit similar relationships with FC. However, the correlation between FC-Florbetapir IC weights and amyloid deposition was stronger than the correlation with FC-Flortaucipir IC weights and tau deposition. These results suggest a prominent role of amyloid deposition on functional connectivity.

	Cognitively Normal (CN, *n* = 27)	Cognitively Impaired (CI, *n* = 6)	*p*-value
Age years mean (SD)	69.8 (6.1)	73.7 (12.7)	0.26
# Female N (%)	17 (62.9%)	1 (20%)	< 0.05
# Florbetapir Positive N (%)	5 (18.5%)	5 (83.3%)	< 0.01
Florbetapir Cortical SUVR Mean (SD)	1.08 (0.10)	1.37 (0.26)	< 0.0001
Flortaucipir MTL SUVR Mean (SD)	1.14 (0.11)	1.43 (0.09)	< 0.0000001

Table1. Participant Information.

FC-Florbetapir hybrid IC

A. Corr = 0.78 , p < 0.001

B.

C. Corr = -0.33, p < 0.01

D. Corr = -0.38, p < 0.01

E. Florbetapir pattern - RSN Order

F. FC pattern - RSN Order
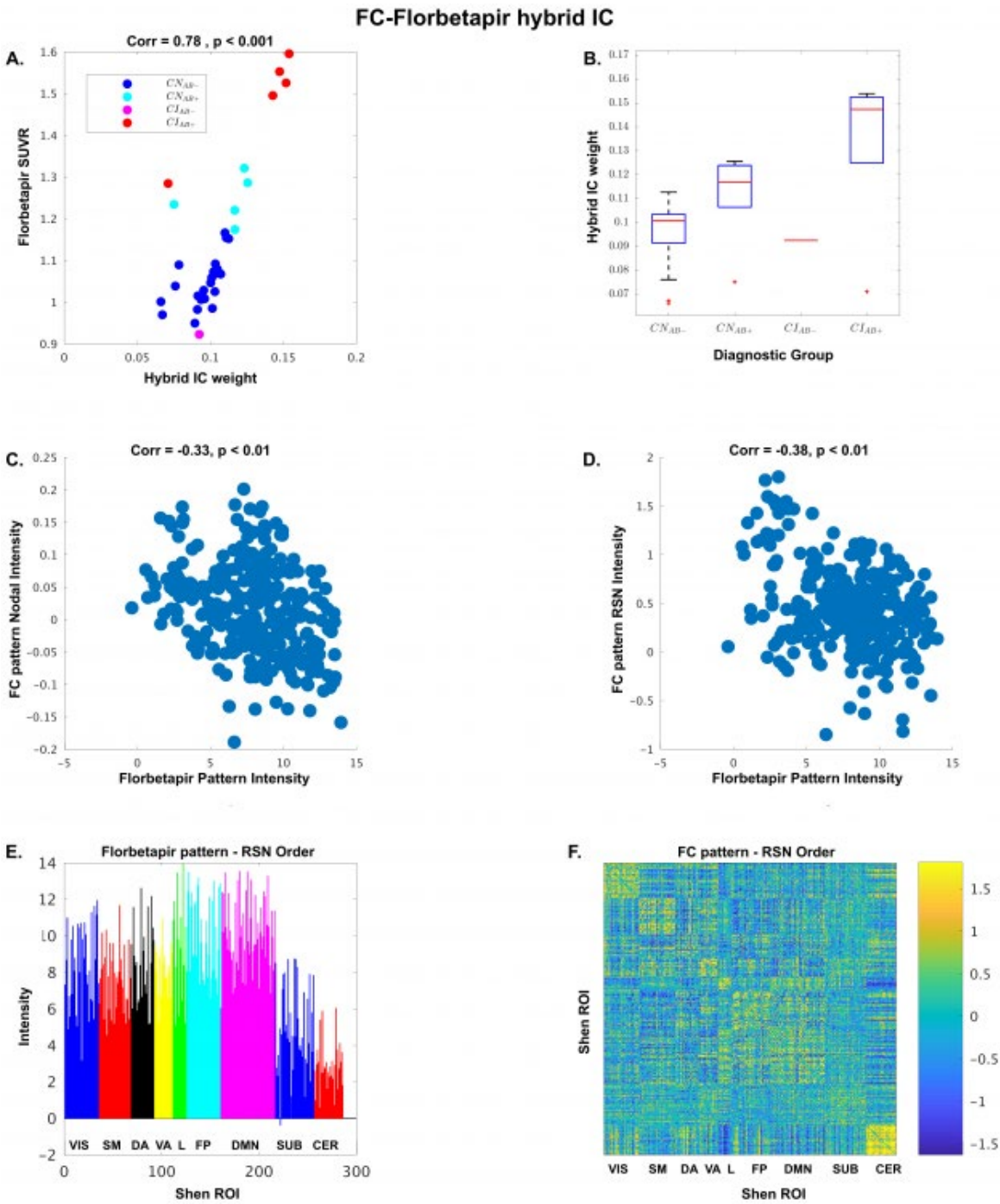
Figure1: FC-Florbetapir IC
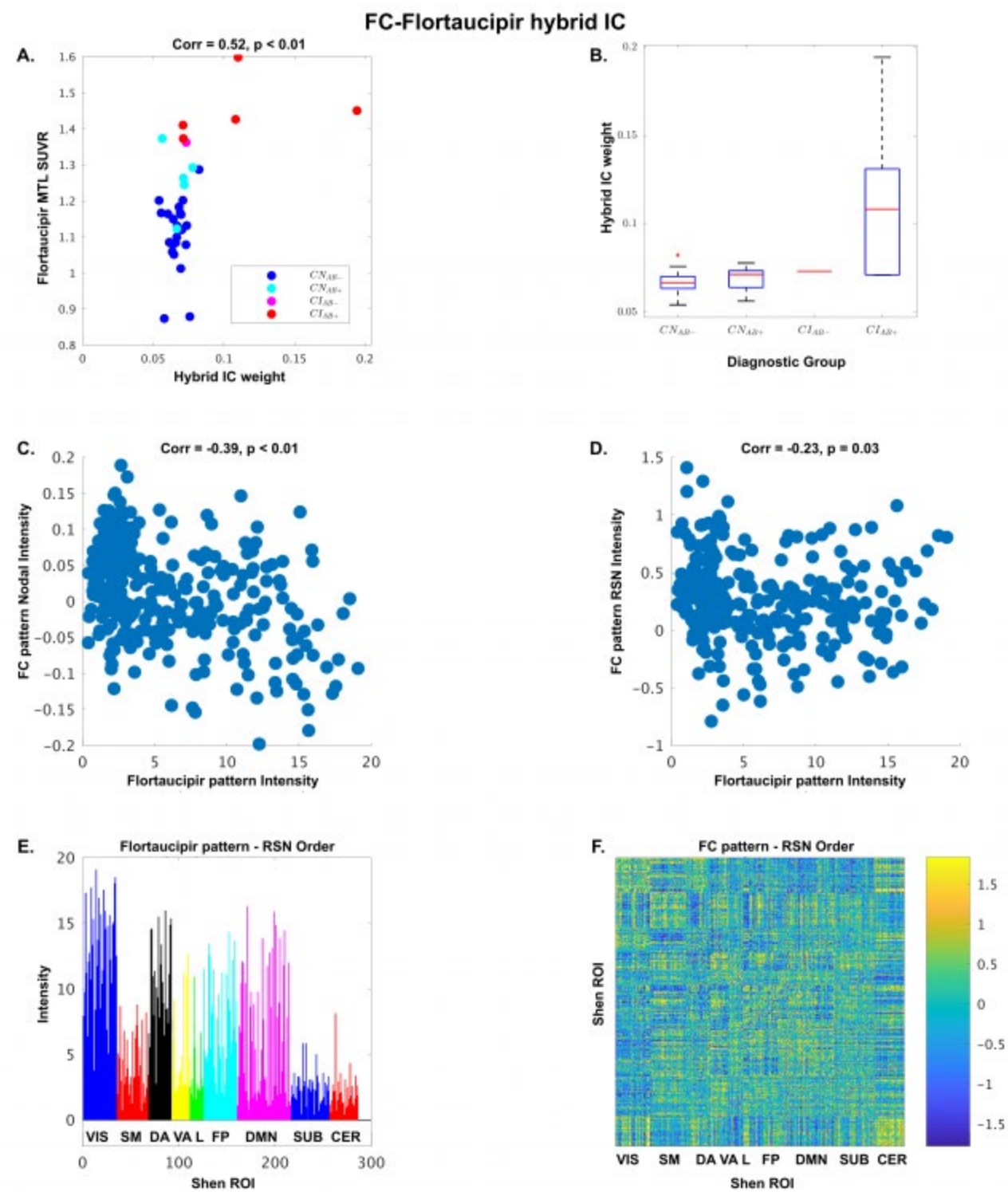
Figure2: FC-Flortaucipir IC

P45: Joint reconstruction method for longitudinal Tau-PET imaging

Amal Tiss[1,2], Yoann Petibon[2,3], Jinsong Ouyang[2,3], Alvin Ihsani[4], Aurélie Kas[1,5], Marie-Odile Habert[1,5], Keith Johnson[2,3,6], <u>Georges El Fakhri</u>[2,3]

[1]*Université Sorbonne, UMR_S 1146, UMR 7371, Laboratoire d'Imagerie Biomédicale (LIB), Paris, France*
[2]*Gordon Center for Medical Imaging, Department of Radiology, Massachusetts General Hospital, Boston, MA, US*
[3]*Department of Radiology, Harvard Medical School, Boston, MA, US*
[4]*NVIDIA, Westford, MA, US*
[5]*AP-HP, Department of Nuclear Medicine, Groupe hospitalier Pitié-Salpêtrière, Paris, France*
[6]*Department of Neurology, Massachusetts General Hospital, Harvard Medical School, Boston, MA, US*

The appearance of excessive amounts of the paired helical filament (PHF) Tau protein has been linked to the process of cognitive decline seen in dementia caused by Alzheimer's disease (AD). The tracer [^{18}F] AV-1451 used in Positron Emission Tomography (PET) permits the observation of the distribution of PHF-Tau in vivo. To determine the rate of Tau deposition in the brain, the conventional approach involves scanning the subject at least two times (between 2-3 years apart) and reconstructing the images separately. The difference image is used to derive region-specific rates of accumulation that are statistically analyzed to find significant differences. However, the difference image suffers from an increased intensity variation making this approach inadequate for analysis of Tau in very early AD.

We propose a joint longitudinal image reconstruction where the Tau deposition difference image is reconstructed directly from the sinograms' measurements leading to a lower intensity variation. This approach introduces a linear temporal dependency and accounts for spatial alignment, and the different injected doses.

We validated the reconstruction method by using phantom data and by inserting simulated lesions in real data at different intensity levels. We computed the sensitivity index in images reconstructed separately and jointly. As expected, the index is higher for the joint reconstruction, especially for lower lesion contrast (over 30% higher for lesions inserted with 3% contrast).

We additionally reconstructed the data from 12 subjects using both methods. We then measured the mean and the standard deviation of the ΔSUVR in different brain regions. The coefficient of variation was systematically lower with our proposed method averaging 90% against 227% for the conventional method.

Our proposed joint longitudinal reconstruction method paves the way for shorter inter-scan time and smaller sample size for hypothesis testing on progression of AD-related Tauopathy thanks to its higher sensitivity and lower intensity variation.

Keywords: *longitudinal PET reconstruction, dual PET reconstruction, Tau Imaging*

P46: Associations between quantitative susceptibility mapping and measures of amyloid and tau in patients with Alzheimer's disease

Suzanne Baker[1], Renaud La Joie[2], Chunlei Liu[3], Yann Cobigo[2], Viktoriya Bourakova[2], Theresa Harrison[3], Gil Rabinovici[2], William Jagust[1,3]

[1]*Lawrence Berkeley National Laboratory, Berkeley, CA, US*
[2]*University of California, San Francisco, San Francisco, CA, US*
[3]*University of California, Berkeley, Berkeley, CA, US*

Introduction: Iron accumulation in the brain has been associated with neurodegeneration, neuritic plaques and neurofibrillary tangles. MRI quantitative susceptibility mapping (QSM) has the potential to measure iron in vivo. We explored the relationship between QSM, amyloid, and tau.

Methods: 20 subjects (7M/5F healthy controls (HC) age 52-69, 3M/5F AD patients age 50-67) underwent QSM-MRIs on a 3T Siemens Trio scanner at UCSF (TR=44ms, 8 echoes, TE=4ms, echo spacing=5ms, flip angle=15°). QSM reconstruction was performed in STI Suite V3.0; white matter, whole cortex and lateral and inferior lateral ventricles were explored as possible reference regions. AD subjects underwent 0-90min PIB scans, and 80-100min Flortaucipir scans. DVR (35-90min) with cerebellar gray reference region was used to quantify amyloid, SUVR with inferior cerebellar gray reference region for tau. A voxelwise comparison was performed between QSM in healthy controls and ADs in template space. Correlations between QSM/PIB and QSM/Flortaucipir were done using freesurfer-defined ROIs in native space.

Results: A significant difference ($p<0.001$, uncorrected) for AD>HC QSM was found in bilateral amygdala, hippocampus, anterior cingulate, pallidum, thalamus, substantia nigra and dentate nucleus. QSM reference region had minimal impact on these results. Positive correlations within AD patients between QSM versus Flortaucipir and QSM versus PIB can be seen in figure 1. Although correlations between QSM and Flortaucipir were more abundant, these correlations were dependent on use of inferior and lateral ventricles as reference region for QSM and diminished when white matter or whole cortex were used as reference region. PIB correlations did not increase with different QSM reference regions.

Conclusion: QSM more highly correlates with Flortaucipir than PIB, however this is highly dependent on QSM reference region and warrants further investigation.

Figure 1

Correlation between QSM and Flortaucipir in AD subjects
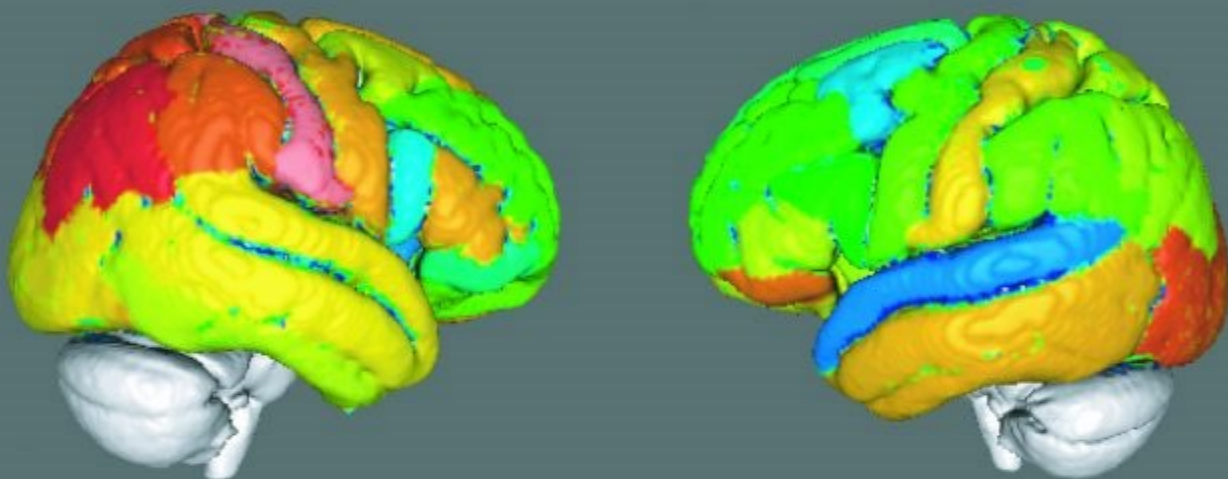
Correlation between QSM and PIB in AD subjects
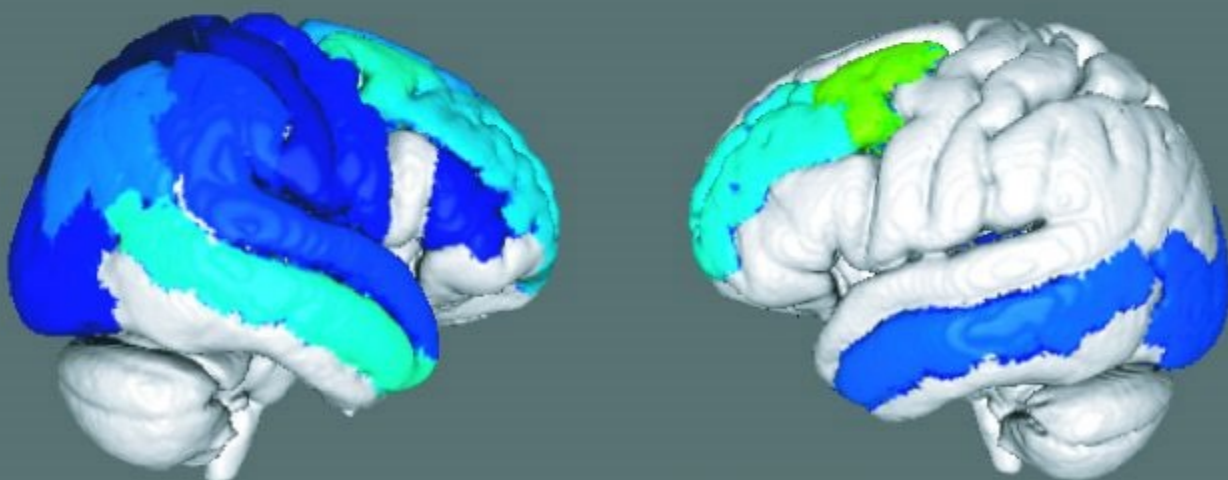
Keywords: *QSM Iron tau amyloid*

P47: The relationship between Aβ-related hippocampal activity and metabolism in impaired individuals

Matthew Scott[1], Bernard Hanseeuw[2,8], Willem Huijbers[1,7], Olivia Hampton[1], Lyssa Manning[1], Jasmeer Chhatwal[1], Rachel Buckley[1,4,5,6], Keith Johnson[2], Reisa Sperling[3,4], Aaron Schultz[1]

[1]*Department of Neurology, Massachusetts General Hospital, Harvard Medical School, Boston, MA, US*
[2]*Department of Radiology, Massachusetts General Hospital, Harvard Medical School, Boston, MA, US*
[3]*Department of Neurology, Brigham and Women's Hospital, Harvard Medical School, Boston, MA, US*
[4]*Center for Alzheimer Research and Treatment, Brigham and Women's Hospital, Harvard Medical School, Boston, MA, US*
[5]*Florey Institute of Neuroscience and Mental Health, Melbourne, Australia*
[6]*Melbourne School of Psychological Sciences, University of Melbourne, Melbourne, Australia*
[7]*Jheronimus Academy of Data Science, Department of Cognitive Science and Artificial Intelligence, Tilburg University, Tilburg, The Netherlands*
[8]*Cliniques Universitaires Saint-Luc, Brussels, Belgium*

Introduction: We have documented both Aβ associated hippocampal hyper-activity and hypo-metabolism in overlapping cohorts of individuals with MCI. Here, we investigate whether these sources of hippocampal information reflect a unified source of Aβ related variance or independent effects of the AD pathological cascade. Using hippocampal activity (HA), metabolism (HM), and volume (HV) imaging data from individuals with a range of impairment, we explore the connection amongst these markers of hippocampal integrity in relation to Aβ.

Methods: Forty-three participants underwent FDG-PET, PiB-PET, structural MRI, and functional MRI. Impairment classification included a mean CDR threshold ≥ 0.4 over three years. Linear and logistic regression models as well as partial correlations were computed to explore the relationships amongst HA, HM, HV, and dichotomous Aβ.

Results: Models and statistical results are shown in table 2. Without an Aβ covariate, HA did not have a significant relationship with either HM or HV (r=-0.195, **p**=.223; r=-0.192, **p**=.230 respectively). However, HM and HV had a significant, positive association (r=0.351, **p**=.024). Aβ positivity was found to be significantly related to HA, HM, and HV (β=0.807 **p**=.008; β=-0.988, **p**=.001; β=-0.849, **p**=.003). With all three measures predicting Aβ, HM and HV showed the strongest effects (β=-1.337, **p**=.021; β=-1.102, **p**=.048) followed by a marginal effect of HA (β=0.887, **p**=.077).

Conclusion: All three hippocampal measures showed associations with Aβ, although the effect of HA on Aβ was independent of both HM and HV. These findings are consistent with a selective sensitivity of fMRI to potential excitotoxic Aβ effects that is independent of and not dependent on background metabolic activity. While there is no direct evidence of excitotoxicity relative to other explanations such as compensatory mechanisms, our findings demonstrate that fMRI can detect a unique source of Aβ variance. Further investigation is warranted into the mechanistic relationship between Aβ and hippocampal activity.

Age *(SD)*	72.56 *(7.76)*
% Female	32.56
CDR *(SD)*	0.52 *(0.11)*
MMSE *(SD)*	27.09 *(2.20)*
% Aβ+	48.84
N	43

Table 1. Demographic Information

Aβ status was determined using a PiB DVR threshold of 1.186; CDR = Clinical Dementia Rating; MMSE = Mini-Mental State Examination

Table 2. Models and statistical output

	Correlated measures:		
	Activity	Metabolism	Volume
Activity		$r = -0.195$ $p = .223$	$r = -0.192$ $p = .230$
Metabolism	$r = -0.195$ $p = .223$		$r = 0.351$ $p = .024^*$
Volume	$r = -0.192$ $p = .230$	$r = 0.351$ $p = .024^*$	

	Dependent variables:		
	Activity	Metabolism	Volume
Aβ+	$\beta = 0.807$ $p = .008^{**}$	$\beta = -0.988$ $p < .001^{***}$	$\beta = -0.849$ $p = .003^{**}$

	Dependent variable:			
	Aβ	Aβ	Aβ	Aβ
Activity	$\beta = 0.970$ $p = .040^*$		$\beta = 0.937$ $p = .048^*$	$\beta = 0.887$ $p = .077^{\#}$
Volume	$\beta = -1.093$ $p = .017^*$	$\beta = -1.162$ $p = .024^*$		$\beta = -1.102$ $p = .048^*$
Metabolism		$\beta = -1.396$ $p = .010^*$	$\beta = -1.324$ $p = .001^{**}$	$\beta = -1.337$ $p = .021^*$

Key:	$^{\#}p<0.1$; $^*p<0.05$; $^{**}p<0.01$; $^{***}p<0.001$

Three sets of models are presented above. First, partial correlation coefficients and *p*-values amongst HA, HM, and HV are presented. Next, beta-estimates and *p*-values of linear regression models using dichotomous Aβ to predict HA, HV, and HM are shown. Lastly, combinations of HA, HV, and HM are used to determine dichotomous Aβ using logistic regression. In all models, age and sex were used as covariates.

P48: Centiloid scale in practice: effect of different SUVR reference regions and comparison of Centiloid cut-offs

Kate Adamczuk[1], Mehul Sampat[1], Maureen Runkle[2], Beth Gorman[2], Joyce Suhy[1], David Scott[1]

[1]Bioclinica, Newark, CA, US
[2]Bioclinica, Philadelphia, PA, US

Background: Centiloid (CL) conversion aligns amyloid PET measures across tracers[1]. A CL pipeline converts PET measures to their PiB equivalent and linearly transforms onto a scale anchored by calibrated means of young controls (YC) and Alzheimer's disease (AD) subjects. We evaluated the impact of reference region and compared positivity cut-offs for FDA-approved amyloid tracers.

Methods: Calibration datasets were processed via Bioclinica (BC) SUVR method with whole-cerebellum (WC) and subcortical white matter (SWM) reference regions. FreeSurfer MRI segmentation was used to calculate SUVR from co-registered, motion-corrected, averaged, smoothed PET. Correlation coefficient (R^2) from linear regression between published SUVR and BC-SUVR was used to evaluate reliability. If R^2 was >0.7, BC-method was considered well-correlated and linear regression between BC-SUVR and published CL was used. SOT-SUVR[2,3] cut-offs were converted to CLs and compared against 3 SD above YC CL mean.

Results: Standard and BC-SUVRs strongly correlated for WC. (Florbetapir R²=0.96, Florbetaben R²=0.98, Flutemetamol R²=0.98). SWM yielded weaker correlations that still met the reliability criterion (Florbetapir R²=0.72, Florbetaben R²=0.88, Flutemetamol R²=0.91).

Mean WC-CL in YC was 0.4±9.8 for Florbetapir, -2.0±5.4 for Florbetaben, and -1.6±7.4 for Flutemetamol versus published CL values of 1.8±10.8 for Florbetapir, -0.3±6.8 for Florbetaben, and -1.0±7.2 for Flutemetamol, yielding variance ratios of 0.91, 0.79, and 1.03, respectively. Mean WC-CL in AD was 53.7±51.7 for Florbetapir, 68.1±54.2 for Florbetaben, and 51.2±49.4 for Flutemetamol.

SOT-SUVR cut-off of 1.11[2] for Florbetapir converted to 25 CL, Florbetaben 1.45[3] converted to 62 CL, and Flutemetamol 1.20[2] converted to 37 CL. 3 SD above YC CL mean suggested cut-offs of 30 for Florbetapir, 14 for Florbetaben, and 21 for Flutemetamol.

Conclusion: Positivity cut-offs differ among tracers even after CL conversion.

References

1. Klunk et al., Alzheimers Dement 2015
2. Landau et al., Eur J Nucl Med Mol Imaging 2014
3. Sabri et al., Clin Transl Imaging 2015

Keywords: *Centiloid, SUVR, white matter, cerebellum, cut-off*

P49: Amyloid-beta imaging in glial cells

Krupal Jethava[1], Priya Prakash[1], Gaurav Chopra[1,2]

[1]*Department of Chemistry, Purdue University, West Lafayette, IN, US*
[2]*Purdue Institute for Integrative Neuroscience, Purdue University, West Lafayette, IN, US*

Introduction: Amyloid-β (Aβ) and α-synuclein (aSyn) accumulation are one of the pathological markers of neurodegenerative diseases so understanding and/or imaging deposition of these toxic protein fragments and its degradation became a central focus in the neuroscience. In this regard, the actions of resident macrophages of the central nervous system called microglia have a critical role to play in phagocytosis of protein debris. But, the specificity of microglial phagocytosis towards aSyn and Aβ peptides and the mechanisms involved are currently not known mainly due to lack of available tools. Available tools are not pH-responsive, so they suffer from some disadvantages. Thus, there is a need for some advanced tools for Aβ imaging and to investigate real-time Aβ phagocytosis that would enhance the understanding in the AD.

Methods: We have developed a novel imaging tool i.e. pH-dependent fluorescent conjugates of aSyn and Aβ peptides that are non-fluorescent outside or inside the cells in the physiological pH of ~7.4 but only fluoresce brightly within the acidic intracellular phagosomal organelles of the cells. We have also developed pH-responsive Near Infrared (NIR) dye conjugate with Aβ for **in vivo** imaging. Additionally, we have developed pH-responsive alpha-synuclein conjugate (monomer/fibril) and characterized by spectroscopic methods.

Results: The functionality of the pH-dependent a
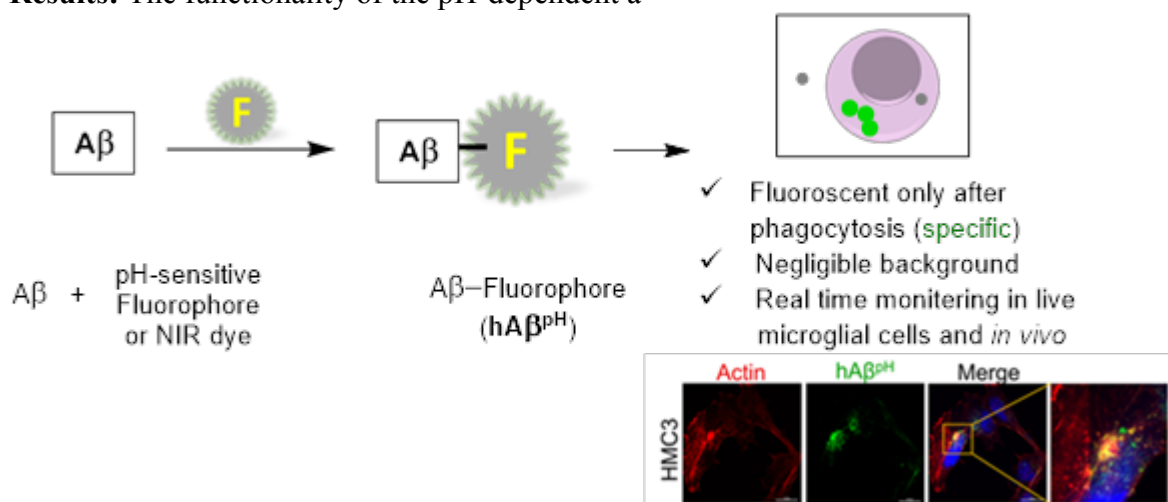
Syn and Aβ sensors has been demonstrated in murine BV2, N9 cells, human HMC3 cells, and primary rodent microglial cells under inflammatory conditions. The ability of phagocytic or non-phagocytic microglia to internalize hAβpH was observed by live cell imaging instrument. The difference in nature between phagocytic and non-phagocytic microglial cells suggesting that our hAβpH reporter would be useful to investigate the phenotypic difference in those cells and could open-up new avenue in the in Aβ imaging and understand neurodegenerative diseases.

Keywords: *Amyloid-beta, alpha-synuclein, Microglial phagocytosis, neurodegenerative diseases*

P50: Preliminary longitudinal evaluation of the novel tau tracer [18F]MK-6240

Tharick Pascoal[1], Mira Chamoun, Min Su Kang, Sulantha Mathotaarachchi, Andréa Benedet, Joseph Therriault, Jean-Paul Souvy, Serge Gauthier, Pedro Rosa-Neto

[1]*McGill University, Montreal, QC, Canada*

Objective: To assess region-of-interest and voxel-wise longitudinal changes and the utility for clinical trials of the novel neurofibrillary tangles' tracer [^{18}F]MK-6240.

Methods: Nineteen individuals (10 cognitively unimpaired (CU) and 9 cognitively impaired (CI)) underwent positron emission tomography (PET) [^{18}F]AZD4694 at baseline and [^{18}F]MK-6240 at baseline and 1-year follow-up. [^{18}F]AZD4694 and [^{18}F]MK-6240 standardized uptake value ratios (SUVRs) used the cerebellum grey matter as the reference region and were calculated between 40 to 70 min and 90 to 110 min post-injection, respectively. Paired t-test assessed the differences between baseline and follow-up bindings. Sample size and voxel-wise (new method) sample size calculations were performed.

Results: All CI and 1 CU were amyloid positive. In CI, there was no significant increase in [^{18}F]MK-6240 uptake over 1 year. In CU, we found a significant increase in [^{18}F]MK-6240 uptake in clusters in the posterior cingulate, parietal, and frontal cortices (Fig. 1). We did not find significant correlations between baseline [^{18}F]AZD4694 and [^{18}F]MK-6240 changes. In CU, we found that a clinical trial would require approximately 260 individuals per arm to test a 25% drug effect on [^{18}F]MK-6240 accumulation (Fig. 2). Voxel-wise sample size calculation avoided sample size overestimation by removing the bias imposed by traditionally anatomically defined regions-of-interest within specific brain regions (Fig. 3).

Figure 1

[^{18}F]MK-6240 ACCUMULATION OVER 12-MONTH IN CN INDIVIDUALS

Baseline SUVR   Increase SUVR   Paired t-test

CN

MCI/AD

SUVR 0 — 4   Δ SUVR 0.05 — 0.3   t value -10 — -2
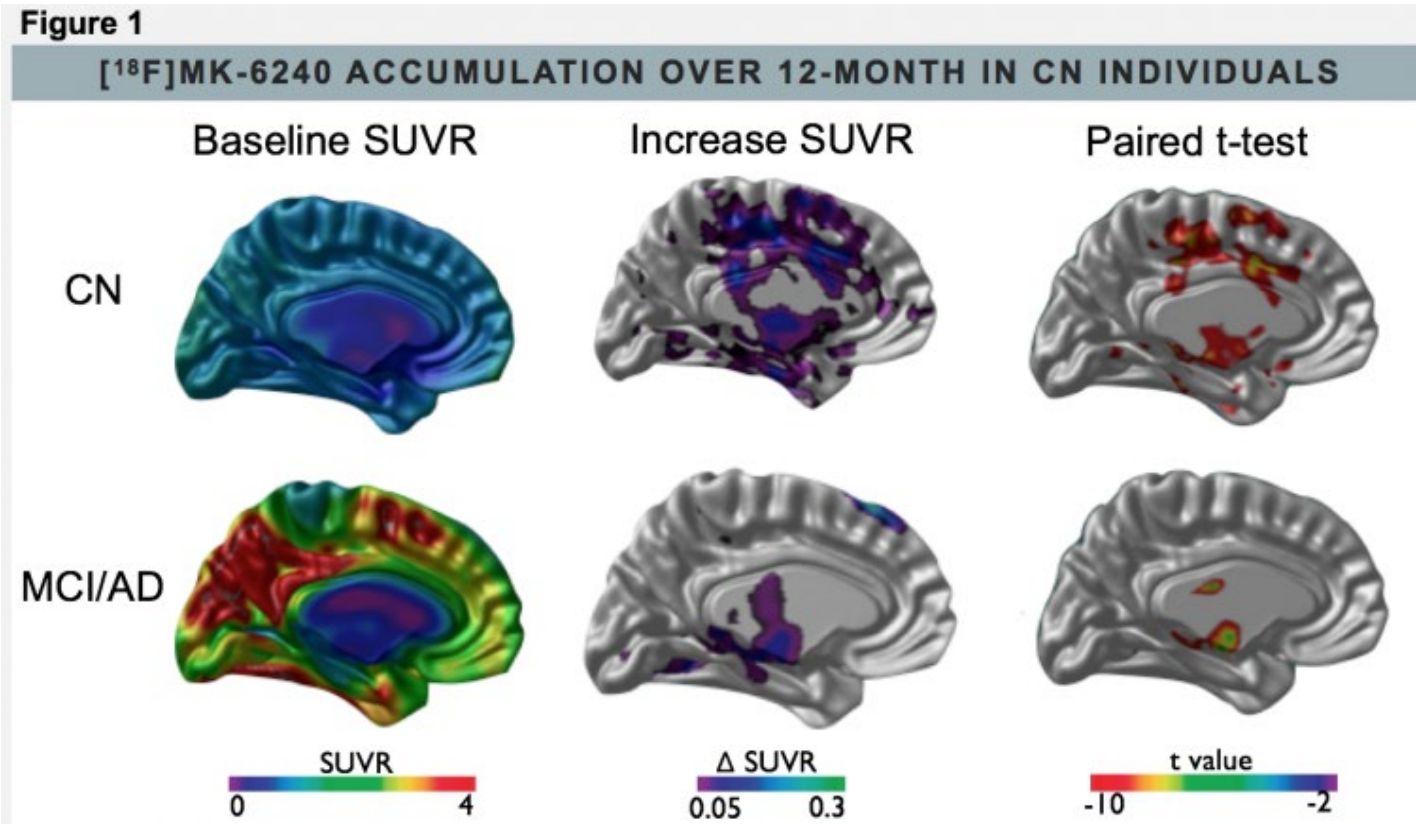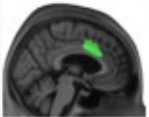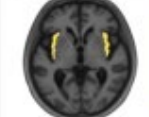
Figure 2

STANDARD ANATOMICAL ROI-BASED SAMPLE SIZE CALCULATION

Region	Power	Drug effect	Significance	Sample by arm
ACC	80%	25%	0.05	260
Frontal	80%	25%	0.05	1001
Insula	80%	25%	0.05	1120
Hippocampus	80%	25%	0.05	3594

Figure 3

VOXEL-WISE POWER CALCULATION

Sample size needed in the cluster -> n = 100 by arm

Sample size by study arm
80 — 500

Sample size needed in the cluster -> n = 250 by arm

Power = 80%

Power = 95%

Hypothesized drug effect = 25%; Significance level = 0.05
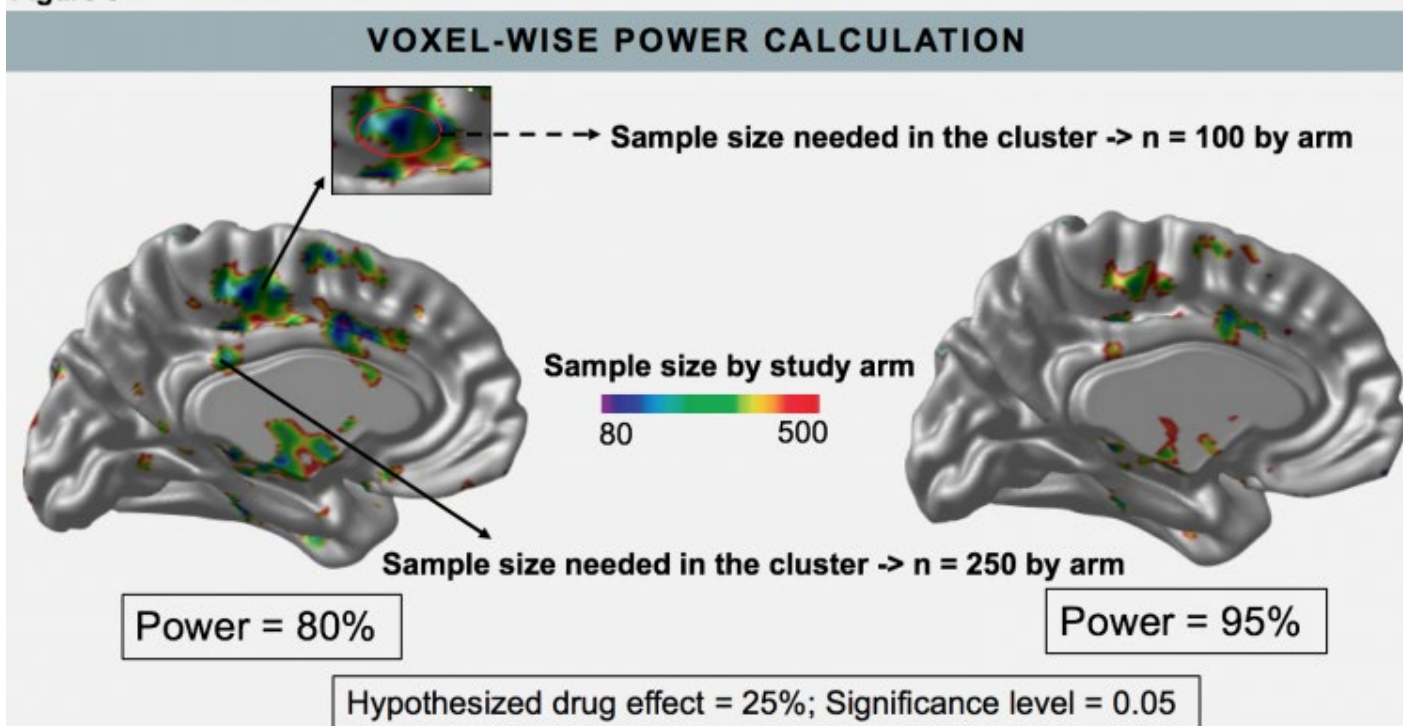
Conclusions: In this preliminary analysis, our results highlight [18F]MK-6240 as a valuable tool for testing the effects of disease-modifying interventions on tau accumulation in presymptomatic individuals predominantly amyloid negative. [18F]MK-6240 accumulation did not associate with baseline amyloid load (subthreshold). Voxel-wise sample size calculation has the potential to significantly increase the statistical power of clinical trials designed to use voxel-based outcomes.

P51: NODDI modeling reveals neurite orientation and dispersion differences in white matter tracts of beta-amyloid positive individuals

Jack Hunt[1,6,7], Nicholas Vogt[1,6,8], Douglas Dean, III[2], Tobey Betthauser[1], Bradley Christian[2,4], Sterling Johnson[1,2,3,5], Andrew Alexander[2,4], Barbara Bendlin[1,2,3]

[1]*Wisconsin Alzheimer's Disease Research Center, Madison, WI, US*
[2]*Waisman Center, Madison, WI, US*
[3]*Wisconsin Alzheimer's Institute, Madison, WI, US*
[4]*University of Wisconsin Department of Medical Physics, Madison, WI, US*
[5]*Geriatric Research Education and Clinical Center, William S. Middleton Veterans Hospital, Madison, WI, US*
[6]*University of Wisconsin Medical Scientist Training Program, Madison, WI, US*
[7]*University of Wisconsin Program in Cellular and Molecular Biology, Madison, WI, US*
[8]*University of Wisconsin Neuroscience Training Program, Madison, WI, US*

Background: Disruption of white matter microstructure (WMM) is an early pathological change in Alzheimer's disease (AD). However, the association between b-amyloid (Ab) accumulation and disrupted WMM is not fully understood. Advances in modelling complex diffusion in white matter tracts (WMTs) are expected to provide new information about neural injury associated with Ab accumulation. This study incorporated measures derived from the Neurite Orientation Dispersion and Density Imaging (NODDI) model to more specifically characterize WMM in Ab+ individuals.

Methods: 187 subjects (164 cognitively normal, 15 MCI, 8 AD) were included in the present study. Participants underwent multi-shell diffusion-weighted MRI and [^{11}C]PiB PET imaging. WMM measures were determined with NODDI (orientation dispersion index, ODI; neurite density index, NDI) or DTI (fractional anisotropy, FA; mean diffusivity, MD) modelling. Ab status was determined by averaging [^{11}C]PiB DVR across 8 cortical regions with a threshold of >1.19 for amyloid positivity as previously described (Johnson , etal. 2014). Probability-weighted average DWI metrics for WMTs were extracted using the JHU white matter tractography atlas. Linear fixed-effects models were employed including age, sex, and time between DWI and PET imaging as covariates.

Results: Ab positivity was significantly associated with decreased ODI in several WMTs (Table 1, Figure 1) and with increased MD in two of the same tracts (Table 2). No significant associations with NDI or FA were observed.

Conclusion: Using [^{11}C]PiB PET and NODDI, we interrogated the relationship between Ab and WMM. Amyloid positivity was most consistently associated with lower ODI in WMTs compared with other DWI metrics. Altered ODI may indicate decreased neurite complexity or, tentatively, gliosis and may represent a sensitive measure of amyloid-related axonal pathology. Further studies are needed to determine the temporal staging of neural degeneration in AD pathogenesis.

Table 1. Summary of linear regression model coefficient estimates and standard errors for NODDI metrics

	NDI SLFP	ODI SLFP	NDI SLFT	ODI SLFT	NDI CCG	ODI CCG	NDI CHB	ODI CHB	NDI ILF	ODI ILF	NDI UF	ODI UF
Amyloid Positive	-0.133	-0.420*	-0.170	-0.425*	-0.183	-0.460**	-0.237	-0.009	-0.302#	-0.715**	-0.089	-0.087
	(0.157)	(0.164)	(0.156)	(0.164)	(0.151)	(0.165)	(0.157)	(0.159)	(0.155)	(0.159)	(0.153)	(0.169)
Observations	188	188	188	188	188	188	188	188	188	188	188	188
R^2	0.149	0.071	0.157	0.074	0.217	0.062	0.151	0.133	0.173	0.133	0.196	0.019
Adjusted R^2	0.126	0.046	0.134	0.048	0.195	0.037	0.128	0.109	0.151	0.109	0.174	-0.008
Residual Std. Error (df = 182)	0.935	0.977	0.931	0.976	0.897	0.982	0.934	0.944	0.922	0.944	0.909	1.004

Notes:
# $p < 0.1$; * $p < 0.05$; ** $p < 0.01$; p-values are uncorrected for multiple comparisons
All models control for age, sex, time between DWI and PET measurements and DWI scanner
ODI, Orientation Dispersion Index; NDI, Neurite Density Index
SLFP, Superior Longitudinal Fasciculus - Parietal; SLFT, Superior Longitudinal Fasciculus - Temporal;
CCG, Cingulum Bundle - Cingulum Portion; CHB, Cingulum Bundle - Hippocampal Portion;
ILF, Inferior Longitudinal Fasciculus; UF, Uncinate Fasciculus
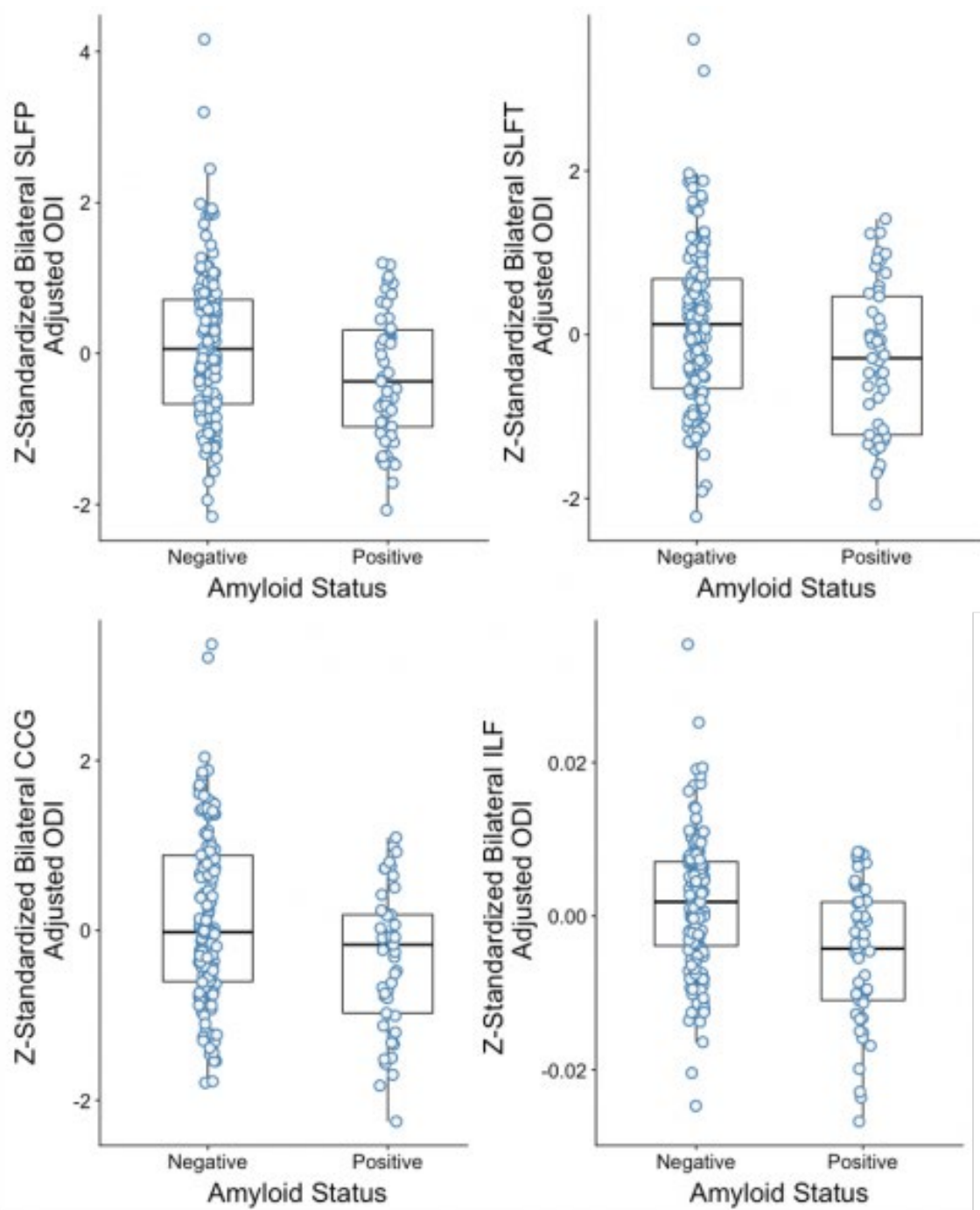
Figure 1. Significant association between amyloid status and NODDI metrics in white matter tracts of interest. Significantly decreased orientation dispersion index (ODI) was observed in the parietal and temporal portions of the superior longitudinal fasciculus (SLFP, SLFT), the cingulate portion of the cingulum bundle (CCG) and inferior longitudinal fasciculus (ILF) are shown here. White matter microstructure measures are Z-normalized and adjusted for age, sex, DWI scanner and time between PET and DWI scans.

Table 2. Summary of linear regression model Z-standarized coefficient estimates and standard errors for DTI metrics

	FA SLFP	MD SLFP	FA SLFT	MD SLFT	FA CCG	MD CCG	FA CHB	MD CHB	FA ILF	MD ILF	FA UF	MD UF
Amyloid Positive	0.103	0.162	0.087	0.237	0.068	0.292*	-0.083	0.196	0.113	0.398**	-0.002	0.008
	(0.156)	(0.145)	(0.158)	(0.148)	(0.154)	(0.144)	(0.152)	(0.143)	(0.155)	(0.141)	(0.004)	(0.005)
Observations	188	188	188	188	188	188	188	188	188	188	188	188
R^2	0.158	0.277	0.143	0.243	0.180	0.286	0.202	0.299	0.170	0.316	0.182	0.372
Adjusted R^2	0.135	0.257	0.119	0.222	0.157	0.267	0.180	0.280	0.147	0.298	0.160	0.355
Residual Std. Error (df = 182)	0.930	0.862	0.938	0.882	0.918	0.856	0.905	0.849	0.923	0.838	0.021	0.030

Notes:
# $p < 0.1$; * $p < 0.05$; ** $p < 0.01$; p-values are uncorrected for multiple comparisons
All models control for age, sex, time between DWI and PET measurements and DWI scanner
FA, Fractional Anisotropy; MD, Mean Diffusivity
SLFP, Superior Longitudinal Fasciculus - Parietal; SLFT, Superior Longitudinal Fasciculus - Temporal;
CCG, Cingulum Bundle - Cingulum Portion; CHB, Cingulum Bundle - Hippocampal Portion;
ILF, Inferior Longitudinal Fasciculus; UF, Uncinate Fasciculus

Wednesday, January 16, 2019 - 03:30 pm - 05:15 pm

Podium Session

Session 2: Methods

CHAIRS: Robert Koeppe, Mark Lubberink

03:30 pm - 05:15 pm	Session 2: Methods	CHAIRS: **Robert Koeppe**, University of Michigan Medical School, Ann Arbor, MI, US **Mark Lubberink**, Uppsala University, Uppsala, Sweden	Page
3:30	Variability of uptake in potential reference regions for longitudinal flortaucipir-PET analysis	**Jungho Cha**, University of California, San Francisco, San Francisco, CA, US	159
3:45	Test-retest repeatability of [18F]Flortaucipir PET in Alzheimer's disease and controls	**Tessa Timmers**, Amsterdam UMC, Amsterdam, The Netherlands	163
4:00	AmyloidIQ demonstrates increased power in longitudinal Amyloid PET studies	**Alex Whittington**, Invicro, Boston, MA, US	166
4:15	Regionalized spatial association between PiB and FTP PET assessed via variography	**Tobias Estime**, Massachusetts General Hospital, Boston, MA, US	168
4:30	Evaluation of the Centiloid scale for use in multi-amyloid PET tracer, multi-center trials	**Jacob Hesterman**, Invicro, Boston, MA, US	170
4:45	A comparison of partial volume correction techniques for measuring change in Serial AV-1451 Tau PET SUVR	**Christopher Schwarz**, Mayo Clinic, Rochester, MN, US	173
5:00	Detecting the earlier stages of amyloid deposition	**Tengfei Guo**, Helen Wills Neuroscience Institute, University of California, Berkeley, CA, US	177
05:15 pm - 05:45 pm	Discussion		

Variability of uptake in potential reference regions for longitudinal flortaucipir-PET analysis

Jungho Cha[1], Mijin Park[2], Yeong-Hun Park[2], Suzanne Baker[3], Renaud La Joie[1], Viktoriya Bourakova[1], Julie Pham[1], Kiran Chaudhary[1], Laura Fenton[4], Mustafa Janabi[3], James O'Neil[3], Bruce Miller[1], William Jagust[3,4], Jong-Min Lee[2], Gil Rabinovici[1]

[1]*Memory and Aging Center, Department of Neurology, University of California, San Francisco, San Francisco, CA, US*
[2]*Department of Biomedical Engineering, Hanyang University, Seoul, Korea*
[3]*Molecular Biophysics and Integrated Bioimaging, Lawrence Berkeley National Laboratory, Berkeley, CA, US*
[4]*Helen Wills Neuroscience Institute, University of California, Berkeley, Berkeley, CA, US*

Objective: To evaluate the variability of tracer retention in potential reference regions applied to longitudinal flortaucipir (FTP)-PET.

Methods: FTP-PET, and T1-weighted MRI were obtained for 64 participants, including 42 cognitively normal controls (NC, 21 PiB-, and 21 PiB+, (PiB+=global DVR>1.065)), and 22 PiB+ patients with MCI/AD (Table 1). Individual SUV images were generated using FTP-PET 80-100min volumes, injected dose of tracer, and participant weight. We examined 21 ROIs derived from three major regions, including cerebellum, WM, and brainstem (Figure 1). These regions were extracted using Freesurfer and SUIT template. The 20 ROIs were created by evaluating sub-regions, morphological erosions, and different thresholded probabilities of GM or WM. We created a combined criterion by averaging two outcomes to compare the stability of reference region SUVs over time: coefficient of variation (CV), and effect size (Cohen's d). Each outcome was normalized using rank-based scaling. We examined sampling variability of the combined criterion using bootstrap procedures (1000 times), and calculated p-values based on the confidence intervals for the bootstrap difference between the best reference and each reference.

Results: Inferior cerebellum GM with probability thresholded above 0.5 showed the lowest CV (CV%=7.39±0.89, Table 2). Inferior cerebellum GM with 5 times erosion showed the smallest effect size between scans (Cohen's d:-0.07, Table 2). Inferior cerebellum GM with 3 times erosions showed the lowest when combining both outcomes (Figure 2). Although variations of references did not differ significantly from each other, but most WM, whole cerebellum, brainstem regions showed higher variability than cerebellum GM and inferior cerebellum GM (Figure 2).

Conclusions: Inferior cerebellum GM with morphological erosions showed the greatest inter-scan stability in SUV and thus may be suitable as reference regions for longitudinal tau PET analyses.

Table 1. Demographics of subjects.

	Normal Controls (PiB-)	Normal Controls (PiB+)	MCI/AD (PiB+)
n	21	21	22
Age (years)	78.38±5.37	75.95±3.87	64.23±10.3
Sex (m/f)	8/13	7/14	8/14
Education (years)	16.61±1.83	16.33±1.56	17.05±2.06
Years btwn tau scans	1.96±0.62	1.78±0.56	1.29±0.31
PiB DVR at tau TP1	1.02±0.03	1.30±0.23	1.55±0.23

Data are presented as mean±SD.
PiB positivity were classified based on global DVR > 1.065.

Figure 1. 21 Reference regions
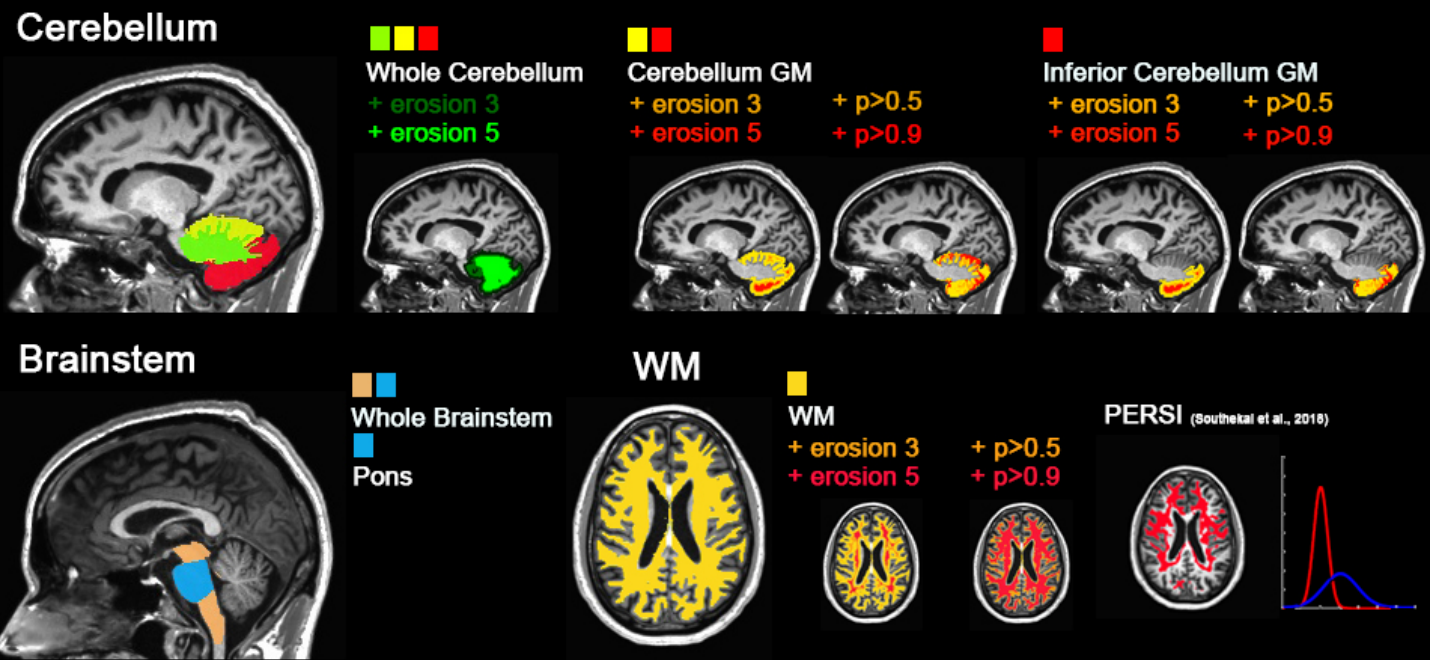
Table 2. Coefficient of variance (%) and effect size of differences in SUVs between scans in ROIs.

Reference regions	CV	Cohen's d
Whole Cerebellum	7.52±0.88	-0.14
Whole Cerebellum with erosion 3	7.71±0.88	-0.12
Whole Cerebellum with erosion 5	7.80±0.87	-0.12
Cerebellum GM	7.48±0.88	-0.13
Cerebellum GM with erosion 3	7.73±0.88	-0.10
Cerebellum GM with erosion 5	7.93±0.88	-0.08
Cerebellum GM (p>0.5)	7.41±0.88	-0.13
Cerebellum GM (p>0.9)	7.42±0.87	-0.13
Inf Cerebellum GM	7.51±0.88	-0.13
Inf Cerebellum GM with erosion 3	7.74±0.88	-0.09
Inf Cerebellum GM with erosion 5	7.90±0.87	**-0.07**
Inf Cerebellum GM (p>0.5)	**7.39±0.89**	-0.15
Inf Cerebellum GM (p>0.9)	7.41±0.88	-0.16
WM	7.88±0.91	-0.10
WM with erosion 3	7.99±0.93	-0.17
WM with erosion 5	8.07±0.97	-0.22
WM (p>0.5)	7.85±0.90	-0.09
WM (p>0.9)	7.82±0.90	-0.12
PERSI	7.75±0.90	-0.14
Brainstem	7.75±0.89	-0.20
Pons	7.85±0.88	-0.18

Data are presented as mean±SE.
Bold values were the lowest value of variance in each measure

Figure 2. Combined criterion are shown with their 83% confidence intervals using 1000 bootstrapping. The right column showed p-values using confidence intervals for the bootstrap differences between the best reference and each ROI

ROIs	Sum of weighted scores (83% CIs)	p value
Inf Cerebellum GM with erosion 3		NA
Cerebellum GM with erosion 3		0.572
Cerebellum GM (p>0.9)		0.733
Inf Cerebellum GM		0.54
Cerebellum GM (p>0.5)		0.367
Whole Cerebellum with erosion 3		0.391
Inf Cerebellum GM (p>0.5)		0.642
Cerebellum GM		0.599
WM (p>0.5)		0.394
Inf Cerebellum GM (p>0.9)		0.318
Inf Cerebellum GM with erosion 5		0.296
Cerebellum GM with erosion 5		0.116
WM (p>0.9)		0.336
Whole Cerebellum		0.362
Whole Cerebellum with erosion 5		0.254
WM		0.313
PERSI (Southekal et al., 2018)		0.306
Brainstem		0.154
Pons		0.155
WM with erosion 3		0.133
WM with erosion 5		0.095

Keywords: *longitudinal tau-PET, reference regions*

Test-retest repeatability of [18F]Flortaucipir PET in Alzheimer's disease and controls

Tessa Timmers[1,2], Rik Ossenkoppele[1,3], Denise Visser[2], Hayel Tuncel[2], Emma E. Wolters[1,2], Sander C.J. Verfaillie[1,2], Wiesje M. van der Flier[1,4], Ronald Boellaard[2], Sandeep S.V. Golla[2], Bart N.M. van Berckel[2]

[1]*Alzheimer Center Amsterdam, Department of Neurology, Amsterdam Neuroscience, Amsterdam UMC, Amsterdam, The Netherlands*
[2]*Department of Radiology & Nuclear Medicine, Amsterdam Neuroscience, Amsterdam UMC, Amsterdam, The Netherlands*
[3]*Clinical Memory Research Unit, Lund University, Lund, Sweden*
[4]*Department of Epidemiology and Biostatistics, Amsterdam UMC, Amsterdam, The Netherlands*

Background: Knowledge of test-retest properties of the tau PET tracer [18F]Flortaucipir is of great importance when studying the natural time course of tau accumulation and when monitoring therapeutic effects in drug intervention studies. The aim of this study was to investigate the test-retest (TRT) repeatability of various parametric methods for [18F]Flortaucipir PET in patients with Alzheimer's disease (AD) and cognitively healthy controls.

Methods: We included 8 subjects with AD dementia or mild cognitive impairment (MCI) due to AD (all amyloid positive, age 65±11, 57% female, MMSE 23±3) and 3 controls (age 58±7, 67% female, MMSE 28±0). All underwent two 130 minute dynamic [18F]Flortaucipir PET scans within 4 weeks. Data were analyzed using basis function based reference region models (RPM, SRTM2) and Reference Logan (RLogan), as well as standardized uptake value ratios (SUVrs: time intervals 40-60, 80-100 and 110-130 minutes post-injection) with cerebellar gray matter as reference region. We obtained DVR or SUVr for three Hammers atlas-based regions-of-interest (ROIs), reflecting early (medial temporal), intermediate (lateral temporal) and late (global cortical) tau deposition. TRT repeatability (%) was defined as (test-retest) / (average (test + retest)) * 100.

Results: For all models and across ROIs, mean TRT repeatability ranged from (%±SD) 1.3%±1.0 to 5.4%±3.0 (Table 1, Figure 1). TRT in in semi-quantitative models (e.g. SUVr) was approximately 1.5 – 2 times larger than in full quantitative models. For simplified reference tissue methods, TRT repeatability was comparable amongst all ROIs, whilst for all SUVr time intervals TRT repeatability was best in the global region (Figure 2).

Conclusions: Test-retest repeatability was excellent for all models used, however semi-quantitative methods performed slightly worse than simplified reference tissue methods.

global cortical
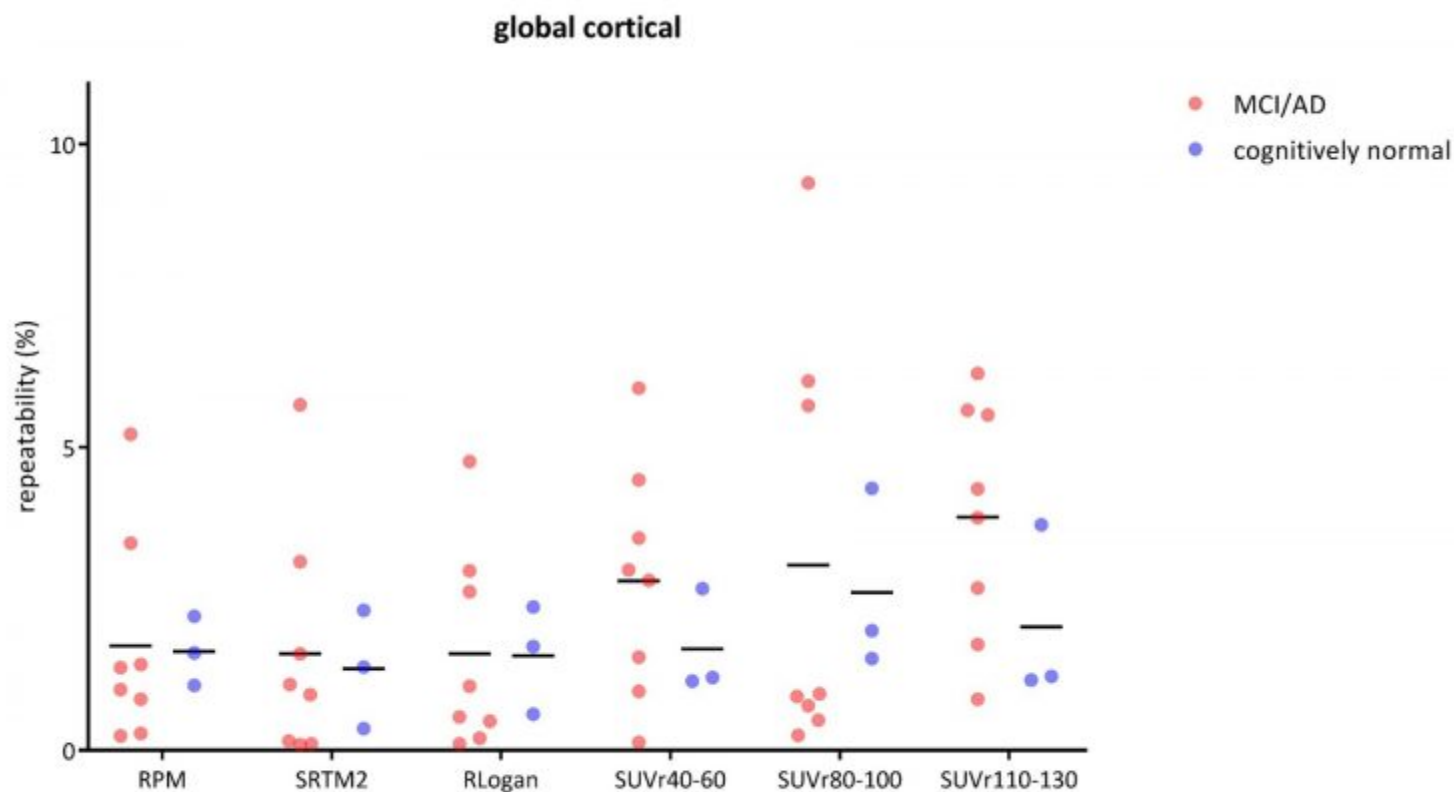
Figure 1: test-retest repeatability (%) for simplified reference tissue methods and semi-quantitative methods
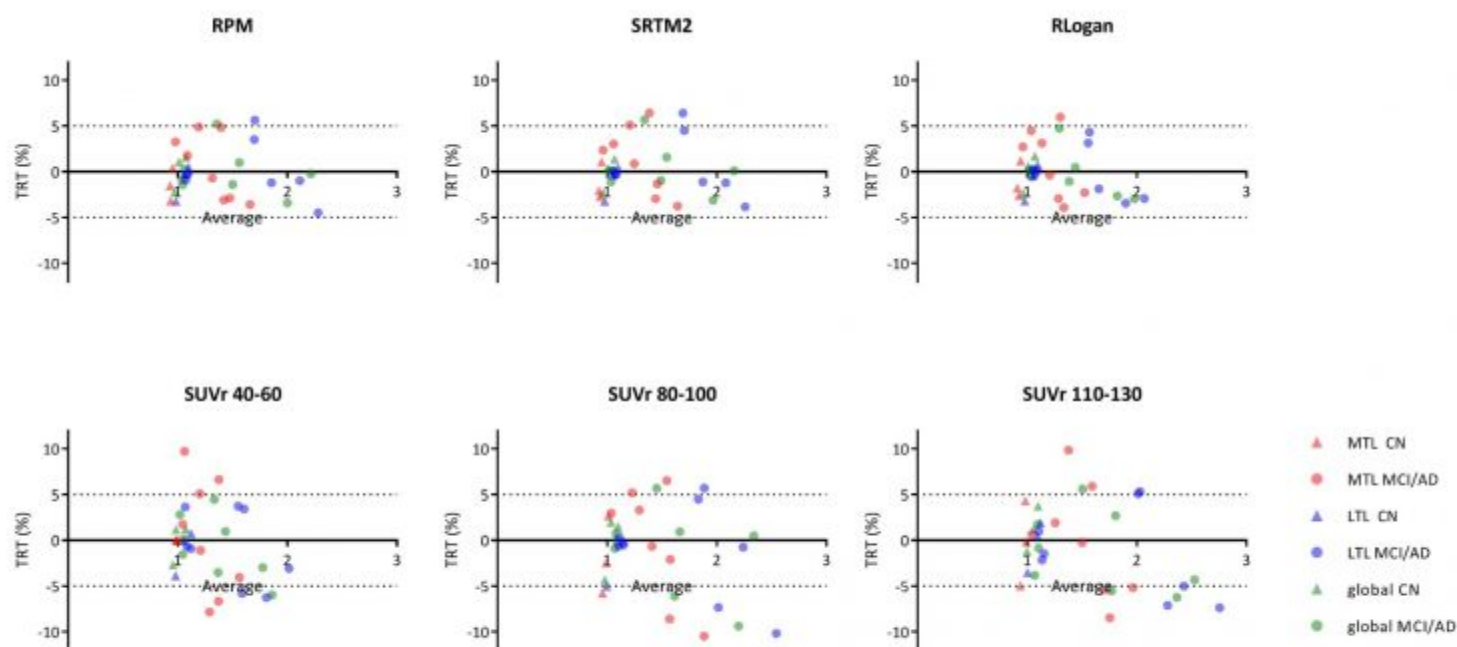
Figure 2: Bland-Altman plots of (a-c) DVR (simplified reference models) and SUVr (semi-quantitative models)

	RPM DVR	SRTM2 DVR	RLogan DVR	SUVr40-60	SUVr80-100	SUVr110-130
MCI/AD						
MTL						
test	1.3 ± 0.2	1.3 ± 0.2	1.2 ± 0.2	1.3 ± 0.2	1.5 ± 0.3	1.5 ± 0.3
retest	1.3 ± 0.2	1.3 ± 0.2	1.2 ± 0.2	1.3 ± 0.2	1.4 ± 0.2	1.5 ± 0.3
TRT repeatability (%)	**3.1 ± 1.4**	**3.2 ± 1.8**	**3.2 ± 1.6**	**5.4 ± 3.0**	**5.0 ± 3.4**	**4.7 ± 3.5**
LTL						
test	1.6 ± 0.5	1.6 ± 0.5	1.5 ± 0.4	1.5 ± 0.4	1.8 ± 0.6	1.9 ± 0.7
retest	1.6 ± 0.5	1.6 ± 0.5	1.5 ± 0.4	1.5 ± 0.3	1.7 ± 0.5	1.8 ± 0.6
TRT repeatability (%)	**2.1 ± 2.1**	**2.2 ± 2.4**	**2.1 ± 1.6**	**3.4 ± 2.0**	**3.7 ± 3.8**	**4.3 ± 2.5**
Global cortical						
test	1.5 ± 0.5	1.4 ± 0.4	1.4 ± 0.4	1.4 ± 0.3	1.6 ± 0.5	1.7 ± 0.6
retest	1.5 ± 0.4	1.5 ± 0.4	1.4 ± 0.3	1.4 ± 0.3	1.6 ± 0.5	1.6 ± 0.5
TRT repeatability (%)	**1.7 ± 1.7**	**1.6 ± 1.9**	**1.6 ± 1.7**	**2.8 ± 1.9**	**3.1 ± 3.5**	**3.9 ± 1.9**
Controls						
MTL						
test	0.9 ± 0.0	0.9 ± 0.0	0.9 ± 0.0	1.0 ± 0.0	1.0 ± 0.0	1.0 ± 0.0
retest	0.9 ± 0.0	0.9 ± 0.0	0.9 ± 0.0	1.0 ± 0.0	1.0 ± 0.0	1.0 ± 0.0
TRT repeatability (%)	**1.7 ± 1.4**	**1.9 ± 0.8**	**1.8 ± 0.7**	**1.4 ± 0.6**	**3.6 ± 1.9**	**3.1 ± 2.6**
LTL						
test	1.1 ± 0.0	1.0 ± 0.1	1.0 ± 0.0	1.1 ± 0.1	1.1 ± 0.1	1.1 ± 0.0
retest	1.0 ± 0.1	1.0 ± 0.1	1.0 ± 0.1	1.0 ± 0.1	1.1 ± 0.1	1.1 ± 0.1
TRT repeatability (%)	**1.3 ± 1.6**	**1.3 ± 1.6**	**1.5 ± 1.5**	**1.6 ± 2.0**	**2.0 ± 2.6**	**2.0 ± 1.5**
Global cortical						
test	1.0 ± 0.0	1.0 ± 0.0	1.0 ± 0.0	1.0 ± 0.1	1.0 ± 0.0	1.0 ± 0.0
retest	1.0 ± 0.1	1.0 ± 0.1	1.0 ± 0.1	1.0 ± 0.1	1.0 ± 0.1	1.1 ± 0.1
TRT repeatability (%)	**1.6 ± 0.6**	**1.3 ± 1.0**	**1.6 ± 0.9**	**1.7 ± 0.9**	**2.6 ± 1.5**	**2.0 ± 1.5**

Table 1: Mean ± SD per method for test and retest, and TRT repeatability (%) for 3 ROIs

AmyloidIQ demonstrates increased power in longitudinal Amyloid PET studies

Alex Whittington[1,2], John Seibyl[1], Jacob Hesterman[1], Roger N. Gunn[1,2]

[1]*Invicro, Boston, MA, US*
[2]*Imperial College London, London, UK*

Introduction: Amyloid PET is used in clinical trials of anti-amyloid therapeutics as a biomarker for the amyloid-β (Aβ) burden. We investigate the application of both SUVR and Amyloid[IQ] analytical approaches to longitudinal Aβ imaging data to assess their power as quantification methods in clinical imaging trials.

Methods: 266 subjects with longitudinal [^{18}F]Florbetapir PET data (baseline plus at least two follow up scans in the interval 2 to 7 years for each subject) and corresponding structural T1-weighted MRI data were downloaded from the ADNI database. For each [^{18}F]Florbetapir PET scan, Amyloid[IQ] was used to calculate Amyloid Load (Aβ$_L$) and a composite SUVR (without PVC and using grey matter Cerebellum as a reference region) was also calculated. Effect sizes (Hedges' g) between baseline and follow-up scans were calculated for both outcome measures. A linear regression was performed on each subject's data to estimate the rate of change of Aβ accumulation and enable an assessment of this in the context of the overall disease trajectory.

Results: Amyloid load produced bigger effect sizes between follow-up and baseline scans for all timepoints as compared to SUVR [2yr:26%, 3yr:32%, 4yr:114%, 5yr:227%, 6yr:11% , 7yr:49% increase] (Figure 1). When exploring the rates of change of Aβ accumulation as a function of time in the overall disease process, there was less variability in the rate of change of Amyloid load compared to SUVR as demonstrated by the increased coherence of the gradient plots (Figure 2). By directly plotting the gradient and its associated confidence interval it is evident that Amyloid Load provides increased power to measure change along the disease trajectory (Figure 3).

Conclusion: Amyloid[IQ] provides increased power to detect changes in longitudinal Aβ imaging studies and therefore has significant value for disease understanding and clinical trials of novel therapeutics in AD.
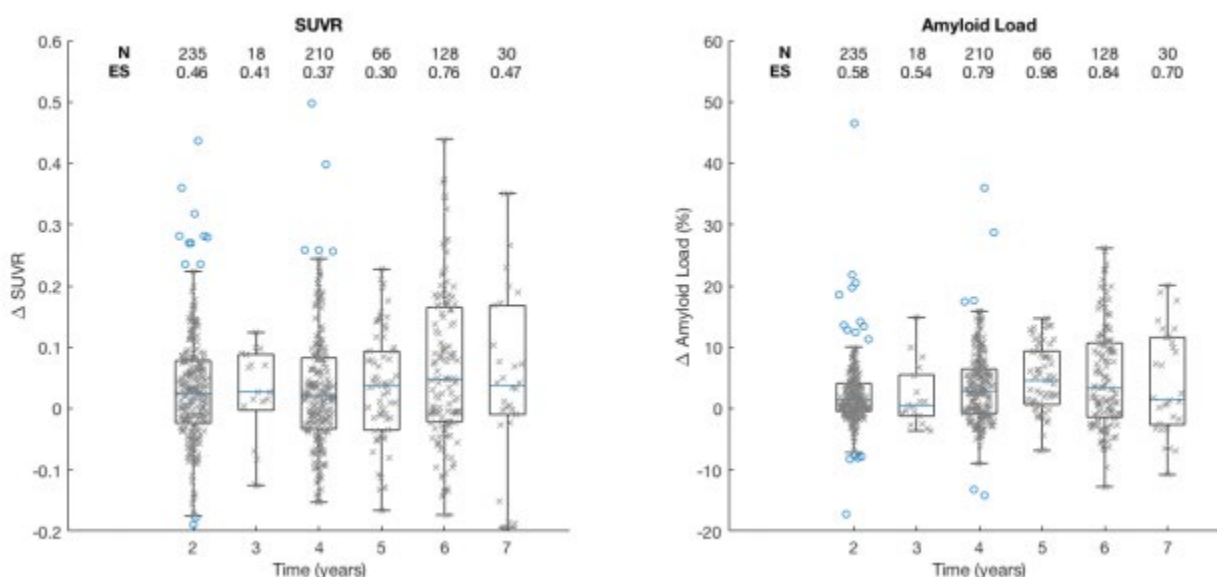
Figure 1
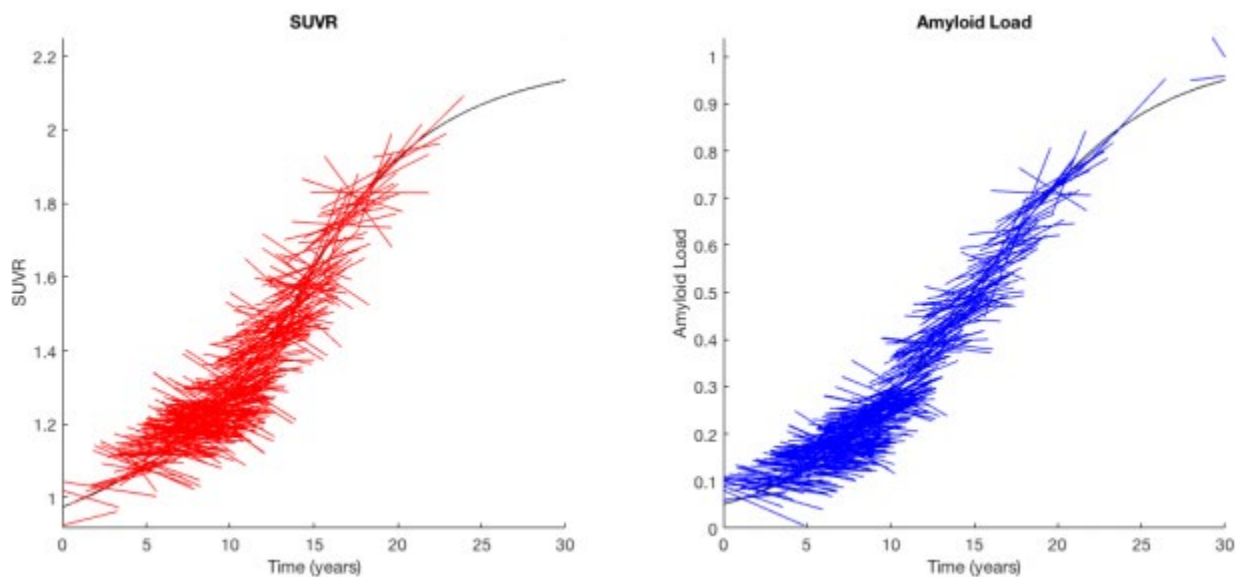
Figure 2
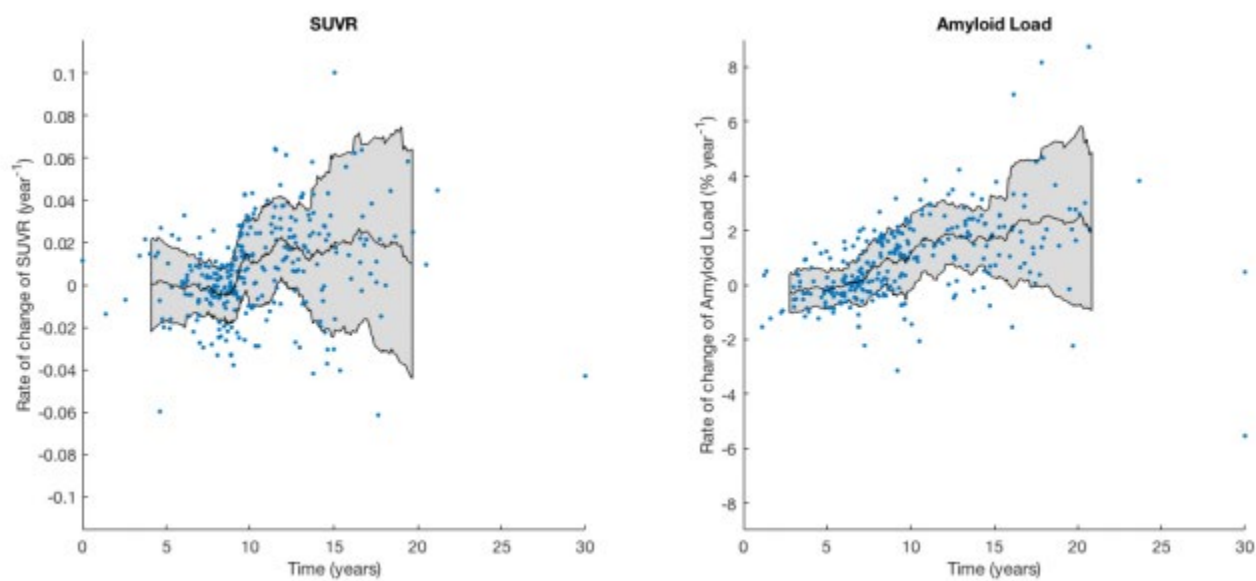
Figure 3

Regionalized spatial association between PiB and FTP PET assessed via variography

Tobias Estime[1], Justin Sanchez[1], Alex Becker[1], Keith Johnson[1]

[1]*Massachusetts General Hospital, Boston, MA, US*

Background: Alzheimer's Disease is characterized by the presence of two distinct abnormal protein aggregates—amyloid-beta plaques and tau neurofibrillary tangles—distributed across areas of the brain in patterns that vary across individuals with age and other factors. Here, we use variography on PiB PET imaging of amyloid and FTP imaging of tau to reveal spatial associations between these proteopathies in temporal cortex.

Methods: We carry out spatial variography with FTP and corresponding PiB PET data from a population of 182 participants, ranging from ages 21-86 with varying degrees of impairment. Sampling partial volume corrected PiB DVR and FTP SUVR at collocated surface vertices aggregated to 6mm resolution, we compute empirical auto-variograms for PiB DVR, FTP SUVR, and cross-variograms for both measures. We model these variograms and compute correlograms from these models to assess spatial cross-correlation (clustering) between PiB and FTP via bivariate Global and Local Moran's **I** analyses, which are done without regard to intensity normalization using reference region.

Results: Auto-variography results show that spatial patterns in FTP and separately in PiB PET are structured—as opposed to exhibiting spatial randomness—and are similar across subjects. Furthermore, via cross-variography, we find that high PiB DVR vertices correspond to high FTP SUVR at neighboring vertices. In our analysis of spatial cross-correlation between the two signals, we find that clustering between PiB and FTP PET across subjects is positively correlated with neocortical PiB FLR ($r = 0.31$, $p < 0.001$) as well as mean inferior temporal FTP SUVR ($r = 0.37$, $p < 0.001$). Furthermore, we find that spatial clustering between high PiB DVR and high FTP SUVR occurs most frequently in the inferior temporal gyrus.

Conclusion: Our findings provide evidence for regionalized spatial association between amyloid and tau, which may support mechanisms proposing their interaction in Alzheimer's pathology.

Figure 1 – Example Cross-variogram between PiB DVR and FTP SUVR
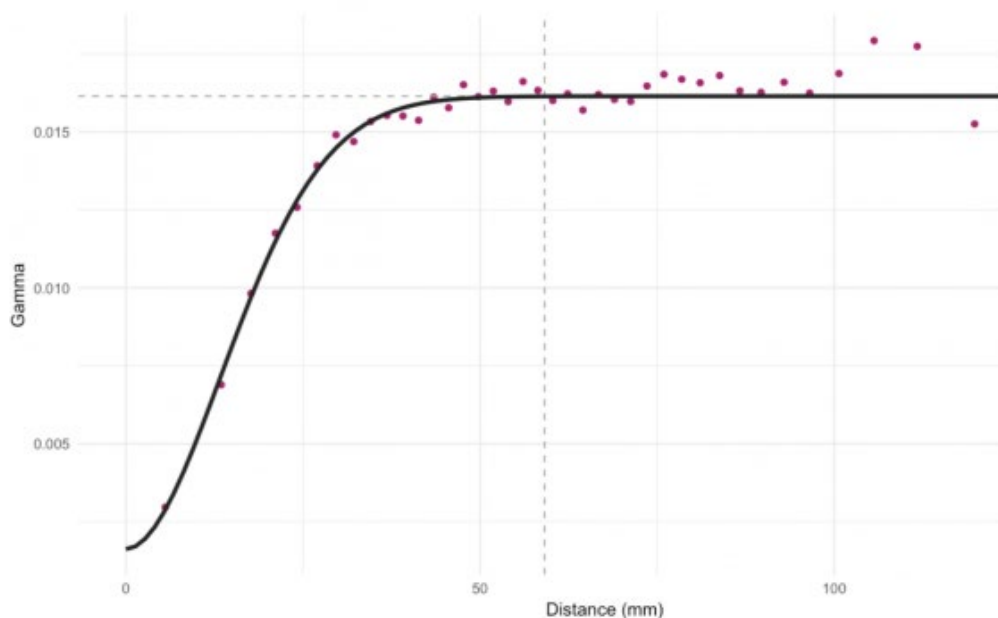
This cross-variogram for the right temporal cortex of a single subject represents the spatial relationship between two variables, PiB DVR and FTP SUVR, as a function of distance. As the distance between any two surface vertices increases, PiB DVR and FTP SUVR values at those vertices are less correlated—the variance (gamma) between the variables increases. This variogram is modeled by the "stable" variogram model, which describes the range encompassing exponential and gaussian spatial processes we observe exclusively throughout our variables and throughout our population when a distance-dependent relationship is present. Here, the vertical dotted line indicates the range of the variogram, the distance beyond which no distance-dependent correlation exists between the two variables, as variance beyond this distance remains constant (indicated by the horizontal dotted line).

Figure 2 – Fraction of population with clustering of high PiB DVR and high FTP SUVR by PiB FLR quartiles
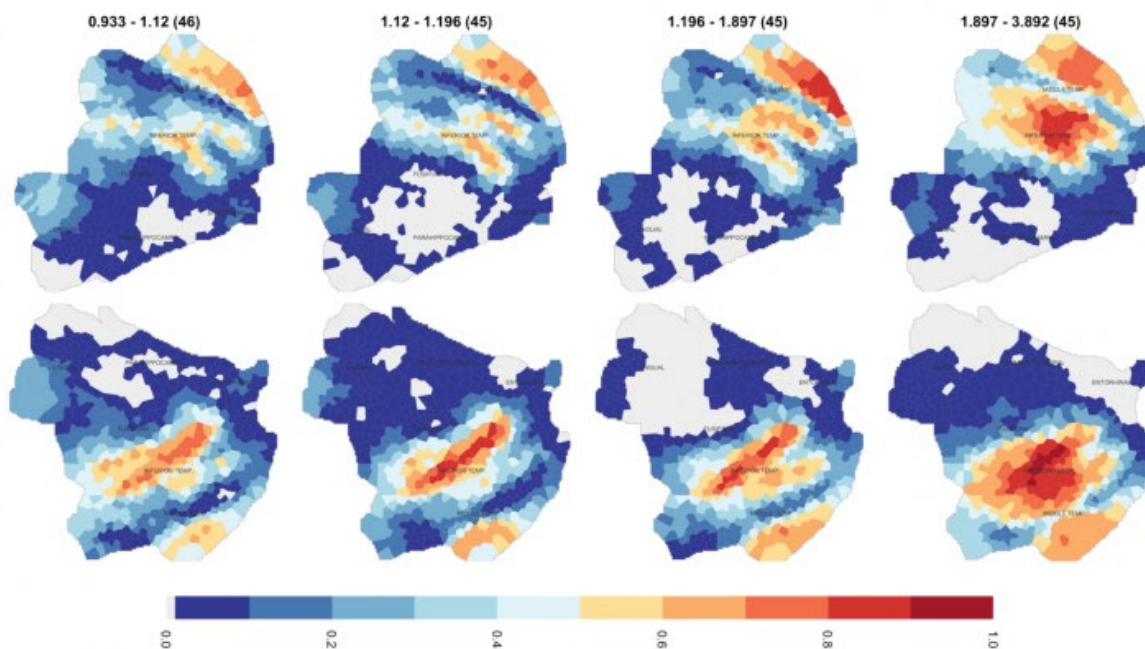
Local Moran's *I* analysis allows locating high clustering—defined as high PiB DVR at any given vertex with high FTP SUVR at neighboring vertices. The spatial dependence used to characterize neighboring vertices is the correlogram, the normalized reciprocal of the variogram. These maps locate the prevalence of statistically significant (Bonferroni-corrected p = 0.05) high clusters by PiB FLR on flattened representations of MRI volumes.

Evaluation of the Centiloid scale for use in multi-amyloid PET tracer, multi-center trials

Jacob Hesterman[1], Olivier Barret[1], Heather Ovens[1], Ryan Petrulli[1], Udo Eichenlaub[2], Andrew Stephens[3], Roger Gunn[1], John Seibyl[1]

[1]*Invicro, Boston, MA, US*
[2]*Roche Diagnostics GmbH, Penzberg, Germany*
[3]*Life Molecular Imaging GmbH, Berlin, Germany*

The Centiloid scale enables mapping of PET SUVR values to a common unit, regardless of tracer and analysis methodology and has been proposed as a method to standardize the quantification of different amyloid tracers for use in multi-center clinical trials. The publication of reference data (http://www.gaain.org/centiloid-project) for commonly used amyloid PET tracers, including [^{18}F]-Florbetapir, [^{18}F]-Florbetaben and [^{18}F]-Flutemetamol, has enabled the mapping of SUVR data into the Centiloid scale for multi-tracer applications. This paper assesses Centiloid-derived cutoffs across these three amyloid tracers for determination of amyloid positivity. 200 scans with associated radiological reads (100 Ab- /100 Ab+) were randomly selected from independent data sets for each tracer and composite SUVR was calculated with a PET-only analysis pipeline, widely used for eligibility determination, before mapping into the Centiloid scale. ROC-based analyses were used to determine an optimal Centiloid threshold using visual read as the gold standard and ROC Accuracy as the figure of merit. This optimization was performed for each tracer separately and for data pooled across all three tracers. Optimal thresholds of 38.0, 42.2, and 34.0 were found, corresponding to ROC Accuracy measures of 0.968, 0.981, and 0.987, for [^{18}F]- Florbetapir, [^{18}F]- Florbetaben and [^{18}F]- Flutemetamol, respectively. For pooled data, an optimal threshold of 34.1 CL was identified. This threshold results in an ROC accuracy of 0.952, an AUC of 0.978, and Cohen's D of 3.24. A plot showing all data on a common Centiloid scale with positive (green) and negative (red) reads indicated is included. This study suggests that a single Centiloid threshold may enable successful quantitative assessment of amyloid positivity from data spanning multiple tracers for utility as a robust enrollment criteria in multi-center amyloid clinical trials.
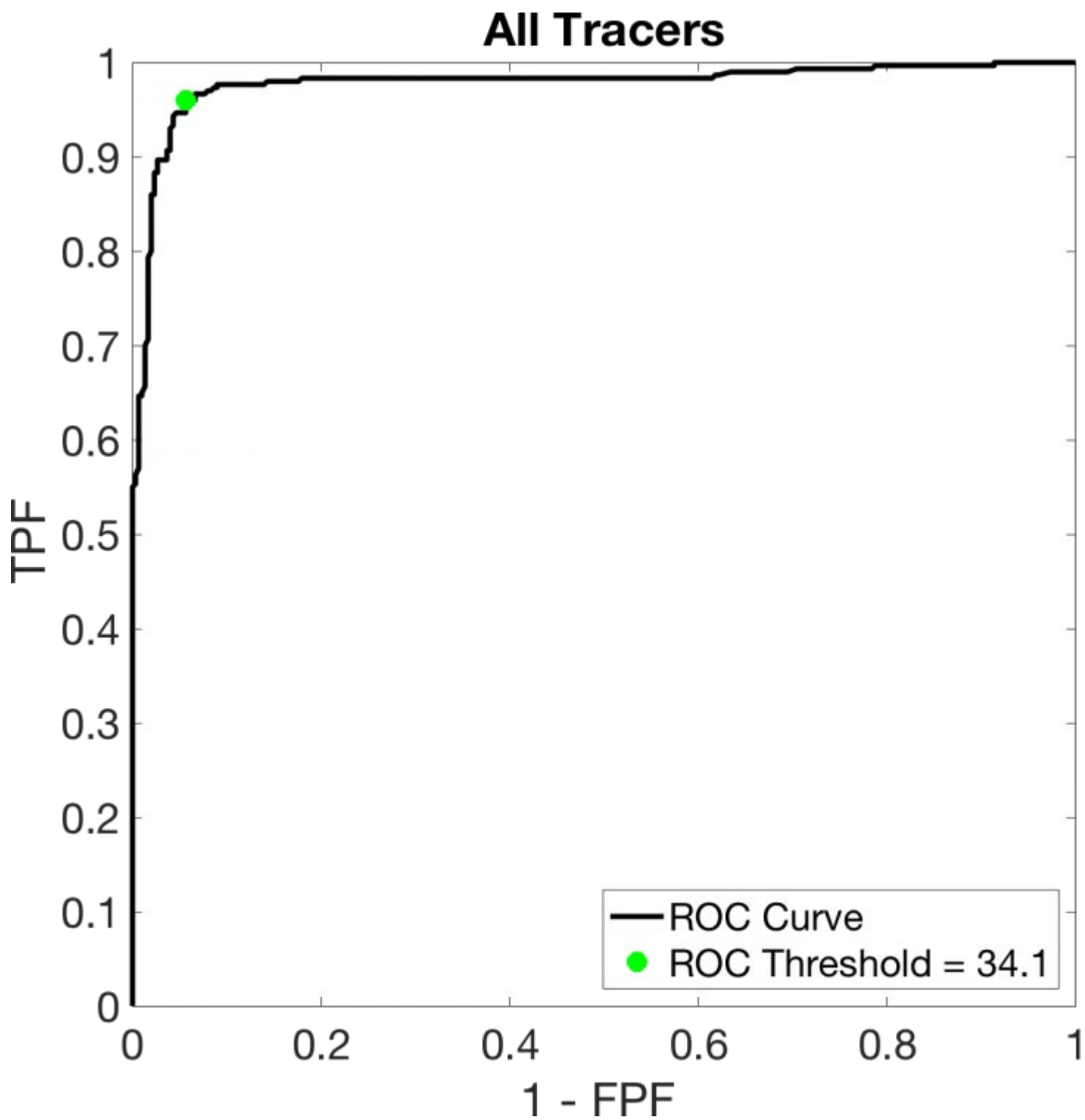
Figure 1: ROC curve from tracer-pooled data with optimal Centiloid threshold identified.
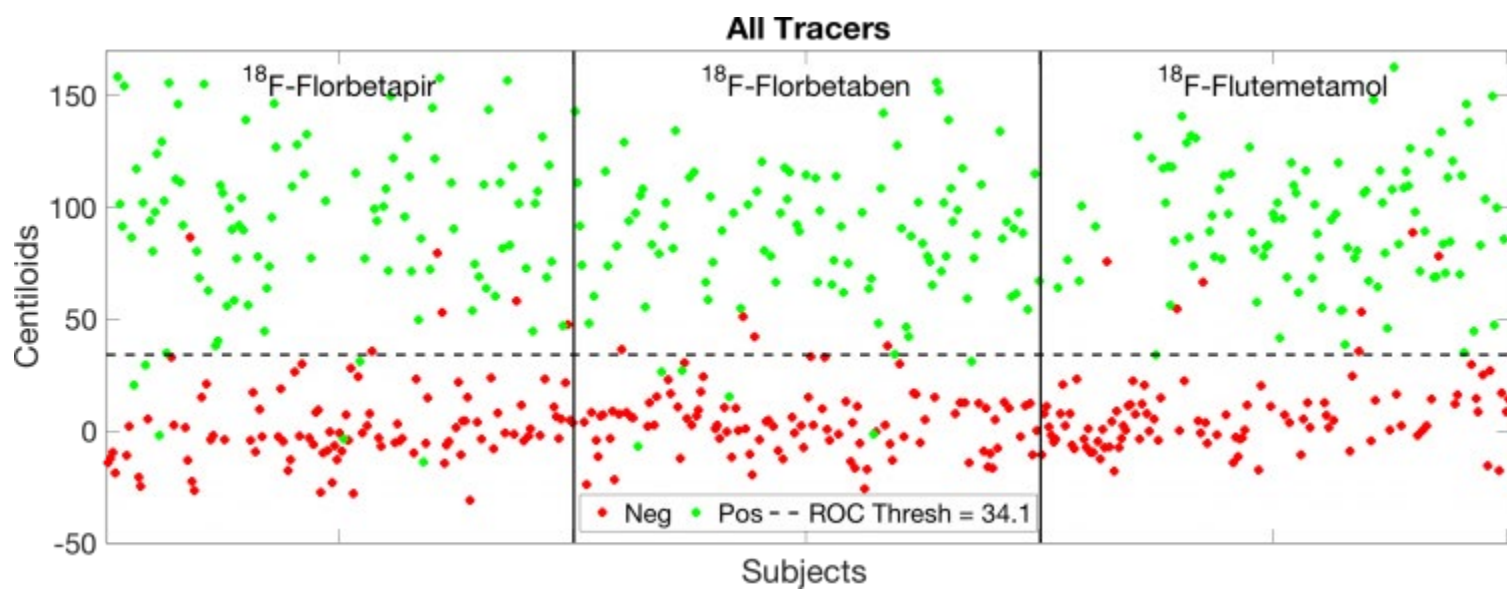
Figure 2: Data across tracer on a common Centiloid scale.

Keywords: *Centiloid, eligibility, multi-center, quantitation, multi-tracer*

A comparison of partial volume correction techniques for measuring change in Serial AV-1451 Tau PET SUVR

Christopher Schwarz[1], Jeffrey Gunter[1], Val Lowe[1], Stephen Weigand[1], Prashanthi Vemuri[1], Matthew Senjem[1], Jennifer Whitwell[1], Keith Josephs[1], Ronald Petersen[1], David Knopman[1], Clifford Jack[1]

[1]*Mayo Clinic, Rochester, MN, US*

Background: We have previously shown that Rousset-style (GTM) partial volume correction (PVC) has relatively poor reliability for measuring change in PiB (amyloid) PET, compared to no-PVC or voxel-based PVC. GTM is popular for tau PET analyses, but its suitability for measuring change in AV-1451 signal has not been tested. Here, we compare the performance of: no PVC, 2-compartment (Meltzer-style), 3-compartment (Müller-Gärtner-style), and multiple implementations of GTM (Mayo, FreeSurfer, Baker et. al. 2017).

Methods: We performed comparisons in Mayo Clinic participants (n=62) each with 3 visits (within 3 years) including AV-1451 PET and MRI. We measured SUVR in: a) a temporal-lobe cortical composite region (amygdala, fusiform, inferior/middle temporal, entorhinal, parahippocampal), b) entorhinal cortex, c) inferior temporal cortex, using each PVC option with both cross-sectional and longitudinal variations of a) Mayo in-house SPM12/MCALT/ANTs-based pipelines, and b) FreeSurfer 6.0. An 8mm PSF was assumed. For each reference region (cerebellar crus/GM/whole, pons, supratentorial-WM), we used linear mixed-effects regression to model intra-subject log(SUVR) and estimated the coefficient of variation ($CV=\sigma/\mu$) using the residual SD of the model. We also compared methods' abilities to differentiate cognitively impaired (n=54) from unimpaired (n=8) participants, both longitudinally and at baseline.

Conclusions: Inferior-temporal and composite target regions were significantly more reliable than entorhinal in most comparisons. Their cross-sectional and longitudinal group-differences were somewhat larger vs. entorhinal, but not significantly. Differences across reference regions were relatively minimal. Measurements using GTM PVC were less reliable than voxel-based or no PVC, and GTM did not significantly increase cross-sectional or longitudinal group-wise differences. This finding was consistent across all implementations and combinations of target/reference regions, and it matches our previous findings for longitudinal amyloid PET. From these data, we recommend using either no PVC or voxel-based PVC for analysis of change in AV-1451 PET. Cross-sectionally, there were no significant differences across PVC methods.

Longitudinal reliability when measuring tau PET SUVR over time

PVC Method

None
2-Comp.
3-Comp.
GTM
GTM_Baker

Error bars show 95% confidence interval

Difference between slopes (Annual SUVR % change)
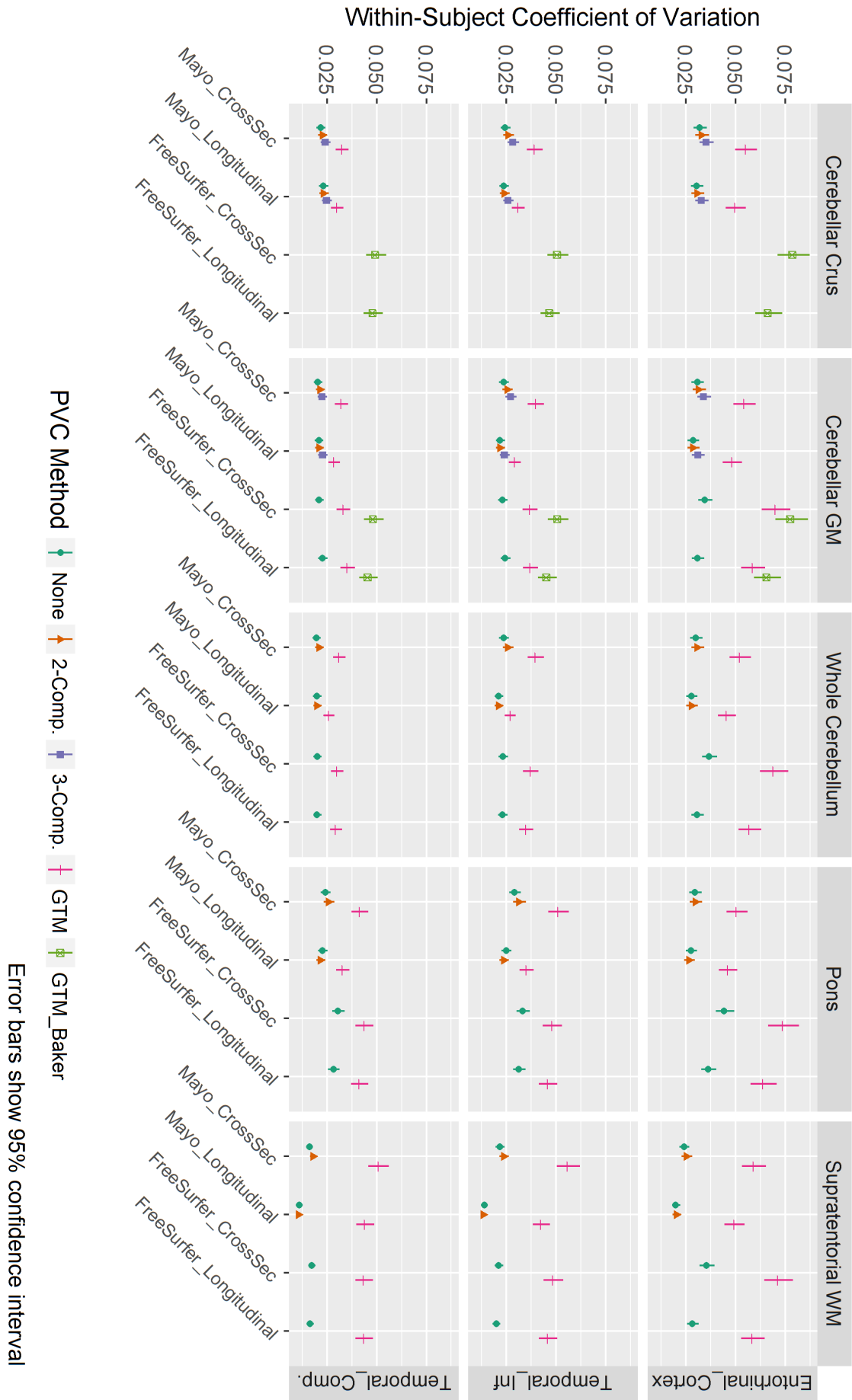
Difference in % slope(impaired) - % slope(unimpaired)
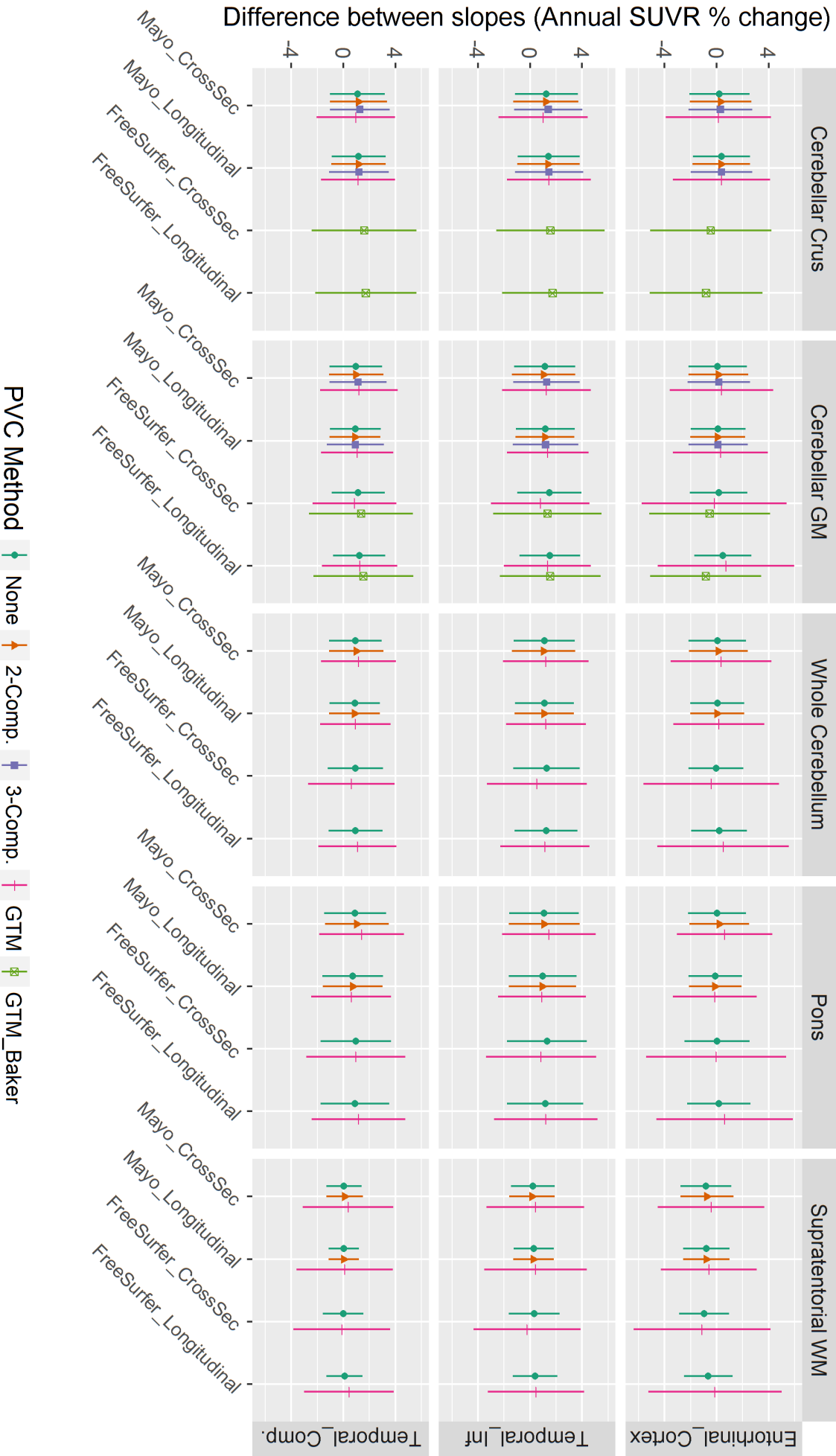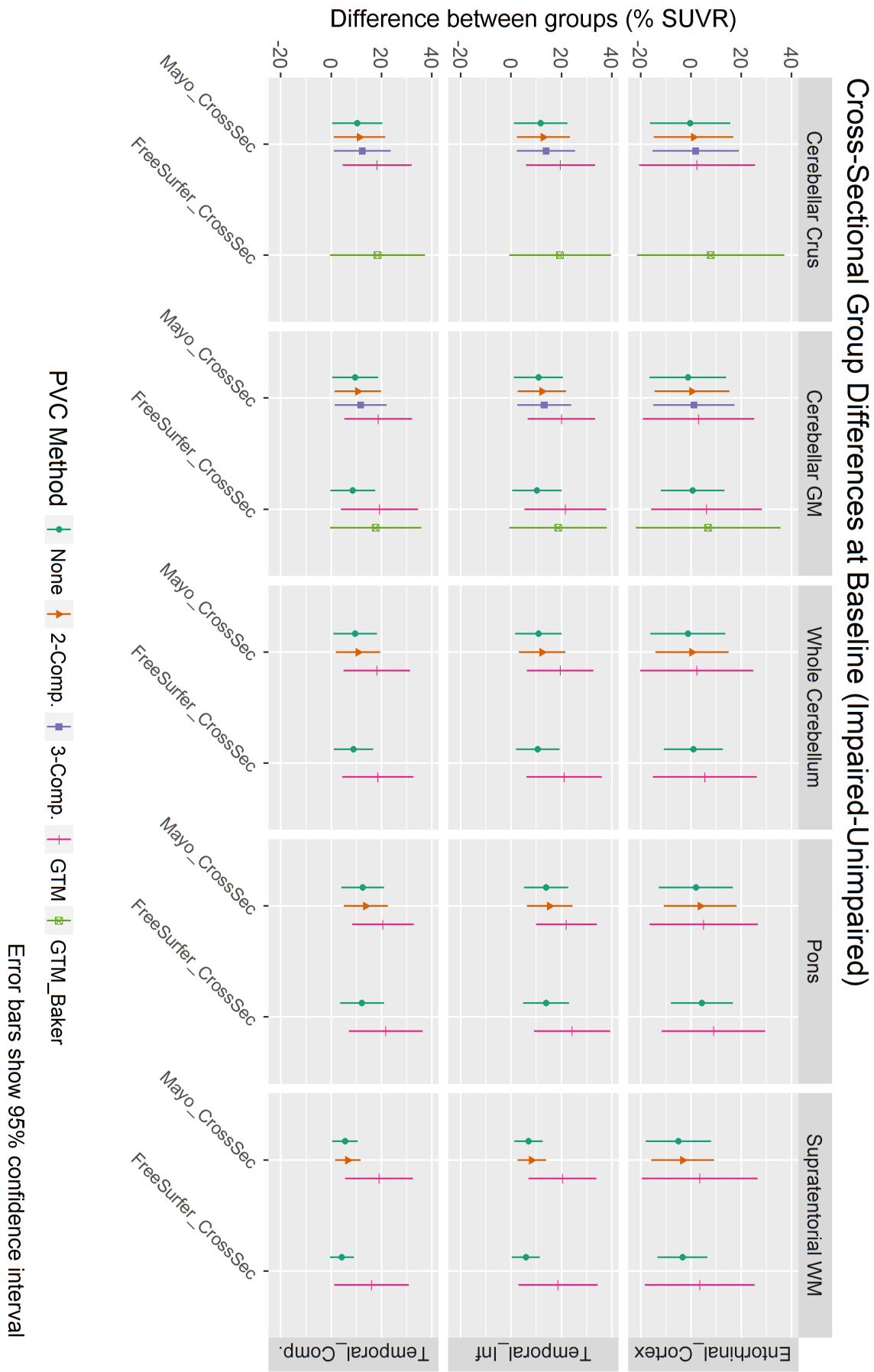
PVC Method

None 2-Comp. 3-Comp. GTM GTM_Baker

Error bars show 95% confidence interval

Cross-Sectional Group Differences at Baseline (Impaired-Unimpaired)

Difference between groups (% SUVR)

PVC Method
- None
- 2-Comp.
- 3-Comp.
- GTM
- GTM_Baker

Error bars show 95% confidence interval

Detecting the earlier stages of amyloid deposition

Tengfei Guo[1,2], Susan Landau[1,2], William Jagust[1,2]

[1]*Helen Wills Neuroscience Institute, University of California, Berkeley, CA, US*
[2]*Molecular Biophysics and Integrated Bioimaging, Lawrence Berkeley National Laboratory, Berkeley, CA, US*

We used ADNI ^{18}F-florbetapir PET data to determine whether a single brain ROI would be more sensitive to amyloid-β (Aβ) deposition, and to predict cognitive decline in cognitively normal (CN) older adults. We ranked SUVRs of all subregions making up the cortical COMPOSITE region to determine the region with the highest SUVR in COMPOSITE+ individuals, which we found to be the bank of the superior temporal sulcus (BANKSSTS) (Fig.1 A). The positivity threshold for BANKSSTS was defined as being above the 1st percentile of SUVR in the COMPOSITE+ CN population. The CN cohort was then divided into three different amyloidosis stages, stage0: BANKSSTS-/COMPOSITE-, stage1: BANKSSTS+/COMPOSITE-, and stage2: BANKSSTS+/COMPOSITE+. Linear mixed effect (LME) models were used to investigate the effect of amyloidosis stage upon the subsequent longitudinal change in memory and executive function.

CN individuals with baseline PET and subsequent longitudinal cognitive tests were classified as (Fig.1 B) stage0 (n=191), stage1 (n=64) and stage2 (n=99). Individuals at stage1 and stage2 had more decline in memory (Fig.1 C) and executive function (Fig.1 D) than stage0 over more than 4 years of mean follow-up. LME results revealed that rates of memory decline at stage1 (-0.0550±0.0129) and stage2 (-0.1058±0.0115) were 2.55 (p=0.0279) and 4.90 (p<0.0001) times faster than stage0 (-0.0216±0.0080) respectively (Fig. 2A). Stage1 (-0.0326±0.0173, p=0.0397) and stage2 (-0.0747±0.0155, p<0.0001) showed rates of executive function decline significantly lower than zero, but stage0 (-0.0132±0.0107) had no significant negative rate of executive function (Fig. 2B).

Nominally Aβ negative individuals with high florbetapir uptake in BANKSSTS are at increased risk of cognitive decline, probably show earlier stages of Aβ deposition, and may be suitable early stage subjects for amyloid-lowering interventions.
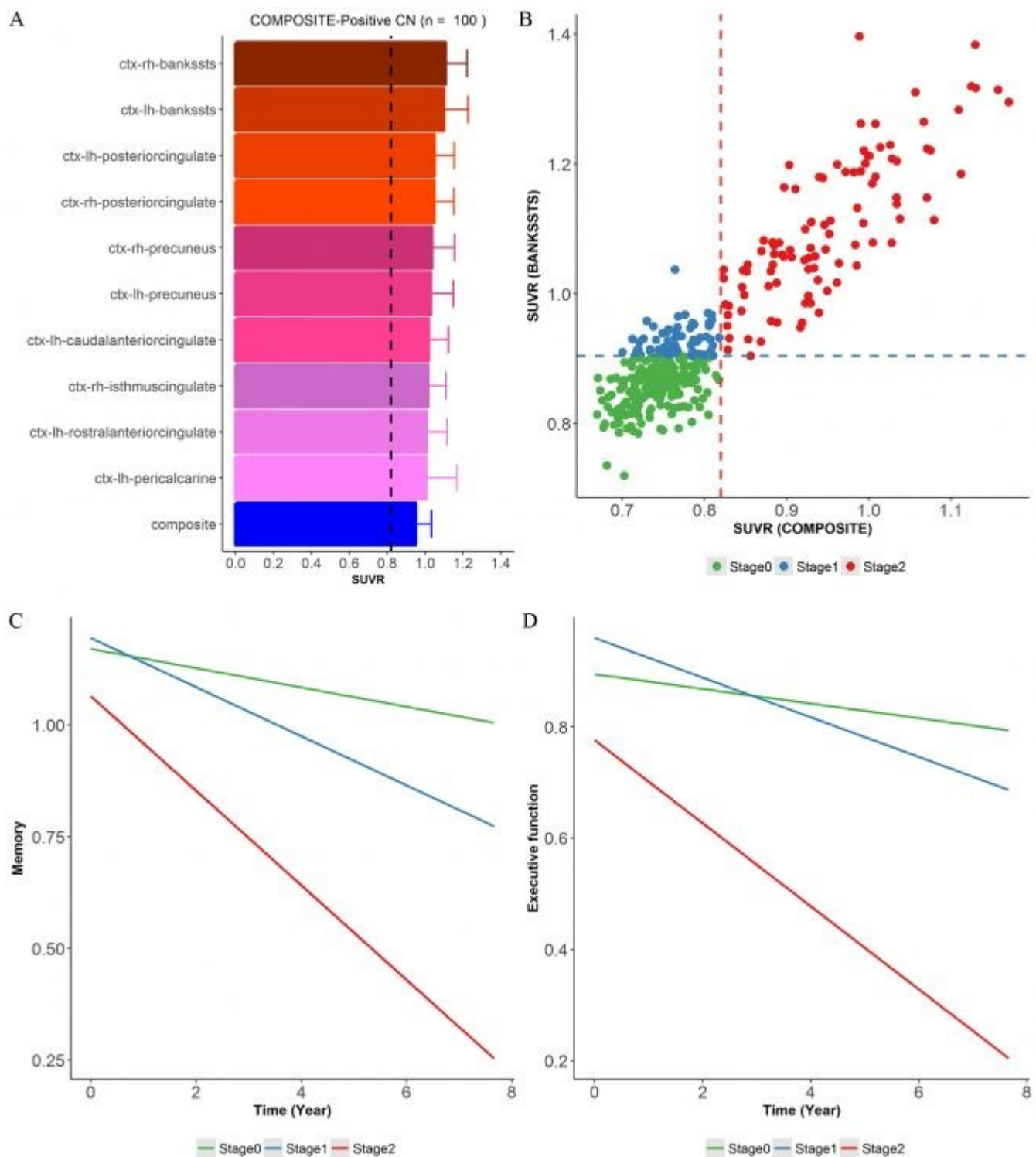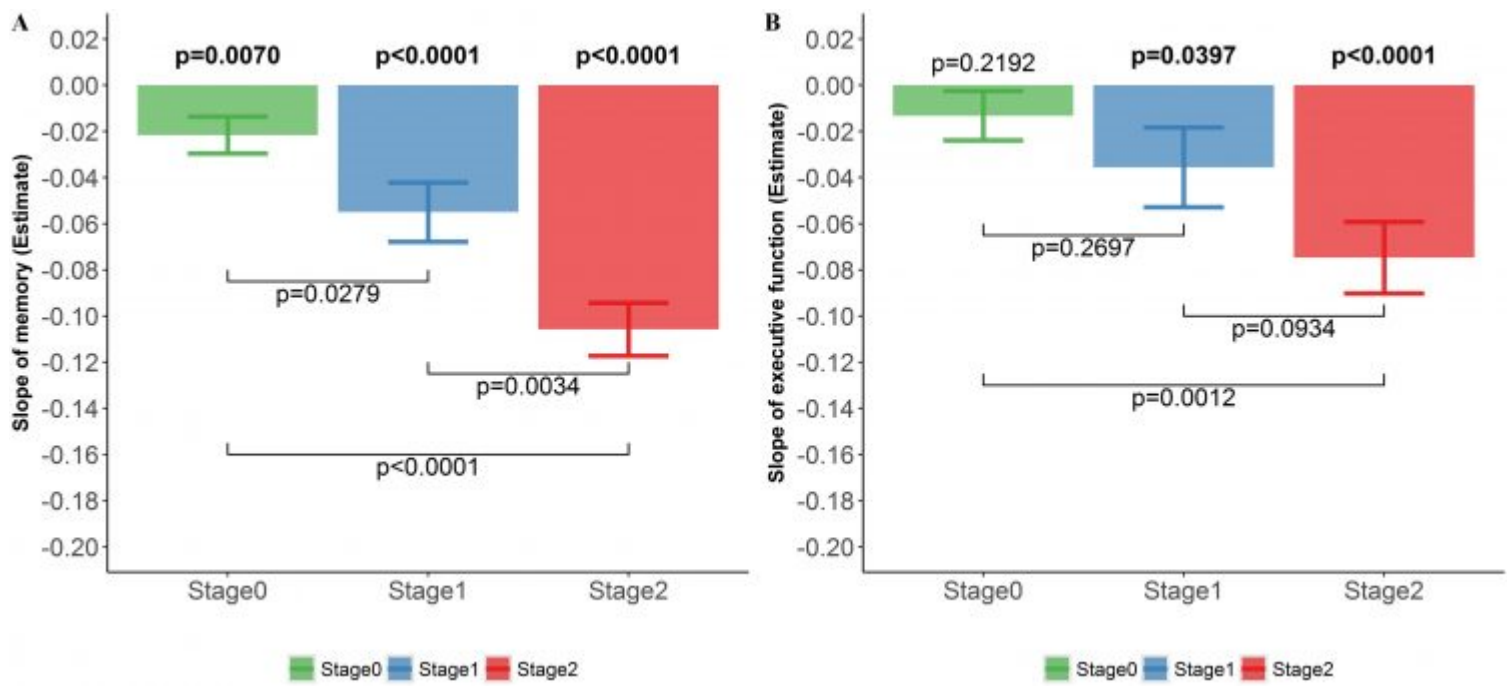
Wednesday, January 16, 2019 - 05:45 pm - 06:15 pm

Keynote Presentation

Carson, Richard

Quantitative brain PET: is SUVR the best we can do?

Richard Carson

Yale PET Center, Departments of Radiology and Biomedical Imaging and of Biomedical Engineering, Yale University, New Haven, CT, US

PET imaging allows the production of high resolution images of radiopharmaceutical distribution in humans and animals. With the use of appropriate radiopharmaceuticals combined with tracer kinetic modeling, relevant physiological parameters such as volume of distribution (VT) and binding potential (BPND) can be quantified *in vivo*. The development of appropriate modeling methodology typically requires dynamic scans plus arterial input function measurement including assays of radiolabeled metabolites. Ideally, additional validation studies are also performed, including *in vivo* blocking studies and *in vivo/ex vivo/in vitro* correlations. Ultimately, to facilitate clinical utility, simplified methodology is developed, e.g., calculating standard uptake values (SUV) and their ratios (SUVR) to an appropriate (or useful) reference region. That process produces a clinically feasible approach but may suffer from increased variability or biased values which can differ in various patient populations or in different patient states.

This presentation will include:

- novel tracer validation and optimization, using as an example 11C-UCB-J, the new SV2A agent used to assess synaptic density

- characterizing and optimizing a simplified quantification method using SUV and SUVR, including the inherent assumptions of these approaches

- examples of imaging paradigms where simplified approaches can provide misleading results, and

- the impact of these issues for amyloid and tau imaging.

Keywords: *Quantitative Brain PET*

THURSDAY, January 17, 2019

	Thursday, January 17, 2019		Page
8:30	**SESSION 3:** **Neuropathological validation of amyloid and tau tracers**	CHAIRS: **Laetitia Lemoine**, Karolinska Institute, Stockholm, Sweden **Rik Vandenberghe**, KU Leuven, Leuven, Belgium	182
10:15	**POSTER SESSION 2A** and Coffee Break		188
11:00	**SESSION 4:** **In vivo-postmortem correlates of flortaucipir PET**	CHAIRS: **Teresa Gomez-Isla**, Massachusetts General Hospital, Boston, MA, US **David Wolk**, University of Pennsylvania, Philadelphia, PA, US	296
12:30	Keynote Lecture	**Michel Goedert**, MRC Lab of Molecular Biology, Cambridge, UK	307
1:15	Lunch		
2:45	**SESSION 5:** **Modeling amyloid & tau relationships and spread**	CHAIRS: **Elizabeth Mormino**, Stanford University, Palo Alto, CA, US **Michel Grothe**, DZNE, Rostock, Germany	308
4:45	**POSTER SESSION 2B** and Coffee Break		
5:30-7:30	Networking Reception		

Thursday, January 17, 2019 - 08:30 am - 09:45 am

Podium Session

Session 3: Neuropathological validation of amyloid and tau tracers

CHAIRS: Laetitia Lemoine, Rik Vandenberghe

08:30 am - 09:45 am	Session 3: Neuropathological validation of amyloid and tau tracers	CHAIRS: Laetitia Lemoine, Karolinska Institute, Stockholm, Sweden Rik Vandenberghe, KU Leuven, Leuven, Belgium	Page
8:30	Neuropathologic correlates of [11C]PiB PET and [11C]altropane dopamine transporter PET in the Lewy body diseases	**Stephen Gomperts**, Massachusetts General Hospital, Boston, MA, US	183
8:45	Postmortem analyses of PiB and Flutemetamol integrated density measures in diffuse and neuritic plaques in Alzheimer's disease	**Milos Ikonomovic**, University of Pittsburgh, Pittsburgh, PA, US	184
9:00	In vitro characterisation of 3H-MK6240 in human autopsy brain tissue in comparison to the first generation tau PET tracers.	**Mona-Lisa Malarte**, Karolinska Institute, Stockholm, Sweden	185
9:15	Postmortem binding study of 18F-AV1451 in semantic variant primary progressive aphasia	**Rik Vandenberghe**, University Hospitals Leuven, Leuven, Belgium	186
9:30	Neuropathologic maturity of neurofibrillary tangles: implications for tau PET imaging	**Melissa Murray**, Mayo Clinic Jacksonville, Jacksonville, FL, US	187
09:45 am - 10:15 am	Discussion		

Neuropathologic correlates of [11C]PiB PET and [11C]altropane dopamine transporter PET in the Lewy body diseases

Stephen Gomperts[1], Julia Shirvan[1], Nathan Clement[2], Rong Ye[1], Samantha Katz[3], Aaron Schultz[3], Keith Johnson[1,3], Matthew Frosch[2], John Growdon[1]

[1]*Massachusetts General Hospital, Department of Neurology, Boston, MA, US*
[2]*Massachusetts General Hospital, Department of Pathology, Boston, MA, US*
[3]*Massachusetts General Hospital, Department of Radiology, Boston, MA, US*

Background: Although the defining pathological changes in the Lewy body diseases - Parkinson disease (PD), PD dementia (PDD) and dementia with Lewy Bodies (DLB) - are aggregates of α-synuclein that accumulate in neurons in stereotypical brain regions including the substantia nigra, neuropathologic changes characteristic of Alzheimer's disease, including Aβ-amyloid plaques and neurofibrillary tangles, are commonly observed at autopsy in both PDD and DLB. In this study, we sought to validate amyloid and dopamine transporter (DAT) imaging biomarkers of Lewy body diseases against postmortem neuropathological findings in a cohort of cognitively impaired parkinsonian patients.

Methods: 4 cognitively normal PD, 4 PD with cognitive impairments, and 10 DLB who underwent amyloid imaging with [11C]PiB and DAT imaging with [11C]altropane came to autopsy and underwent evaluation. All 18 had annual neurological examinations. All cognitively normal PD subjects developed cognitive impairment prior to death. Neuropathological examinations assessed and scored Braak Lewy bodies, Thal amyloid distribution, CERAD neuritic amyloid plaques, Braak neurofibrillary tangles, and cerebral amyloid angiopathy, as well as total amyloid plaque burden in superior frontal, superior parietal, occipital and inferior temporal cortical regions.

Results: All 18 patients met neuropathologic criteria for Lewy body disease; the DAT concentration was low in each case. All patients with elevated [11C]PiB retention had Aβ-amyloid deposits at autopsy. [11C]PiB retention correlated weakly with neuritic plaque burden but significantly with total plaque burden in both occipital and superior parietal regions. [11C]PiB retention also significantly correlated with the severity of both Braak stages of neurofibrillary tangle and Lewy body scores. Neuritic plaque burden was significantly associated with the severity of tangle pathology.

Conclusion: Antemortem [11C]altropane and [11C]PiB scans accurately reflect substantia nigra degeneration and cortical amyloid deposits seen at autopsy. In the Lewy body diseases, the magnitude of [11C]PiB retention predicts the severity of neurofibrillary tangle and Lewy body pathologies.

Postmortem analyses of PiB and Flutemetamol integrated density measures in diffuse and neuritic plaques in Alzheimer's disease

Milos Ikonomovic[1], Chris Buckley[2], Eric Abrahamson[1], Chester Mathis[1], William Klunk[1], Gill Farrar[2]

[1]*University of Pittsburgh, Pittsburgh, PA, US*
[2]*GE Healthcare, Amersham, UK*

Background: Specificity/sensitivity of amyloid PET radioligands for neuritic plaques (NP) is high, however imaging-to-autopsy studies produced some false positive results in cases with infrequent NPs but with substantial diffuse plaques (DP). Thus, the contribution of DPs to amyloid PET signal needs to be investigated. High retention of [C-11]PiB and [F-18]Flutemetamol (Vizamyl) in the striatum, where DP predominate, indicates that these ligands can bind to diffuse amyloid. However, in cortical areas such as frontal cortex (FC), with mixed DP and NP, contribution of different plaque types to ligands' binding is unclear.

Methods: We used highly fluorescent derivatives of PiB (6-CN-PiB) and Flutemetamol (CN-Flute) applied to tissue sections from striatum (caudate, CD) and FC from 10 definite AD cases. Percent area occupied by plaques and integrated density (combined plaque percent area coverage and fluorescent intensity of plaques) were calculated for each case/region/ligand.

Results: Percent area coverage of total plaques was similar in CD and FC for both ligands (CN-Flute: CD=3.79±0.64; FC=5.81±1.18; 2-tailed t-test p=0.15; 6-CN-PiB: CD=3.12±0.48; FC=5.25±2.20 2-tailed t-test p=0.08). In contrast, integrated density values were greater in FC compared to the CD for both ligands (CN-Flute: CD=5024±490.3, FC=11742±568.2, 2-tailed t-test p<0.0001; 6-CN-PiB: CD=4846±258, FC=12425±551, 2-tailed t-test p=0.002).

Discussion: [C-11]PiB and [F-18]Flutemetamol PET retention in vivo likely depends on both the size and fibrillar density of plaques in brain regions analyzed. In two brain regions with similar total plaque burden, the region with predominant NPs yields higher integrated density values. However, large swaths of DPs could yield PET ligands' retention levels similar to those detected in the much smaller volumes of NPs. Thus, amyloid PET may correlate better with NIA-AA 2012 AD neuropathology criteria that incorporate both CERAD (NP) and Thal phases (all types of Aβ plaques).

Keywords: *Vizamyl, PiB, PET, amyloid, diffuse plaques*

In vitro characterisation of 3H-MK6240 in human autopsy brain tissue in comparison to the first generation tau PET tracers

Mona-Lisa Malarte[1], Agneta Nordberg[1,2], Laetitia Lemoine[1]

[1]Center of Alzheimer Research, Department of Neurobiology, Care Sciences and Society, Karolinska Institute, Stockholm, Sweden
[2]Theme Aging, Karolinska University Hospital Huddinge, Stockholm, Sweden

The first-generation tau tracers, including THK family and Flortaucipir, bind to at least 2 binding sites in human autopsy brain tissue and display different binding properties compared to another first generation tau tracer, the PBB3. In silico modeling suggest at least 4 binding sites on the tau fibrils (Murugan et al. 2018). The aim of this study was to characterise the binding properties of the MK6240, a second-generation tau tracer, and to compare its binding properties with first-generation tau tracers using binding assay on tissue homogenates and autoradiography on large frozen sections from the same post-mortem human brain tissue.

Methods: Regional distribution (in temporal, parietal and frontal cortex, hippocampus, thalamus, caudate nucleus and cerebellum) was carried out on 6 AD cases (3 EOAD, 3 LOAD) and 7 control cases, using a fixed concentration of ^{3}H-MK6240 (0.5 nM). Competition with increasing concentrations of unlabelled THK5351, THK5117, Flortaucipir respectively, was performed in temporal brain homogenates from 2 AD cases using 3H-MK6240. Autoradiography with ^{3}H-MK6240 and unlabelled MK6240 was also performed.

Results: Regional binding of ^{3}H-MK6240 showed low binding in the caudate nucleus and higher binding in cortical regions in EOAD compared to LOAD. Good discrimination between AD and control were observed. Competition binding assay showed that ^{3}H-MK6240 compete with Flortaucipir, and with lower affinity with THK compounds. Unlabelled MK6240 did not compete with ^{3}H-THK5351. Autoradiography confirmed the results of the regional distribution in tissue homogenates.

Conclusion: First and second-generation tau PET tracers display several binding sites to tau with different affinities. ^{3}H-MK6240 seems to discriminate EOAD and LOAD. Future studies will also incorporate other second-generation tau tracers to extend the understanding of their binding properties and relationship in AD as well as in non-AD tauopathies.

Postmortem binding study of 18F-AV1451 in semantic variant primary progressive aphasia

Rik Vandenberghe[1,2], Jolien Schaeverbeke[2], Sofie Celen[2], Alicja Ronisz[2], Kim Serdons[1], Koen Van Laere[1,2], Dietmar Thal[1,2], Guy Bormans[2]

[1]*University Hospitals Leuven, Leuven, Belgium*
[2]*KU Leuven, Leuven, Belgium*

Introduction: ^{18}F-THK5351 and ^{18}F-AV1451 PET consistently show high retention in the anterior temporal lobe in primary progressive aphasia semantic variant (PPA SV). PPA SV is most commonly due to TDP43 proteinopathy. We conducted an in vitro autoradiography binding study in PPA SV.

Methods: Cases were selected from the UZ/KU Leuven Brain BioBank based on both the clinical syndrome and the neuropathological diagnosis. Five cases had a clinical diagnosis of PPA SV, two a clinical diagnosis of AD, and two cases were controls. Neuropathologically, three of the SV had FTLD-TDP43, one SV had AD, and one SV had Pick's disease. Sections were obtained from the anterior part of the right inferior temporal gyrus. The in vitro binding study was performed according to the method described by Xia et al. with some minor modifications: Each air-dried frozen section was incubated with 0.4 µCi ^{18}F-AV1451 (200 µL per section) in presence/absence of 10 µM authentic reference material or 10 µM deprenyl at room temperature for 60 minutes. Autoradiograms were obtained by exposing the slides overnight to a high-performance phosphor storage super-resolution screen. The screens were read using a Cyclone Plus system and analyzed using Optiquant software.

Results: None of the PPA SV due to FTLD-TDP4 showed binding on autoradiography. In contrast, PPA SV due to Pick's disease or due to AD showed strong cortical binding, which was displaceable by the cold compound. Co-incubation with deprenyl did not affect the binding levels. The two typical AD cases showed the expected pattern, with strong cortical binding, which could be blocked by the cold compound. This binding was not affected by deprenyl. The two controls did not show any binding.

Conclusion: Binding to non-tau aggregates does not seem to be responsible for the strong PET signal that is seen systematically in PPA SV in vivo.

Keywords: *tau PET - Autoradiography - TDP43 proteinopathy - semantic dementia*

Neuropathologic maturity of neurofibrillary tangles: implications for tau PET imaging

Jolien Schaeverbeke[1], Fadi Hanna-Al-Shaikh[1], Tyler Bruinsma[2], Amanda Liesinger[1], Geoff Curran[2], Bradley Boeve MD[3], David Knopman MD[3], Neill Graff-Radford[5], Ronald Petersen MD, PhD[3], Clifford Jack, Jr.[4], Val J. Lowe[2], Ping Fang[2], Melissa Murray[1]

[1]*Mayo Clinic Jacksonville, Department of Neuroscience, Jacksonville, FL, US*
[2]*Mayo Clinic Rochester, Department of Nuclear Medicine, Rochester, MN, US*
[3]*Mayo Clinic Rochester, Department of Neurology, Rochester, MN, US*
[4]*Mayo Clinic Rochester, Department of Radiology, Rochester, MN, US*
[5]*Mayo Clinic Jacksonville, Department of Neurology, Jacksonville, FL, US*

Background: Neurofibrillary pathology underlying Alzheimer's disease (AD) develops progressively in the perikaryal space of the neuron. Maturity of a neurofibrillary tangle (NFT) is strongly associated with cognitive decline. Our goal was to investigate the relationship between tau maturity and tau PET utilizing autoradiographic and immunohistochemical methods.

Methods: A total of 149 neuropathologically-diagnosed AD cases were selected from the Florida Autopsied Multi-Ethnic (FLAME) cohort to undergo autoradiographic tau binding using AV-1451. The hippocampus was immunohistochemically examined with antibodies to early tau (CP13, phospho-epitope) and mature tau (Ab39, conformational epitope to NFTs). A pan-amyloid-β antibody (33.1.1) was also assessed. Slides and autoradiographs were digitized to facilitate quantification using Aperio ePathology system. Two linear regression models were built to assess association between tau burden and autoradiographic binding with age and sex as covariates.

Results: Visually, autoradiographic tau binding patterns were closely related to the perikaryal/somal tau pathology with less autoradiographic binding observed in ares of neuritic pathology (i.e. extrasomal tau). Areas of extracellular ghost tangles did not readily bind AV-1451. Tau pathology in the subiculum was nearly double the burden observed in the CA1 subsector of the hippocampus. Linear regression modeling of autoradiographic binding in the CA1 revealed an association with more mature tau ($p<0.001$), but not early tau ($p=0.470$) or amyloid-β ($p=0.442$). Linear regression modeling of autoradiographic binding in the subiculum revealed an association with more mature tau ($p=0.002$), but not early tau ($p=0.662$) or amyloid-β ($p=0.084$).

Conclusions: Visual comparison of autoradiographic images and tau supports the hypothesis that AV-1451 may not readily bind to extrasomal tau. Autoradiographic labeling of AV-1451 was quantitatively associated with both early and mature tau markers, but only mature tau survived adjustment. However, visual assessment revealed there may be an upper limit to this association, as a paucity of binding observed in the most advanced NFT lesions.

Keywords: *tangle, neuropathology, hippocampus, Alzheimer's disease, tau maturity*

Thursday, January 17, 2019 - 10:15 am - 11:00 am
Poster Session 2A

Board #	Poster Title	Authors	Presenter	Page
85	Item-level analysis of the Cognitive Function Index by screening amyloid PET in the A4 Study	Amariglio | Sikkes | Marshall | Buckley | Gatchel | Johnson | Rentz | Donohue | Raman | Sun | Yaari | Holdridge | Grill | Aisen | Sperling	**Amariglio, Rebecca**	240
97	Regional tau and atrophy: domain-specific relationships with cognition	Digma | Reas | Brewer | Banks	**Banks, Sarah**	263
90	Amyloid burden and hippocampal function	Beason-Held | Shafer | Bilgel | Wong | Resnick	**Beason-Held, Lori**	251
86	Cross-sectional and longitudinal effects of asymmetric amyloid deposition on memory in Baltimore Longitudinal Study of Aging (BLSA) participants	Brinson | Bilgel | An | Huang | Wong | Resnick	**Brinson, Zabecca**	241
62	Determination of FTD candidates in an MCI-SNAP cohort by PET amyloid and MRI structural analysis	Buckley | Esteban | Wilkens | Wolk	**Buckley, Christopher**	194
63	Striatal amyloid load predicts conversion from aMCI to pAD	Buckley | Chedumbarum-Pillay | Jenkinson | Smith | Beach | Thal | Wolk	**Buckley, Christopher**	196
88	CSF tau biomarkers correlate with [18F]MK6240 SUVR in Alzheimer's disease related areas	Chamoun | Kang | Pascoal | Benedet | Mathotaarachchi | Therriault | Savard | Thomas | Bouhachi | Hsiao | Massarweh | Soucy | Gauthier | Rosa-Neto	**Chamoun, Mira**	247
60	18F-Florbetaben and 18F-Flutemetamol PET beta-amyloid binding expressed in centiloids	Cho | Choe | Kim | Kim | Kim | Jang | Kim | Jung | Na | Park | Seo	**Cho, Soo Hyun**	191
105	Amyloid-β and cortical atrophy in adults with Down Syndrome	Cody | Tudorascu | Lao | Cohen | Zaman | Laymon | Johnson | Klunk | Handen | Christian	**Cody, Karly**	279
106	Relationship between intracranial blood flow and beta-amyloid assessed with PiB PET	Cody | Betthauser | Koscik | Rivera-Rivera | Berman | Cary | Hoffman | Clark | Chin | Barnhart | Bendlin | Johnson | Wieben | Christian | Johnson	**Cody, Karly**	282
83	In-vivo tau burden correlates with subregional atrophy in medial temporal lobe in amyloid negative individuals	Das | Xie | Wisse | Cui | Ittyerah | Yushkevich | Wolk	**Das, Sandhitsu**	236
110	Amyloid-sex interaction effect on cognitive decline: Differential effects on memory versus executive functioning are not mediated by temporal lobe atrophy	Gavett | Fletcher | Mungas | DeCarli	**DeCarli, Charles**	291
107	Personalizing the use of the ATN framework in clinical research: integrating the clinical phenotype and biomarkers in a case series across the MCI/dementia spectrum	Dickerson | McGinnis | Quimby | Hochberg | Brickhouse | Collins | Putcha | Eldaief | Wong | Frosch | Das | McMillan | Yuschkevich | de Flores | Wisse | Xie | Wolk	**Dickerson, Brad**	285
68	Amyloid deposition and hippocampal atrophy in non-demented elderly subjects over 85 years	Treyer | Meyer | Buchmann | Crameri | Studer | Saake | Gruber | Unschuld | Nitsch | Hock | Gietl	**Gietl, Anton**	204
98	Inferior temporal tau is associated with greater prospective cortical thinning in clinically-normal older adults	Hampton | Scott | Buckley | Chhatwal | Jacobs | Hanseeuw | Johnson | Sperling | Schultz	**Hampton, Olivia**	265
89	Diagnostic accuracy of [18F]RO948 PET for differentiating AD from other neurodegenerative disorders	Hansson | Stomrud | Borroni | Klein | Strandberg | Smith	**Hansson, Oskar**	248
72	Longitudinal 18F-APN-1607 (18F-PM-PBB3) PET in the rTg4510 mouse model of tauopathy	Hsiao | Huang | Lin | Yang	**Hsiao, Ing-Tsung**	212
104	Sex-specific effects of APOE-e4 genotype on amyloid burden and cognitive function	Isenberg | Aslanyan | Pa	**Isenberg, Lisette**	278
87	Regional sex-differences in tau pathology in asymptomatic individuals with elevated amyloid	Jacobs | Buckley | Mormino | Schultz | Raman | Donohue | Sun | Marek | Seibyl | Mintun | Shcherbinin | Pontecorvo | Rowe | VanDyck |	**Jacobs, Heidi**	244

Board #	Poster Title	Authors	Presenter	Page
		Salloway | Jack | Yaari | Holdridge | Aisen | Sperling | Johnson		
75	AV1451 and THK5351 PET with pathology correlations in a patient with Sporadic Creutzfeldt-Jakob Disease	Kim | Cho | Park | Jang | Ryu | Choi | Moon | Oh | Oh | Na | Lyoo | Kim | Choi | Seo	**Kim, Hee Jin**	219
74	Pearls and pitfalls of using centiloids in interventional anti-amyloid studies – an examination of amyloid reductions in the gantenerumab open label extension studies	Klein | Delmar | Abi-Saab | Andjelkovic | Ristic | Voyle | Hesterman | Seibyl | Marek | Baudler | Fontoura | Doody	**Klein, Gregory**	217
67	Vascular medical treatment influences the association between vascular burden and amyloid pathology in middle-to-late-aged cognitively healthy individuals at risk for AD	Köbe | Gonneaud | Pichet Binette | Meyer | McSweeney | Rosa-Neto | Breitner | Poirier | Villeneuve | (PREVENT-AD) Research Group	**Köbe, Theresa**	202
65	Novel tau PET ligand compound series for detecting 4-repeat tau lesions	Koga | Svensson | Sohn | Dickson	**Koga, Shunsuke**	200
95	Quantitative gradient recalled echo (qGRE) MRI identifies significant neuronal loss in the hippocampal subfields related to cognitive impairment in mild Alzheimer's disease	Kothapalli | Benzinger | Hassenstab | Goyal | Morris | Yablonskiy	**Kothapalli, Satya**	258
99	Lower left ventricular ejection fraction relates to increased cerebrospinal fluid biomarker evidence of neurodegeneration in older adults	Kresge | Liu | Gupta | Osborn | Acosta | Bell | Pechman | Gifford | Mendes | Wang | Blennow | Zetterberg | Hohman | Jefferson	**Kresge, Hailey**	269
108	The ATN framework in ADNI: How do different A,T, and N biomarkers influence the definition of AD pathology and cognitive trajectories?	Landau | Korman | Shaw | Trojanowski | Jagust	**Landau, Susan**	286
76	Associations among amyloid, tau, cerebrovascular disease, and neurodegeneration across cognitive stages in the Alzheimer's continuum	Lao | Kreisl | Brickman	**Lao, Patrick**	221
73	Healthy brain structural connectome predicts regional tau accumulation in amyloid-positive mild cognitive impairment patients	Lee | Shin | Na | Seo | Seong	**Lee, Wha Jin**	214
91	Ante-post mortem binding of THK5317 and its vitro comparability with MK-6240 in a case of FTLD	Lemoine | Chiotis | Leuzy | Graff | Nennesmo | Nordberg	**Lemoine, Laetitia**	252
96	Predictors for β-amyloid positivity in cognitively impaired patients. Data from the Imaging Dementia—Evidence for Amyloid Scanning (IDEAS) Study	Lesman-Segev | Hanna | La Joie | Iaccarino | Siegel | Hillner | Whitmer | Carrillo | Edwards | Chaudhary | Gatsonis | Rabinovici	**Lesman-Segev, Orit**	260
103	Asymmetric tau and focal amyloid PET in an autopsy-confirmed case of AD presenting as primary progressive aphasia	Martersteck | Sridhar | Coventry | Mesulam | Rogalski	**Martersteck, Adam**	275
80	Cross-sectional associations between temporal tau and cortical thickness across the lifespan	Moody | Jacobs | Sidwell | Hanseeuw | Katz | Sanchez | Mayblyum | Estime | Sepulcre | Satizabal | Pase | Beiser | Demissie | Daniluk | Schaefer | Peets | Price | Sperling | DeCarli | Seshadri | Johnson	**Moody, Kirsten**	229
100	ApoE4 as a moderating factor between mild traumatic brain injury and tau deposition in the temporal cortex	Munro | Chen | Rundle | Cullum | Rodrigue | Park	**Munro, Catherine**	270
102	Initial clinical evaluation of [18F] PI-2620 as a potent PET radiotracer imaging tau protein	Oh | Oh | Lee | Oh | Roh | Chung | Lee | Lee | Kim	**Oh, Minyoung**	274
84	Distinct tau PET patterns in atrophy-defined subtypes of Alzheimer's disease	Ossenkoppele | Lyoo | Rabinovici | Hansson	**Ossenkoppele, Rik**	239
70	[18F]AV1451 deposition pattern across the Alzheimer's disease spectrum – characterization at the individual level	Pichet Binette | Gonneaud | Villeneuve | Neuroimaging Initiative	**Pichet Binette, Alexa**	206

Board #	Poster Title	Authors	Presenter	Page
69	Association between elevated brain tau pathology and subsequent cognitive decline among non-demented PSEN1 E280A mutation carriers: Preliminary findings from the COLBOS project	Quiroz | Sperling | Guzman-Velez | Hanseeuw | Pardilla-Delgado | Bocanegra | Vila-Castelar | Baena | Artola | Sanchez | Hampton | Fuller | Ramirez-Gomez | Gatchel | Schultz | Arbo-leda-Velasquez | Lopera | Reiman | Johnson	**Quiroz, Yakeel**	205
71	BLAzER: A versatile and efficient workflow for analyzing PET neuroimaging data in AD	Raman | Grandhi | Murchison | Kennedy | Landau | Roberson | McConathy	**Raman, Fabio**	209
64	Evaluation of [18F]GTP1 (Genentech tau probe 1) Extent and Load for assessing tau burden in Alzheimer's disease	Sanabria Bohorquez | Baker | Manser | Toth | Marik | Weimer	**Sanabria Bohorquez, Sandra**	198
92	Tau and amyloid protein accumulation affect distinct white matter fiber tracts in Alzheimer's disease	Savard | Kang | Pascoal | Mathotaarachchi | Therriault | Chamoun | Lessa Benedet | M. Thomas | Parsons | Tissot | Lussier | Gauthier | Rosa-Neto	**Savard, Melissa**	253
93	Plasma neurofilament light chain concentrations in relation to [18F]florbetapir and [18F]flortaucipir PET in AD	Lessa Benedet | Leuzy | A. Pascoal | Mathotaarachchi | Savard | Therriault | Kang | Chamoun | Schöll | J. Ashton | Gauthier | Zetterberg | Rosa-Neto | Blennow | for the Alzheimer's Disease Neuroimaging Initiative	**Savard, Melissa**	255
61	Modelling tau pathology progression in Alzheimer's disease: Preliminary results and parameters required at a minimum to inform the model	Soucy | Hortelan | Benali	**Soucy, Jean-Paul**	193
81	Amyloid-dependent and –independent effects of Tau on clinical function in AD	Therriault | Pascoal | Sefranek | Mathotaarachchi | Savard | Benedet | Chamoun | Kang | Gauthier | Rosa-Neto	**Therriault, Joseph**	232
82	Voxel-wise receiver operating characteristic analysis reveals clinically relevant sites of amyloid-beta deposition	Therriault | Pascoal | Leuzy | Collij | Lessa Benedet | Mathotaarachchi | Kang | Alves | Massarweh | Soucy | Gauthier | Rosa-Neto	**Therriault, Joseph**	234
94	APOEε4 potentiates the relationship between amyloid-β and tau pathologies in a dose-dependent manner	Parsons | Therriault | Benedet | Pascoal | Mathotaarachchi | Savard | Kang | Chamoun | Soucy | Massarweh | Saha-Chaudhuri | Poirier | Gauthier | Rosa-Neto	**Therriault, Joseph**	257
77	Association between neuroinflammation (level) and cognitive performance	Thomas | Chamoun | Pascoal | Savard | Nazar | Sbeiti | Olmand | Mathotaarachchi | Kang | Therriault | Gauthier | Rosa-Neto	**Thomas, Emilie**	223
109	Neuropsychiatric symptoms are correlated with tau deposition in the AD spectrum	Tissot | Pascoal | Therriault | Chamoun | Lussier | Savard | Mathotaarachchi | Lessa Benedet | Thomas | Parsons | Rosa-Neto | Gauthier	**Tissot, Cécile**	289
111	Molecular imaging discordance with CSF AD biomarkers in atypical AD	Townley	**Townley, Ryan**	292
66	Comparable associations between memory impairment and hippocampal [18F]flortaucipir signal after optimization	Wolters | Ossenkoppele | Golla | Verfaillie | Timmers | Visser | Tuncel | Coomans | Scheltens | Windhorst | van der Flier | Boellaard | van Berckel	**Wolters, Emma**	201
101	A longitudinal examination of amyloid burden and myelin content in major white matter tracts	Yang | Dean III | Vogt | Jonaitis | Hunt | Merluzzi | Kohli | Christian | Oh | Betthauser | Asthana | Johnson | Alexander | Bendlin	**Yang, Kao Lee**	271
78	Relationship of amyloid-beta and neuro-fibrillary tau deposition in Down syndrome using [11C]PiB and [18F]AV-1451 PET	Zammit | Tudorascu | Cody | Laymon | Cohen | Minhas | Ellison | Sabbagh | Zaman | Johnson | Mathis | Klunk | Handen | Christian	**Zammit, Matt**	224
79	Amyloid accumulation in the striatum is more rapid than in the cortex early in Down syndrome and can serve as a marker for early intervention	Zammit | Cody | Betthauser | Tudorascu | Lao | Laymon | Cohen | Murali | Minhas | Zaman | Johnson | Mathis | Klunk | Handen | Christian	**Zammit, Matt**	227

P60: 18F-Florbetaben and 18F-Flutemetamol PET beta-amyloid binding expressed in centiloids

Soo Hyun Cho[1,2], Yeong Sim Choe[1,6], Hee Jin Kim[1,2], Si Eun Kim[1,3], Seung Joo Kim[1,2], Hyemin Jang[1,2], Jun Pyo Kim[1,2], Young Hee Jung[1,2], Duk L. Na[1,2,5,6], Seongbeom Park[1,2], Sang Won Seo[1,2,6]

[1]*Departments of Neurology, Samsung Medical Center, Sungkyunkwan University School of Medicine, Seoul, Korea*
[2]*Neuroscience Center, Samsung Medical Center, Korea, Korea*
[3]*Departments of Neurology, Inje University College of Medicine, Haeundae Paik Hospital, Busan, Korea*
[4]*Department of Neurology, Kangwon National University Hospital, Kangwon National University College of Medicine, Chuncheon, Korea*
[5]*Stem Cell & Regenerative Medicine Institute, Samsung Medical Center, Seoul, Korea*
[6]*Department of Health Sciences and Technology, SAIHST, Sungkyunkwan University, Seoul, Korea*
[7]*Department of Clinical Research Design & Evaluation, SAIHST, Sungkyunkwan University, Seoul, Korea*

Purpose: The Centiloid (CL) method enables quantitative values from Aβ-amyloid (Aβ) imaging of multiple tracers and methods. We compare florbetaben (FBB) and flutemetamol (FMM) head to head using the Centiloid method with zero CL set as an average in young controls (YC) and 100 CL the average in subjects with Alzheimer's disease cognitive impairment (ADCI). We assessed CL units with several reference regions: cerebellar gray (CG), whole cerebellum (WC), WC with brainstem (WC + B) and pons.

Methods: Paired FBB and FMM PET scans were obtained in 20 ADCI, 16 OC and 20 YC aged under 40 years. To generate global cortical target (CTX) volume of interests (VOI), each averaged AD-CTX was generated in MNI-152 space and averaged OC-CTX image was subtracted. The Centiloid methods were applied to establish a conversion from FBB /FMM SUVr values obtained from CTX VOIs.

Results: FBB and FMM retention has no apparent difference between ADCI and OC in amyloid deposition pattern. CTX VOI SUVR from FBB and FMM were highly well correlated each other at four different reference regions. The correlation coefficient for each reference were WC ($r = 0.94$), WC+B ($r = 0.94$), pons ($r = 0.91$) and CG ($r = 0.89$). In order to find the appropriate reference region, we compare the effect size of Centiloid (CL) values between ADCI and YC and compare the variance of CL values in YC group. Taken together, our fingdings show that when we try to convert amyloid PET SUVR to CL unit using FBB and FMM ligands, WC, WC+B and CG could be used as reference regions.

Conclusions: FBB is strongly correlated with FMM and results can be expressed in CL units directly. The WC, WC + B and CG are reliable reference regions when we convert FBB and FMM SUVR into CL units.
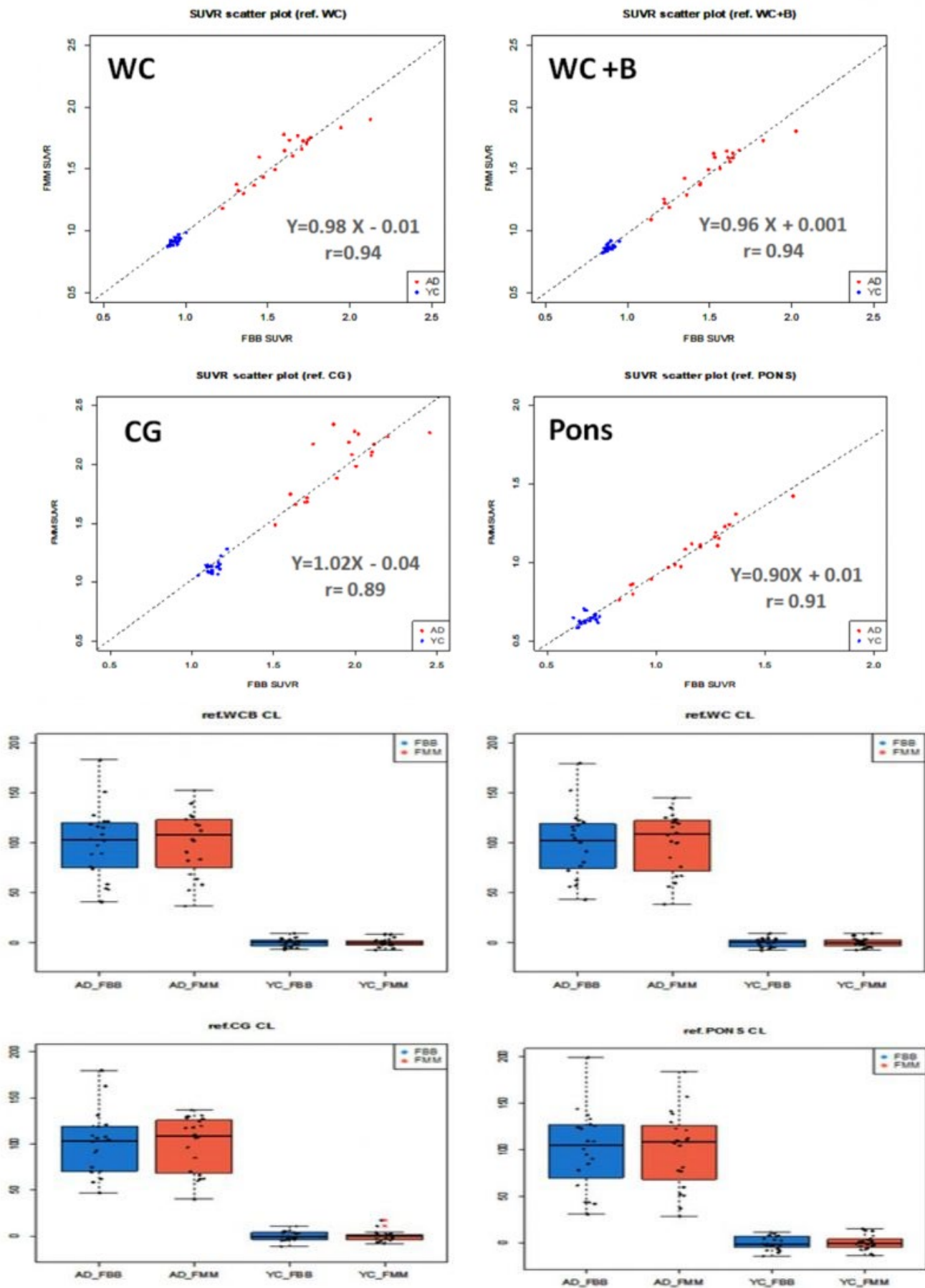
SUVR scatter plot (ref. WC)

SUVR scatter plot (ref. WC+B)

SUVR scatter plot (ref. CG)

SUVR scatter plot (ref. PONS)

ret.WCB CL

ret.WC CL

ref.CG CL

ref.PONS CL

P61: Modelling tau pathology progression in Alzheimer's disease: Preliminary results and parameters required at a minimum to inform the model

Jean-Paul Soucy[1], Valentine Hortelan[1,2], Habib Benali[1]

[1]*PERFORM Centre, Concorda University, Montréal, QC, Canada*
[2]*Université de Liège, Liège, Belgium*

Neurodegenerative diseases typically show microscopic misfolded/insoluble protein aggregates inside/outside of neurons. Many such particles behave as prions. Their regional brain concentration at any given time is constrained by a complex system of molecular biological, chemical, physical and anatomical parameters, including: a) production rates and accumulation of normal proteins and degradation of polymers and misfolded proteins; b) efficiency, rate and duration of the nucleation-elongation process leading to aggregates, which can adopt different conformations linked to variant amino acids sequences and local chemical conditions at the time of their formation; c) movement/propagation of these in neural tissues, by intra/extra-cellular anisotropic diffusion, axonal transport and synaptic release and uptake. Understanding how those parameters influence distribution of aggregates over time could help identify events targetable for progression-blocking therapies. We worked on computational models describing those events in the case of Alzheimer's related tauopathy.

We developed a literature-based model of tau nucleation-elongation. Spreading mechanisms were modeled for monomers and polymers using heat and mass transport equations, their parameters calibrated with diffusor tensors data from DWI. Using numerical simulations we estimated the spatiotemporal evolution of proteins concentration.

For validation, 33 Alzheimer's subjects were selected from ADNI, each with 2 PET tau studies scans, a T1 structural MRI and a DWI MR study (at time 1). PET 2 is the ground truth to which Default Mode Network progression simulation results were compared.

Progression between PET1/2 in DMN was **not** significant (t test p: 0.98) due to a balanced mix (17/16) of subjects with increasing/decreasing tau concentrations. Simulations and PET 2 differed significantly (t test p: 0.003). Improvements will at least need better biological data on aggregates formation rates/conformation, their relation to monomers, data on the effect of cells/axonal losses (decreasing SUVRs and transport), calibration of simulation iterations to disease running time and local impact of amyloid concentrations.

Keywords: *Alzheimer, tau, progression, modelling*

P62: Determination of FTD candidates in an MCI-SNAP cohort by PET amyloid and MRI structural analysis

Christopher Buckley[1], Eva Esteban[1,2], Paul Wilkens[3], David Wolk[4]

[1]GE healthcare, Amersham, UK
[2]University of Surrey, Guilford, UK
[3]GE Healthcare, Marlborough, MA, US
[4]University of Pennsylvania Health Ststem, Pennsylvania, PA, US

Introduction: In a 3-year aMCI outcome study, baseline PET amyloid imaging status was used to assess conversion rate to probable AD. While amyloid positivity was a significant and independent predictor of conversion, a fraction (23%) of the amyloid-negative subjects (MCI–SNAP) also converted, hence the question: **what condition gave rise to their conversion to dementia**?

In a post-hoc analysis, the number of amyloid negative subjects who were candidates for Frontotemporal Dementia (FTD) based on their right-hemisphere temporal pole to occipital lobe cortical thickness were determined to examine this as an alternate disease hypothesis.
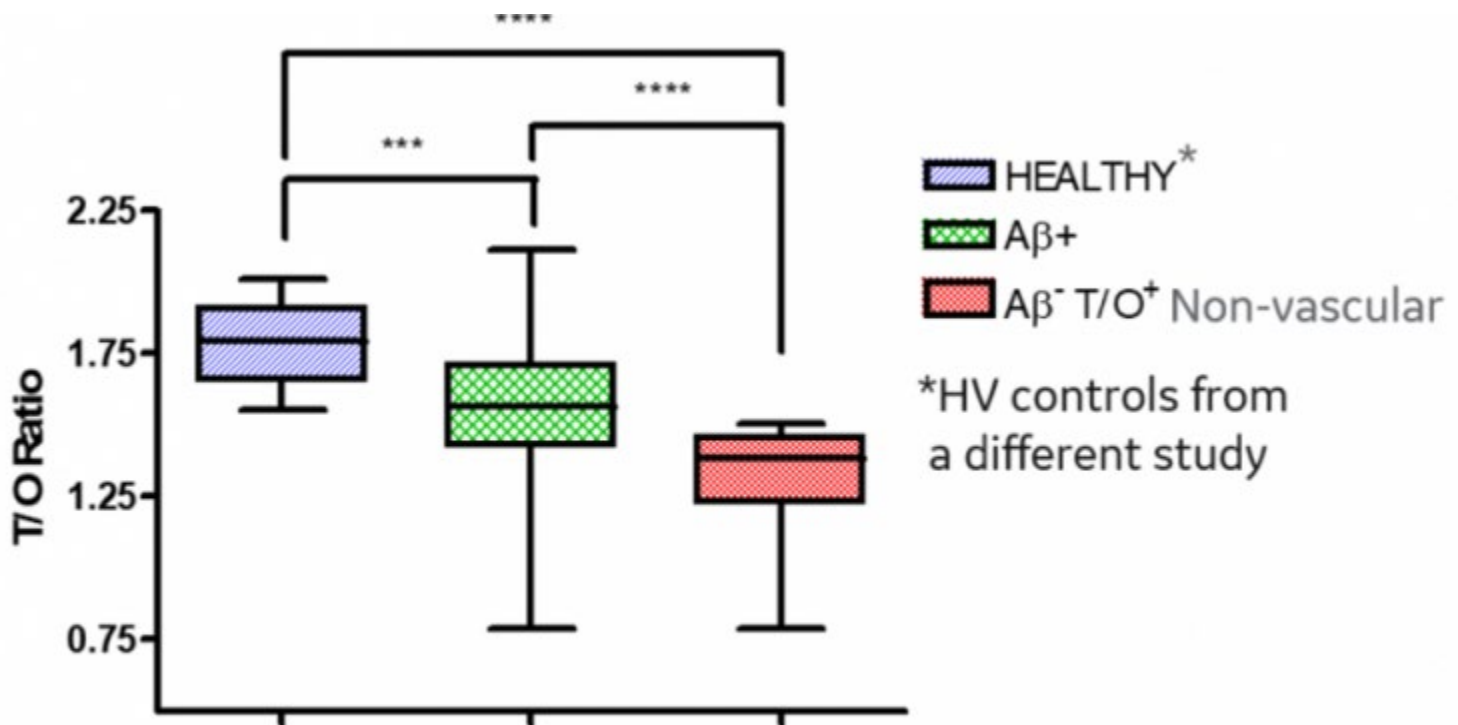
Figure 1. Temporal/Occipital cortical thickness ratios for HV, MCI Aβ+ and MCI Aβ- T/O+ subjects

Methods: [^{18}F]flutemetamol images from the study were quantified using Cortex ID^{TM} with a composite cortical region and were divided into amyloid positive and amyloid negative by the mean +2SD of age-equivalent healthy controls. MRI images were analysed using Freesurfer v6.0 with the Deskian/Killiany VOI atlas to extract the ratio of temporal pole cortical thickness (T) to lateral occipital region cortical thickness (O). A threshold of T/O ratio mean-2SD was obtained from a separate healthy cohort and used to identify aMCI subjects below the threshold ratio of 1.51 for the commonly affected right hemisphere in FTD (Figure 1).

Results: Of 232 subjects in this aMCI study, 222 had MRIs suitable for analysis. Of these, 101 were amyloid positive and 121 were negative. There were 32 subjects who had a T/O ratio below threshold. Of these, 12 converted to dementia within three years.

Discussion: Of the possible non-AD dementia sub-types, only behavioural-variant FTD (bvFTD) has preferential decreased temporal pole cortical thickness. Further, bvFTDs dement at a younger age than other dementia types and the **rate** of cognitive decline is faster. Figures 2 and 3 indicate this in the study cohort and are supportive evidence that A- MCI-SNAP subjects with T/O+ baseline imaging biomarker may be bvFTD sub-
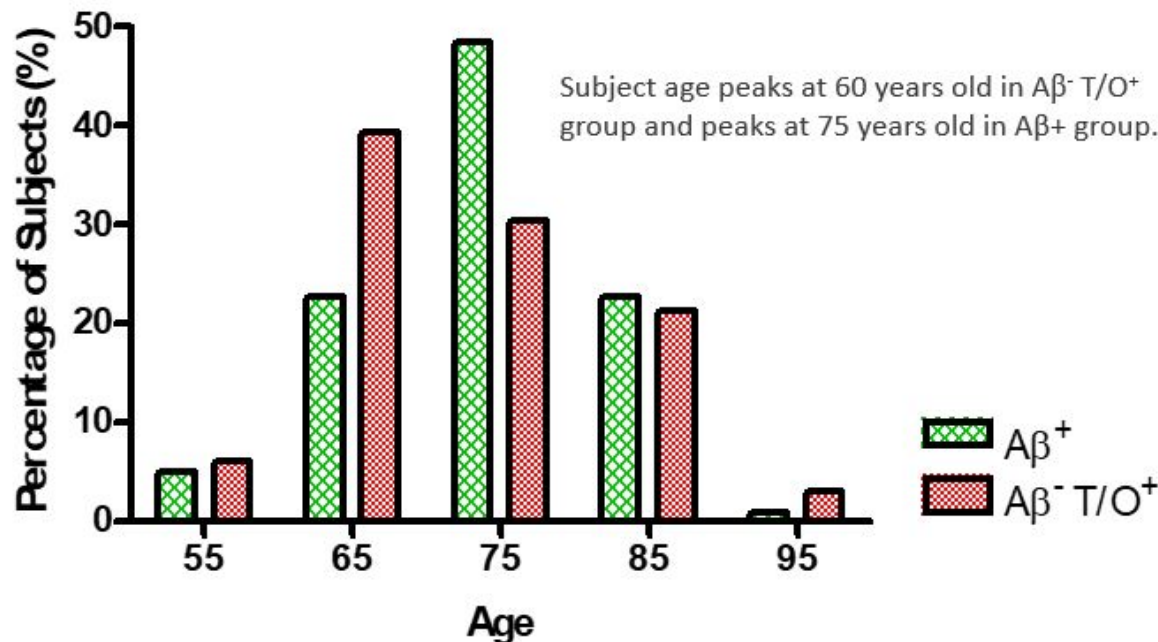
Figure 2. Age distribution A-, T/O+ compared to A+. Results are concordant with younger symptom manifestation in FTD pathology compared to Aβ+ AD pathology·

types.
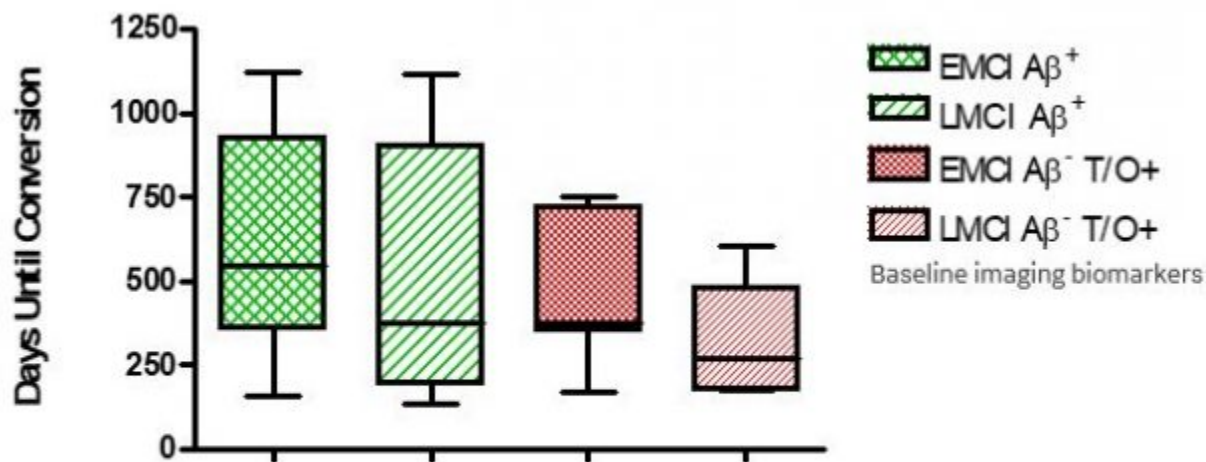
Figure 3. Faster conversion rate for early MCI (EMCI) and late MCI (LMCI) Aβ- T/O+ subjects compared to Aβ+ group, concordant with fast progression of FTD pathology*.

Keywords: *FTD, SNAP, MCI, outcome, A-*

P63: Striatal amyloid load predicts conversion from aMCI to pAD

Christopher Buckley[1], Lovena Chedumbarum-Pillay[1,2], Mark Jenkinson[2], Adrian Smith[1], Thomas Beach[3], Dietmar Thal[4], David Wolk[5]

[1]*GE Healthcare, Amersham, UK*
[2]*University of Oxford, Oxford, UK*
[3]*Banner Health Research Institute, Sun City, AZ, US*
[4]*KU Leuven, Leuven, Belgium*
[5]*University of Pennsylvania Health System, Pennsylvania, PA, US*

Introduction: In a 3-year aMCI outcome study, baseline amyloid imaging status was used to assess conversion rate to probable AD (pAD). While amyloid positivity was a significant and independent predictor of conversion, 45.9% of baseline blinded image evaluation (BIE) amyloid positive subjects (A+) did not convert. Here in a post-hoc analysis we examine how the conversion status of these A+ candidates are associated with the degree of striatal uptake of [18F]flutemetamol.

Methods - Image Processing & Analysis: Anterior striatum and pons VOI masks were processed with baseline PET and T1-w MR images in FSL v5.0.9 to derive bilateral striatal SUVr_pons ratios.

Results and discussion: Of the 98 aMCI BIE A+ subjects, 83 were amenable for processing with FSL. 43 of these A+ subjects converted to pAD within three years. The converters had a mean (sd) bilateral striatal SUVr_pons of 0.647 (0.069), while non-converters had a mean (sd) of 0.581 (0.071) associating conversion with higher uptake (p=0.0006, Wilcoxon rank-sum test). [Figure 1]. It is notable that the converters have a striatal uptake indicating amyloid phase > 3 [Thal et.al.].

The striatal uptake of [18F]flutemetamol was significantly higher in the BIE amyloid positive subjects who converted from aMCI to pAD, compared to those who remained aMCI in the 3 year time period. Also, we see an increase separation in the SUVr when we consider late MCIs (LMCI) only [Figure 2]. These results show that striatal uptake in A+ subjects has value as a predictive metric in aMCI to AD conversion.

Bilateral Striatal SUVr__pons:
Correlation with Conversion Status in BIE Amyloid Positive Cohort

p=0.000592

A+,Non-Conv.
n=39

A+,Conv.
n=43

Figure 1

Bilateral Striatal SUVr__pons:
Correlation with Conversion Status in BIE Amyloid Positive LMCI Cohort

p=0.002

Non-Conv.
n=22
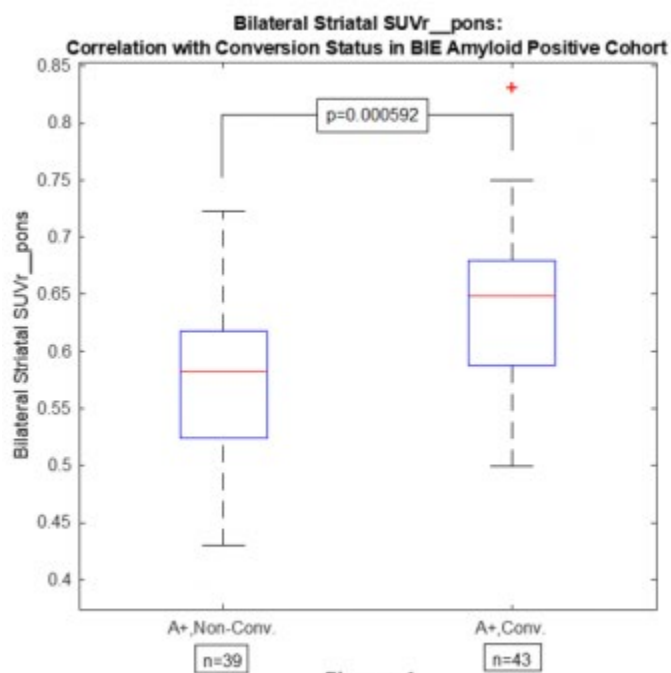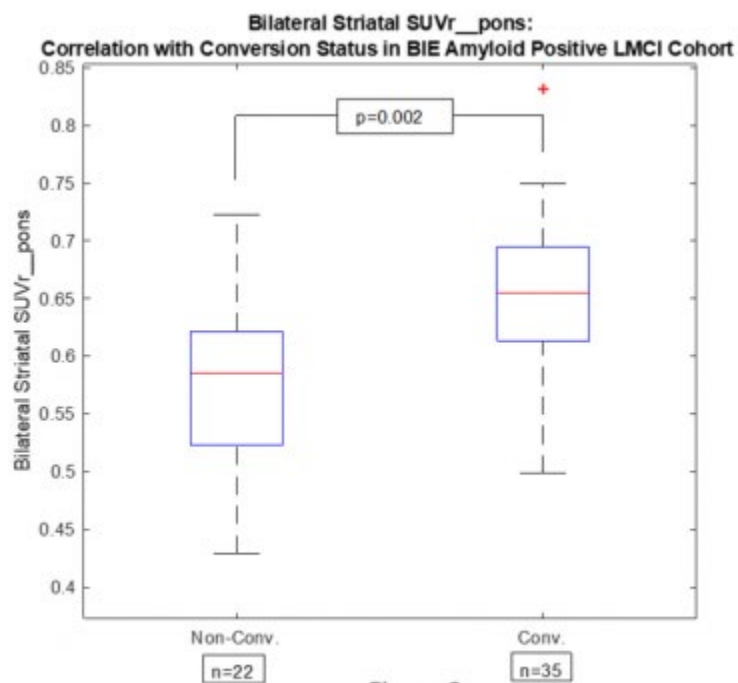
Conv.
n=35

Figure 2

References: Thal et.al. Acta Neuropathologica 2018;136(4):557-567

Keywords: *Striatum, aMCI, conversion, SUVR*

P64: Evaluation of [18F]GTP1 (Genentech tau probe 1) Extent and Load for assessing tau burden in Alzheimer's disease

Sandra Sanabria Bohorquez[1], Suzanne Baker[1,2], Paul Manser[1], Balazs Toth[1], Jan Marik[1], Robby Weimer[1]

[1]Genentech, Inc., South San Francicso, CA, US
[2]Molecular Biophysics and Integrated Bioimaging, Lawrence Berkeley National Lab, Berkeley, CA, US, Berkeley, CA, US

Objective: To evaluate the performance of SUVR, Extent and Load metrics for detecting [18F]GTP1 longitudinal change in Alzheimer's disease (AD).

Methods: [18F]GTP1 imaging was performed at baseline and 12 months in amyloid negative and positive healthy volunteers (HV; n[BL/12m]=7/2 and 8/7, respectively), and amyloid positive prodromal (Prod; n=27/18; MMSE 24-30, CDR = 0.5) and mild/moderate (MM; n=38/27; MMSE 22-30, CDR = 0.5-2) AD patients. Images were converted into SUVR using the cerebellum gray as reference. Extent was defined as the percentage of voxels within an ROI above a threshold and Load was calculated as the sum of these voxels SUVR divided by the number of voxels in the ROI (Weimer et al. HAI 2017). Threshold values were derived based on: (1) the HV voxelwise SUVR distribution in the whole gray matter, (2) ability to discriminate HV vs. AD in a temporal ROI (Jack et al. 2017), and (3) the individual scans cerebellum uptake distribution. Methods 1&2 estimate a unique threshold for all subjects and scans. Method 3 estimates a scan specific threshold calculated as the mean plus two standard deviations within the cerebellum.

Results: Figure 1 illustrates the results from the threshold estimation methods. The values from method 1 were 1.4 or 1.5 SUVR (HV distribution 95 or 97.5%ile, respectively) and method 2 resulted in a threshold of 1.25 SUVR. Method 3 resulted in thresholds values that could vary between timepoints. Figure 2 shows the metrics measured change (Δ) at 12 months. The average ΔExtent andΔLoad were larger yet the %variance of the change (%CV=100%SD/average) was lower using method 3 when compared to methods 1 and 2. Additionally, method 3 ΔExtent and ΔLoad %CVs were lower than ΔSUVR %CV.

Conclusion: Extent and Load metrics derived from scan specific thresholds provide an opportunity to reduce variability in longitudinal tau PET measurements.
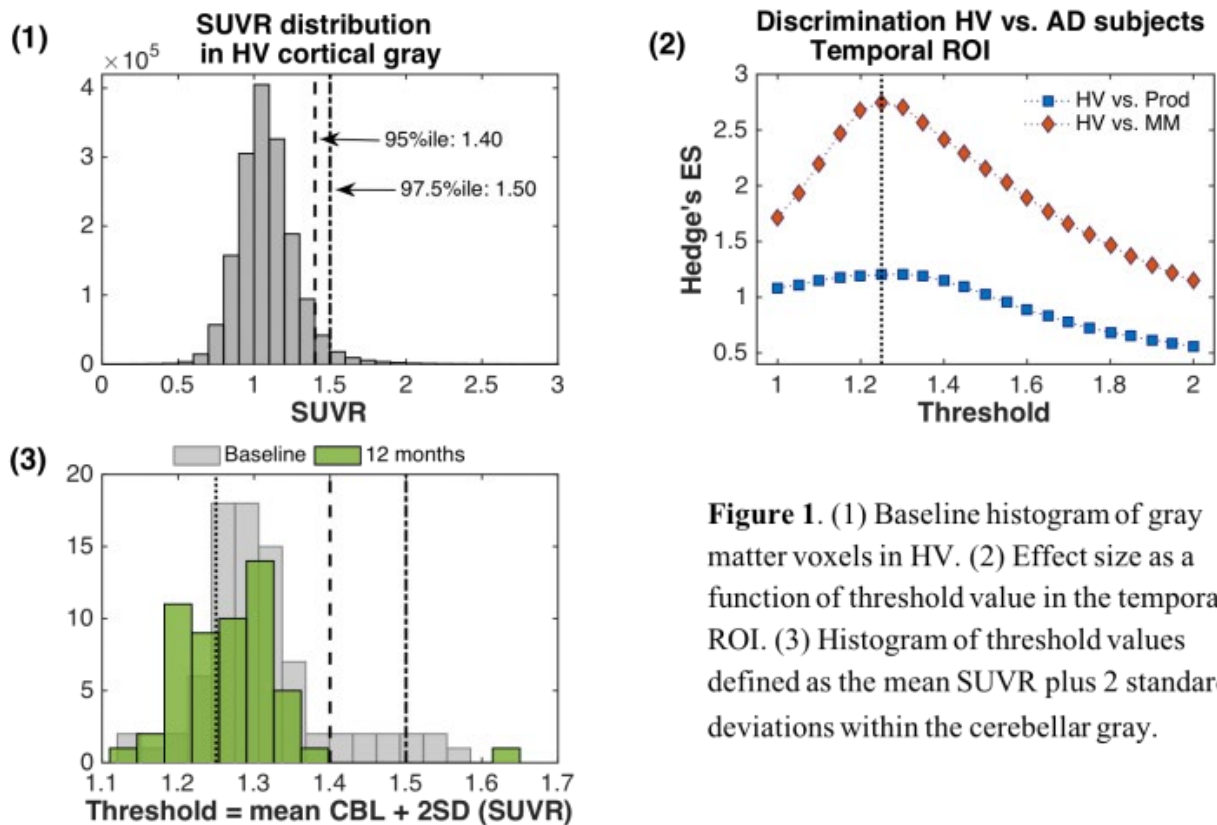
Figure 1. (1) Baseline histogram of gray matter voxels in HV. (2) Effect size as a function of threshold value in the temporal ROI. (3) Histogram of threshold values defined as the mean SUVR plus 2 standard deviations within the cerebellar gray.
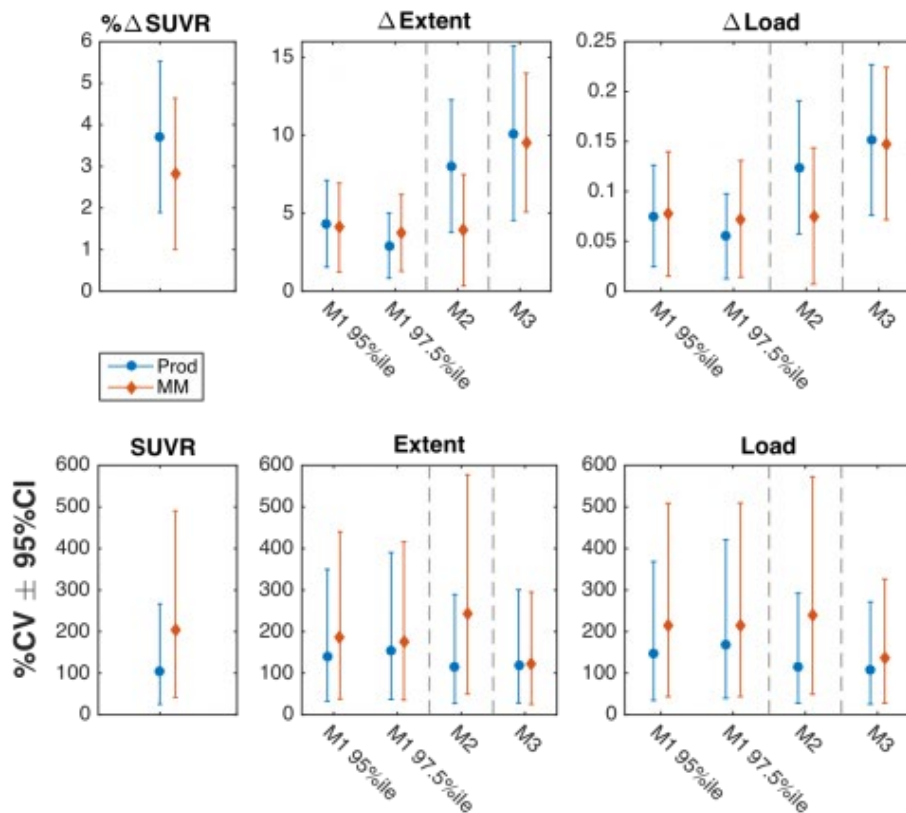
Figure 2. Top: Measured SUVR, extent and load change (Δ) in prodromal (n=18) and mild/moderate (n=27) subjects at 12 months relative to baseline. Bottom: Comparison of measured percentage variance (%CV) of ΔSUVR, Δextent and Δload as function of threshold. Thresholds for extent and load calculated using Method 1 (M1), Method 2 (M2) and Method 3 (M3).

Keywords: *Tau PET imaging, tau pathology changes, disease progression, tau PET quantification*

P65: Novel tau PET ligand compound series for detecting 4-repeat tau lesions

<u>Shunsuke Koga</u>[1], Samuel Svensson[2], Dan Sohn[2], Dennis Dickson[1]

[1]*Department of Neuroscience, Mayo Clinic, Jacksonville, FL, US*
[2]*CBD Solutions, Center for Molecular Medicine, Stockholm, Sweden*

Background: Tau PET tracers have been widely used in clinical research. It is challenging to interpret results of patients with 4-repeat tauopathies, such as progressive supranuclear palsy (PSP) and corticobasal degeneration (CBD), because their affected brain regions are also common sites of off-target binding of the tau PET tracers, and straight filaments in both diseases are not preferentially bound by these tracers compared with pair-helical filaments observed in Alzheimer's disease (AD) brains. CBD Solutions and its collaborators have developed a series of compounds (CBD2001, CBD2017, CBD2115, CBD2133, and CBD2134) to detect 4-repeat tau with less off-target binding.

Method: In the present study, we have characterized **in vitro** radioligand binding profile to recombinant 4-repeat tau and $Abeta_{1-42}$ fibrils. We performed tau ligand fluorescence staining with anti-tau or anti-α-synuclein antibodies, as well as autoradiography in brain sections from AD, PSP, CBD, and Pick disease. To assess possible binding to α-synuclein pathology, brain sections from dementia with Lewy bodies and multiple system atrophy (MSA) were also examined. For select ligands, in vitro autoradiography was performed.

Results: The compounds bound with low nanomolar affinity to recombinant 4-repeat tau fibrils. THK-5117and PBB3 were able to fully compete with [^{3}H]CBD2134 binding to recombinant 4-repeat tau fibrils. All compounds labeled neurofibrillary tangles in AD as well as coiled bodies and tufted astrocytes in PSP by fluorescence staining. Of those, CBD2017 had broader binding spectrum compared with other compounds; CBD2017 also detected Pick bodies in Pick disease, astrocytic plaques in CBD, and glial cytoplasmic inclusions in MSA. Lewy bodies and Lewy neurites were not detected by any compounds.

Discussion: Our current chemical scaffolds has no stilbene or diene chemical moieties, and preliminary data of a series of tau PET tracers show that they may be a promising candidates for detecting tau lesions in patients with 4-repeat tauopathies.

Keywords: *[3H]CBD2134, CBD2017, Autoradiography, Progressive supranuclear palsy, Corticobasal degeneration*

P66: Comparable associations between memory impairment and hippocampal [18F]flortaucipir signal after optimization

<u>Emma E Wolters</u>[1,2], Rik Ossenkoppele[2,3], Sandeep SV Golla[1], Sander CJ Verfaillie[1], Tessa Timmers[1,2], Denise Visser[1], Hayel Tuncel[1], Emma M Coomans[1], Philip Scheltens[2], Albert D Windhorst[1], Wiesje M van der Flier[2,4], Ronald Boellaard[1], Bart NM van Berckel[1]

[1]*Department of Radiology & Nuclear Medicine, Amsterdam Neuroscience, Vrije Universiteit Amsterdam, Amsterdam UMC, Amsterdam, The Netherlands*
[2]*Alzheimer Center Amsterdam, Department of Neurology, Amsterdam Neuroscience, Vrije Universiteit Amsterdam, Amsterdam UMC, Amsterdam, The Netherlands*
[3]*Clinical Memory Research Unit, Lund University, Lund, Sweden*
[4]*Department of Epidemiology and Biostatistics, Vrije Universiteit Amsterdam, Amsterdam UMC, Amsterdam, The Netherlands*

Background: Off-target [18F]flortaucipir binding in the choroid plexus may cause spill-in into the anatomically proximate hippocampus, which could hamper associations with memory performance. We compared three different approaches to optimize the quantification of hippocampal [18F]flortaucipir signal using a semi-automated technique, and assessed which method showed the best correlates with cognitive performance.

Methods: 130 minute dynamic [18F]flortaucipir PET scans were performed in 109 subjects (n=45 controls with subjective cognitive decline (SCD), n=64 with cognitive impairment (mild cognitive impairment (MCI)/ Alzheimer's disease (AD) dementia). We extracted hippocampal binding potential (BP_{ND}) using receptor parametric mapping (reference region cerebellar grey matter). Three hippocampal volumes of interest(VOIs) were generated: a 100% hippocampal VOI (Hammers atlas-based), and eroding a percentage of the highest hippocampus BP_{ND} voxels (i.e. lowering spill-in) resulting in optimized 50% and 40% hippocampal VOIs. The eroded VOIs were corrected for partial volume (PVC) using Van Cittert iterative deconvolution and HYPR denoising (HDH). Cognitive performance was assessed with Rey auditory verbal learning delayed recall corrected for immediate recall(% remembered). We performed receiver operating characteristic analyses to investigate which method could best discriminate controls and MCI/AD. Subsequently, we performed non-parametric linear regressions to investigate associations between the hippocampal [18F]flortaucipir BP_{ND} VOIs and delayed recall(% remembered), adjusted for age, gender and education.

Results: We found higher hippocampal BP_{ND} in MCI/AD (BP_{ND}=0.27±0.15) compared to SCD (BP_{ND}= 0.07±0.13) and all methods showed comparable discriminative effects ($AUC_{100\%}$=0.850 (CI=0.777–0.928); $AUC_{50\%}$=0.831 (CI=0.748–0.914); $AUC_{40\%}$=0.820 (CI=0.735–0.906). Across groups, higher [18F]flortaucipir BP_{ND} was related to more severe memory impairment with comparable effect sizes for all hippocampal VOIs(standardized betas; $\beta_{100\%}$=-0.588, $\beta_{50\%=}$ -0.582, $\beta_{40\%}$ -0.573, all p<0.001).

Conclusions: The combination of HDH PVC and eroding of hippocampal tau load does not result in stronger associations with cognitive correlates. Both discrimination in diagnosis and associations between hippocampal [18F]flortaucipir BP_{ND} and memory impairment were comparable for all methods.

P67: Vascular medical treatment influences the association between vascular burden and amyloid pathology in middle-to-late-aged cognitively healthy individuals at risk for Alzheimer's disease

Theresa Köbe[1,2], Julie Gonneaud[1,2], Alexa Pichet Binette[1,2,4], Pierre-François Meyer[1,2], Melissa McSweeney[1,2], Pedro Rosa-Neto[1,2,3,4], John C. S. Breitner[1,2,4], Jude Poirier[1,2], Sylvia Villeneuve[1,2,3,4], for the Presymptomatic Evaluation of Novel or Experimental Treatments for Alzheimer Disease (PREVENT-AD) Research Group (PREVENT-AD) Research Group[2]

[1]*Department of Psychiatry, McGill University, Montreal, QC, Canada*
[2]*Douglas Mental Health University Institute, Studies on Prevention of Alzheimer's Disease (StoP-AD) Centre, Montreal, QC, Canada*
[3]*Department of Neurology and Neurosurgery, McGill University, Montreal, QC, Canada*
[4]*McGill Centre for Integrative Neuroscience, McGill University, Montreal, QC, Canada*

Objective: The influence of vascular risk factors (VRF) on Alzheimer's disease (AD) pathophysiology remains inconclusive. This study aims to examine the associations of lipids, blood pressure and combined VRF scores with Aß and **tau** pathology in the preclinical disease stage, considering the moderating impact of vascular drug treatment.

Methods: Cognitively healthy individuals with family history of AD from the PREVENT-AD cohort were included (mean age: 62 years). Aß-PET [^{18}F-NAV-4694] and **tau**-PET [^{18}F-AV-1451] scans were obtained from 120 individuals to examine the association between lipids [total cholesterol, high-density lipoprotein (HDL), low-density lipoprotein (LDL) cholesterol], blood pressure [systolic and diastolic blood pressure, pulse pressure], combined VRF scores [CAIDE, FCRP, FHS-CVD (see Figure1 legend)] and global Aß and entorhinal **tau** SUVR. Individuals were binarized for vascular medication (dyslipidemia and/or hypertensive drugs) to test for interaction effects, using linear regression models. Post-hoc analyses assessed within-group effects. All models were corrected for age, sex and time difference between VRF and PET measurements, while secondary models also included correction for apolipoprotein E ε4 (APOEε4) status. The analyses were repeated using CSF Aβ$_{1-42}$ and p-**tau** biomarkers in 162 PREVENT-AD individuals (67 also included in the PET analyses).

Results: In most analyses, we found interactions between VRF and vascular medical treatment on Aß burden (Figure1). In non-treated participants, higher levels of total cholesterol, LDL, systolic blood pressure, pulse pressure and all combined VRF scores were associated with higher Aß-PET deposition (all $p_{non-treated} \leq 0.04$). Similarly, total cholesterol, LDL and the CAIDE risk score were related to lower Aβ$_{1-42}$ in the CSF in non-treated participants only (all $p_{non-treated} \leq 0.02$). All associations were independent of APOEε4 (data not shown). No associations were found between VRF and **tau**.

Conclusions: Dyslipidemia and hypertensive drugs modify the relationship between VRF and Aß, such that increased vascular burden was only associated with Aß pathology in non-treated individuals.
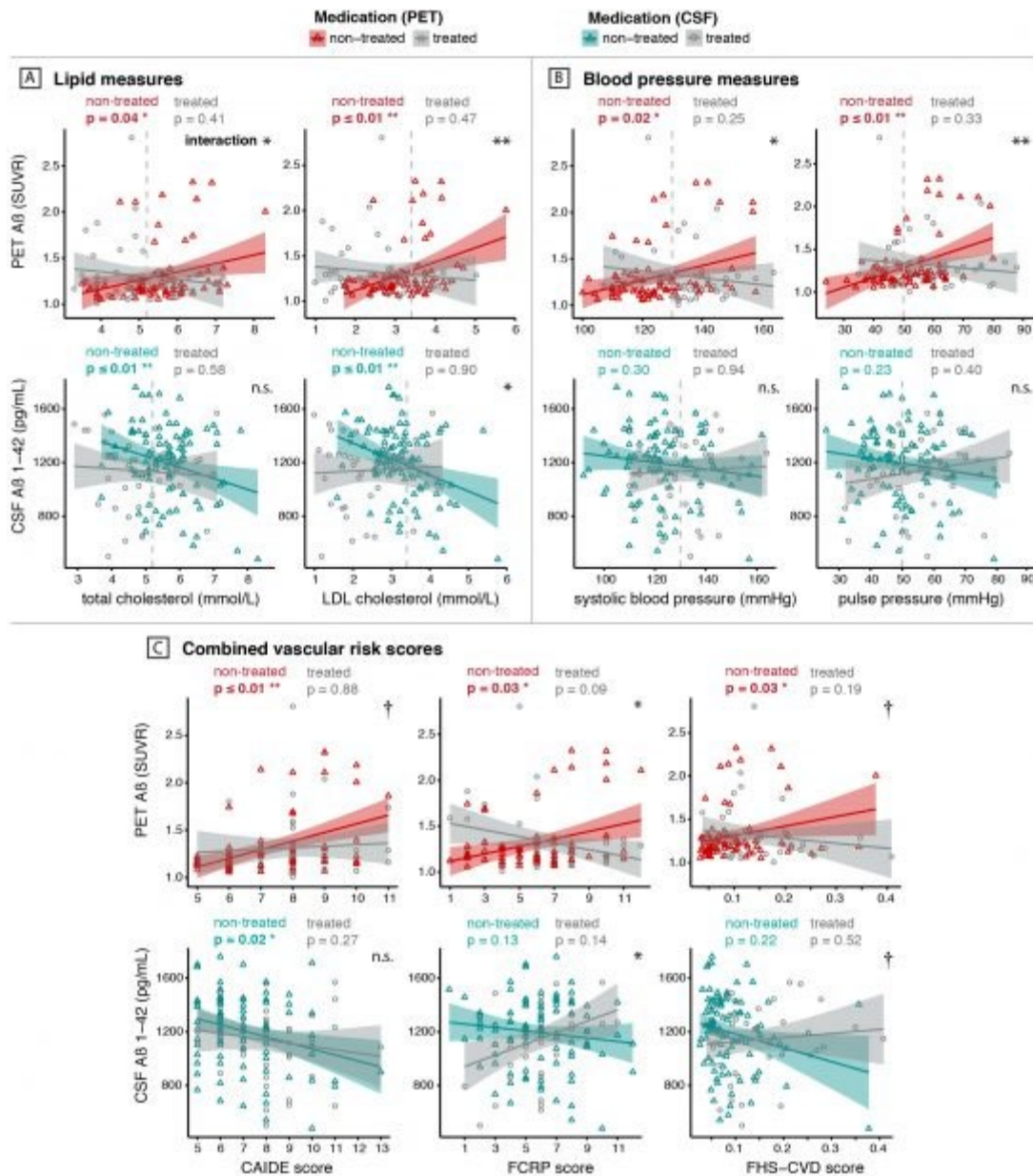
Figure1. Association between vascular risk factors and Aβ in treated and non-treated participants.

Concentrations of plasma lipids (A, total cholesterol and LDL cholesterol), blood pressure (B, systolic blood pressure and pulse pressure) and combined vascular risk scores (C, CAIDE, FCRP and FHS-CVD scores) are individually plotted against global cerebral Aβ standard uptake value ratios (SUVR) measured with PET (upper panels in red and gray) and $Aβ_{1-42}$ measured in CSF (lower panels in cyan and gray) (unadjusted raw data is shown). Statistics were obtained with linear regression analyses controlled for age, sex and time difference between VRF and PET/ CSF assessments. Interaction effects between VRF and vascular medical treatment are indicated within the graphs (upper right corner, ** ≤ 0.001, * ≤ 0.05, † ≤ 0.1). Shaded areas represent 95% confidence intervals for regression lines' slopes. Dotted lines represent the thresholds for elevated values in the different VRF: >5.2 mmol/L for total cholesterol, >3.4 mmol/L for LDL, ≥130 mmHg for systolic blood pressure and >50 mmHg for pulse pressure. CAIDE, cardiovascular risk factors, aging and dementia risk score (including age, education, sex, systolic blood pressure, body mass index, total cholesterol, physical activity and APOEε4); FCRP, Framingham Coronary Risk Profile (including age, sex, hypertension, HDL, LDL, smoking and diabetes); FHS-CVD, Framingham general CVD risk score (including age, systolic blood pressure, total cholesterol, HDL, smoking, and diabetes, stratified for sex and treatment for hypertension).

P68: Amyloid deposition and hippocampal atrophy in non-demented elderly subjects over 85 years

Valerie Treyer[1,4], Rafael Meyer[1,5], Andreas Buchmann[1], Giovanni Crameri[1], Sandro Studer[1], Antje Saake[1], Esmeralda Gruber[1], Paul Unschuld[1,3], Roger Nitsch[1,2], Christoph Hock[1,2], Anton Gietl[1]

[1]*Institute for Regenerative Medicine (IREM), University of Zurich, Schlieren, Switzerland*
[2]*Neurimmune, Schlieren-Zurich, Schlieren, Switzerland*
[3]*Hospital for Psychogeriatric Medicine, University of Zurich, Zurich, Switzerland*
[4]*Department of Nuclear Medicine, University Hospital of Zurich, Zurich, Switzerland*
[5]*Psychiatric Services Aargau, Brugg, Switzerland*

Background: A considerable number of individuals have preserved cognition and maintain a high level of everyday function even at very high age. We characterized such a population with respect to markers for Alzheimer's disease and explored lifestyle factors and personality traits.

Methods: 49 participants (average age of 87.8/range: 85 to 94 years) without dementia received neuropsychological testing and underwent a PET/MR (Signa PET/MR GE Healthcare) scan with 18F-Flutemetamol. Images were processed with PMOD NeuroTool. Volumes of amygdala, anterior and posterior hippocampus were manually outlined.

Results: Participants had 14.12 years of education (SD 2.9) and a MMSE score of 28.37 (SD 1.8). Six were ApoE epsilon 4 carrier with three e2/e4 combinations. There were no correlations between cortical or regional amyloid-load with hippocampal or amygdala volume. Distribution of amyloid-load was as follows: Quartile 1:1.09 -1.29, Q2:1.29–1.4, Q3: 1.4–1.6 Q4:1.6–3.2. Neither MMSE nor neuropsychological performances did correlate with brain beta-amyloidosis. Measures of memory performance (VLMT) showed no correlations with anterior hippocampus but posterior hippocampal volume correlated negatively with immediate recall after presentation of an intrusion list (rho =-0.309, p=0.035) and recognition (rho=-0.325, p=0.024). The 6 E4 carriers showed better performance in word recall compared to non-carrier (median 6.19 vs. 8.5, U=208.5, p=0.007). NEOFFI measures of neuroticism and extraversion were significantly different over the 4-quartiles for amyloid SUVR. Participants in the highest quartile showed reduced extraversion compared to quartiles 1-3. However, participants in Q1-Q3 showed a significant positive correlation with extraversion (rho=0.402, p=0.014).

Discussion: Our results show that amyloid-deposition and hippocampal atrophy occur frequently at higher age in non-demented healthy subjects. However, the typical association of amyloid with hippocampal volume loss and impaired memory function, which characterizes the pathway to Alzheimer's disease, is no longer present. This could point to yet undiscovered protective or modifying factors.

Keywords: *Amyloid, memory, oldest-old, hippocampus volume, personality*

P69: Association between elevated brain tau pathology and subsequent cognitive decline among non-demented PSEN1 E280A mutation carriers: Preliminary findings from the COLBOS project

Yakeel Quiroz[1,2,3], Reisa Sperling[1,3,4], Edmarie Guzman-Velez[1], Bernard Hanseeuw[1], Enmanuelle Pardilla-Delgado[1], Yamile Bocanegra[2], Clara Vila-Castelar[1], Ana Baena[1,2], Arabiye Artola[1], Justin Sanchez[1], Olivia Hampton[1], Joshua Fuller[1], Liliana Ramirez-Gomez[1], Jennifer Gatchel[1], Aaron Schultz[1], Joseph Arboleda-Velasquez[5], Francisco Lopera[2], Eric Reiman[6], Keith Johnson[1]

[1]*Massachusetts General Hospital, Harvard Medical School, Boston, MA, US*
[2]*Grupo de Neurociencias, Universidad de Antioquia, Medellin, CO*
[3]*Athinoula A. Martinos Center for Biomedical Imaging, Charlestown, MA, US*
[4]*Brigham and Women's Hospital, Harvard Medical School, Boston, MA, US*
[5]*Schepens Eye Research Institute of Mass Eye and Ear, Boston, MA, US*
[6]*Banner Alzheimer's Institute, Phoenix, MA, US*

Objective: While brain imaging markers have been used in early detection and tracking of Alzheimer's disease (AD) pathology, their ability to predict subsequent cognitive decline remains to be determined. In this study, we compared the utility of baseline tau vs. amyloid PET to predict cognitive decline in non-demented Presenilin-1 (PSEN1) E280A mutation carriers from the Colombian autosomal dominant AD (ADAD) kindred.

Methods: Exploratory analyses were conducted with baseline biomarker and longitudinal cognitive data from thirteen non-demented individuals, aged 30-45 years (5 unimpaired carriers, 2 mildly impaired carriers, and 6 age-matched non-carriers), as part of the Colombia-Boston Longitudinal Biomarker Study (COLBOS Project). All subjects had one parent with the PSEN-1 mutation, and thus bore a 50% risk of carrying it themselves. Baseline cerebral-to-cerebellar Pittsburgh Compound B (PiB) DVRs and Flortaucipir (FTP) SUVRs were related to 2-year subsequent decline on the Alzheimer's Prevention Initiative (API) preclinical ADAD cognitive composite, previously found to be sensitive to preclinical progression. Spearman correlations were used to estimate the relationship between baseline biomarker measures and subsequent cognitive decline in mutation carriers.

Results: In carriers, baseline entorhinal cortex (EC) and inferior temporal lobe (IT) tau SUVRs were associated with decline on the cognitive composite (EC: r= -.85, p=.01; IT: r= -.89, p=.008); PiB DVRs were not (r= -.58, p=.18).

Conclusions: Preliminary findings support a relationship between baseline tau PET measurements and subsequent cognitive decline among non-demented mutation carriers from the Colombian kindred with ADAD. Findings also suggest that tau PET measurements may be better prognostic indicators of AD-related cognitive decline than amyloid PET in ADAD mutation carriers. Research with larger samples is needed to further clarify the prognostic value of these biomarkers and measure longer-term associations in unimpaired individuals at risk for autosomal dominant and late-onset AD.

P70: [18F]AV1451 deposition pattern across the Alzheimer's disease spectrum – characterization at the individual level

Alexa Pichet Binette[1,3], Julie Gonneaud[2,3], Sylvia Villeneuve[2,3], Alzheimer's Disease Neuroimaging Initiative[4]

[1]*Integrated Program in Neuroscience, McGill University, Montreal, QC, Canada*
[2]*Department of Psychiatry, McGill University, Montreal, QC, Canada*
[3]*Douglas Mental Health Research Institute, StoP-AD Centre, Montreal, QC, Canada*
[4]*Alzheimer's Disease Neuroimaging Initiative, CA, US*

Background: The extent to which older adults follow a typical pattern of tau-PET deposition is not clear. We focused on inter-individual pattern of [18F]AV1451-PET binding across Braak stages and single brain regions in participants along the AD spectrum.

Methods: We included 166 Aβ-negative (113 cognitively normal [CN], 33 eMCI, and 20 lMCI/AD) and 129 Aβ-positive (72 CN, 30 eMCI and 27 lMCI/AD) participants from ADNI with a [18F]AV1451-PET scan. SUVRs were extracted in composite regions approximating Braak stages and in the Freesurfer Desikan atlas regions as more fine-grained measurements. In each region, we derived liberal and conservative thresholds using Gaussian-mixture models (GMM) across all participants (respectively 50% and 90% probability to be in high SUVR distribution). We then examined the distribution of elevated SUVR across all regions at the subject-level.

Results: Even when applying liberal thresholds for positivity, only 4% of Aβ-negative participants had elevated SUVR in Braak I/entorhinal and/or in further stages (Fig.1A). In Aβ-positive subjects, 17% CN, 43% EMCI and 67% LMCI/AD had elevated SUVR in Braak I (Fig.1B and Fig.2). Among these individuals, only 50% of LMCI/AD had elevated SUVRs in further stages compared to 92% in EMCI. Using smaller regions, [18F]AV1451 spreading became evident in LMCI/AD and 8% of CN showed focal cortical binding in the absence of elevated entorhinal SUVR (Fig.2).

Conclusions: Almost no Aβ-negative individuals have elevated tau, regardless of clinical diagnosis. All Aβ-positive participants followed the expected pattern of tau spreading, when using composite Braak regions, but only 50% of LMCI/AD showed abnormal binding outside of the entorhinal cortex even with liberal thresholds. Using smaller regions revealed widespread tau in LMCI/AD. Furthermore, some CN individuals did not follow the expected spatiotemporal progression of tau. This unexpected focal binding in CN might indicate non-AD neurodegenerative disease or false positive results.

Figure 1

A. Amyloid-negative
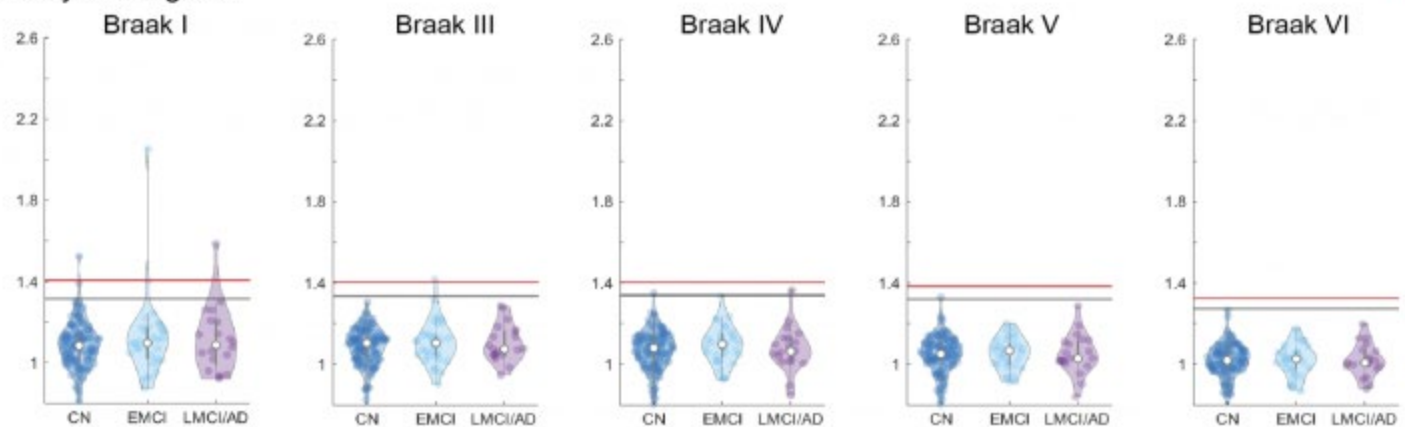
B. Amyloid-positive
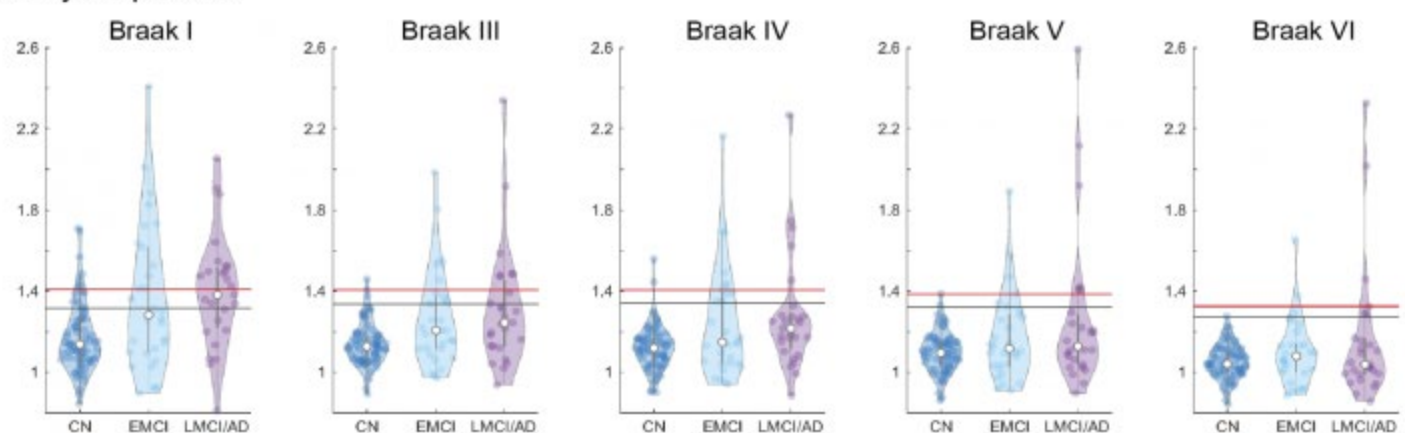
GMM did not yield two distributions in the hippocampus (Braak II), and thus was removed from the analyses. Mean SUVR in Braak stages I, III, IV, V and VI in Aβ-negative individuals (**1A**) and Aβ-positive (**1B**). Grey lines represent the liberal threshold and red lines the conservative threshold.

Figure 2

A. [18F]AV1451 SUVRs
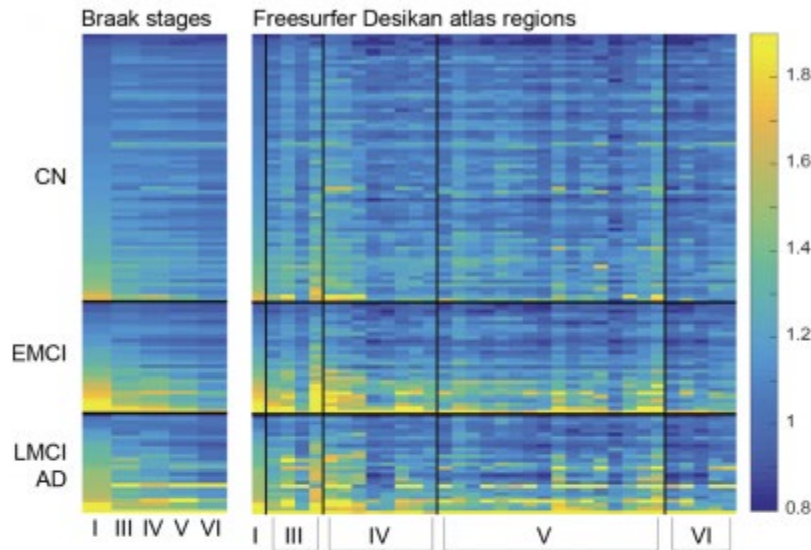
B. Thresholds
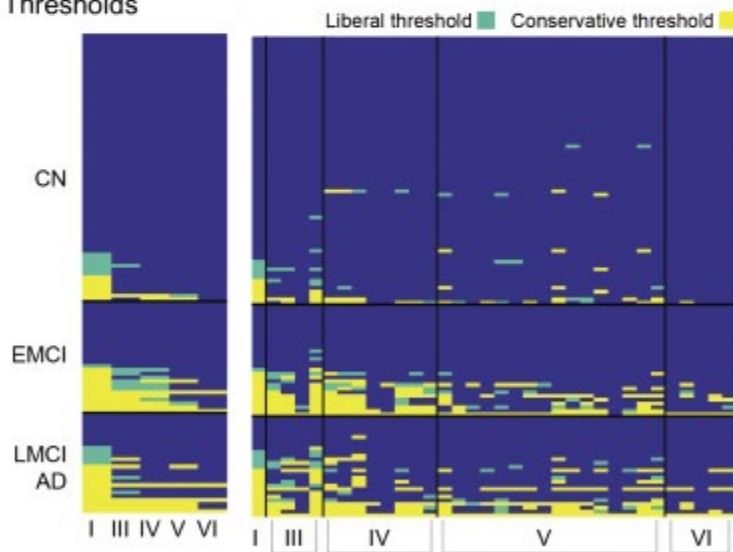
GMM did not yield two distributions in the hippocampus (Braak II), and thus was removed from the analyses. Composite Braak regions are on the left and single brain regions on the right. All matrices are ordered based on Braak I.
2A. [18F]AV1451 SUVR in brain regions (columns) across all Aβ-positive participants (rows). **2B.** Thresholded matrices showing brain regions (columns) where Aβ-positive participants (rows) are positive either on the liberal (green) and conservative (yellow) positivity thresholds.

Keywords: *tau, Braak*

P71: BLAzER: A versatile and efficient workflow for analyzing PET neuroimaging data in Alzheimer's disease

Fabio Raman[1,2], Sameera Grandhi[1,2], Chad Murchison[2,3], Richard Kennedy[2,3], Susan Landau[4], Erik Roberson[2,5,6], Jon McConathy[1,2]

[1]*The University of Alabama at Birmingham, Department of Radiology, Birmingham, AL, US*
[2]*The University of Alabama at Birmingham, Alzheimer's Disease Center, Birmingham, AL, US*
[3]*The University of Alabama at Birmingham, Department of Biostatistics, Birmingham, AL, US*
[4]*The University of California at Berkeley, Helen Wills Neuroscience Institute, Berkeley, CA, US*
[5]*The University of Alabama at Birmingham, Department of Neurology, Birmingham, AL, US*
[6]*The University of Alabama at Birmingham, Center for Neurodegeneration and Experimental Therapeutics, Birmingham, AL, US*

Objective: The semi-automated Biomarker Localization, Analysis, Visualization, Extraction, and Registration (BLAzER) workflow allows for rapid evaluation of amyloid– and tau–PET images, combining features well-suited for both clinical and research workflow. The purpose of the study was to assess BLAzER for regional brain PET quantification using participants with different cognitive statuses from the Alzheimer's Disease Neuroimaging Initiative (ADNI) dataset. Additionally, we determined whether different segmentation inputs, FreeSurfer and Neuroreader, can be used and provide similar results with our workflow.

Methods: 127 amyloid–PET and 55 tau–PET studies along with corresponding volumetric MRI were selected from ADNI. The BLAzER workflow begins with segmentation of MR images by FreeSurfer v6.0.0 (Boston, MA) or Neuroreader (Horsens, Denmark). Segmented output files along with source MR and PET scans are then visualized and quantified using an automated workflow on FDA-approved software (MIM v6.6.13, Cleveland, OH), enabling quality control to ensure optimal registration (Figure 1).

Results: For efficiency, Neuroreader was faster than FreeSurfer on a per case basis (15 min/case vs. 12 hours/case) yet slower for total processing time for batches of studies (45.5 vs. 12 hours) due to parallelizing on FreeSurfer. For reproducibility, all amyloid– and tau–PET showed strong agreement between operators (ICC>0.97). For global accuracy, BLAzER showed strong agreement with ADNI for amyloid–PET (r=0.9922, p<0.001) with tight 95% CI (–1.7 to 4.9%) and small bias (1.6%, Figure 2). For regional accuracy, BLAzER similarly showed strong agreement with ADNI across Braak staging regions for tau–PET (r>0.97, p<0.001, Figure 3). Finally, upon comparison, Neuroreader and FreeSurfer gave similar results (r=0.9841, p<0.001) despite systematic bias (4.0%) as cases showed similar dichotomization results after correcting with logistic regression (83 vs. 84 amyloid+ participants).

Conclusions: BLAzER provides an efficient workflow for regional brain PET quantification. FDA-approved components and the ability to visualize registration reduces barriers between research and clinical applications.
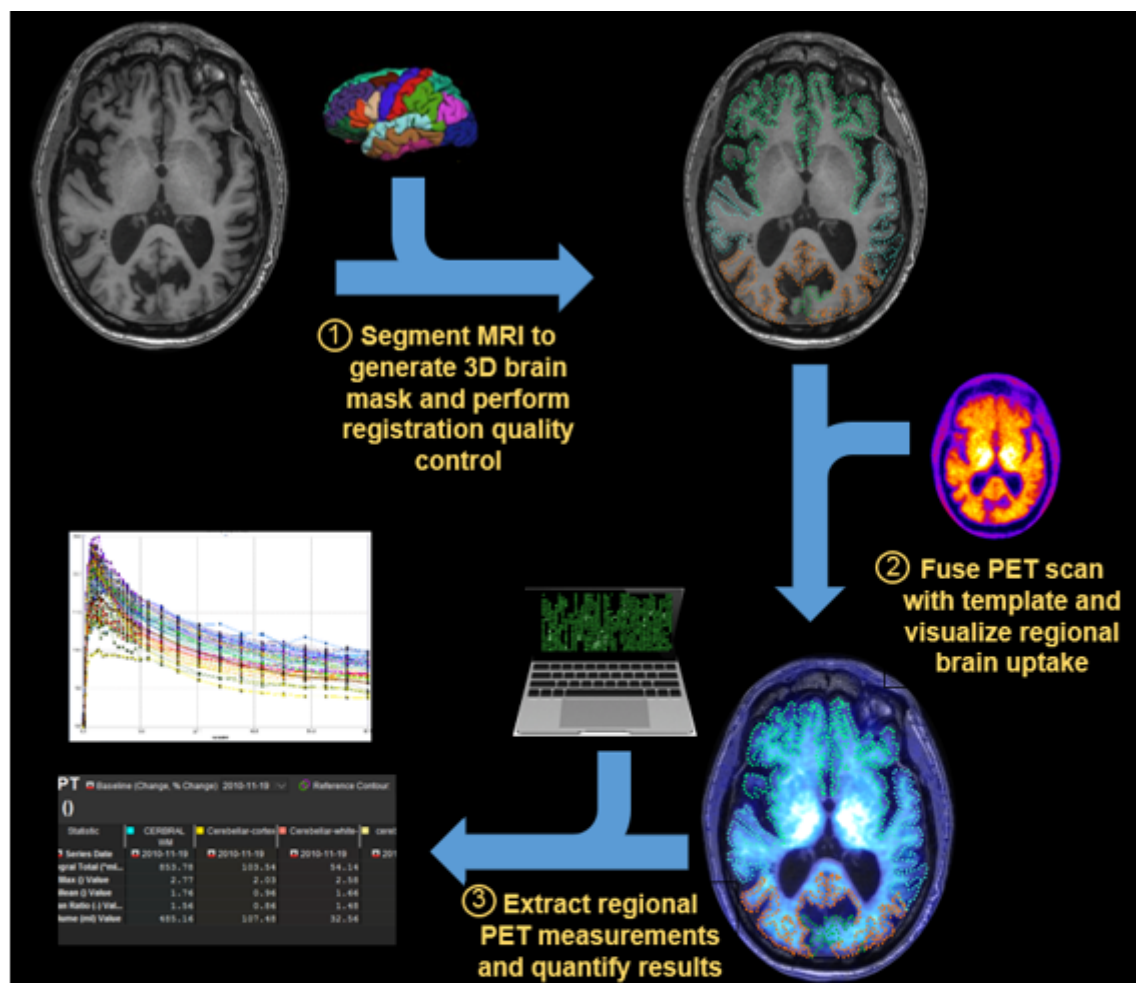
Figure 1. Schematic diagram of semi-automated BLAzER workflow with 1) segmentation of 3D volumetric MRI and registration of resulting brain mask to original MRI to ensure quality control ; 2) fusion of raw PET, volumetric MRI, and brain mask to allow for visualization of regional brain uptake of PET radiotracer; 3) Extraction and graphical representation of quantitative PET measurements.
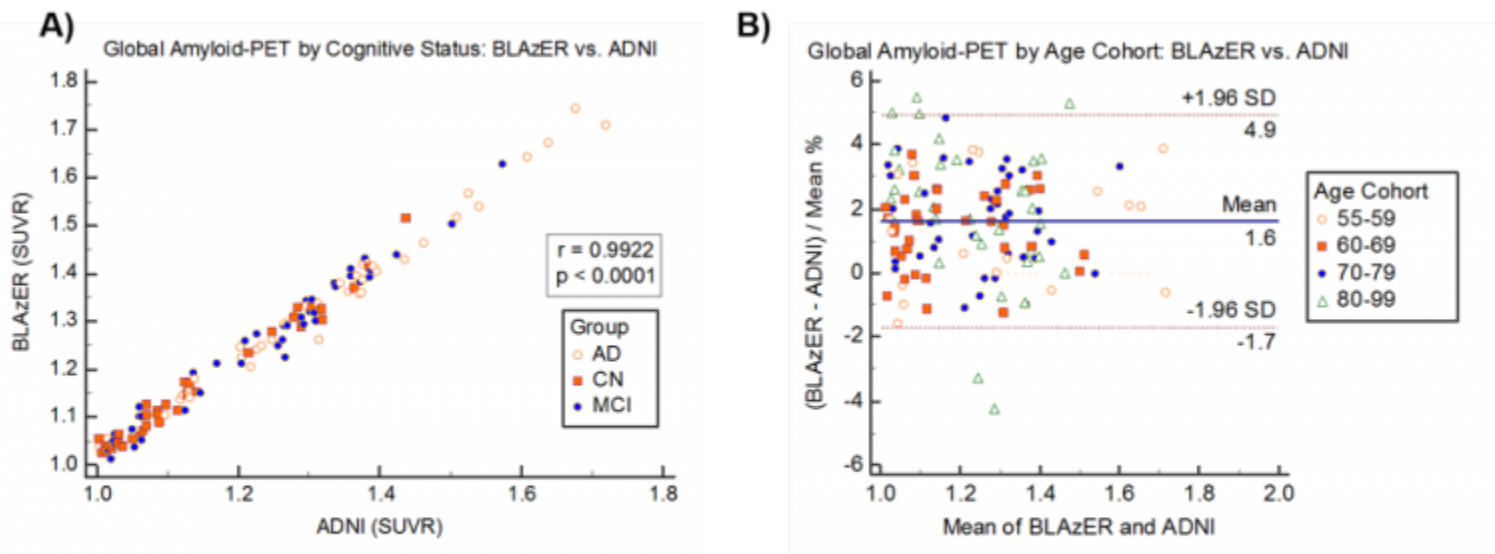
Figure 2. Comparison of BLAzER vs. ADNI for florbetapir-PET, showing A) univariate Pearson correlation across cognitively normal, MCI, and AD cohorts and B) Bland-Altman with 95% confidence intervals with mean percent difference across four age cohorts.
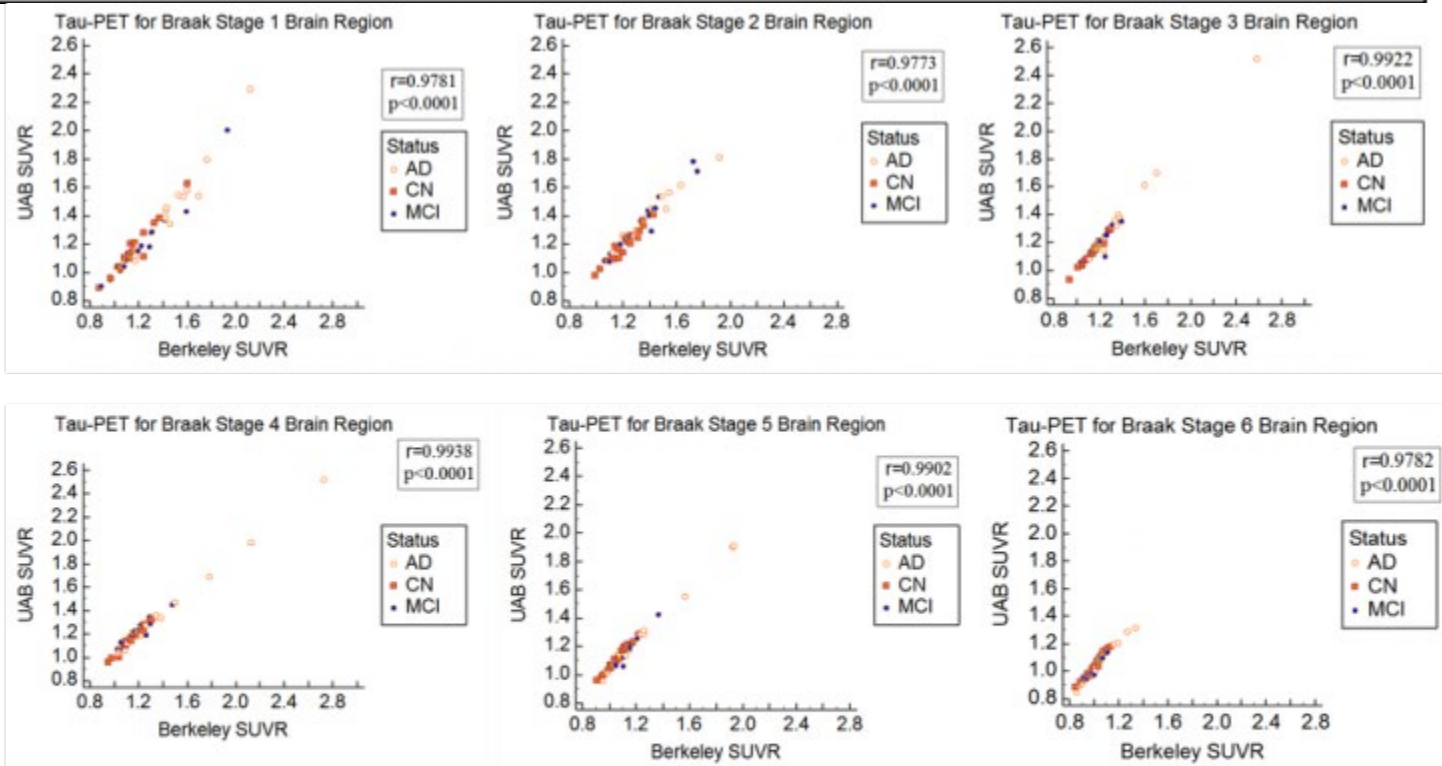
Figure 3. Comparison of our BLAzER workflow (UAB) to the ADNI reference (Berkeley) for tau-PET across the regions representing the pathological Braak stages, showing univariate Pearson correlation for cognitively normal (CN), mild cognitive impairment (MCI), and Alzheimer's disease (AD) participants.

Keywords: *PET quantification, FDA-approved, Registration Quality Control*

P72: Longitudinal 18F-APN-1607 (18F-PM-PBB3) PET in the rTg4510 mouse model of tauopathy

Ing-Tsung Hsiao[1,2], Kuo-Lun Huang[3], Kun-Ju Lin[1,2], Qing-Fang Yang[1]

[1]*Department of Medical Imaging and Radiological Sciences & Healthy Aging Center, Chang Gung University, Tau-Yuan, Taiwan*
[2]*Department of Nuclear Medicine, Chang Gung Memorial Hospital, Taoyuan, Taiwan*
[3]*Department of Neurology, Chang Gung Memorial Hospital, Taoyuan, Taiwan*

Background: The rTg(tet-o-TauP301L)4510 (rTg4510) bi-transgenic mouse is a widely used model of tauopathy. In this model 4-repeat tau deposits in brain over time. We performed the first longitudinal study of tau deposition in rTg4510 mice using the novel tracer ^{18}F-APN-1607 which detects 4R tau.

Methods: Fifteen Tg4510 mice were investigated longitudinally with MRI and ^{18}F-APN-1607 PET from 2-8 months of age. Each mouse was scanned monthly from 40-70 min post-injection, a time window previously determined as optimal in a dynamic and cross-sectional study. Individual PET images were spatially normalized to a mouse brain MRI template using rigid matching, and regions of interest for cortex, striatum, fornix, and hippocampus were delineated for quantitation. SUVRs were calculated for each ROI using the whole cerebellum as reference region.

Results: Using the 2 mo images as baseline, regional SUVRs showed only a trend toward increase at 4 months of age but a significant increase at 5mos and thereafter (Figure 1). The overall mean tau binding progression rate was 9.5%, 8.9%, 10.8% and 11% per month for cortex, striatum, fornix, and hippocampus, respectively.

Conclusion: The novel tau tracer ^{18}F-APN-1607 successfully characterized tau deposition in rTg4510 mice quantitatively. Longitudinal imaging with ^{18}F-APN-1607 may be useful for studying the course of pathology in this model and especially the effect of putative treatments for tauopathy.
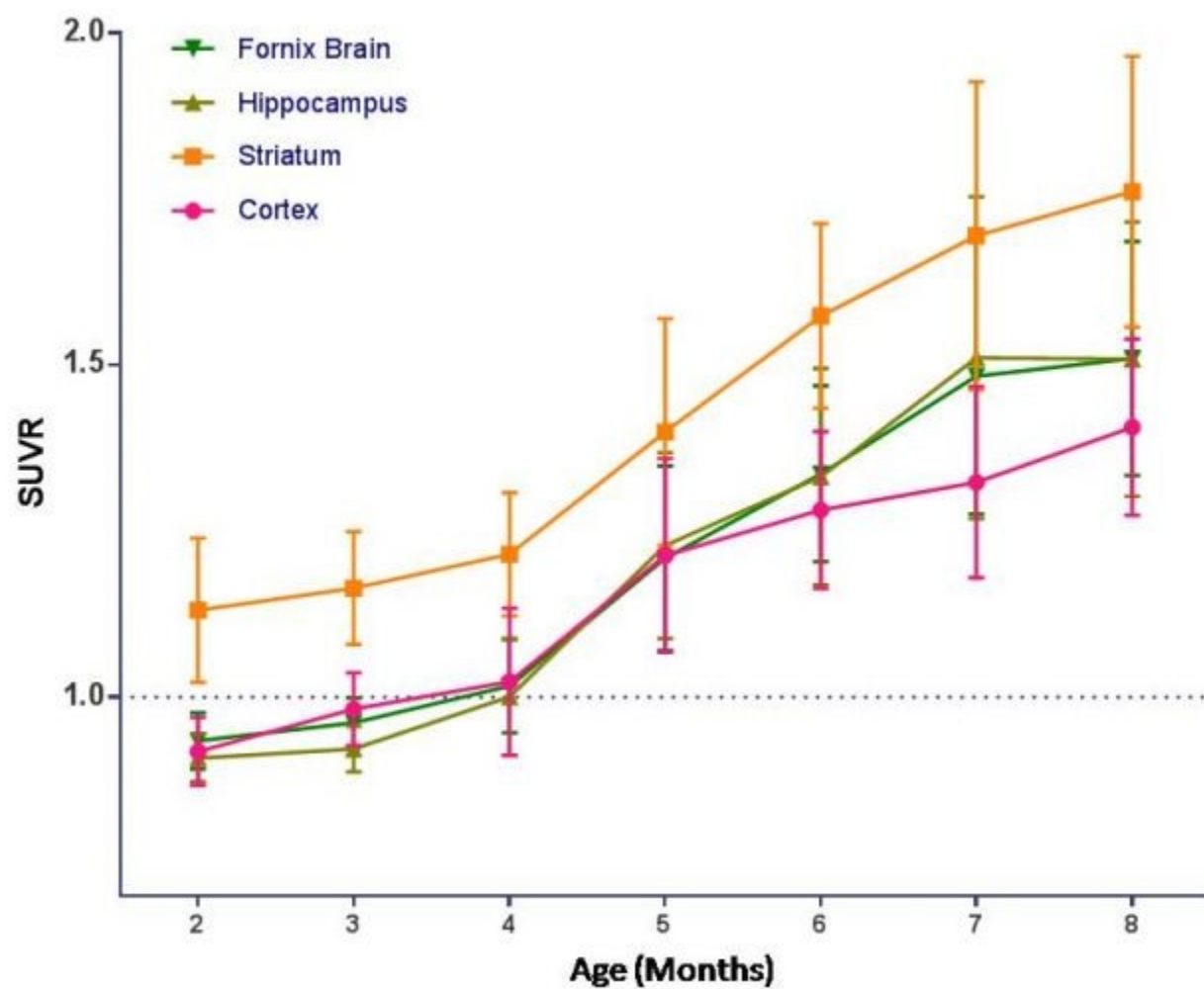
Figure 1. The mean regional SUVR plot over time for the 8 months duration in the longitudinal study

P73: Healthy brain structural connectome predicts regional tau accumulation in amyloid-positive mild cognitive impairment patients

Wha Jin Lee[1], Jeong-Hyeon Shin[1], Duk L. Na[2,3], Sang Won Seo[2,3], Joon-Kyung Seong[1]

[1]*School of Biomedical Engineering, Korea University, Seoul, Korea*
[2]*Department of Neurology, Sungkyunkwan University School of Medicine, Samsung Medical Center, Seoul, Korea*
[3]*Neuroscience Center, Samsung Medical Center, Seoul, Korea*

Objective & Background: Although a large amount of evidence has recently shown that the topographical patterns of tau pathology reflect spreading of tau via cell-to-cell synaptic transmission, the process still remains unclear at whole-brain connectivity level. We therefore sought to investigate how structural connectivity in health predicts region-by-region tau deposition patterns in MCI patients, and further how amyloid pathology affects this transneuronal spreading of tau.

Methods: We exploited the recently developed positron-emission tomography (PET) tracer AV1451 for in vivo imaging of tau pathology, which is combined with healthy structural connectome extracted using established diffusion tensor imaging (DTI) methods. We specifically included the total number of 197 participants, including 130 cognitively normal subjects, 42 patients with EMCI, and 25 patients with LMCI, of which MRI and PET images were downloaded from the ADNI database. Also, diffusion weighted MR images of 70 healthy subjects were employed to derive healthy structural connectome using seed regions easily damaged in the prodromal stages of Alzheimer's disease (AD). For each EMCI and LMCI, special regions were identified as "epicenters" having most similar spatial distributions between healthy structural connectome and the disease-associated tau pathology map.

Results: Graph theoretical analyses showed that tau deposition increases in the regions network topologically close to epicenters, which validates the transneuronal spreading model. Furthermore, tau spreading patterns along synaptic connectivity showed strong correlation with modular organization of healthy structural connectome in amyloid-positive but not in amyloid-negative patients with MCI. The structural connectivity in health also predicts cognitive impairment through accumulated tau pathology in amyloid-positive patients with MCI.

Conclusion: Our results proposed that diffusing pattern of tau, known as critical AD pathogenesis, can be predicted in the prodromal stages of AD through healthy whole-brain connectome, providing evidence that higher amyloid pathology amplifies the transneuronal spread and facilitates cognitive declines.
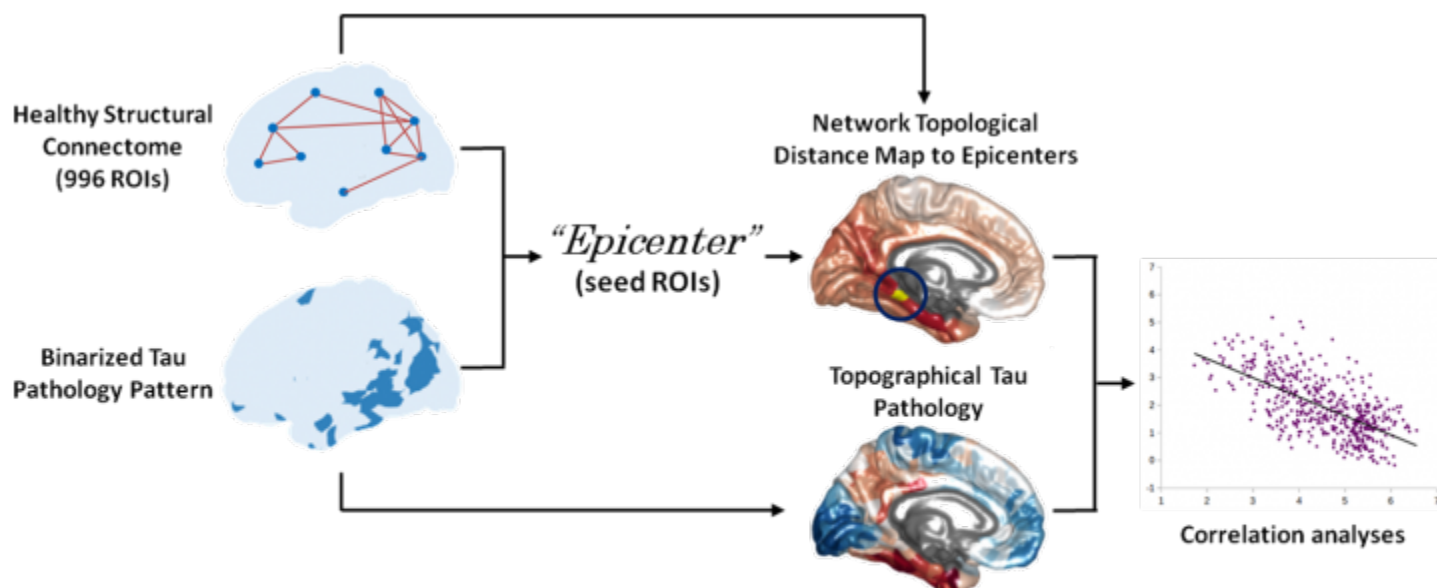
Figure 1. Study overview. Epicenters whose structural connectivity most resembled the tau pathology pattern were identified. For each epicenter, network topological distance map was calculated and correlated with the topographical tau pathology pattern to validate a transneuronal spread model of network-based tau accumulation.
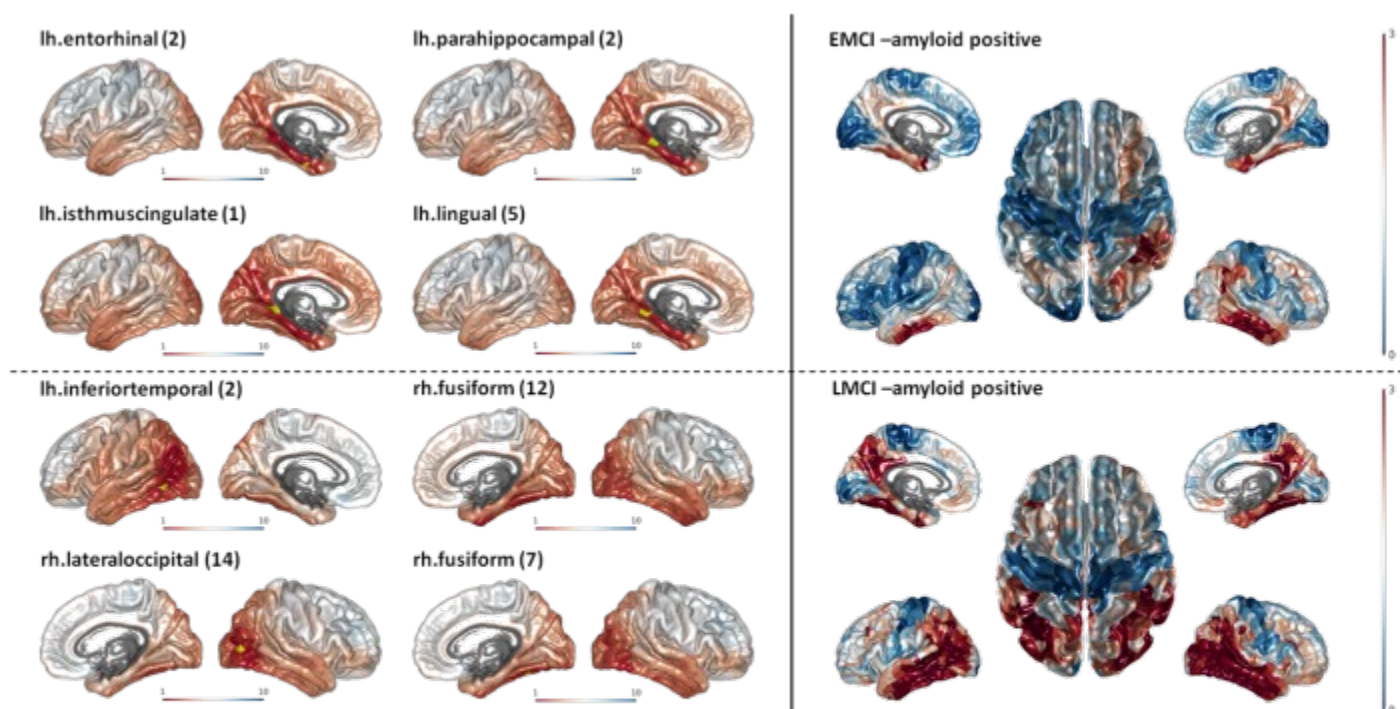
Figure 2. Network topological distance map to epicenters and topographical tau pathology. Left figures represent network topological distance map to the identified epicenters based on the shortest path length, and right figures represent the group-level topographical map of tau pathology. The upper/lower panels correspond to EMCI/LMCI, respectively. Yellow regions in left figures denote epicenters.

lh, left hemisphere; rh, right hemisphere; EMCI, early mild cognitive impairment; LMCI, late mild cognitive impairment;
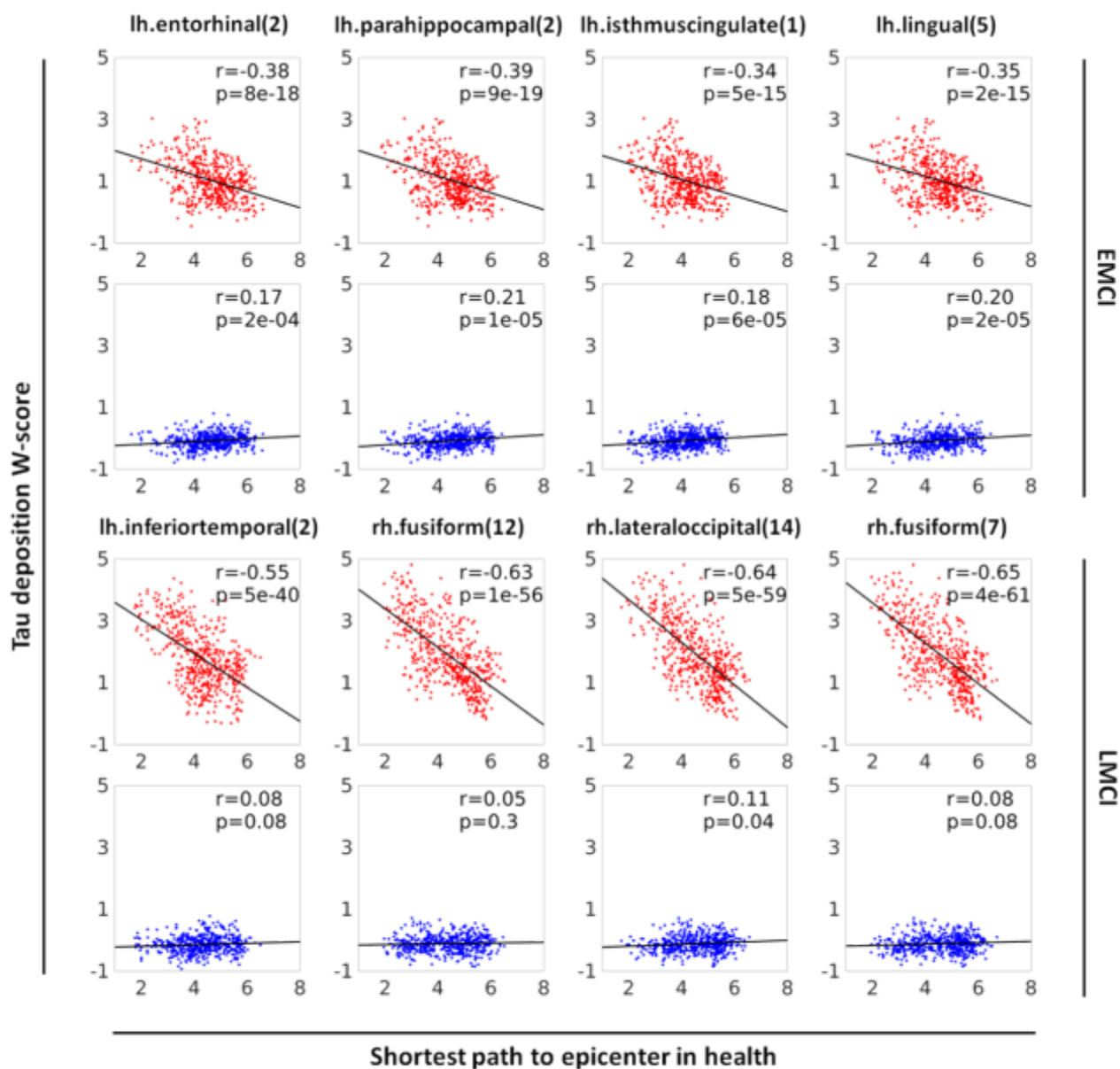
Figure 3. Correlations between network topological distance map and topographical tau pathology. Red color denotes relationship among amyloid-positive patients and blue color denotes amyloid-negative patients. The upper/lower panels correspond to EMCI/LMCI, respectively.

lh, left hemisphere; rh, right hemisphere; EMCI, early mild cognitive impairment; LMCI, late mild cognitive impairment;

Keywords: *healthy structural connectome, mild cognitive impairment, network-based tau accumulation, amyloid, diffusion tensor imaging*

P74: Pearls and pitfalls of using centiloids in interventional anti-amyloid studies – an examination of amyloid reductions in the gantenerumab open label extension studies

Gregory Klein[1], Paul Delmar[2], Danielle Abi-Saab[2], Mirjana Andjelkovic[2], Smiljana Ristic[2], Nicola Voyle[2], Jacob Hesterman[3], John Seibyl[3], Ken Marek[3], Monika Baudler[3], Paulo Fontoura[2], Rachelle Doody[2]

[1]*Roche Pharma Research and Early Development, Basel, Switzerland*
[2]*Roche/Genentech Product Development, Neuroscience, Basel, Switzerland*
[3]*Invicro, LLC, Boston, MA, US*

Background: Gantenerumab is a fully human monoclonal antibody currently under evaluation for the treatment of early Alzheimer's Disease at titrated doses to 1200 mg subcutaneous monthly in the Scarlet RoAD (SR, NCT01224106) and Marguerite RoAD (MR, NCT02051608) open label extension (OLE) studies. The antibody has demonstrated high levels of amyloid reduction measured with florbetapir PET and a cerebellar grey reference region. A 71 centiloid reduction was seen after 2 years treatment in previously untreated MR patients, and a 56 centiloid reduction was seen overall in all OLE patients. In principle, similar centiloid baseline and amyloid reduction values should be obtained using different SUVR pipelines, however, this is yet to be examined in an interventional study with large amyloid reductions. Here, we examine the generalizability of the centiloid method by comparing centiloid values at baseline and week 104, using different processing pipelines and reference regions.

Methods: Template- and native-space methods were used to compute SUVR measures of OLE baseline and week 104 of the OLE data using a variety of reference regions including cerebellum, white matter and pons. Centiloid transformations were calculated for each pipeline using the methods described by Klunk. Analysis focused on the combined group of 39 SR and MR patients who received follow-up scans at the week 104 visit.

Results: Baseline centiloid values varied considerably over processing pipelines, ranged from 65.6 to 102.6. Methods using cerebellar reference regions had consistently lower baseline values (mean 75.4) compared to methods using white matter, pons or brainstem (mean 98.2). Centiloid change at week 104 was less variable (mean -54.8, range -41.5 to -60.1].

Conclusions: While centiloid methods for florbetapir appear to offer more intuitive and comparative interpretations of amyloid reductions in interventional clinical trials, caution should be used when comparing baseline centiloid values obtained with different processing pipelines and reference regions.
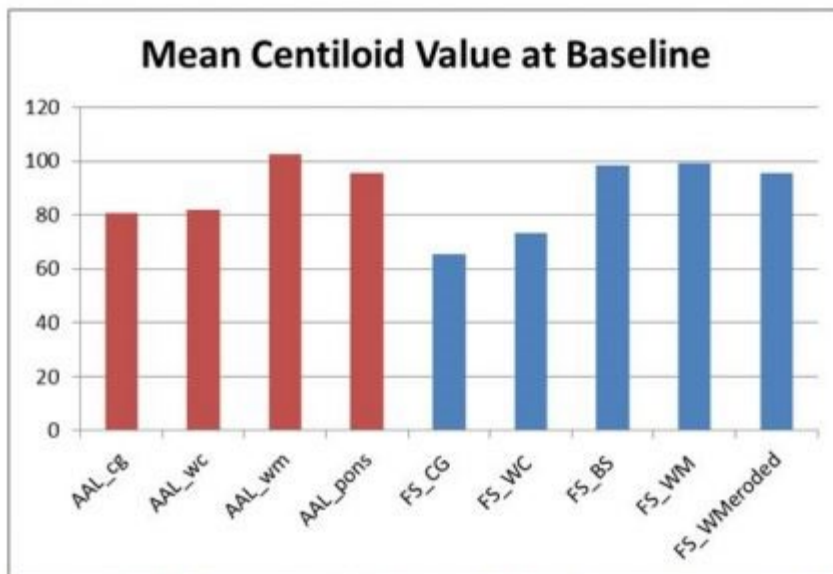
Figure 1. Mean baseline amyloid load for 39 OLE patients who received a scan at week 104. Centiloid values for the template-space approach using an AAL atlas are shown in red using reference regions: cerebellar grey (AAL_cg), whole cerebellum (AAL_wc), white matter (AAL_wm), pons (AAL_pons). Freesurfer native-space approach results are shown in blue using reference regions: cerebellar grey (FS_cg), whole cerebellum (FS_wc), brainstem (FS_bs), white matter (FS_wm), and eroded white matter (FS_WMeroded).
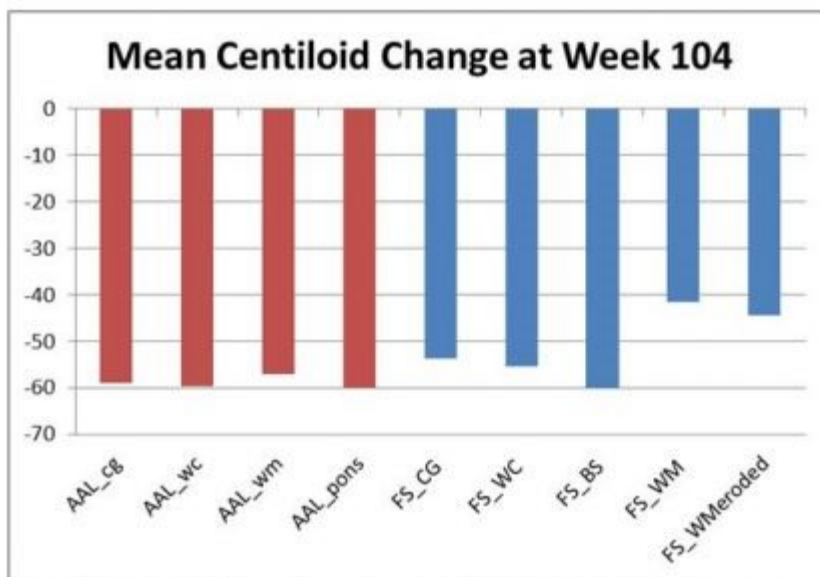
Figure 2. Mean amyloid load change for at week 104. Amyloid burden change was more consistent between different processing pipelines than for baseline values seen in Fig 1. Amyloid burden change was less using a white matter reference region using the Freesurfer approach, which may be due to partial volume effects or actual change in the reference region uptake over time.

P75: AV1451 and THK5351 PET with pathology correlations in a patient with Sporadic Creutzfeldt-Jakob Disease

Hee Jin Kim[1,2], Hanna Cho[4], Seongbeom Park[1,2], Hyemin Jang[1,2], Young Hoon Ryu[4], Jae Yong Choi[4], Seung Hwan Moon[5], Seung Jun Oh[6], Minyoung Oh[6], Duk L Na[1,2], Chul Hyoung Lyoo[3], Jae Seung Kim[6], Kyung Chan Choi[7], Sang Won Seo[1,2]

[1]*Department of Neurology, Samsung Medical Center, Sungkyunkwan University School of Medicine, Seoul, Korea*
[2]*Neuroscience Center, Samsung Medical Center, Seoul, Korea*
[3]*Department of Neurology, Gangnam Severance Hospital, Yonsei University College of Medicine, Seoul, Korea*
[4]*Department of Nuclear Medicine, Gangnam Severance Hospital, Yonsei University College of Medicine, Seoul, Korea*
[5]*Department of Nuclear Medicine, Samsung Medical Center, Sungkyunkwan University School of Medicine, Seoul, Korea*
[6]*Department of Nuclear Medicine, Asan Medical Center, University of Ulsan College of Medicine, Seoul, Seoul, Korea*
[7]*Department of Pathology, Chuncheon Sacred Heart Hospital, Hallym University College of Medicine, Chuncheon, Korea*

Background: ^{18}F-AV1451 and ^{18}F-THK5351 tau tracers have high affinity for paired helical filament tau, yet diverse off-target bindings have been reported. A previous head-to-head comparison suggested that ^{18}F-AV1451 is more specific to Alzheimer disease type tau while THK5351 may mirror non-specific neurodegeneration. Especially, ^{18}F-THK5351 has high affinity to MAOB as ingestion of MAOB inhibitor (selegiline) reduced ^{18}F-THK5351 uptake in human brains. We performed imaging-pathological correlation study in a Creutzfeldt-Jakob-Disease (CJD) patient.

Methods: We performed diffusion weighted image, ^{18}F-Florbetaben, ^{18}F-AV1451, and ^{18}F-THK5351 PET in a 67-year-old man with CJD. After the patient died, immunohistochemistry against amyloid-ß, and phosphorylated tau, GFAP, and MAO-B stains were performed.

Results: Diffusion weighted image showed cortical diffusion restriction in the left temporo-parieto-occipital area. ^{18}F-florbetaben PET revealed amyloid negative. ^{18}F-AV1451 PET showed focal uptake only in the left occipital white-matter region. However, ^{18}F-THK-5351 PET showed diffuse high uptake on the left temporo-parieto-occipital regions, which largely overlapped with the diffusion restricted regions. Postmortem study revealed definite diagnosis for CJD as we found micro-vacuolar degeneration and immunoreactive for PrP[sc] (3F4 and 1C5 antibody). There was no evidence of neurofibrillary tangle in the left occipital cortex. Severe gliosis was observed in the left occipital cortex as GFAP stain showed abundant astrocytosis which was reactive for MAOB stain.

Conclusions: Our findings suggested that increased THK-5351, but not AV1451, uptake in a patient with CJD might represent MAOB activity through increased reactive astrocytosis.
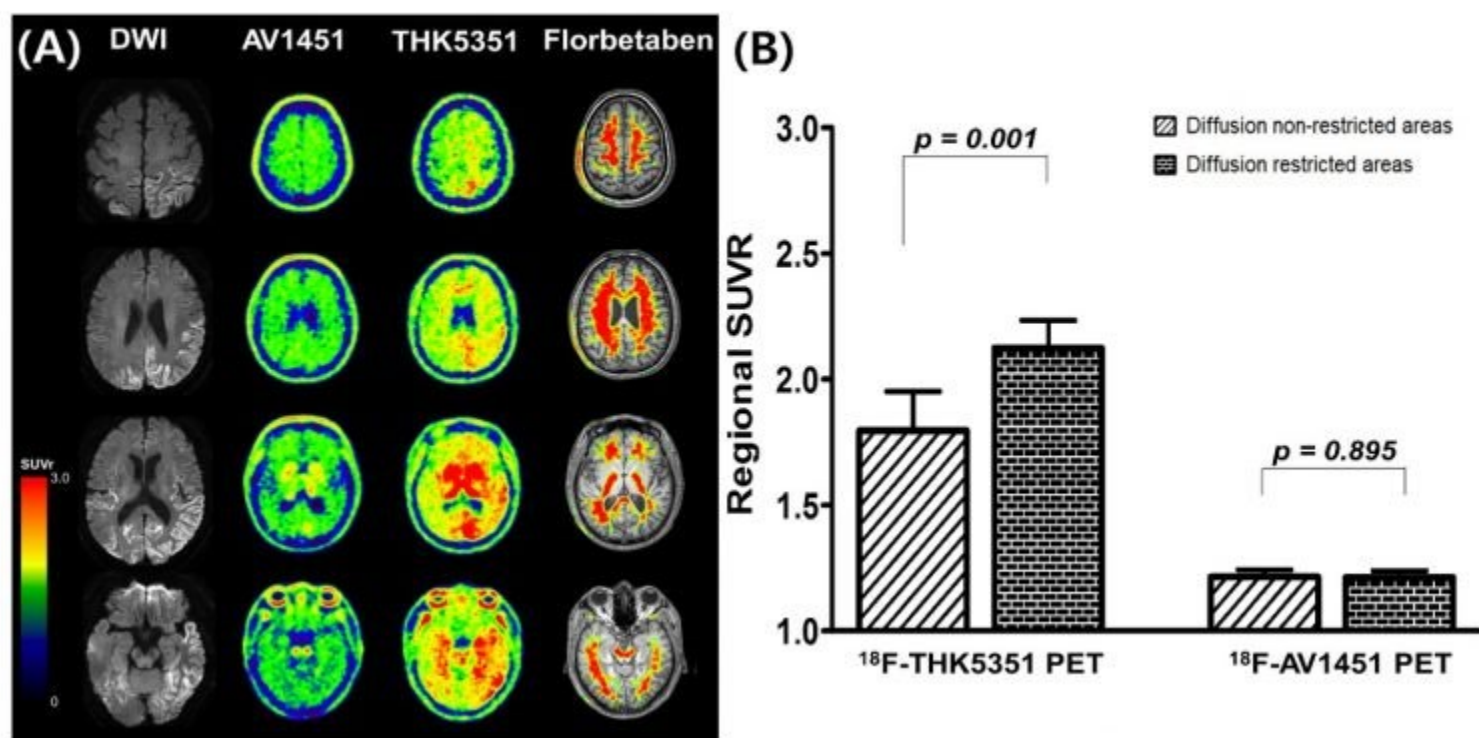
Figure 1. (A) Diffusion weighted images (DWI), tau (AV-1451 and THK-5351), and amyloid (florbetaben) PET images. (B) Regional SUVR of THK-5351 and AV-1451 in diffusion non-restricted and restricted areas.
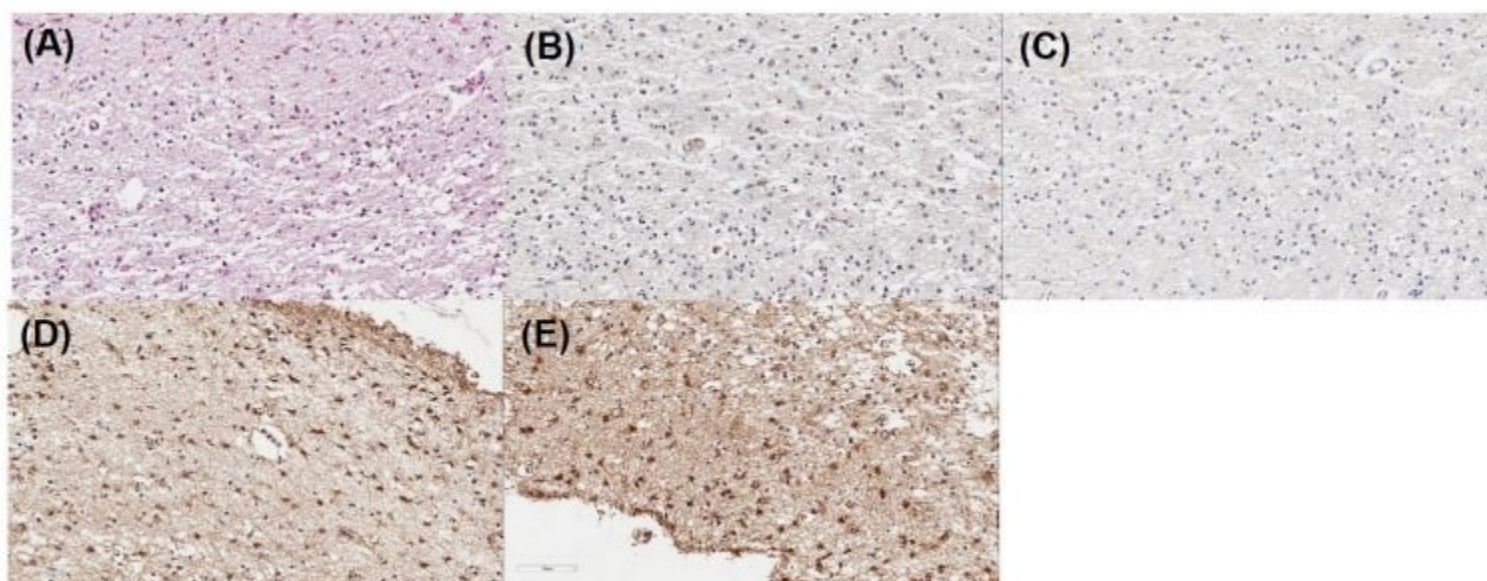
Figure 2. (A) H&E stain shows neuronal loss and vacuolation. (B-C) Immunohistochemistry against amyloid-ß and phosphorylated tau shows no amyloid plaque and no neurofibrillary tangle, respectively. (D) GFAP stain shows active astrocytosis and (E) MAOB stain showed increased MAOB activity.

P76: Associations among amyloid, tau, cerebrovascular disease, and neurodegeneration across cognitive stages in the Alzheimer's continuum

Patrick Lao[1], William Kreisl[1], Adam Brickman[1]

[1]Columbia University Medical Center, New York, NY, US

Background: The aim of this study was to determine the spatial pattern of and relationships among amyloid and tau accumulation, neurodegeneration, and small vessel cerebrovascular disease (CVD) across cognitive stages.

Methods: Florbetaben positivity was determined for amyloid burden, MK6240 SUVR for tau burden, cortical thickness (CT) for neurodegeneration, and whole-brain white matter hyperintensity (WMH) volume for small vessel CVD. Regions of interest (ROIs) included entorhinal cortex, medial temporal cortex, and parietal cortex to approximate early, middle, and late Braak stages, respectively. Clinical Dementia Rating (CDR) scores were used to stage participants into normal cognition (CDR=0), mild cognitive impairment (MCI; CDR=0.5), or mild clinical Alzheimer's disease (AD, CDR=1) groups. T-tests were performed for tau, WMH, and CT between Florbetaben negative control (n=19;75±9yrs), Florbetaben positive control (n=7;70±9yrs), and Florbetaben positive MCI/AD groups (n=13;69±11yrs). General linear models were performed pairwise between tau, WMH, and CT. Scan acquisition is ongoing, allowing for greater power to test interactions between biomarker and group.

Results: Tau was evident in entorhinal cortex in nearly all participants, in medial/lateral temporal cortex among amyloid positive individuals only, and in frontoparietal cortex with greater CDR. Tau was higher across groups (Florbetaben negative controls<Florbetaben positive controls<Florbetaben positive MCI/AD) and CT was lower (Florbetaben positive MCI/AD<Florbetaben negative controls). WMH did not differ between groups. There was a negative association of tau SUVR with CT in the entorhinal cortex, medial temporal cortex, and parietal cortex. Across ROIs, there were non-significant positive associations of tau with WMH, and non-significant negative associations of WMH with CT.

Conclusion: MK6240 patterns approximate Braak staging across cognitive stages, defined by the CDR. While amyloid positive participants had evidence of neurodegeneration only with MCI/AD, tau showed an association with neurodegeneration even in early Braak stage ROIs. Vascular biomarkers may contribute to AD progression by affecting tau and neurodegeneration directly.
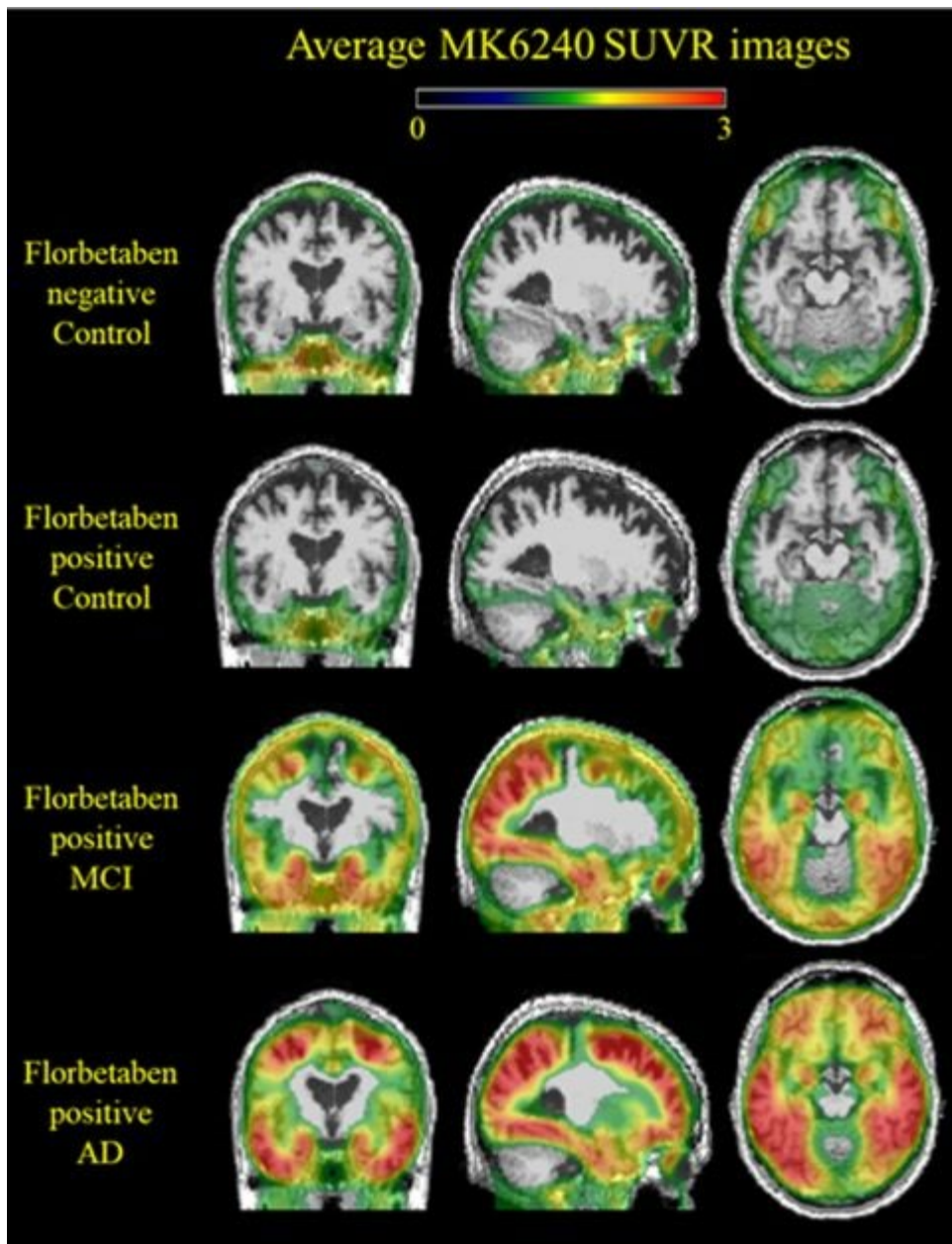
Average MK6240 SUVR images in MNI space for Florbetaben negative controls, Florbetaben positive controls, and Florbetaben positive MCI and AD demonstrating an increase in magnitude and a cross-sectional spread across Braak regions of tau binding. SUVR values below 1.25 have been greyed out.

P77: Association between neuroinflammation (level) and cognitive performance

Emilie Thomas[1], Mira Chamoun[1], Tharick Pascoal[1], Melissa Savard[1], Rim Nazar[1], Sarah Sbeiti[1], Miloudza Olmand[1], Sulantha Mathotaarachchi[1], Min Su Kang[1], Joseph Therriault[1], Serge Gauthier[1], Pedro Rosa-Neto[1]

[1]*McGill Center for Studies in Aging, Montreal, QC, Canada*

Background and objective: previous studies using PET have supported the concept that neuroinflammation measured as 18K translocator protein (TSPO) availability affects cognitive performance across the spectrum of Alzheimer's disease (AD) clinical presentations. However, most of these results were ontained in patients high and mixed affinity binders. The goal of this study was to determine, in living patients, whether the neuroinflammation load is associated with cognitive performance in high affinity binders.

Methods: Participants were between 65 and 85 years old (average: 72.9, SD: 5.1) and have an average of 14.2 years of education (SD: 3.8). The sample included 22 cognitively healthy elderly (CH) and 7 patients (3 people diagnosed with mild cognitive impairment (MCI) and 4 patients suffering from AD dementia). The positron emission tomography (PET) for neuroinflammation was performed with [11C]PBR-28 radiopharmaceutical. Additionally, all participants had detailed clinical and neuropsychological assessments and MRI. MRI was conducted to provide structural information for the PET analysis. Quantification of [11C]PBR-28 was performed with individual voxel maps. Our hypothesis was evaluated with linear regression models including cognitive performance on the Montreal Cognitive Assessment (MoCA) and on the Rey Auditory Verbal Learning Test (RAVLT) as independent variables.

Preliminary results: The global cognitive functioning, as measured by the MoCA, is negatively correlated with high concentration of neuroinflammation [11C]PBR-28 when adjusted for age and gender (figure 1). The results highlight a specific accumulation of neuroinflammation in the posterior cingulated cortex, precuneus and left enthorinal cortex. Another preliminary analysis also reveals a negative association between performance on the RAVLT and the accumulation of neuroinflammation (figure 2).

Conclusions: Consistent with our hypothesis, these preliminary results suggest that neuroinflammation plays a role in cognitive performance. This is particularly important for the development of new and effective disease modification therapies for neurodegenerative diseases.

Keywords: *Neuroinflammation imaging, PET, Alzheimer's disease, cognitive performance*

P78: Relationship of amyloid-beta and neurofibrillary tau deposition in Down syndrome using [11C]PiB and [18F]AV-1451 PET

Matt Zammit[1], Dana Tudorascu[2], Karly Cody[1], Charles Laymon[2], Ann Cohen[2], Davneet Minhas[2], Paul Ellison[1], Marwan Sabbagh[3], Shahid Zaman[4], Sterling Johnson[1], Chester Mathis[2], William Klunk[2], Ben Handen[2], Bradley Christian[1]

[1]*University of Wisconsin-Madison, Madison, WI, US*
[2]*University of Pittsburgh, Pittsburgh, PA, US*
[3]*Barrow Neurological Institute, Phoenix, AZ, US*
[4]*University of Cambridge, Cambridge, UK*

Background: Adults with Down syndrome (DS) are at high-risk to reveal Alzheimer's disease (AD) pathology in part due to the triplication of chromosome 21 encoding the amyloid precursor protein. Our previous studies have assessed longitudinal changes in amyloid-beta (Aβ) accumulation in DS. This cross-sectional PET study aims to assess in DS the relationship of global Aβ to regional tau characterized by Braak staging.

Methods: We report on 92 participants with DS that underwent [^{11}C]PiB and [^{18}F]AV-1451 PET scans in addition to T1-weighted structural MRI. ROI definition was performed using FreeSurfer (v5.3.0). SUVR images were generated from PET data (50-70 minute post-injection (p.i.) [^{11}C]PiB; 80-100 minute p.i. [^{18}F]AV-1451) using cerebellar gray matter as the region for normalization. Multiple linear regression models (adjusted for chronological age, sex, and performance site) were used to examine associations between regional AV-1451 SUVR (based on regions associated with Braak stages 1-6) and global PiB SUVR (as both a continuous and dichotomous variable).

Results: Global PiB retention showed statistically significant associations with AV-1451 retention (all $p<0.05$; presented as slope estimates and 95% CI's) in each Braak region (Table 1.1). The inclusion of sex in the regression did not influence model variability. Two outliers were observed displaying high AV-1451 retention in Braak region 6. Associations between global PiB and Braak regional AV-1451 retention remained significant ($p<0.05$) after repeating the analysis while excluding the outliers (Figure 1). As a dichotomous variable, comparing PiB status to AV-1451 retention in each Braak region also showed significant associations (all $p<0.05$; Table 1.2).

Discussion: This cross-sectional analysis provides insight into the relationship between global Aβ and regional tau deposition in DS. Future work will involve performing longitudinal tau scans to investigate changes in tau in relation to amyloid.

Table 1.1. Comparison of global PiB (treated as a continuous variable) to regional Braak AV-1451:

Braak Region	Slope estimate (β)	95% CI for β
Braak 1	0.50	(0.36, 0.64)
Braak 2	0.45	(0.32, 0.58)
Braak 3	0.70	(0.57, 0.82)
Braak 4	0.49	(0.38, 0.59)
Braak 5	0.65	(0.51, 0.78)
Braak 6	0.62	(0.46, 0.78)

Table 1.2. Comparison of global PiB (treated as a dichotomous variable) to regional Braak AV-1451:

Braak Region	Slope estimate (β)	95% CI for β
Braak 1	0.23	(0.11, 0.34)
Braak 2	0.22	(0.11, 0.32)
Braak 3	0.24	(0.11, 0.37)
Braak 4	0.17	(0.06, 0.27)
Braak 5	0.20	(0.06, 0.33)
Braak 6	0.17	(0.02, 0.31)

Figure 1. Cross-sectional comparison between global PiB and regional AV-1451. Analysis for Braak region 6 is displayed alongside the repeated analysis excluding the outliers.
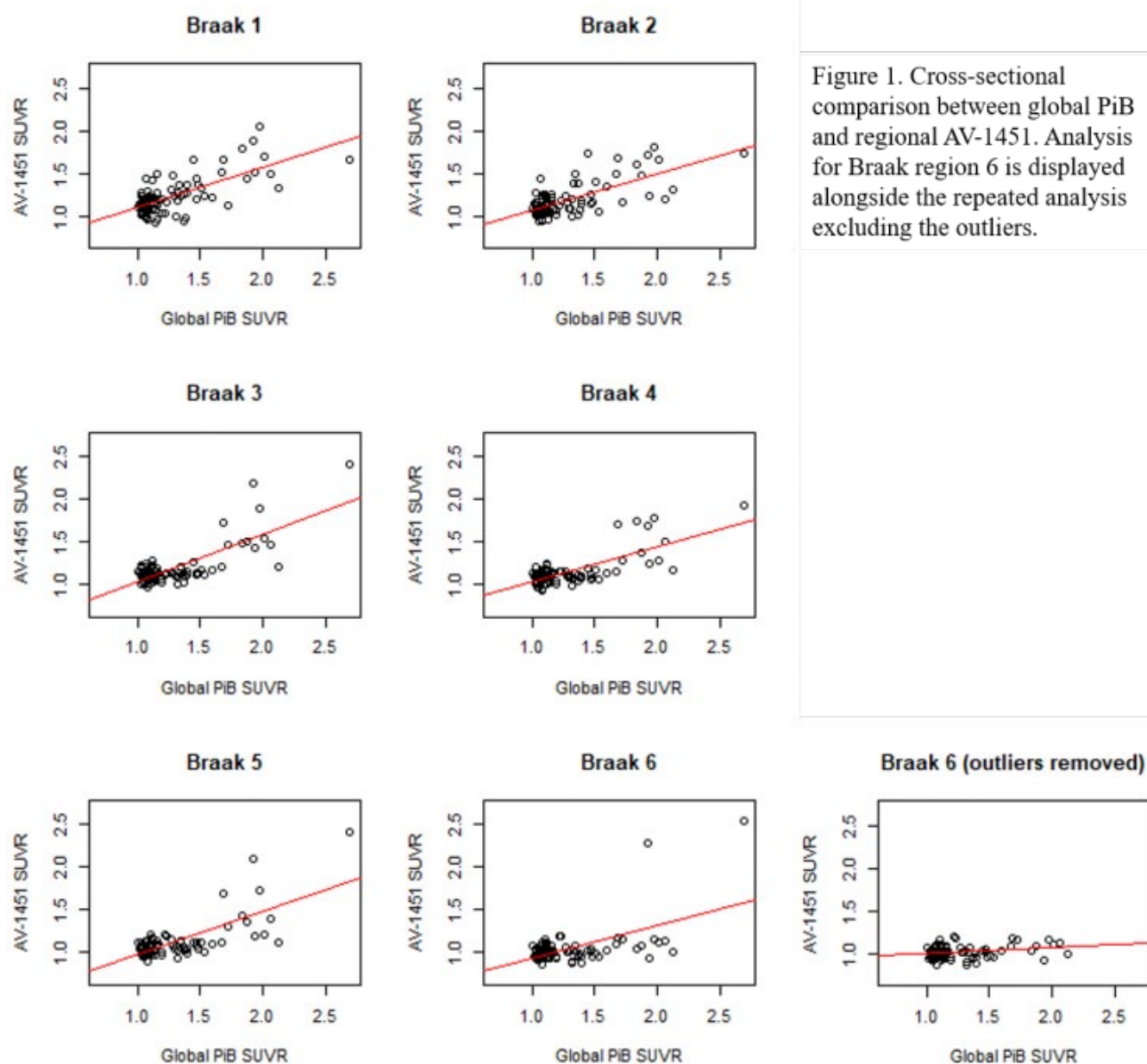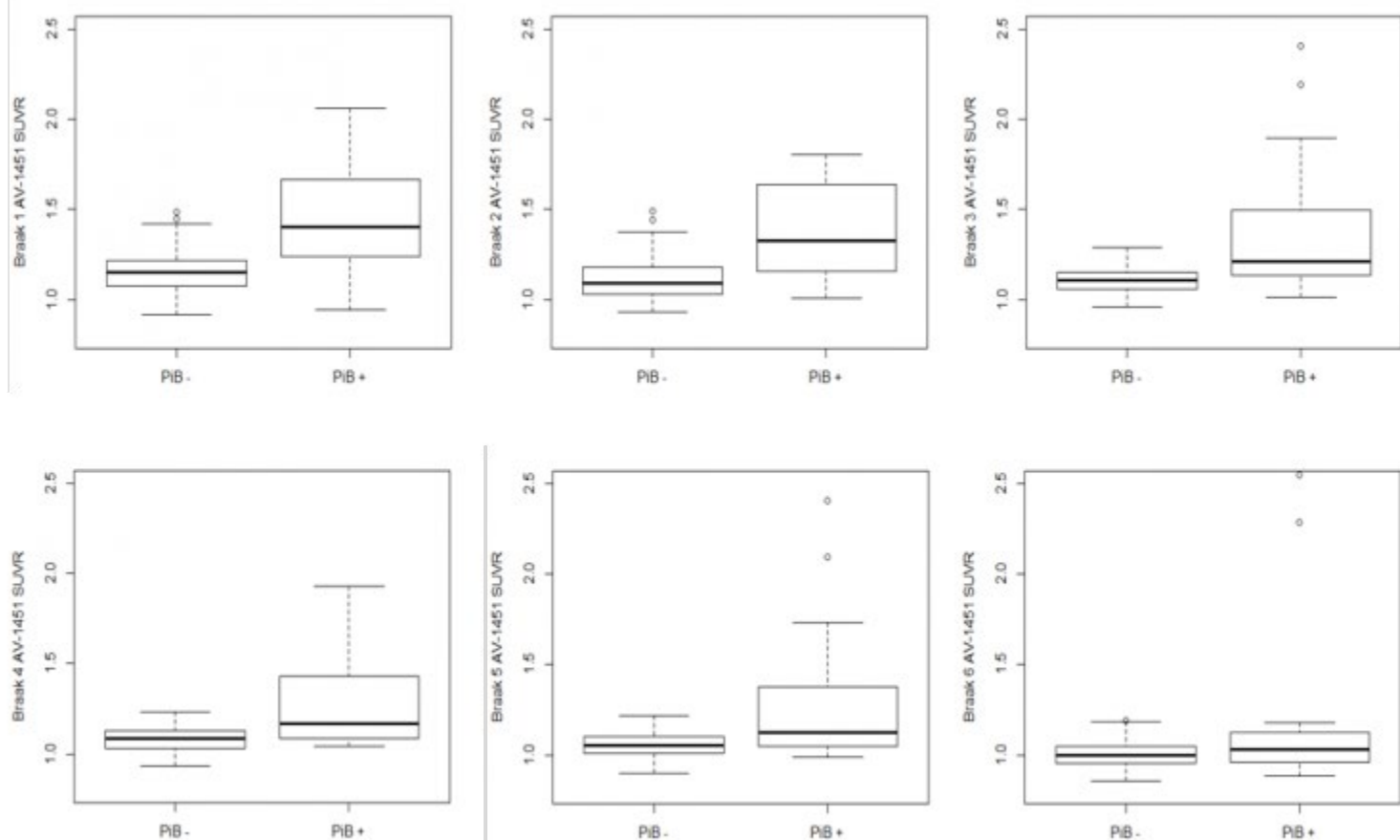
Figure 2. Comparison of regional Braak AV-1451 based on PiB status. PiB(+) was classified based on global PiB retention ≥ 1.36 SUVR.

P79: Amyloid accumulation in the striatum is more rapid than in the cortex early in Down syndrome and can serve as a marker for early intervention

<u>Matt Zammit</u>[1], Karly Cody[1], Tobey Betthauser[1], Dana Tudorascu[2], Patrick Lao[3], Charles Laymon[2], Ann Cohen[2], Dhanabalan Murali[1], Davneet Minhas[2], Shahid Zaman[4], Sterling Johnson[1], Chester Mathis[2], William Klunk[2], Ben Handen[2], Bradley Christian[1]

[1]*University of Wisconsin-Madison, Madison, WI, US*
[2]*University of Pittsburgh, Pittsburgh, PA, US*
[3]*Columbia University, New York, NY, US*
[4]*University of Cambridge, Cambridge, UK*

Background: Individuals with Down syndrome (DS) show increased production of the amyloid precursor protein (APP) and are at risk to develop Alzheimer's disease. Our previous PiB PET studies in DS have shown amyloid-beta (Aβ) deposition occurs predominantly in the striatum before the cortex. This study assesses whether striatal Aβ deposition occurs more rapidly than cortical deposition in DS by evaluating longitudinal PiB SUVR change.

Methods: In ongoing longitudinal PET studies, 34 adults with DS (subset of N=160) underwent three [^{11}C]PiB scans (performed 2-3 years apart) in addition to structural T1w-MRI. ROIs were defined using FreeSurfer (v5.3.0). SUVR images were generated from summed 50-70 minute PET frames using cerebellar gray matter as the reference region. Mean SUVRs were extracted for the striatum and target cortical ROIs (anterior cingulate, superior frontal gyrus, orbitofrontal gyrus, insula, lateral temporal gyrus, parietal cortex, posterior cingulate, precuneus) weighted by region volume. Participants were classified as PiB(+) if at least one ROI exceeded its SUVR threshold. Longitudinal change in SUVR were compared across participants based on their PiB status (PiB(-), PiB converter, or PiB(+)).

Results: Between all cycles, PiB converters displayed significantly greater SUVR change in the striatum than in the cortex (two-sample paired t-test; Cycle 1-2: p=0.008, Cycle 2-3: p=0.001). Participants that remained either PiB(-) or PiB(+) between cycles showed no significant difference between striatal and cortical accumulation (all p>0.05).

Discussion: These results suggest that in DS, changes in Aβ accumulates are greater in the striatum during the early stages of amyloid accumulation compared to cortical regions. Once the transition from PiB-converter to PiB(+) occurs, no difference between striatal and cortical Aβ change is noticed. This analysis reveals that the striatum may be more vulnerable to Aβ plaque formation and identifies the striatum as a potential marker for early intervention in DS.
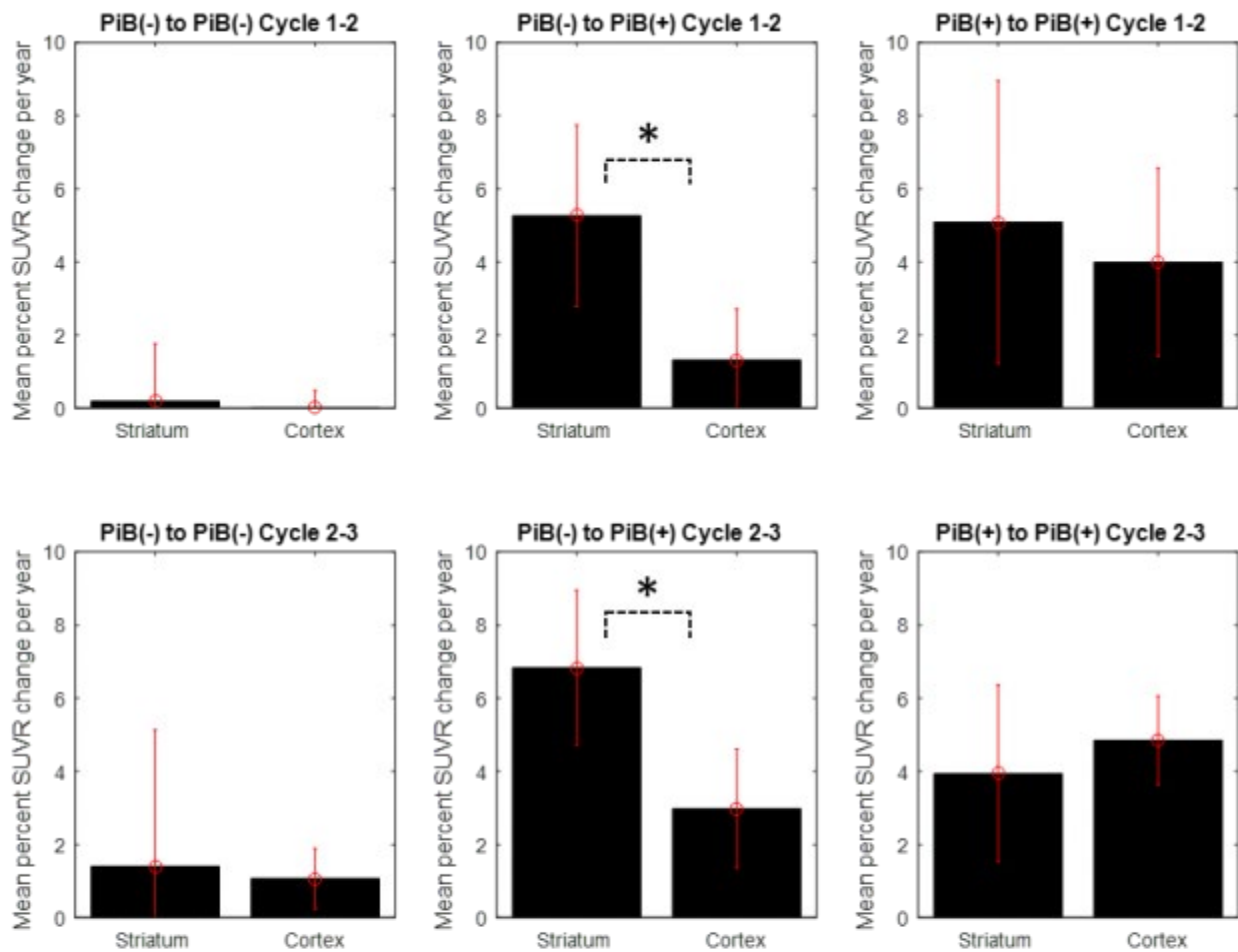
Figure 1. Mean percent SUVR change per year compared between the striatum and the cortex. Error bars represent the 95% confidence interval of the mean. Participants classified as a PiB-converter in cycles 1-2 were re-classified as PiB(+) before the start of cycle 3. Between cycles 1-2, n=21 participants remained PiB(-), 6 converted from PiB(-) to PiB(+), and 7 were PiB(+) at both time points. Between cycles 2-3, n=13 participants remained PiB(-), 8 converted from PiB(-) to PiB(+), and 13 were PiB(+) at both time points.

P80: Cross-sectional associations between temporal tau and cortical thickness across the lifespan

Kirsten Moody[1], Heidi Jacobs[1,3], Amanda Sidwell[1], Bernard Hanseeuw[1,4], Samantha Katz[1], Justin Sanchez[1], Danielle Mayblyum[1], Tobias Estime[1], Jorge Sepulcre[1], Claudia Satizabal[5,6], Matthew Pase[6,7,9], Alexa Beiser[5,6,7], Serkalem Demissie[7], Daniel Daniluk[6,7], Colin Schaefer[6,7], Bryanne Peets[6,7], Julie Price[1], Reisa Sperling[1,2], Charles DeCarli[8], Sudha Seshadri[6,7], Keith Johnson[1]

[1]*Department of Neurology, Radiology, and the Athinoula A. Martinos Center for Biomedical Imaging, Massachusetts General Hospital, Harvard Medical School, Boston, MA, US*
[2]*Center for Alzheimer's Research and Treatment, Brigham and Women's Hospital, Harvard Medical School, Boston, MA, US*
[3]*Maastricht University, Maastricht, The Netherlands*
[4]*Cliniques Universitaires Saint-Luc, Brussels, Belgium*
[5]*Department of Neurology, Boston University School of Medicine, Boston, MA, US*
[6]*The Framingham Heart Study, Framingham, MA, US*
[7]*Boston University, School of Public Health, Boston, MA, US*
[8]*University of California, Davis, Davis, CA, US*
[9]*Melbourne Dementia Research Centre, The Florey Institute for Neuroscience and Mental Health, Victoria, Australia*

Objectives: Aging and Alzheimer's disease are associated with cortical thinning, amyloid and tau pathology. Increased tau binding is related to cortical thinning in temporoparietal regions in impaired individuals in the context of amyloidosis. Given that tau can occur in middle adulthood in the absence of elevated amyloid, we aimed to investigate associations between tau and cortical thickness (CT) across the lifespan independent of amyloid.

Methods: We studied 400 clinically normal (CN) and 70 clinically impaired (CDR>0) participants with T1-MPRAGE, [18F]Flortaucipir (FTP) and PIB-PET data from the Harvard Aging Brain Study, Framingham Heart Study and patient studies (Table 1). FTP SUVR and CT were measured in six temporal regions: entorhinal, fusiform, inferior, middle, superior temporal, and parahippocampal cortices. Pearson correlations examined tau-CT associations in four CN age quartiles and the impaired group (FDR-adjusted). Correlations were compared with Fisher's r-to-z-test.

Results: The CN age groups differed in amyloid and sex proportions ($p<0.001$, $p=0.049$), but not in education, MMSE, or APOE status. Right-sided CT and tau correlations were apparent in all age groups, while left-sided correlations were only significant in quartile 4 (Fig. 1). Bilateral patterns were observed in quartile 4 and the impaired group (Fig. 2).

In left and right entorhinal cortices, the correlation strength differed between quartiles 2 and 3 ($p=0.004$, $p=0.030$). In the left superior temporal cortex, the correlation strength differed between quartile groups 3 and 4 ($p=0.025$). Correcting for amyloid revealed similar patterns.

Conclusions: Concurrent relationships between tau and CT, independent of amyloid, were observed in CN participants at older ages and the oldest group (≥75 years) showed bilateral patterns, similar to the impaired group. This is consistent with close links between tau and CT, and suggests that cortical thinning is a slower process than tau accumulation.

	Clinically Normal	Quartile 1	Quartile 2	Quartile 3	Quartile 4	Impaired (CDR>0)
N	400	100	101	101	98	70
[†]Age, y [range]	65.1 ± 13.4 [20,92]	47.5 ± 7.3 [20,55]	60.5 ± 3.2 [56,65]	70.4 ± 2.0 [66,74]	81.7 ± 4.3 [75,92]	74.6 ± 9.5 [55,90]
Male, n (%)	185 (46)	57 (57)	41 (41)	40 (40)	47 (48)	37 (53)
ApoE4, n (%)	80/339 (24)	20/78 (26)	18/87 (21)	30/98 (31)	23/91 (25)	9/24 (38)
[†]Global Aβ, DVR	1.28 ± 0.34	1.11 ± 0.06	1.18 ± 0.16	1.35 ± 0.38	1.47 ± 0.45	1.90 ± 0.63
[†]MMSE	29.3 ± 0.96	29.5 ± 0.82	29.4 ± 0.88	29.4 ± 0.86	29.0 ± 1.19	26.3 ±3.48
[†]Education, y	15.8 ± 2.73	15.8 ± 2.26	15.4 ± 2.31	16.4 ± 2.87	15.8 ± 2.27	15.9 ± 0.64
[††]Bilateral ETC tau	1.29 ± 0.30	1.18 ± 0.22	1.16 ± 0.20	1.34 ± 0.28	1.47 ± 0.37	1.98 ± 0.64
[††]Bilateral ITC tau	1.38 ± 0.20	1.24 ± 0.14	1.32 ± 0.15	1.44 ± 0.17	1.53 ± 0.21	2.06 ± 0.80

[†]mean ± SD

[††]tau burden is defined by [^{18}F]-Flortaucipir PET SUVR Partial-Volume Corrected (PVC)

MMSE = mini-mental state examination; DVR=distribution volume ratio, ETC=entorhinal cortex, ITC=inferior temporal cortex

Table 1. Participant characteristics of clinically normal (Age Quartiles) and cognitively impaired subjects (CDR>0).
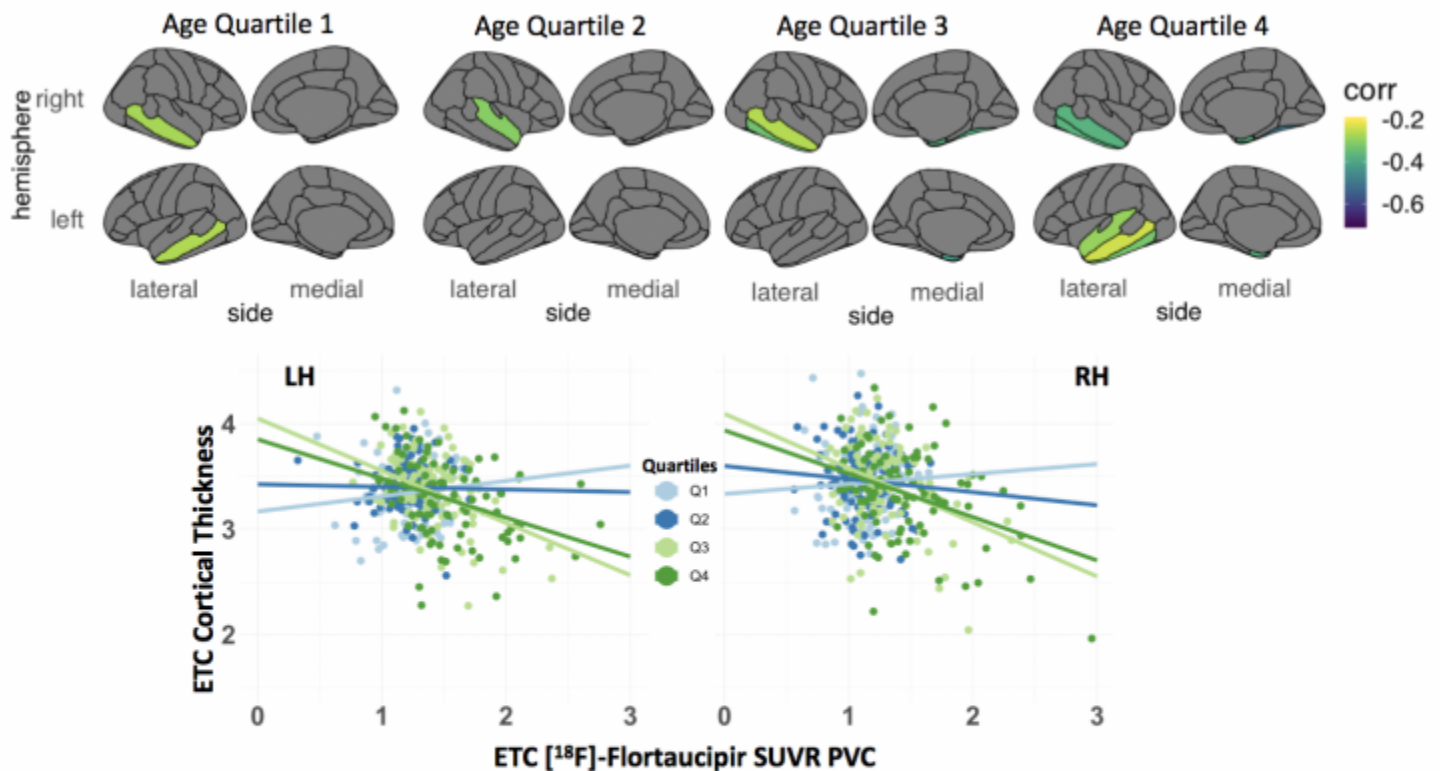
Figure 1. (Top row) Correlations between temporal lobe tau and cortical thickness across the different age quartiles in CN subjects. Brain surfaces show the significant correlation coefficients after adjustment for multiple comparisons using the FDR-approach. Note: correlation between right middle temporal cortical thickness and tau was borderline significant in age quartile 2. (Bottom row) Relationship between tau SUVR and cortical thickness in the left (LH) and right (RH) entorhinal cortex (ETC). Colors indicate the age quartiles. The correlation strength differed between quartiles 2 and 3 (left: -0.02 to -0.41, p=0.004; right: -0.08 to -0.37, p=0.030).
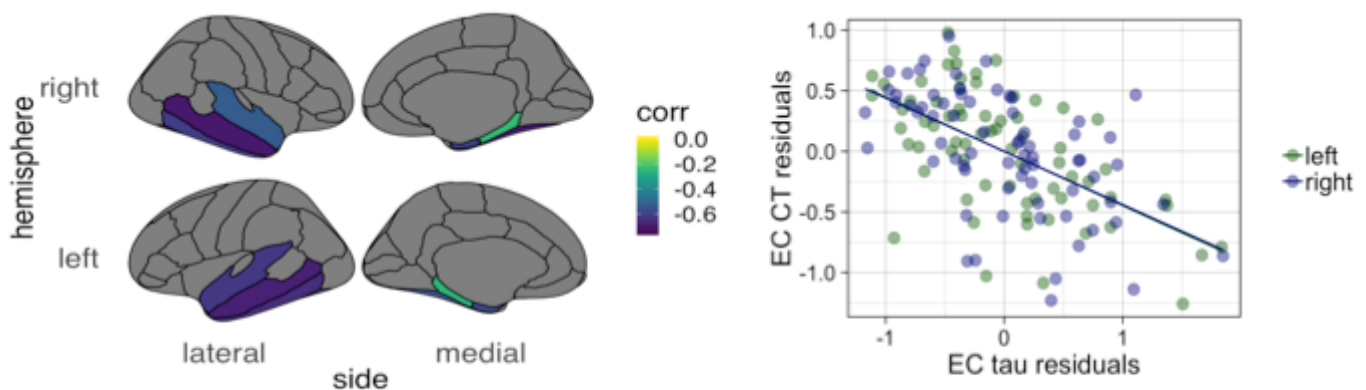
Figure 2. Correlations between temporal tau and cortical thickness in impaired individuals with CDR>0, corrected for age and with FDR-adjustment. Scatterplot depicts the association between left and right entorhinal cortical thickness and tau, residualized for age.

Keywords: *cortical thickness, tau pathology, Flortaucipir, aging*

P81: Amyloid-dependent and –independent effects of Tau on clinical function in Alzheimer's disease

Joseph Therriault[1], Tharick Pascoal[1,2], Marcus Sefranek[1,2], Sulantha Mathotaarachchi[1,2], Melissa Savard[1,2], Andrea Benedet[1,2], Mira Chamoun[1,2], Min Su Kang[1,2], Serge Gauthier[1,2], Pedro Rosa-Neto[1,2]

[1]*Translational Neuroimaging Lab, Montreal, QC, Canada*
[2]*McGill Center for Studies in Aging, Montreal, QC, Canada*

In recent years, frameworks that propose "amyloid-dependent" and "amyloid-independent" phases of AD have emerged, in which cerebral amyloid burden becomes less related to Alzheimer's clinical presentation with further disease progression. However, work from animal models has suggested that the molecular interaction between amyloid-β and tau peptides leads to neuronal and synaptic dysfunction, which are closely associated with cognitive impairment.

For the present study, we assessed cognitively normal (n=125), amnestic MCI (n=67) and AD (n=23) individuals from the ADNI who had undergone T1-weighted magnetic resonance imaging, [18F]florbetapir amyloid-β and [18F]AV1451 tau PET imaging as well as clinical assessments. Voxel-wise regression models evaluated the main and interactive effects of [18F]florbetapir and [18F]AV1451 SUVRs on clinical status, as measured by the Clinical Dementia Rating (CDR) Sum of Boxes.

A significant synergistic effect of [18F]florbetapir and [18F]AV1451 SUVR in the precuneus, anterior and posterior cingulate (including the retrosplenial cortex), lateral temporal, medial prefrontal, orbitofrontal, frontal pole, and basal forebrain cortices was associated with worse clinical status across the Alzheimer's disease spectrum (**P** < 0.001). Alternatively, within this interaction model, the independent effect of [18F]AV1451 SUVR in medial temporal, cuneus, and right superior parietal was associated with higher CDR Sum of Boxes. No independent effects of [18F]florbetapir SUVR on clinical status were observed (figure 1).

Our results demonstrated dissociable regional relationships between the synergistic effects of amyloid and tau deposition, as well as the independent contribution of tau deposition to clinical function (figure 2). Our results contribute to existing sequential models of Alzheimer's disease progression by providing evidence that amyloid exacerbates the deleterious effects of tau on clinical symptoms.
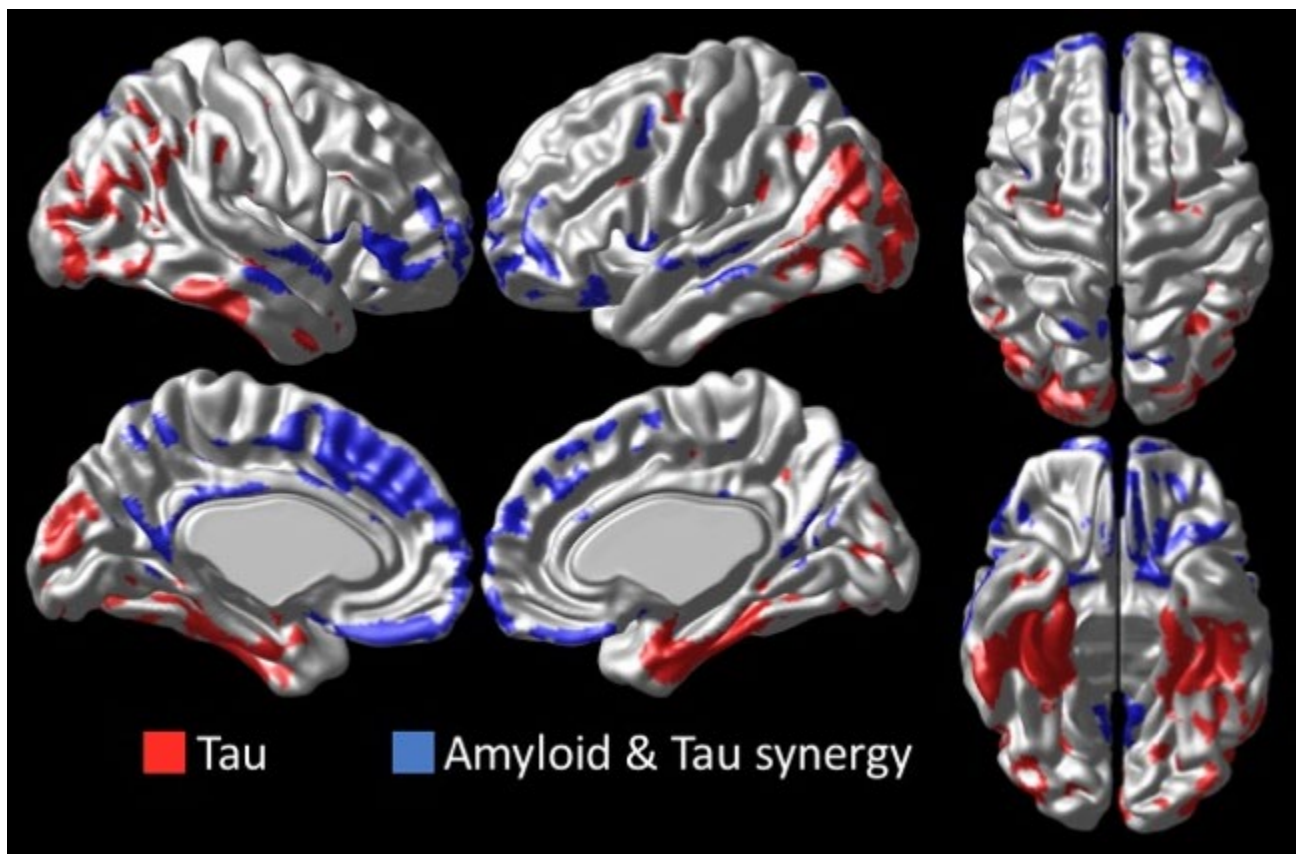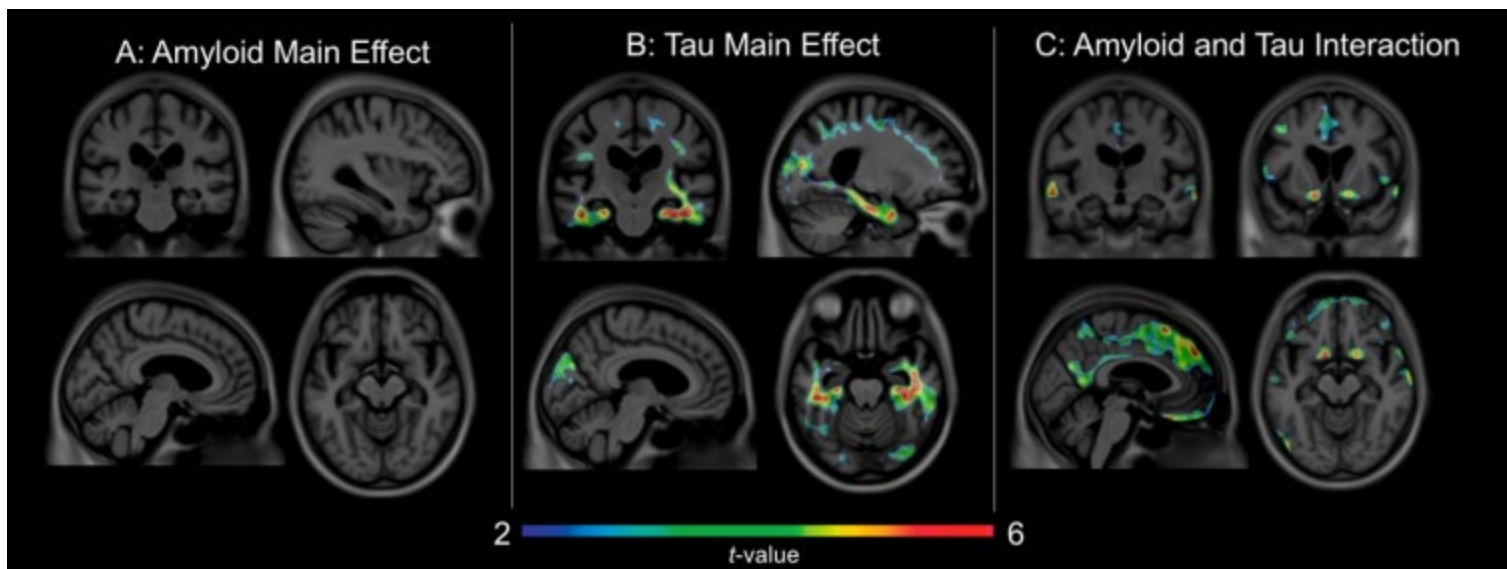
P82: Voxel-wise receiver operating characteristic analysis reveals clinically relevant sites of amyloid-beta deposition

Joseph Therriault[1,2], Tharick Pascoal[1,2], Antoine Leuzy[1], Lyduine Collij[4], Andrea Lessa Benedet[1,2], Sulantha Mathotaarachchi[1,2], Min Su Kang[1,2], Isadora Alves[4], Gassan Massarweh[3], Jean-Paul Soucy[3], Serge Gauthier[2], Pedro Rosa-Neto[2]

[1]*Translational Neuroimaging Lab, Montreal, QC, Canada*
[2]*McGill Center for Studies in Aging, Montreal, QC, Canada*
[3]*Montreal Neurological Institute, Montreal, QC, Canada*
[4]*VU Medical Center, Amsterdam, The Netherlands*

Aims: To assess the contributions of the regional distribution of amyloid pathology to AD severity.

Methods: We assessed cognitively normal (n=302), and AD (n=224) individuals who underwent [^{18}F]Florbetapir PET, cognitively normal (n = 106) and AD (n = 98) individuals scanned with [^{11}C]PiB and cognitively normal (n = 70) and AD (n = 30) scanned with [^{18}F]AZD4694 and cognitively normal (n=199) and AD (204) scanned with [^{18}F]Flutemetamol. In order to identify the brain regions that optimally differentiated controls from AD patients, we conducted a ROC curve in every brain voxel using the VoxelStats toolbox [1]. Then, parametric maps of area under the curve were generated for each amyloid imaging agent (Figure 1). Area under the curve values were highest in clusters in the AD signature regions including the precuneus, posterior cingulate, lateral temporal, and medial prefrontal cortices, as well as the striatum. Next, to determine if amyloid burden in these structures is related to AD severity, we conducted linear regressions assessing the relationship between amyloid burden from AD signature regions and the standard neocortical composite mask and brain metabolism as assessed by [^{18}F]FDG uptake in MCI (n = 502). We compared the slopes and adjusted R^2 of each model.

Results: In MCI, we observed stronger relationships between brain metabolism and amyloid in AD signature regions than with global amyloid burden (figure 2). Similarly, we observed stronger relationships between cognitive dysfunction and amyloid in AD signature regions than we did with global amyloid burden (figure 3).

Conclusion: Our results suggest that amyloid deposition in vulnerable regions is more closely associated with AD severity. Studies examining the relationships between amyloid and cognition may benefit from assessing amyloid burden in AD signature regions rather than global amyloid burden.

Area Under the Curve
0.7 — 0.95

[18F]Florbetapir   [18F]Flutafuranol   [11C]PiB   [18F]Flutemetamol
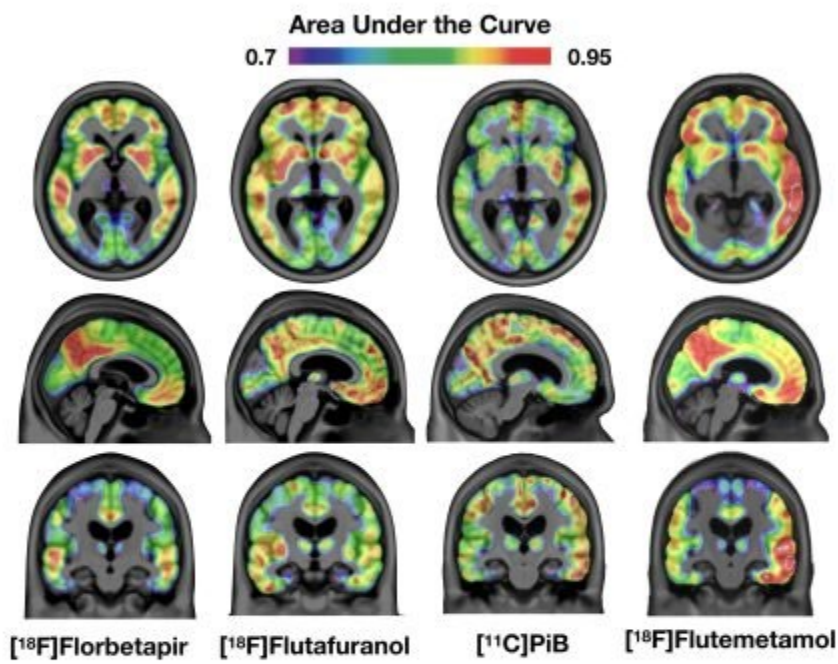
Figure 2: Results of voxel-wise linear regressions testing the relationship between Aβ PET uptake and FDG uptake. Aβ in AD-signature regions was related to more widespread metabolic decline than AB from a neocortical composite mask.

Neocortical Aβ Deposition

AD-Signature Aβ Deposition
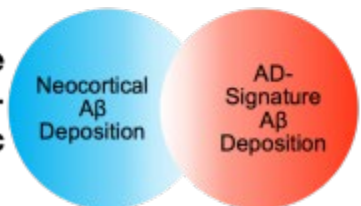
Keywords: *Amyloid PET, Receiver Operating Characteristic Curve, Amyloid Regional Distribution*

P83: In-vivo tau burden correlates with subregional atrophy in medial temporal lobe in amyloid negative individuals

Sandhitsu Das[1], Long Xie[1], Laura Wisse[1], Salena Cui[2], Ranjit Ittyerah[1], Paul Yushkevich[1], David Wolk[1]

[1]*University of Pennsylvania, Philadelphia, PA, US*
[2]*Jefferson University, Philadelphia, PA, US*

Introduction: We investigated the relationship between a measure of in-vivo burden of tau pathology in medial temporal lobe (MTL) and structural atrophy in MTL subregions as well as memory performance in Amyloid-β negative individuals.

Methods: Data from 185 participants from ADNI with mixed clinical status (cognitive normal, MCI, AD dementia) were divided into Amyloid positive (A+) and negative (A-) groups based on Florbetapir-PET imaging. In-vivo tau burden was estimated as the average SUVR within a composite ROI of MTL cortical regions, computed from Flortaucipir-PET imaging. Subregional atrophy was measured from high-resolution T2-MRI including hippocampal subfield volume (CA1, DG, Subiculum) and thickness for entorhinal, perirhinal (divided into BA35 and BA36) and parahippocampal cortices. Tau burden and atrophy or logical memory measures were correlated separately in both groups.

Results: In the A- group, correlations of tau burden were strongest for BA35 and ERC thickness with subiculum and CA1 less strongly correlated within the hippocampus. More widespread correlations were found in the A+ group, but BA35 again being the strongest. Regional thickness analysis correlating point-wise thickness with MTL tau burden displayed overlapping strong BA35/ERC correlations in the A+ and A- groups with somewhat more medial CA (near CA2) thinning in the A- relative to more lateral CA (overlapping CA1) in the A+ group (see Figure). BA35, ERC, and MTL tau burden correlated with logical memory scores in the A- group.

Discussion: These results provide first **in-vivo** evidence of correlation of tau burden in MTL with atrophy at a **subregional** level in A- individuals. Strongest effects in BA35, also described as transentorhinal cortex and the site of earliest tau pathology in Alzheimer's disease, followed by ERC and CA1 subfield of hippocampus, mimic the progression of tau pathology along Braak stages. These findings support the potential sensitivity of Flortaucipir-PET to primary age related tauopathy (PART).

ROI	Atrophy vs. tau A- p-value	Atrophy vs. tau A- partial correlation	Atrophy/tau vs. memory A- p-value	Atrophy/tau vs. memory A- partial correlation
BA35	4.00E-05	-0.38	0.00056	0.32
BA36	0.00452	-0.27	0.0382	0.2
ERC	8.00E-05	-0.36	1.00E-04	0.36
PHC	0.18497	-0.13	0.25032	0.11
CA1	0.00432	-0.27	0.04896	0.19
DG	0.05972	-0.18	0.17492	0.13
SUB	0.00977	-0.25	0.08574	0.17
MTL Tau			0.00641	-0.26
ROI	Atrophy vs. tau A+ p-value	Atrophy vs. tau A+ partial correlation	Atrophy/tau vs. memory A+ p-value	Atrophy/tau vs. memory A+ partial correlation
BA35	3.00E-05	-0.48	4.00E-08	0.6
BA36	0.00098	-0.39	0.00029	0.42
ERC	0.00074	-0.39	0.00034	0.42
PHC	0.26053	-0.14	0.17411	0.17
CA1	0.00023	-0.43	1.00E-05	0.5
DG	0.00044	-0.41	0.00077	0.4
SUB	0.00169	-0.37	0.00051	0.41
MTL Tau			4.70E-08	-0.6

Correlation of subregional atrophy with tau burden as well as correlation of atrophy and tau with memory performance. Covariates include time between pairs of correlated variables, age, ICV for volume, and education for memory correlations. Top rows show A- and bottom rows show A+.

Amyloid+   Amyloid-

Superior view

CA

T-stat

+5

0

-5

ERC

Antero-inferior view

BA35

Antero-superior view

T-statistic map of correlation between tau burden and local thickness in left MTL, with time between MRI and PET scans and age as covariates. Red arrows point to the significant clusters around different subregions circumscribed with black contours . There is considerable overlap between A+ and A- clusters. However, a cluster in A- indicated by the red circle extends into supero-medial aspects of CA, near CA2.

P84: Distinct tau PET patterns in atrophy-defined subtypes of Alzheimer's disease

Rik Ossenkoppele[1,2], Chul H. Lyoo[3], Gil Rabinovici[4], Oskar Hansson[1]

[1]*Lund University, Clinical Memory Research Unit., Lund, Sweden*
[2]*VU University Medical Center, Department of Neurology and Alzheimer Center, Amsterdam Neuroscience, Amsterdam, The Netherlands*
[3]*Department of Neurology, Gangnam Severance Hospital, Yonsei University College of Medicine, Seoul, KP*
[4]*Department of Neurology, University of California San Francisco, Memory and Aging Center, San Francisco, CA, US*

Based on differential patterns of brain atrophy, structural magnetic resonance imaging studies have identified four reproducible subtypes of Alzheimer's disease: i) "typical", ii) "limbic-predominant", iii) "hippocampal-sparing", and iv) "mild atrophy". The factors underlying these atrophy-defined subtypes are largely unexplained. Previous studies have shown that the distribution of amyloid-β pathology is virtually the same across subtypes. We therefore aimed to examine whether tau pathology could help explain differences in atrophy patterns. We used a clustering method to replicate **in vivo** the four subtypes based on magnetic resonance imaging defined atrophy in medial temporal, posterior and frontal brain regions of 260 amyloid-β positive patients with Alzheimer's disease. We then tested whether the subtypes differed on [^{18}F]flortauicpir (tau) positron emission tomography, white matter hyperintensity burden and rate of global cognitive decline. We found the greatest tau load in hippocampal-sparing (neocortical-predominant) and typical (temporal-predominant) patients, while limbic-predominant patients showed particularly high entorhinal tau pathology. Typical Alzheimer's disease patients had the most pronounced white matter hyperintensity load compared to the other subtypes, while hippocampal-sparing Alzheimer's disease patients showed the most rapid global cognitive decline. In conclusion, the distribution of tau pathology differed in a biologically and clinically meaningful manner among distinct atrophy-defined subtypes of Alzheimer's disease.

Keywords: *Tau, PET, MRI, heterogeneity*

P85: Item-level analysis of the Cognitive Function Index by screening amyloid PET in the A4 Study

Rebecca Amariglio[1,2], Sietske Sikkes[2,6], Gad Marshall[1,2], Rachel Buckley[2,7], Jennifer Gatchel[2], Keith Johnson[1,2], Dorene Rentz[1,2], Michael Donohue[3,4], Rema Raman[3,4], Chung-Kai Sun[3,4], Roy Yaari[5], Karen Holdridge[5], Joshua Grill[8], Paul Aisen[4], Reisa Sperling[1]

[1]*Brigham and Women's Hospital, 02115, MA, US*
[2]*Massachusetts General Hospital, Boston, MA, US*
[3]*Alzheimer's Therapeutic Research Institute, San Diego, CA, US*
[4]*University of Southern California, San Diego, CA, US*
[5]*Lilly Research Laboratories, Indianapolis, IN, US*
[6]*VU Amsterdam, Amsterdam, The Netherlands*
[7]*University of Melbourne, Melbourne, Australia*
[8]*University of California Irvine, Irvine, CA, US*

Background: The Cognitive Function Index (CFI) is a participant and study partner reported functional assessment, previously shown to track with clinical progression. Preliminary report of the A4 Study screen data showed a relationship between the CFI total score and brain amyloid status. In this study, we aimed to further understand the relationship between amyloid status and item-level responses on the CFI.

Methods: 4486 (CDR=0; MMSE 25-30) participants (ages 65-85) who were screened as part of the A4 Study completed amyloid PET imaging. The CFI was administered to both the participant and a study partner prior to amyloid PET imaging. Participants were classified as elevated amyloid (Ab+; n=1323) or non-elevated amyloid (Ab-; n=3163). For each item of the CFI, odds of endorsement by Ab status was assessed for participant and study partner report.

Results: Independent of Ab status, participants reported a higher level of endorsement compared to the study partners for nearly all CFI items with the largest difference for 'trouble following the news' (OR=6.35; 95% CI, 4.92, 8.21; p<0.001). Ab+ increased the odds of greater endorsement on the majority of CFI items in comparison to Ab- (for both participant and study partner report), with the highest odds ratios for 'a substantial decline in memory' (OR=1.59; 95% CI, 1.39, 1.84; p<0.001), 'seen a doctor' (OR= 1.68; 95% CI 1.35, 2.09; p<0.001), and 'work performance' (OR= 1.71, 95% CI, 1.19, 2.44; p=0.0034).

Conclusions: Cognitively normal Ab+ individuals and their study partners report changes across a variety of everyday cognitive tasks compared to Ab-. This suggests a person may notice very subtle changes in one's own cognitive functioning that can be corroborated by an observer. These findings have implications for the types of questions that may be most valuable to ask when starting to screen along the preclinical stage of Alzheimer's disease.

Keywords: *subjective report, A4 Study, amyloid*

P86: Cross-sectional and longitudinal effects of asymmetric amyloid deposition on memory in Baltimore Longitudinal Study of Aging (BLSA) participants

Zabecca Brinson[1], Murat Bilgel[2], Yang An[2], Chiung-Wei Huang[2], Dean Wong[3,4,5,6,7], Susan Resnick[2]

[1]*Russell H Morgan Department of Radiology and Radiological Science, Brain PET Clinical Research Training Program, The Johns Hopkins University School of Medicine, Baltimore, MD, US*
[2]*Laboratory of Behavioral Neuroscience, National Institute on Aging, Baltimore, MD, US*
[3]*Department of Neurology, The Johns Hopkins University School of Medicine, Baltimore, MD, US*
[4]*Solomon Snyder Department of Neuroscience, The Johns Hopkins University School of Medicine, Baltimore, MD, US*
[5]*Russell H Morgan Department of Radiology and Radiological Science, Division of Nuclear Medicine and Molecular Imaging/High Resolution Brain PET, The Johns Hopkins University School of Medicine, Baltimore, MD, US*
[6]*Department of Psychiatry and Behavioral Sciences, The Johns Hopkins University School of Medicine, Baltimore, MD, US*
[7]*Department of Environmental Health and Engineering, Johns Hopkins Bloomberg School of Public Health, Baltimore, MD, US*

Introduction: Previous research has suggested associations between asymmetric amyloid deposition and cognition in certain pathological conditions but data are limited in cognitively normal individuals. We investigated cross-sectional and longitudinal effects of baseline asymmetric brain amyloid deposition on memory among 183 cognitively normal NIH-NIA Baltimore Longitudinal Study of Aging participants using PET-PiB imaging.

Methods: Baseline asymmetry scores of mean DVRs were calculated for 10 regions as (Left−Right DVR)/(Left+Right DVR), converted to z-scores, and categorized as "No asymmetry" (NA) if within 0.5 SD from 0, "R>L" if <−0.5, and "L>R" if >0.5. Memory composite z-scores were calculated as mean of immediate and delayed free recall z-scores on the California Verbal Learning Test. Participants were PiB+ if mean cortical DVR>1.062. Using memory as the outcome, linear mixed effects models included age, sex, time since baseline, PiB status, asymmetry group, and their interactions.

Results: Baseline memory was lower in L>R compared to NA within PiB- for mean cortical (β=−0.339 (−0.673, −0.005)), frontal grey matter (GM) (β=−0.335 (−0.664, −0.007)), parietal GM (β=−0.396 (−0.770, −0.022)), temporal GM (β=−0.430 (−0.766, −0.094)), and lateral frontal GM (β=−0.403 (−0.721, −0.084)). Similarly, baseline memory was lower in PiB- with L>R compared with R>L in precuneus (β=−0.707 (−1.150, −0.265)), parietal GM (β=−0.533 (−1.030, −0.036)), medial frontal GM (β=−0.498 (−0.891, −0.106)). Significant time x asymmetry x PiB status interactions indicated L>R asymmetry had a greater impact on memory decline in PiB+ vs. PiB- (NA vs. L>R: posterior cingulate gyrus, β=−0.132 (−0.257, −0.007), temporal GM, β=−0.312 (−0.569, −0.054), medial frontal GM, β=−0.204 (−0.406, −0.001); R>L vs. L>R: temporal GM, β=−0.313 (−0.569, −0.057), lateral temporal GM, β=−0.239 (−0.474, −0.004)).

Conclusions: Our results demonstrate that baseline L>R PiB uptake is associated with lower baseline memory scores and greater longitudinal memory decline. Future research directions include investigation of asymmetry as a risk for cognitive impairment.

Table 1. Demographic characteristics of the participants

	All participants			Participants with >1 visit		
	PiB neg N=129	PiB pos N=54	p.overall	PiB neg N=101	PiB pos N=35	p.overall
Demographics:						
Baseline Age	74.9 (7.73)	78.3 (7.53)	0.006	75.2 (7.50)	79.8 (7.34)	0.002
Sex:			0.505			0.329
Female	66 (51.2%)	24 (44.4%)		52 (51.5%)	14 (40.0%)	
Male	63 (48.8%)	30 (55.6%)		49 (48.5%)	21 (60.0%)	
Race:			0.905			0.887
Nonwhite	29 (22.5%)	11 (20.4%)		20 (19.8%)	8 (22.9%)	
white	100 (77.5%)	43 (79.6%)		81 (80.2%)	27 (77.1%)	
Education	17.3 (2.20)	16.8 (2.31)	0.159	17.4 (2.19)	17.0 (1.93)	0.315
ApoE4:			0.015			0.111
e4 carriers	32 (25.0%)	24 (44.4%)		24 (24.0%)	14 (40.0%)	
e4 non-carriers	96 (75.0%)	30 (55.6%)		76 (76.0%)	21 (60.0%)	
Follow-up time:						
Years	3.97 (3.47)	2.83 (3.17)	0.032	5.07 (3.12)	4.36 (2.96)	0.231

Figure 1. Distribution of Mean Cortical baseline asymmetry scores by asymmetry group
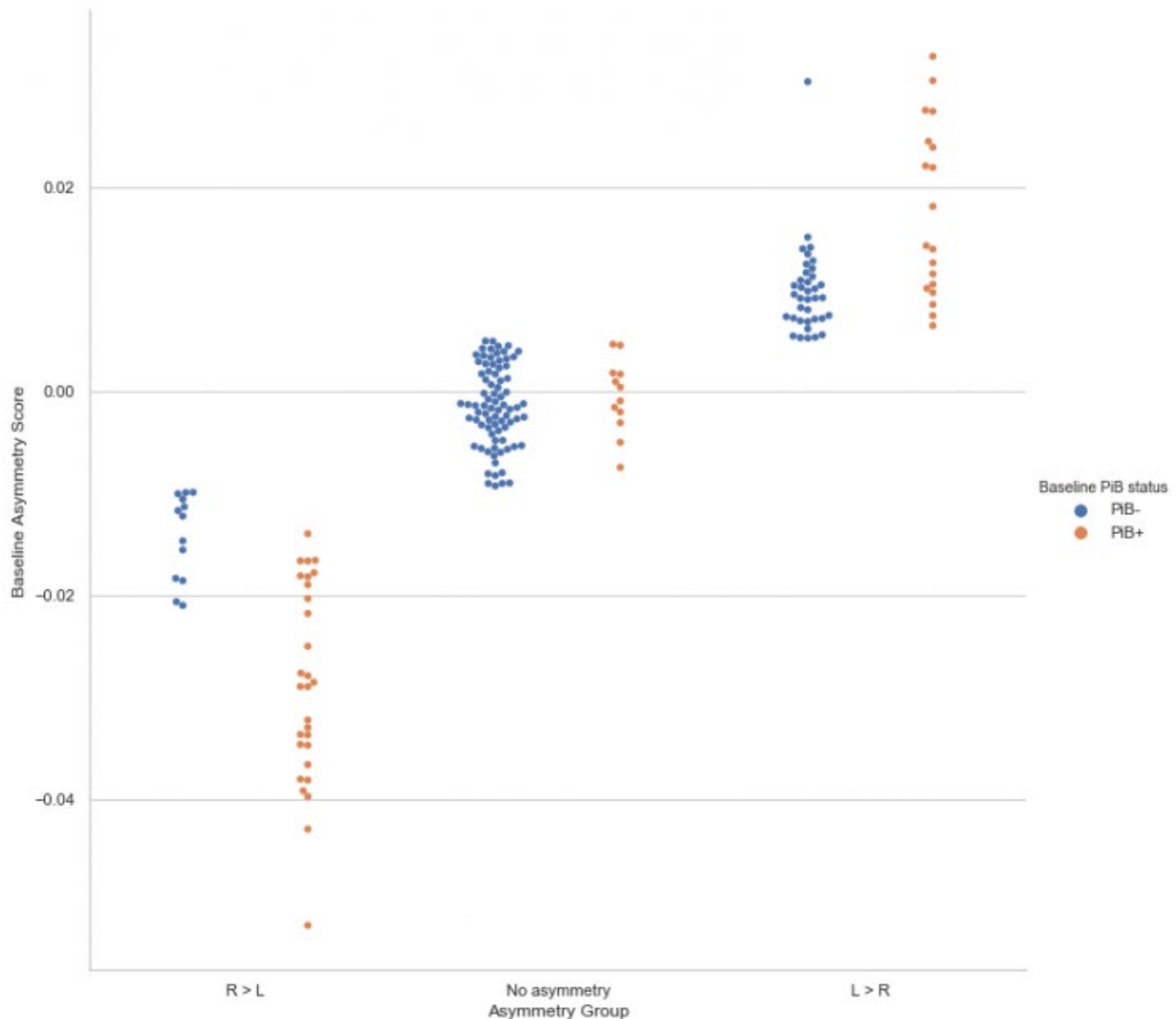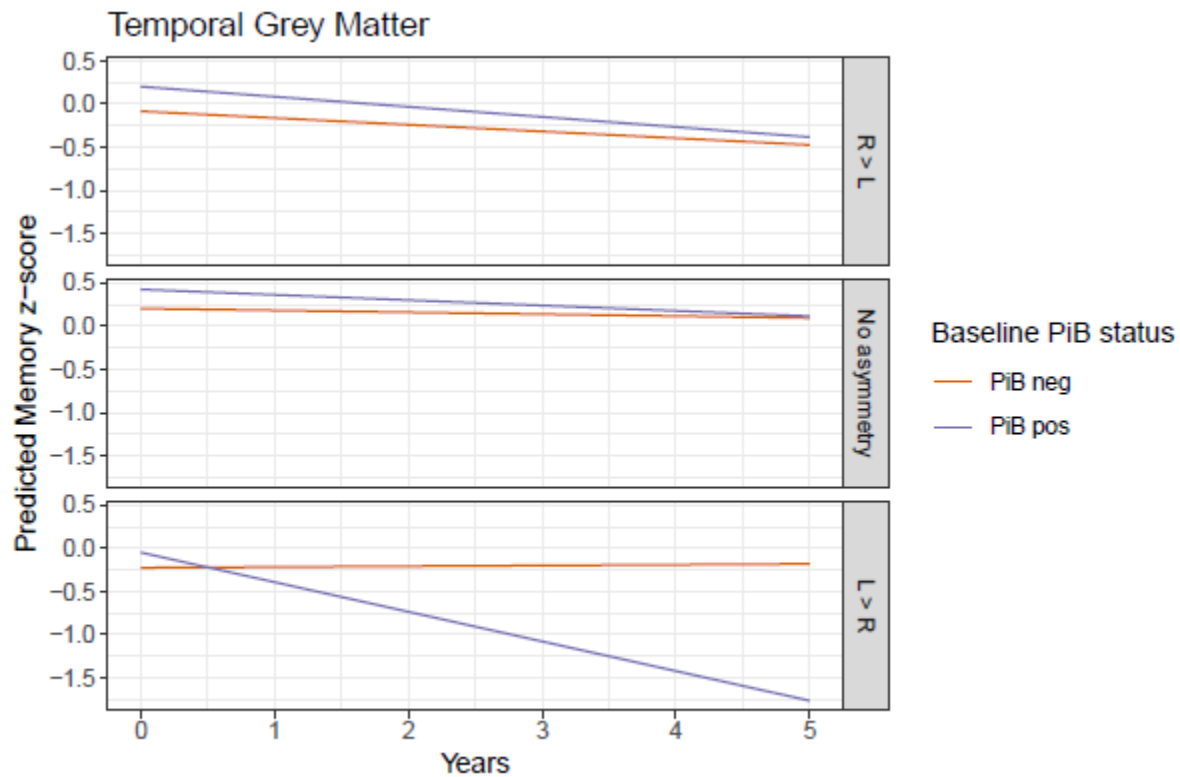
Figure 2. Predicted longitudinal effects of baseline asymmetry on memory

---

Keywords: *memory, cognition, longitudinal studies, amyloid imaging, asymmetry*

P87: Regional sex-differences in tau pathology in asymptomatic individuals with elevated amyloid

<u>Heidi Jacobs</u>[1], Rachel Buckley[15,16], Elizabeth Mormino[9], Aaron Schultz[1], Rema Raman[2], Michael Donohue[3], Chung-Kai Sun[4], Kenneth Marek[5], John Seibyl[6], Mark Mintun[7], Sergey Shcherbinin[7], Michael Pontecorvo[8], Chris Rowe[10], Chris VanDyck[11], Stephen Salloway[12], Cliff Jack[13], Roy Yaari[14], Karen Holdridge[7], Paul Aisen[3], Reisa Sperling[15], Keith Johnson[1]

[1]*Department of Radiology, Division of Molecular Imaging and Nuclear Medicine, Massachusetts General Hospital / Harvard Medical School, Boston, MA, US*
[2]*University of Southern California, San Diego, CA, US*
[3]*Alzheimer's Therapeutic Research Institute, San Diego, CA, US*
[4]*University of Southern California, Los Angeles, CA, US*
[5]*Molecular Neuroimaging, A Division of inviCRO, New Haven, CT, US*
[6]*Invicro, New Haven, CT, US*
[7]*Eli Lilly and Company, Indianapolis, IN, US*
[8]*Avid Radiopharmaceuticals, Philadelphia, PA, US*
[9]*Stanford Medicine, Neurology & Neurological Sciences, Stanford, CA, US*
[10]*Austin Health, Melbourne, Australia*
[11]*Yale School of Medicine, New Haven, CT, US*
[12]*Alpert Medical School of Brown University, USA, RI, US*
[13]*Mayo Clinic, Rochester, MN, US*
[14]*Lilly Research Laboratories, Indianapolis, IN, US*
[15]*Center for Alzheimer Research and Treatment, Brighma and Women's Hospital, Harvard Medical School, Boston, MA, US*
[16]*The Florey Institute and Melbourne School of Psychological Science,The University of Melbourne, Melbourne, Australia*

Background: Women may be at greater risk for accumulating Alzheimer's disease (AD) pathology and cognitive decline than males. The modulation of these sex-specific associations by the apolipoprotein ε (APOEε) gene has shown to be dependent on the presence of amyloidosis. We set out to investigate sex-differences in tau pathology and potential modulation by APOEε4 in asymptomatic individuals with elevated amyloid (Aβ) who were enrolled in the A4 study.

Methods: Florbetapir and Flortaucipir-PET data were collected in 384 Aβ-positive cognitively normal individuals (mean age: 72.12 years (range: 65-86), Figure 1). Regression analyses examined main effects of ε4-status and sex differences on regional tau burden across all regions of the cortical mantle, and their interaction. Covariates were age, APOEε4 or sex and neocortical Aβ. Comparisons were adjusted with a False Discovery Rate (FDR) approach.

Results: Males were older than females, and ε4-carriers were younger than non-carriers (p<0.001). There were no sex-differences in neocortical Aβ or global tau (p=0.77, p=0.58). Sex-differences in regional tau were observed across the cortical mantle, also when controlling for Aβ (Figure 2 & 3; Cohen's d range:0.28-0.44; e.g.:11.8% higher rostral middle frontal tau in females versus males). While we observed more regions showing greater tau in females than males compared to the opposite contrast, the effects sizes in both directions were of similar magnitude.

ε4-carriers had higher Aβ (p<0.001) than non-carriers. APOEε4 groups did not differ on global tau, but carriers

displayed greater tau binding in medial and lateral temporal regions than non-carriers. No ε4-related regional differences remained present when controlling for Aβ. No significant "sex by APOEε4" or "sex by Aβ" effects were detected.

Conclusion: Regional sex-differences in tau pathology occur independent of Aβ and APOEε4 genotype. These findings suggest that accrual of tau pathology exhibits sex-specific regional vulnerabilities of which the biological correlates remain unclear.

Figure 1

Means (sd)	APOEε4 carriers (n = 218)		APOEε4 non-carriers (n= 166)	
	F (n=129)	M (n=89)	F (n=93)	M (n=73)
Age (years)	70.56 (4.08)	72.98 (5.03)	72.46 (5.06)	73.37 (4.82)
Education (years)	15.61 (2.69)	16.54 (2.75)	15.77 (2.74)	17.12 (3.05)
MMSE (score)	28.63 (1.18)	28.33 (1.43)	28.97 (1.21)	28.41 (1.54)
Neocortical amyloid	1.35 (0.17)	1.37 (0.17)	1.26 (0.17)	1.26 (0.15)
Entorhinal tau	1.59 (0.45)	1.56 (0.39)	1.48 (0.41)	1.41 (0.30)
Inferior temporal tau	1.57 (0.34)	1.57 (0.27)	1.50 (0.25)	1.49 (0.24)
Global tau	1.31 (0.16)	1.31 (0.13)	1.30 (0.13)	1.27 (0.12)

F=females, M=males;

Figure 2
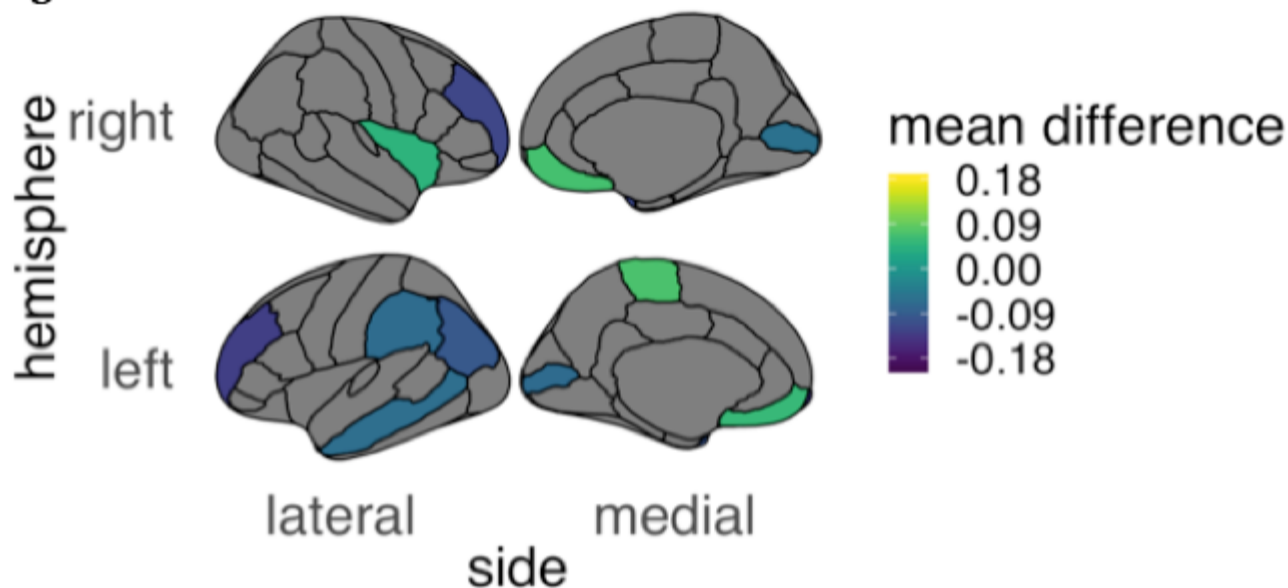
Note: significant differences between males and females in regional tau binding, adjusted for amyloid, APOEε4 and age. Yellow-green: M>F, blue-purple: F>M. Analyses were controlled for multiple comparisons using the FDR-approach.

Figure 3
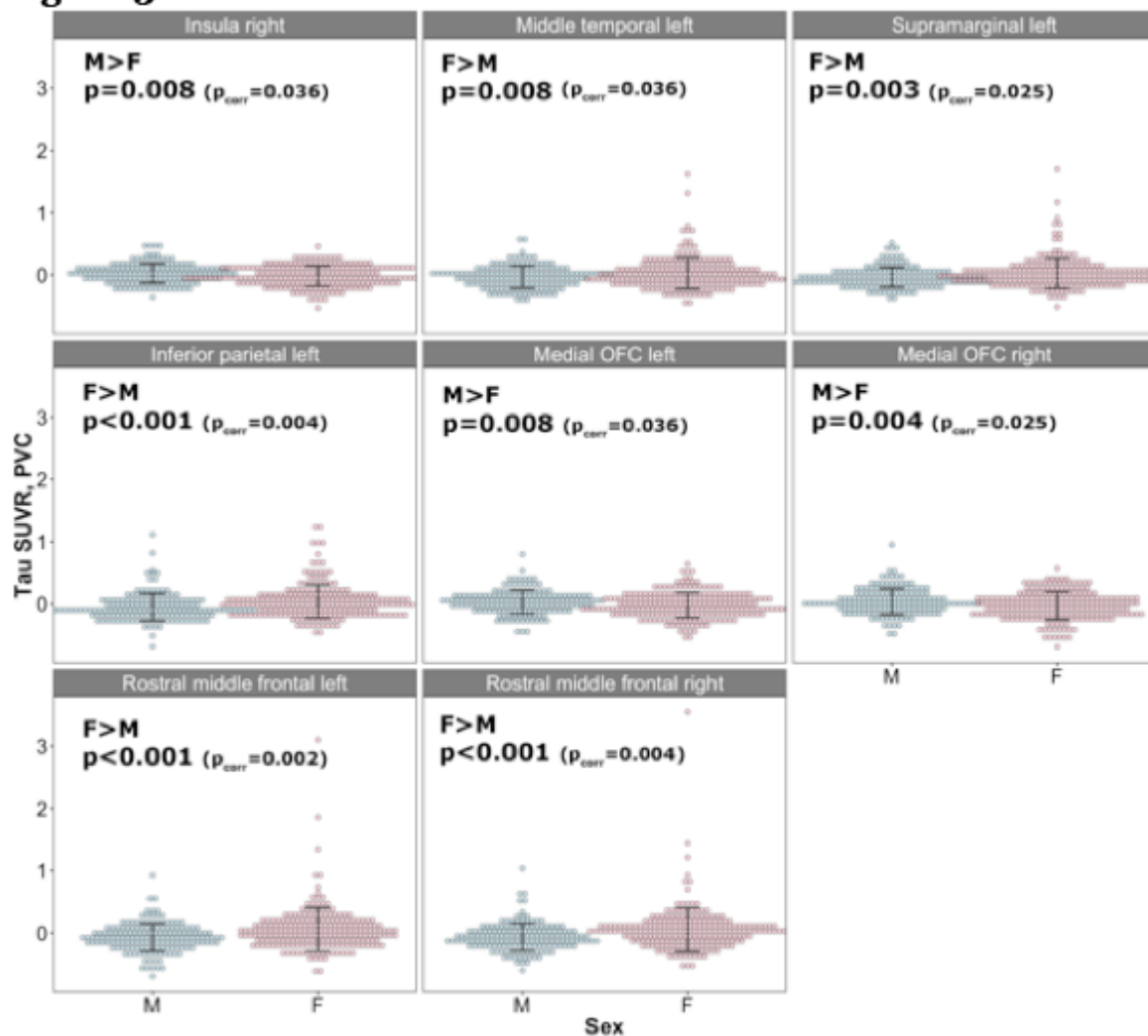
Note: distributions of regional tau pathology in males and females from selected regions of Figure 2. Values are adjusted for age, APOEε4 and amyloid. All plotted regions were significantly different between males and females, after FDR-correction (p_corr). F=females, M=males.

P88: CSF tau biomarkers correlate with [18F]MK6240 SUVR in AD related areas

Mira Chamoun[1,2], Min Su Kang[1,2], Tharick A. Pascoal[1,2], Andréa L. Benedet[1,2,3], Sulantha Mathotaarachchi[1,2], Joseph Therriault[1,2], Melissa Savard[1,2], Emilie Thomas[1,2], Reda Bouhachi[6], Chris Hsiao[6], Gassan Massarweh[6], Jean-Paul Soucy[6], Serge Gauthier[2,4], Pedro Rosa-Neto[1,2,5,6]

[1]*Translational Neuroimaging Laboratory, McGill University Research Centre for Studies in Aging, Montreal, QC, Canada*
[2]*Douglas Hospital Research Centre, McGill University, Montreal, QC, Canada*
[3]*CAPES Foundation, Ministry of Education of Brazil, Brasília, Brazil*
[4]*Alzheimer's Disease Research Unit, McGill University Research Centre for Studies in Aging, Montreal, QC, Canada*
[5]*Department of Neurology and Neurosurgery, McGill University, Montreal, QC, Canada*
[6]*Montreal Neurological Institute, Montreal, QC, Canada*

Voxelwise association between [18F]MK6240 and CSF p-tau

Background: Cerebrospinal fluid (CSF) markers of tau and imaging tau load measured with [18F]AV-1451 have revealed significant associations in various cortical regions. PET imaging of the tau load with [18F] MK6240 presents a promising imaging agent due to its high selectivity to pathologic tau deposits in the AD brain and its sensitivity in early detection of tau pathology. Here, we studied for the first time the association between the novel tau imaging agent [18F]MK6240 and the CSF total-tau (t-tau) and phosphorylated-tau (p-tau) levels.

Methods: In this observational study all participants had complete cognitive assessments and clinical CSF biomarkers measurement of Aβ and tau and PET imaging biomarkers of Aβ ([18F]AZD4669) and tau ([18F]MK6240). [18F]AZD4669 and [18F]MK6240 binding outcomes were calculated using SUVR40-70 SUVR90-110, respectively using the cerebellum as reference region.

Results: We studied 34 individuals AD (N=13; MMSE=18), MCI (N=5; MMSE=26), FTD (N=4; MMSE=27), CN (N=12, MMSE=29); aged 44 to 78 yo. We observed that CSF p-tau and t-tau were highly correlated with [18F]MK6240 in typical AD-related brain regions. The regions with the highest correlation were the hippocampus (p-tau; p=0.004, t-tau: p=0.002) the mediobasal temporal lobe (p-tau; p=0.0003, t-tau: p<0.0001) and the striatum (p-tau: p=0.003, t-tau: p=0.003). Additionally, as expected, CSF Aβ and [18F]AZD4669 were reversely correlated.

Conclusions: The associations between CSF t-tau or p-tau with [18F]MK6240 support the concept that pair helical filament availability and monomeric forms of CSF p-tau and t-tau reflects the brain tau pathology in vivo.

Keywords: *CSF, p-tau, t-tau, [18F]MK6240, Alzheimer's disease*
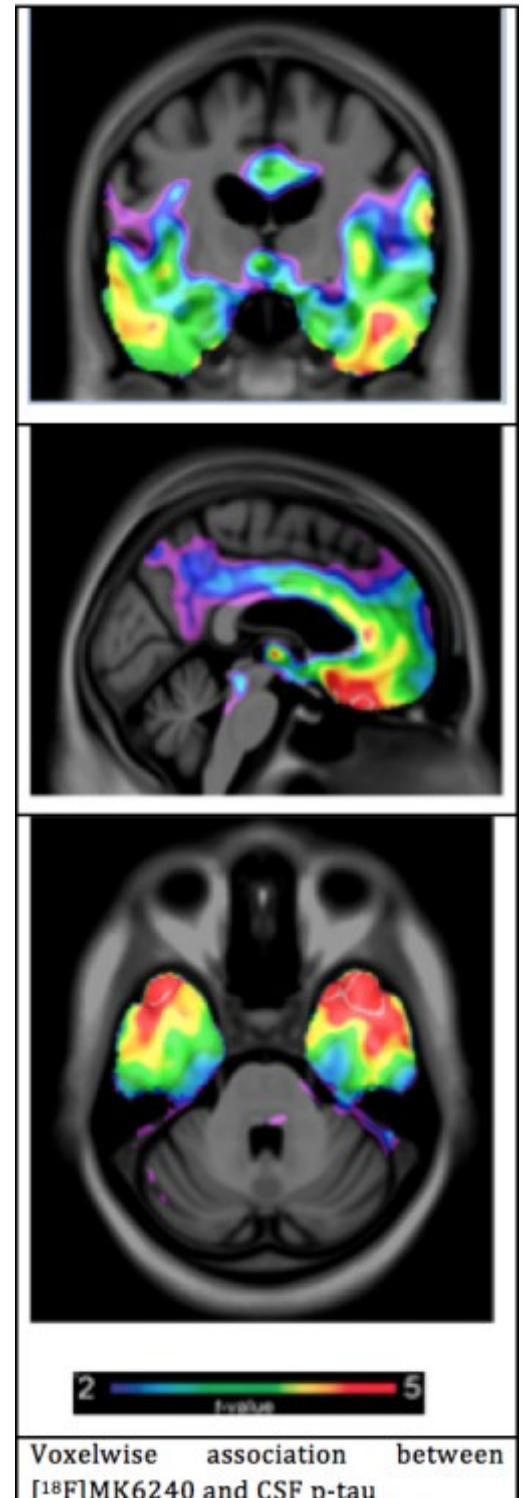
P89: Diagnostic accuracy of [18F]RO948 PET for differentiating Alzheimer's disease from other neurodegenerative disorders

Oskar Hansson[1], Erik Stomrud[1], Edilio Borroni[2], Gregory Klein[2], Olof Strandberg[1], Ruben Smith[1]

[1]*Clinical Memory Research Unit, Dept of Clinical Sciences Malmö, Lund University, Lund, Sweden*
[2]*Roche Pharma Research and Early Development, Basel, Switzerland*

Aim: The aim was to examine the discriminative accuracy of [^{18}F]RO948 PET for AD versus non-AD neurodegenerative disorders.

Methods: In this cross-sectional study, 297 participants have been included to date in the Swedish BioFINDER-2 study (between June 2017 and September 2018). The study population included 88 cognitively normal controls, 100 patients with mild cognitive impairment (52% amyloid-β+ [i.e. "MCI-due-to-AD"]), 58 patients with AD dementia and 51 patients with various non-AD neurodegenerative disorders (Table 1).

The index test was the [^{18}F]RO948 PET SUVR in four pre-defined regions-of-interest (ROIs) spanning Braak stages I-VI. Cut-points for "tau-positivity" were determined using the mean +2 standard deviations observed in controls (Figure 1) and Youden index for the contrast AD dementia versus controls.

The reference standard was the clinical diagnosis determined at the specialized memory centers. In the primary analysis, the discriminative accuracy (i.e. sensitivity and specificity) of [^{18}F]RO948 was examined for AD dementia versus all non-AD neurodegenerative disorders. In secondary analyses, the area-under-the-curve (AUC) of [^{18}F]RO948 SUVR was compared with three established MRI measures (hippocampal volumes and AD-signature and whole-brain cortical thickness).

Results: [^{18}F]RO948 uptake in the medial-basal and lateral temporal cortex(stages I-IV) showed 81% sensitivity and 93% specificity using the threshold based on controls (SUVR=1.31), and 84% sensitivity and 93% specificity using the Youden index derived cut-off (SUVR=1.29) for distinguishing AD dementia from all non-AD neurodegenerative disorders. The age-adjusted AUCs for all four [^{18}F]RO948 ROIs were higher (AUC range: 0.90-0.95) compared to the three volumetric MRI measures (AUC range: 0.50-0.52, all ROIs p<0.001) (Figure 2). Diagnostic performance of the four [^{18}F]RO948 ROIs were lower in MCI-due-to-AD (AUC range: 0.69-0.75).

Conclusion: [^{18}F]RO948 PET is a promising tool for distinguishing AD from other neurodegenerative disorders, especially at the dementia stage, and could support the diagnostic process in patients with cognitive, behavioral and/or motor symptoms.

	Controls	MCI	AD	Other dementias
n	88	100	58	51
Age	64.1 ± 14.7	68.7 ± 9.1	73.6 ± 7.3	70.1 ± 3.5
Sex (% Male)	53.4	48.0	48.3	62.8
Education	12.4 ± 4.0	12.5 ± 4.7	12.4 ± 5.0	12.1 ± 3.5
MMSE	28.8 ± 1.2	27.1 ± 2.5	20.3 ± 4.2	24.4 ± 4.4
Aβ+ (No., Total No., %)	28/88 (31.8)	52/100 (52.0)	58/58 (100)	10/51 (19.6)
ApoE4 heteroz (%)	43	52	67	31
ApoE4 homoz (%)	5	6	10	6
SUVR Stage I-II	1.17 ± 0.21	1.32 ± 0.36	1.93 ± 0.47	1.21 ± 0.21
SUVR Stage I-IV	1.17± 0.15	1.29 ± 0.32	2.04 ± 0.75	1.21 ± 0.17
SUVR Stage III-IV	1.17 ± 0.15	1.28 ± 0.32	2.04 ± 0.78	1.22 ± 0.17
SUVR Stage V-VI	1.05 ± 0.10	1.07 ± 0.14	1.45 ± 0.46	1.07 ± 0.11
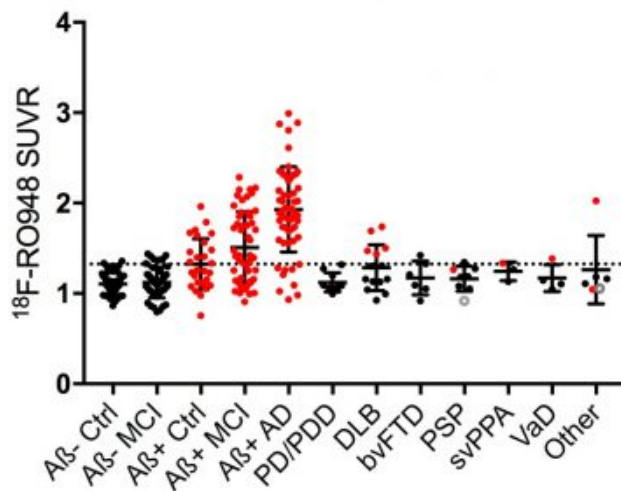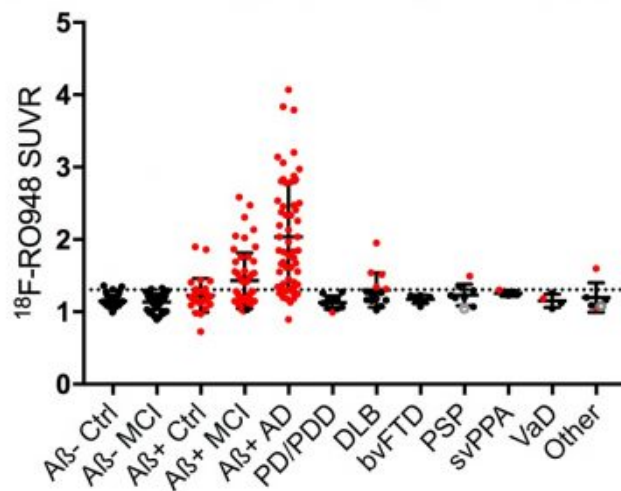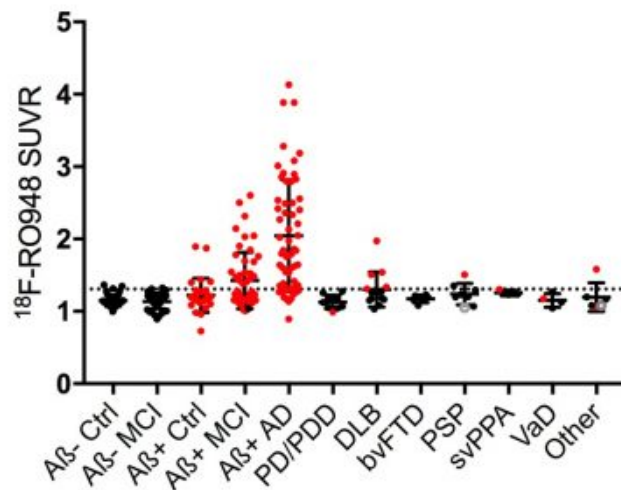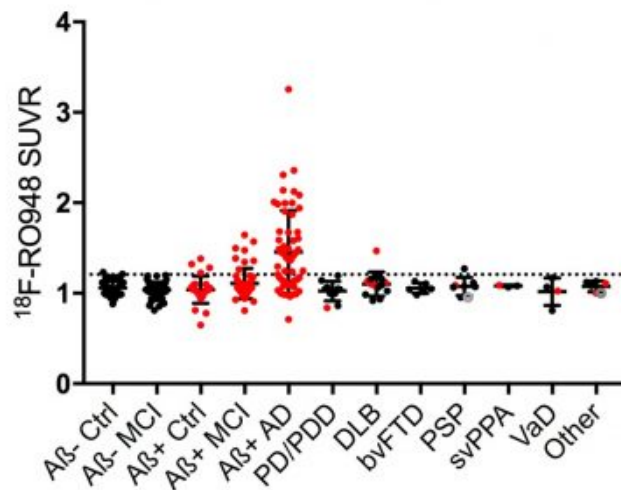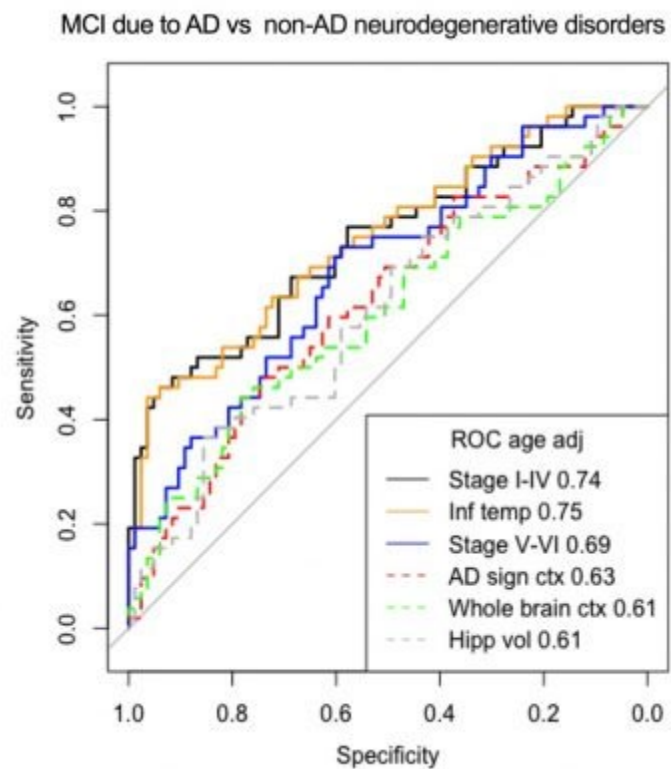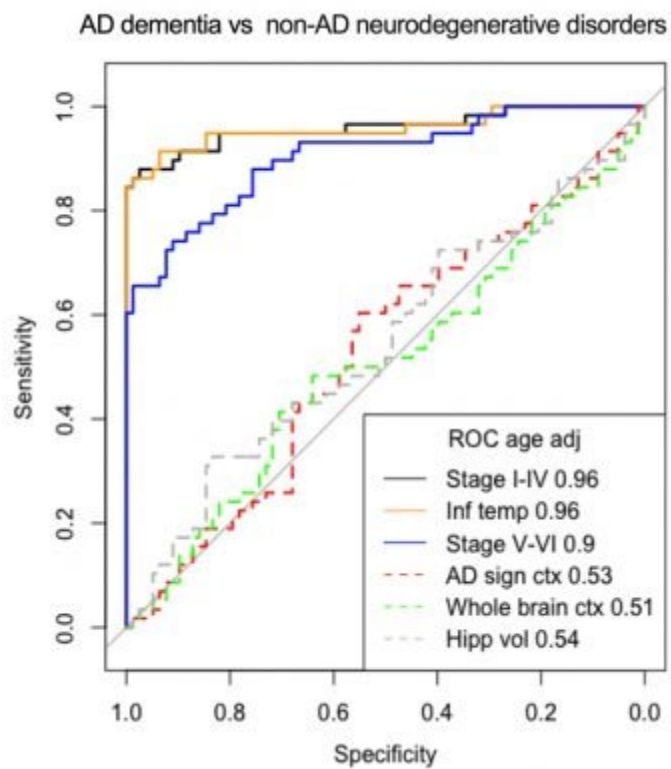
AD dementia vs non-AD neurodegenerative disorders

ROC age adj
Stage I-IV 0.96
Inf temp 0.96
Stage V-VI 0.9
AD sign ctx 0.53
Whole brain ctx 0.51
Hipp vol 0.54

MCI due to AD vs non-AD neurodegenerative disorders

ROC age adj
Stage I-IV 0.74
Inf temp 0.75
Stage V-VI 0.69
AD sign ctx 0.63
Whole brain ctx 0.61
Hipp vol 0.61

P90: Amyloid burden and hippocampal function

Lori Beason-Held[1], Andrea Shafer[1], Murat Bilgel[1], Dean Wong[2], Susan Resnick[1]

[1]*National Institute on Aging Intramural Research Program, NIH, Baltimore, MD, US*
[2]*Johns Hopkins University, Baltimore, MD, US*

Introduction: Functional connectivity changes are associated with amyloid accumulation in Alzheimer's dementia and the prodromal stage of the disease, often involving the temporal lobe of the brain. Here, we examine activation and functional connectivity patterns of different regions of the hippocampus during memory encoding in cognitively normal amyloid positive individuals, relative to those who are amyloid negative.

Methods: We used cross-sectional data from 48 participants (16 PiB+, and 32 age and sex matched PiB-) enrolled in the Baltimore Longitudinal Study of Aging who had both 11C-Pittsburgh compound B (PiB) dynamic amyloid PET and fMRI task activation scans. The fMRI scans were collected during an associative face-scene (Face Place; FP) memory encoding task. Regional activation patterns and functional connectivity of the hippocampus were assessed in the PiB+ group relative to the PiB- group.

Results: When examining the overall pattern of task activation (Novel FP pairs vs. fixation condition), the PiB+ group showed bilateral decreased activation of the hippocampal head. When examining the memory-specific activation pattern (Novel FP pairs vs. Repeated FP pairs), the PiB+ group showed increased activation of the hippocampal body/tail. Functional connectivity analyses of these regions demonstrated decreased connectivity of both the hippocampal head and body in the PiB+ group.

Conclusions: Activation differences are seen in the PiB+ group relative to PiB- group. The overall task activation pattern showed decreased activation of the hippocampal head, whereas the memory-specific activation results showed increased activation of the hippocampal body and tail in the PiB+ group. Although both increased and decreased activation levels were observed in the hippocampus of cognitively normal PiB+ individuals, functional connectivity of this region was consistently decreased in those with cortical amyloid burden.

P91: Ante-post mortem binding of THK5317 and its vitro comparability with MK-6240 in a case of FTLD

Laetitia Lemoine[1], Konstantinos Chiotis[1,2], Antoine Leuzy[1], Caroline Graff[1,3], Inger Nennesmo[4], Agneta Nordberg[1,3]

[1]*Division of clinical geriatrics, department of Neurobiology, Care Sciences and Society, Karolinska Institute, Stockholm, Sweden*
[2]*Theme Neurology, Karolinska University Hospital, Stockholm, Sweden*
[3]*Theme Aging, Karolinska University Hospital, Stockholm, Sweden*
[4]*Department of Pathology, Karolinska University Hospital, Stockholm, Sweden*

Introduction: Significant progress has been made with respect to tau PET imaging, with so called first-generation ligands (e.g. 18F-THK5317) having been used extensively in research studies and second-generation compounds (e.g. 18F-MK-6240) now entering the field. An open question, however, is whether a subset of these tracers will prove interchangeable, or whether a range of compounds will be required to characterize different tauopathies.

Aims: To compare ante-mortem PET and post-mortem autoradiographic findings with THK5317 (S-form of THK5117) in a case clinically diagnosed as frontotemporal lobar degeneration (FTLD). In addition, we aimed to compare THK5117 and MK-6240 autoradiograms in this case, and in an additional case with Alzheimer's disease (AD).

Methods: For in vivo 18F-THK5317 PET, a Logan reference distribution volume ratio image was created using the interval 30- to 60-minutes and the cerebellar cortex as a reference tissue. 18F-FDG and 11C-PIB PET were also performed. In vitro autoradiography was performed on paraffin fixed sections (10μ thick) with 3H-THK5117 (4nM) and 3H-MK-6240 (0.5nM). Non-specific binding was determined with 1μm MK-6240 and 10 μm THK5117 unlabelled compound.

Results: In combination with neuropsychological and CSF findings (normal Aβ1-42 and p-tau, increased neurofilament light), in vivo PET (18F-THK5317, 18F-FDG, and 11C-PIB) findings showed a pattern suggestive of FTLD. At autopsy, however, tau-positive globose neurofibrillary tangles were observed, suggesting a diagnosis of corticobasal degeneration. In vitro, autoradiographic studies using both 3H-THK5117 and 3H-MK-6240 showed that the binding pattern in this case differed from that seen in AD tissue. In the both cases, however, semi-quantitative analysis showed higher binding when using 3H-THK5117.

Conclusions: In vitro THK5117 and MK6240 showed a similar binding pattern, at least in the AD case. Some in vivo-in vitro discrepancies were observed and further in vitro investigations (both autoradiography and immunostaining) are required to understand what underlies specific binding in this FTLD case.

P92: Tau and amyloid protein accumulation affect distinct white matter fiber tracts in Alzheimer's disease

Melissa Savard[1,2], Min Su Kang[1,2], Tharick Pascoal[1,2], Sulantha Mathotaarachchi[1,2], Joseph Therriault[1,2], Mira Chamoun[1,2], Andrea Lessa Benedet[1,2], Emilie M. Thomas[1,2], Marlee Parsons[1,2], Cecile Tissot[1,2], Firoza Lussier[1,2], Serge Gauthier[1,2], Pedro Rosa-Neto[1,2]

[1]*McGill University Research Centre for Studies in Aging, Verdun, QC, Canada*
[2]*Translational Neuroimaging Laboratory, McGill University, Verdun, QC, Canada*

Intro: Tau and amyloid protein accumulation are the hallmarks of Alzheimer Disease neuropathology. While many studies have investigated their relationship to Grey Matter (GM), little is known about their effect on White Matter (WM). We used diffusion imaging (DWI) in combination with PET imaging to investigate the relationship between amyloid, tau, and whole-brain WM fiber density and cross-section.

Method: Preliminary data from 76 participants from the Triad cohort were analysed. All participants (CN = 34, CN at risk for AD = 19, MCI due to AD = 15 and probable AD = 8) underwent an Amyloid PET scan ($[^{18}F]$AZD4694) a Tau PET scan ($[^{18}F]$MK6240), a structural MRI and a multi-shell diffusion MRI. Global averaged SUVR values were calculated in individual native GM mask. DWI sequences were analysed using the Fixel-Based analysis from the MrTrix3 package (http://www.mrtrix.org/), enabling us to obtain a voxelwise measure of WM fibre density (FD) and cross-section (FC).

Results: High amyloid load was associated with a broad reduction of WM integrity including large association fibres (cingulum and uncinate fasciculus), the corpus callosum (genu), projection fibres (internal capsule, posterior thalamic radiation, anterior corona radiata) and short association fibres (hippocampal, frontal, and temporal WM gyri). In contrast, the negative association with a high load of Tau was more localized to posterior parts of the brain such as the angular and supramarginal gyrus, the parietal lobules and the precuneus, but also to the temporal and fusiform gyri, the thalamus, the putamen and the amygdala.

Conclusion: Our results indicate a negative relationship between misfolded proteins and the WM microstructure and support a framework where different pathology could have distinct deleterious effects on WM.
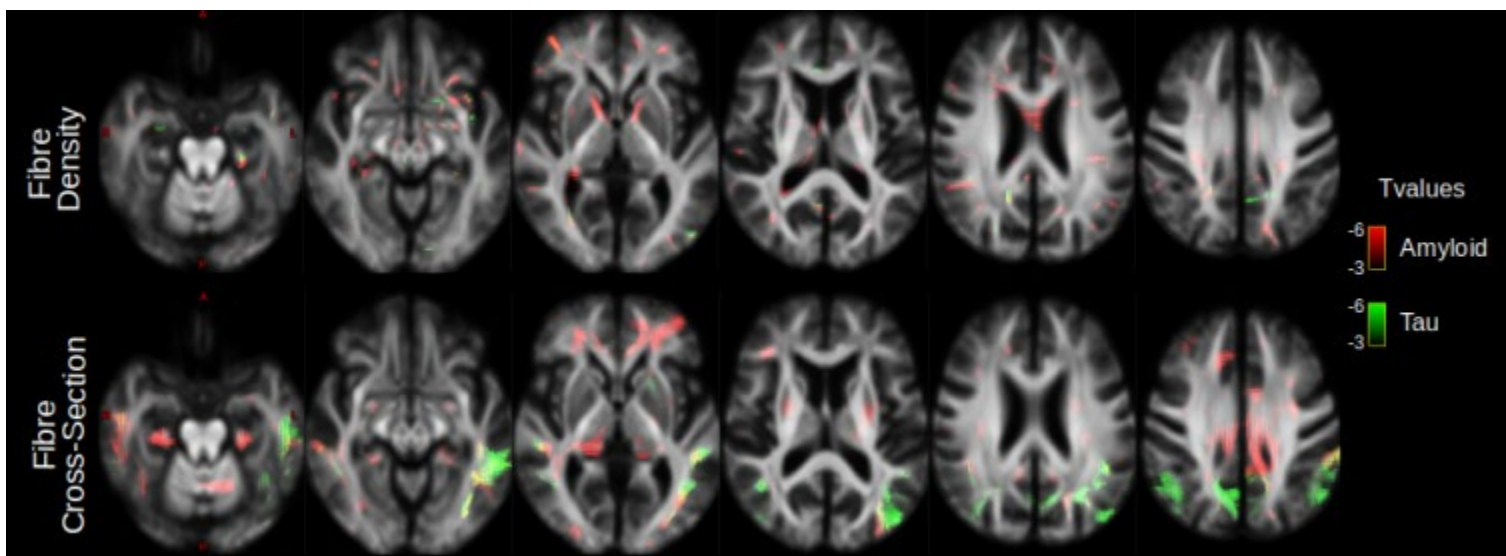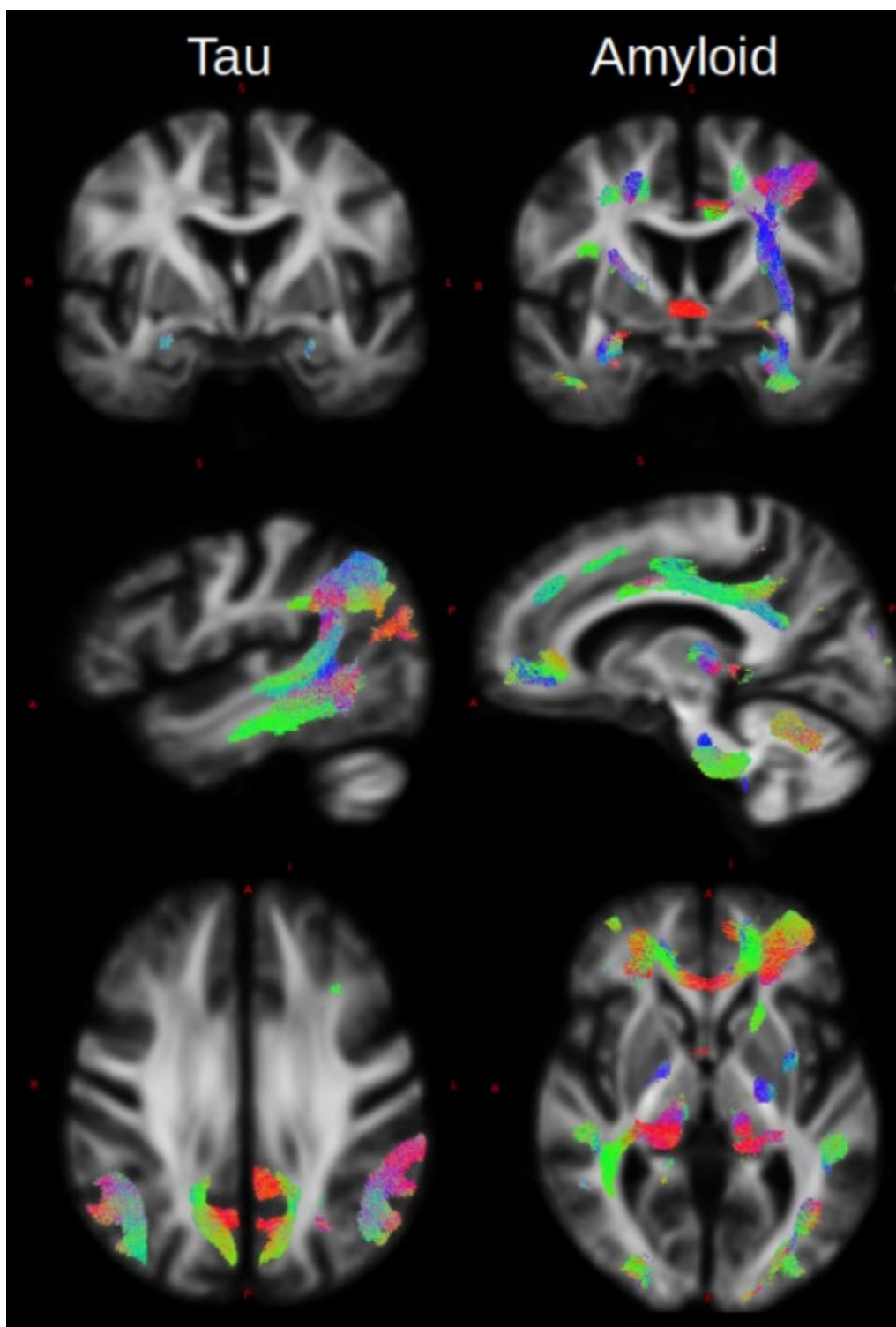
Keywords: *White Matter, Diffusion MRI, Amyloid, Tau*

P93: Plasma neurofilament light chain concentrations in relation to [18F]florbetapir and [18F]flortaucipir PET in Alzheimer's disease

Andrea Lessa Benedet[1,2], Antoine Leuzy[3,4], Tharick A. Pascoal[1], Sulantha Mathotaarachchi[1], Melissa Savard[1], Joseph Therriault[1], Min Su Kang[1], Mira Chamoun[1], Michael Schöll[3,4,5,6], Nicholas J. Ashton[3,4], Serge Gauthier[7], Henrik Zetterberg[3,8,9,10], Pedro Rosa-Neto[1,7,11,12], Kaj Blennow[3,8], for the Alzheimer's Disease Neuroimaging Initiative[14]

[1]*Translational Neuroimaging Laboratory, McGill Centre for Studies in Aging, McGill University, Montreal, QC, Canada*
[2]*CAPES Foundation, Ministry of Education of Brazil, Brasilia, Brazil*
[3]*Department of Psychiatry and Neurochemistry, Institute of Neuroscience & Physiology, the Sahlgrenska Academy at the University of Gothenburg, Mölndal, Sweden*
[4]*Wallenberg Centre for Molecular and Translational Medicine, University of Gothenburg, Gothenburg, Sweden*
[5]*Clinical Memory Research Unit, Department of Clinical Sciences, Malmö, Lund University, Malmö, Sweden*
[6]*Department of Neurodegenerative Disease, UCL Institute of Neurology, London, UK*
[7]*Alzheimer's Disease Research Unit, The McGill University Research Centre for Studies in Aging, Montreal, McGill University, Montreal, QC, Canada*
[8]*Clinical Neurochemistry Laboratory, Sahlgrenska University Hospital, Mölndal, Sweden*
[9]*Department of Molecular Neuroscience, UCL Institute of Neurology, Queen Square, London, UK*
[10]*UK Dementia Research Institute at UCL, London, UK*
[11]*Montreal Neurological Institute, Montreal, QC, Canada*
[12]*Department of Neurology and Neurosurgery, Montreal, QC, Canada*
[13]*University of California San Francisco, San Francisco, CA, US*
[14]*Alzheimer's Disease Neuroimaging Initiative, Washington, DC, US*

Introduction: Neurofilament light (NfL) is a marker of neuroaxonal injury and has been shown to be elevated in the cerebrospinal fluid (CSF) of patients with Alzheimer's disease (AD) and related conditions, as well as in cognitively unimpaired (CU) elderly. CSF NfL levels have also been shown to correlate with CSF levels of both amyloid and tau. Recently, plasma NfL (p-NfL) has also been described as global marker of neurodegeneration. No studies, however, have examined the relationship between plasma NfL and imaging-based measures of amyloid and tau pathology.

Aims: To investigate the cross-sectional association between plasma NfL levels and [^{18}F]florbetapir and [^{18}F]flortaucipir PET in a mixed cohort using data from the Alzheimer's Disease Neuroimaging Initiative.

Methods: 203 patients (114 CU, 67 mild cognitive impairment (MCI) and 22 AD) with longitudinal plasma NfL, measured using an in house Single molecule array method, and single time point [^{18}F]florbetapir and [^{18}F]flortaucipir PET were included. Rate of change in plasma NfL was calculated; for PET, standard uptake value ratios (SUVR) were determined using the cerebellar cortex as reference tissue. Linear regression was implemented at the voxel level, using VoxelStats, in order to examine the association between plasma NfL and PET-based measures.

Results: As compared to CU and MCI subjects, the rate of change in plasma NfL was greater among AD patients ($P<0.001$). Using cross-sectional plasma NfL, associations were confined to [^{18}F]florbetapir among CU subjects, and were seen primarily in the posterior cingulate and medial prefrontal cortex (Fig.1). By contrast, widespread associations within lateral temporo-parietal and frontal regions were observed when using the rate of change in plasma NfL; these, however, were confined to [^{18}F]flortaucipir in the AD group (Fig.2).

Conclusion: These findings suggest that plasma NfL may prove an early marker of amyloid-related neuronal injury, with its increase over time more closely related to tau-mediated neurodegeneration.
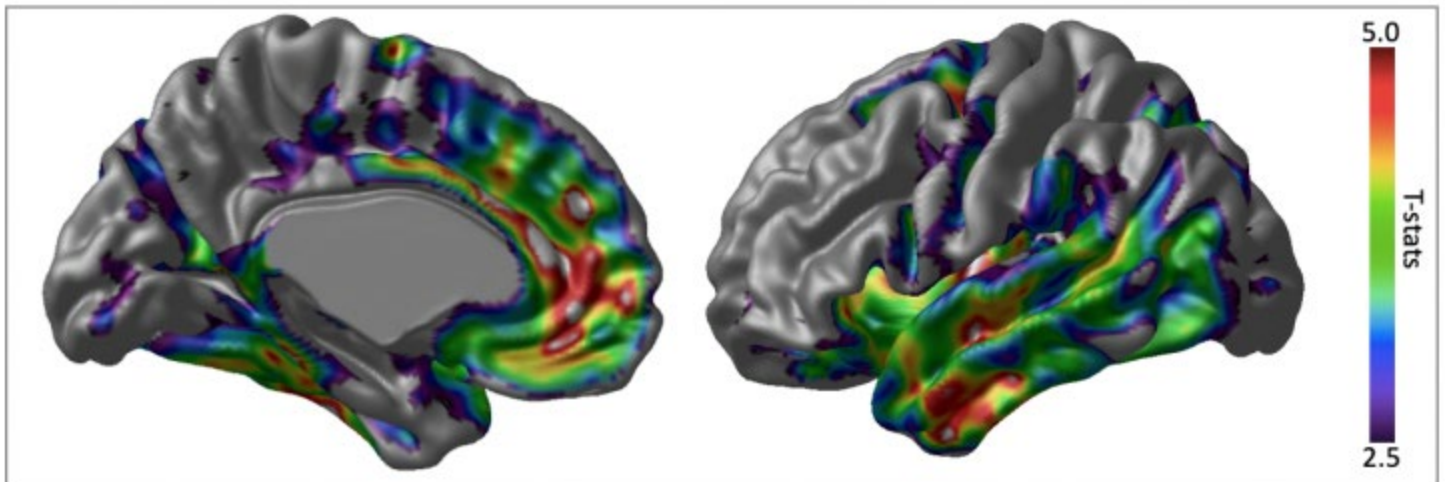
Figure 1. 3D T-statistical maps showing the brain regions where plasma NfL shows the highest association with [18F]florbetapir PET cross-sectionally in cognitively unimpaired elderly.
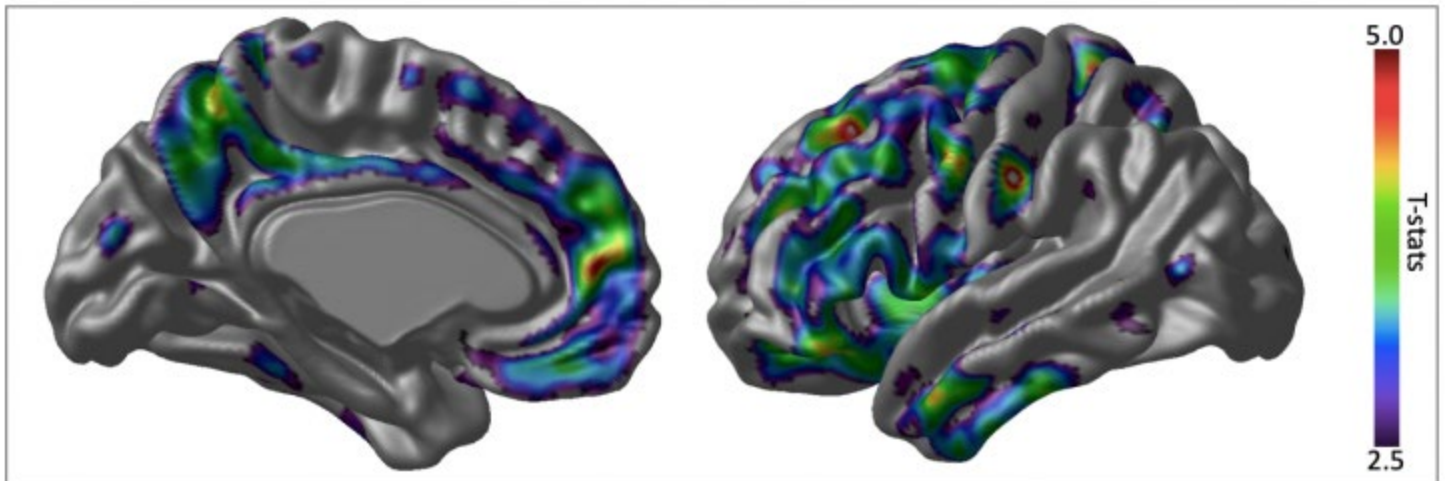
Figure 2. 3D T-statistical maps showing the brain regions where the rate of change in plasma NfL shows the highest association with [18F]flortaucipir PET in Alzheimer's disease patients.

P94: APOEε4 potentiates the relationship between amyloid-β and tau pathologies in a dose-dependent manner

Marlee Parsons[1,2,3], Joseph Therriault[1,3,4], Andrea Benedet[1,3,4], Tharick Pascoal[1,3,4], Sulantha Mathotaarachchi[1], Melissa Savard[1], Min Su Kang[1,3,4], Mira Chamoun[1,3,4], Jean-Paul Soucy[3,4], Gassan Massarweh[3,6], Paramita Saha-Chaudhuri[7], Judes Poirier[5], Serge Gauthier[1,4,5], Pedro Rosa-Neto[1,3,4,5]

[1]*Translational Neuroimaging Laboratory, The McGill University Research Centre for Studies in Aging, Alzheimer's Disease Research Unit, Douglas Hospital, McGill University, Montreal, QC, Canada*
[2]*Department of Experimental Medicine, McGill University, Montreal, QC, Canada*
[3]*Montreal Neurological Institute, Montreal, QC, Canada*
[4]*Department of Neurology and Neurosurgery, McGill University, Montreal, QC, Canada*
[5]*Department of Psychiatry, McGill University, Montreal, QC, Canada*
[6]*Department of Radiochemistry, McGill University, Montreal, QC, Canada*
[7]*Department of Epidemiology and Biostatistics, McGill University, Montreal, QC, Canada*

Background: APOEε4 is an important risk factor for Alzheimer's disease and is involved in the accumulation of cerebral amyloid-β. However, it is unclear whether APOEε4 is related to other Alzheimer's disease pathologies such as tau.

Methods: We assessed 207 individuals scanned with [18F]AV1451 and [18F]florbetapir, as well as 487 individuals who underwent lumbar puncture for CSF phosphorylated tau and [18F]florbetapir PET. All individuals were genotyped for APOEε4. The interaction models were built to test whether main and interactive effects between APOEε4 and amyloid-β PET SUVR are associated with Tau-PET uptake. APOEε4 allele status was treated as a categorical variable in a dose dependent manner, with ε3ε3<ε3ε4<ε4ε4. Because patients with AD were more likely to be APOEε4 carriers, we adjusted the model for age and clinical diagnosis.

Results: Voxel-wise analyses revealed a dose-dependent interaction between APOE ε4 and amyloid SUVR on [18F]AV1451 uptake across the cerebral cortex (Figure1). In subjects with CSF measures of phosphorylated tau, the synergistic effect between APOEε4 and neocortical [18F]florbetapir SUVR was related to increased CSF p-tau. A dose dependent effect of APOEε4 was also observed, with heterozygotes (b3=49.4, se=12.4, p<0.0001) and homozygotes (b3= 63.4, se=26.89, p=0.01) having different slopes (Figure2).

Conclusions: Our study provides support for a more integrative model of the role of APOEε4 in Alzheimer's disease pathogenesis.

P95: Quantitative gradient recalled echo (qGRE) MRI identifies significant neuronal loss in the hippocampal subfields related to cognitive impairment in mild Alzheimer's disease

Satya Kothapalli[1], Tammie Benzinger[1,2], Jason Hassenstab[2,3], Manu Goyal[1,3], John Morris[2,3], Dmitriy Yablonskiy[1]

[1]*Department of Radiology, Washington University in St. Louis, Saint Louis, MO, US*
[2]*Knight Alzheimer's Disease Research Center, Washington University in St. Louis, Saint Louis, MO, US*
[3]*Department of Neurology, Washington University in St. Louis, Saint Louis, MO, US*

Quantifying neuronal loss in hippocampal subfields is important as they are related to different biological functions. It was recently demonstrated (Wen, et al, PNAS-2018) that the qGRE MRI (Ulrich, Yablonskiy, MRM-2016) provides in-vivo information on human brain tissue cellular composition. In particular, the R2t* metric of qGRE signal determines the neuronal index (NI) – a parameter proportional to the neuronal density of the remaining (after atrophy) tissue. In healthy human hippocampus NI=0.3-0.5, whereas NI=0 corresponds to total neuronal loss. Herein, we investigate the neuronal composition of the hippocampal subfields in three groups of participants recruited from the Knight Alzheimer Disease Research Center: (1) cognitively normal (Clinical Dementia Rating (CDR)=0, amyloid-beta "negative" ($A\beta$)=0) (n=21), (2) preclinical AD (CDR=0, $A\beta$ "positive" =1) (n=9), and (3) mild AD (CDR<=1, $A\beta$=1) (n=9). Segmentation of hippocampal subfields was performed on T1-weighted MRI using Freesurfer6.0. In addition to regional NI we also compared normalized (by intracranial volume) regional volumes (NV) and cognitive tests.

Results: NI measurements in CA1, CA2, CA4, GC-DG, molecular layer, and HP tail subfields showed significantly stronger correlations with all cognitive tests (verbal fluency (**R**>0.35; **P**<0.01), verbal memory (**R**>0.35; **P**<0.01), working memory (**R**>0.35; **P**<0.01); attention (**R**<-0.35; **P**<0.01)) than NV in the respective regions (Fig. 1). NI measurements also demonstrated significant differences between normal and mild AD groups (**P**<0.05) in all subfields except in para/presubiculum and hippocampal-amygdala transition area (HATA), indicating significant neuron loss in mild AD participants (Fig. 2). The mean NI for the mild AD group was decreased by 20% (para/presubiculum), 30% (subiculum), 50% (CA1), 64% (CA2), 45% (CA3/4), 48% (GC-DG), 27% (HATA), 21% (fimbria), 46% (molecular layer), 48% (hippocampal fissure), and 19% (HP tail) as compared to normal.

In conclusion, qGRE method identifies neuronal loss in mild AD that defines loss of cognitive function not recognized by measurement of tissue atrophy.

Figure 1. Pearson R values of regression analysis of Normalized Volume (left) and Neuronal Index (right) vs cognitive tests (37 subjects included): Animal naming (ANIMALS), Trailmaking Test part A (TMA), Free and Cued Selective Reminding test free recall (SRTfree), and WAIS-III letter number sequencing (Lettnum). Red highlights R values greater than 0.4 and yellow highlights R values between 0.3-0.4.

#	Normalized Volume (NV)				Neuronal Index (NI)			
#	ANIMALS	TMA	SRTfree	Lettnum	ANIMALS	TMA	SRTfree	Lettnum
CA1	0.25	-0.26	0.23	0.33	0.46	-0.47	0.37	0.47
CA2	-0.01	-0.03	0.02	0.10	0.45	-0.37	0.43	0.41
CA4	0.24	-0.28	0.24	0.26	0.41	-0.43	0.46	0.42
GC-DG	0.24	-0.24	0.21	0.27	0.45	-0.46	0.45	0.47
HATA	0.09	-0.16	0.07	0.26	0.28	-0.18	0.06	0.13
Fimbria	0.33	-0.34	0.11	0.14	0.17	-0.26	0.23	0.25
Molecular layer	0.23	-0.27	0.16	0.28	0.36	-0.39	0.37	0.44
Hippocampal fissure	0.11	-0.07	0.29	0.21	0.32	-0.39	0.34	0.28
HP tail	0.12	-0.19	0.06	0.18	0.38	-0.31	0.37	0.54

Figure 2. Group differences between Normal (n=21), Preclinical (n=9), and mild AD groups (n=9) defined by Neuronal Index in hippocampal subfields. "ns" means no significant difference, * represents P<0.05, and ** represents P<0.01.
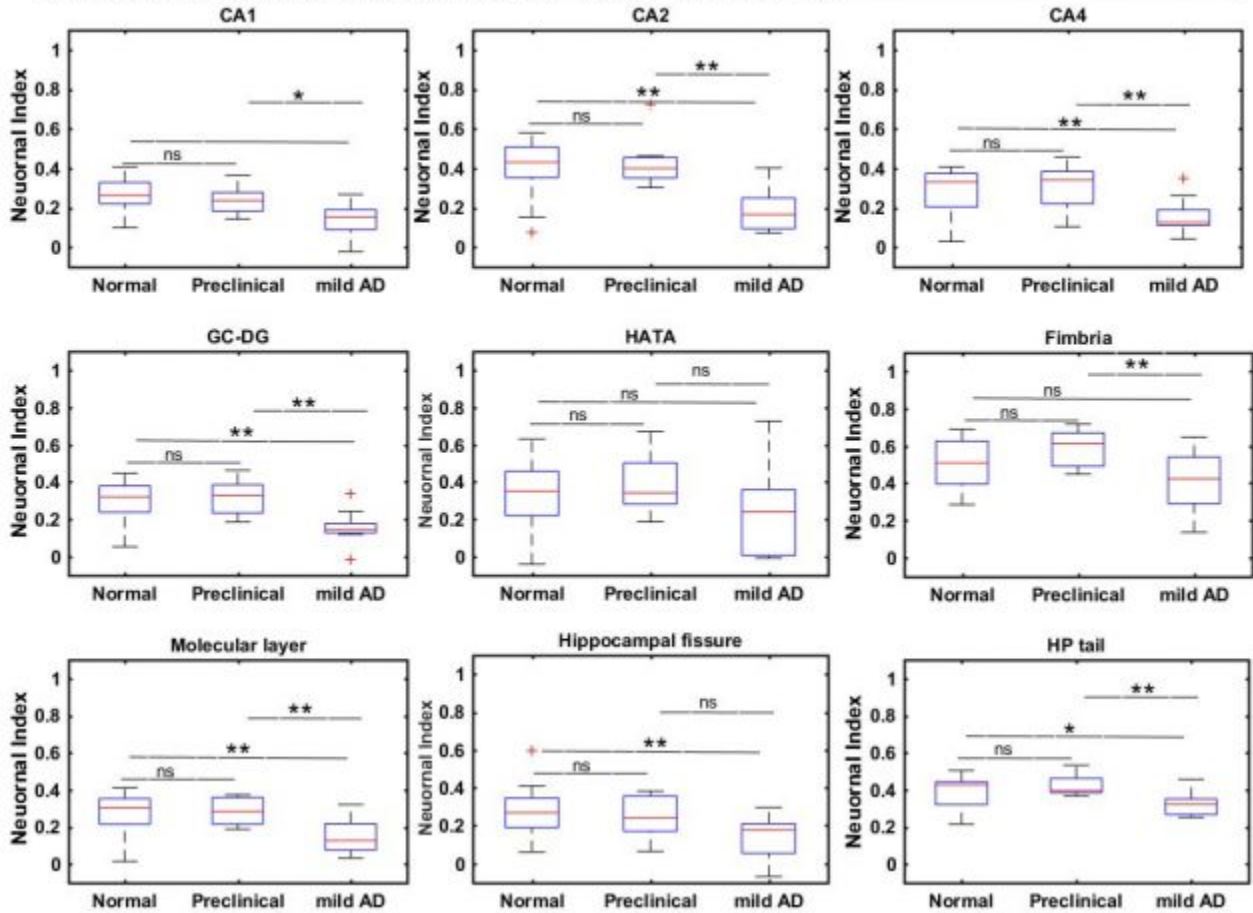
P96: Predictors for β-amyloid positivity in cognitively impaired patients. Data from the Imaging Dementia—Evidence for Amyloid Scanning (IDEAS) Study

Orit Lesman-Segev[1], Lucy Hanna[2], Renaud La Joie[1], Leonardo Iaccarino[1], Barry Siegel[3], Bruce Hillner[4], Rachel Whitmer[5,6], Maria Carrillo[7], Lauren Edwards[1], Kiran Chaudhary[1], Constantine Gatsonis[2,8], Gil Rabinovici[1,9,10]

[1]*Memory and Aging Center, University of California San Francisco, San Francisco, CA, US*
[2]*Center for Statistical Sciences, Brown University School of Public Health, Providence, RI, US*
[3]*Edward Mallinckrodt Institute of Radiology, Washington University School of Medicine, St. Louis, MO, US*
[4]*Department of Medicine, Virginia Commonwealth University, Richmond, VA, US*
[5]*Division of Research, Kaiser Permanente, Sacramento, CA, US*
[6]*Department of Public Health Sciences University of California Davis, Sacramento, CA, US*
[7]*Alzheimer's Association, Chicago, IL, US*
[8]*Department of Biostatistics, Brown University School of Public Health, Providence, RI, US*
[9]*Life Sciences Division, Lawrence Berkeley National Laboratory, Berkeley, CA, US*
[10]*Helen Wills Neuroscience Institute, University of California Berkeley, Berkeley, CA, US*

Table 1: Descriptive characteristics of the IDEAS study population (n=11398)

		MCI (n=6898)		Dementia (n=4500)	
Amyloid status		Positive, n=3817 (55.3%)	Negative, n=3081 (44.7%)	Positive, n=3154 (70%)	Negative, n=1346 (30%)
Demographics	Age, mean [range]	75.9 [65-98]	74.4 [65-105]	76.8 [65-98]	76.4 [65-97]
	Female sex	1907 (50%)	1516 (49.2%)	1715 (54.4%)	662 (49.2%)
	Race is Caucasian	3506 (91.9%)	2693 (87.4%)	2734 (86.7%)	1088 (80.8%)
	Race is Hispanic	91 (2.4%)	118 (3.8%)	157 (5%)	87 (6.5%)
	Bachelor's degree or higher	1874 (49.1%)	1441 (46.8%)	1192 (37.8%)	461 (34.2%)
	High school	1794 (47%)	1519 (49.3%)	1665 (52.8%)	716 (53.2%)
	Less than high school	149 (3.9%)	121 (3.9%)	297 (9.4%)	169 (12.6%)
	Family history of AD	508 (13.3%)	353 (11.5%)	375 (11.9%)	114 (8.5%)
Severity	Modified MMSE*, mean [range]	26.1 [0-30]	27 [0-30]	21.1 [0-30]	22.8 [0-30]

%- Percentages represent the fraction out of the total number of amyloid positive/negative patients.

Abbreviations: MCI – Mild Cognitive Impairment; IDEAS – Imaging Dementia Evidence for Amyloid scanning; AD – Alzheimer's disease;

*modified MMSE – modified Mini Mental State Examination. For missing MMSE scores that had MoCA scores, MMSE was converted from MoCA as described at Bergeron et-al, 2017.

Table 2: Results of univariate logistic regression models

	Predictor	MCI, odds ratio (range)		Dementia, odds ratio (range)	
Demographics	Age (per year)	**1.043**	**(1.03-1.05)**	1.009	(1.00-1.02)
	Female sex	1.031	(0.94-1.13)	**1.231**	**(1.08-1.40)**
	Race is Caucasian	**1.624**	**(1.39-1.90)**	**1.544**	**(1.30-1.83)**
	Race is Hispanic	**0.613**	**(0.46-0.81)**	**0.758**	**(0.58-0.99)**
	Bachelor's degree or higher vs. Less than high school	1.056	(0.28-1.36)	**1.471**	**(1.18-1.83)**
	High school vs less than high school	0.959	(0.75-1.23)	**1.323**	**(1.07-1.63)**
	Family history of AD	**1.186**	**(1.03-1.37)**	**1.458**	**(1.17-1.82)**
Medical history	Hypertension	0.922	(0.84-1.01)	0.886	(0.78-1.01)
	Ischemic heart disease	0.975	(0.83-1.15)	**0.741**	**(0.61-0.90)**
	History of dyslipidemia	0.995	(0.90-1.10)	0.972	(0.86-1.11)
	Diabetes	**0.618**	**(0.54-0.70)**	**0.644**	**(0.55-0.76)**
	Current or former smoker	0.912	(0.80-1.03)	0.899	(0.76-1.07)
	Cerebrovascular disease	0.860	(0.69-1.08)	0.816	(0.63-1.05)
	Past stroke or TIA	**0.783**	**(0.67-0.92)**	**0.657**	**(0.54-0.80)**
	Depression	**0.726**	**(0.64-0.82)**	1.158	(0.96-1.39)
	Bipolar	**0.451**	**(0.31-0.66)**	**0.299**	**(0.19-0.47)**
	Past TBI	0.804	(0.64-1.01)	1.113	(0.81-1.52)
	MS	**0.175**	**(0.08-0.40)**	0.426	(0.12-1.47)
	Seizures	0.804	(0.64-1.01)	**0.579**	**(0.41-0.82)**
	COPD	**0.663**	**(0.51-0.86)**	**0.633**	**(0.45-0.89)**
Modified MMSE*		**0.882**	**(0.87-0.90)**	**0.934**	**(0.92-0.95)**

Statistically significant odds ratios are bolded.

Abbreviations: MCI – Mild Cognitive Impairment; IDEAS – Imaging Dementia Evidence for Amyloid scanning; TIA – transient ischemic attack; TBI- traumatic brain injury; MS – multiple sclerosis; COPD – chronic obstructive pulmonary disease; AD – Alzheimer's disease;

*modified MMSE – modified Mini Mental State Examination. For patients that did not have a MMSE score but had MoCA score, MMSE was converted from MoCA as described at Bergeron et-al, 2017.

Background: We aim to identify predictors for β-amyloid positivity in the practice-based IDEAS study.

Methods: 11,398 cognitively impaired patients from the Imaging Dementia-Evidence for Amyloid Scanning (IDEAS) study were included from 595 sites across the US (6,898 Mild-Cognitive-Impairment [MCI], 4,500 dementia). All patients were aged≥65, meeting published appropriate use criteria (AUC) for amyloid-PET that had completed pre-PET assessment and an amyloid scan read as positive or negative by local radiologist. Using univariate logistic regression models, we investigated the relationship between i) amyloid positivity and ii) demographic factors; medical history; family history of Alzheimer's disease (AD); and dementia severity (modified MMSE).

Results: A total of 3817 (55%) of patients with MCI and 3154 (70%) of patients with dementia were β-amyloid positive (table 1). Caucasian race and family history of AD were associated with higher β-amyloid positivity rates for both patients with MCI (odds-ratio [OR] 1.624, 1.186 respectively) and dementia (OR=1.544, 1.458, table 2). Increased age was associated with higher rates of β-amyloid positivity in patients with MCI (OR=1.043 per-year) while female sex and higher education were associated with higher rates in patients with dementia

(OR=1.231, 1.471 for bachelor's or higher vs lower). Hispanic race, higher MMSE and diabetes, TIA/stroke, bipolar disorder or Chronic-Obstructive-Pulmonary-Disease were associated with lower rates of β-amyloid positivity in both MCI and dementia groups. History of depression and multiple sclerosis were negatively associated with β-amyloid positivity in patients with MCI, and history of cardiac ischemia and seizures were negatively associated with β-amyloid positivity in patients with dementia.

Conclusions: In the practice-based IDEAS study, Caucasian race and family history of AD had the highest OR for β-amyloid positivity. Hispanic race and relevant co-morbidities were associated with a lower risk for β-amyloid-PET positivity. These results may set the ground for prediction models associated with amyloid positivity in the AUC population

---

Keywords: *β-amyloid, PET, predictors*

P97: Regional tau and atrophy: domain-specific relationships with cognition

Leonardino Digma[1], Emilie Reas[1], James Brewer[1], Sarah Banks[1]

[1]*University of California, San Diego, La Jolla, CA, US*

Background: Although late-onset Alzheimer's disease (AD) patients usually present with primary memory impairment, they also demonstrate deficits in other cognitive domains. It is thought that tau predates atrophy, and both follow networks underlying cognition. Here, we report tau and atrophy patterns as they relate to different aspects of cognition.

Methods: We analyzed data from 131 amyloid-positive ADNI participants with diagnoses of cognitively normal, mild cognitive impairment, or AD. We first performed voxel-wise regressions (**p** < 0.001, uncorrected) between tau (AV1451-PET) and scores on cognitive tests of memory, executive function, semantic fluency, naming and clock drawing, and between atrophy (structural-MRI) and cognitive test scores. Next, we calculated Simpson overlap coefficients to assess spatial overlap in the tau-cognition and atrophy-cognition pattern for each test. Lastly, we performed partial correlations between tau or atrophy and each cognitive test. We performed Wilcoxon's rank-sum test on these partial correlations to compare the strengths of the associations. Analyses were adjusted for age and sex.

Results: Tau and atrophy were both significantly related to performance on each cognitive test (except atrophy and clock-copying). Patterns of tau-cognition statistical maps recapitulated known structure-function localizations (e.g., predominant left-sided laterality for language tests; Figure 1). Atrophy-cognition patterns overlapped with tau-cognition patterns (overlap coefficient: range 0.69-0.96). However, tau-cognition patterns were larger and more topographically extensive than atrophy-cognition patterns. Wilcoxon's test revealed that tau-cognition associations were stronger than atrophy-cognition associations (**p**=0.002; Figure 2D).
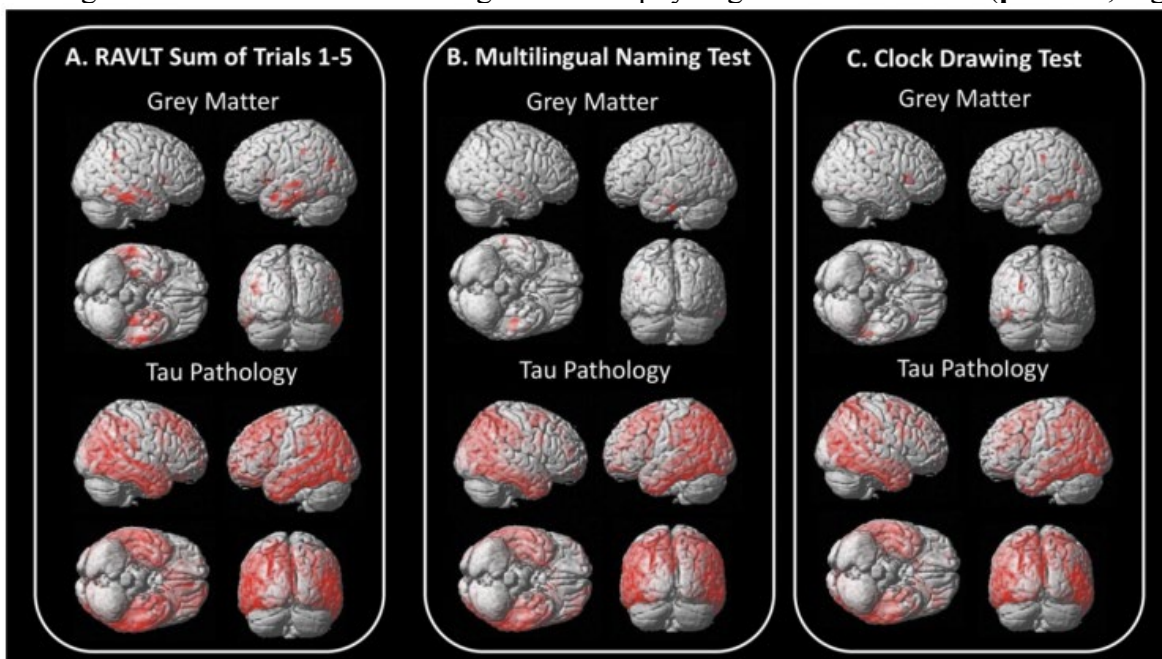
Figure 1. Tau and atrophy are associated with cognition. Results from voxel-wise regressions between cognitive tests and either atrophy or tau. A subset of cognitive tests for (A) learning and memory (RAVLT sum of trials 1 to 5), (B) naming (Multilingual Naming Test) and (C) constructional abilities (Clock Drawing Test) are displayed. Age and sex were included as covariates in all models. For analyses involving atrophy, voxel values were normalized by the sum of the grey matter, white matter, and CSF probability masks to correct for head size. Statistical maps are thresholded at p<0.001, uncorrected. RAVLT = Rey Auditory Verbal Learning Test.
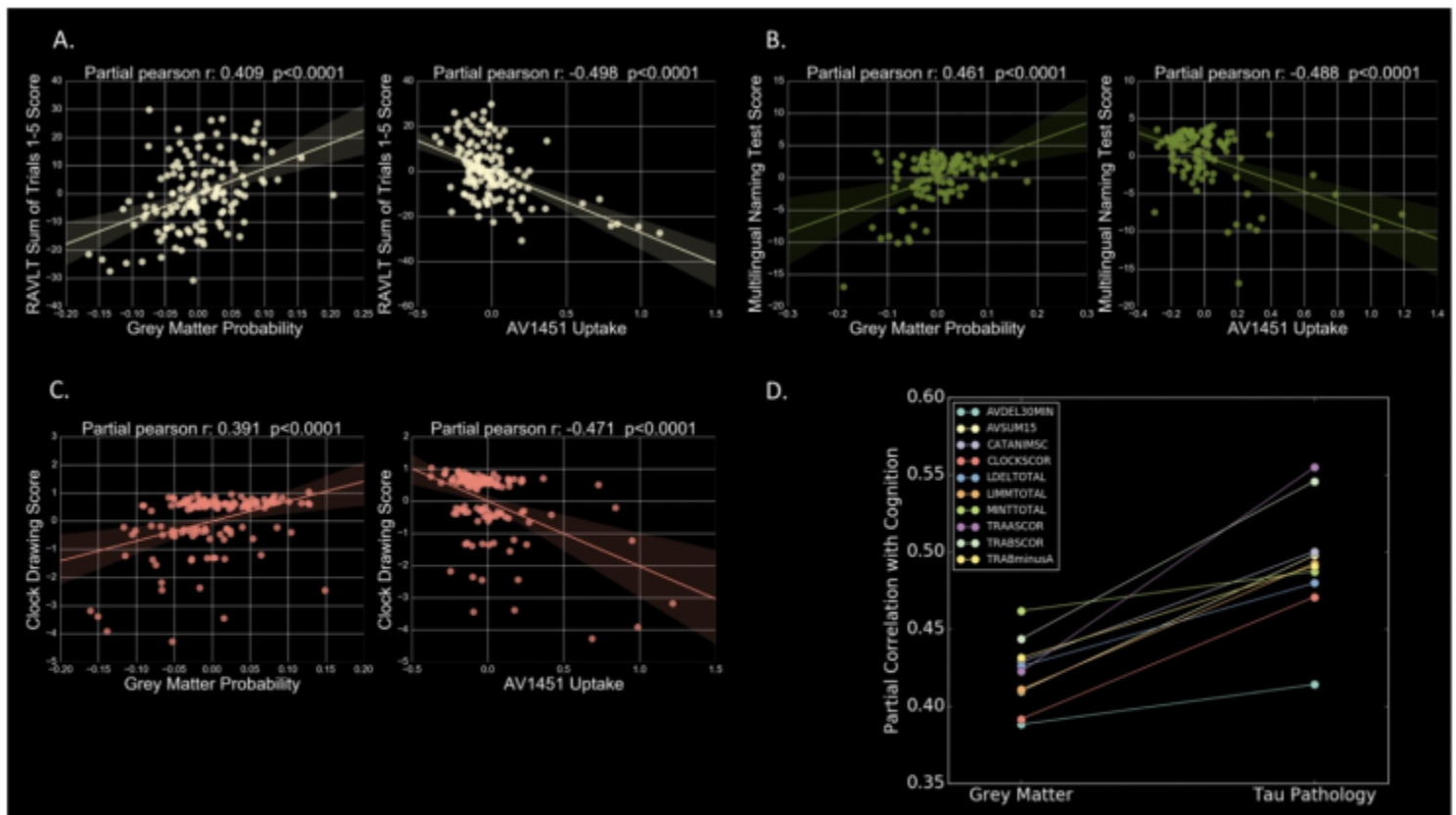
Figure 2. Tau is more strongly related to cognition than atrophy. Examples of partial correlation between atrophy or tau and performance on (A) learning and memory (RAVLT sum of trials 1 to 5), (B) naming (Multilingual Naming Test) and (C) constructional abilities (Clock Drawing Score) are shown. For each individual, atrophy or tau measures were derived by averaging the grey matter probability or AV1451 SUVR values from significant clusters from the voxel-wise regression analyses. All measures have been residualized by age and sex. (D) Comparison of partial correlations reveals that the tau-cognition relationships are stronger than atrophy-cognition relationships (Wilcoxon rank-sum test p=0.002); RAVLT = Rey Auditory Verbal Learning Test.

Discussion: Our data indicate that tau and atrophy are related to performance in several cognitive domains. Furthermore, we found that the tau-cognition relationships overlap, exceed, and are stronger than the atrophy-cognition relationships. These findings are consistent with the notion that tau contributes to the breakdown of cognitive networks, and may precede atrophy in the progression of AD.

Keywords: *cognition; tau PET; atrophy; Alzheimer's disease*

P98: Inferior temporal tau is associated with greater prospective cortical thinning in clinically-normal older adults

Olivia Hampton[1,3], Matthew Scott[1,3], Rachel Buckley[1,3,5,7], Jasmeer Chhatwal[1,3,6], Heidi Jacobs[2,3,4,8], Bernard Hanseeuw[1,2,3,9], Keith Johnson[1,2,3,4,6], Reisa Sperling[1,3,6], Aaron Schultz[1,3,4]

[1]*Department of Neurology, Massachusetts General Hospital, Boston, MA, US*
[2]*Department of Radiology, Massachusetts General Hospital, Boston, MA, US*
[3]*Harvard Medical School, Boston, MA, US*
[4]*Athinoula A. Martinos Center for Biomedical Imaging, Boston, MA, US*
[5]*Florey Institutes of Neuroscience and Mental Health, Melbourne, Australia*
[6]*Center for Alzheimer Research and Treatment, Department of Neurology, Brigham and Women's Hospital, Boston, MA, US*
[7]*Melbourne School of Psychological Science, University of Melbourne, Melbourne, Australia*
[8]*School for Mental Health and Neuroscience, Alzheimer Centre Limburg, Maastricht University, Maastricht, The Netherlands*
[9]*Cliniques Universitaires Saint-Luc, Institute of Neurosciences, Université Catholique de Louvain, Brussels, Belgium*

Introduction: Previous tau-PET research in the HABS cohort used retrospective structural MRI to investigate relationships between tau-PET and cortical thinning (LaPoint et al., 2017). We extended these initial findings in the same clinically-normal cohort using both retrospective and prospective structural imaging.

Methods: Longitudinal T1-weighted MRI scans were processed using the FreeSurfer (FS) v6 longitudinal pipeline (Reuter et al., 2012). 111 participants had at least 3 MRI time points over a period of 4.4 ± 1.0 years that straddled acquisition of 18F Fluortaucipir-PET (FTP-PET; see Table 1). FS-based thickness ROIs were averaged across hemispheres. FTP-PET was processed via an FS-based pipeline, and GTM-PVC corrected inferior temporal (IT) SUVr, normalized by cerebellar gray, was used for analyses.

Linear mixed models were used to assess relationships between IT FTP-PET signal and 1) overall rate of change in thickness, 2) change of thickness in retrospective versus prospective tau time frames, and 3) the difference in rates of thinning between retrospective and prospective periods. Age and sex were included as covariates.

Results: We found significant relationships between IT FTP-PET and cortical thinning across multiple AD-vulnerable regions in the midline and temporal lobe (ps < 0.005). For many of these regions, the rate of thinning was greater in the prospective period rather than the retrospective period. Lastly, inferior temporal and entorhinal thinning demonstrated statistically different post-tau versus pre-tau slopes (ps < 0.05).

Conclusion: The pattern of observed results shows a clear relationship between inferior temporal tau burden and longitudinal atrophy in multiple key AD regions. Furthermore, the rates of thinning were generally higher in prospective data than in retrospective data, congruent with the hypothesis that tau pathology precedes and is associated with accelerated rates of atrophy. Additional follow-up, particularly with longitudinal tau imaging, is needed to confirm these results.

Table 1. Demographics table

Participants

N	111
Age	75.57
Sex (% Female)	54.95
CDR (SD)	0.0285 (0.12)
MMSE (SD)	29.26 (0.95)
% APOE e4 carriers	32.73
% PiB+	30.83

MRI

Timepoints (SD)	3.48 (0.63)
Range in years (SD)	4.46 (1.05)

CDR = Clinical Dementia Rating, MMSE = Mini Mental State Exam, PiB positivity determined by DVR threshold of 1.186

Figure 1: Results of cortical thinning over time predicted by tau
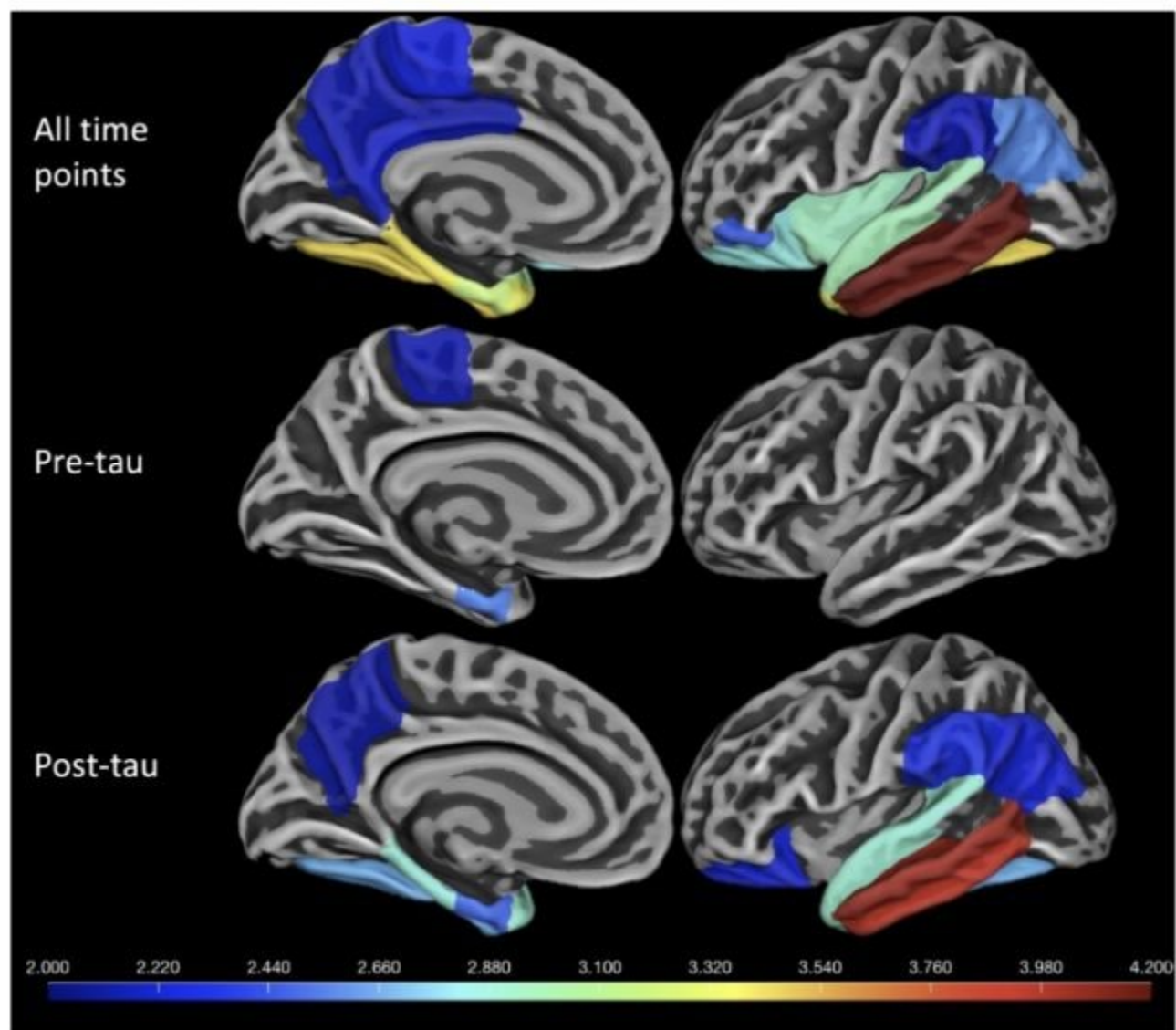
The figure depicts significant FS ROIs ($p < 0.05$) of the cortical thinning predicted by tau over all time. These regions were used to model the pre-tau and post-tau analyses, also above. The color bar describes t-values of the models.

Figure 2: Difference in retrospective versus prospective cortical thinning predicted by tau
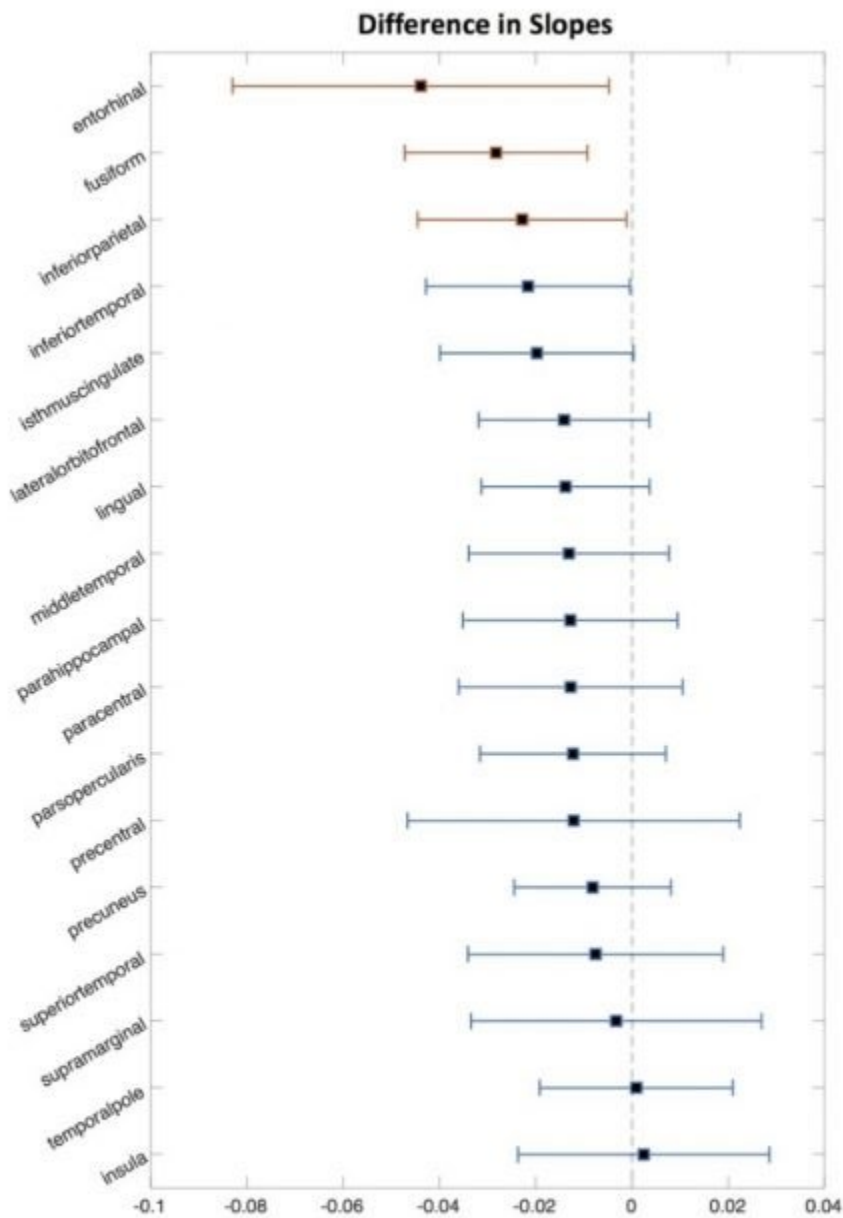
Forest plot showing the difference of retrospective and prospective slopes predicted by tau for significant ROIs from the across all time points model ($p < 0.05$; see Figure 1). Regions with significant slope differences are colored in red ($p < 0.05$). Error bars are based on beta-estimates and standard errors.

Keywords: *Alzheimer's disease, Atrophy, Tau, Longitudinal, Aging*

P99: Lower left ventricular ejection fraction relates to increased cerebrospinal fluid biomarker evidence of neurodegeneration in older adults

Hailey Kresge[1], Dandan Liu[1], Deepak Gupta[1], Katie E. Osborn[1], Lealani Mae Acosta[1], Susan Bell[1], Kimberly Pechman[1], Katherine Gifford[1], Lisa Mendes[1], Thomas Wang[1], Kaj Blennow[2], Henrik Zetterberg[2], Timothy Hohman[1], Angela Jefferson[1]

[1]*Vanderbilt University Medical Center, Nashville, TN, US*
[2]*The Sahlgrenska Academy at University of Gothenburg, Mölndal, Sweden*

Objective: Cardiac dysfunction is associated with abnormal brain aging, but the exact neuropathological underpinnings are unknown. Subclinical reductions in cardiac function are associated with decreased cerebral blood flow, which places the aging brain at risk for Alzheimer's disease (AD) pathology and neurodegeneration. This study investigates the association between subclinical cardiac dysfunction, measured by left ventricular ejection fraction (LVEF), and cerebrospinal fluid (CSF) biomarkers of AD (beta-amyloid$_{42}$ (Ab$_{42}$), hyperphosphorylated tau (p-tau)) and neurodegeneration (total tau (t-tau)).

Methods: Vanderbilt Memory & Aging Project participants free of clinical dementia, stroke, and heart failure (n=152, 72±6 years, 68% male) underwent echocardiogram to quantify LVEF and lumbar puncture to measure CSF levels of Ab$_{42}$, p-tau, and t-tau. Linear regressions with ordinary least square estimates related LVEF to each CSF biomarker, adjusting for age, sex, race/ethnicity, education, Framingham Stroke Risk Profile, cognitive diagnosis, and apolipoprotein E e4 allele status. Secondary models tested an **LVEF x cognitive diagnosis** interaction and then stratified by diagnosis (normal cognition (NC), mild cognitive impairment (MCI)).

Results: In main effect models LVEF related to CSF Ab$_{42}$ levels (β=-6.50, p=0.04), but results were attenuated after excluding participants with prevalent cardiovascular disease and atrial fibrillation (p-values>0.06). LVEF was unrelated to t-tau (p=0.79) or p-tau (p=0.47). We observed an interaction between LVEF and cognitive diagnosis on CSF t-tau (p=0.004) and p-tau levels (p=0.002), whereby lower LVEF was associated with increased t-tau (β=-9.74, p=0.01) and p-tau (β=-1.41, p=0.003) in NC but not MCI participants (p-values>0.13).

Conclusions: Among cognitively normal older adults free of heart failure and stroke, subclinical LVEF reductions relate to greater molecular evidence of hyperphosphorylation and neurodegeneration. Results suggest modest age-related changes in cardiovascular function may have implications for abnormal biochemical changes in the brain in late life, presumably through subtle reductions in blood flow delivery to the brain.

P100: ApoE4 as a moderating factor between mild traumatic brain injury and tau deposition in the temporal cortex

Catherine Munro[1,2], Xi Chen[2], Melissa Rundle[2], C Munro Cullum[1], Karen Rodrigue[2], Denise Park[2]

[1]*University of Texas Southwestern Medical Center, Dallas, TX, US*
[2]*University of Texas at Dallas, Dallas, TX, US*

It is well known through both animal and human studies that carriers of the apolipoprotein e4 (ApoE4) allele are at increased risk for developing Alzheimer's disease (AD) pathophysiology (e.g., amyloid and tau proteins) (Liraz et al., 2013). Previous history of traumatic brain injury (TBI) has also been associated with increases in these proteins and has been shown to be a risk factor for diagnosis of AD (Ramos-Cejudo et al., 2018). These findings raise the possibility that a link might exist between history of mild TBI (mTBI) and long-term increases in AD pathophysiology that may be moderated by ApoE4. Any relationship between tau and ApoE4 in this context is poorly understood, but if an association were present it would likely be in regions sensitive to pathology (e.g., the temporal lobe). We obtained a self-reported history of mTBI from 46 cognitively-normal adults (ages 55-87), using the OSU TBI questionnaire. Regional tau burden was assessed using Flortaucipir PET imaging (Johnson et al., 2016)in five bilateral regions of the temporal lobe: entorhinal, inferior temporal, middle temporal, superior temporal, and transverse temporal cortices. A linear regression model was used to predict regional tau burden based on the interaction between ApoE4 carrier status and total number of mTBI (controlling for age, sex, and amyloid burden). The interaction was significant for the transverse temporal cortices in both the left (F=2.414, df=5, p=0.043, R^2=0.531, interaction p=0.030) and the right (F=3.523, df=5, p = 0.009; R^2=0.435, interaction p=0.040) hemispheres, even after FDR correction. The transverse temporal cortices are specialized for processing auditory and semantic information. The interaction occurred because the impact of self-reported mTBI was much greater for ApoE4 carriers compared to noncarriers. We cautiously suggest that the findings provide evidence that ApoE4 carriers may be more susceptible to tau deposition associated with mild head injuries.

Keywords: *traumatic brain injury, tau, PET, ApoE4*

P101: A longitudinal examination of amyloid burden and myelin content in major white matter tracts

Kao Lee Yang[1], Douglas C. Dean III[2], Nicholas M. Vogt[1], Erin M. Jonaitis[1,3], Jack Hunt[1], Andrew P. Merluzzi[4], Akshay Kohli[1], Bradley T. Christian[2,5], Jennifer Oh[1], Tobey J. Betthauser[1], Sanjay Asthana[1,3,6], Sterling C. Johnson[1,2,3], Andrew L. Alexander[2,5], Barbara B. Bendlin[1,2,3]

[1]*Wisconsin Alzheimer's Disease Research Center, Madison, WI, US*
[2]*Waisman Center, Madison, WI, US*
[3]*Wisconsin Alzheimer's Institute, Madison, WI, US*
[4]*Potomac Institute for Policy Studies, Arlington, VA, US*
[5]*Department of Medical Physics, Madison, WI, US*
[6]*Geriatric Research, Education, and Clinical Center, William S. Middleton Veterans Hospital, Madison, WI, US*

Background: White matter alterations are associated with cortical β-amyloid (Aβ) aggregation and thought to be an early feature of Alzheimer's disease (AD). This study explored longitudinal associations between Aβ and myelin content.

Methods: Participants were recruited from the Wisconsin Registry for Alzheimer's Prevention and Wisconsin Alzheimer's Disease Research Center. This analysis included data from 50 cognitively unimpaired participants (MMSE: Median, Range = 30.00, 27-30) with baseline [C-11]PiB scans and up to 3 time points of multicomponent driven equilibrium single pulse observation of T1 and T2 (mcDESPOT) imaging. Global Aβ burden was operationalized as the average PiB DVR (Logan graphical analysis, cerebellum GM reference region) across 8 bilateral ROIs: anterior/posterior cingulate, precuneus, and angular, supramarginal, middle, frontal middle orbital, and superior temporal gyri. Myelin content was indexed by myelin water fraction (MWF), derived from mcDESPOT scans. Associations between Aβ and mean MWF were tested using linear mixed effects models. One model was fitted for MWF in each of these tracts: uncinate fasciculus, superior and inferior longitudinal fasciculi, forceps major and minor, and cingulum bundle. Models included random intercepts and time-related slopes for each subject and fixed effects of: baseline age, time since baseline, PiB DVR (mean-centered), APOE4 positivity, sex, and interactions of age*PiB and time*PiB. Models were fitted in SPSS 25.0 and considered significant at unadjusted $p<.05$.

Results: Sample characteristics are displayed in Table 1. Significant fixed effects of time were observed in several white matter tracts (Table 2). Baseline Aβ burden was not associated with longitudinal MWF alterations and there were no significant interaction effects.

Conclusion: MWF decreased over time, though there were no associations between baseline Aβ burden and longitudinal myelin content. Results should be interpreted with caution since this study was completed in a cognitively unimpaired cohort. Additional studies are needed that include participants along the AD spectrum.

Table 1. Participant characteristics at baseline visit.

Characteristics	Value
Female, %	64 (N=50)
MMSE, Median ± SD	30.00 ± 0.68 (range: 27 – 30)
Education (years), M ± SD	16.48± 2.65
APOE4 positivity, %	38
White/Caucasian, %	98
Positive parental history of AD, %	66
Age at time of PET, M ± SD	62.20 ± 6.00
Global PiB (mean of 8 bilateral regions), DVR	1.13 ±.18

Abbreviations: MMSE = mini mental state examination; APOE4 = apolipoprotein E allele 4;
AD = Alzheimer's disease; PiB = [C-11] Pittsburgh Compound B; PET = positron emission tomography;
DVR = distribution volume ratio.

Table 2. Associations between baseline amyloid and longitudinal MWF in white matter tracts.

Covariates	ILF	SLF	Cingulum portion A	Cingulum portion B	Forceps Major	Forceps Minor	Uncinate Fasciculus
Model A							
Intercept	.1904*	.2070*	.1842*	.1282*	.2168*	.2197*	.0940
Global PiB	-.1552	.0216	-.1633	-.3333	.0819	-.1742	-.5772
Time	-.0005*	-.0006*	-.0007*	-.0002	-.0004*	-.0007*	-.0006*
Age	-.0007	-.0010	-.0008	-.0006	-.0012	-.0007	.0004
Sex	-.0029	-.0003	-.0005	.0103	.0072	.0004	-.0046
APOE4	-.0007	-.0052	.0029	-.0082	-.0022	.0082	-.0005
Age*PiB	.0022	-.0000	.0024	.0051	-.0009	.0026	.0086
Model B							
Intercept	.1938*	.1814	.1379*	.1322*	.1712*	.2060*	.1440
Global PiB	-.0167	-.0081	-.0775	.0026	-.0160	-.0447	.0135
Time	-.0005*	-.0005*	-.0007*	-.0003*	-.0003	-.0010*	-.0007*
Age	-.0007	-.0007	-.0001	-.0007	-.0007	-.0003	-.0004
Sex	-.0104	-.0087	-.0054	-.0053	-.0009	-.0006	-.0156
APOE4	.0053	.0040	.0189	.0074	.0065	.0084	.0134
Time*PiB	.0001	.0005	.0020	-.0001	.0014	.0014	-.0010

*$p<.05$

All reported values are β estimates from linear mixed effects models with each white matter tract as the response variable. All models were fitted using the maximum likelihood (ML) estimation and unstructured covariance matrix in SPSS version 25.0 with the MIXED command. Models included random intercepts and time-related slopes for each subject and fixed effects for global PiB burden at baseline visit (mean-centered), age at baseline visit, time since baseline visit (in months), sex, APOE4 positivity, and an Age*PiB interaction (Model A) or Time*PiB interaction (Model B).

Abbreviations: MWF = myelin water fraction; ILF = inferior longitudinal fasciculus; SLF = superior longitudinal fasciculus; Cingulum portion A = portion of cingulum projecting into cingulate gyrus; Cingulum portion B = cingulum portion projecting into medial temporal lobe; PiB = [C-11] Pittsburgh Compound B; APOE4 = apolipoprotein E allele 4.

Keywords: *[C-11] PiB, myelin content, cognitively unimpaired*

P102: Initial clinical evaluation of [18F] PI-2620 as a potent PET radiotracer imaging tau protein

Minyoung Oh[1], Seung Jun Oh[1], Sang Ju Lee[1], Jungsu S. Oh[1], Jee Hoon Roh[2], Sun Ju Chung[2], Jae-Hong Lee[2], Chong Sik Lee[2], Jae Seung Kim[1]

[1]Department of Nuclear Medicine, Asan Medical Center, University of Ulsan College of Medicine, Seoul, Korea
[2]Department of Neurology, Asan Medical Center, University of Ulsan College of Medicine, Seoul, Korea

PET is a useful tool for detecting the presence and extent of tau accumulation in the brain. Most first generation tau PET tracers, however, have limitations regarding high off-target binding and detection for tau in non-AD tauopathies. The purpose of this study is to evaluate the potential clinical utility of [18F]PI-2620, a novel tau PET tracer with a high binding affinity for aggregated tau in AD and non-AD tauopathies.

Twenty participants diagnosed with 3 probable AD, 3 Semantic Dementia (SD), 2 behavioral variant of Frontotemporal Dementia (bvFTD), 1 Primary Progressive Aphasia (PPA), 3 Progressive Supranuclear Palsy (PSP), 3 Corticobasal Syndrome (CBS), 2 Dementia with Lewy body (DLB), as well as 3 healthy controls (HC) were enrolled. They underwent a 60-90 min static brain PET scan after 259MBq intravenous injection of [18F]PI-2620, as well as Florbetaben PET to establish Aβ status (Aβ-/Aβ+), MRI, neuropsychiatric test, and safety evaluation.

All of participants showed no increased off-target binding in basal ganglia as noted for first generation tau tracers, but faint uptake in the substantia nigra and choroid plexus on [18F]PI-2620 PET images. Three Aβ+ AD patients showed diverse cortical [18F]PI-2620 uptake in temporoparietal cortex. Aβ+ DLB and PPA patients also showed increased [18F]PI-2620 uptake in temporoparietal cortex. PSP patients showed faint uptake in the globus pallidus. All of patients with CBS, SD and bvFTDs showed no significant [18F]PI-2620 uptake in the brain. There was no drug related adverse reaction in all of participants after injection of [18F]PI-2620.

In this phase 0 study, [18F]PI-2620 PET seems to be sensitive tool to detect tau deposits in patients with Aβ+ AD and Aβ+ non-AD tauopathies. Furthermore, our studies show [18F]PI-2620 is not affected by potentially confounding "off-target" binding. Further study with a large sample size is needed to conclude regarding [18F]PI-2620 binding in Aβ- tauopathy.

Keywords: *Positron emission tomography, Alzheimer's disease, non-AD tauopathies, tau*

P103: Asymmetric tau and focal amyloid PET in an autopsy-confirmed case of Alzheimer's disease presenting as primary progressive aphasia

Adam Martersteck[1,2], Jaiashre Sridhar[1], Christina Coventry[1], M.-Marsel Mesulam[1,3], Emily Rogalski[1,4]

[1]*Mesulam Center for Cognitive Neurology and Alzheimer's Disease, Northwestern University Feinberg School of Medicine, Chicago, IL, US*
[2]*Department of Radiology, Northwestern University Feinberg School of Medicine, Chicago, IL, US*
[3]*Department of Neurology, Northwestern University Feinberg School of Medicine, Chicago, IL, US*
[4]*Department of Psychiatry and Behavioral Sciences, Northwestern University Feinberg School of Medicine, Chicago, IL, US*

Background: A participant clinically diagnosed with the agrammatic variant of primary progressive aphasia (PPA) completed research visits at six-month intervals over the course of two years. The participant received a neuropsychological battery and structural MRI at each visit. They received a ^{18}F-florbetapir amyloid PET and ^{18}F-flortaucipir tau PET scan 19 months and 13 months before death, respectively.

Objective: To examine the progression of atrophy, tau and amyloid PET deposition in a unique case of PPA with autopsy-confirmed Alzheimer's disease (AD).

Methods: Freesurfer (v6.0.0) was used to reconstruct T_1-weighted MRI scans, generate atrophy maps compared to 35 normal controls, and provide segmentations for the modified Müller-Gärtner partial volume correction (PVC) for PET.

Results: There was a marked progression of cortical atrophy over 6 month intervals (Figure 1). The amyloid PET load (with and without PVC) was focal in the left superior temporal and middle frontal gyrus, with higher retention in the left than right (Figure 2A). The tau PET scan was asymmetric with expected language network predominance (Figure 2B). Using an identical method as a previous study of aging, typical and atypical dementia (Maass et al., **Neuroimage,** 2017), this participant had higher inferior temporal tau PET retention (left and right SUVR = 4.6; left SUVR = 5.5) than most participants scanned with flortaucipir PET. The autopsy reported histopathologic alterations consistent with AD (Thaal, A3; Braak, B3; CERAD, C3) and no other co-pathologies.

Conclusions: Utilizing biomarkers of amyloid, tau, and neurodegeneration, this case of agrammatic variant PPA with underlying AD demonstrates 1) a rapid progression of cortical atrophy, 2) a pattern of focal amyloid retention not previously reported, and 3) an asymmetric tau load found within the perisylvian language network, consistent with atrophy at last visit. Future directions will include correlations between imaging and post mortem measurements of pathology.

Figure 1.
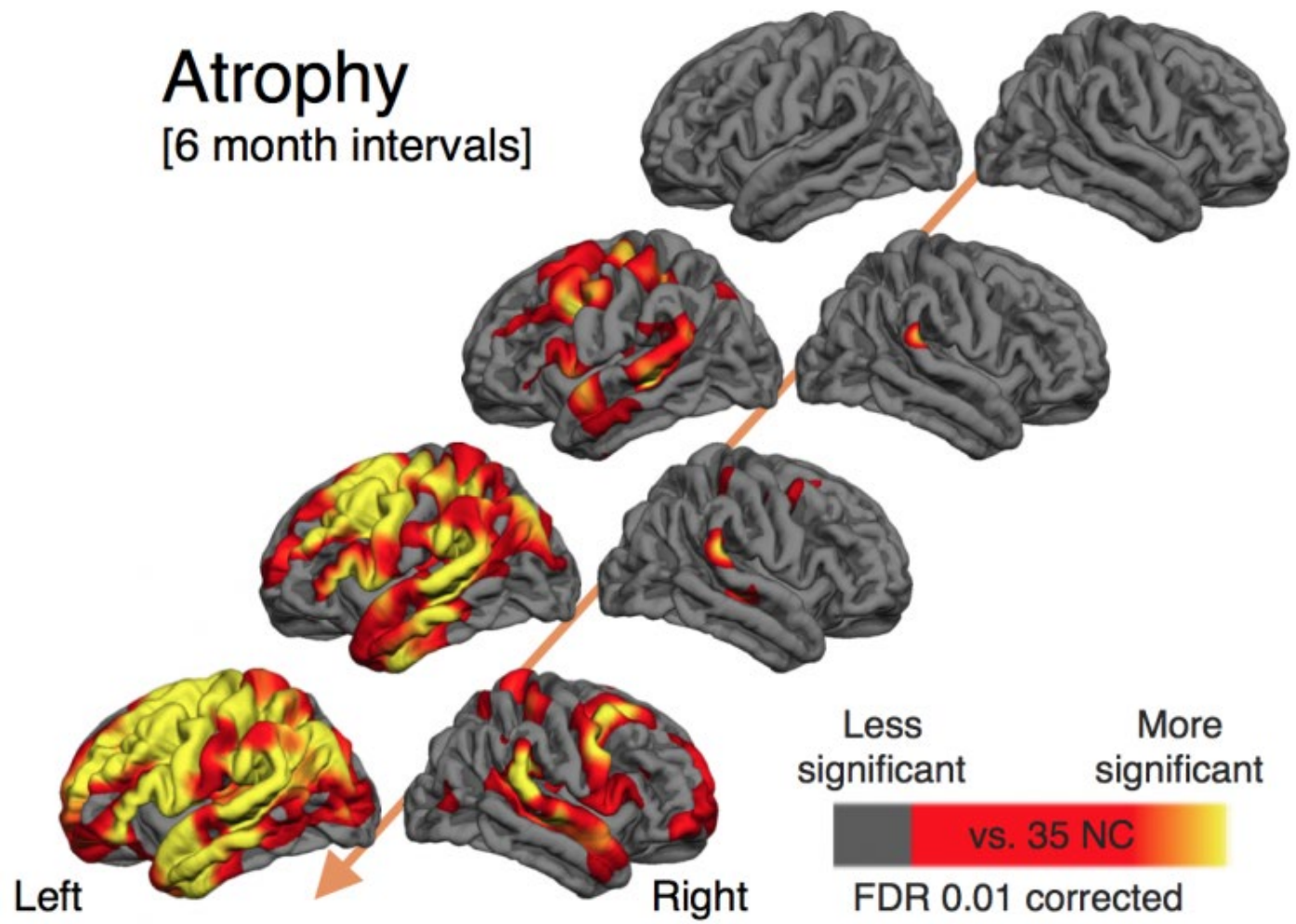
Atrophy
[6 month intervals]

Less significant — More significant

vs. 35 NC

FDR 0.01 corrected

Left

Right

Figure 2.

A

^{18}F-florbetapir amyloid PET

Left   Right

Whole cerebellar SUVR

1.2   1.4   1.6   1.8   2

B

^{18}F-flortaucipir tau PET

Left   Right

Grey cerebellar SUVR

2   3   4   5   6
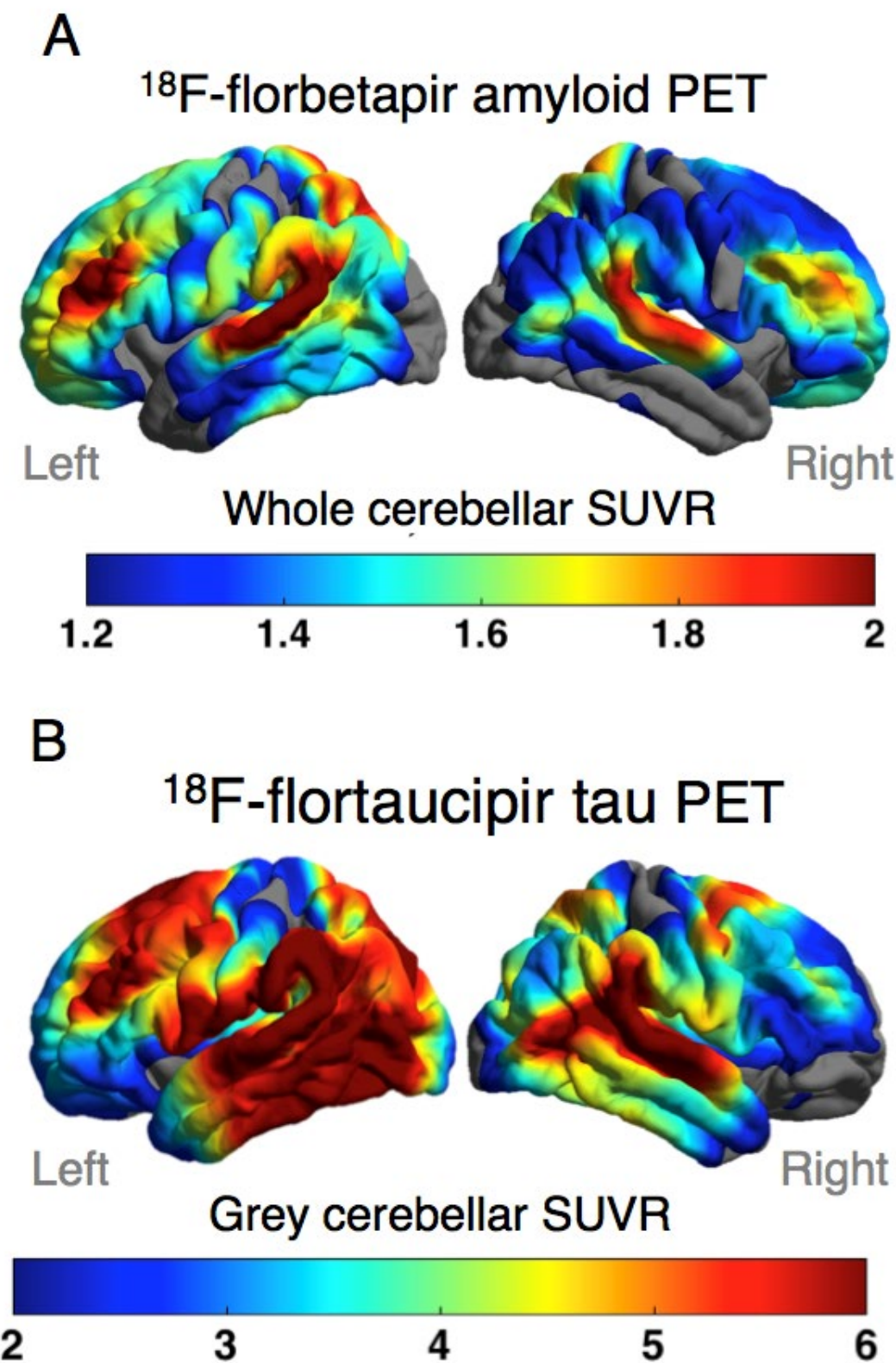
P104: Sex-specific effects of APOE-e4 genotype on amyloid burden and cognitive function

Lisette Isenberg[1], Vahan Aslanyan[1], Judy Pa[1]

[1]*University of Southern California, Los Angeles, CA, US*

Introduction: APOE-e4 allele carriers and sex have been linked to increased risk for developing AD. However, the number of APOE-e4 alleles (gene dose effects), sex, and their relationship to AD biomarkers remains understudied. Here we investigate dose dependent effects of APOE-e4 on amyloid burden and cognition in a subset of ADNI participants.

Methods: We examined cross-sectional cognitive and florbetapir PET data in participants who were cognitively normal (N=318), MCI (N=475) or AD (N=187) with known APOE-e4 genotype. ROI analyses were conducted for sites of known amyloid aggregation, including precuneus, medial orbital frontal cortex, middle frontal cortex and anterior and poster cingulate cortex. MMSE and a memory composite score were evaluated to identify clinically meaningful differences associated with sex, amyloid level and APOE-e4 genotype.

Results: ROI analyses showed higher amyloid levels in all brain regions ($p<.0001$) for women across diagnoses in a dose-dependent fashion, with the exception of homozygous women AD patients. Across diagnoses, women carriers, irrespective of dose show higher amyloid levels than all men. Further, in homozygous MCI women only, amyloid level is similar to all women carriers with AD. MMSE and memory composite scores support these findings, suggesting homozygous MCI women show marked deficits relative to heterozygous women and men ($p<.0001$).

Conclusion: Dose effects suggest sex-specific risk by APOE-e4, such that female carriers show greater amyloid accumulation than their male counterparts, until AD. Additionally, MCI homozygous women show levels of amyloid burden proximal to single and double e4 female AD allele carriers, as well as significantly poorer global cognition and memory performance. This finding suggests that greater levels of amyloid accumulation may exist for homozygous women, which corresponds to poorer performance on memory and global cognition measures, but not a clinical diagnosis of AD, indicating potential reserve mechanisms should be explored in this population.

Keywords: *Genetics, Sex, Amyloid, APOE, Cognition*

P105: Amyloid-β and cortical atrophy in adults with Down Syndrome

<u>Karly Cody</u>[1], Dana Tudorascu[2], Patrick Lao[3], Annie Cohen[2], Shahid Zaman[4], Charles Laymon[2], Sterling Johnson[1], William Klunk[2], Benjamin Handen[2], Bradley Christian[1]

[1]*University of Wisconsin, School of Medicine and Public Health, Madison, WI, US*
[2]*University of Pittsburgh, School of Medicine and Public Health, Pittsburgh, PA, US*
[3]*Columbia University, School of Medicine and Public Health, New York City, NY, US*
[4]*University of Cambridge, Cambridge, UK*

Introduction: In Down syndrome (DS) the triplicate copy of amyloid precursor protein gene results in an over production of amyloid-β (Aβ) and consequently, an increased risk for Alzheimer's disease (AD) and dementia. This study investigated the relationship between AD-related cortical atrophy and amyloid accumulation in non-demented adults with DS.

Methods: 100 non-demented adults with DS (36.1± 7.6 years) underwent [^{11}C]PiB PET and anatomical T1-weighted MRI scans. Cortical thicknesses of eight AD-vulnerable ROIs were obtained from MR T1-weighted images using FreeSurfer (v5.3.0). Parametric PiB SUVR images were generated with cerebellar gray matter as a reference region. Vertex-wise analysis was performed using general linear models to 1) examine the relationship between cortical thickness and age and 2) to investigate PiB status group (Aβ- vs Aβ+) differences in cortical thickness. Linear regressions were used on a subset of participants (n=42) with longitudinal imaging to investigate the age-adjusted PiB status group differences on percent cortical thinning per year in cortical regions known to be affected early on in the AD pathological cascade.

Results: Vertex-based analysis revealed significant age-related cortical thinning throughout the cortex (Figure 1), and clusters of significant cortical thinning in the Aβ+ compared to Aβ- group (Figure 2). Compared to the Aβ- group, the Aβ+ group showed significant (**p**<.05) decreases in AD-related regions of cortical thickness over time (Table 1).

Conclusion: The presence of Aβ in adults with DS is associated with a pattern of cortical thinning in regions known to be affected early on in the AD pathological cascade. In the context of our longitudinal amyloid findings, these results suggest that, in addition to age, Aβ aggregation may have a modifying effect on neurodegeneration.
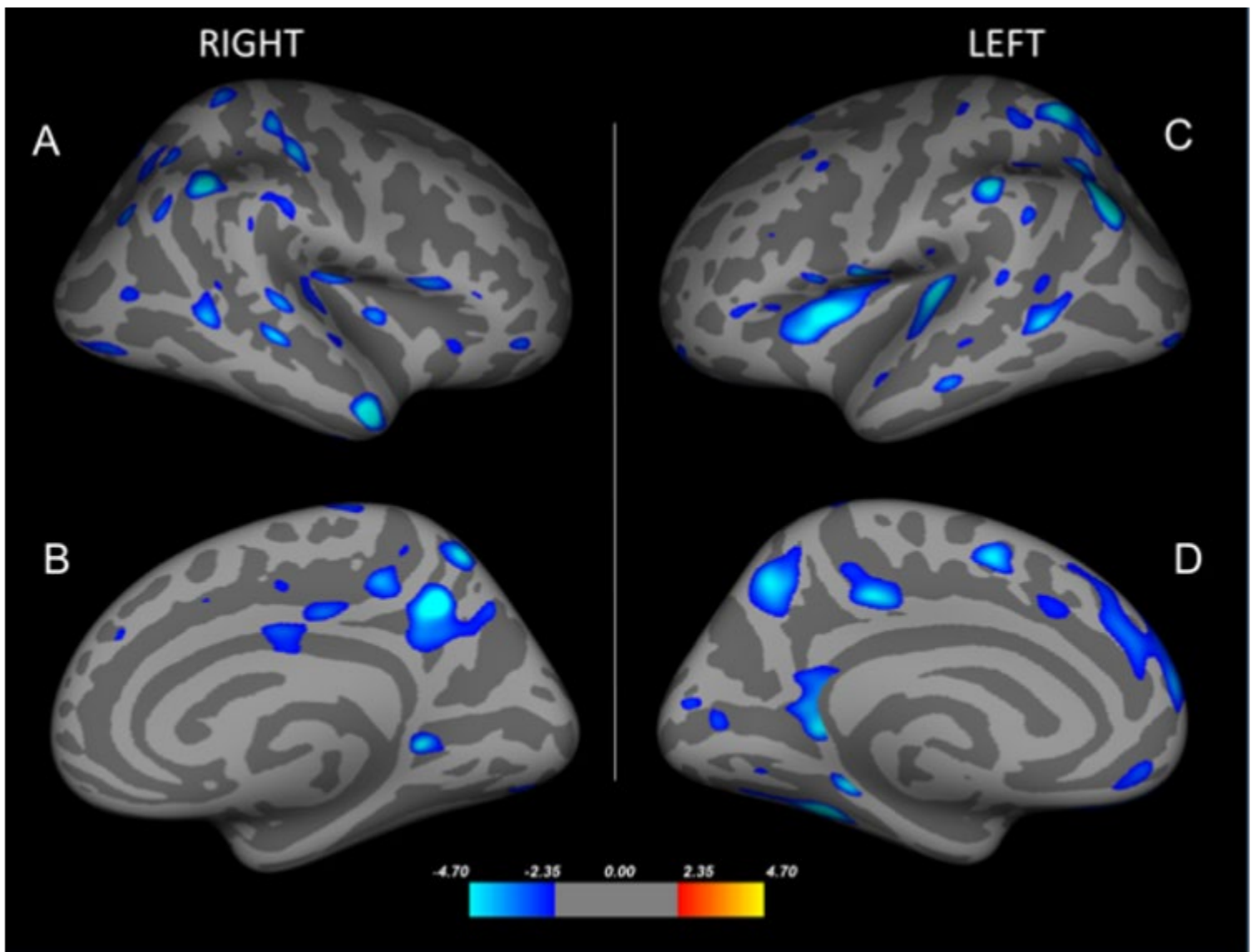
Figure 1. A-D: Vertex-based analysis (*P* < 0.05, FDR corrected). Right lateral (A) and medial (B), and left lateral (C) and medial (D) view of adults(n=100) with DS. The value of the color scale represents the significance of the difference in thickness as - log 10 (*p*-value) with blue-light blue indicating thinning cortex with increasing age.
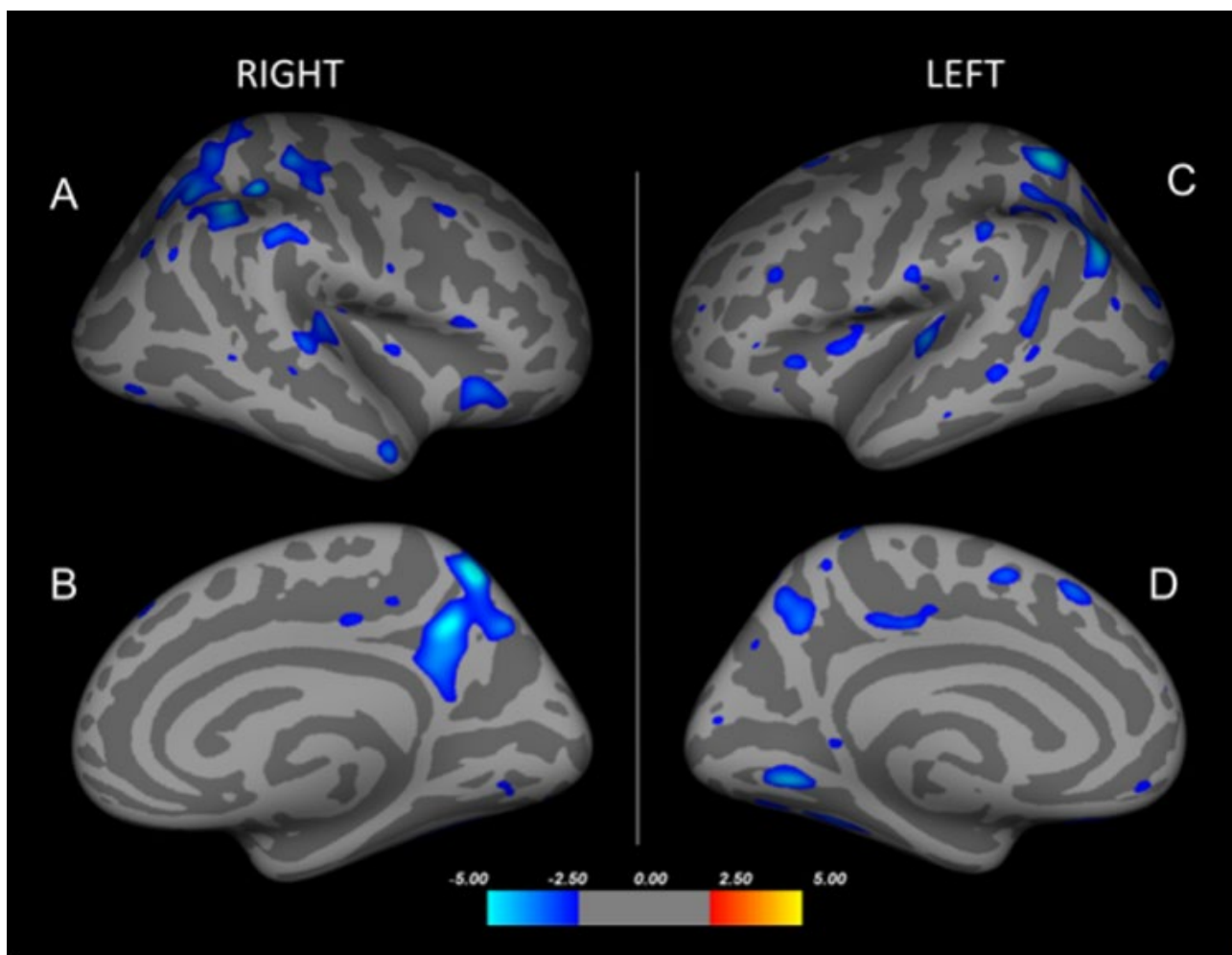
Figure 2. A-D: Vertex-based analysis (P < 0.05, FDR corrected). Right lateral (A) and medial (B), and left lateral (C) and medial (D) view of Aβ- vs Aβ+ groups. The value of the color scale represents the significance of the difference in thickness as - log 10 (p-value) with blue-light blue indicating thinner cortex in the Aβ+ group relative to the Aβ- group.

Table 1

Main effect of Aβ on changes in cortical thickness over time *,**

Region of Thickness (mm)	Aβ-, n=33	Aβ+, n=9	P
Entorhinal	.027 (.03)	-.113 (.06)	.055
Parahippocampal	.059 (.02)	-.047 (.05)	.057
Fusiform	.012 (.02)	-.097 (.04)	.028
Cingulate Isthmus	.011 (.02)	-.151 (.04)	.001
Posterior Cingulate	-.033 (.02)	-.142 (.04)	.011
Precuneus	-.034 (.02)	-.066 (.04)	.497
Supramarginal	.016 (.02)	-.064 (.04)	.076
Inferior Parietal	.001 (.02)	-.059 (.04)	.193

*All values are adjusted for age and time between scans (mean (SD); 4.48(1.7) years)

**All values were corrected for multiple comparisons (Bonferroni, α=.05)

P106: Relationship between intracranial blood flow and beta-amyloid assessed with PiB PET

<u>Karly Cody</u>[1], Tobey Betthauser[1], Rebecca Koscik[1], Leonardo Rivera-Rivera[2], Sara Berman[1], Paul Cary[1], Carson Hoffman[2], Lindsay Clark[1], Nathanial Chin[1], Todd Barnhart[2], Barbara Bendlin[1], Kevin Johnson[2], Oliver Wieben[2], Bradley Christian[2], Sterling Johnson[1]

[1]*Alzheimer's Disease Research Center, University of Wisconsin School of Medicine and Public Health, Madison, WI, US*
[2]*Department of Medical Physics, University of Wisconsin-Madison, Madison, WI, US*

Introduction: Poor intracranial arterial health, resulting from cerebrovascular disease, may contribute to AD pathophysiologic processes like amyloid accumulation. This study investigated the relationship between measures of intracranial blood flow (ICBF), cardiovascular risk factors (CVRFs), and beta-amyloid plaque accumulation.

Methods: 148 cognitively unimpaired older adults (Table 1) underwent [^{11}C]PiB PET and MR imaging. 4D flow MRI was used to estimate ICBF features, particularly left and right averaged, mean ICBF of the middle cerebral artery (MCA), inferior internal carotid artery (ICAi), and superior internal carotid artery (ICAs). Amyloid burden was assessed by taking the mean PiB DVR (Logan graphical analysis, cerebellum GM) across 8 bilateral cortical regions, and PiB positivity was determined using a previously defined global PiB DVR threshold of 1.19. Partial correlations between global PiB DVR, MRI flow metrics, and CVRF were examined. Linear regression was used to examine associations between ICBF measures and global PiB DVR, adjusting for age and gender.

Results: No significant differences in ICBF or CVRFs were observed between PiB status groups (Table 1). After adjusting for age and sex, correlations between ICBF, CVRFs, and global PiB were not significant (Table 2). Linear regressions, adjusted for age and gender, revealed no significant relationships between ICBF and global PiB. The strongest association was a marginal (**p**=0.057) positive relationship between MCA mean flow and global PiB accumulation (Table 3).

Conclusion: In this late-middle aged cohort, there is no detectable link between 4D flow MRI measured-ICBF and global PiB or CVRFs and global PiB. The age range and limited time frame between 4D flow MRI and PiB PET imaging may have precluded the detection of a relationship between arterial health and amyloid burden in this population. Longitudinal image collection and analysis is ongoing.

Table 1. Sample Characteristics

Measure	Total sample	PiB(+)	PiB(-)	p^{+}
n	148	42, 28.4%	106, 74.6%	---
Females n, %	92, 62%	24, 57%	68, 64%	.456[++]
Age at MRI, yr	65.38 (7.40)	68.37 (7.51)	64.20 (7.05)	.002
Years between MRI and PiB PET	2.10 (2.41)	1.65 (2.09)	2.27 (2.51)	.162
Global PiB DVR	1.19 (.24)	1.52 (.23)	1.06 (.05)	<.001
Body Mass Index (kg/m^2)	28.01 (5.29)	27.31 (5.12)	28.40 (5.35)	.258
Total Cholesterol (mmol/L)*	207.00 (41.59)	210.05 (41.69)	205.77 (41.69)	.580
Systolic BP (mm Hg)**	127.94 (16.47)	128.76 (17.05)	127.61 (16.30)	.702
Diastolic BP (mm Hg)**	76.84 (7.16)	75.52 (6.10)	77.38 (7.51)	.158
MCA mean flow (mL/min)	1.88 (.46)	1.95 (.52)	1.86 (.42)	.253
Inferior ICA mean flow (mL/min)***	3.46 (.68)	3.46 (.56)	3.48 (.76)	.978
Superior ICA mean flow (mL/min)***	3.41 (.75)	3.45 (.72)	3.41 (.81)	.702

Table 1. Values represent Mean (Standard Deviation), unless otherwise indicated
* Of the total sample,13 subjects were missing cholesterol, n=135
** Of the total sample, 5 subjects were missing blood pressure, n=140
*** Of the total sample 6 subjects were missing ICA data, n=142
[+] p, Significance (2-tailed) of difference between PiB(+) and PiB(-) groups; Independent samples T-Test
[++] p, Significance (2 tailed) of difference between PiB(+) and PiB(-) groups; Chi Square, Fisher's Exact Test

Table 2.				Partial Correlations (n=131*)									
Control Variables			1.	2.	3.	4.	5.	6.	7.	8.	9.	10
Age, Gender	1. Global PiB DVR	Correlation	⎯	.045	.093	.103	.091	-.029	-.115	-.091	.065	.063
		Sig. (2-tailed)		.603	.286	.240	.296	.743	.189	.298	.458	.471
	2. Inferior ICA Mean Flow (mL/min)	Correlation		⎯	.881	.756	-.005	-.100	-.011	-.048	.059	.069
		Sig. (2-tailed)			.000	.000	.950	.251	.901	.585	.500	.429
	3. Superior ICA Mean Flow (mL/min)	Correlation			⎯	.779	.013	-.049	-.014	-.080	.047	.019
		Sig. (2-tailed)				.000	.883	.576	.871	.362	.595	.831
	4. MCA Mean Flow (mL/min)	Correlation				⎯	-.013	-.096	-.029	-.045	.043	.093
		Sig. (2-tailed)					.883	.270	.742	.608	.627	.289
	5. Systolic BP (mmHg)	Correlation					⎯	.712	.187	.170	-.111	-.174
		Sig. (2-tailed)						.000	.031	.050	.202	.045
	6. Diastolic BP (mmHg)	Correlation						⎯	.276	.201	-.127	-.162
		Sig. (2-tailed)							.001	.021	.146	.063
	7. BMI (kg/m^2)	Correlation							⎯	.284	-.471	-.024
		Sig. (2-tailed)								.001	.000	.785
	8. Triglycerides (mg/dL)	Correlation								⎯	-.529	.074
		Sig. (2-tailed)									.000	.398
	9. HDL Cholesterol (mg/dL)	Correlation									⎯	.082
		Sig. (2-tailed)										.348
	10. LDL Cholesterol (mg/dL)	Correlation										⎯
		Sig. (2-tailed)										

†All bolded values represent significant (p<.05) correlations between measures, adjusting for age and gender.
*As noted in Table 1, several subjects had incomplete data; n=131 represents all subjects with complete data across all measures.

Table 2. No significant correlations were observed between global PiB amyloid deposition and intracranial blood flow or between global PiB amyloid deposition and cardiovascular risk factors when adjusting for the effects of age and gender. Notably, measures of intracranial blood flow and cardiovascular risk were significantly intra-correlated.

Table 3. Association Between Blood Flow and Global PiB, Adjusting for Age and Gender

Model: Global PiB DVR = Intercept + β_{age}*age + β_{gender}*gender + β_{ICBF}*ICBF

Model Predictor	n	β (SE)	t	ΔR^2	p
MCA Mean Flow	148	.080 (.04)	1.92	.111	.057
Inferior ICA Mean Flow	142	.023 (.00)	.788	.086	.432
Superior ICA Mean Flow	142	.036 (.03)	1.36	.095	.176

P107: Personalizing the use of the ATN framework in clinical research: integrating the clinical phenotype and biomarkers in a case series across the MCI/dementia spectrum

Brad Dickerson[1,2], Scott McGinnis[1,2], Megan Quimby[1], Daisy Hochberg[1], Mike Brickhouse[1], Jessica Collins[1,2], Deepti Putcha[1], Mark Eldaief[1], Bonnie Wong[1,2], Matthew Frosch[2,3], Sandy Das[4], Corey McMillan[4], Paul Yuschkevich[4], Robin de Flores[4], Laura Wisse[4], Long Xie[4], David Wolk[4]

[1]*MGH Frontotemporal Disorders Unit, Boston, MA, US*
[2]*Massachusetts ADRC, Boston, MA, US*
[3]*C. S. Kubik Laboratory for Neuropathology, Boston, MA, US*
[4]*Perelman School of Medicine, University of Pennsylvania, Philadelphia, PA, US*

A new research framework was published in 2018 for Alzheimer's disease that defines the disease using biomarkers of Amyloid, Tau, and Neurodegeneration (ATN). We are evaluating the framework in the context of a series of patients with MCI or Dementia. We report on a series of 50 patients, some of whom have come to autopsy. For each case, independent raters blind to each case reviewed the clinical history and office-based cognitive neuropsychiatric examination, then determined and rated confidence in the clinical syndrome. Biomarker status and likely neuropathology were predicted from this information. Neuropsychological testing was then evaluated and confidence in the clinical syndrome was again rated, and biomarker status and likely neuropathology were predicted from this clinical information. Next, the MRI scan was reviewed and rated for evidence of neurodegeneration. Molecular biomarker status and likely neuropathology were predicted from this clinical and MRI information. Finally, CSF and/or amyloid and tau PET images were reviewed and likely neuropathology was again predicted. Analyses are ongoing but preliminary results indicate that clinical information provides strong and often accurate hypotheses for biomarker results and likely neuropathology. The addition of MRI scan information provides further value in predicting molecular biomarker results and likely neuropathology. Molecular biomarkers provide additional information, especially in cases with clinical phenotypes that are atypical and in older patients. In conclusion, clinical information and patterns of atrophy on MRI lead to enhanced prediction of likely pathology beyond using ATN alone. These findings suggest that, at least in symptomatic patients, the ATN framework should be considered in clinical context when aiming to comprehensively classify individual patients.

Keywords: *ATN, amyloid, tau, neurodegeneration, Alzheimer's disease*

P108: The ATN framework in ADNI: How do different A,T, and N biomarkers influence the definition of AD pathology and cognitive trajectories?

Susan Landau[1], Deniz Korman[1], Leslie Shaw[2], John Trojanowski[2], William Jagust[1]

[1]*University of California, Berkeley, Berkeley, CA, US*
[2]*University of Pennsylvania, Philadelphia, PA, US*

Objectives: The 2018 NIA-AA AD Research Framework defines AD by the presence of abnormal Aβ [A], tau [T], and neurodegeneration [N], independent of cognitive symptoms. Importantly, PET, CSF, and/or structural MRI measurements can be used to define A+/-, T+/-, and N+/- status; but it is unclear how the use of different biomarkers affects operationalization of the ATN framework. Here, we examined agreement in ATN definition across different biomarkers in non-demented ADNI participants, and their impact on cognitive trajectories.

Methods: 221 non-demented ADNI participants (130 cognitively normal, 91 MCI) were classified as A+/-, T+/-, and N+/- using concurrent (1) PET (cortical florbetapir or florbetaben [A], inferolateral temporal flortaucipir [T], FDG in AD-specific regions [N]) and (2) CSF (CSF $A\beta_{1-42}$ [A], CSF p-tau$_{181p}$ [T], CSF t-tau [N] using the Roche Elecsys assay) measurements, as well as two variations using hippocampal volume [N]. We applied biomarker-specific thresholds and examined agreement across PET-based versus CSF-based assessments of ATN status, and ATN associations with ongoing cognitive change.

Results: Agreement between CSF and PET +/- status was highest for A (78%) than for T (52%) and N (55%). Across PET and CSF definitions of ATN, membership was generally consistent with previous reports, but PET-defined ATN membership differed from CSF-defined ATN membership (κ=0.31, p<0.001; Figure 1). The use of hippocampal volume to define [N] had minimal impact on group membership. Both PET- and CSF-defined ATN status were independently associated with cognitive change (p<0.01; Figure 2), primarily due to cognitive decline in preclinical AD (A+T+) participants. In a multiple regression model, only PET-defined ATN status remained significant (p=0.009).

Conclusion: ATN membership and predictive value were both influenced by whether PET or CSF was used to assess pathophysiology. The operationalization of the ATN framework across biomarkers is highly threshold dependent but also influenced by differing biomarker substrates.

ATN category membership varies across PET and CSF biomarkers
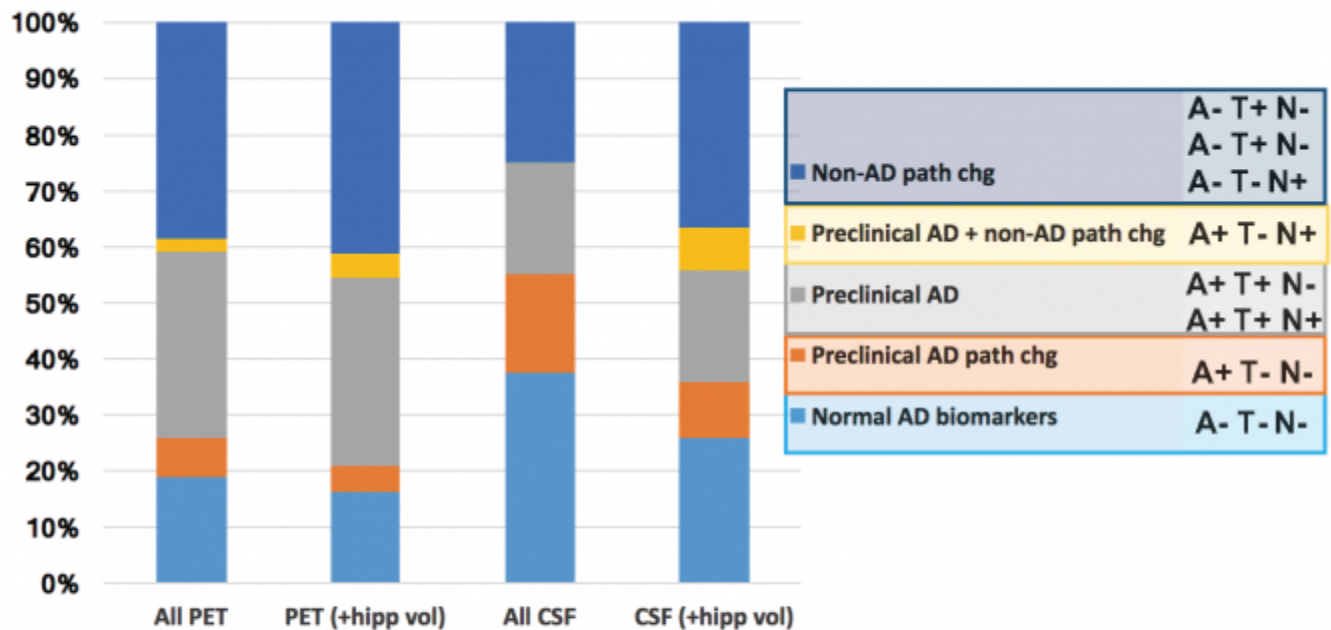
Figure 1. The 8 ATN subgroups were further condensed into 5 clinical categories based on the presence/absence of AD and non-AD pathologic change (Jack et al. Alz & Dementia 2018). Bar plots illustrate percentages of 221 non-demented (Normal, MCI) ADNI participants making up each ATN category (colored bars) across PET and CSF biomarker definitions of ATN (category axis). "All PET" and "All CSF" definitions of ATN are shown, with/without including hippocampal volume as [N]. The biomarker-specific thresholds for defining +/- status included autopsy-validated (florbetapir, florbetaben), ROC-based (CSF), and 90th percentile of abnormality in AD patients (flortaucipir, hippocampal volume, FDG) methods.
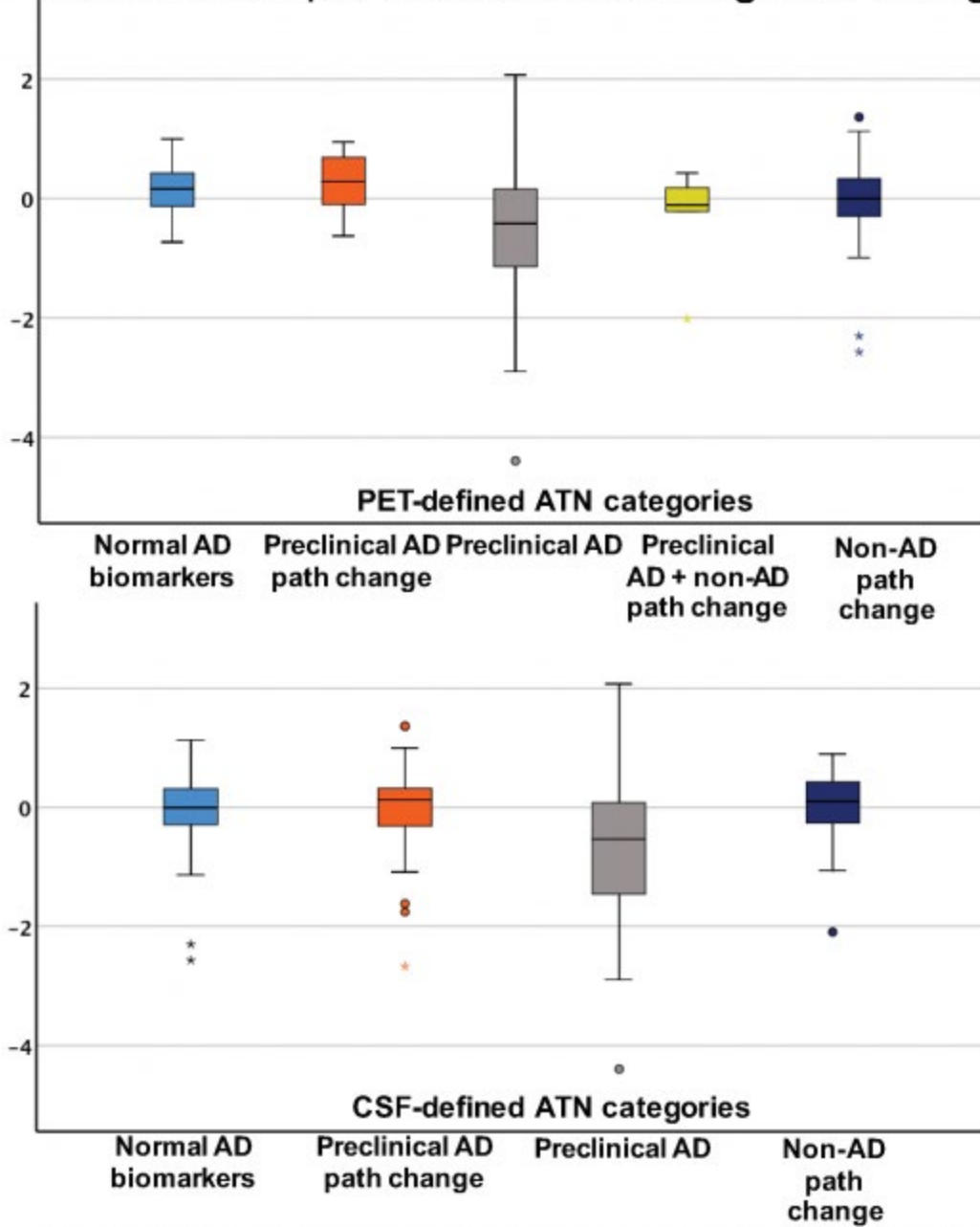
Figure 2. In univariate models with all 221 non-demented ADNI subjects, PET-defined and CSF-defined ATN status were each associated with cognitive change (p<0.01), primarily due to cognitive decline in A+T+ subjects (grey bars, top and bottom). In a multiple regression model, only PET-defined ATN status remained a significant predictor of longitudinal cognitive change (p=0.009) and had a greater effect size ($\eta_p^2=0.063$) than CSF ATN status ($\eta_p^2=0.032$).

P109: Neuropsychiatric symptoms are correlated with tau deposition in the Alzheimer's disease spectrum

Cécile Tissot[1,2], Tharick Ali Pascoal[1,2], Joseph Therriault[1,2], Mira Chamoun[1,2], Firoza Lussier[1,2], Melissa Savard[1,2], Sulantha Mathotaarachchi[1,2], Andrea Lessa Benedet[1,2], Emilie M. Thomas[1], Marlee Parsons[1,2], Pedro Rosa-Neto[1,2], Serge Gauthier[1,3]

[1]McGill University Center for Studies in Aging, Verdun, QC, Canada
[2]Translational Neuroimaging Laboratory McGill University, Verdun, QC, Canada
[3]Douglas Mental Health Research Center, Verdun, QC, Canada

Introduction: Neuropsychiatric Inventory-Questionnaire (NPI-Q) is a survey addressed to informants to assess the participant's neuropsychiatric symptoms (NPS) and their impact on the participant and their informant. Although NPS has been closely related to the clinical progression to dementia in carriers of Alzheimer's disease (AD) pathophysiology, the relationship between NPS and brain amyloid and tau pathologies is still unclear. Here we test the relationship between tau aggregates in the brain and NPS within the AD clinical spectrum.

Methods: 75 individuals (CN = 56, MCI = 5, AD = 11) underwent positron emission tomography (PET) amyloid [^{18}F]AZD4694 and tau [^{18}F]MK-6240. [^{18}F]AZD4694 and [^{18}F]MK-6240 standardized uptake value ratios (SUVRs) used the cerebellum grey matter as the reference region and were calculated between 40-70 min and 90-110 min post-injection, respectively. A voxel based regression model evaluated the relationship between the accumulation of a biomarker, using [^{18}F]MK6240 or [^{18}F]AZD4694 PET scans, and the NPI-Q scores. The model's covariates were age, gender, years of education and diagnosis of participants.

Results: We did no find association between NPI-Q scores and brain amyloid deposition. However, we found a strong association between tau accumulation and NPI-Q scores in several brain regions: the most impacted one is the frontal lobe, specifically the right frontal pole, spreading to more medial regions. Additional areas showing association between tau deposition and NPI-Q were precuneus and right temporal pole.

Conclusion: These preliminary results show a strong correlation between NPS and tau aggregation in regions of the brain known to be involved with self-consciousness and holistic thoughts, and also recognized as AD-related regions. This aligns with the idea that tau is more closely related with cognitive and behavioral symptoms than amyloid. This study demonstrates NPS correlate with neurofibrillary tangles and it is thus important to assess in the context of AD clinical spectrum.

[18F]MK6240 accumulation correlates with neuropsychiatric symptoms across the Alzheimer's disease spectrum
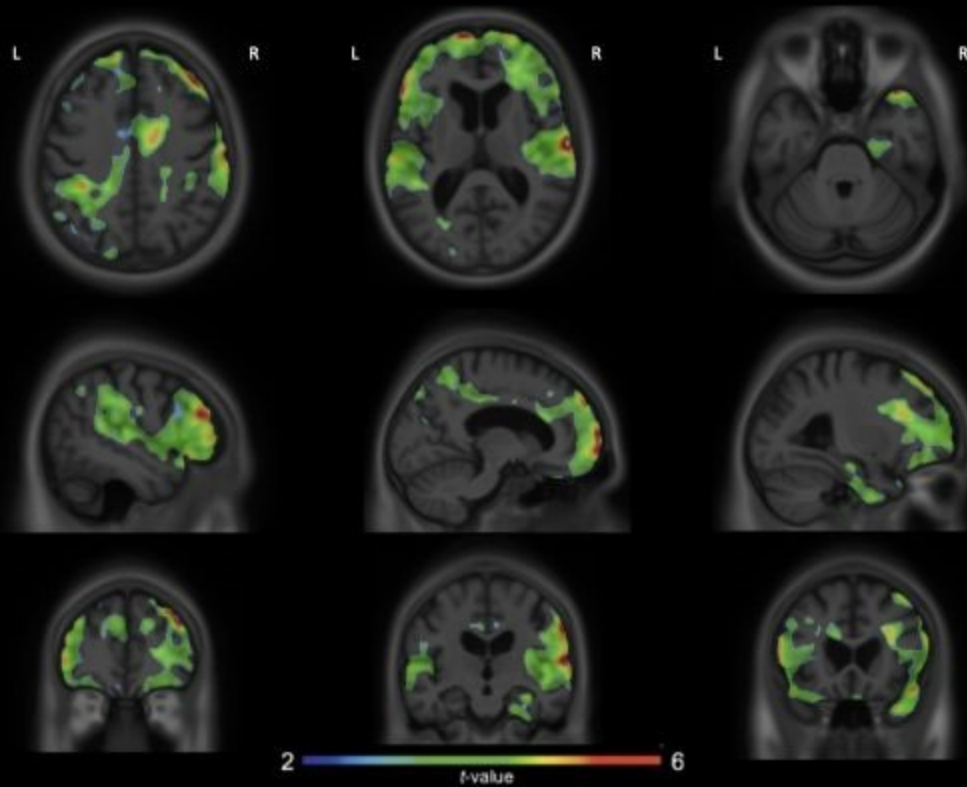
Keywords: *tau, alzheimer's spectrum, neuropsychiatric symptoms*

P110: Amyloid-sex interaction effect on cognitive decline: Differential effects on memory versus executive functioning are not mediated by temporal lobe atrophy

Brandon Gavett[1], Evan Fletcher[2], Dan Mungas[2], Charles DeCarli[2]

[1]*University of Western Australia, School of Psychological Science, Perth, Australia*
[2]*University of California at Davis, Alzheimer's Disease Center, Sacramento, CA, US*

Brain b-amyloid (Ab) deposition appears to be a more important risk factor for global cognitive decline in women than in men (Buckley et al., 2018). The current study sought to determine whether this interaction effect is manifest similarly in the subdomains of memory and executive functioning, and whether temporal lobe atrophy – which we have found uniquely influences cognitive decline – mediates this interaction effect. Participants at the UC Davis Alzheimer's Disease Center underwent amyloid PET imaging, annual cognitive assessment, and at least two MRI scans. A Bayesian multilevel latent variable model was run using Mplus version 8 for each outcome (memory and executive). Specified models treated Ab (absent/present), sex, and the Ab-sex interaction as predictors, annualized temporal lobe atrophy rate as the mediator, and cognitive slopes as outcomes. Covariates included age at baseline, years of education, and apolipoprotein e4 status. For memory (n = 92), Ab-positivity (estimate = -0.042), the Ab-sex interaction (estimate = 0.070), and temporal lobe atrophy (estimate = 0.012) exerted the strongest effects on memory slope. However, there was no evidence to suggest that the interaction effect between Ab and sex was mediated by temporal lobe atrophy. For executive functioning (n = 102), males declined more rapidly than females (estimate = -0.030), but neither Ab-positivity (estimate = -0.020), the Ab-sex interaction (estimate = 0.024), nor temporal lobe atrophy (estimate=0.009) strongly influenced executive functioning slope. Again, temporal lobe atrophy exerted negligible mediation effects. The results are partially consistent with those reported by Buckley et al. (2018) in that our evidence suggests that the effect of Ab on cognitive decline depends on sex; however, this effect was stronger for memory slope than for executive functioning slope. The results also revealed that temporal lobe atrophy may not be the primary mechanism underlying the relationship between Ab and cognitive decline.

Keywords: *amyloid, memory, executive functioning, temporal lobe, sex*

P111: Molecular imaging discordance with CSF AD biomarkers in atypical Alzheimer's disease

Ryan Townley

[1]Mayo Clinic, Rochester, MN, US

Background: Posterior cortical atrophy (PCA) and dysexecutive Alzheimer's disease (dAD) are two atypical variants of Alzheimer's disease. AD proteins are the predominant pathology found in both variants at autopsy, but studies looking at ante mortem cerebrospinal fluid (CSF) biomarkers have suggested some cases were non-AD due to inconclusive biomarkers. We aimed to evaluate these atypical AD variants with CSF biomarkers and molecular imaging. Of particular interest, those with atypical CSF profiles but positive molecular imaging are highlighted.

Methods: Twenty-five patients were seen at Mayo Clinic for the initial evaluation and diagnosis of dAD or PCA. CSF biomarkers were measured clinically to assist with initial diagnosis. Patients were subsequently enrolled into the Alzheimer's Disease Research Center (ADRC) or the Molecular and Structural Imaging in Atypical Alzheimer's Disease study for longitudinal molecular imaging at 12 month intervals.

Results: Demographics of the participants and biomarker results are shown in Table 1. Tau-PET SUVR was inversely correlated with cognitive scores and younger age of onset (Figure 1A-D). Five patients had CSF p-tau < 61 with positive tau-PET imaging (mean SUVR 2.11); 8 patients had CSF Aβ1-42 > 500 with average amyloid-PET SUVR of 2.17 (exemplar of each atypical CSF group shown in Figure 2A-B). Longitudinal imaging was available in 13/25 patients (8 with 2 scans and 5 with 3 scans) but no significant changes from baseline scan were found across groups.

Conclusions: Atypical CSF profiles should be further investigated with molecular imaging if suspicion for AD is high. Tau-PET SUVR captured disease severity better than CSF or amyloid-PET. Age of onset, driven mostly by dAD patients, was inversely associated with tau-PET SUVR and tau-PET SUVR was inversely associated with lower cognitive scores. One possible interpretation of these data is that dAD involves failure of large scale brain networks, mainly the frontoparietal working memory networks.
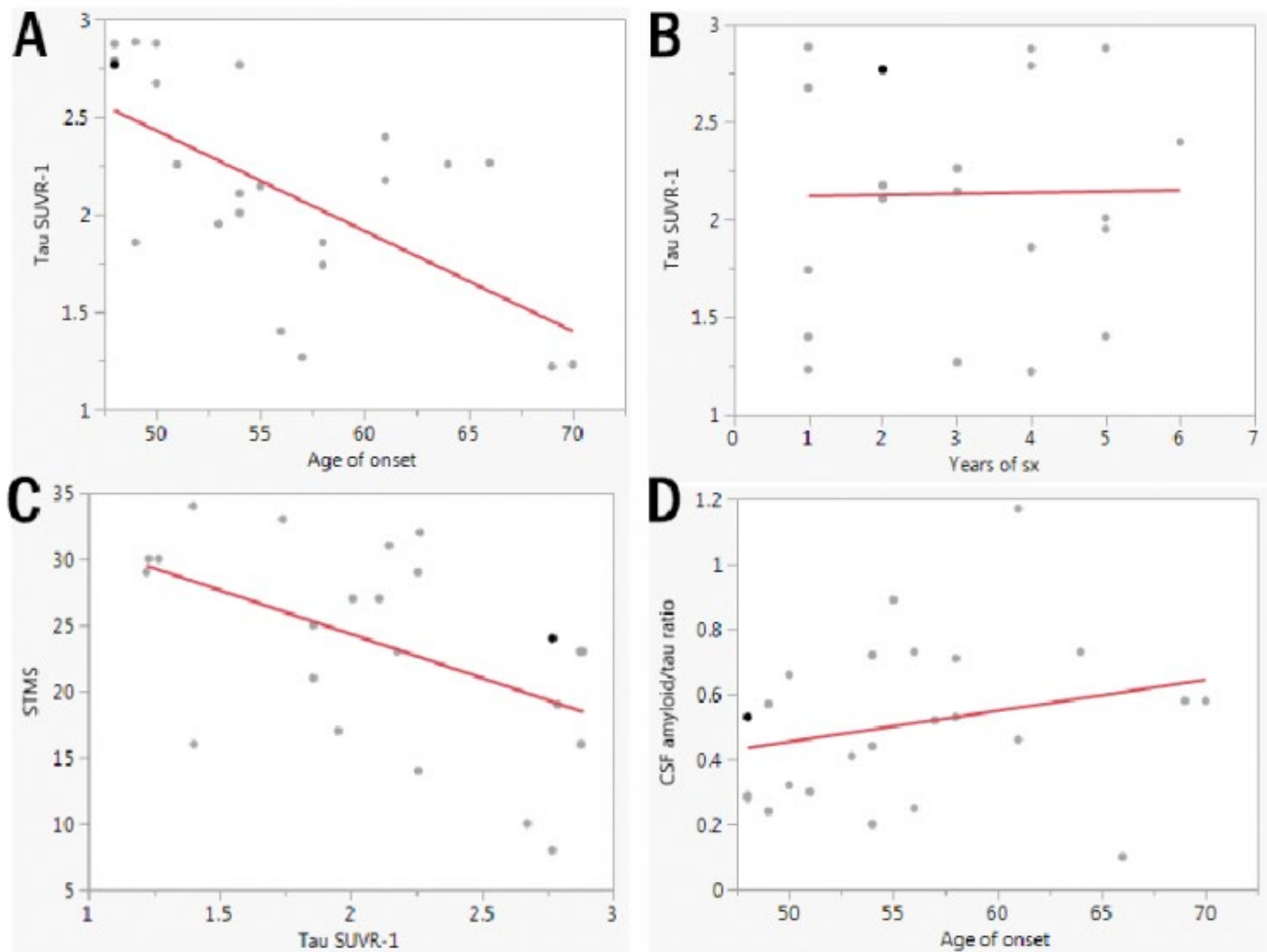
Figure 1: A) Tau-PET SUVR by age of onset with, $p < 0.001$ (R^2 adjusted 0.35). When separated by diagnosis (not shown), dAD group, $p < 0.001$ (R^2 adjusted 0.59) and PCA group, $p = 0.21$ (R^2 adujsted 0.21). B) Tau-PET SUVR by years of symptoms prior to tau-PET scan, $p = 0.93$. C) Cognitive score by Tau-PET SUVR, $p < 0.01$ (R^2 adjusted 0.23). D) CSF biomarkers by age of onset, best exemplified by amyloid/tau ratio, $p = 0.23$ (R^2 adjusted 0.02).

Figure 2: FDG-PET scan (left) with Z scores from 0-7, Tau-PET (middle) scale 0-2.5 (abnormal SUVR > 1.23), Amyloid-PET (right) scale 0-3 (abnormal SUVR > 1.44). A) A 48yoF with a 2 year history of dysexecutive impairment, diagnosed as dAD with CSF biomarkers: Aβ1-42 - 328, t-tau - 316, p-tau - 43, Aβ1-42/Tau Index - 0.53. B) A 61yoM with a 2 year history of visual difficulties diagnosed as PCA with CSF biomarkers: Aβ1-42- 785 , t-tau - 367, p-tau - 71, Aβ 1-42/Tau Index - 1.17.

Table 1: Demographics and Biomarker Data Between Diagnostic Groups

	dAD	PCA
N	16	8
Gender, F:M	9:7	7:1
Age of onset, median (IQR)	54 (49-56)	62.5 (55-68.25)**
Sx Duration, mean (SD)	2.9 (1.5)	3.4 (1.6)
Education, mean (SD)	14.1 (2.4)	15.1 (2.8)
STMS, median (IQR)	23.5 (16.8-29.3)	29 (17-30)
CSF Aβ1-42, median (IQR)	434.2 (307-538.8)	394.9 (329.1-507.6)
CSF Total Tau, median (IQR)	455.9 (333.4-923.4)	464.2 (368.7-858.3)
CSF p-tau, median (IQR)	75.9 (61.4-98.5)	72.0 (62.0-107.9)
CSF Aβ1-42/Tau Index, mean (SD)	0.49 (0.21)	0.54 (0.31)
Tau-PET SUVR, mean (SD)	2.21 (0.59)	1.96 (0.47)
Amyloid-PET SUVR, mean (SD)	2.28 (0.32)	2.12 (0.42)

Typically accepted values for abnormal CSF AD biomarkers: Aβ1-42 < 500, total tau > 450, p-tau > 61, Aβ1-42/Tau index < 1.0. Positive molecular imaging: Tau-PET SUVR > 1.23, Amyloid-PET SUVR > 1.44. STMS: Short Test of Mental Status, scored out of 38, a score < 30 is consistent with dementia. All variables were non-significant between the two groups except for age of onset, p< 0.001**

Thursday, January 17, 2019 - 11:00 am - 12:00 pm

Podium Session

Session 4: In vivo-postmortem correlates of flortaucipir PET

CHAIRS: Teresa Gomez-Isla, David Wolk

11:00 am - 12:00 pm	Session 4: In vivo-postmortem correlates of flortaucipir PET	CHAIRS: **Teresa Gomez-Isla**, Massachusetts General Hospital, Boston, MA, US **David Wolk**, University of Pennsylvania, Philadelphia, PA, US	Page
11:00	Pathologic correlations of in vivo [18F]-AV-1451 imaging in autopsy-confirmed Alzheimer's disease, Frontotemporal lobar degeneration with TDP-43 inclusions and control cases.	**Cinthya Aguero**, MassGeneral Institute for NeuroDegenerative Disease, Charlestown, MA, Charlestown, MA, US	296
11:15	[18F]Flortaucipir PET and pathology correlations in Alzheimer's disease, non-Alzheimer's tauopathies, and other neurodegenerative diseases	**David Soleimani-Meigooni**, University of California, San Francisco, San Francisco, CA, US	297
11:30	Tau PET imaging correlates with neuropathology	**Val Lowe**, Mayo Clinic, Rochester, MN, US	301
11:45	Relationships between flortaucipir PET signal and tau neurofibrillary tangle pathology at autopsy	**Mark Mintun**, Avid Radiopharmaceuticals, Philadelphia, PA, US	304
12:00 pm - 12:30 pm	Discussion		

Pathologic correlations of in vivo [18F]-AV-1451 imaging in autopsy-confirmed Alzheimer's disease, Frontotemporal lobar degeneration with TDP-43 inclusions and control cases.

Cinthya Aguero[1,2], Maeva Dhaynaut[3,4], Ana C. Amaral[1,2], Nicholas Heng[1,3], Prianca Ramanan[1,2], Marc D. Normandin[3,4], Samantha Katz[2,3], Derek H. Oakley[1,2,5], Keith A. Johnson[2,3], Matthew P. Frosch[1,2,5], Teresa Gómez-Isla[1,2]

[1]*MassGeneral Institute for NeuroDegenerative Disease, Charlestown, MA, Charlestown, MA, US*
[2]*Department of Neurology, Massachusetts General Hospital, Boston, MA, Boston, MA, US*
[3]*Department of Radiology, Massachusetts General Hospital, Boston, MA, Boston, MA, US*
[4]*Gordon Center for Medical Imaging, Division of Nuclear Medicine and Molecular Imaging, Massachusetts General Hospital, Boston, MA, Boston, MA, US*
[5]*C.S. Kubik Laboratory for Neuropathology, Massachusetts General Hospital, Boston, MA, Boston, MA, US*

Background: Data from studies -including our own- on legacy postmortem material showed that [^{18}F]-AV-1451 (T807, Flortaucipir) binds with strong affinity to tau aggregates in AD brains, and those that form as a function of age. But our data also suggested that AV-1451 has relatively low affinity for tau aggregates in non-AD tauopathies, and exhibits strong off-target binding to neuromelanin- and melanin-containing cells, and some weaker binding to blood products. Neuroimaging–pathologic correlation studies conducted on postmortem material from individuals imaged while alive are now critical to accurately interpret tau neuroimaging in clinical settings.

Goal: To study the correlation between **in vivo** [^{18}F]-AV-1451 retention and postmortem burden of tau aggregates in multiple regions of interest (ROIs) in four individuals imaged while alive who came to autopsy (one AD, one mixed AD/LBD, one FTLD-TDP-43 and one healthy control).

Methods: Comparison of antemortem [^{18}F]-AV-1451 standardized uptake value ratios (SUVRs) with autoradiographic and quantitative tau measures in matching ROIs at postmortem (load of tau aggregates as detected by immunohistochemistry and measures of different soluble tau species as reported by Western Blot and ELISA).

Results: Autoradiography experiments confirmed strong tracer binding to tangle-containing brain slices in the two AD cases. Slices from the FTLD-TDP43 case and the control showed no AV-1451 binding with the exception of incidental binding to entorhinal cortex (age-related tangles) and the substantia nigra and choroid plexus (off-target to neuromelanin-containing neurons and calcifications, respectively). Comparisons of **in vivo** [^{18}F]-AV-1451 retention values and quantitative pathological and biochemical tau measures in matching ROIs at postmortem confirmed a significant correlation between antemortem tracer binding and postmortem tangle burden in the two AD cases.

Conclusion: Neuroimaging–pathologic correlation studies are key to unequivocally confirm the potential utility of tau PET tracers for the reliable detection/quantification of tau aggregates in AD and related tauopathies and disease-progression tracking.

[18F]Flortaucipir PET and pathology correlations in Alzheimer's disease, non-Alzheimer's tauopathies, and other neurodegenerative diseases

David Soleimani-Meigooni[1], Leonardo Iaccarino[1], Renaud La Joie[1], Viktoriya Bourakova[1], Orit Lesman-Segev[1], Suzanne Baker[2,3], Mustafa Janabi[3], Rana Eser[1], Eva Larsen[1], Salvatore Spina[1], William Seeley[1], Lea Grinberg[1], William Jagust[2,3], Gil Rabinovici[1]

[1]Memory and Aging Center, University of California, San Francisco, San Francisco, CA, US
[2]Helen Wills Neuroscience Institute, University of California, Berkeley, Berkeley, CA, US
[3]Molecular Biophysics and Integrated Bioimaging, Lawrence Berkeley National Laboratory, Berkeley, CA, US

Introduction: Correlation of [^{18}F]Flortaucipir PET (FTP) to autopsy diagnosis and post-mortem tau pathology is limited. We aimed to determine if FTP can: 1. Discriminate AD from non-AD autopsy diagnoses, 2. Distinguish non-AD tauopathies from frontotemporal lobar degeneration (FTLD) caused by TDP-43 or FUS, 3. Detect early-stage neurofibrillary tangle (NFT) pathology.

Methods: Ten patients, who received FTP during life, underwent autopsy. 1. Neuroimaging: FTP 80-100 minute SUVR images were created using an inferior cerebellar gray matter reference, and age-adjusted Z-score (W-score) maps were generated from a dataset of 88 [^{11}C]PiB PET-negative controls (mean age 66.1, S.D. 19.9). We extracted SUVRs from ROIs corresponding to Braak stages I (entorhinal cortex), I/II, III/IV, V/VI, and compared these values to 14 young controls (mean age 26.2, S.D. 4.6) used as a standard for tau-negativity. 2. Neuropathology: Blinded autopsies and immunohistochemistry for beta-amyloid, tau, TDP-43, and alpha-synuclein were completed. Primary and secondary neuropathologic diagnoses and Braak stages were assigned (Table 1).

Results: FTP binding was highest in patients with AD primary pathology (Figure 1A). Among patients with non-AD primary pathology, tracer binding was higher in FTLD-tau (progressive supranuclear palsy, corticobasal degeneration, MAPT P301L) compared to FTLD-TDP and -FUS (Figure 1A). Non-AD pathology had unique FTP binding patterns; FTLD-TDP and -FUS had low-level off-target binding in frontal white matter (Figure 1B). Across all ROIs, patients with primary AD pathology (Braak VI) had clearly elevated SUVRs compared to patients with non-AD pathology and controls (Figure 2). FTP binding in patients with Braak I-IV pathology showed no elevation compared to young controls.

Conclusions: FTP was able to distinguish AD and non-AD primary pathology at autopsy. AD had high tracer binding, FTLD-tau had intermediate binding, and FTLD-TDP and -FUS had lower binding. Patients with Braak I-IV stage NFT pathology did not show elevated FTP SUVR compared to young controls.

Table 1: Characteristics of patients who received autopsy

Clinical diagnosis	Age at PET	Time: PET to Autopsy (Months)	Gender	MMSE at PET	CDR at PET	[¹¹C]PiB PET	1° & 2° pathology	Pathology: Braak Stage; ABC score; ADNC level
MCI (amnestic, multi-domain)	60	12.2	Male	26	1	Neg.	PSP, AD	II; A1, B1, C1; Low
AD (logopenic PPA)	53	36.1	Female	16	0.5	N/a	AD, LBD	VI; A3, B3, C3; High
AD (logopenic PPA)	73	37.7	Male	22	0.5	Pos.	AD, LBD	VI; A3, B3, C3; High
AD/PD	71	7.9	Male	22	2	Pos.	AD, LBD	VI; A2, B3, C3; High
bvFTD	68	3.8	Male	29	1	Neg.	AGD, vascular	III; A0, B2, C0; Not ADNC
bvFTD	48	20.5	Female	26	1	Neg.	TDP-43 type B (C9orf72), AD	III; A1, B1, C0; Low
bvFTD (frontal)	67	35.7	Male	5	2	Pos.	FTLD-tau (MAPT P301L mutation), AD	IV; A3, B2, C3; Intermediate
bvFTD (frontal)	34	12.0	Male	22	2	N/a	FTLD-FUS with MND	0; A0, B0, C0; Not ADNC
Non-fluent PPA	74	29.4	Female	27	0.5	Neg.	PSP, AD	II; A1, B1, C0; Low
PSP	63	9.0	Female	16	3	Neg.	CBD, vascular	I; A0, B1, C0; Not ADNC

AD = Alzheimer's disease; ADNC = Alzheimer's disease neuropathological change; AGD = argyrophilic grain disease; bvFTD = behavioral variant frontotemporal dementia; CBD = corticobasal degeneration; CDR = Clinical Dementia Rating; FTLD = frontotemporal lobar degeneration; LBD = Lewy body disease; MCI = mild cognitive impairment; MMSE = Mini-Mental State Examination; MND = motor neuron disease; PD = Parkinson's disease; PPA = primary progressive aphasia; PSP = progressive supranuclear palsy

Figure 1: A. Individual [18F]Flortaucipir PET W-score maps for patients with Alzheimer's disease (AD) primary pathology (right box) and non-AD primary pathology (left). W-score maps share a common threshold (1.65), but the maximum level of the color scale was adapted due to very high tracer binding in patients with AD primary pathology versus lower binding in patients with non-AD primary pathology.
B. SUVR images for patients with corticobasal degeneration (CBD), progressive supranuclear palsy (PSP), FTLD-TDP43 type B, and FTLD-FUS pathology on autopsy. The arrows highlight areas of higher tracer retention on the SUVR images.

AGD = argyrophilic grain disease
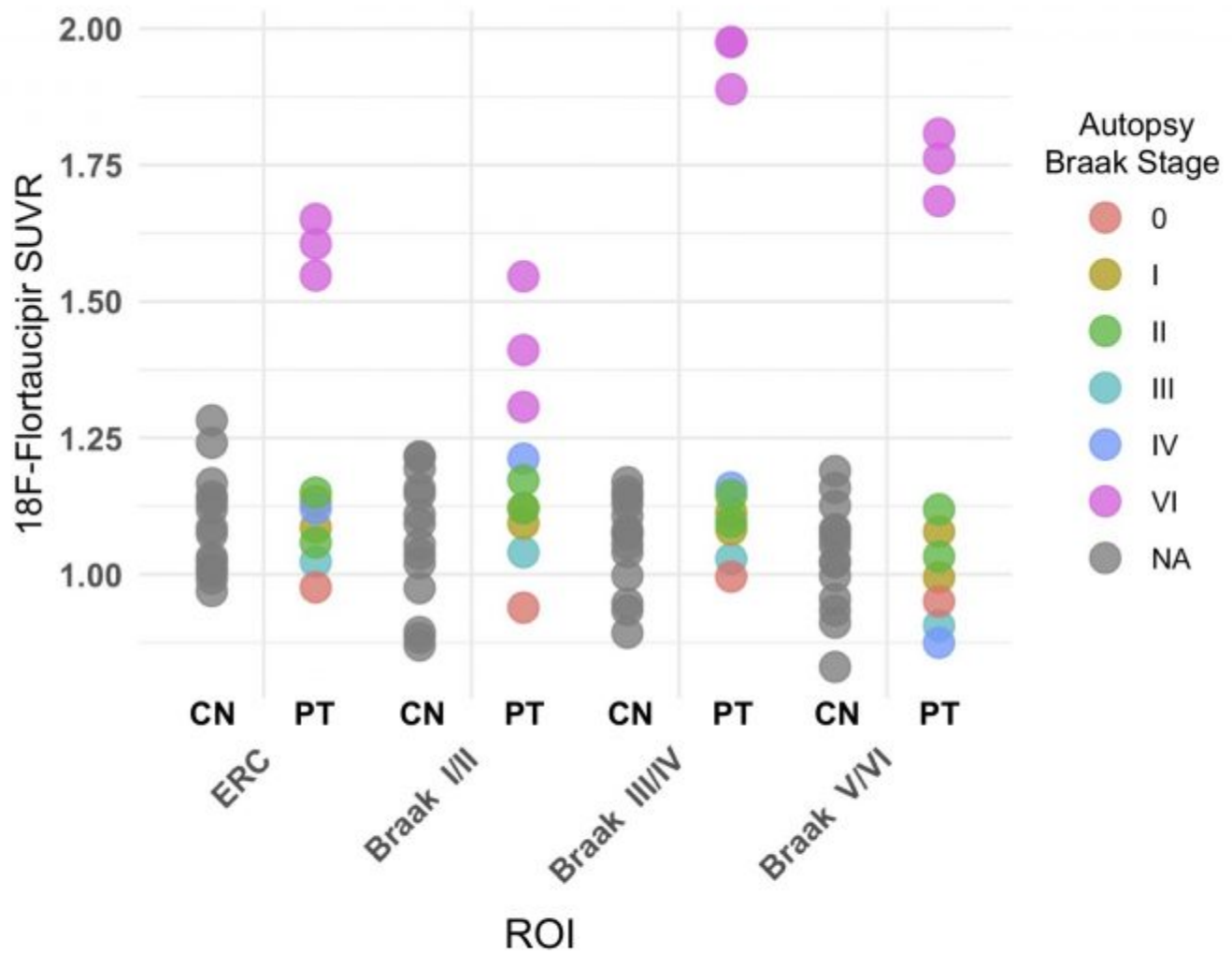CVD = cerebrovascular disease
LBD = Lewy body disease

Figure 2: [18F]Flortaucipir PET SUVRs at regions of interest (ROI) corresponding to Braak stages I (entorhinal cortex or ERC), I/II, III/IV, V/VI for patients (PT, colored dots) and young, cognitively normal controls (CN, gray dots). Each patient is color coded by Braak neurofibrillary degeneration stage found on autopsy.

Tau PET imaging correlates with neuropathology

Val Lowe[1], Emily Lundt[1], Sabrina Albertson[1], Nancy Scott[1], Hoon Kee Min Min[1], Ping Fang[1], Scott Przybelski[1], Matthew Senjem[1], Christopher Schwarz[1], Joseph Parisi[1], Kejal Kantarci[1], Bradley Boeve[1], David Jones[1], David Knopman[1], Clifford Jack[1], Dennis Dickson[2], Ronald Petersen[1], Melissa Murray[2]

[1]*Mayo Clinic, Rochester, MN, US*
[2]*Mayo Clinic, Jacksonville, FL, US*

Background: Tau PET findings may be better understood by correlation with autopsy data. We evaluated tau PET in a group of participants from a population study who had brain autopsy using a multi-region ROI that is most consistent with tau deposition topography along the spectrum of normal aging to early AD.

Methods: Autopsies were performed on 26 participants from the Mayo Clinic who had ante-mortem tau PET with Flortaucipir within 30 months. Autopsy diagnosis and Braak NFT Stage of the participants were compared to tau PET imaging findings. Tau PET standardized uptake value ratios (SUVr) were determined by a composite multi-region target comprised of regions of interest (ROI) (amygdala, entorhinal cortex, fusiform, parahippocampal, and inferior temporal and middle temporal gyri) normalized to the bilateral cerebellar crus gray matter (positive when SUVr values > 1.25).

Results: Autopsy diagnoses included AD (N=10), AD (early) (N=1), pathologic aging (N=1), PART (N=3), LBD (N=9), hippocampal sclerosis/TDP (N=1), and probable globular glial tauopathy (N=1). Tau PET categorized all participants in the AD and early AD groups as positive. Five LBD, one PART, and the hippocampal sclerosis/TDP and the probable globular glial tauopathy participants were also tau PET positive. (Figure 1) Those with Braak Stages of 4 or greater were all tau PET positive. (Figure 2)

Conclusions: Positive tau PET signal seen with Flortaucipir with an AD composite multi-region target reflects Braak stage 4 or greater neuropathology. Participants with LBD had positive tau signal in the AD-centric multi region ROI but the signal intensity was low (not greater than 1.5 in this group). Participants with PART, hippocampal sclerosis/TDP, and probable globular glial tauopathy had minimal signal. A secondary pathologic diagnosis of AD or AD spectrum disease can be the cause of minimally positive Flortaucipir signal.

Figure 1. Autopsy diagnoses compared to tau PET SUVr.

Tau PET SUVr was positive in all AD (and early AD) participants (cut-point shown by vertical dotted line). The primary pathologic diagnoses are shown on the "y" axis with the secondary pathologic diagnoses shown by shapes as denoted by those seen in the call-out box.
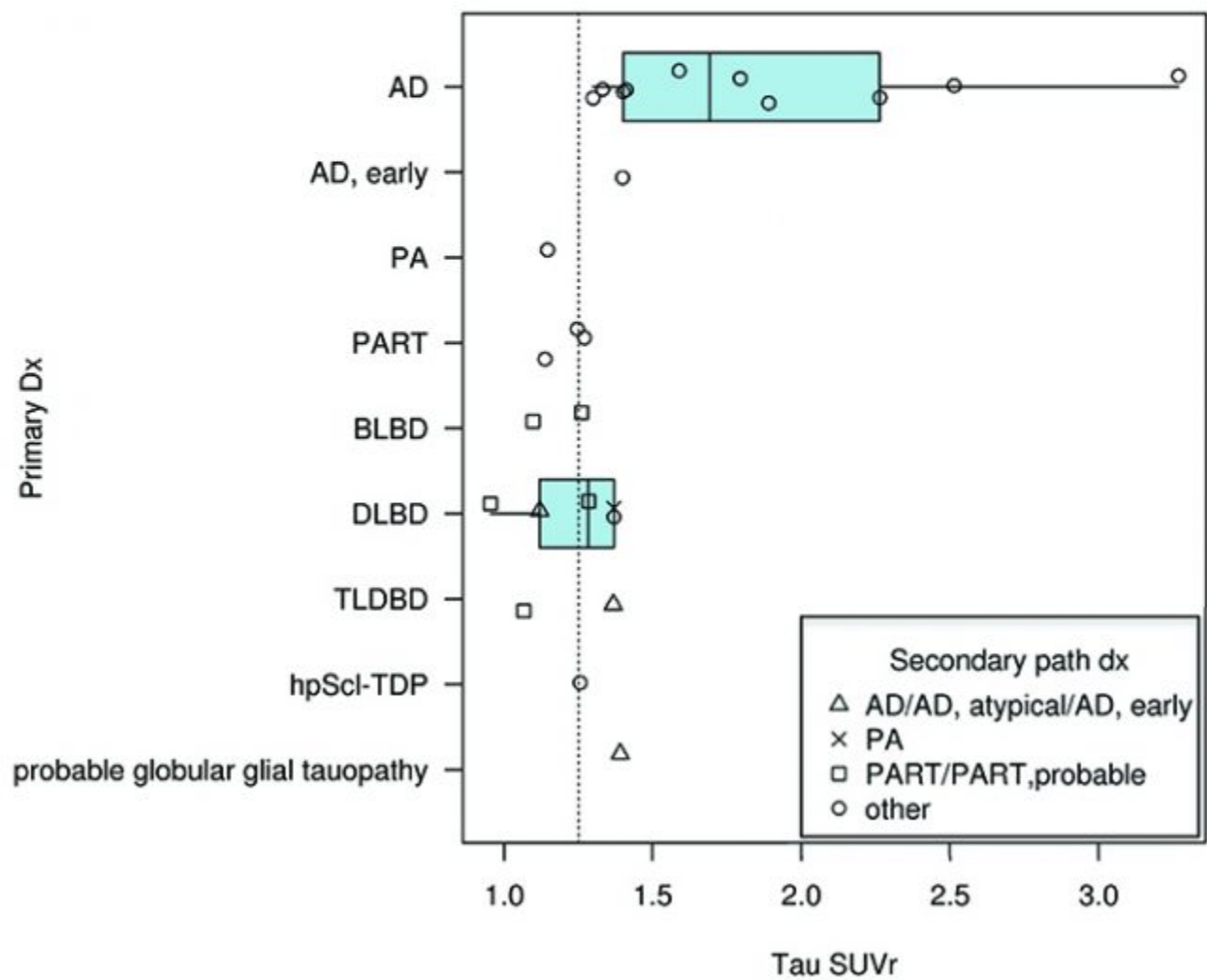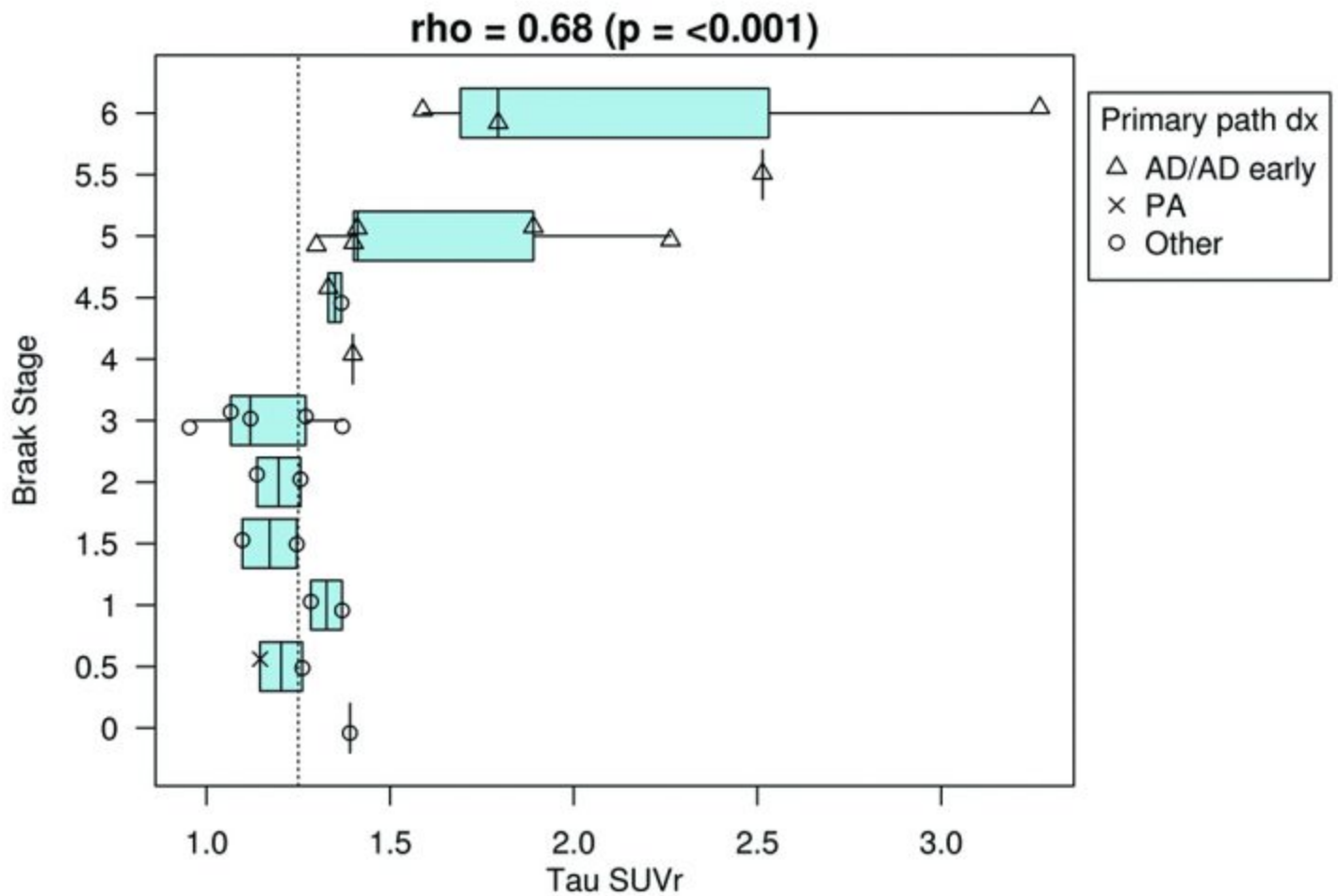
Figure 2. Braak NFT stage compared to tau PET SUVr.

Tau PET SUVr positively correlated with Braak stage. The primary pathologic diagnoses from autopsy are shown by shapes as seen in the call-out box.

Relationships between flortaucipir PET signal and tau neurofibrillary tangle pathology at autopsy

Mark Mintun[1], Michael Devous[1], Adam Fleisher[1], Ming Lu[1], Thomas G. Beach[2], Thomas J. Montine[3], Geidy Serrano[2], Craig Curtis[8], Allison Perrin[4], Stephen Salloway[5], Stephen Thein[6], Charles Wellman[1,7], Ian Kennedy[1], Michael Navitsky[1], Sudeepti Southekal[1], Anupa Arora[1], Patricia Aldea Stevenson[1], Matthew Flitter[1], Michael Pontecorvo[1]

[1]*Avid Radiopharmaceuticals, Philadelphia, PA, US*
[2]*Banner Sun Health Research Institute, Sun City, AZ, US*
[3]*Stanford Unitersity, Stanford, CA, US*
[4]*Banner Alzheimer's Institute, Phoenix, AZ, US*
[5]*Butler Hospital, Providence, RI, US*
[6]*Pacific Research Network, Inc., San Diego, CA, US*
[7]*Hospice of the Western Reserve, Cleveland, OH, US*
[8]*Compass Research, Orlando, FL, US*

Objective: Evaluate the correlation between flortaucipir PET quantitation and global/regional NFT pathology at autopsy

Methods: 67 terminally ill patients underwent PET imaging (20 min acquisition, 80 min after ~370 MBq iv flortaucipir F 18) and were followed to autopsy. The first 3 patients (frontrunners) were considered exploratory and were evaluated prior to conclusion of the study. The remaining 64 cases comprised the primary analysis population (PAP) for this Phase III study.

A 2-expert panel provided a neuropathologic diagnosis following NIA-AA recommendations (Hyman, 2012) for all cases. In the frontrunners, the same tissue blocks were also used to measure phosphorylated paired helical filament (PHF) tau tissue concentrations with an antibody (AT8) capture assay.

PET images were motion- and time-corrected and summed over the 20 min period. For quantitation, images were fitted to MNI template space and VOIs including a weighted large neocortical composite and unweighted AAL regions were applied. SUVr was calculated in the PAP scans using a statistically derived white matter reference region. For the frontrunners, VOIs were also individually drawn in the individual PET scan native space to match the regions sampled for pathology; SUVrs were calculated relative to cerebellum.

Results: In the PAP, the composite SUVr was significantly higher in subjects with Braak V/VI NFT pathology vs subjects with Braak stage 0-4 at autopsy. In the frontrunners, the regional analysis showed highly significant correlation to the PHF tau concentrations in the corresponding brain tissue samples (Figure 1). Additional analyses are ongoing to explore how quantitation of selective regions corresponds to Braak II through IV pathology. Finally, other analyses will explore potential relationships between regional PET results and regional NFT scoring.

Conclusions: While additional data will be reviewed, the results to date suggest quantitative flortaucipir PET may be useful in estimating pattern and density of AD type NFT tau.
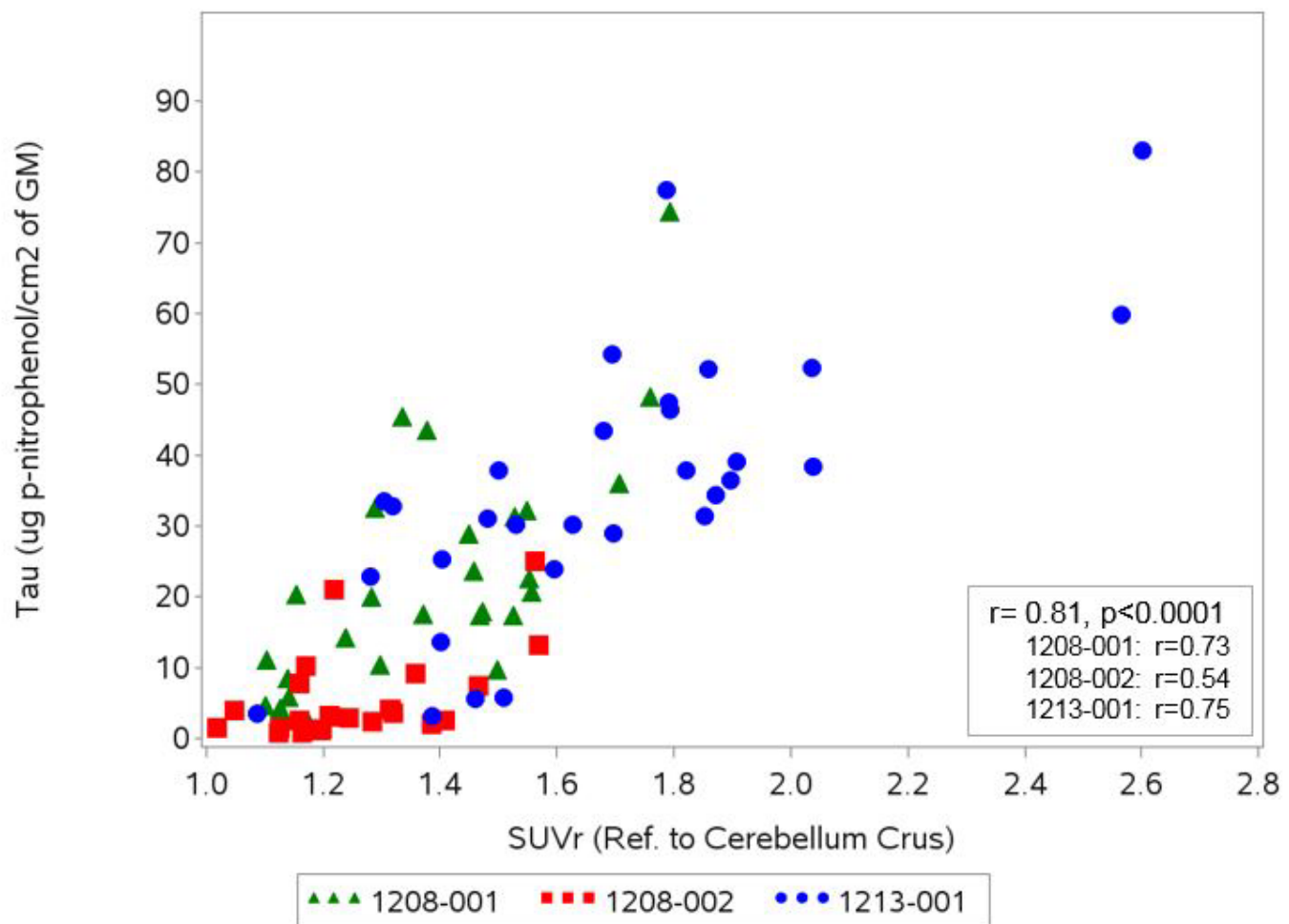
Associations shown between regional flortaucipir SUVr and PHF tau tissue concentration values at autopsy in three front runner participants in the autopsy trial.

Thursday, January 17, 2019 - 12:30 pm - 01:00 pm

Keynote Lecture

Goedert, Michel

Conformers of assembled Tau

Michel Goedert

MRC Laboratory of Molecular Biology, Cambridge, UK

The ordered assembly of tau protein into abnormal filamentous inclusions underlies a large number of human neurodegenerative diseases. Filament morphologies and isoform compositions often differ between diseases. Together with experimental studies, this has led to the suggestion that multiple conformers of aggregated tau exist. Electron cryo-microscopy (cryo-EM) can be used to determine the high-resolution structures of amyloid filaments from human brain. Paired helical and straight tau filaments of Alzheimer's disease are ultrastructural polymorphs. Each filament core is composed of two identical protofilaments extending from G273/304-E380 (in the numbering of the 441 amino acid isoform of human tau), which adopt a combined cross-β/β-helix structure. They comprise the end of the first or second repeat (R1 or R2), the whole of R3 and R4, as well as 12 amino acids after R4. By contrast, the core of the narrow tau filaments of Pick's disease consists of a single protofilament that extends from K254-F378 of three-repeat tau, which adopt a cross-β structure. It comprises the distal 21 amino acids of R1, all of R3 and R4, as well as 10 amino acids after R4. The wide tau filaments of Pick's disease, which are in the minority, consist of two protofilaments linked by anti-parallel stacking of C322-S324. These findings show that filamentous tau protein adopts distinct folds in different human neurodegenerative diseases, establishing the existence of multiple conformers of aggregated tau. We also used cryo-EM to characterise filaments that were assembled from recombinant full-length human tau with three (2N3R) or four (2N4R) repeats in the presence of heparin. Their structures differ from those of Alzheimer's and Pick's diseases, which have larger cores with different repeat compositions.

Keywords: *Conformers, assembled Tau*

Thursday, January 17, 2019 - 02:45 pm - 04:15 pm

Podium Session

Session 5: Modeling amyloid and tau relationships and spread

CHAIRS: Michel Grothe, Elizabeth Mormino

02:45 pm - 04:15 pm	Session 5: Modeling amyloid and tau relationships and spread	CHAIRS: Elizabeth Mormino, Stanford University, Palo Alto, CA, US Michel Grothe, German Center for Neurodegenerative Diseases, Rostock, Germany	Page
2:45	Data-driven characterization of cross-sectional and longitudinal molecular imaging in aging and Alzheimer's disease	**Hugo Botha**, Mayo Clinic, Rochester, MN, US	308
3:00	The cortical site of origin and initial spread of medial temporal tauopathy assessed with positron emission tomography	**Justin Sanchez**, Massachusetts General Hospital, Boston, MA, US	312
3:15	Amyloid and tau pathology are related to functional signal homogeneity and isolation of the hippocampus in cognitively healthy older adults	**Theresa Harrison**, University of California Berkeley, Berkeley, CA, US	316
3:30	Cross-method identification of earliest regions to display amyloid burden	**Isadora Lopes Alves**, VU University Medical Center, Amsterdam University Medical Centers, Amsterdam, The Netherlands	319
3:45	Tau organization precedes Aβ deposition across the brain cortex	**Tharick Pascoal**, McGill University, Montreal, QC, Canada	323
4:00	Increased task activation and amyloid independently explain advanced tau pathology in older adults	**Anne Maass**, German Center for Neurodegenerative Diseases, Magdeburg, Germany	326
04:15 pm - 04:45 pm	Discussion		

Data-driven characterization of cross-sectional and longitudinal molecular imaging in aging and Alzheimer's disease

<u>Hugo Botha</u>[1], Jonathan Graff-Radford[1], Mary Machulda[1], Scott Przybelski[1], Matthew Senjem[1], Christopher Schwarz[1], Prashanthi Vemuri[1], Kejal Kantarci[1], Bradley Boeve[1], Ronald Petersen[1], David Knopman[1], Val Lowe[1], Clifford Jack Jr[1], David Jones[1]

[1]*Mayo Clinic, Rochester, MN, US*

Background: Quantifying amyloid and tau accumulation remains challenging, especially in light of phenotypic heterogeneity and variability in off-target binding. We used data driven approach to identify Alzheimer's disease (AD) related and off-target amyloid and tau PET binding patterns. We show the utility of this technique for cross sectional and longitudinal group analyses, as well as the characterization of participant level findings.

Methods: Spatial independent component analysis (ICA) was used to characterize the patterns of amyloid (11C-PiB) and tau (AV-1451) PET binding in a large sample spanning the aging-Alzheimer's disease spectrum. Parameters from the ICA decomposition were then used to project longitudinal data points into the ICA space. Component scores were used to assess the relationship between behavioral measures and the magnitude/extent of tau PET binding.

Results: 880 participants were included in the cross-sectional analysis (734 CN, 56 MCI, 85 AD, 5 other), of whom 87 had longitudinal data available. Four independent amyloid PET components, including one AD component, and thirty-four tau PET components were identified, including nine AD components (Figure 1). Cross-sectional scores on the temporal component correlated with age in CNs, but not in impaired participants, and higher loads were associated with greater cognitive impairment (Figure 2). Participant level amyloid and tau component scores appeared to capture the heterogeneity in on-target and off-target binding (Figure 2). Comparing scores on the AD amyloid and temporal tau components revealed a sigmoidal relationship in both cross-sectional and longitudinal analyses (Figure 3).

Conclusions: The data driven approach was able to capture the spatial pattern and uptake magnitude. Using this framework, we were able to show the sigmoidal relationship between amyloid and temporal tau uptake. Specifically, initial low-level temporal tau accumulation in the absence of amyloidosis, followed by amyloid accumulation without much change in tau, before pronounced tau accumulation occurs with little change amyloid.
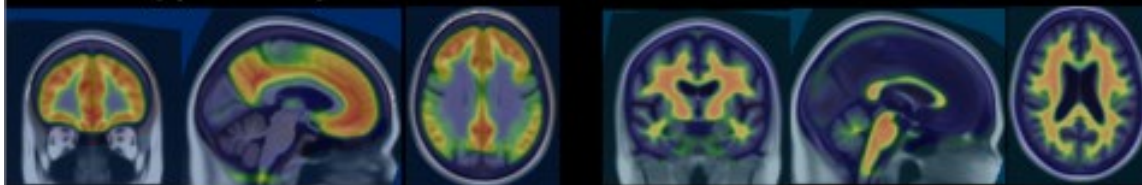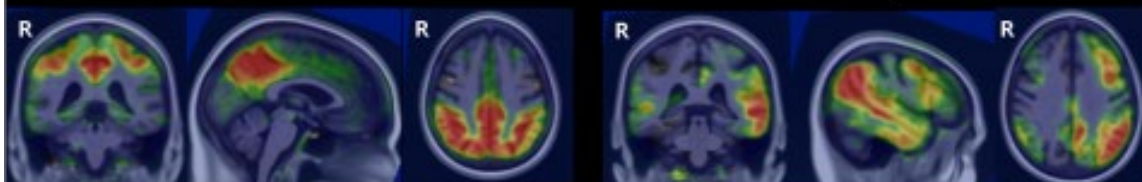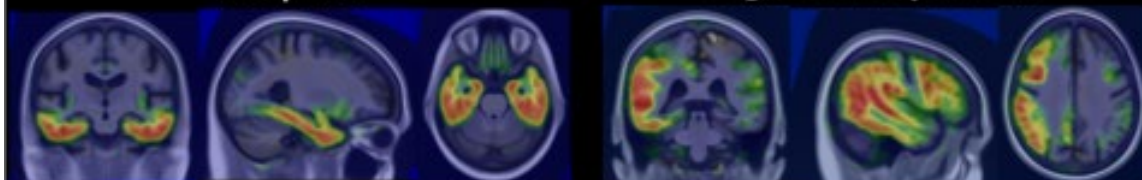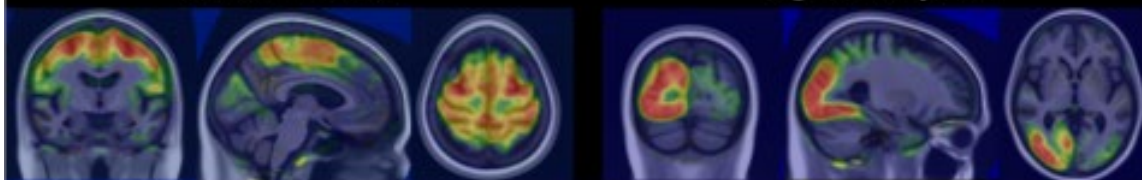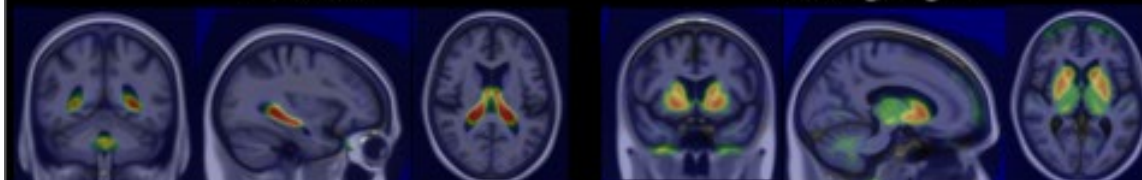
Figure 1: Representative views of notable Alzheimer's disease and off-target components Amyloid PET ICA revealed a single, AD-related component which included regions typically sampled when calculating global PiB SUVRs. In fact, scores on this component were highly correlated with global PiB SUVRs (R^2 0.96). Also shown is the white matter amyloid component. The temporal tau component included core Braak-staging areas. Several tau components appeared to capture atypical AD phenotypes (e.g. occipital, frontal parietal) and scores on these components were negative correlated with age.
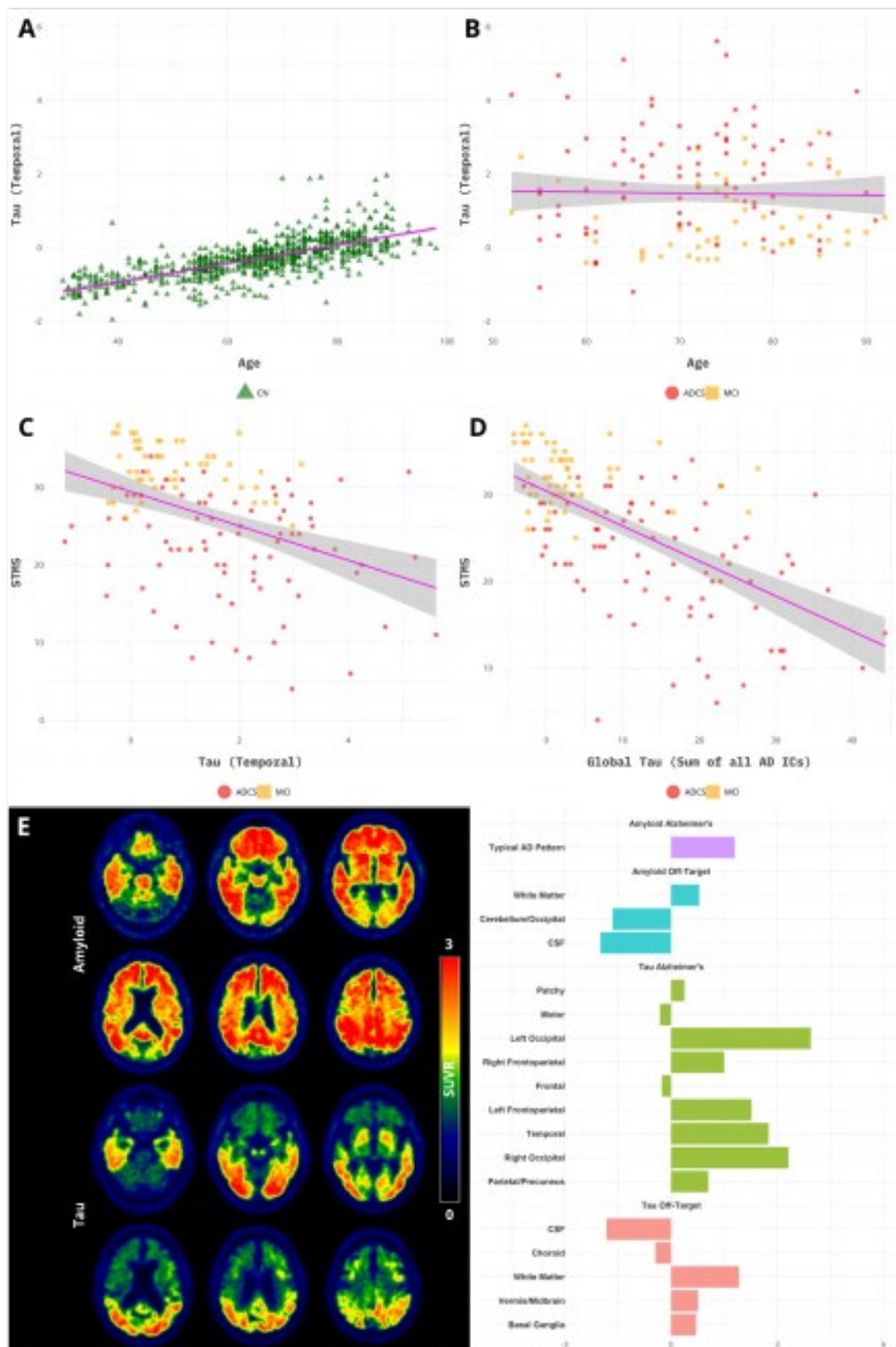
Figure 2: Relationship between clinical data and component scores

(A) Among cognitively normal participants, increasing age was associated with higher scores on the temporal tau component (R^2 0.51, p<0.001), possibly reflecting age-related tau accumulation. (B) There was no age-score relationship among cognitively impaired patients for this component. (C) Higher temporal tau IC scores were associated with worse performance on the short test of mental status (STMS) (R^2 0.15, p<0.001) (D) However, prediction of cognitive performance improved when total IC score for all AD-related components were considered (R^2 0.35, p<0.001). (E) PET images for a participant with posterior cortical atrophy. The breakdown of scores for core AD-related and off-target components capture the spatial pattern of tau PET binding, with the highest scores in the occipital components.
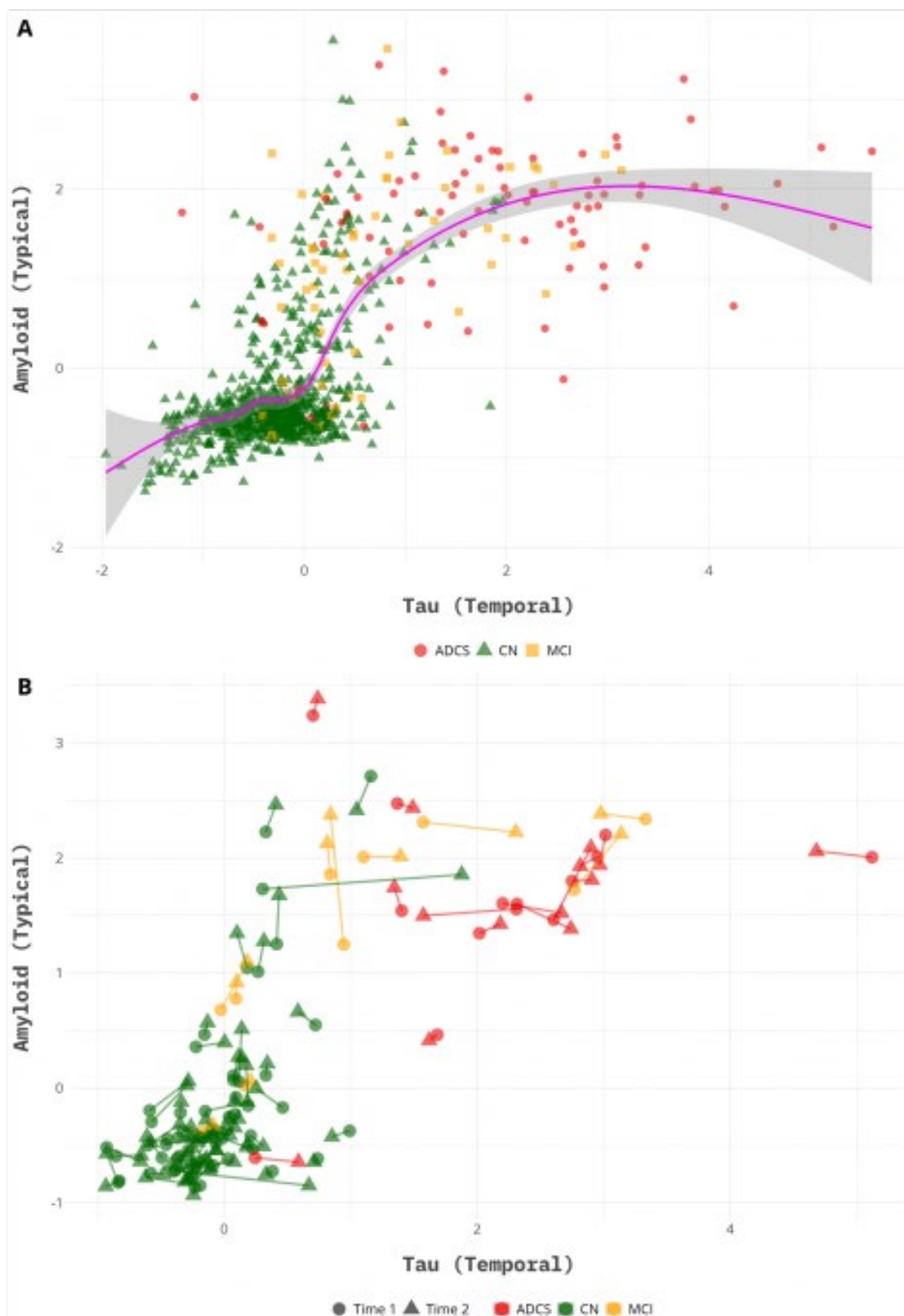
Figure 3: Sigmoidal relationship between scores on the temporal tau and typical amyloid components
(A) Cross sectional scores on the typical AD amyloid and the temporal tau components are shown, fitted with a generalized additive model with penalized regression splines, revealing a sigmoidal relationship. (B) Amyloid and temporal tau scores for participants with two time-points, supporting the sigmoidal relationship suggested by the cross-sectional analysis. Note the increasing amyloid scores with little to no change in tau scores in the middle section, as well as the increase in tau with relatively stable amyloid scores in the upper portion.

The cortical site of origin and initial spread of medial temporal tauopathy assessed with positron emission tomography

Justin Sanchez[1], Alex Becker[1], Tobias Estime[1], Samantha Katz[1], Danielle Mayblyum[1], Kirsten Moody[1], Alexa Beiser[4,5], Claudia Satizabal[4,5], Charles DeCarli[6], Ron Killiany[4], Heidi Jacobs[1,3], Shu Jiang[1], Aaron Schultz[1], Yakeel Quiroz[1,7], Dorene Rentz[1,2], Reisa Sperling[1,2], Sudha Seshadri[4,5], Jean Augustinack[1], Julie Price[1], Keith Johnson[1,2]

[1]*Massachusetts General Hospital, Boston, MA, US*
[2]*Brigham and Women's Hospital, Boston, MA, US*
[3]*Maastricht University, Maastricht, The Netherlands*
[4]*Boston University School of Medicine, Boston, MA, US*
[5]*The Framingham Heart Study, Framingham, MA, US*
[6]*University of California, Davis, Davis, CA, US*
[7]*Grupo de Neurociencias, Universidad de Antioquia, Medellin, CO*

Background: Tau-PET enables in-vivo characterization of the magnitude and anatomic distribution of tauopathy. We employ a combination of cross-sectional and longitudinal data in regions-of-interest and surface vertices to assess the earliest detectable PET evidence of pathologic cortical tau deposition and propagation.

Methods: 443 Harvard Aging Brain and Framingham Heart Study participants underwent 18F-flortaucipir (FTP) and 11C-PiB-PET; 104 had follow-up FTP-PET (Table1). We identified rhinal cortex (RC) on the basis of MTL sulcal anatomy, hypothesizing it to be the first site of PET-detectable cortical tauopathy, and inferior temporal cortex (IT) as a proxy for neocortical tauopathy. Gaussian mixture modeling (GMM) identified subgroups with elevated regional and vertex-wise FTP SUVr (white-matter reference, PVC) in cohorts defined by Ab and diagnosis. Baseline and follow-up scans were classified by GMM as RC+/- and IT+/-; exact binomial test compared the likelihood of different transitions. Relationship between baseline PiB and annualized FTP change (dTau) was assessed with linear regression.

Results: In low-Ab clinically normal (CN) participants, GMM identified a high-RC-tau mode that was older (p=0.001) and had higher PiB (p=0.039) than the low-RC-tau low-Ab mode (Fig1A). By contrast, IT-tau was unimodal in low-Ab (Fig1B). Both RC- and IT-tau were bimodal in high-Ab CN; IT-tau was bimodal in MCI-AD, whereas RC-tau was unimodal. This pattern was confirmed with vertex-wise analysis (Fig1C-D). On follow-up, the most likely transitions were from RC-/IT- to RC+/IT- and from RC+/IT- to RC+/IT+ (Fig2A). Baseline PiB was associated with dTau in IT (p<0.001) but not RC (p=0.472) (Fig2B).

Conclusions: These cross-sectional and longitudinal data demonstrate a temporal progression of pathologic tau deposition beginning in rhinal cortex, spreading to inferior temporal cortex in the presence of high levels of beta-amyloid, and continuing to additional cortical regions with clinical impairment. Future analyses will investigate associations between RC tau, age, and prospective amyloid-mediated AD pathologic change.

	Low-Aβ CN	High-Aβ CN	MCI-AD
Baseline cohort (N=443)			
N	327	61	55
Age	60.8 ± 14.6 (21-93)	75.3 ± 7.5 (58-92)	71.4 ± 9.5 (50-90)
Females, N (%)	170 (52)	36 (59)	23 (42)
Education (Years)	15.2 ± 3.2 (2-20)	16.1 ± 2.7 (12-20)	16.3 ± 2.5 (12-20)
Neocortical (FLR) PiB (PVC DVR)	1.14 ± 0.07 (0.9-1.4)	1.9 ± 0.39 (1.4-2.9)	2.27 ± 0.6 (1.1-3.4)
Longitudinal cohort (N=104)			
N (% of baseline N)	66 (20)	27 (44)	11 (20)
Age	72.1 ± 12.3 (28-90)	77.6 ± 5.2 (68-88)	65.5 ± 10.5 (50-86)
Females, N (%)	42 (64)	14 (52)	3 (27)
Education (Years)	15 ± 3.6 (5-20)	16.3 ± 2.8 (12-20)	15.5 ± 2.6 (12-20)
Neocortical (FLR) PiB (PVC DVR)	1.16 ± 0.07 (1.0-1.4)	2.08 ± 0.41 (1.4-2.9)	2.4 ± 0.28 (1.9-2.8)
FTP follow-up time (Years)	2.3 ± 0.5 (1.1-3.5)	1.9 ± 0.5 (0.7-3.1)	1.9 ± 1.0 (0.9-3.6)

Table 1: Participant characteristics
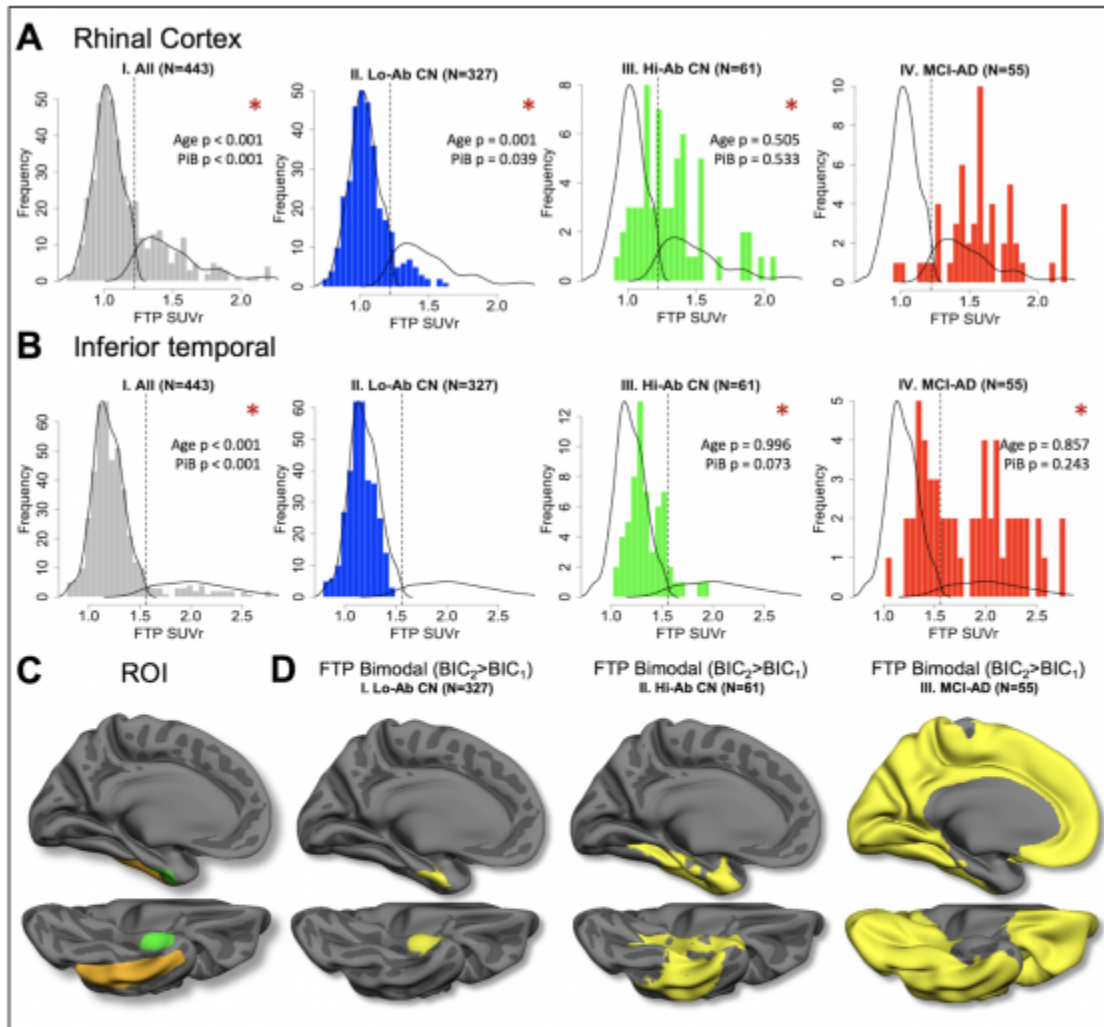
Figure 1: Cross-sectional tau PET bimodality

(A-B) Rhinal cortex tau, but not inferior temporal tau, is bimodal in low-Aβ. Distribution (density and histogram) of FTP PET SUVrs in full sample (I) and cohorts defined by Aβ and diagnosis (II-IV); density estimates (black traces) correspond to full sample distribution; dashed vertical lines indicate thresholds derived from full sample two-component GMM. * indicates bimodal distributions (likelihood-ratio test with bootstrap $p<0.01$); p-values for t-tests of age and PiB differences between high- and low-FTP modes are given for bimodal distributions.

(C-D) Vertex-wise analysis shows anatomic specificity of cohort bimodality. (C) RC (green) and IT (orange) labels projected on left hemisphere surface in medial (top) and inferior (bottom) views. (D) Surface maps showing vertex-wise tests of FTP bimodality in same cohorts (I-III) as (A) and (B) II-IV; yellow indicates vertices where FTP distribution is bimodal ($p<0.005$). In low-Aβ CN (I), bimodality is anatomically restricted to a set of vertices surrounding anterior collateral sulcus, corresponding to RC; in hi-Aβ CN, FTP bimodality extends to neocortex (IT) is seen; in MCI-AD, FTP bimodality extends to rest of cortex.
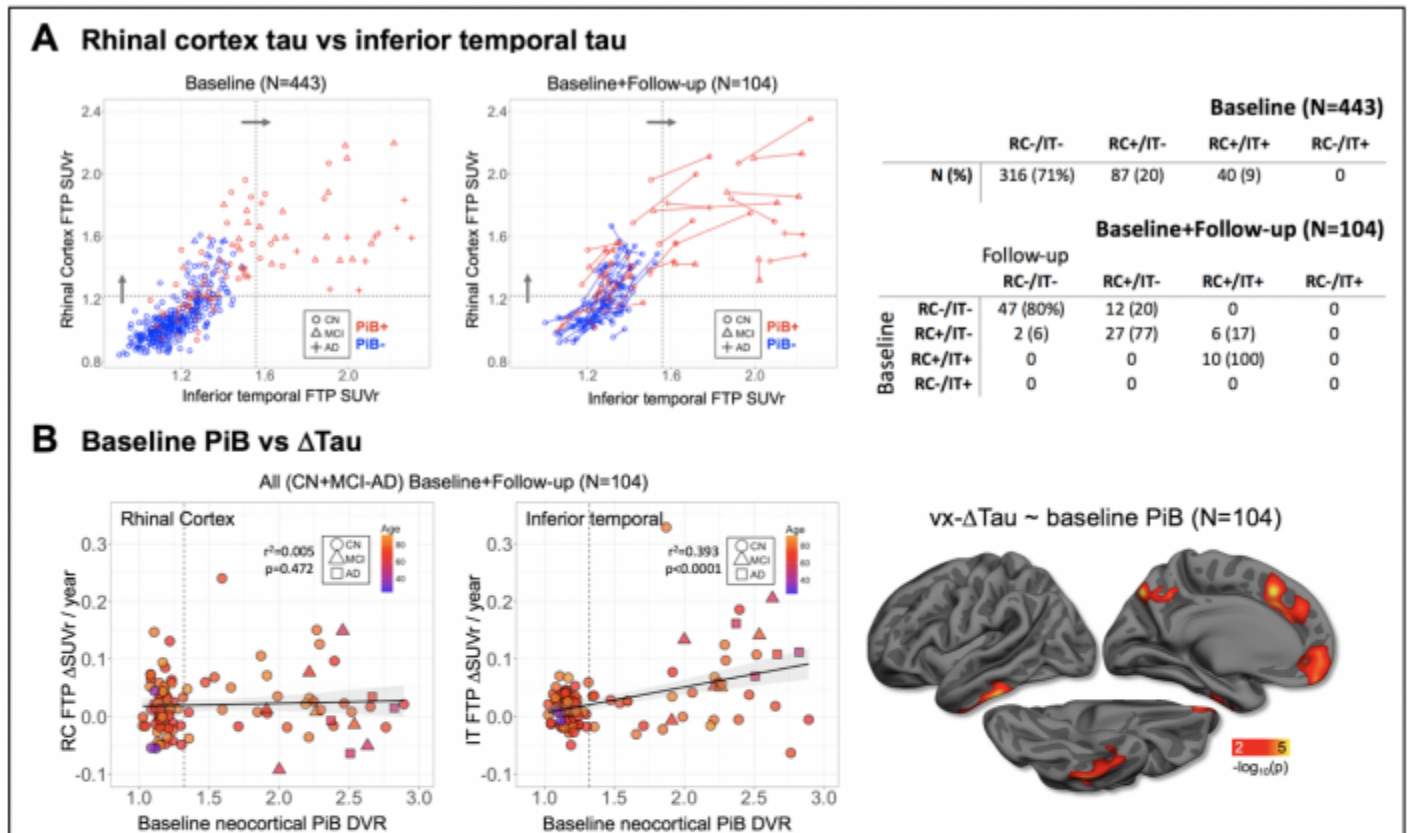
Figure 2: Longitudinal tau PET measures

(A) Rhinal cortex tau accumulation precedes inferior temporal cortex tau accumulation. Baseline (left) and baseline + follow-up (middle) scatter plots of inferior temporal (IT) vs rhinal cortex (RC) tau; dotted lines indicate SUVr thresholds from 2-component GMM in full sample for each ROI; diagnosis (shape) and PiB status (color) encoded. Frequencies (N%) of participants of each tau-PET classification, based on RC and IT tau, at baseline (top) and at follow-up for a given baseline tau-PET classification (bottom). The most likely transitions observed were from RC-/IT- to RC+/IT- (p<0.001) and from RC+/IT- to RC+/IT+ (p=0.035).

(B) Baseline PiB predicts subsequent tau accumulation in inferior temporal, but not rhinal cortex. Scatter plots of baseline neocortical (FLR) PiB DVR (PVC) vs annualized FTP SUVr change (ΔTau) in RC (left) and IT (center); vertical dashed line indicates high-Aβ threshold (1.3). Vertex-wise analysis (right) confirms baseline PiB is associated with ΔTau in neocortex, but not medial temporal allocortex.

Keywords: *tau PET, longitudinal, medial temporal, rhinal cortex*

Amyloid and tau pathology are related to functional signal homogeneity and isolation of the hippocampus in cognitively healthy older adults

Theresa Harrison[1], Jenna Adams[1], Anne Maass[1,2], Richard Du[1], Suzanne Baker[3], William Jagust[1,3]

[1]*University of California Berkeley, Berkeley, CA, US*
[2]*German Center for Neurodegenerative Diseases, Magdeburg, Germany*
[3]*Lawrence Berkeley National Laboratory, Berkeley, CA, US*

Background: The hippocampus is targeted by tau pathology in aging and AD. We used measures of hippocampal local resting state fMRI (rs-fMRI) signal synchrony with PET measures of amyloid and tau to explore mechanisms through which tau may exert functional and cognitive effects on the aging brain.

Methods: Eighty-nine older adults (OA; 77±6.1 years, 63% F, 44% PiB+) and 50 young adults (YA; 25±4.4 years, 50% F) underwent 3T rs-fMRI; OA also had PiB and FTP scans. rs-fMRI data were processed to calculate voxelwise regional homogeneity (ReHo), a measure of local functional synchrony, and for conventional functional connectivity (FC) analyses. Mean group ReHo images were created for YA and OA using DARTEL tools for normalization. Mean ReHo in native space was calculated in FreeSurfer-derived ROIs. Global PiB DVR and partial volume corrected FTP SUVR regional values were calculated for OA. Memory performance was measured using an episodic memory domain score.

Results: In YA, areas of high ReHo include lateral parietotemoporal junction, lateral frontal, precuneus and primary visual areas (Fig 1A). In contrast, high ReHo regions in OA include the temporal lobe (Fig 1B). ROI data also reveal that ReHo increases with age in temporal lobe, including hippocampus (r=0.35, p<0.001). Higher hippocampal ReHo is predicted by PiB (p=0.02) and FTP (p=0.01) in models adjusting for age, sex and hippocampal volume (Fig 2). Higher hippocampal ReHo is associated with lower FC between hippocampus and cortex (r=-0.3 p=0.004). Worse memory performance is predicted by higher hippocampal ReHo (r=-0.29, p=0.01, Fig 3).

Conclusions: ReHo increases with aging in the temporal lobe, including the hippocampus. Higher hippocampal ReHo is associated with greater burdens of amyloid and tau pathology, decreased functional connectivity of the hippocampus to cortical regions and worse memory. ReHo may be an important measure of hippocampal functional isolation leading to behavioral deficits.
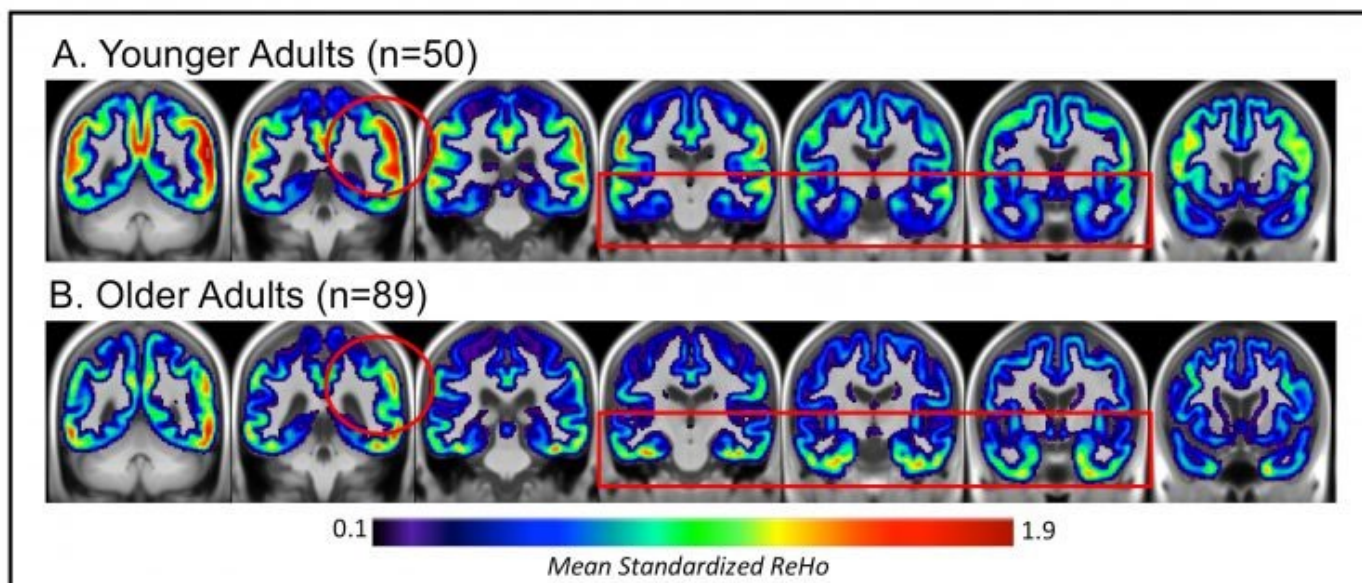
Figure 1. Patterns of high and low ReHo change with age. A) Voxelwise group mean standardized ReHo in younger adults (YA) in group-specific gray matter (GM) mask. **B)** Voxelwise group mean standardized ReHo in older adults (OA) in group-specific GM mask. On average, areas of highest ReHo in YA have lower ReHo values in OA (red circles). ReHo increases in temporal lobe in OA (red boxes).
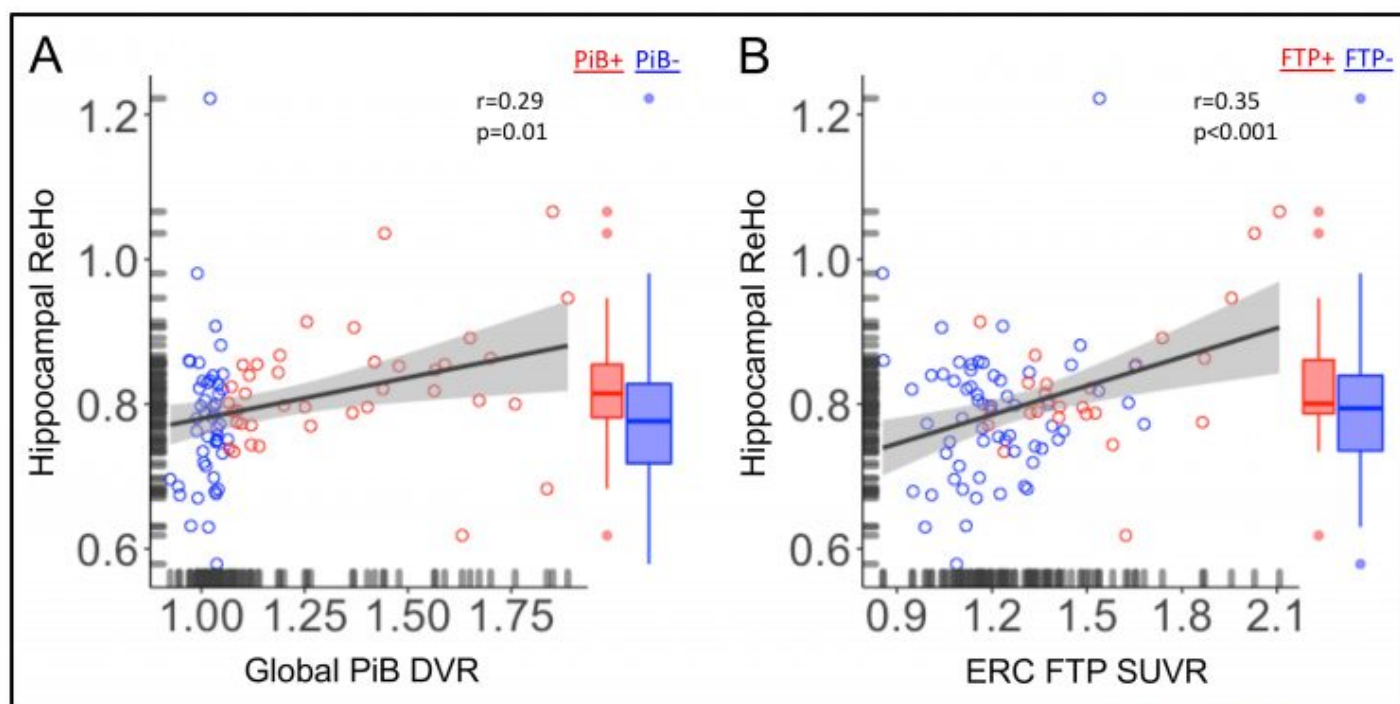
Figure 2. Amyloid- and tau-PET measures are related to hippocampal ReHo. A) Global PiB DVR (PiB+ in red, PiB- in blue; threshold DVR=1.065) predicts hippocampal ReHo. This relationship remains significant in a model adjusting for age, sex and hippocampal volume. **B)** Entorhinal flortaucipir (ERC FTP) SUVR (FTP+ in red, FTP- in blue; threshold SUVR=1.26 in Braak III/IV) predicts hippocampal ReHo. This relationship remains significant in a model adjusting for age, sex and hippocampal volume.
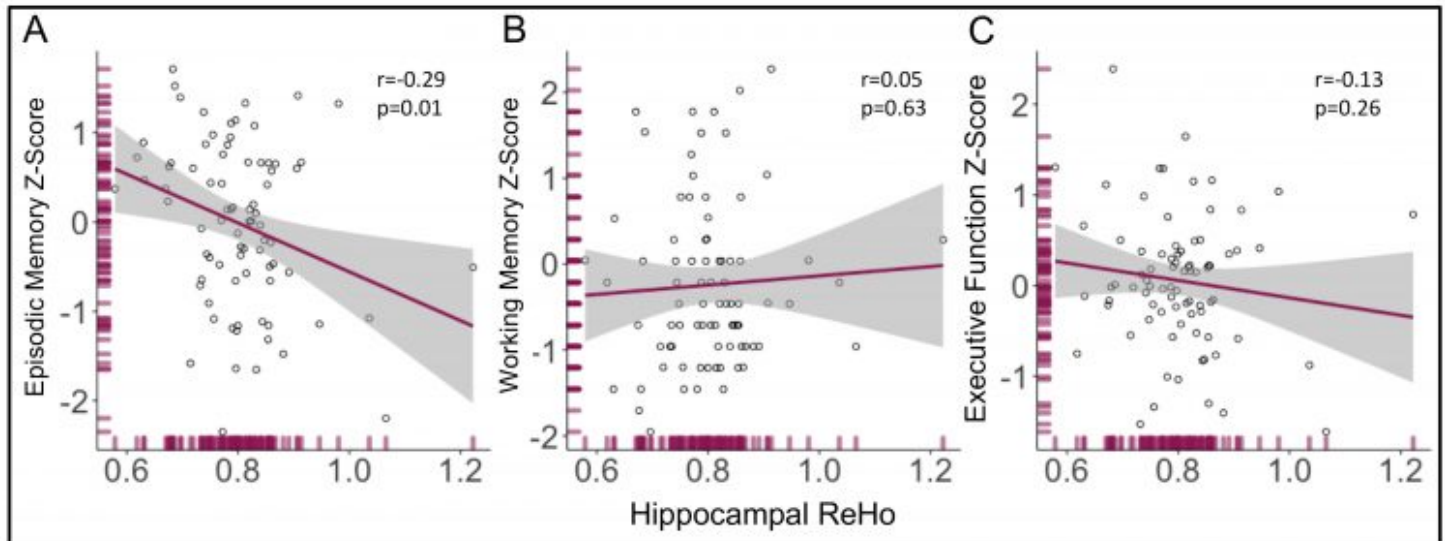
Figure 3. Hippocampal ReHo is related to episodic memory but not to working memory or executive functioning. A) ReHo in the hippocampus predicts an episodic memory z-score comprised of visual and verbal short and long delay recall performance. This relationship is still significant (p=0.02) in a model that adjusts for age, sex and hippocampal volume. There is no significant relationship between hippocampal ReHo and a working memory z-score based on digit symbol performance **(B)** or an executive functioning z-score comprised of digit symbol, Trails B-A and Stroop performance **(C)**.

Cross-method identification of earliest regions to display amyloid burden

Isadora Lopes Alves[1], Leon Aksman[2], Marco Lorenzi[3], Lyduine Collij[1], Fiona Heeman[1], Gemma Salvadó[4], Pawel Markiewicz[2], Frederik Barkhof[1,2], on behalf of the AMYPAD Consortium

[1]Department of Radiology and Nuclear Medicine, VU University Medical Center, Amsterdam Universy Medical Centers, Amsterdam, The Netherlands
[2]Institute of Neurology and Healthcare Engineering, University College London, London, UK
[3]Asclepios Research Project, Université Côte d'Azur, Inria, Nice, France
[4]BarcelonaBeta Brain Research Center, Barcelona, Spain
[5]This work has received support from the EU-EFPIA Innovative Medicines Initiatives 2 Joint Undertaking (grant No 115952), Brussels, Belgium

Background: Brain amyloid-β plaque accumulation might be the first detectable pathological change in Alzheimer's disease. Understanding of the accumulation process itself is limited, while increasingly relevant for anti-amyloid trials. This study applied two independent methodologies to determine the earliest changes detectable with amyloid PET.

Methods: [^{11}C]PIB scans of 493 cognitively normal (CN) subjects in the OASIS-3 data-set were included, and regional standard uptake value ratios (SUVR) were extracted using the PET unified pipeline (https://github.com/ysu001/PUP). Next, two methods were used to determine the ordering of regional pathology observable in amyloid PET. The first was a frequentist approach (FA), determining the regional frequency of positivity across the population and assuming higher frequency reflects earlier involvement. Regional positivity was determined when SUVR>1.31. The second was the probabilistic and data-driven event-based model (EBM), where the probability of biomarker abnormality is determined from the observed distributions across groups (-/+ on global amyloid PET). The resulting ordering of regional amyloid abnormalities was compared between methods.

Results: The FA shows the cingulate, precuneus and orbitofrontal as the earliest regions displaying amyloid burden (Figure 1), while EBM identified three blocks of events (Figure 2): the first corresponding to FA plus lateral parietal, frontal and lateral temporal, the second involving insula, and the third affecting remaining temporal and occipital regions. In addition, the distributions between groups (global +/-) observed in the EBM algorithm (Figure 3) point to cingulate, precuneus, orbitofrontal and insula as regions where signal is already higher even among amyloid negative scans, supporting their earlier involvement.

Conclusion: Two independent methodologies point to cingulate, precuneus and orbitofrontal as the first regions to show amyloid burden, even prior to global amyloid positivity. These results indicate the possibility of detecting amyloid pathology at the regional level, supporting earlier diagnosis and targeted inclusion of CN subjects in anti-amyloid preventive trials.
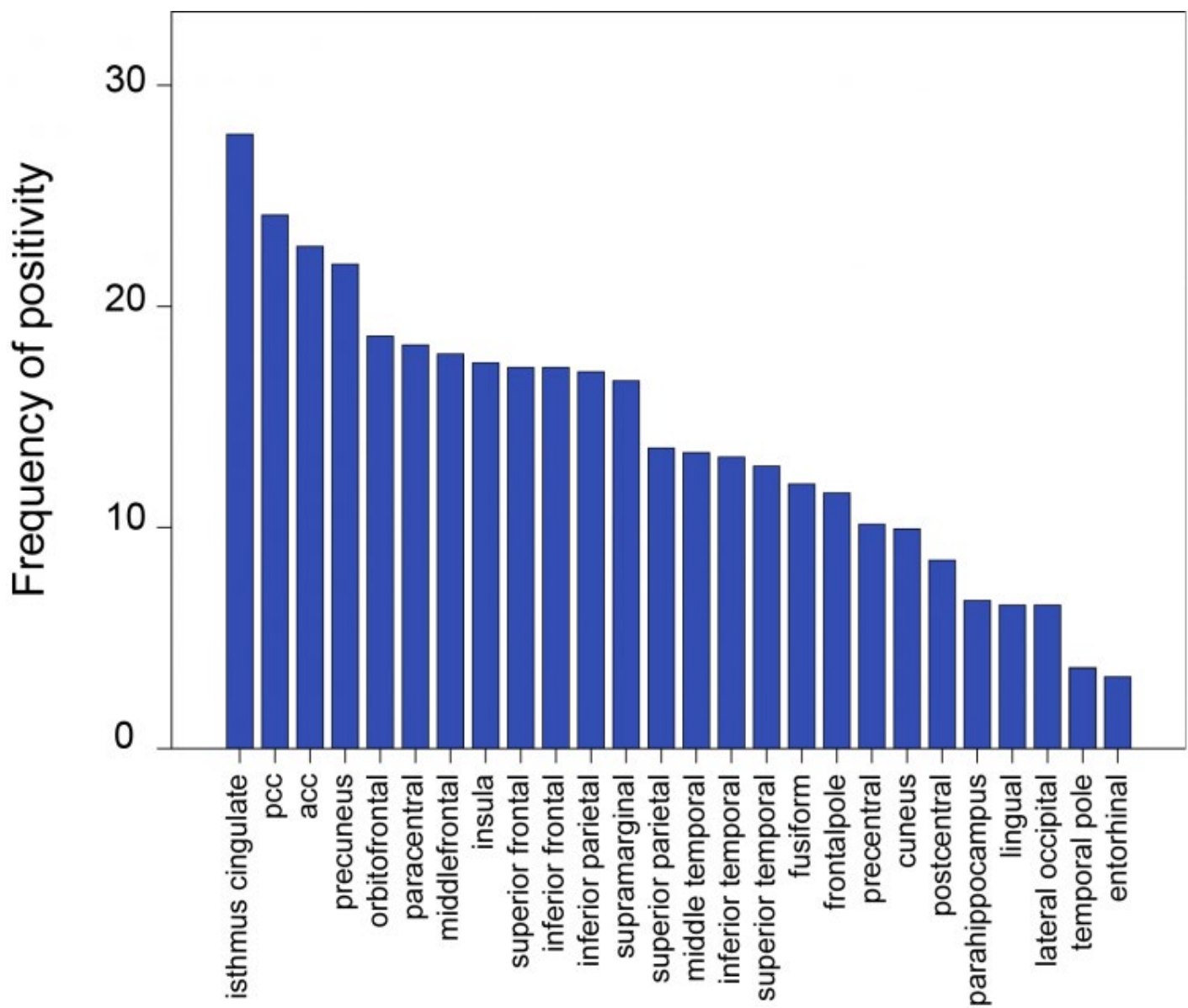
Figure 1. *Frequency of regional positivity across 493 cognitively healthy subjects. A global cut-off of 1.31 was applied to all regions equally.*
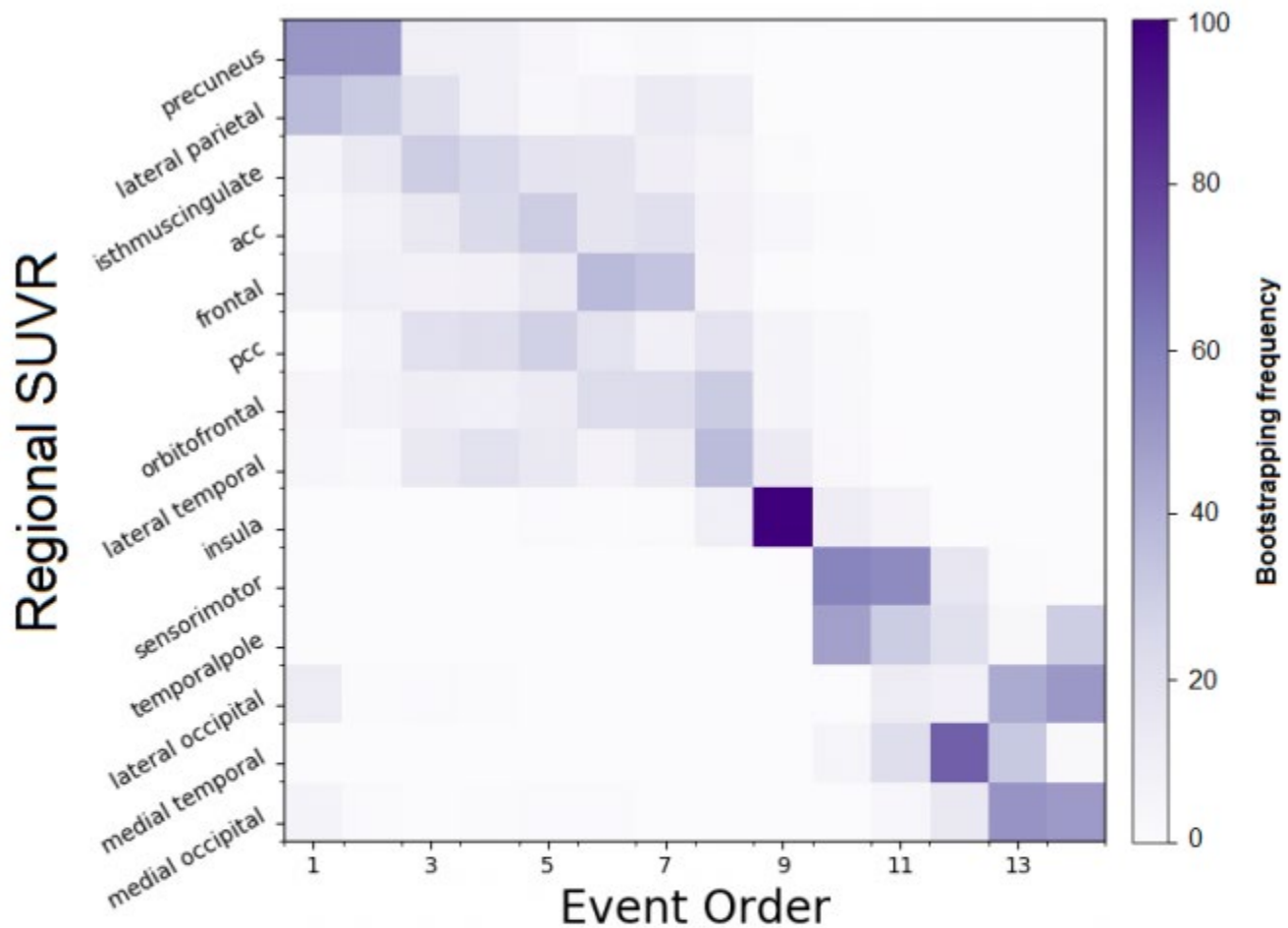
Figure 2. EBM biomarker ordering of the path towards global amyloid positivity. Effects of sex, APOE4 carriership and race were removed via a general linear model. A mixture of two normal distributions was fitted to each biomarker (see Figure 3), describing the likelihood of an abnormal measurement given either normal or abnormal global SUVR. EBM finds the most likely biomarker ordering using a probability function that relies on these distributions rather than pre-specified abnormality cut-points.
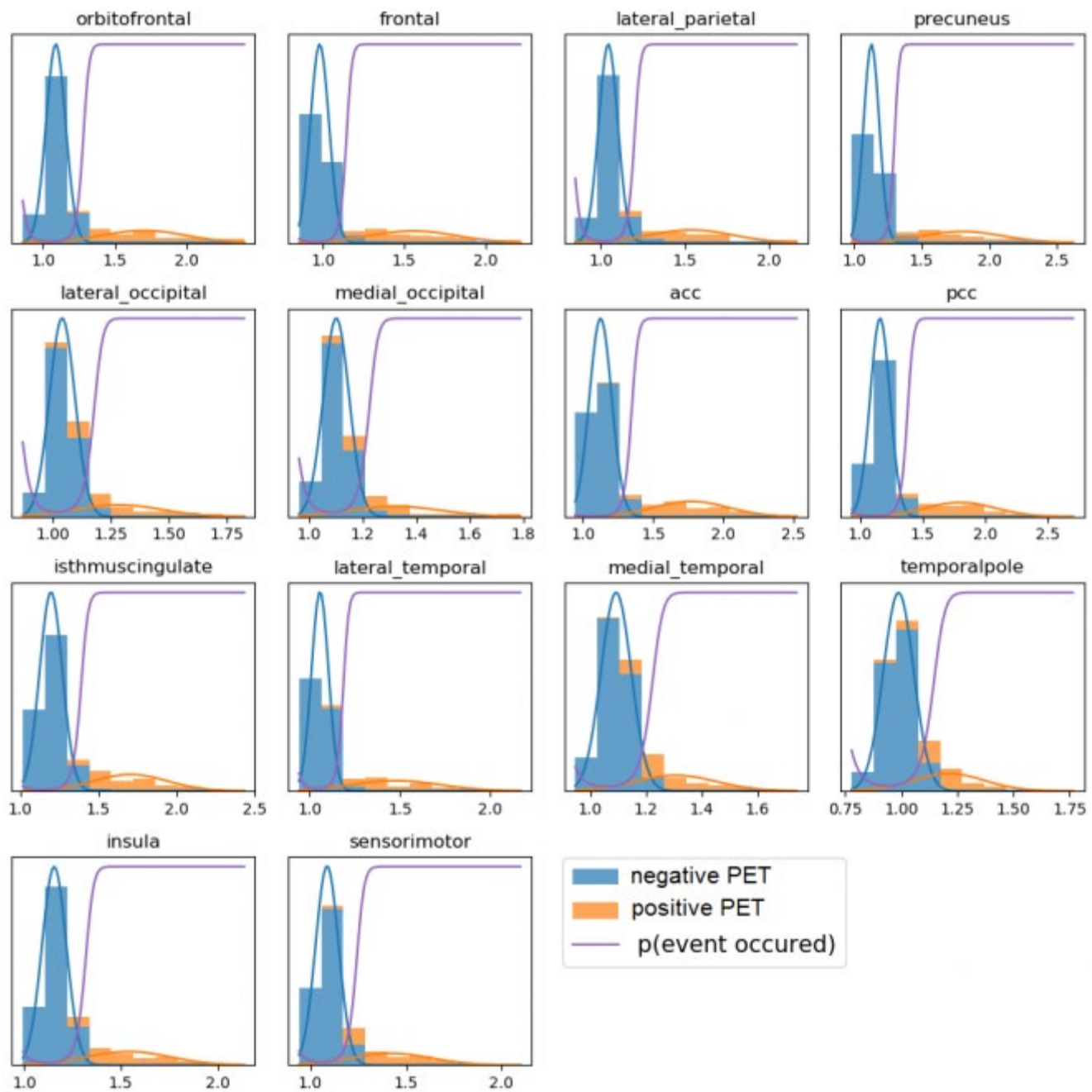
Figure 3. Regional SUVR distributions describing the likelihood of an abnormal measurement given either negative or positive global SUVR.

Tau organization precedes Aβ deposition across the brain cortex

Tharick Pascoal[1], Mira Chamoun[1], Andréa Benedet[1], Guilherme Schu[1], Min Su Kang[1], Sulantha Mathotaarachchi[1], Joseph Therriault[1], Firoza Lussier[1], Cecile Tissot[1], Emilie Thomas[1], Jean-Paul Soucy[1], Eduardo Zimmer[1], Serge Gauthier[1], Pedro Rosa-Neto[1]

[1]*McGill University, Montreal, QC, Canada*

Background: Although the most widely accepted model of Alzheimer's disease (AD) progression suggest that amyloid triggers a cascade of events leading to dementia, histopathological evidence showed tau before amyloid deposition in some brain regions. Histopathological studies suggest tau neuroanatomical signatures associated with AD, which initiate in the transentorhinal cortex spreading to the neocortex. Here, using a tau tracer with sub-nanomolar affinity to tangles and a novel statistical framework, we tested the hypothesis that subthreshold tau organization starts before amyloid deposition.

Methods: We studied 146 individuals across the AD spectrum (Young=26(mean age=44y.o), Elderly CN = 59 (mean age=74y.o), MCI=29, AD=24) with [18F]AZD4694 and [18F]MK-6240 (standardized uptake value ratios (SUVRs) used the cerebellum grey matter as the reference region). Firstly, we subsample randomly PET data of subjects 10000 times, generating 10000 networks for a group of interest. Afterward, using the generated networks, we define a representative MBN as being the group-wise mean Pearson correlation matrix FDR corrected at $P < 0.05$.

Results: We found that amyloid negative young and elderly CN individuals presented visually similar patterns of [18F]MK-6240 uptake (Fig.1), whereas MCI and AD individuals showed clear binding in posterior cingulate, precuneus, temporal, and parietal cortices. In MCI and AD, network analysis revealed a clear pattern of amyloid and tau organization in the regions where these proteinopathies were abnormal in these groups. Although amyloid did not present cortical organization in young, elderly CN amyloid negative individuals, tau pathology showed organization within brain regions corresponding to Braak stages V (Fig.2).

Conclusions: Our finding suggests that tau organization occurs in brain regions proposed by Braak to be affected by tau pathology in late AD stages before any evidence of amyloid deposition. Whereas subthreshold tau accumulation starts first, the presence of amyloid deposition is necessary for the development of high tau pathological levels.
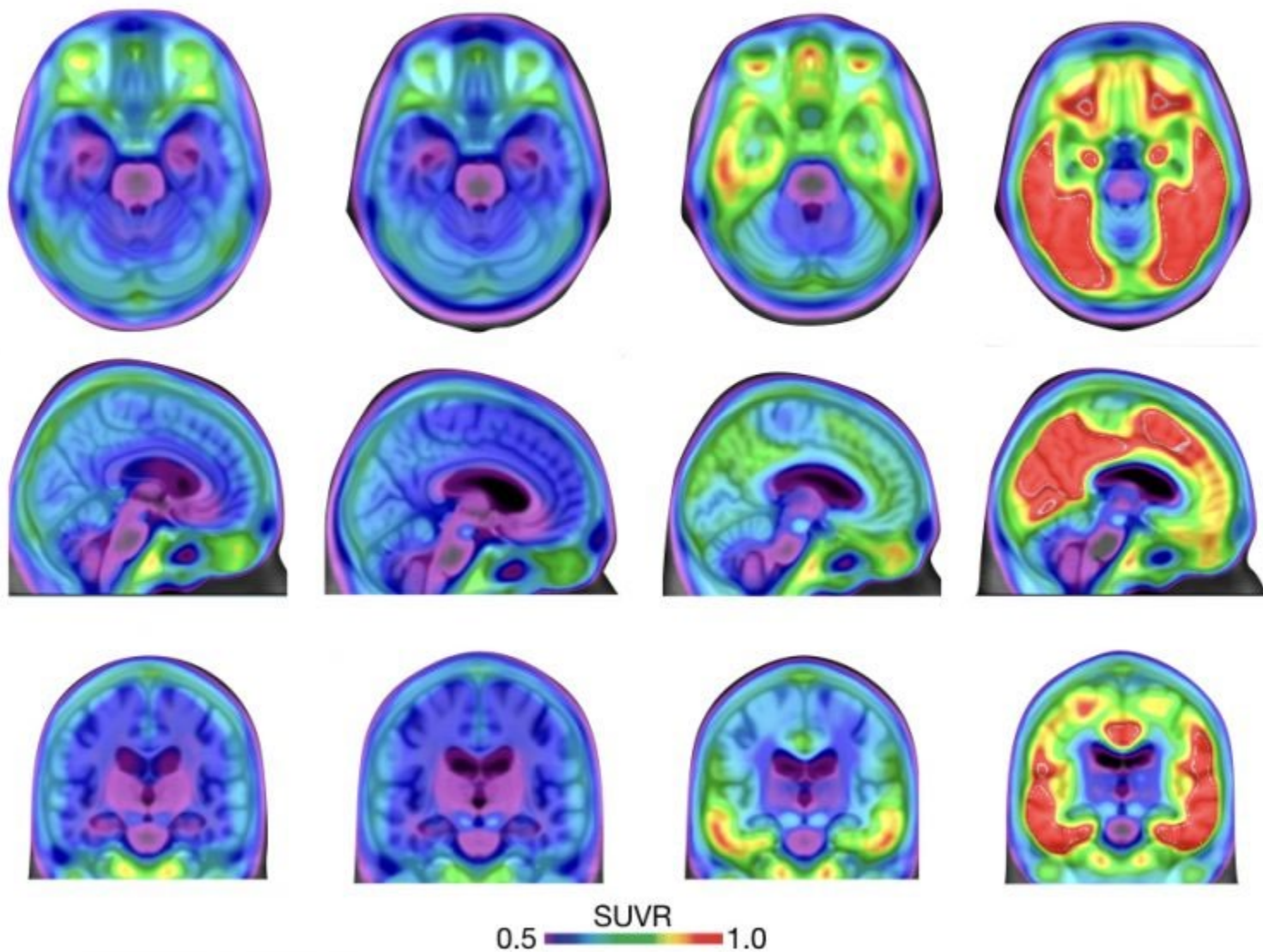
Figure 1

CN young	CN Elderly Aβ -	MCI	AD

SUVR
0.5 ————— 1.0

Figure 2

Keywords: *Amyloid pathology, tau pathology*

Increased task activation and amyloid independently explain advanced tau pathology in older adults

Anne Maass[1,2], David Berron[1,3], Theresa Harrison[2], Jenna Adams[2], Renaud La Joie[4], Taylor Mellinger[2,4], Rachel Bell[2], Kaitlin Swinnerton[2], Suzanne Baker[5], Ben Inglis[6], Gil Rabinovici[4], Emrah Duzel[1], William Jagust[2]

[1]*German Center for Neurodegenerative Diseases, Magdeburg, Germany*
[2]*Helen Wills Neuroscience Institute, UC Berkeley, Berkeley, CA, US*
[3]*Clinical Memory Research Unit, Lund University, Lund, Sweden*
[4]*Memory and Aging Center, University of California, San Francisco, CA, US*
[5]*Molecular Biophysics and Integrated Bioimaging, Lawrence Berkeley National Lab, Berkeley, CA, US*
[6]*Henry H. Wheeler, Jr. Brain Imaging Center, UC Berkeley, Berkeley, CA, US*

Objectives: Previous work, mainly in animals, indicates associations between aberrant activation, tau and $A\beta$ accumulation and also suggests that $A\beta$ accelerates the spread of tangles from the **anterior-temporal** (**AT**) lobe to **posterior-medial** (**PM**) regions. We tested in cognitively normal older adults (OA) how tau, $A\beta$ and activation measures are related using a task that specifically engages AT and PM networks (Fig.2A)

Methods: Fifty OA (78±6yrs) underwent [^{11}C]PiB-PET (24 $A\beta^-$/25 $A\beta^+$), [^{18}F]FTP-PET (32 Tau$^-$/17 Tau$^+$) and 3T fMRI (see Fig.1 for Methods) while they performed a memory task on object and scene images. Group-specific effects of $A\beta$ and tau on activation in AT and PM regions were tested with ANOVAs. A stepwise regression was run to identify the best predictor(s) (among activity measures and global $A\beta$) of PM FTP SUVR.

Results: Tau+ OA showed higher activation than Tau- OA during both object and scene processing in AT regions (p=.044; not shown). In PM regions that usually do not activate for objects, Tau+ OA showed increased activation during object processing (p=.016; Fig.2B), resulting in diminished functional domain-specificity or dedifferentiation. No significant activity differences were seen between $A\beta^-$ and $A\beta^+$ OA. Correlational analyses confirmed a positive association between PM activation and FTP SUVR but not PiB DVR (Fig. 2C/D). PM FTP SUVR was best predicted by object activation in PM ROIs and global PiB DVR (Table1) with no interactive effect of activity and $A\beta$.

Conclusions: Advanced tau pathology in old age is related to aberrant activation and loss of functional specificity in PM regions. $A\beta$ might initiate the spread of tau from the temporal lobe to connected PM regions, followed by tau-induced aberrant activation and further protein accumulation. Alternatively, temporal lobe tau might lead to a compensatory shift of processing load to the PM system manifesting as hyperactivation leading to protein accumulation.

Figure 1
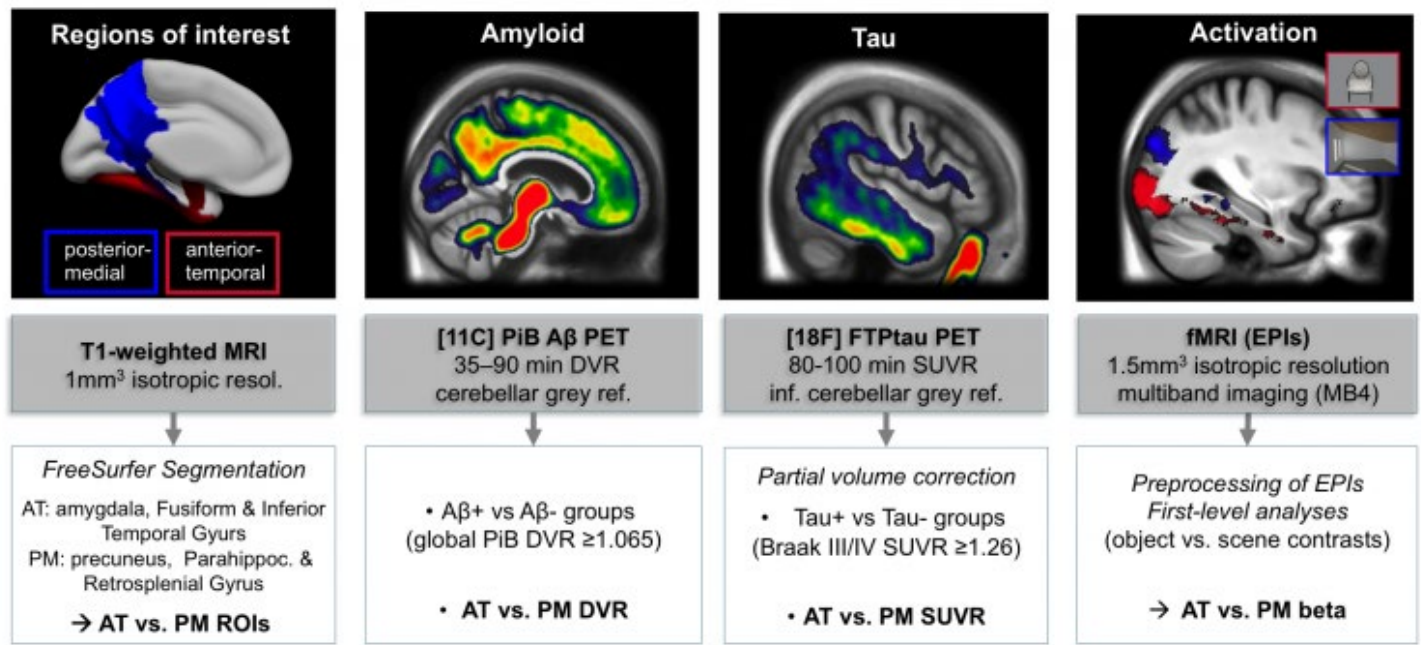
Overview of data and main processing steps. AT and PM PET and activity measures were derived as average across the *a priori* defined regions of interest (ROIs) shown in the left panel that were derived by FreeSurfer segmentation.

Figure 2

A. Domain-specific Activation
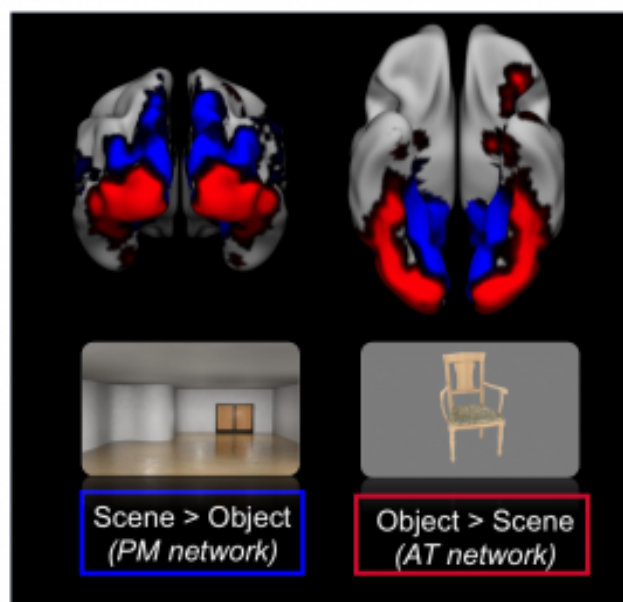
B. Tau+ elderly show increased activation
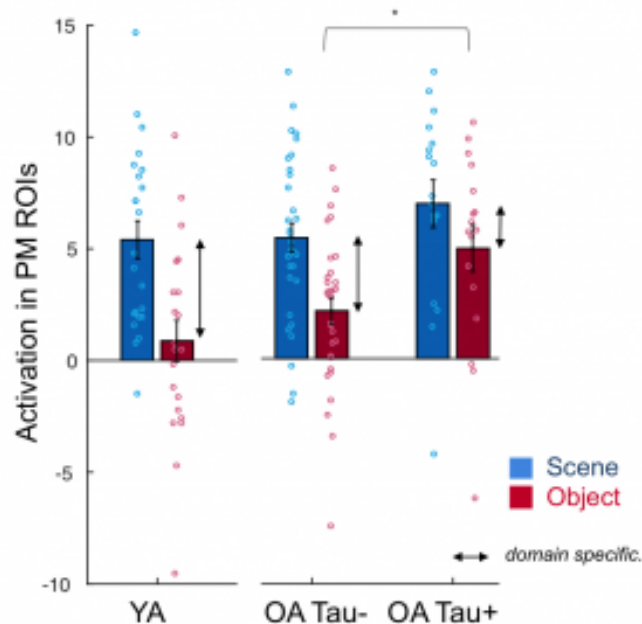
C. Tau vs Activation
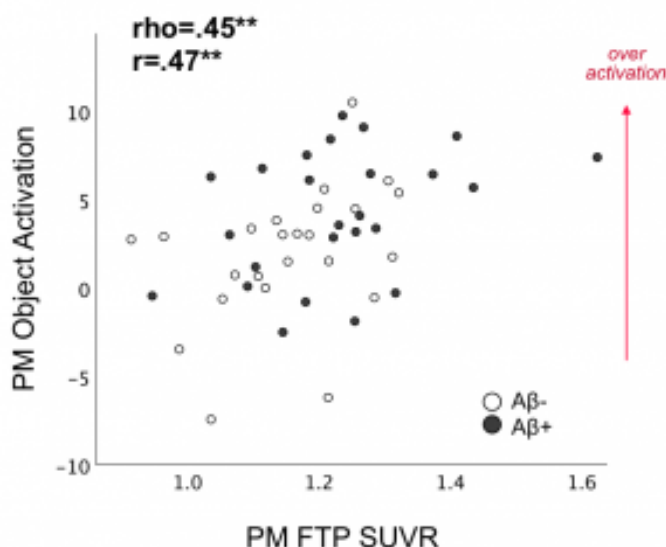
D. Aβ vs Activation
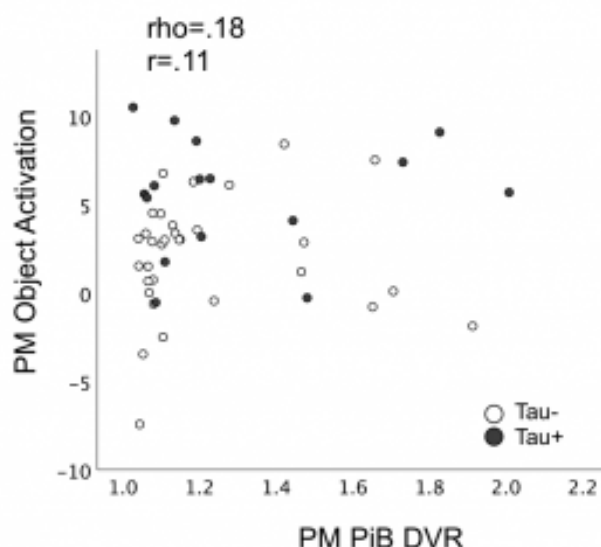
Increased tau (but not Aβ) relates to aberrant activation and reduced functional domain-specificity.

(A) One-sample *t*-test contrasts in older adults (n=49; cluster corrected) showing preferential AT (anterior-temporal) and PM (posterior-medial) regional activation for object and scene processing, respectively. **(B)** Tau+ OA (n=17) showed object-specific overactivation in PM regions of interest (domain x group interaction: $F(1,45)=4.7$, $p=.036$, *post-hoc* $t(47)=2.5$, $p=.016$). This yielded to reduced functional domain specificity ($p=.032$; illustrated as arrow). Tau+ OA also exhibited general overactivation in AT regions ($F(1,45)=4.3$; $p=.044$, not shown). **(C)** Higher PM tau measures were related to higher activation during object processing, whereas no such association was seen for PM Aβ PET load and activity **(D)**. For *a-priori* defined AT and PM ROIs , see Fig.1

Table 1. General linear models predicting PM tau burden by global Aβ and activation

Model	Parameter	B (unstand.)	SE	t	p	Partial η^2
1.	Age_FMRI	-.003	.003	-1.146	.258	.029
	Gender	.064	.033	1.943	.058	.079
	PM Object Activation	**.013**	**.004**	**3.120**	**.003**	**.181**
	Global Aβ	**.178**	**.070**	**2.539**	**.015**	**.128**
2.	PM Object Activation	-.003	.020	-.131	.897	.000
	Global Aβ	.132	.091	1.454	.153	.047
	Aβ * PM Object Activation	.013	.017	.793	.432	.014

Global Aβ was measured as PiB DVR across cortical regions. Activation denotes the mean beta derived from PM ROIs for the object vs. baseline contrast. A stepwise regression revealed PM object activation and global Aβ as best predictors of PM tau. Model 1: $F(4,44)=6.4$, Adjusted $R^2 = .310$. Model 2: $F(5,43)=5.2$, Adjusted $R^2 =.304$. The second model was run to test for an interactive effect of Aβ and activation in predicting tau load and also included age and gender as covariates (parameter estimates not shown).

Keywords: *tau progression, hyperactivation, posterior-medial, aging*

FRIDAY, January 18, 2019

	Friday, January 18, 2019		Page
8:30	**SESSION 6:** **PET and fluid biomarkers**	CHAIRS: **Oskar Hansson**, Lund University, Lund, Sweden **Susan Landau**, University of California, Berkeley, Berkeley, CA, US	332
10:00	**POSTER SESSION 3A** and Coffee Break		341
10:45	**SESSION 7:** **Multi-modality: cognitively normal**	CHAIRS: **William Jagust**, University of California, Berkeley, Berkeley, CA, US **Tobey Betthauser**, Univ. of Wisconsin-Madison, Madison, WI, US	444
12:30	Keynote Lecture	**John Trojanowski**, University of Pennsylvania, Philadelphia, PA, US	462
1:15	Lunch		
2:30	**SESSION 8:** **Multi-modality: patient populations**	CHAIRS: **Ann Cohen**, University of Pittsburgh, Pittsburgh, PA, US **Keith Johnson**, Massachusetts General Hospital, Boston, MA, US	463
4:15	**POSTER SESSION 3B** and Coffee Break		
5:00	Awards Ceremony		
5:05	**SESSION 9:** **Clinical applications**	CHAIRS: **Pedro Rosa-Neto**, McGill University, Montreal, QC, Canada **Gil Rabinovici**, University of California, San Francisco, CA, US	482

Friday, January 18, 2019 - 08:30 am - 09:30 am

Podium Session

Session 6: PET and fluid biomarkers

CHAIRS: Oskar Hansson, Susan Landau

08:30 am - 09:30 am	Session 6: PET and fluid biomarkers	CHAIRS: **Oskar Hansson**, Lund University, Lund, Sweden **Susan Landau**, University of California, Berkeley, Berkeley, CA, US	Page
8:30	Longitudinal investigation of concordant vs. discordant amyloid CSF/PET biomarkers	**Arianna Sala**, Karolinska Institute, Stockholm, Sweden	333
8:45	CSF and PET tau measures in different stages of Alzheimer's disease	**Niklas Mattsson**, Lund University, Lund, Sweden	334
9:00	Predicting brain amyloidosis using peripheral blood-based gene expression and early stage neurodegeneration biomarkers	**Apoorva Bharthur Sanjay**, Indiana University School of Medicine, Indianapolis, IN, US	337
9:15	Friend or foe? Regional dependent roles of neuroinflammation in Alzheimer's disease pathophysiology	**Min Su Kang**, McGill University Research Centre for Studies in Aging, Verdun, QC, Canada	340
09:30 am - 10:00 am	Discussion		

Longitudinal investigation of concordant vs. discordant amyloid CSF/PET biomarkers

Arianna Sala[1,2,3], Agneta Nordberg[1,4], Elena Rodriguez-Vieitez[1]

[1]*Division of Clinical Geriatrics, Department of Neurobiology, Care Sciences and Society, Karolinska Institute, Stockholm, Sweden*
[2]*Vita-Salute San Raffaele University, Milan, Italy*
[3]*In vivo human molecular and structural neuroimaging Unit, Division of Neuroscience, IRCCS San Raffaele Scientific Institute, Milan, Italy*
[4]*Theme Aging, Karolinska University Hospital, Stockholm, Sweden*

While Florbetapir-PET and CSF-Aβ42 usually provide highly concordant information, mismatch between these measures has been consistently reported in a minority of cases. Here, we tested the hypothesis that discordance is due to differences in amyloid processing and kinetics in the CSF vs. in the brain, whereby CSF represents a dynamic measure of **ongoing** amyloid accumulation, while PET provides end-stage information on **resulting** amyloid accumulation. Consequently, we hypothesized that the earliest stage of amyloid deposition consists of isolated CSF+/PET- cases only.

We retrospectively selected N=846 cases from ADNI, ranging from cognitively normal to overtly demented, with Florbetapir-PET and CSF-Aβ42 measurements obtained within 3 months. We additionally collected available longitudinal PET/CSF follow-up data (2 years: N=592-PET, N=285-CSF; 4 years: N=340-PET; 6 years: N=127-PET).

In accordance with our hypothesis, baseline CSF-Aβ42 levels significantly and consistently predicted rate of amyloid plaque deposition as measured by change in Florbetapir-PET over 2-, 4- and 6-year follow-up intervals (p<0.001), also outperforming the predictive ability of baseline Florbetapir-PET.

Contrarily to our hypothesis: (i) isolated Florbetapir-PET positivity was present since the earliest disease stages, however being less prevalent (3.1%) than isolated CSF-Aβ42 positivity (9.8%); (ii) concordant negative cases progressed towards not only isolated CSF-Aβ42 positivity (8.4%) but also isolated Florbetarpir-PET positivity (3.4%), these proportions being consistent with cross-sectional values; (iii) among discordant cases, while the majority progressed towards full biomarker concordance, 25-48% presented a persistent discordant biomarker profile, still after 2-year follow-up.

Our results suggest that the hypothesis whereby CSF represents a dynamic measure of ongoing amyloid accumulation may only partially account for biomarkers mismatches. Since amyloid PET tracers bind to dense-core fibrillary plaques and not to diffuse plaques, protofibrils or oligomers, biological factors underlying individual differences in the conformation of amyloid aggregates may partly explain the observed discordance, advocating for the need for diverse biomarkers for patient stratification.

CSF and PET tau measures in different stages of Alzheimer's disease

<u>Niklas Mattsson</u>[1], Ruben Smith[1], Rik Ossenkoppele[1], Sebastian Palmqvist[1], Olof Strandberg[1], Erik Stomrud[1], Oskar Hansson[1]

[1]*Lund University, Lund, Sweden*

Background: CSF tau and tau PET may have different dynamics during the course of AD.

Method: 62 cognitively unimpaired (CU, 41 AB+), 32 MCI (29 AB+), 45 AD dementia (42 AB+), and 75 non-AD neurodegenerative patients (21 AB+) from the BioFINDER study were examined with CSF biomarkers (T-tau and P-tau using automated Euroimmun ELISAs) and tau PET imaging (18F-Flortaucipir). 60 subjects had an additional early CSF sample (mean 3.7 years before PET). Associations were tested between biomarkers, diagnosis, atrophy and cognition.

Results: CSF tau markers were changed already in CU AB+, while 18F-Flortaucipir was changed in MCI/AD (Fig 1A), giving a discrepancy between CSF and PET with a proportion isolated CSF+ subjects (Fig 1B). At a priori cut-points, P-tau was the marker with greatest sensitivity for CU AB+ (46.3%) and MCI AB+ (93.1%), while 18F-Flortaucipir (in inferior temporal cortex) had the greatest sensitivity for AD AB+ (100%). T-tau and P-tau had high accuracy for CU AB+, MCI AB+, and AD AB+ (AUC 0.91-1.00) versus CU AB-. 18F-Flortaucipir had high accuracy for MCI AB+ (AUC 0.82-0.94) and AD AB+ (AUC 0.95-1.00). In the CU subset that had two CSF samples and were 18F-Flortaucipir negative at follow-up, the sensitivity was 23-40% for CU AB+ using the early CSF tau measure, and longitudinal rates of CSF tau were increased in CU AB+ (Fig 2A). 18F-Flortaucipir was more strongly associated with MMSE and atrophy, compared to CSF tau (Fig 2B-C). High 18F-Flortaucipir (but not CSF tau) was associated with longitudinal decline in MMSE in MCI/AD (Fig 2D). P-tau and 18F-Flortaucipir had similar accuracy for AD versus non-AD ND (Fig 3A-B).

Discussion: CSF T-tau and P-tau are changed very early in AD, possibly reflecting altered tau secretion. 18F-Flortaucipir is likely a more accurate measure of tau aggregation and tracks the disease during the symptomatic stages.
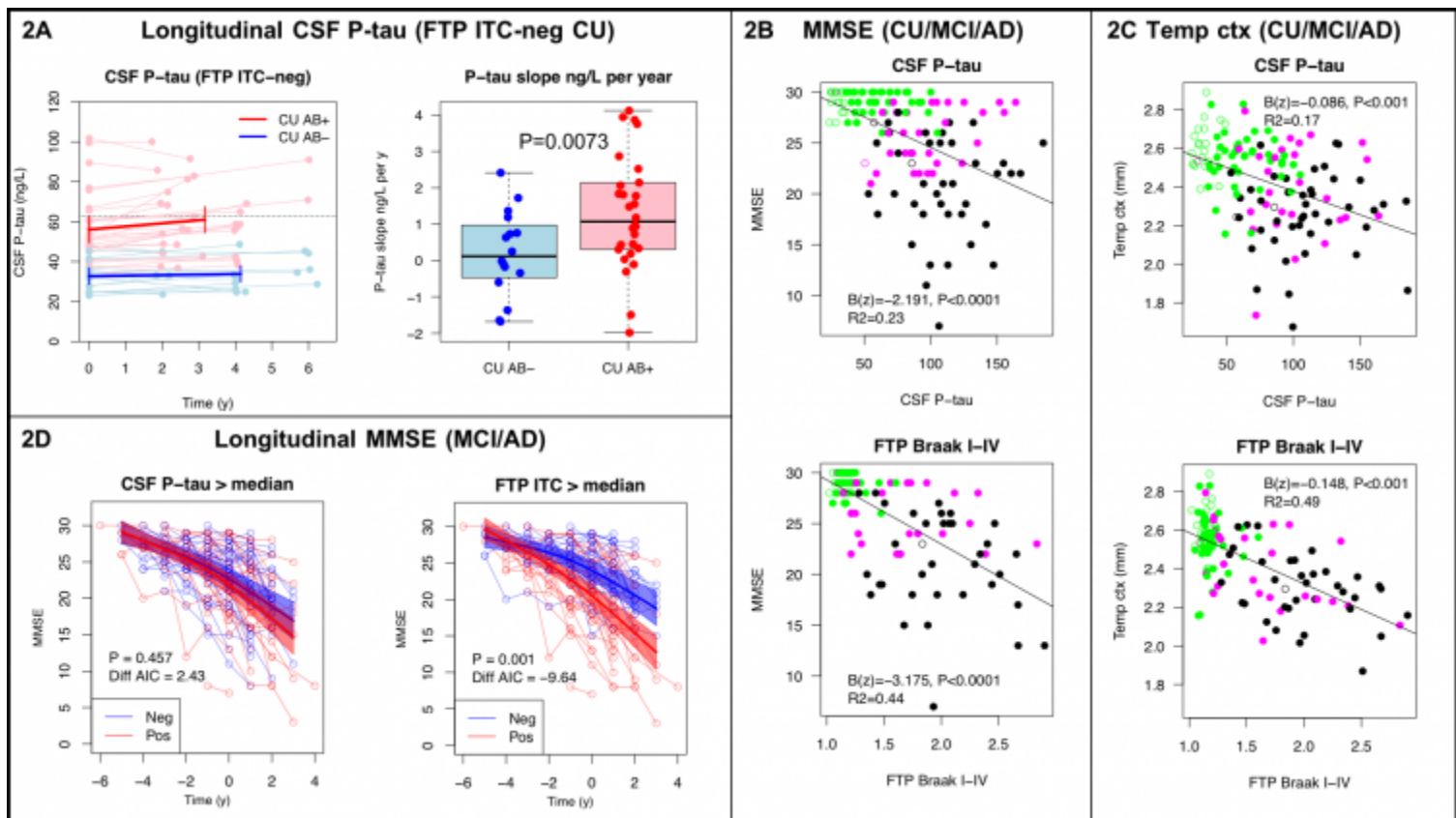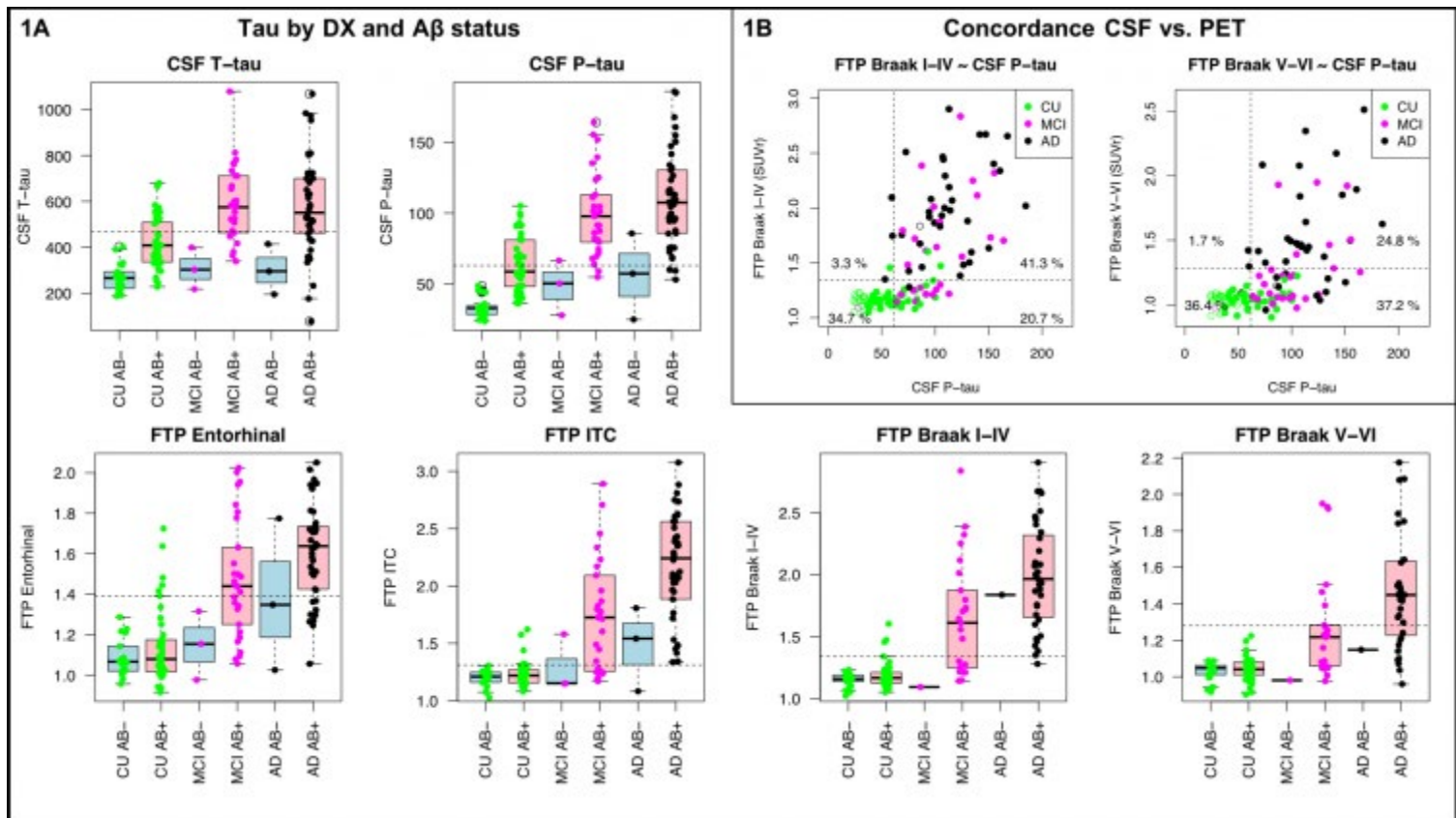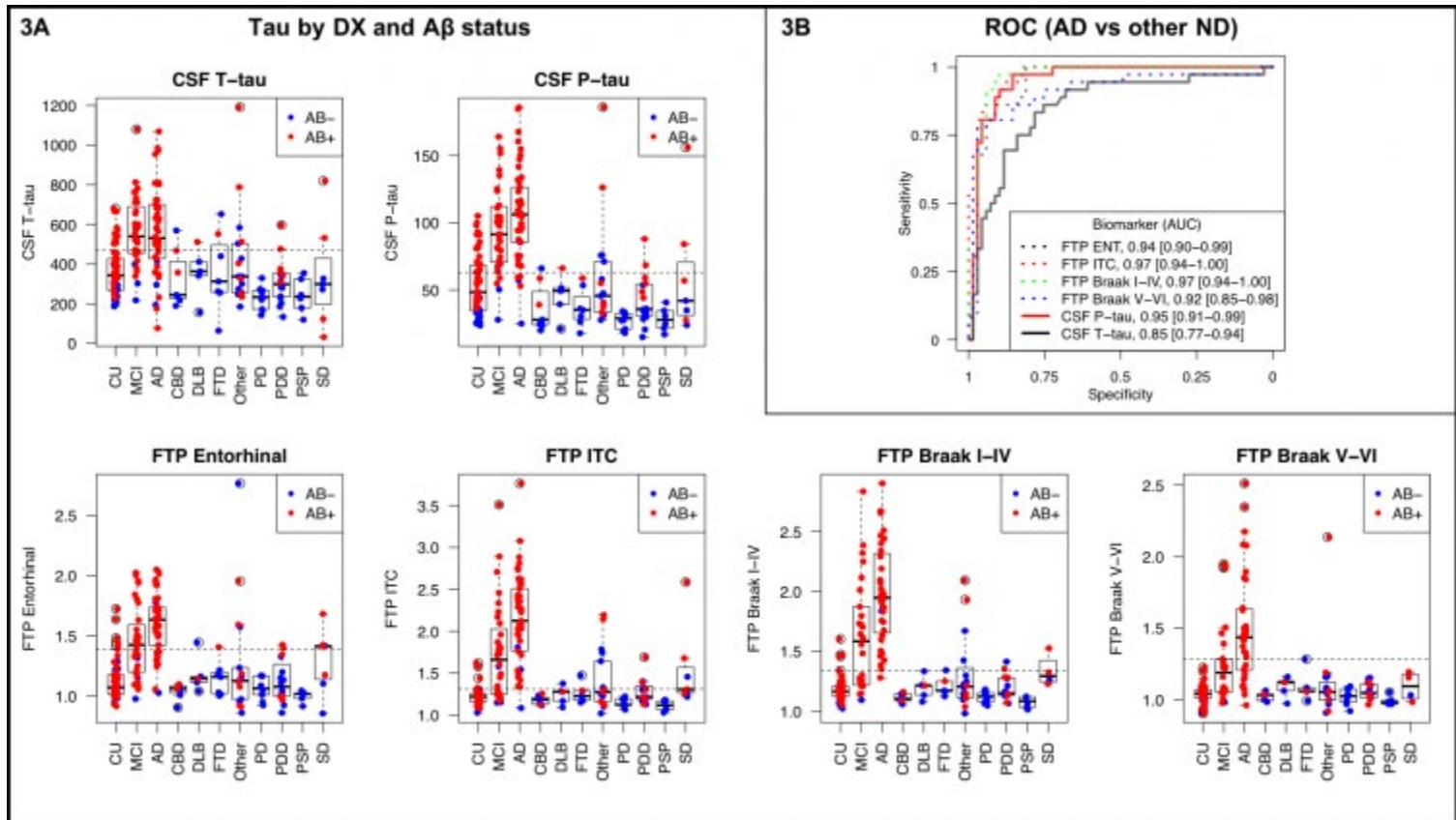
Keywords: *tau, biomarker, CSF, PET, flortaucipir*

Predicting brain amyloidosis using peripheral blood-based gene expression and early stage neurodegeneration biomarkers

Apoorva Bharthur Sanjay[1], Liana Apostolova[1], Diana Svaldi[1], Andrew Saykin[1], Kristy Hwang[2], Naira Goukasian[2], Tugce Durant[1]

[1]*Indiana University School Of Medicine, Indianapolis, IN, US*
[2]*UCLA, Los Angeles, CA, US*

Objective: Amyloid deposition is known to have genetic association, however, much of the heritability remains unexplained. Peripheral blood allows for evaluation of genetic contributions to Amyloid deposition that may not be strictly neuronal. We evaluate the efficacy of using peripheral blood mRNA levels and neuroimaging biomarkers in predicting amyloidosis.

Methods: Peripheral-blood-mRNA and structural-MRI scans (1.5T MRI, UCLA ADRC) were obtained from 108 mild cognitive impairment (amnestic & non-amnestic) and 52 cognitively normal controls (CN) participating in the ImaGene study. 70 subjects underwent F^{18}-Flutemetamol PET scans. Baseline $\log_2$-transformed mRNA levels were correlated with hippocampal volume and ranked by the absolute value of correlation. The top 10 transcripts were used to develop a multimodal classifier for predicting brain amyloidosis (PET standard uptake value ratio (SUVR) ≥ 1.27 after normalization to whole cerebellum). Additionally, entorhinal thickness extracted using Freesurfer6.0, was included as a predictor (left/right separate), representing an early-stage region of neurodegeneration. We used a support-vector-machine (SVM) algorithm on 57 subjects with both neuroimaging and gene expression data to build a classifier, validating using leave-one-out cross-validation. Selected features from the classifier were assessed for significant diagnostic group differences (ANOVA, $p<0.05$) and/or significant ($p<0.05$) linear associations with Amyloid-SUVR.

Results: The SVM classifier chose 6 features, 4 mRNA transcripts (Table1) and 2 Entorhinal thickness measures, achieving an AUC=0.77(fig1). VRK3 and TNFSF9 exhibited a diagnostic group effect. VRK3 and Entorhinal thickness exhibited significant associations with SUVR (Fig2).

Conclusions: Classifier results agree with animal studies suggesting that genes involved in immune response, including clearance and neuroinflammation play a large role in amyloid deposition. VRK3 is a kinase that has been associated with reducing apoptosis and amyloid accumulation. TNFSF9 belongs to the tumor necrosis factor superfamily that play a major role in neuroinflammation. Early stage neurodegeneration measures were predictive of and associated with amyloid deposition

Figures

Measure	aMCI (n=20)	CN (n=26)	naMCI (n=11)	p-value (ANOVA)
Age(years) Mean (SD)	67.6 (8.4)	69.46 (7.93)	67.09 (9.45)	n.s
EDU(years) Mean (SD)	14.95 (2.42)	17.23 (2.23)	16.45 (3.62)	0.01*
SUVR	1.4 (0.37)	1.14 (0.29)	1.21 (0.46)	0.057
Left entorhinal thickness(mm) Mean (SD)	2.91 (0.58)	3.27 (0.55)	3.38 (0.55)	0.04*
Right Entorhinal Thickness(mm) Mean (SD)	3.08 (0.70)	3.25 (0.55)	3.39 (0.56)	n.s.
TNFSF9 Mean (SD)	6.94 (0.13)	7.06 (0.19)	6.95 (0.19)	0.04*
VRK3 Mean (SD)	7.57 (0.22)	7.78 (0.27)	7.63 (0.23)	0.006*
TCEA2 Mean (SD)	6.89 (0.08)	6.89 (0.14)	6.86 (0.11)	n.s
SYNE1 Mean (SD)	6.59 (0.08)	6.62 (0.09)	6.63 (0.06)	n.s

Brain Amyloidosis Classifier
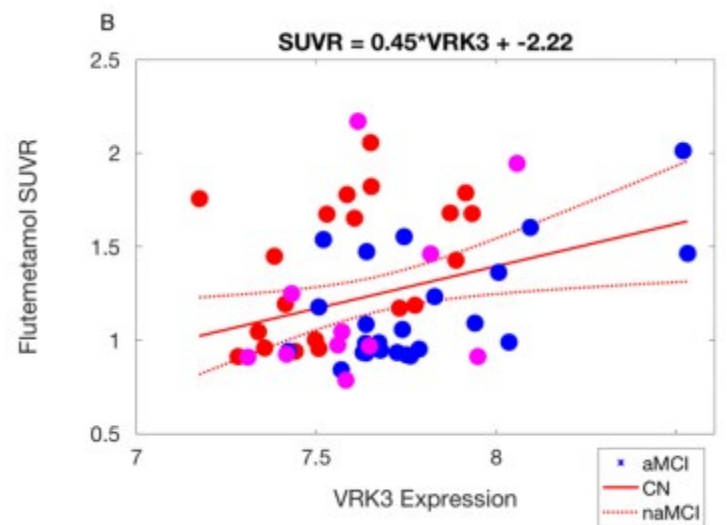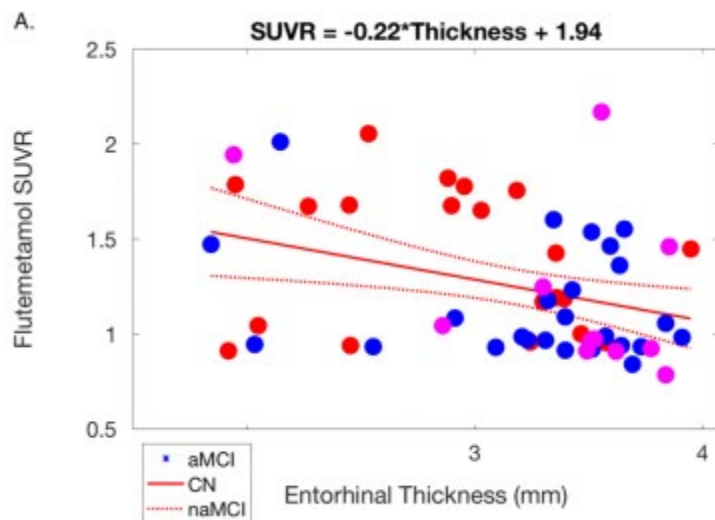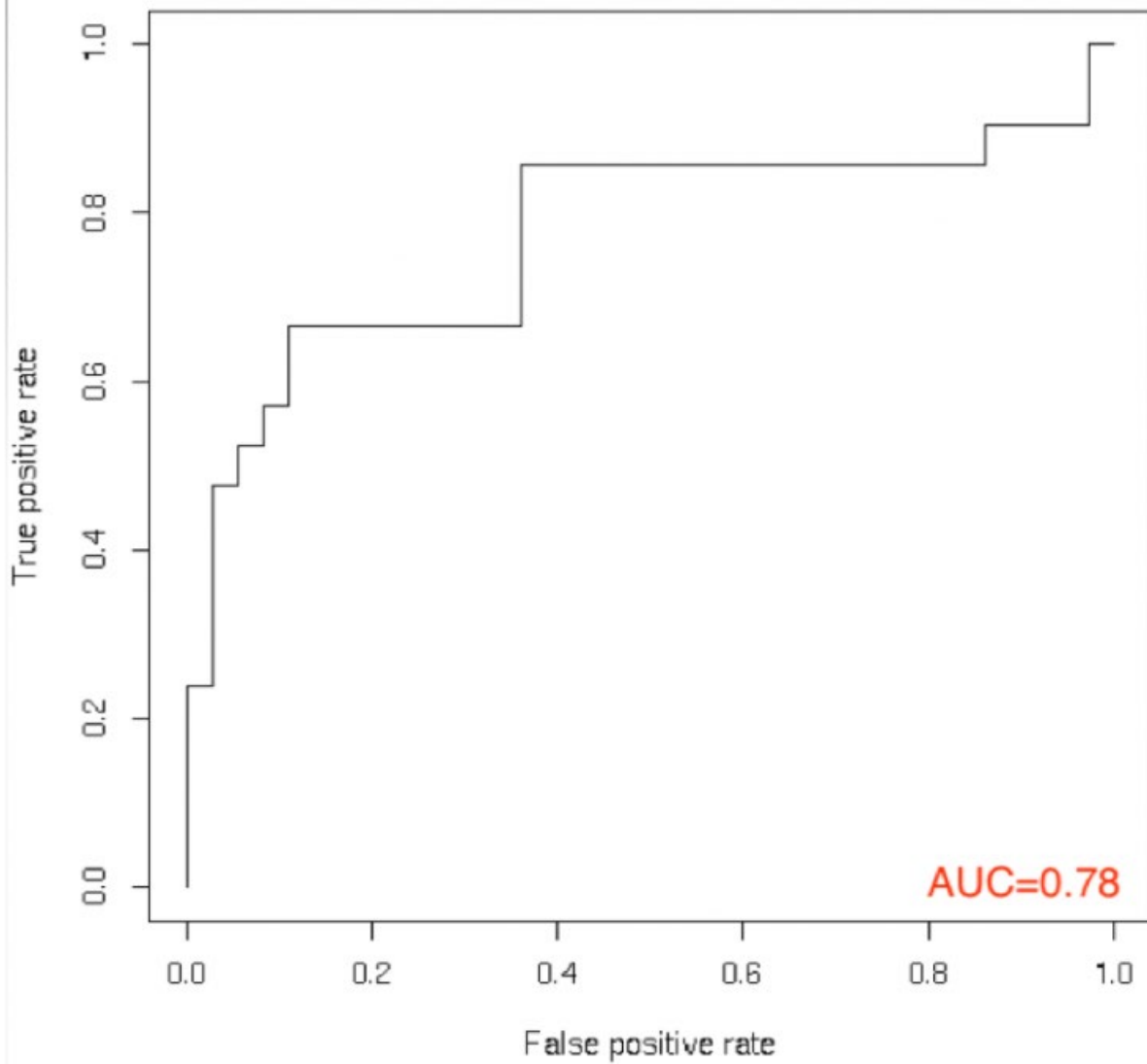
AUC=0.78

A. SUVR = -0.22*Thickness + 1.94

B SUVR = 0.45*VRK3 + -2.22

Friend or foe? Regional dependent roles of neuroinflammation in Alzheimer's disease pathophysiology

Min Su Kang[1,2,3], Mira Chamoun[1,2], Sulantha Mathotaarachchi[1,2], Meïlissa Savard[1,2], Tharick A. Pascoal[1,2], Andreìa L. Benedet[1,2], Joseph Therriault[1,2], Emilie Thomas[1,2], Cecile Tissot[1,2], Jean-Paul Soucy[3], Serge Gauthier[1,2], Gassan Massarweh[3], Pedro Rosa-Neto[1,2,3]

[1]*Translational Neuroimaging laboratory - McGill Centre for Studying in Aging, Verdun, QC, Canada*
[2]*Brain Imaging Centre – Douglas Research Centre, Verdun, QC, Canada*
[3]*McConnell Brain Imaging Centre – McGill University, Montreal, QC, Canada*

Background: Understanding the complex dynamic of the multi-facets pathophysiology of Alzheimer's disease (AD) that leads to cognitive decline is crucial in developing successful therapeutic strategies. Here, we aimed to reveal the association among the major targets of AD clinical trials - amyloid ([^{18}F]NAV4694), tau ([^{18}F]MK6240), and neuroinflammation ([^{11}C]PBR28) – through multimodal PET study. We hypothesized a regional dependent association between TSPO expression and amyloid and tau, which led to differential effects of TSPO expression on cognitive measures.

Methods: Total 34 participants (25 CN, 5 MCI, and 4 AD) with high-affinity binder for TSPO from TRIAD cohort underwent 3 PET scans and MMSE and CDR-SoB. MCI and AD patients were combined as one group. Static 40–60min [^{18}F]NAV4694 and 90-110min [^{18}F]MK6240 SUVR images were generated. Dynamic 60min [^{11}C]PBR28 images were processed to BP$_{ND}$ based on SRTM. All PET images were normalized to ADNI template, used cerebellar grey as a reference region, and adjusted for age, gender, education, and APOE.

Results: Compared to CN, MCI/AD had significantly greater amyloid, tau, and TSPO expression. The association between TSPO expression and amyloid and tau was significantly different in MCI/AD compared to CN such that there was a negative association in frontal, parietal, and lateral temporal cortex but positive association in entorhinal, fusiform cortex, and parahippocampal gyrus. Effectively, we observed a significant effect of TSPO expression on better MMSE and CDR-SoB in frontal, parietal, and lateral temporal cortex but worsening scores in parahippcampal gyrus, entorhinal, and fusiform cortex in MCI/AD compared to CN.

Conclusion: Our study revealed differential effects of neuroinflammation in AD pathophysiology and cognition that depends on regions. The increased neuroinflammation showed downregulating amyloid and tau and better cognition in frontal, parietal, and lateral temporal in MCI/AD. In contrast, it showed detrimental roles upregulating amyloid and tau and worsening cognition in basal temporal regions.

Board #	Poster Title	Authors	Presenter	Page
153	A preliminary analysis of the association between cerebral blood flow and amyloid and tau PET binding in older adults	Albrecht | Isenberg | Stradford | Monreal | Jann | Pa	**Albrecht, Daniel**	405
125	Cerebrospinal fluid synaptic vesicle glycoprotein 2A in Alzheimer's disease	Ashton | Höglund | Leuzy | Heurling | Hansson | Schöll | Zetterberg | Blennow	**Ashton, Nicholas**	356
131	Spatially compact components of non-negative matrix factorization applied to AV-1451 PET images reveal distinct demographic associations	Bilgel | Ziontz | Shafer | Wong | Resnick	**Bilgel, Murat**	366
151	Comparing amyloid PET tracers and interpretation strategies: A multicenter study	Bischof | Bartenstein | Barthel | van Berckel | Doré | van Eimeren | Forster | Hammes | Lammertsma | Minoshima | Rowe | Sabri | Seibyl | van Laere | Vandenberghe | Villemagne | Yakushev | Drzezga	**Bischof, Gérard**	402
154	Random forests of amyloid PET may pinpoint key brain regions predictive of MoCA score	Zukotynski | Gaudet | Kuo | Adamo | Goubran | Scott | Bocti | Borrie | Chertkow | Frayne | Hsiung | Laforce | Noseworthy | Prato | Sahlas | Smith | Sossi | Thiel | Soucy | Tardif | Black	**Black, Sandra**	408
145	Early localized network dysfunction in APOE ε4 carriers without biomarker evidence of Alzheimer's disease	Butt | Strain | Wisch | Schindler | Fagan | Curchaga | Benzinger | Ances	**Butt, Omar**	396
132	Independent contributions of hippocampal activity, amyloid burden, and retrospective decline to Subjective Cognitive Decline	Chen | Jingting | Farrell | Park	**Chen, Xi**	369
121	Disease progression modeling from preclinical stages of Alzheimer's disease (AD) to AD dementia	Cho | Woo | Kim | Kim | Kim | Kim | Jang | Kim | Kim | Jung | Kim | Lockhart | Ossenkoppele | Landau | Jagust | Weiner | Na | Seo	**Cho, Soo Hyun**	348
149	Longitudinal associations between Aβ and glucose metabolism in a normal elderly population	Tudorascu | Yu | Anderson | Snitz | Minhas | Laymon | Lopresti | Mathis | Aizenstein | Klunk | Cohen	**Cohen, Ann**	400
150	Associations between Aβ, tau, and cerebrovascular reactivity in a non-demented elderly population	Cohen | Huppert | Tudorascu | Snitz | Laymon | Lopresti | Mathis | Nadkarni | Lopez | Aizenstein | Klunk | Reis	**Cohen, Ann**	401
137	Staging cortical amyloid deposition using PET imaging	Collij | Heeman | Salvadó | Altomare | de Wilde | Konijnenberg | van Buchem | Yaqub | Markiewicz | Golla | Wottschel | Wink | Visser | Lammertsma | Scheltens | van der Flier | Boellaard | van Berckel | Gispert | Schmidt | Barkhof | Lopes Alves | AMYPAD consortium	**Collij, Lyduine**	379
129	Tau deposition in amyloid negative subjects: the application of the AT(N) model in the Geneva Memory Center experience	Dodich | Frisoni | Andryszak | Scheffler | Mendes | Assal | Schibli | Schwarz | Rakotomiaramanana | Gold | Zekry | Lovblad | Chicherio | Boccardi | Unschuld | Garibotto	**Dodich, Alessandra**	363
165	Chronic low-grade inflammation associates with lower TSPO binding in elderly individuals without dementia	Ekblad | Toppala | Tuisku | Helin | Marjamäki | Laine | Jula | Viitanen | Rinne	**Ekblad, Laura**	428
142	The BIN1 rs744373 SNP is associated with increased tau-PET levels and worse memory independent of amyloid	Franzmeier | Neitzel | Rubinski | Ewers	**Franzmeier, Nicolai**	388
167	F18-PI2620 Tau PET in three memory clinic patients with uncertain CSF biomarker profiles	Frolov | Sha | Fredericks | Nadiadwala | Azevedo | Hall | Toueg | Castillo | Deutsch | Greicius | Davidzon | Zaharchuk | Chin | Mormino	**Frolov, Alexander**	433
157	Beta-amyloid accumulation in non-demented elderly individuals correlates with baseline beta-amyloid load, ApoE genotype and age	Gietl | Treyer | Buchmann | Meyer | Saake | Gruber | Mu | Unschuld | Buck | Nitsch | Hock	**Gietl, Anton**	412

163	Prediction of brain age using resting-state functional connectivity suggests accelerated aging in the preclinical phase of autosomal dominant Alzheimer's disease, irrespectively of amyloid pathology	Gonneaud | Vachon-Presseau | Baria | Pichet Binette | Benzinger | Morris | Bateman | Breitner | Poirier | Villeneuve | Study Group | Research Group	**Gonneaud, Julie**	422
156	Relation of cardiovascular risk factors to markers of pathology and memory in autosomal-dominant Alzheimer's disease	Martínez | Guzmán-Vélez | Padilla-Delgado | Vila-Castelar | Fuller | Artola | Sperling | Quiroz	**Guzmán-Vélez, Edmarie**	411
147	Image features and clinical associations of the novel tau PET tracer 18F-APN-1607 in Alzheimer's disease	Hsu | Lin | Hsiao | Lian | Huang | Huang | Yen	**Hsu, Jung-Lung**	398
143	Optimal scanning time for the novel tau PET Tracer 18F-APN-1607	Huang | Hsiao | Lin | Lian | Hsu | Huang	**Huang, Chin-Chang**	392
171	Application of amyloid and tau classification system in subcortical vascular cognitive impairment patients	Jang | Kim | Park | Park | Choe | Cho | Lyoo | Lee | Kim | Cho | Kim | Kim | Jung | Ryu | Choi | Moon | Seong | DeCarli | Weiner | Lockhart | Na | Seo	**Jang, Hyemin**	442
128	Clinical significance of amyloid β positivity in patients with probable cerebral amyloid angiopathy markers	Jang. | Jang | Kim | Werring | Lee | Choe | Park | Lee | Kim | Kim | Cho | Kim | Kim | Charidimou | Na | Seo	**Jang, Young Kyoung**	360
166	Cognitive trajectory of subcortical vascular cognitive impairment	Kim | Woo | Jang | Cho | Kim | Lee | Kim | Kim | Lee | Kim | Seo	**Kim, Hee Jin**	431
170	Modeling PiB PET trajectory groups identifies a subgroup with PiB beta-amyloid accumulation near age 50 and predicts MK-6240 SUVR	Koscik | Betthauser | Jonaitis | Clark | Allison | Mueller | Hermann | Poetter | Sanson | Shouel | Chin | Christian | Johnson	**Koscik, Rebecca**	438
158	Identification of rapid amyloid accumulators: A longitudinal PET amyloid study	Koychev | Vaci | Bilgel | An | Albert | Resnick	**Koychev, Ivan**	413
152	Amyloid and memory impairment have additive effects on microglial activation but not tau pathology	Kreisl | Tao | Zou | Johnson | Tomljanovic | Razlighi | Brickman | Lee | Stern	**Kreisl, William Charles**	403
148	Safety, biodistribution and radiation dosimetry for the tau PET Tracer 18F-APN-1607 in healthy human subjects	Lin | Hsiao | Lian | Huang | Hsu | Huang | Yen	**Lin, Kun-Ju**	399
164	Vascular risk factors and multimodal neuroimaging biomarkers: Preliminary analyses from a biracial older adult cohort	Lockhart | Craft | Sachs | Rapp | Jung | Whitlow | Hayden | Hughes	**Lockhart, Samuel**	425
134	Influence of apolipoprotein-E (APOE) genotype on amyloid trajectories in a longitudinal subject cohort	Lopresti | Campbell | Yu | Snitz | Anderson | Aizenstein | Minhas | Kolibash | Cohen | Mathis | Klunk | Lopez | Tudorascu	**Lopresti, Brian**	372
135	A follow-up report on the prevalence and magnitude of amyloid positivity between cognitively normal elderly Japanese and Americans	Yu | Lopresti | Ihara | Cui | Aizenstein | Higashiyama | Fukuda | Koizumi | Minhas | Lopez | Klunk | Mathis | Miyamoto | Kuller | Sekikawa	**Lopresti, Brian**	374
130	Characterizing the spatial distribution of cross-sectional [18F]GTP1 (Genentech tau probe 1) SUVR using multivariate statistical analysis and machine learning	Manser | Sanabria Bohorquez | Baker | Toth | Teng | Marik | Weimer	**Manser, Paul**	364
146	Association between retinal thickness and brain β-amyloid accumulation in individuals with Subjective Cognitive Decline: data from the FACEHBI study	Marquié | Monté-Rubio | Rodríguez-Gómez | Sanabria | Castilla-Martí | Martínez | Alegret | Pérez-Cordón | Lomeña | Pavia | Gismondi | Bullich | Vivas-Larruy | Tejero | Gómez-Chiari | Orellana | Valero | Ruiz | Tárraga | Boada	**Marquié, Marta**	397
136	Association of in vivo [F-18]AV-1451 with [C-11]PiB, [F-18]FDG hypometabolism, and cortical atrophy in chronic TBI subjects	Minhas | Mountz | Laymon | Lopresti | Beers | Sharpless | Puccio | Edelman | Mathis | Okonkwo	**Minhas, Davneet**	376
124	Association of subjective cognitive decline and gait slowing with Aβ deposition in cognitively normal individuals	Nadkarni | Perera | Snitz | Mathis | DeKosky | Klunk | Lopez	**Nadkarni, Neelesh**	353

168	Differential associations of cortisol plasma level with glucose metabolism, hippocampal atrophy, and amyloid deposition across Alzheimer's disease stages	Oh | Leung | Canli | Slifstein	**Oh, Hwamee**	435
133	Amyloid and tau accumulate across distinct spatial networks and are differentially associated with brain connectivity	Pereira | Ossenkoppele | Palmqvist | Strandberg | Smith | Westman | Hansson	**Pereira, Joana**	371
144	Associations between behavioral factors and Alzheimer's pathology: Findings from cognitively normal older adults at risk of AD and presymptomatic ADAD mutation carriers	Pichet Binette | Gonneaud | Ozlen | Bedetti | Morris | Bateman | Benzinger | Poirier | Breitner | Villeneuve | Research Group | Study Group	**Pichet Binette, Alexa**	393
141	[11C]PIB PET is associated with the brain biopsy amyloid β load and CSF amyloid β levels in subjects with normal pressure hydrocephalus	Rinne | Suotunen | Rummukainen | Herukka | Nerg | Koivisto | Rauramaa | Nagren | Hiltunen | Alzfuzoff | Rinne | Jääskeläinen | Soininen | Leinonen	**Rinne, Juha**	386
122	Metabolism mediates the effect of tau on cognition in mild cognitive impairment and dementia	Rodriguez-Vieitez | Mazrina | Chiotis | Colato | Nordberg	**Rodriguez-Vieitez, Elena**	351
123	Patterns of cerebral tau deposition across Alzheimer's disease stages: A study comparing 18F-THK5317 and 18F-AV-1451 PET tracers	Rodriguez-Vieitez | Colato | Chiotis | Mazrina | Nordberg	**Rodriguez-Vieitez, Elena**	352
126	Longitudinal evaluation of [18F]MK-6240 in Alzheimer's disease and cognitively normal adults: preliminary results at 6 & 12 months	Salinas | Purohit | Lohith | Struyk | Martarello | Beaver	**Salinas, Cristian**	357
160	Derivation of amyloid PET centiloid cut-offs using core AD CSF biomarkers including the whole Alzheimer's continuum: a joint analysis in ALFA and ADNI	Salvadó | Brugulat-Serrat | Falcon | Pavia | Niñerola | Perissinotti | Lomeña | Zetterberg | Blennow | Molinuevo | Gispert | ADNI, TRIBEKA Consortium and ALFA study	**Salvadó, Gemma**	417
161	SSRI reduces CSF Ab42 in healthy older adults and transgenic mice: dose, duration and baseline amyloid effects	Sheline | Snider | Lee | Linn | Fagan | Yan | Aselcioglu | Waligorska | Korecka | Morris | Shaw | Cirrito	**Sheline, Yvette**	420
162	Determination of the optimal scanning time point for the assessment of tau deposition in Alzheimer's disease using [18F]PI-2620 PET	Bullich | Mueller | Barret | Berndt | Madonia | Seibyl | Marek | Stephens	**Stephens, Andrew**	421
138	PET analysis of verubecestat effect on amyloid load in mild-to-moderate Alzheimer's disease patients (EPOCH trial)	Sur | Adamczuk | Sampat | Kost | Scott | Suhy | Egan	**Sur, Cyrille**	382
139	Effect of verubecestat on amyloid load in prodromal Alzheimer's disease patients: Results from the PhIII APECS trial	Sur | Kost | Adamczuk | Scott | Suhy | Egan	**Sur, Cyrille**	383
127	Subicular volume as a surrogate marker of beta-amyloid associated episodic memory variation at high age	Schroeder | Van Bergen | Schreiner | Meyer | Kagerer | Vionnet | Gietl | Treyer | Buck | Kaufmann | Nitsch | Pruessmann | Hock | Unschuld	**Unschuld, Paul**	359
120	Longitudinal [18F]AV-1451 PET imaging in primary progressive apraxia of speech	Utianski | Martin | Schwarz | Hugo | Duffy | Petersen | Clark | Machulda | Butts | Jack, Jr. | Lowe | Whitwell | Josephs	**Utianski, Rene**	344
159	Age-of-onset dependent associations between [18F]Flortaucipir PET and cognitive impairment in AD	Visser | Wolters | Verfaillie | Ossenkoppele | Timmers | Tuncel | Golla | Boellaard | Windhorst | Scheltens | van der Flier | van Berckel	**Visser, Denise**	414
155	Comparison of objective and self-reported sleep, tau, and Aβ in healthy older adults	Winer | Fenton | Harrison | Maass | Baker | Jagust	**Winer, Joseph**	409
169	Cerebral small vessel disease is associated with medial temporal lobe hyperconnectivity in pre-clinical AD	Wu | Tudorascu | Mathis | Lopresti | Cohen | Snitz | Klunk | Aizenstein	**Wu, Minjie**	436
140	AV1451 retention is associated with hippocampal volume and memory declines in cognitively normal older adults	Ziontz | Bilgel | Shafer | June | Wong | Resnick	**Ziontz, Jacob**	384

P120: Longitudinal [18F]AV-1451 PET imaging in primary progressive apraxia of speech

Rene Utianski[1], Peter Martin[1], Christopher Schwarz[1], Botha Hugo[1], Joseph Duffy[1], Ronald Petersen[1], Heather Clark[1], Mary Machulda[1], Alissa Butts[1], Clifford Jack, Jr.[1], Val Lowe[1], Jennifer Whitwell[1], Keith Josephs[1]

[1]*Mayo Clinic, Rochester, MN, US*

Rationale: When apraxia of speech (AOS; planning and/or programming deficit) is the presenting symptom of a neurodegenerative condition in the absence of aphasia (language deficit), it is referred to as primary progressive apraxia of speech (PPAOS). PPAOS is strongly associated with 4-repeat tau. We previously described cross-sectional patterns of increased [18F]AV-1451 uptake in PPAOS compared to healthy controls and those who developed aphasia (Utianski **et al**. 2018). Here, we assess changes over time in previously-identified cortical regions and their relationship with clinical presentation.

Methods: Thirteen patients, who were diagnosed with PPAOS (5 female) at presentation underwent AV-1451 PET imaging at two annual visits. Five of these patients had developed aphasia by the time of the baseline scan. AV-1451 uptake was assessed as cortical to cerebellar crus ratios (SUVR) in cortical regions of interest. A single hierarchical linear model (HLM) compared PPAOS patients to 52 cognitively-unimpaired controls (21 female) from the Mayo Clinic Study of Aging. Annualized SUVR change was the outcome, predicted by region and clinical status, age-adjusted. Person-specific effects accounted for intra-subject correlations, and contralateral regions were included as repeated measures. Changes in clinical measures were assessed using paired t-tests.

Results: Median age was 72, with a median of 4 years disease duration at initial testing. There were significant changes in AOS, aphasia, and cognitive severity scores between visits. Changes in SUVR were greater for patients than controls (Figure 1). Larger changes were seen in the 5 patients with aphasia at first visit than those without (Figure 2). The strongest changes in PPAOS patients were in the dentate nucleus of the cerebellum, pallidum, and precentral gyrus, per the HLM (Figure 3).

Conclusions: While the biological mechanisms of AV-1451 signal in non-AD tauopathies are unknown, this study demonstrates clinically-meaningful signal changes in patients with PPAOS, possibly related to concomitant aphasia.
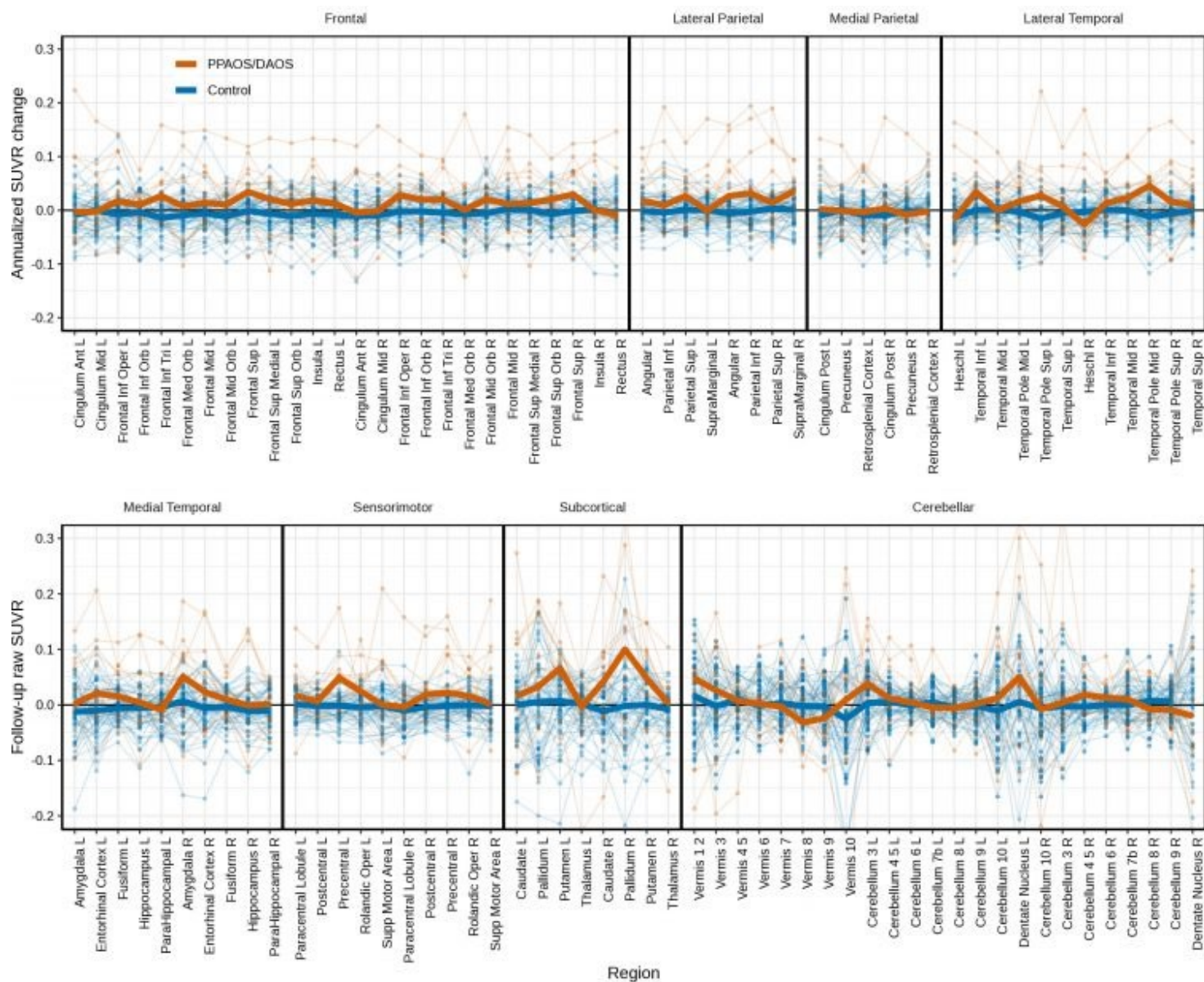
Figure 1

Spaghetti plots of individual change in AV-1451 PET SUVRs (annualized) for patients and controls for all available ROIs, with median values overlaid as heavy lines in each group.

Note: PPAOS = Primary Progressive Apraxia of Speech; DAOS = Dominant Apraxia of Speech or PPAOS who had developed aphasia.
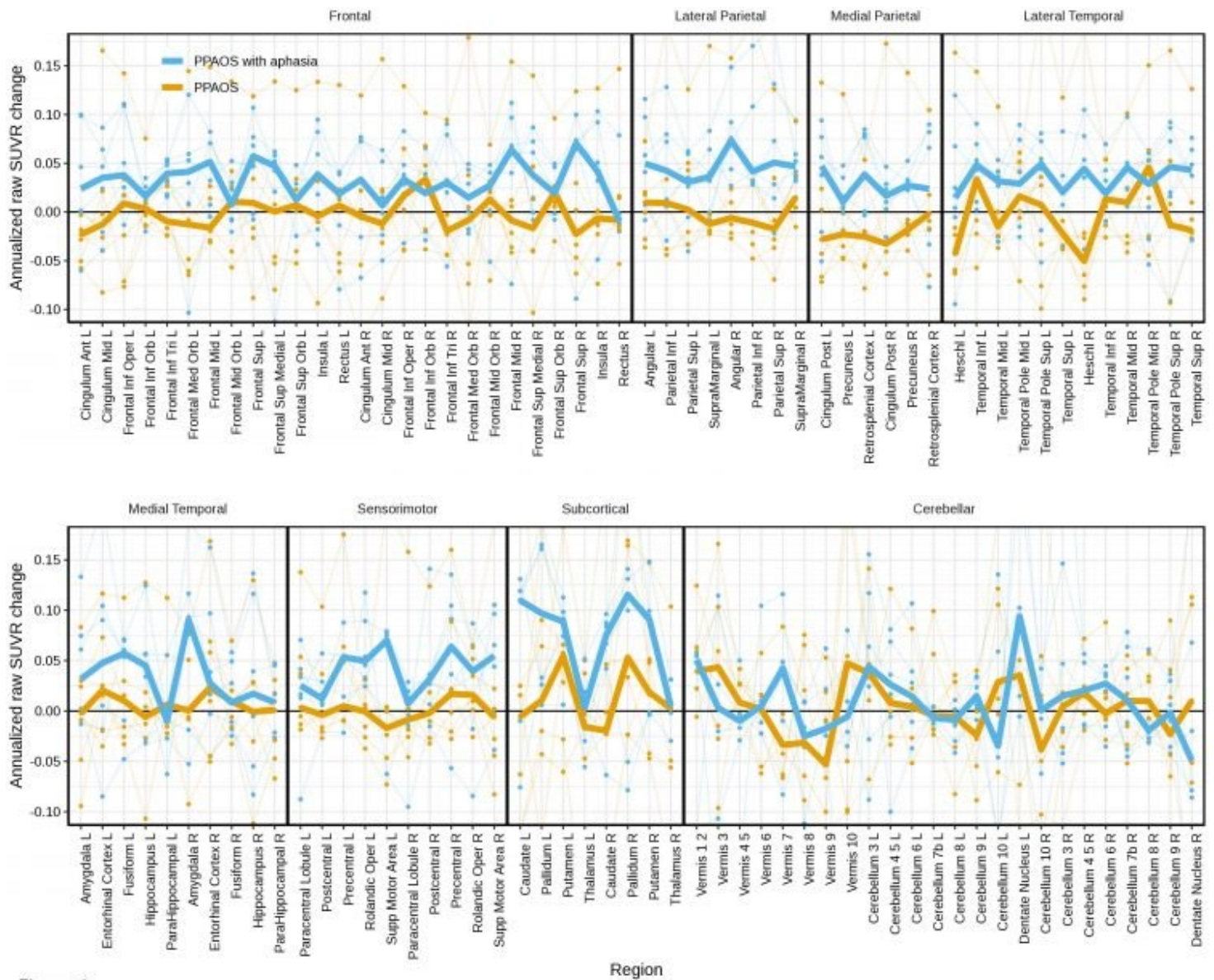
Figure 2

Spaghetti plot of individual change in SUVRs (annualized) for patients for all available ROIs, with median values overlaid as heavy lines in each group. This provides support for a possible relationship between aphasia and trajectory of SUVR. Not surprisingly, greater uptake is observed in the frontal and parietal regions in patients with aphasia, but both hemispheres do appear to be affected.
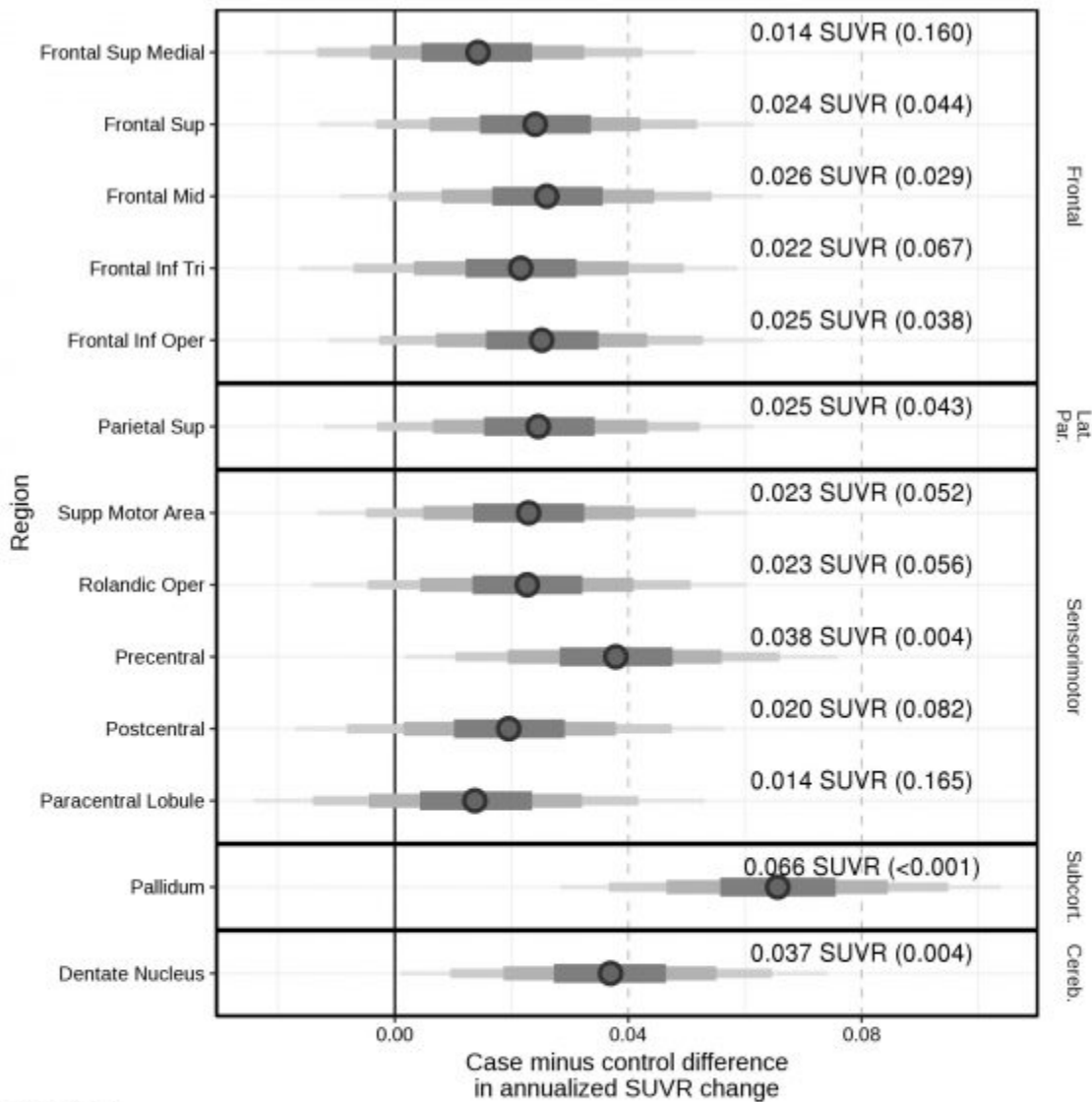
Figure 3

The posterior estimated difference between patients and controls estimated using a single hierarchical linear model predicting SUVR change by region and disease, including age and per-person adjustments. Results showed weak evidence in the parietal and frontal superior medial regions, moderate evidence in most other ROIs, and strong evidence in the pallidum, dentate nucleus of the cerebellum, and precentral regions of larger annualized increase in SUVr in patients with PPAOS than in controls. The bars, moving out from the median (circle) in each row, cover 50%, 80%, 95%, and 99% of the posterior samples. Numerical values are median estimates (posterior probability of difference).

P121: Disease progression modeling from preclinical stages of Alzheimer's disease (AD) to AD dementia

<u>Soo Hyun Cho</u>[1,3], Sookyoung Woo[2], Seon-woo Kim[2], Hee Jin Kim[1,3], Si Eun Kim[1,4], Seung Joo Kim[1,3], Hyemin Jang[1,3], Yeshin Kim[1,5], Jun Pyo Kim[1,3], Young Hee Jung[1,3], Changsoo Kim[6], Samuel Lockhart[7], Rik Ossenkoppele[8], Susan Landau[9], William Jagust[9], Michael Weiner[10], Duk L. Na[1,3,11], Sang Won Seo[1,3,11,12]

[1]*Departments of Neurology, Samsung Medical Center, Sungkyunkwan University School of Medicine, Seoul, Korea*
[2]*Statistics and Data Center, Samsung Medical Center, Seoul, Korea*
[3]*Neuroscience Center, Samsung Medical Center, Seoul, Korea*
[4]*Department of Neurology, Inje University College of Medicine, Haeundae Paik Hospital, Busan, Korea*
[5]*Department of Neurology, Kangwon National University College of Medicine, Chuncheon-si, Gangwon-do, Korea*
[6]*Department of Preventive Medicine, Yonsei University College of Medicine, Seoul, Korea*
[7]*Internal Medicine - Gerontology and Geriatric Medicine, Wake Forest School of Medicine, Winston-Salem, NC, US*
[8]*Department of Neurology and Alzheimer Center, VU University Medical Center, Neuroscience Campus Amsterdam, Amsterdam, The Netherlands*
[9]*Helen Wills Neuroscience Institute, University of California, Berkeley, Berkeley, CA, US*
[10]*Center for Imaging of Neurodegenerative Diseases, University of California, San Francisco., San Francisco, CA, US*
[11]*Department of Health Sciences and Technology, Samsung Advanced Institute of Health Sciences and Technology, Sungkyunkwan University, Seoul, Korea*
[12]*Department of Clinical Research Design and Evaluation, Samsung Advanced Institute of Health Sciences and Technology, Sungkyunkwan University, Seoul, Korea*

Background: Clinical trials testing treatments for Alzheimer disease (AD) are increasingly focused on from preclinical AD to AD dementia. However, disease progression course has not been studied extensively because of difficulty to follow up for a long time. Using accelerated longitudinal model(ALM), we estimated the disease progression from preclinical AD to AD dementia. We further investigated how interaction between APOE4 and sex have an influence on cognitive decline in AD continuum.

Methods: For the participants in the ADNI, visits are repeated 6, and 12 months after the baseline visit and then annually. Data analysis for this study was performed in June 2017. We analyzed 435 patients who took amyloid PET with positive result. Preclinical AD (N=127) and MCI due to AD (N=308) were followed up during 29.3/24.9 months respectively. There were overlapped intervals between two cohorts and corresponding converted time were calculated using estimated ADAS-cog 13 scores.

Results: Estimated time from preclinical AD to AD dementia using ALM showed that it might take about 15.2 years. In women, APOE4 carriers showed steeper incline in ADAS-cog 13 cog score than APOE4 non-carriers ($p < 0.001$). Men with APOE4 carriers also showed steeper incline in ADAS-cog 13 score than men with APOE4 non-carriers from preclinical AD to AD dementia stage. In addition, women with APOE4 carriers showed steeper incline in ADAS-cog 13 cog score than men with **APOE4** carriers and non-carriers ($p<0.001$).

Conclusion: Our findings provide more understanding of disease natural courses for Alzheimer's continuum and a disease progression course for APOE4 effects by sex. The result meets the need of individualized therapeutic and preventive strategies aimed at ameliorating cognitive decline.
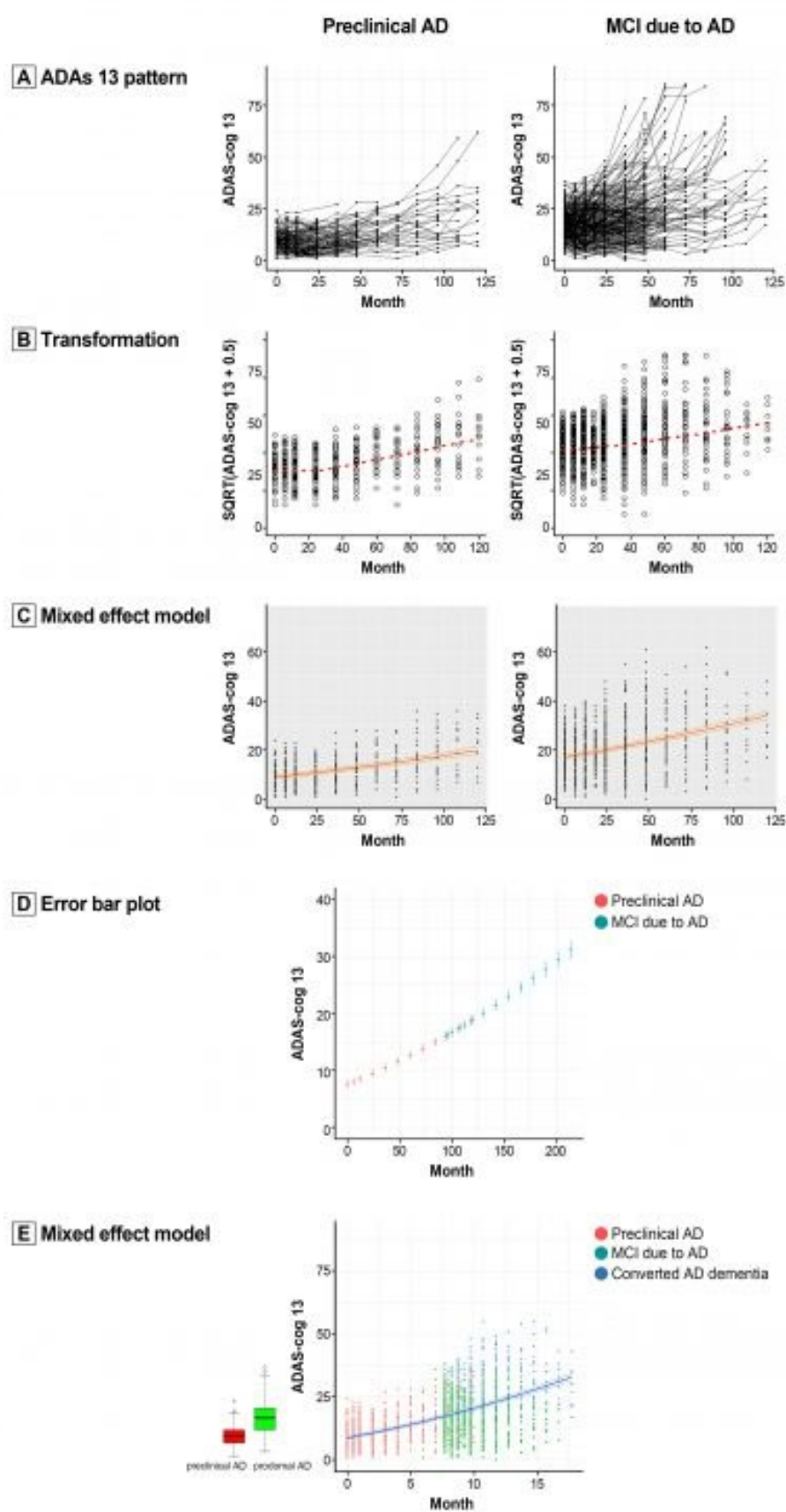
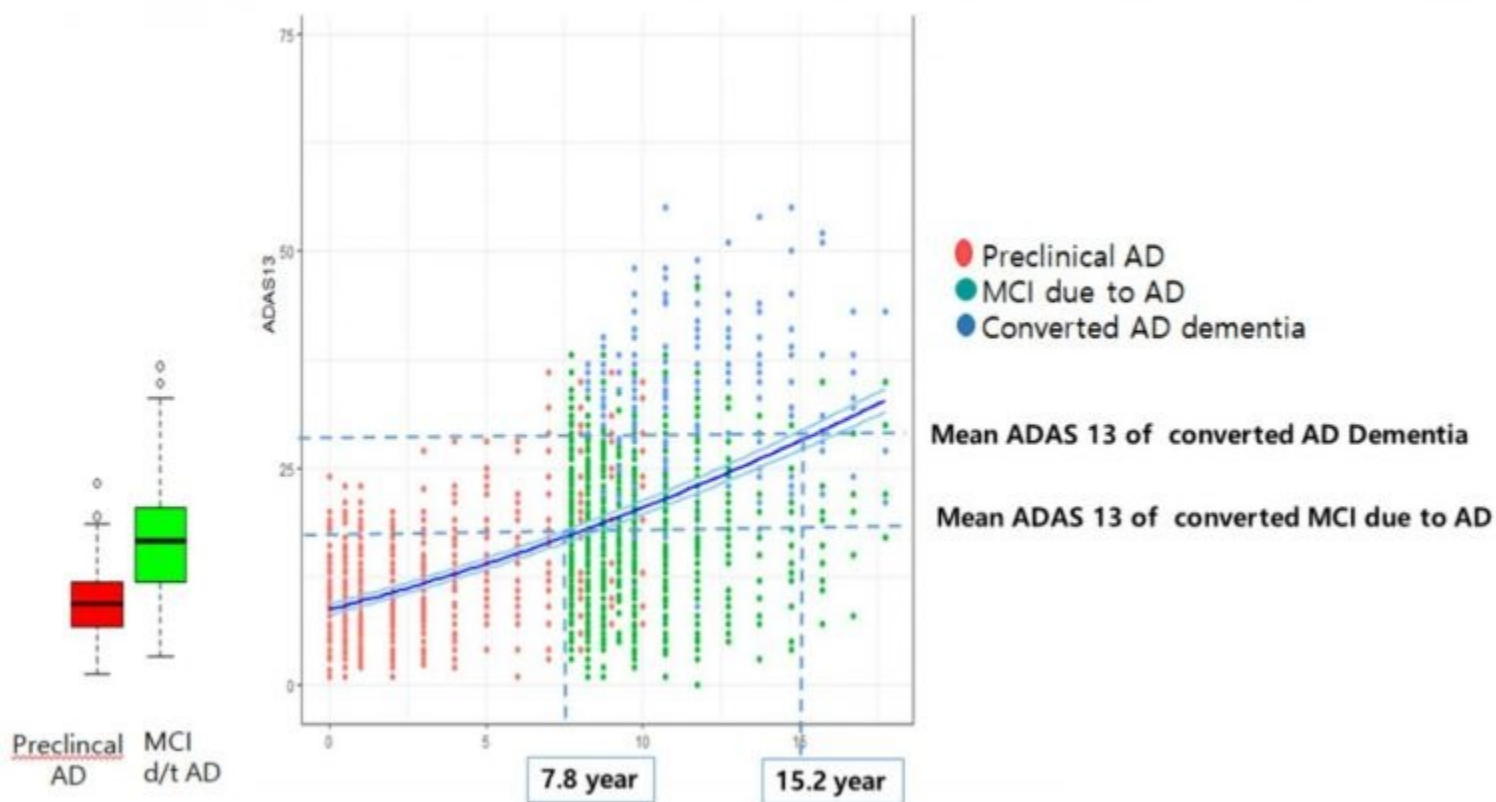Figure 1. Accelerated longitudinal model with ADAS cog 13

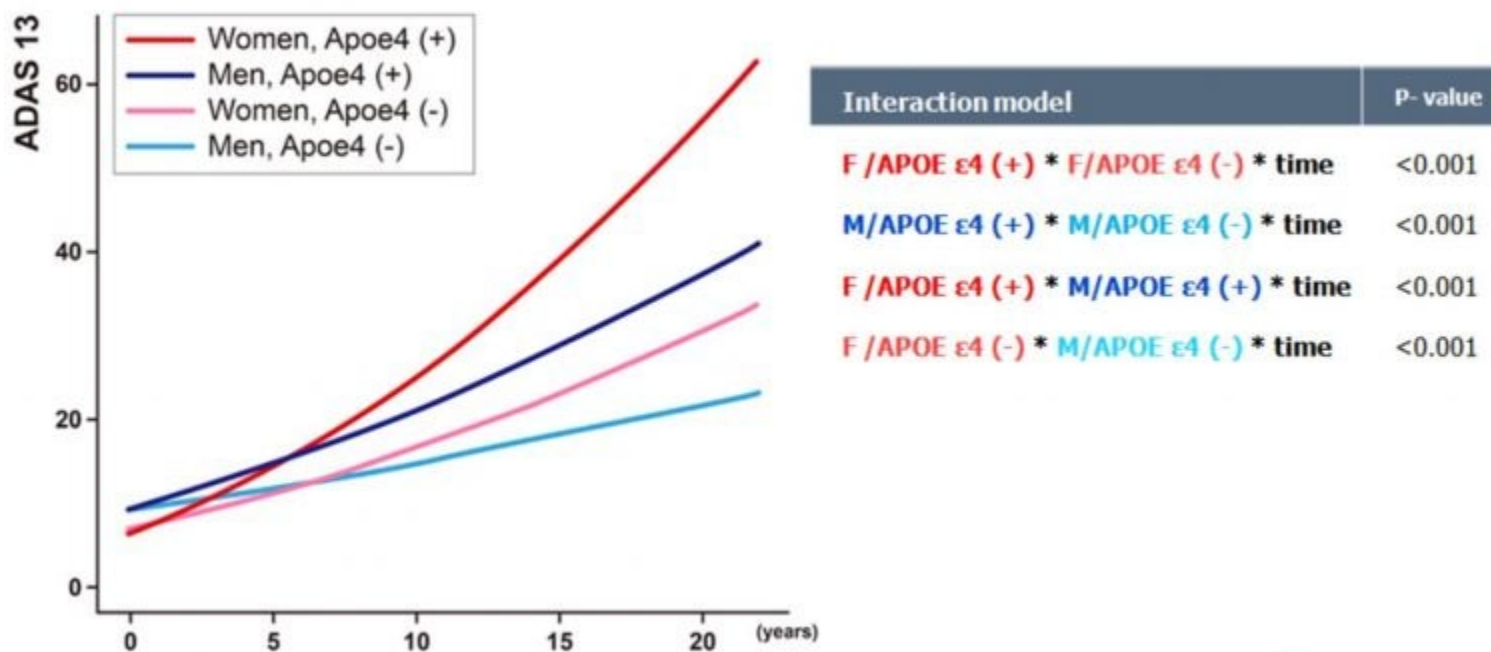Figure 2. Disease progression course modeling from preclinical AD to AD dementia

Figure 3. APOE4 effects on disease progression course by sex

P122: Metabolism mediates the effect of tau on cognition in mild cognitive impairment and dementia

Elena Rodriguez-Vieitez[1], Mariam S. Mazrina[1], Konstantinos Chiotis[1,2], Elisa Colato[1], Agneta Nordberg[1,3]

[1]*Division of Clinical Geriatrics, Department of Neurobiology, Care Sciences and Society, Karolinska Institute, Stockholm, Sweden*
[2]*Theme Neurology, Karolinska University Hospital, Stockholm, Sweden*
[3]*Theme Aging, Karolinska University Hospital, Stockholm, Sweden*

Aim: To investigate the association between tau and cognition via direct and/or indirect (mediated by glucose metabolism) pathways, in a cross-sectional sample of amyloid-negative mild cognitive impairment (Aβneg-MCI), amyloid-positive MCI (prodromal AD) and AD dementia patients.

Methods: We examined 67 patients (35 Aβneg-MCI, 22 prodromal AD, 10 AD dementia; mean age 75.8 [range 56-92] years) and 44 age-matched amyloid-negative controls from ADNI, who had ^{18}F-AV-1451 and ^{18}F-FDG PET scans. Linear regression was used to investigate associations between AV-1451, FDG and cognition. Mediation analysis was applied to explore FDG-mediated effects of AV-1451 on cognition.

Results: When patients were stratified into amyloid-negative (Aβneg-MCI) and amyloid-positive (prodromal AD and AD dementia, or "AD group"), clear differences were observed. While in the AD group AV-1451 had a strong direct negative effect on both episodic memory and global cognition in widespread regions, it only impacted global cognition in Aβneg-MCI restricted to middle/inferior temporal and fusiform gyri. In the AD group, FDG was positively associated to global cognition across widespread regions, and to episodic memory affecting the hippocampus and posterior cingulate cortex. In Aβneg-MCI, FDG showed widespread positive associations with both global cognition and episodic memory.

Hippocampal FDG mediated the effect of AV-1451 on global cognition in the AD group. In Aβneg-MCI, FDG mediated the effect of AV-1451 on both global cognition and episodic memory in parahippocampal, lateral temporal and frontal regions.

Conclusions: Our results show that tau pathology exerts a stronger direct effect on cognition in the presence of Aβ. While the direct effect of tau on cognition was weaker in the absence of Aβ, tau nevertheless had an indirect impact on cognition in Aβneg-MCI patients via the mediational effect of glucose metabolism. Multimodal PET studies may contribute to understanding the pathophysiological mechanisms by which cerebral tau deposits lead to cognitive dysfunction in neurodegenerative diseases.

Keywords: *metabolism, tau, amyloid, mediation, mild cognitive impairment*

P123: Patterns of cerebral tau deposition across Alzheimer's disease stages: A study comparing 18F-THK5317 and 18F-AV-1451 PET tracers

<u>Elena Rodriguez-Vieitez</u>[1], Elisa Colato[1], Konstantinos Chiotis[1,2], Mariam S. Mazrina[1], Agneta Nordberg[1,3]

[1]*Division of Clinical Geriatrics, Department of Neurobiology, Care Sciences and Society, Karolinska Institute, Stockholm, Sweden*
[2]*Theme Neurology, Karolinska University Hospital, Stockholm, Sweden*
[3]*Theme Aging, Karolinska University Hospital, Stockholm, Sweden*

Aim: In-vitro autoradiography studies have shown that the binding properties of different tau PET tracers may depend on the particular conformation, morphology or level of maturity of the tau deposits. However, few **in-vivo** studies have compared the patterns of tau deposition across disease progression as measured by different tau PET tracers. The aim of this study was to compare cross-sectionally the discriminative ability of ^{18}F-THK5317 and ^{18}F-AV-1451 at different stages of Alzheimer's disease (AD), and their correlation with cognition.

Methods: Two cohorts of 29 subjects each (9 healthy control [HC], 11 prodromal AD [pAD], 9 AD dementia [AD]) underwent ^{18}F-THK5317 (Karolinska Institute [KI] cohort) or ^{18}F-AV-1451 (Alzheimer's Disease neuroimaging initiative [ADNI] cohort) tau PET, T1-MRI, and neuropsychological assessments. Regional THK5317 and AV-1451 brain retention (Logan DVR and SUVR, respectively) was quantified with the Hammers atlas using the cerebellum grey matter as reference. Receiver operating characteristic (ROC) analyses were performed to measure the discriminative ability of each tau PET tracer between diagnostic groups. The comparison between tau PET retention at different stages of AD was also investigated using voxel-wise methods. Linear regression was applied to investigate the association between tau and cognition; age and education were covariates.

Results: THK5317 discriminated better than AV-1451 between HC and pAD, while AV-1451 provided better discrimination between pAD and AD stages. Both tracers showed a significant negative association to episodic memory, and AV-1451 had a stronger negative association to global cognition than THK5317.

Conclusions: The results from this study suggest that THK5317 is better able than AV-1451 to capture the early prodromal stage of AD, while AV-1451 performed better at tracking disease progression, showing a stronger correlation with global cognition. Further research is needed to understand whether different tau PET tracers may preferentially bind to different tau conformations at early vs. late stages of AD.

Keywords: *THK5317, AV-1451, tau, cognition, discriminative ability*

P124: Association of subjective cognitive decline and gait slowing with Aβ deposition in cognitively normal individuals

Neelesh Nadkarni[1,2], Subashan Perera[1], Beth Snitz[1,2], Chester Mathis[1], Steven DeKosky[3,4], William Klunk[1,2], Oscar Lopez[1,2]

[1]*University of Pittsburgh School of Medicine, Pittsburgh, PA, US*
[2]*Pittsburgh Alzheimer's Disease Research Center, Pittsburgh, PA, US*
[3]*University of Florida College of Medicine, Gainesville, FL, US*
[4]*Florida Alzheimer's Disease Research Center, Gainesville, FL, US*

Background: Subjective cognitive decline (SCD), an early symptom of AD, is associated with cortical Aβ deposition. Gait slowing precedes cognitive decline in the trajectory to clinical AD, and is also associated with Aβ deposition in dementia-free individuals. SCD could play a role in the association between Aβ and gait speed.

Aim: We examined the cross-sectional relationship among SCD, gait speed and Aβ deposition in cognitively normal individuals.

Methods: SCD severity was quantified on the Memory Functioning Questionnaire (MFQ) on categories that included mnemonic usage (8-items), seriousness of forgetting (18-items) and retrospective functioning (6-items); each item was self-rated on a 1(=always) to 7(=never) scale. Gait speed was measured over 15' walk. Brain Aβ deposition was quantified using Pittsburgh-B (PiB) PET, and PiB-SUVR was averaged over 6 AD-relevant ROIs. We examined interaction between gait speed and each MFQ category on Aβ using linear models, and performed stratified analysis by the median of the MFQ category (lower scores=worse).

Results: In 58 cognitively normal individuals (age: 85.4±3 years; 34.5% female) the mean gait speed was 0.94±0.21 m/sec, mean PiB-SUVR was 1.69±0.43, and MFQ total score was 284.5±42.2 (range:180-365). Interaction between mnemonic usage and gait speed on Aβ deposition was statistically significant (p=0.047). Gait speed correlated significantly with Aβ (r=-0.38, p=0.041) among frequent but not infrequent mnemonic users (r=0.07, p=0.7, Figure 1). Similarly, gait speed correlated with Aβ in those with greater (r=-0.35, p=0.05) but not lesser (r=-0.03, p=0.8) severity of seriousness of forgetting (Figure 2). Findings were qualitatively similar with other MFQ categories, except for retrospective function.

Conclusion: SCD may have a bearing on the association between gait slowing and Aβ pathology in cognitively normal individuals. AD pathology may simultaneously influence subtle cognitive symptoms and motor signs in preclinical AD. Examining cognitive-motor interactions along with AD biomarkers are warranted to further explore these findings.
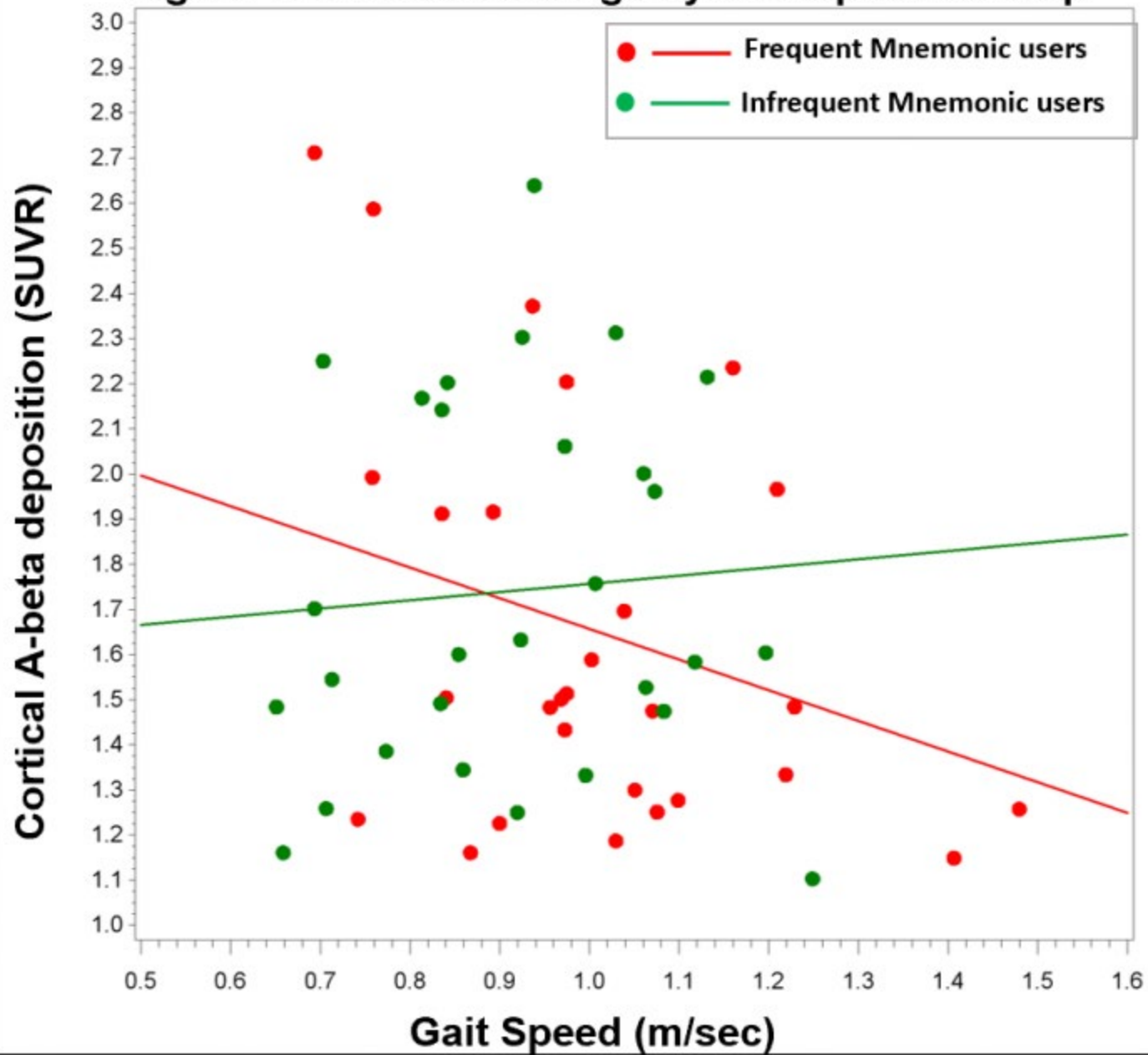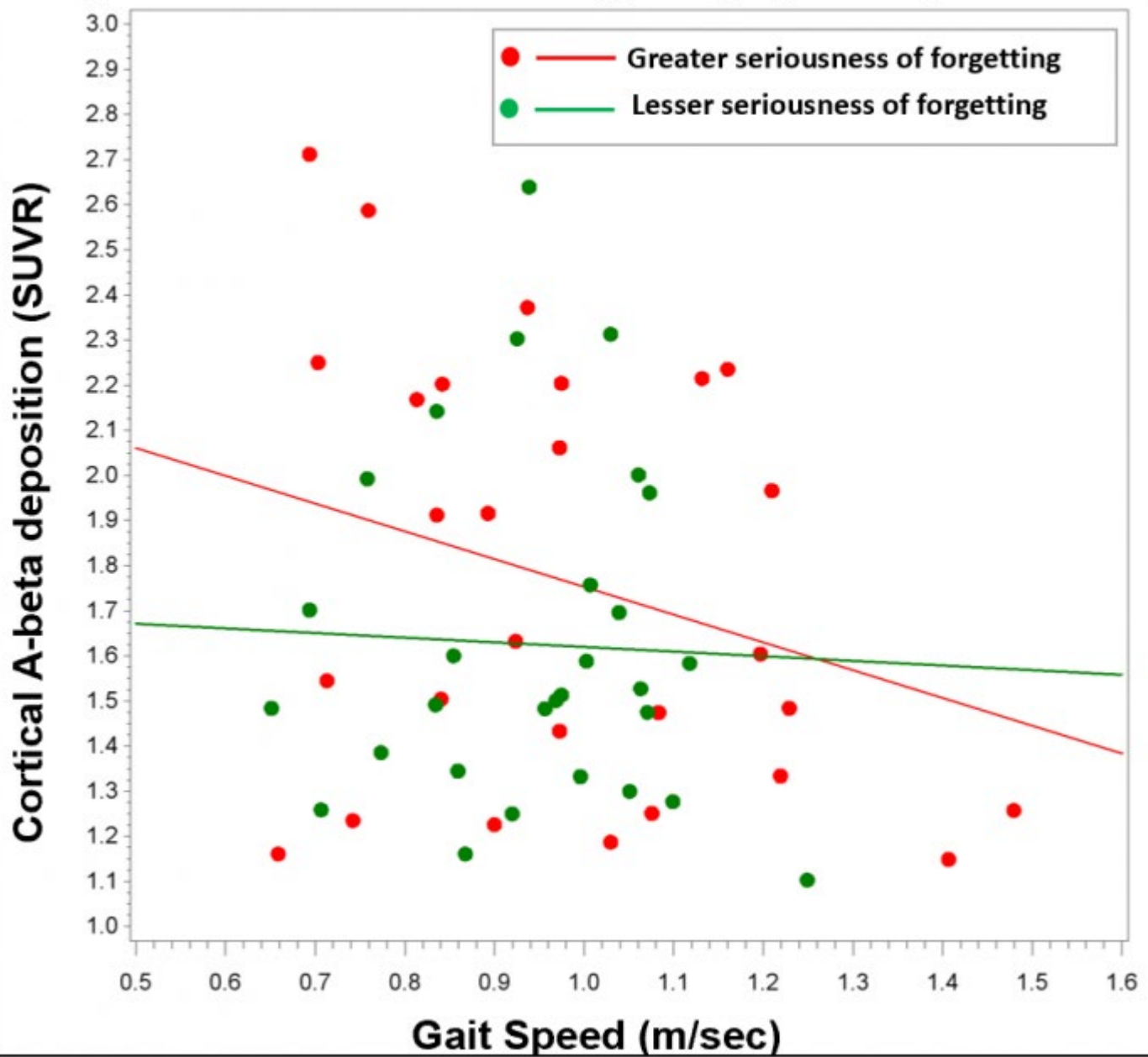
Figure 1: Mnemonic Usage by Gait Speed with Aβ

Figure 2: Seriousness of Forgetting by Gait Speed with Aβ

P125: Cerebrospinal fluid synaptic vesicle glycoprotein 2A in Alzheimer's disease

Nicholas Ashton[1,2,3], Kina Höglund[1,4,8], Antoine Leuzy[1,2], Kerstin Heurling[1,2], Oskar Hansson[5,6], Michael Schöll[1,2,5,7], Henrik Zetterberg[1,8,9,10], Kaj Blennow[1,8]

[1]*Department of Psychiatry and Neurochemistry, Institute of Neuroscience & Physiology, the Sahlgrenska Academy at the University of Gothenburg, Gothenburg, Sweden*
[2]*Wallenberg Centre for Molecular and Translational Medicine, University of Gothenburg, Gothenburg, Sweden*
[3]*King's College London, Institute of Psychiatry, Psychology & Neuroscience, Maurice Wohl Clinical Neuroscience Institute, London, UK*
[4]*Department of Neurobiology, Care Sciences and Society, Center for Alzheimer Disease Research, Neurogeriatrics Division, Karolinska Institute, Novum, Huddinge, Stockholm, Sweden*
[5]*Clinical Memory Research Unit, Lund University, Lund, Sweden*
[6]*Memory Clinic, Skåne University Hospital, Lund, Sweden*
[7]*Department of Neurodegenerative Disease, UCL Institute of Neurology, London, UK*
[8]*Clinical Neurochemistry Laboratory, Sahlgrenska University Hospital, Mölndal, Sweden*
[9]*Department of Molecular Neuroscience, UCL Institute of Neurology, Queen Square, London, UK*
[10]*UK Dementia Research Institute at UCL, London, UK*

Introduction: Measuring synaptic density **in vivo** with positron emission tomography ligands targeting synaptic vesicle protein 2A (SV2A) has received much attention due to its varied research and clinical applications in synaptopathies, especially neurodegenerative disorders. Preliminary findings using [^{11}C]UCB-J in Alzheimer's disease (AD) patients shows decreased ligand uptake, predominantly in the hippocampus. Several candidate cerebrospinal fluid (CSF) biomarkers for synaptic degeneration show a very clear change in AD, but currently there is no assay for CSF SV2A to complement **in vivo** imaging.

Methods: An enzyme-linked immunosorbent assay (ELISA) was developed for the N-terminal region of SV2A and measured in three clinical cohorts. Cohort I (Sahlgrenska University Hospital) consisted of neurochemically defined controls (n=20) and AD patients (n=20). Cohort II (BioFINDER) consisted of biochemically confirmed healthy controls (n=43) and AD patients (n=50), whereas Cohort III (Lariboisière University) consisted of AD (n=87), subjective cognitive decline (n=27), mild cognitive impairment (n=70) and other neurodegenerative disorders (n=50).

Results: In the pilot study (Cohort I), CSF SV2A was significantly decreased in AD patients compared with healthy controls (**P** =0.008). CSF SV2A was correlated highly with CSF Aβ_{42} (**P** =0.008, r =0.486) compared with CSF T-tau (**P** =0.021, **r**=-0.361) and P-tau (**P** =0.025, **r**=-0.355). Further results will examine the replicability of these initial results in a larger cohort (Cohort II) and the performance of CSF SV2A in other neurodegenerative disorders (Cohort III).

Conclusion: Early deliberations surrounding the utility of SV2A PET revolved around its possible use as a marker of neurodegeneration in AD. We have developed an immunological assay to measure SV2A in CSF, with preliminary results indicating decreased levels in AD. Future investigations should determine if concordance exists between CSF and PET measures of SV2A and whether the decrease of CSF SV2A is specific to AD.

Keywords: *SV2A, CSF, Alzheimer's disease, synaptopathies, UCB-J*

P126: Longitudinal evaluation of [18F]MK-6240 in Alzheimer's disease and cognitively normal adults: preliminary results at 6 and 12 months

Cristian Salinas[1], Ajay Purohit[1], Talakad Lohith[2], Arie Struyk[3], Laurent Martarello[1], John Beaver[1]

[1]*Imaging Biomarkers, Biogen, Cambridge, MA, US*
[2]*Translational Biomarkers, Merck & Co., Inc., West Point, PA, US*
[3]*Translational Pharmacology, Merck & Co., Inc., North Wales, PA, US*

Introduction: [^{18}F]MK6240 is a PET radiotracer currently under investigation for the assessment and monitoring of tau pathology in patients with Alzheimer's disease (AD). Here we report preliminary longitudinal data from four AD patients and three healthy adults scanned with [^{18}F]MK6240 at baseline and approximately 6 and 12 month time-points, as well as three AD patients scanned at baseline and 6 months. Baseline scans were acquired in a test-retest design (data reported previously). All seven AD patients were amyloid positive and in the mild to severe range on MMSE.

Results: We first evaluated [^{18}F]MK6240 signal change over time by comparing data obtained at 6 and 12 months to baseline using $SUVR_{90\text{-}120}$ based on the overall tracer uptake in a composite whole brain cortical gray matter region of interest with cerebellar grey matter as reference region. Cortical grey matter SUVR (Figure 1), showed changes of 6.4±8.2% and 6.5±4.5% on average at 6 and 12 month, respectively which is consistent with the 3% annual whole brain SUVR change reported for [^{18}F]AV-1451[1]. No change was detected in the healthy adults at either time-points. We also explored changes in tau distribution over time in the AD patients using several analytical approaches postulated as more sensitive to the pathology spreading hypothesis. These analyses showed changes in [^{18}F]MK6240 uptake ranging from -5% – 17% at 6 mos, and 2% – 12% at 12 mos.

Conclusion: The results from this study provide further evidence that [^{18}F]MK6240 is a valuable tool to measure longitudinal changes in tau in patients with AD, and that the signal observed in healthy adults remain within test-retest variability.
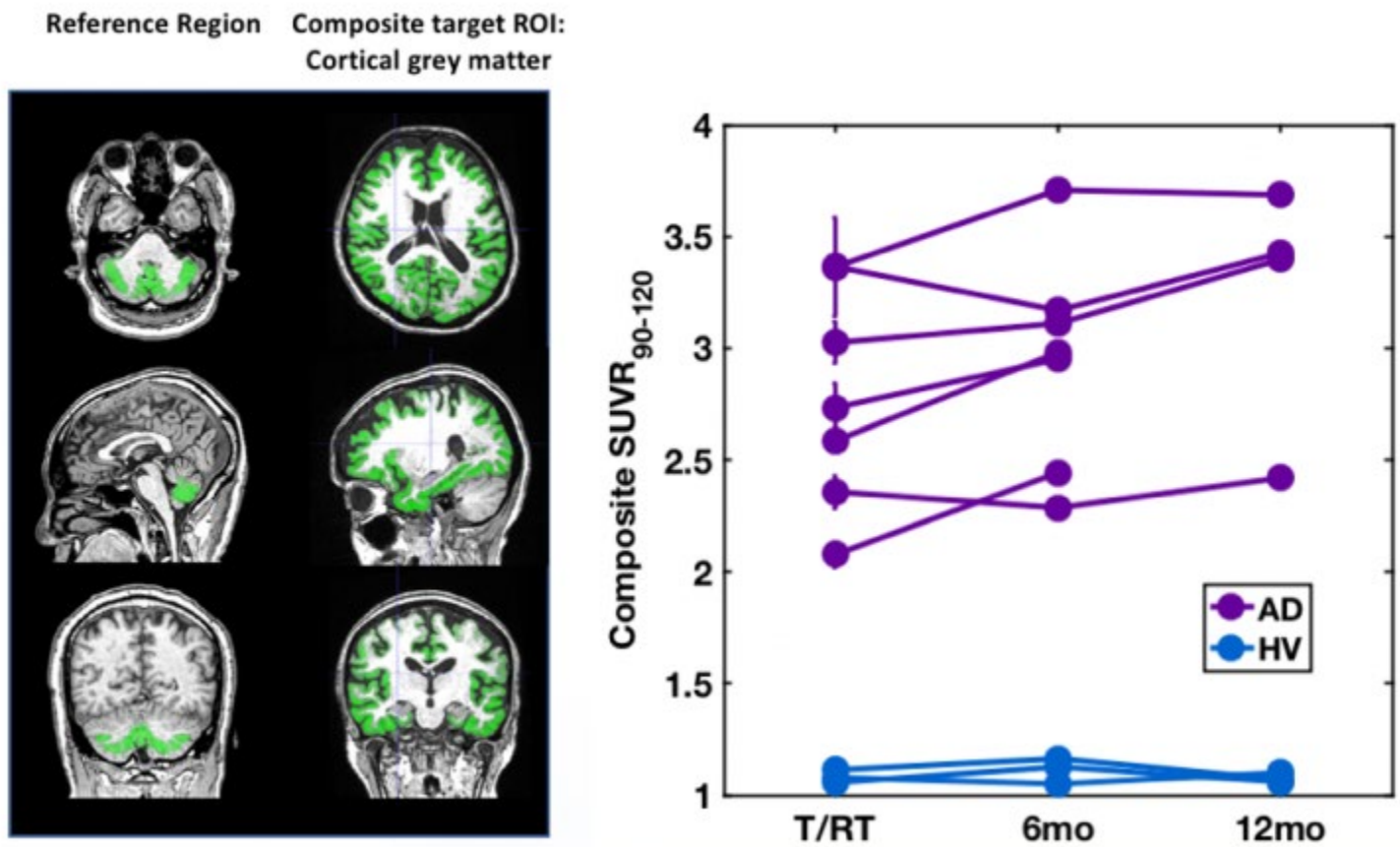
Figure 1: Definition of the reference region, composite target ROI and longitudinal change of the composite SUVR90-120

1. Jack, C.R., Jr. et al. Longitudinal tau PET in ageing and Alzheimer's disease. Brain 141, 1517-1528 (2018).

Keywords: *[18F]MK-6240, Tau, PET, Alzheimer's disease, Longitudinal*

P127: Subicular volume as a surrogate marker of beta-amyloid associated episodic memory variation at high age

Clemens Schroeder[1,2], Jiri Van Bergen[1,2], Simon Schreiner[1,2], Rafael Meyer[1,2], Sonja Kagerer[1,2], Laetitia Vionnet[3], Anton Gietl[1], Valerie Treyer[1,4], Alfred Buck[4], Philipp Kaufmann[4], Roger M. Nitsch[1], Klaas Pruessmann[3], Christoph Hock[1], Paul Unschuld[1,2]

[1]*Institute for Regenerative Medicine (IREM), University of Zurich, Zurich, Switzerland*
[2]*Hospital for Psychogeriatric Medicine, University of Zurich, Zurich, Switzerland*
[3]*Institute for Biomedical Engineering, University of Zurich and ETH Zurich, Zurich, Switzerland*
[4]*Department of Nuclear Medicine, University of Zurich, Zurich, Switzerland*

Background: Atrophy of hippocampal substructures has been suggested to reflect increased risk for progression to aging-related cognitive disorder. This study investigated old-aged, non-demented adults for a relationship between hippocampal substructure-volumes, cortical Aβ burden and episodic-memory (EM) performance within the normal range.

Methods: 61 nondemented old-aged adults (mean age: 70.23(SD6.52) years) were administered a T1-weighted MP2RAGE sequence (TR/TE = 4.8 ms/2.1 ms, voxel size = $0.6mm^{3)}$) on a Philips 7-Tesla Achieva whole-body scanner (32-channel receive coil). 11C-PiB-PET and 18F-Flutemetamol-PET were used for dichotomization of the study population ("high-" versus "low-Aβ ") by standard SUVR positivity-cutoff. The Verbal Learning and Memory Test (VLMT), was used for dichotomization of the study group in high- versus low EM. FreeSurfer (V6.0) was used for assessing volumes of hippocampal subfields. Alpha was adjusted by FDR.

Results: When performing a multiple Analysis of Variance (MANOVA), Mahalanobis distances indicated most distinguished effects on variation of hippocampal subfield volumes for coexistent criteria "high- Aβ" and "low EM" (λ=0.34, **p**=0.039). Secondary analysis indicated a significant interactive effect between Aβ and EM for the subiculum (F(1, 57) = 5.90, **p** = 0.018). Volume of the subiculum was significantly lower in subjects with high-Aβ" and low EM compared to the rest of the study popualtion (F(1, 59) = 16.8, **p**=0.002).

Discussion: Our findings are consistent with reports that aging-related hippocampal pathology may manifest first by atrophy of the subiculum. Moreover, our data suggest that subicular volume might represent a surrogate marker for Aβ-burden related variation in episodic memory at high age.

Keywords: *ultra high field MRI, 11C-PiB-PET, hippocampal subfields, preclinical AD*

P128: Clinical significance of amyloid β positivity in patients with probable cerebral amyloid angiopathy markers

Hyemin Jang.[1], Young Kyoung Jang[1], Hee Jin Kim[1], David John Werring[2], Jin San Lee[3], Yeong Sim Choe[1], Seongbeom Park[1], Juyeon Lee[4], Ko Woon Kim[5], Yeshin Kim[6], Soo Hyun Cho[1], Si Eun Kim[7], Seung Joo Kim[1], Andreas Charidimou[7], Duk L. Na[1], Sang Won Seo[1]

[1]Departments of Neurology, Samsung Medical Center, Sungkyunkwan University School of Medicine, Seoul, Korea, Seoul, Korea
[2]UCL Stroke Research Centre, Department of Brain Repair and Rehabilitation, UCL Institute of Neurology and the National Hospital for Neurology and Neurosurgery, London, UK
[3]Departments of Neurology, KyungHee University School of Medicine, Seoul, Korea
[4]Department of neurology, Chungnam National University School of Medicine, Daejeon, Korea
[5]Department of neurology, Chonbuk National University Hospital, Jeonju, Korea
[6]Department of Neurology, Kangwon National University Hospital, Kangwon National University College of Medicine, Chuncheon, Korea
[7]Departments of Neurology, Inje University College of Medicine, Busan, Korea
[8]Department of Neurology, Massachusetts General Hospital Stroke Research Center, Harvard Medical School, Boston, MA, US

Methods: We recruited 65 patients with CAA markers, defined by the modified Boston criteria for probable CAA. All patients underwent amyloid PET, MRI and neuropsychological tests. We obtained information of CAA markers including lobar intracranial hemorrhage (ICH)/cerebral microbleeds (CMBs) and cortical superficial sederosis (CSS); and ischemic cerebral small vessel disease (CSVD) markers, including lacunes and white matter hyperintensities (WMH). We investigated the effect of Aß positivity on longitudinal cognitive decline using linear mixed effect models.

Results: Among 65 CAA patients, 43(66.2 %) showed Aβ PET positivity. Aβ positive CAA patients had more lobar CMBs (9(2,41) vs. 3(2,8), **p**=0.045) and a higher prevalence of CSS (34.9 vs. 9.1%, **p**=0.025), while Aβ negative CAA patients had more lacunes (1(0,2) vs. 0(0,1), **p**=0.029) and a higher prevalence of severe WMH (45.5 vs. 20.9%, **p**=0.040). Finally, Aβ positivity was associated with faster decline in multiple cognitive domains including language (**p** < 0.001), visuospatial function (**p** < 0.001), and verbal memory (**p** < 0.001) in linear mixed effects models.
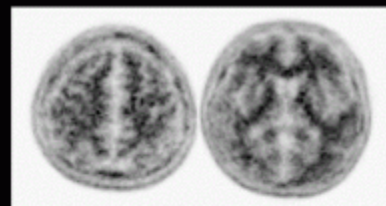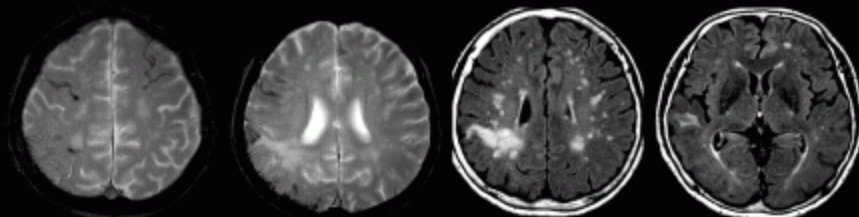
Conclusions: Our findings suggest that a significant proportion of patients with probable CAA in a memory clinic are Aβ PET negative. Aβ positivity in CAA patients is associated with a distinct pattern of MRI CSVD biomarker expression, and a worse cognitive trajectory. Aβ positivity has mechanistic and clinical relevance in CAA, and might represent either advanced CAA or additional AD neuropathologic changes.

Patient 1.
F/70
APOE 2/3

After 1.5 years
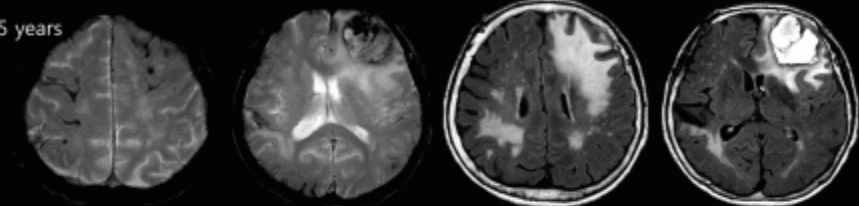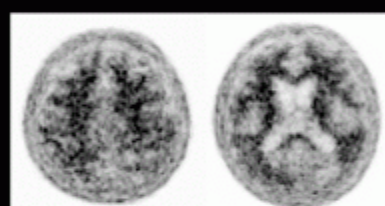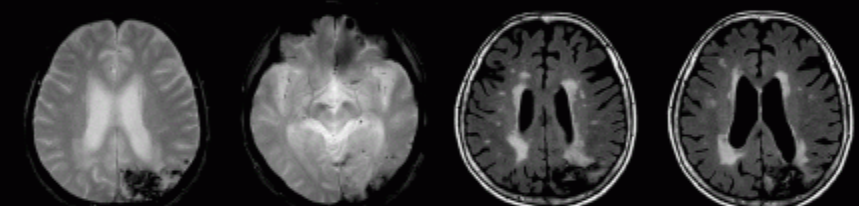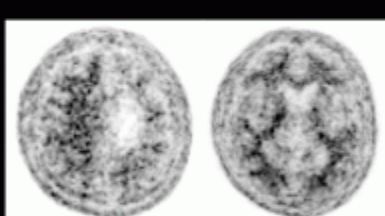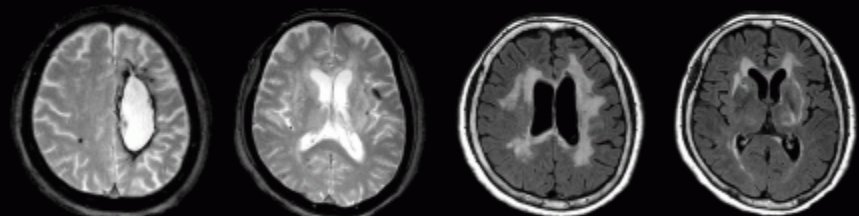
Patient 2.
F/77
APOE 3/3

Patient 3.
F/70
APOE 3/3

Patient 4.
F/78
APOE 3/3

T2*-GRE

FLAIR
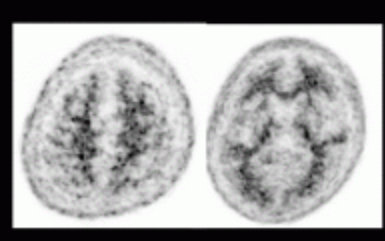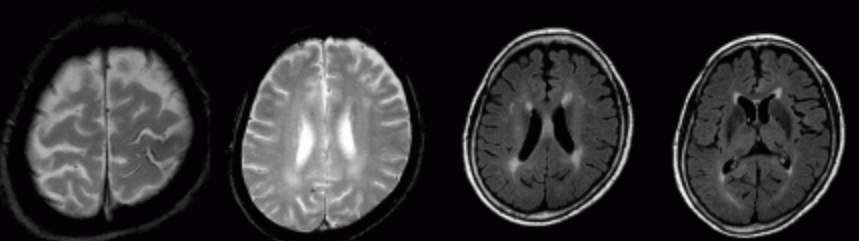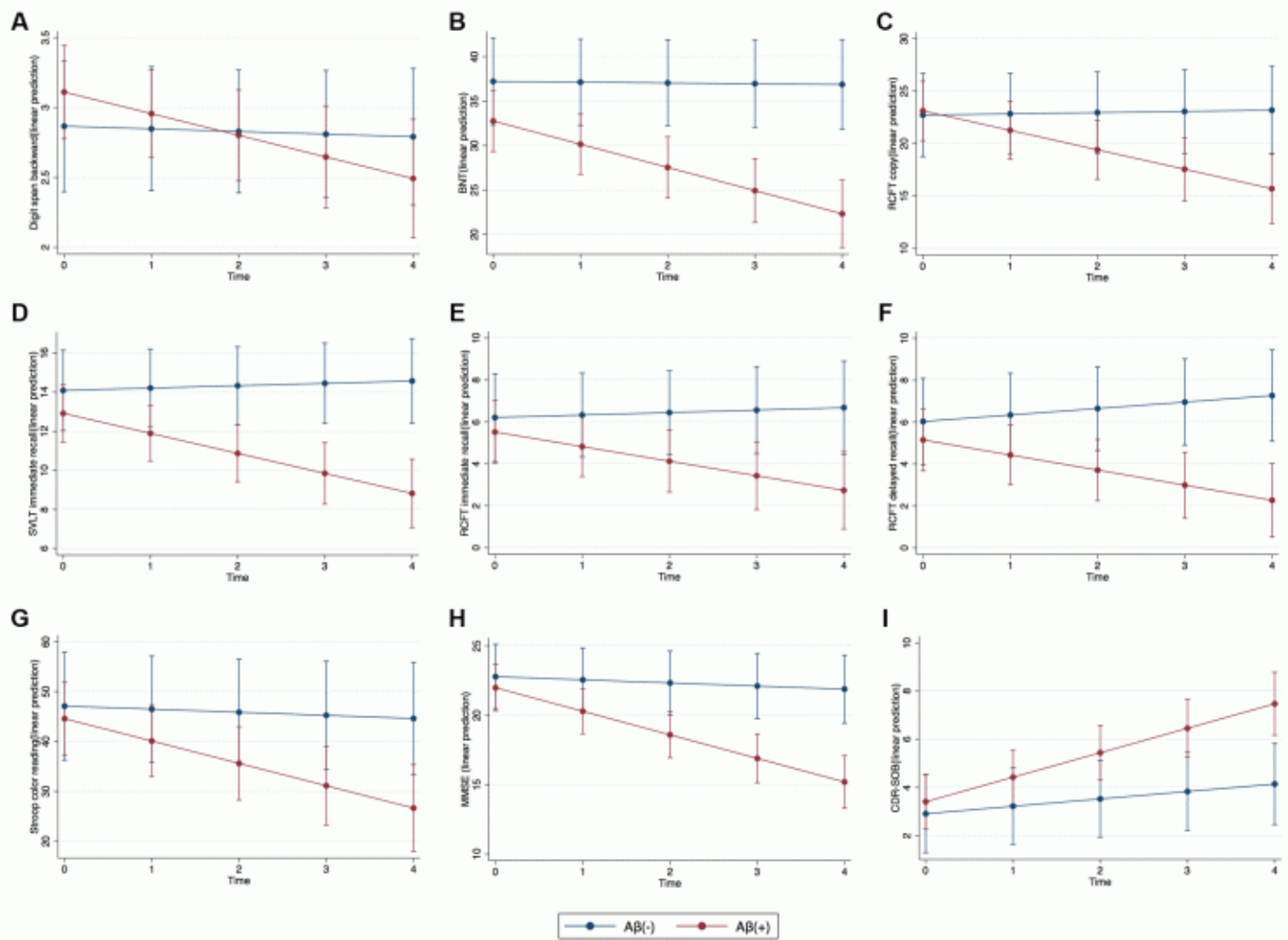
Florbetaben PET

P129: Tau deposition in amyloid negative subjects: the application of the AT(N) model in the Geneva Memory Center experience

<u>Alessandra Dodich</u>[1], Giovanni Frisoni[2,3,4], Paulina Andryszak[3,4], Max Scheffler[5], Aline Mendes[6], Frédéric Assal[7], Roger Schibli[8,9], Adam J Schwarz[10,11,12], Barinjaka Rakotomiaramanana[4], Gabriel Gold[6], Dina Zekry[6], Karl-Olof Lovblad[5], Christian Chicherio[3,7], Marina Boccardi[2,4], Paul Unschuld[13], Valentina Garibotto[1,5]

[1]*Neuroimaging and Innovative Molecular Tracers Laboratory, University of Geneva, Geneva, Switzerland*
[2]*Laboratory of Alzheimer Neuroimaging & Epidemiology, IRCCS Fatebenefratelli, Brescia, Italy*
[3]*Memory Center - Department of Internal Medicine, University Hospital of Geneva, Geneva, Switzerland*
[4]*Laboratory of Neuroimaging of Aging, University of Geneva, Geneva, Switzerland*
[5]*Department of Radiology and Medical informatics, Geneva University Hospital and University of Geneva, Geneva, Switzerland*
[6]*Department of General Internal Medicine, Rehabilitation and Geriatrics, Geneva University Hospital, Geneva, Switzerland*
[7]*Neuropsychology Unit, Department of Neurology, Geneva University Hospital, Geneva, Switzerland*
[8]*Department of Chemistry & Applied Biosciences, Institute of Pharmaceutical Sci, ETH, Zurich, Switzerland*
[9]*Center for Radiopharmaceutical Sciences ETH-PSI-USZ, Paul Scherrer Institut, Villigen, Switzerland*
[10]*Department of Radiology and Imaging Sciences, Indiana University School of Medicine, Indianapolis, IN, US*
[11]*Takeda Pharmaceutical Company Ltd, Cambridge, MA, US*
[12]*Department of Psychological and Brain Sciences, Indiana University, Bloomington, IN, US*
[13]*Institute for Regenerative Medicine, University of Zurich, Zurich, Switzerland*

Objectives: The prevalent neuropathological model of AD postulating that amyloid deposition (A) leads to a cascade characterized by tau aggregation (T) and neurodegeneration (N) has been recently questioned by the discovery of subjects with abnormal (N) or T status, despite normal amyloid burden. We report the results of an ongoing study at the University Hospitals of Geneva aimed at investigating the AT(N) status through PET and structural MRI biomarkers in subjects with subjective cognitive decline (SCD) and objective cognitive impairment.

Methods: Subjects performed an in-depth clinical/neuropsychological evaluation. A and T PET biomarkers as well as MRI measures of (N) were acquired. Subjects were classified as A+/A- and N+/N- according to the presence/absence of amyloid burden and medial temporal atrophy. We compared tau deposition across AN subgroups in regions of interest specifically involved in each Braak pathological stage, and we estimated the Braak staging for each subject through an automatic algorithm.

Results: 70 subjects (14 SCD, 48 mild cognitive impairments, 8 AD dementia) were classified according to the AN status. Significant differences emerged in regions characterizing Braak stage III and Braak stage IV, with A+N+ subjects showing higher tau deposition in comparison to A-N- group. The automatic algorithm showed no tau accumulation (Braak stage 0) in the majority of A-N- subjects (74%). On the other hand, Braak stage VI characterized only A+ subjects and the 64% of A+N+ individuals were classified as Braak stage>3. Eight A- subjects (6 A-N- and 2 A-N+) were classified as Braak staging of I or higher. The analysis in these subjects of the individual picture highlighted substantial heterogeneities both in clinical and imaging findings.

Conclusions: We confirmed a higher tau deposition in A+ subjects. However, a substantial amount of tau pathology, as revealed by Braak staging, characterized a subgroup of A- subjects with and without neurodegeneration.

P130: Characterizing the spatial distribution of cross-sectional [18F]GTP1 (Genentech tau probe 1) SUVR using multivariate statistical analysis and machine learning

Paul Manser[1], Sandra Sanabria Bohorquez[1], Suzanne Baker[2], Balazs Toth[1], Edmond Teng[1], Jan Marik[1], Robby Weimer[1]

[1]*Genentech, South San Francisco, CA, US*
[2]*Lawrence Berkeley National Lab, Berkeley, CA, US*

Objective: To characterize the spatial distribution of cross-sectional tau pathology measured with [^{18}F]GTP1 in Alzheimer's disease (AD) patients and healthy volunteers (HVs).

Methods: [^{18}F]GTP1 scans were performed in amyloid negative and positive healthy volunteers (HV; n=2 and 8, respectively), amyloid positive prodromal (Prod; n=27; MMSE 24-30, CDR = 0.5), mild (Mild; n=19; MMSE 22-30, CDR = 0.5 or 1), and moderate (Mod; n=15; MMSE 22-30, CDR = 0.5-2) AD subjects. Data were quantified using [^{18}F]GTP1 SUVR using the cerebellum as reference. The spatial distribution of [^{18}F]GTP1 SUVR across subjects was summarized with principal component analysis (PCA) using a singular value decomposition. Two elastic net regression models using 3-fold cross-validation were used to find sparse sets of cortical ROIs that together were maximally associated with either AD diagnosis or ADAS-Cog13 scores within AD patients.

Results: PCA results in Figure 1 show that 88% of cross-sectional variability can be explained by the first two principal components (80% and 8%, respectively) which correspond to a whole cortical gray (WCG) SUVR average and a contrast between temporal lobe (TL) and rest-of-brain (RoB). As WCG [^{18}F]GTP1 SUVR increased, TL SUVR tended to increase relative to RoB. However, patients with highest WCG SUVR had a higher RoB SUVR relative to TL. The two elastic net regression models selected similar sets of semi-overlapping ROIs from the TL. Common ROIs selected by the two models included anterior medial temporal lobe, middle and inferior temporal gyri, and fusiform gyrus.

Conclusion: We observed spatial differences in cross-sectional tau pathology that were largely driven by differences between TL relative to RoB. A sparse data-driven subset of TL ROIs were selected as being maximally associated with AD diagnosis and ADAS-Cog13. These results highlight the importance but also variability of tau deposition in the temporal lobe in AD.

Figure 1. Results of principal component analysis on baseline [^{18}F]GTP1 SUVR. Principal component 1 (PC1) explains 80% of variability and is a roughly equally weighted whole cortical grey (WCG) SUVR average. PC2 explains 8% of variability is a contrast between temporal lobe (TL) and rest-of-brain (RoB).
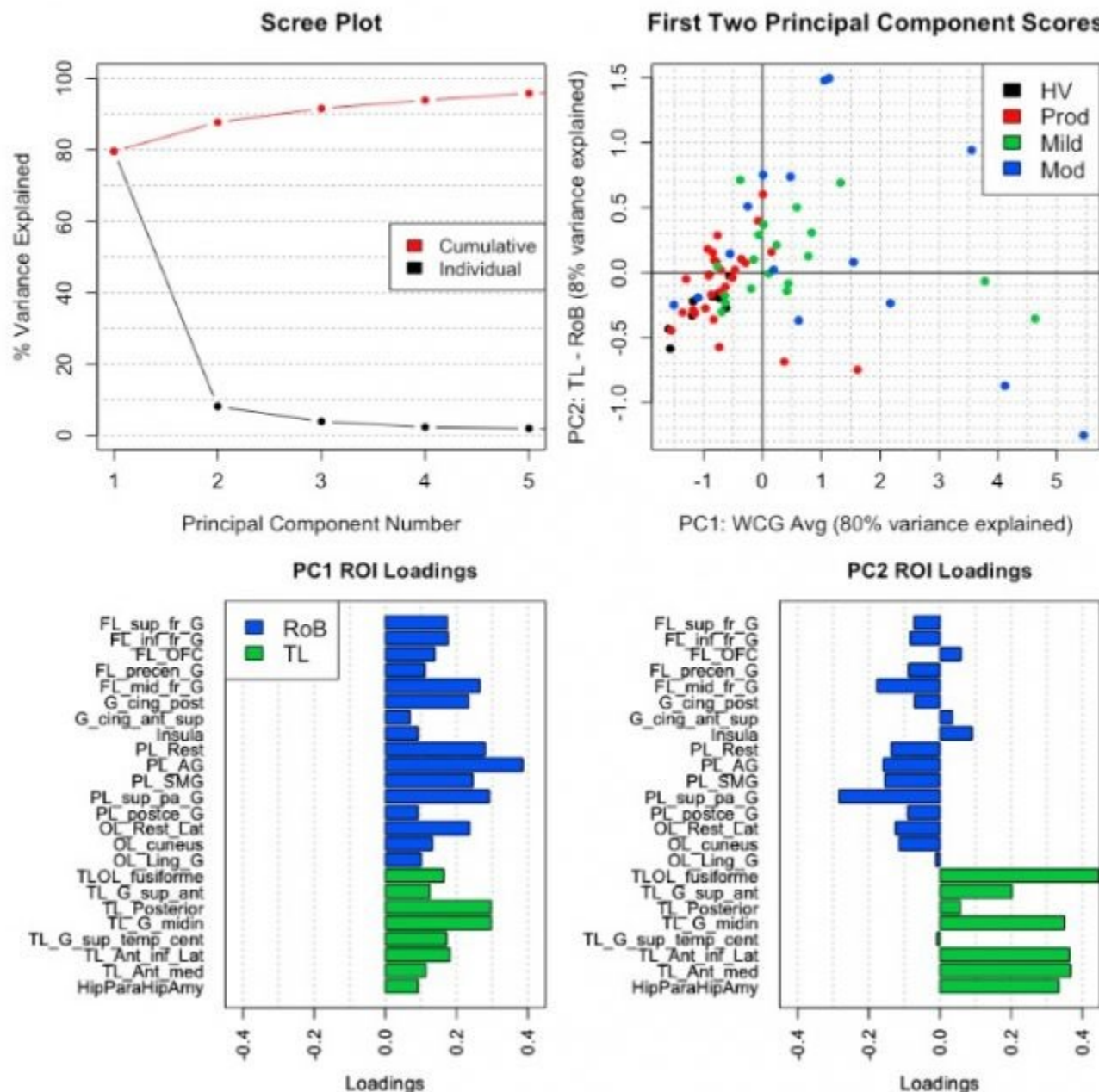
P131: Spatially compact components of non-negative matrix factorization applied to AV-1451 PET images reveal distinct demographic associations

Murat Bilgel[1], Jacob Ziontz[1], Andrea Shafer[1], Dean F. Wong[2], Susan M. Resnick[1]

[1]Laboratory of Behavioral Neuroscience, National Institute on Aging, Baltimore, MD, US
[2]Department of Radiology and Radiological Science, Johns Hopkins University School of Medicine, Baltimore, MD, US

Introduction: Spatial patterns of specific and non-specific AV-1451 binding and their demographic correlates among cognitively normal (CN) individuals remain to be fully elucidated.

Methods: We used data for 55 CN participants from the Baltimore Longitudinal Study of Aging (Table A) with baseline AV-1451-PET and PiB-PET within a year. We spatially normalized Region-Based Voxel-wise (RBV) partial volume corrected AV-1451-SUVR images into MNI space and performed non-negative matrix factorization (NMF) to determine a small number of positive components whose positively-weighted sums best represent the observed images. Using robust linear regression, we characterized the association of each NMF component score with age, sex, race, PiB positivity, and age×PiB status interaction.
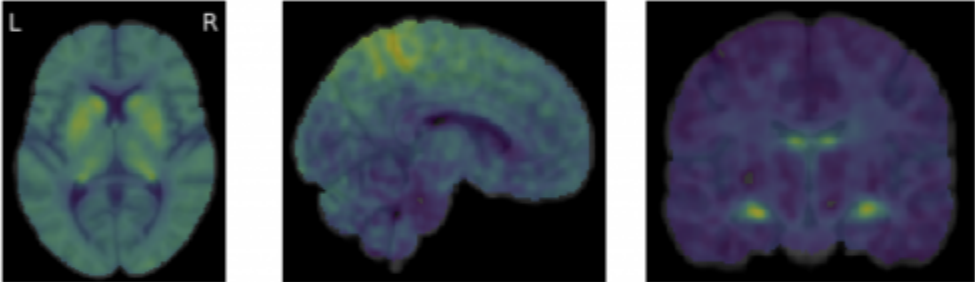
Results: NMF components revealed distinct spatial patterns (Figure 1). Component 1 scores were negatively correlated with second (Pearson's $r=-0.62$, $p<0.001$) and third ($r=-0.26$, $p=0.054$) component scores, whereas no correlation was observed between the latter. Component 1 featured signal throughout the brain, particularly capturing basal ganglia structures, hippocampus, and inferior choroid plexus, and it exhibited positive associations with age ($p=0.007$), PiB positivity ($p=0.018$), and age×PiB ($p=0.002$) (Table B, Figure 2). Component 2 captured the paracentral lobule, precuneus, superior parietal lobule, and possibly meningeal signal spill-over. Age was negatively associated with component 2 scores ($p<0.001$) whereas men had higher scores ($p=0.045$). Component 3 captured the choroid plexus, and scores along this component were negatively associated with age ($p<0.001$).

Discussion: Our results suggest that there is age-associated AV-1451 binding in the basal ganglia among CN individuals, that men may have greater AV-1451 signal in the paracentral lobule and superior parietal cortex, and that choroid plexus AV-1451 signal, thought to represent non-specific binding, is negatively associated with age. Dimensionality-reduction via non-negative matrix factorization yielded spatially compact and interpretable components with distinct demographic associations, enabling us to navigate the multiple comparisons problem in our limited sample.

Table. (A) Participant demographics. **(B)** Results of robust linear regression models investigating the associations of each NMF component scores with age, sex, race, PiB status, and age ✕ PiB status interaction. Estimated regression coefficients are presented with standard errors in parentheses. Statistically significant (i.e., p<0.05) estimates are in red, italicized.

(A)	PiB- N = 41		PiB+ N = 14	
Age at AV-1451 PET, mean (SD)	77.2 (8.89)		79.5 (10.1)	
Female, n (%)	25	(61%)	5	(36%)
Black, n (%)	8	(20%)	4	(29%)

(B)

	Component 1	Component 2	Component 3
Age	*0.054 (0.020)* *p = 0.007*	*-0.18 (0.047)* *p < 0.001*	*-0.13 (0.034)* *p < 0.001*
Male sex	0.44 (0.32) p = 0.17	*1.5 (0.75)* *p = 0.045*	0.37 (0.54) p = 0.50
Black race	0.40 (0.37) p = 0.28	0.89 (0.89) p = 0.31	0.95 (0.64) p = 0.14
PiB positivity	*0.85 (0.36)* *p = 0.018*	0.66 (0.85) p = 0.44	-0.75 (0.62) p = 0.22
Age ✕ PiB status	*0.12 (0.038)* *p = 0.002*	0.045 (0.089) p = 0.61	-0.040 (0.065) p = 0.53

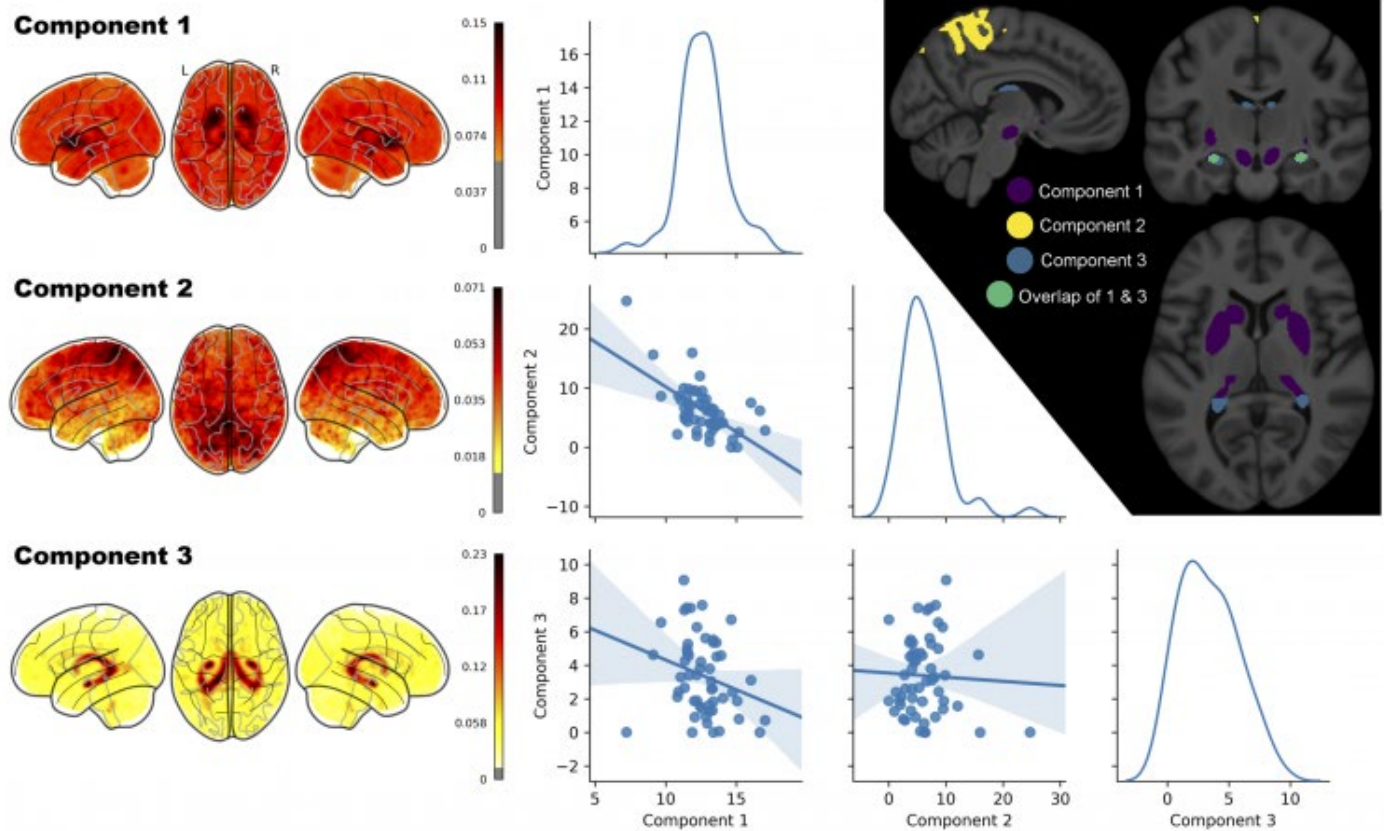**Figure 1.** *Left*: Components obtained from non-negative matrix factorization. *Middle*: Pair plot of scores estimated for each individual per component. Distributions of the scores are presented in the diagonal plots. *Upper right*: The three NMF components binarized at 0.10, 0.05, and 0.15, respectively.
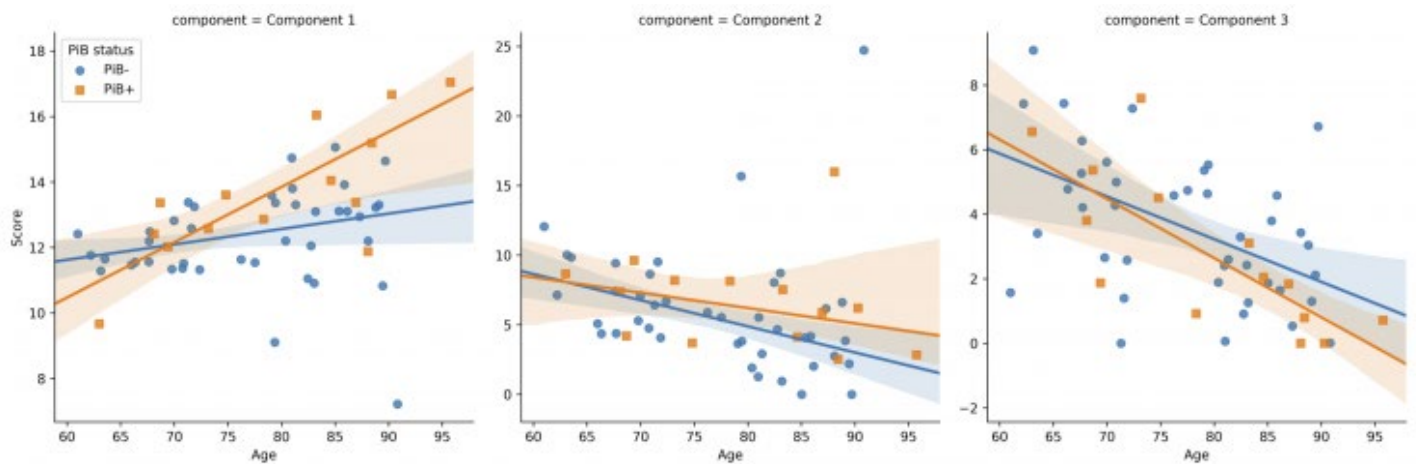

Figure 2. Robust associations of NMF component scores with age by PiB group (not adjusted for sex or race).

P132: Independent contributions of hippocampal activity, amyloid burden, and retrospective decline to Subjective Cognitive Decline

Xi Chen[1], Zhang Jingting[1], Michelle Farrell[2], Denise Park[1]

[1]*Center for Vital Longevity, University of Texas at Dallas, Dallas, TX, US*
[2]*Department of Neurology, Massachusetts General Hospital, Boston, MA, US*

Introduction: Older adults often express feelings of Subjective Cognitive Decline (SCD) which predicts progression to mild cognitive impairment and dementia. In the present study, we investigated the independent and interactive effects of hippocampal activity, amyloid deposition, and actual retrospective memory decline on older adults' reports of memory decline.

Methods: We studied 156 participants (aged 55-93) from the Dallas Lifespan Brain Study. SCD was measured as reports of perceived memory capacity and stability. Individual difference measures used to predict SCD included:

- Hippocampal activity: Participants encoded scene pictures in an fMRI task that was used to extract hippocampal activity during successful encoding relative to baseline (Fig.1).

- Amyloid burden**:** Mean cortical SUVR was measured in 105 participants using florbetapir PET.

- Retrospective memory decline: A difference score between current and retrospective memory with a 4-year interval.

Results: A series of general linear models demonstrated significant independent contributions of hippocampal activity, amyloid, and retrospective decline to SCD (Fig.2). Specifically, lower activation in bilateral hippocampus was the largest contributor to lower perceived memory capacity and stability, particularly for young-old adults (Fig.2a). Additionally, higher amyloid (Fig.2b) and faster decline (Fig.2c) were also associated with greater SCD. No interactions were observed.

Conclusions: The strongest predictor of SCD was decreased hippocampal activation during encoding, with amyloid deposition and retrospective memory decline making additional independent contributions, suggesting that low hippocampal function, associated with worse subsequent memory, predicts SCD regardless of actual decline or amyloid pathology, particularly in young-old adults. The finding shows a surprising sensitivity of participants to inefficient brain activity in a major memory structure that appears to translate into complaints about memory. Future studies with larger samples may further validate the independence of effects observed in our sample, and explore the possibility of multiple concurring but independent mechanisms underlying SCD, which may separately reflect normal and pathological aging.

Fig. 1a. Scene pictures encoded during the subsequent memory fMRI task.
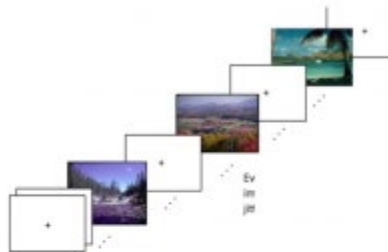
Fig. 1b. Hippocampal activation during encoding (high-confidence remembered > baseline).
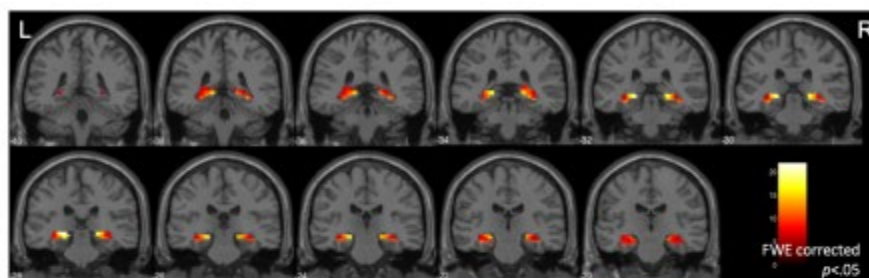
Fig. 1c. Higher hippocampal activation was associated with higher subsequent memory performance.
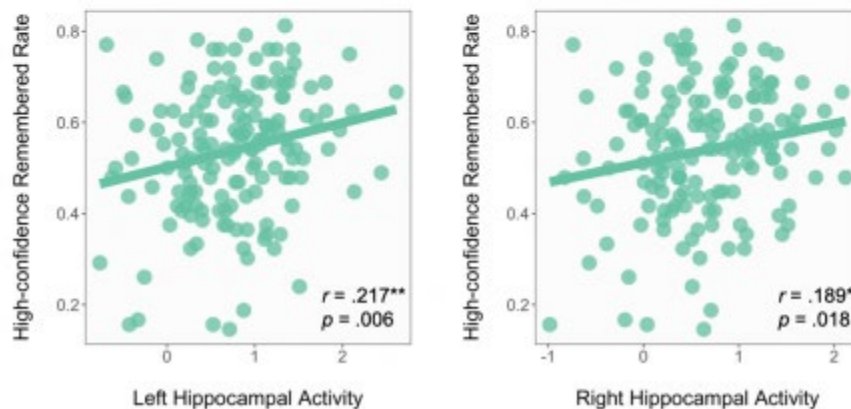
Fig. 2a. Lower hippocampal (HPC) activity was related to lower perceived memory capacity and stability, particularly for young-older adults. Lines in the figure represent the simple slope of the relationship between hippocampal activity and SCD for the particular age.
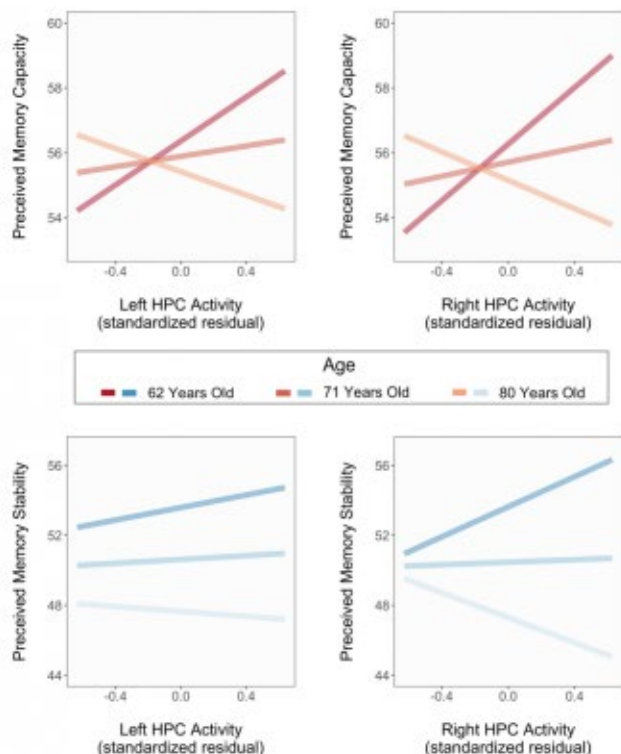
Fig. 2b. Greater amyloid burden was marginally associated with lower perceived memory capacity, and significantly associated with lower perceived memory stability.
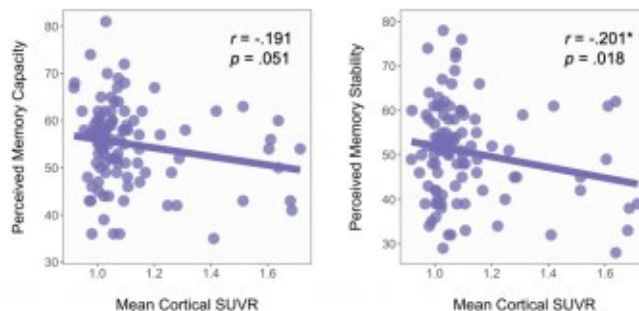
Fig. 2c. Faster retrospective decline predicted lower perceived memory capacity and stability, after controlling for the baseline memory performance.
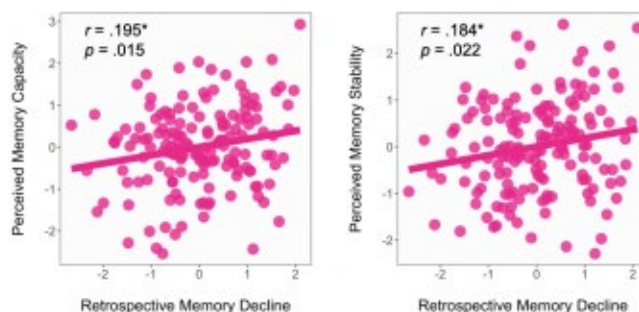
Keywords: *Subjective Cognitive Decline, fMRI, Hippocampus, Amyloid Deposition, Actual Memory Decline*

P133: Amyloid and tau accumulate across distinct spatial networks and are differentially associated with brain connectivity

Joana Pereira[1], Rik Ossenkoppele[2,3], Sebastian Palmqvist[3,4], Tor Olof Strandberg[3], Ruben Smith[3,4], Eric Westman[1], Oskar Hansson[3,5]

[1]*Division of Clinical Geriatrics, Department of Neurobiology, Care Sciences and Society, Karolinska Institute, Stockholm, Sweden*
[2]*Department of Neurology and Alzheimer Center, Neuroscience Campus Amsterdam, VU University Medical Center, Amsterdam, The Netherlands*
[3]*Clinical Memory Research Unit, Department of Clinical Sciences, Lund University, Lund, Sweden*
[4]*Department of Neurology, Skåne University Hospital, Lund, Sweden*
[5]*Memory Clinic, Skåne University Hospital, Malmo, Sweden*

There is increasing evidence that the abnormal accumulation of amyloid and tau does not occur in random brain areas but targets specific spatial networks. However, the relationship between these networks across the entire Alzheimer's disease spectrum has not been explored in a single study including both preclinical and clinical patients. Moreover, it is not known how different amyloid and tau networks are related to functional and anatomical brain connectivity. In this study, we assessed 26 amyloid negative cognitively normal subjects in addition to 32 cognitively normal subjects, 21 patients with mild cognitive impairment and 36 patients with Alzheimer's disease dementia that were all amyloid positive. These individuals underwent ^{18}F-Flortaucipir PET, [18]F- Flutemetamol PET, resting-state functional magnetic resonance, diffusion tensor imaging and neuropsychological testing. Using independent component analyses, we identified a set of 12 amyloid and 10 tau networks. Most of these networks were different for amyloid and tau such as the sensorimotor and temporal networks, although a few converged in brain regions such as the precuneus. The severity of amyloid and tau burden in almost all networks showed significant differences between groups. Both amyloid and tau networks spatially overlapped well with resting-state networks but only the tau networks correlated with decreased white matter integrity. Finally, the tau networks were more closely associated with worse global cognition, memory, executive and visuospatial abilities. Altogether, these findings indicate that amyloid and tau accumulate in different spatial networks but converge in regions like the precuneus, which might be vulnerable to the accumulation of both pathologies. Moreover, our results indicate that amyloid and tau are differentially related to brain connectivity, with both pathologies overlapping well with functional networks but only tau being associated with white matter integrity loss. These findings might lead to a better understanding on the spreading mechanisms of amyloid and tau pathology.

Keywords: *Tau, amyloid, networks, resting-state fMRI, diffusion tensor imaging*

P134: Influence of apolipoprotein-E (APOE) genotype on amyloid trajectories in a longitudinal subject cohort

Brian Lopresti[1], Elizabeth Campbell[1], Zheming Yu[1], Beth Snitz[5], Stewart Anderson[3], Howard Aizenstein[4], Davneet Minhas[1], Sarah Kolibash[1], Ann Cohen[4], Chester Mathis[1], William Klunk[4], Oscar Lopez[5], Dana Tudorascu[2,3,4]

[1]University of Pittsburgh Department of Radiology, Pittsburgh, PA, US
[2]University of Pittsburgh Department of Medicine, Pittsburgh, PA, US
[3]University of Pittsburgh Department of Biostatistics, Pittsburgh, PA, US
[4]University of Pittsburgh Department of Psychiatry, Pittsburgh, PA, US
[5]University of Pittsburgh Department of Neurology, Pittsburgh, PA, US

Introduction: Polymorphic alleles of the APOE gene are established risk modifiers for sporadic AD. Previous studies associate the APOE-e4 allele with an elevated risk of AD, whereas an e2 allele may be protective. Cross-sectional imaging studies show associations between APOE-e4 and Aβ(+) in cognitively normal elderly [1]. This study models the influence of APOE genotype on Aβ trajectories.

Methods: [11C]PiB imaging studies were conducted in 235 subjects (average follow-up =4 years, classified as APOE-e2 (e2e3: n=28), APOE-e4 (e3e4: n=54 and e4e4: n=11), or APOE-e3e3 (n=142). Parametric and non-parametric tests were used to examine group differences in clinical and demographic variables. A mixed model including fixed factors of APOE, age (time-dependent predictor), age squared and their interactions was used to test the associations between APOE and age over time, and to determine the age of Aβ(+) (global SUVR > 1.51[2]) as well as the rate of Aβ accumulation.

Results: Significant group differences were observed for baseline age (p=0.0004), baseline [11C]PiB SUVR (p < 0.001), follow-up interval (p=0.005), proportion of Aβ(+) at baseline (p < 0.001), and prevalence of a not demented diagnosis (p<0.001), Table 1. Modeling of group amyloid trajectories (Figure 1) revealed a much earlier age of Aβ(+) for e4 carriers compared to e3e3 (60.9 vs. 77.5 yrs) and a faster rate of amyloid accumulation at the threshold of Aβ(+) (0.043 vs. 0.029 SUVR/yr). Conversely, e2 carriers showed a later onset of Aβ(+) compared to e3e3 (81.7 yrs) and a similar rate of accumulation (0.035 SUVR/yr).

Conclusion: This study demonstrates that an earlier age of onset and a faster rate of Aβ accumulation are characteristic of APOE-e4, whereas APOE-e2 may have a modest protective effect. More data in APOE-e2 carriers would help to further characterize this association.

[1]Jansen et al. (2018) JAMA 414:1924-38

[2]Cohen et al. (2013) Neuroimage 71:207-215

Table 1. Clinical and demographic variables (mean(SD)) for APOE subject classes

	ε3ε3 (n=142)	ε2 Carriers (n=28)	ε4 Carriers (n=65)	Test Statistic (df), p-value
Age at Baseline (SD)	78.87 (8.92)	75.61 (10.17)	73.52 (9.23)	F: 7.98 (2), p = 0.000445
Baseline [^{11}C]PiB SUVR (SD)	1.56 (0.40)	1.33 (0.35)	1.86 (0.47)	F: 19.03 (2), p << 0.001
Years from Baseline (SD)	4.48 (2.34)	4.03 (2.40)	3.39 (1.80)	F: 5.49 (2), p = 0.00468
Visit Number (SD)	3.23 (0.97)	3.25 (1.40)	2.91 (0.84)	F: 2.45 (2), p = 0.0889
Nonwhite race/ethnicity, No. (%)	10 (7)	3 (11)	6 (9)	Fisher's Exact: p = 0.6837
Female sex, No. (%)	74 (52)	11 (39)	28 (43)	χ^2: 2.44 (2), p = 0.2946
Education (SD)	15.11 (2.66)	15.75 (2.80)	16.09 (3.19)	F: 2.84 (2), p = 0.0602
Median MMSE (IQR)	29 (2)	28 (2)	28 (3.25)	KW: 4.00 (2), p = 0.14
Globally PiB Positive, No. (%)	52 (37)	4 (14)	44 (68)	χ^2: 28.00 (2), p << 0.001
Not Demented Dx, No. (%)	119 (83)	19 (68)	35 (54)	Fisher's Exact: p << 0.001

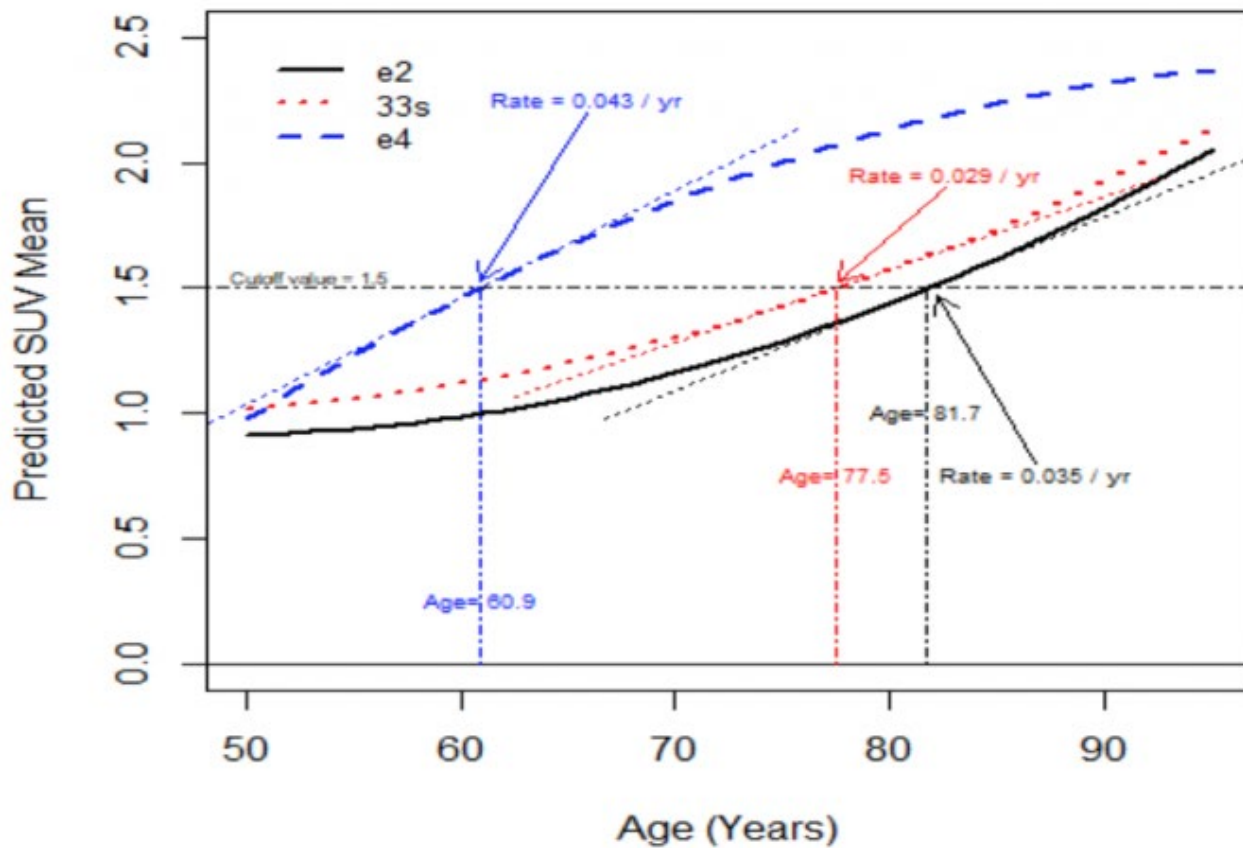**Figure 1.** Models of amyloid trajectories for three APOE subject classes (ε2 carriers, ε4 carriers, and ε3 homozygotes). Shown is the global cortical PiB positivity threshold (1.51 SUVR) showing the age of expected [^{11}C]PiB positivity and the rate of Aβ accumulation at the threshold of positivity.

Keywords: *PiB, APOE, amyloid, aging, longitudinal*

P135: A follow-up report on the prevalence and magnitude of amyloid positivity between cognitively normal elderly Japanese and Americans

Zheming Yu[1], Brian Lopresti[1], Masafumi Ihara[2], Chendi Cui[3], Howard Aizenstein[4], Aya Higashiyama[2], Tetsuya Fukuda[2], Motohiko Koizumi[2], Davneet Minhas[1], Oscar Lopez[5], William Klunk[4], Chester Mathis[1], Yoshihiro Miyamoto[2], Lewis Kuller[3], Akira Sekikawa[3]

[1]University of Pittsburgh Department of Radiology, Pittsburgh, PA, US
[2]National Cerebral and Cardiovascular Center, Suita, Japan
[3]University of Pittsburgh Department of Epidemiology, Pittsburgh, PA, US
[4]University of Pittsburgh Department of Psychiatry, Pittsburgh, PA, US
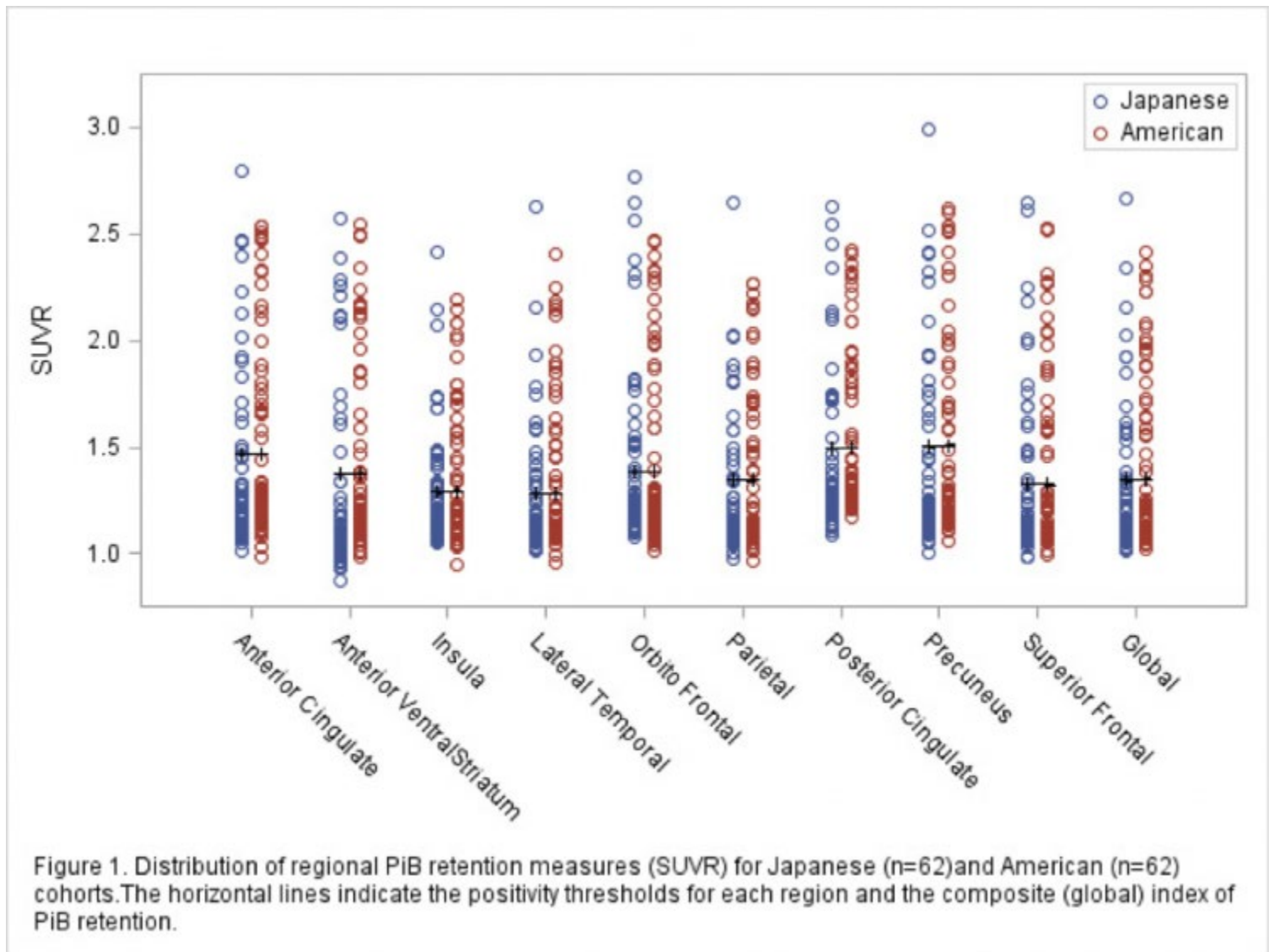*[5]University of Pittsburgh Department of Neurology, Pittsburgh, PA, US*

Background: Epidemiological studies imply a lower prevalence of Alzheimer's Disease (AD) in Japan compared to American and European populations despite the Japanese having greater longevity. We have previously reported a similar prevalence of brain amyloidosis for cognitively normal (CN) elderly Japanese and Americans based on a limited number of participants (n=21). The present study represents an ongoing analysis of PiB retention involving a larger cohort.

Methods: 62 CN elderly Japanese participants (32M/30F) aged 80-89 were recruited from the Suita study and underwent PiB imaging in Japan. Regional and global PiB retention indices were determined. For each Japanese participant, a CN American counterpart was identified from Pittsburgh study cohorts- matched in terms of age, gender, and education. To exclude MCI and dementia, all participants underwent neuropsychological testing and evaluation by experienced neuropsychologists.

Results: Age and gender were well matched between Japanese and American subjects and there were no significant differences in cognition (**P**=0.86). Using the Wilcoxon signed rank test, we observed a trend towards a lower rate of Aβ(+) in Japanese (26% vs 40%, P=0.09), a borderline significant trend in lower global PiB SUVR in Japanese [Median(quantiles) 1.16 (1.10, 1.36) vs 1.22 (1.11, 1.72), **P**=0.06] and significantly lower regional PiB SUVR in Japanese for anterior cingulate [1.23 (1.13, 1.46) vs 1.29 (1.20, 1.86), **P**=0.03], anterior ventral striatum [1.09 (1.01, 1.26) vs 1.22 (1.11, 1.84), **P**=0.003], posterior cingulate [1.27 (1.20, 1.47) vs 1.36 (1.26, 1.86), **P**=0.03], and precuneus [1.21 (1.13, 1.60) vs 1.29 (1.19, 1.98), **P**=0.02].

Conclusion: The current study suggests a similar prevalence of global brain amyloidosis between Japanese and American CN elderly, although a borderline significant trend towards lower global PiB retention in the Japanese group was noted. Interestingly, the Japanese group showed significantly lower PiB retention in some regions associated with early AD pathology.

Figure 1. Distribution of regional PiB retention measures (SUVR) for Japanese (n=62) and American (n=62) cohorts. The horizontal lines indicate the positivity thresholds for each region and the composite (global) index of PiB retention.

P136: Association of in vivo [F-18]AV-1451 with [C-11]PiB, [F-18]FDG hypometabolism, and cortical atrophy in chronic TBI subjects

Davneet Minhas[1], James Mountz[1], Charles Laymon[1], Brian Lopresti[1], Sue Beers[2], Jane Sharpless[3], Ava Puccio[4], Kathryn Edelman[3], Chester Mathis[1], David Okonkwo[4]

[1]*Department of Radiology, University of Pittsburgh, Pittsburgh, PA, US*
[2]*Department of Psychiatry, University of Pittsburgh, Pittsburgh, PA, US*
[3]*Neurotrauma Clinical Trials Center, University of Pittsburgh, Pittsburgh, PA, US*
[4]*Department of Neurosurgery, University of Pittsburgh, Pittsburgh, PA, US*

Background: Traumatic brain injury (TBI) is epidemiologically associated with multiple types of dementia, including Alzheimer's disease (AD). The objective of this work was to examine the topographical distribution and severity of **in vivo** neurofibrillary tau and its colocalization with Aβ plaques, hypometabolism, and cortical atrophy in subjects with a history of TBI.

Methods: Structural T1 MR and [F-18]AV-1451, [C-11]PiB, and [F-18]FDG PET images were acquired in 22 TBI subjects (21-61 years old, 1 female). Subjects were classified into 3 categories based on trauma exposure frequency: **few** (<4 exposures), **intermediate** (4-10 exposures), and **numerous** (>10 exposures). MR images were processed with FreeSurfer v5.3 to generate 68 bilateral neocortical regions-of-interest (ROIs) with associated cortical thickness measures. Standardized uptake value ratio (SUVR) images were created for each radiotracer with FreeSurfer cerebellar grey matter as reference and sampled with neocortical ROIs. AV-1451 and PiB SUVR images were visually classified as positive or negative. For each subject, Pearson correlations were assessed for all ROIs between AV-1451 SUVR and PiB SUVR, FDG SUVR, and cortical thickness.

Results: Two subjects with **numerous** trauma exposures were classified as AV-1451-positive and PiB-positive (Case 1: 60-year old male; Case 2: 54-year old male). In Case 1, AV-1451 SUVR was most prominent in the cuneus (2.39 SUVR) and lateral occipital (2.28 SUVR) regions (Figure 1). In Case 2, [F-18]AV-1451 SUVR was most prominent in the banks of the superior temporal sulcus (3.11 SUVR), precuneus (2.97 SUVR), and parietal (2.86 SUVR). In both cases, increased regional AV-1451 SUVR was significantly correlated with decreased FDG SUVR and decreased cortical thickness, but not PiB SUVR (Figure 2).

Conclusion: While limited by sample size, the topography of AV-1451, PiB, FDG, and cortical atrophy seen in these TBI cases is consistent with patterns previously reported in typical and atypical variants of AD, including posterior cortical atrophy.

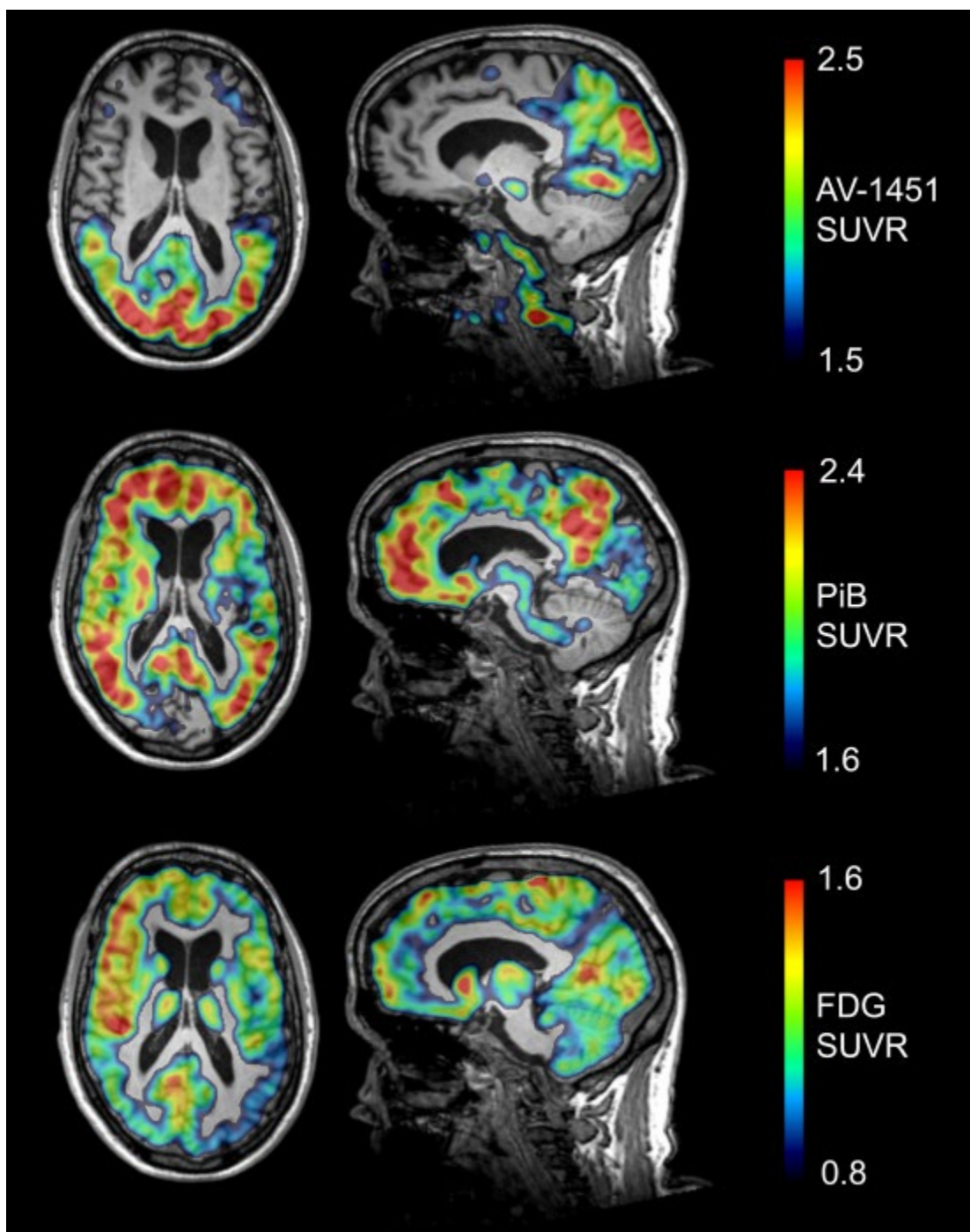Figure 1. Standardized uptake value ratio (SUVR) images of AV-1451, PiB, and FDG from a 60-year old male subject with a history of numerous (>10) traumatic brain injuries.
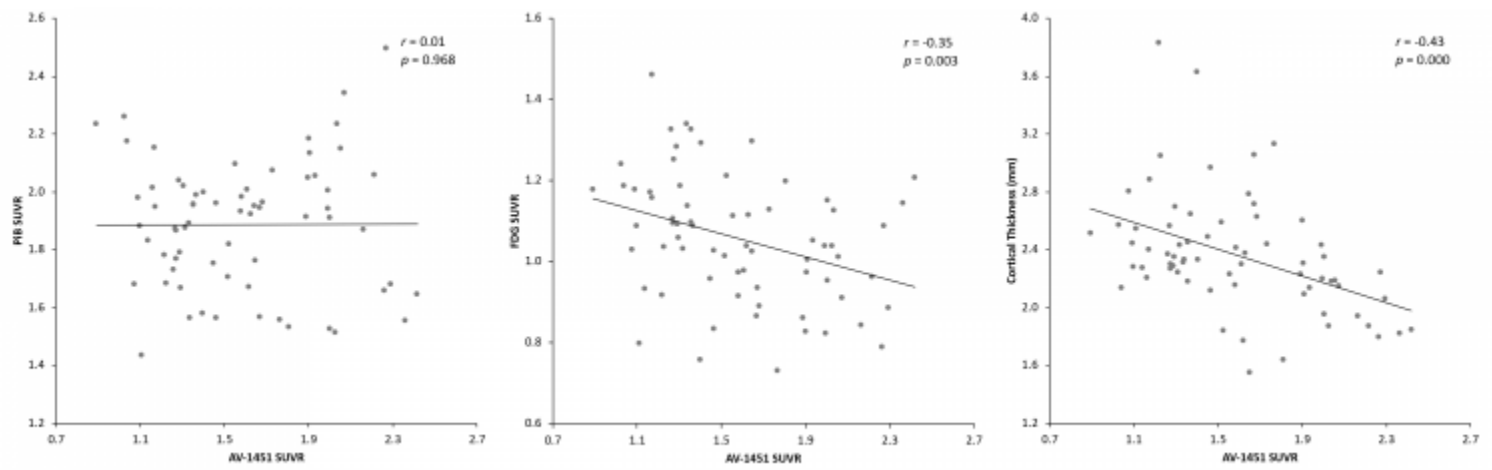
Figure 2. Regional correlations between AV-1451 SUVR and PiB SUVR, FDG SUVR, and cortical thickness for a 60-year old male subject with a history of numerous (>10) traumatic brain injuries.

Keywords: *Traumatic brain injury, AV-1451, PiB, tau, amyloid*

P137: Staging cortical amyloid deposition using PET imaging

Lyduine Collij[1], Fiona Heeman[1], Gemma Salvadó[2], Daniele Altomare[3], Arno de Wilde[3], Elles Konijnenberg[3], Marieke van Buchem[3], Maqsood Yaqub[1], Pawel Markiewicz[4], Sandeep Golla[1], Viktor Wottschel[1], Alle Meije Wink[1], Pieter Jelle Visser[3], Adriaan Lammertsma[1], Philip Scheltens[3], Wiesje van der Flier[3], Ronald Boellaard[1], Bart van Berckel[1], Juan Domingo Gispert[2], Mark Schmidt[5], Frederik Barkhof[1,4], Isadora Lopes Alves[1], On behalf of the AMYPAD consortium

[1]*Radiology and Nuclear Medicine, Amsterdam Neuroscience, VU University Medical Center, Amsterdam UMC, Amsterdam, The Netherlands*
[2]*BarcelonaBeta Brain Research Center, Barcelona, Spain*
[3]*Alzheimer Center, Neurology, Amsterdam Neuroscience, VU University Medical Center, Amsterdam UMC, Amsterdam, The Netherlands*
[4]*Institute of Neurology and Healthcare Engineering, University College London, London, UK*
[5]*Janssen Pharmaceutica, NV, Beerse, Belgium*
[6]*This work has received support from the EU-EFPIA Innovative Medicines Initiatives 2 Joint Undertaking (grant No 115952)., Brussels, Belgium*

Background: Accumulation of amyloid-β (Aβ) plaques in Alzheimer's disease (AD) starts decades before cognitive symptoms. Capturing this process in its earliest stages might be useful for earlier diagnosis and secondary prevention trials. In this context, this study developed and evaluated an **in vivo** model for staging cortical amyloid deposition using PET.

Methods: In total 3025 subjects (1520 controls, 274 SCD, 705 MCI, 422 AD dementia, 104 nonAD dementia) from six cohorts (EMIF-AD, ALFA, ABIDE, ADC, OASIS-3, ADNI) scanned with one of four amyloid radiotracers were included; 993 with longitudinal PET (years: **Mean**=4.04, **SD**=1.81, range=0.85-9.61) (Table 1). The model was constructed from baseline PET scans of 989 cognitively normal subjects, by classifying regions as positive/negative based on tracer-specific cut-offs, ranking their frequency of positivity, and creating 4 clusters (4-stage model). A stage was reached if 50% of its regions were positive. Relationships between baseline stage and CSF $A\beta_{42}$, global PET status (i.e. negative or positive), and follow-up MMSE were assessed, as well as between amyloid stage progression and MMSE decline.

Results: At baseline, 929, 799, 215, 566, and 495 subjects were classified as stage 0-4, respectively. Based on global PET, 1.8%, 5.6%, 33.0%, 72.4%, and 96.0% were positive across stage 0-4, respectively (Figure 1A & B). Increasing cortical amyloid stage was associated with decreasing z-scored CSF $A\beta_{42}$ levels (**F**=267.09, **p**<0.05) (Figure 1C) and with faster progression towards MMSE≤27 (**N**=1267, **p**<0.01). 'Amyloid stage progressors' (**N**=156) reached MMSE≤27 faster (trend, **p**=0.08) than 'non-progressors' (**N**=369). Baseline stage predicted MMSE change when corrected for age and follow-up window (**N**=1346, **p**<0.01) (Figure 3).

Conclusion: The proposed cortical amyloid staging model can detect early (pre-global) amyloid burden, potentially supporting both pre-dementia diagnosis and subject inclusion into anti-amyloid trials. The model could also be used as alternative measure of pathological progression and treatment

Table 1. Baseline Demographics Cohorts

Cohort	ALL (N = 3035)	ALFA (N = 226)	EMIF-AD (N = 190)	ADC (N= 145)				ABIDE (N = 353)			
Diagnostic group	N/A	Controls	Controls	SCD (N = 3)	Impaired (N = 10)	AD Dementia (N = 84)	Non AD Dementia (N = 48)	SCD (N = 128)	Impaired (N = 66)	AD Dementia (N = 106)	Non AD Dementia (N = 53)
Age (SD)	68·36 (8·75)	61·17 (4·83)	70·44 (7·55)	59·76 (1·78)	62·80 (7·65)	62·47 (5·41)	61·77 (5·54)	60·70 (7·97)	66·13 (7·09)	66·69 (7·47)	66·84 (7·16)
Gender (F)	1547 (51·2%)	142 (62·8%)	112 (58·9%)	0 (0·0%)	3 (30·0%)	45 (53·6%)	18 (37·5%)	53 (41·4%)	24 (36·4%)	52 (49·1%)	15 (928·3%)
MMSE (SD)	27·60 (3·08)	29·01 (2·25)	28·99 (1·14)	25·00 (3·46)	25·80 (1·75)	22·78 (3·10)	23·96 (3·72)	27·76 (2·42)	26·94 (2·01)	22·41 (4·24)	24·45 (3·40)
APOE ε4 carriership +	1372 (45·4%)	98 (43·3%)	62 (33·3%)	1 (33·3%)	5 (50·0%)	63 (75·0%)	18 (37·5%)	112 (87·5%)	56 (85·8%)	99 (93·4%)	45 (84·9%)
Global PET +	996 (32·9%)	17 (7·5%)	27 (14·5%)	0 (0·0%)	1 (10·0%)	83 (98·8%)	6 (12·5%)	26 (20·3%)	32 (48·5%)	81 (76·4%)	20 (37·7%)
CSF Aβ42 (SD)	N/A	1352·14 (358·67)	892·28 (317·96)	1277·00 (131·52)	918·80 (318·69)	539·75 (92·56)	939·48 (215·34)	1081·74 (283·94)	906·45 (319·25)	681·61 (276·33)	892·94 (295·90)
CSF T-Tau (SD)	N/A	205·02 (77·47)	412·36 (144·56)	192·67 (180·94)	303·71 (397·04)	569·99 (339·82)	357·38 (213·89)	366·23 (286·48)	476·39 (274·50)	651·77 (368·39)	387·72 (178·33)
CSF P-Tau (SD)	N/A	20·29 (18·79)	N/A	37·00 (35·50)	58·40 (46·83)	77·09 (27·36)	44·05 (18·55)	53·92 (29·84)	65·74 (27·82)	79·04 (35·37)	53·47 (17·88)
CSF Essay	N/A	Elecsys	ELISA	Innotest				Innotest			

Table 1. Baseline Demographics Cohorts (continued)

Cohort	OASIS (FBP) (N = 360)				OASIS (PiB) (N = 572)				ADNI (N = 1179)			
Diagnostic group	Controls (N = 306)	Impaired (N = 23)	AD Dementia (N = 30)	Non AD Dementia (N = 1)	Controls (N = 493)	Impaired (N = 25)	AD Dementia (N = 52)	Non AD Dementia (N = 2)	Controls (N = 305)	SCD (N = 144)	Impaired (N = 580)	AD Dementia (N = 150)
Age (SD)	66·78 (8·53)	71·12 (5·51)	73·70 (6·86)	67·61	64·72 (9·40)	72·78 (7·53)	73·93 (7·71)	65·74 (0·35)	73·78 (6·06)	71·85 (5·59)	71·97 (7·49)	74·43 (8·29)
Gender (F)	164 (53·6%)	16 (69·2%)	18 (60·0%)	1 (100%)	306 (62·1%)	10 (40·0%)	17 (32·%)	1 (50·0%)	158 (51·8%)	85 (59·4%)	245 (42·2%)	62 (41·3%)
MMSE (SD)	29·04 (1·25)	28·48 (1·56)	24·63 (4·00)	19·00	29·13 (1·16)	27·12 (1·94)	25·58 (3·57)	26·50 (3·54)	28·75 (1·78)	29·09 (1·16)	27·43 (2·98)	23·03 (2·09)
APOE ε4 carriership +	102 (33·3%)	6 (26·1%)	23 (76·7%)	1 (100·0%)	167 (33·9%)	10 (40·0%)	28 (53·8%)	1 (50·0%)	76 (24·9%)	32 (22·4%)	272 (46·9%)	96 (64·0%)
Global PET +	82 (26·8%)	12 (52·2%)	26 (86·7%)	1 (100·0%)	89 (18·1%)	9 (36·0%)	44 (84·6%)	2 (100·0%)	56 (18·4%)	27 (18·9%)	239 (941·2%)	118 (78·7%)
CSF Aβ42 (SD)	N/A				N/A				1217·74 (446·65)	1248·86 (423·30)	1008·84 (434·77)	683·18 (321·53)
CSF T-Tau (SD)	N/A				N/A				245·54 (92·63)	237·64 (93·50)	279·88 (130·98)	378·24 (155·18)
CSF P-Tau (SD)	N/A				N/A				22·48 (9·46)	21·61 (9·58)	26·77 (14·53)	37·38 (16·15)
CSF Essay	N/A				N/A				Elecsys			

effects.

Figure 1.

A. Frequency of positivity plot
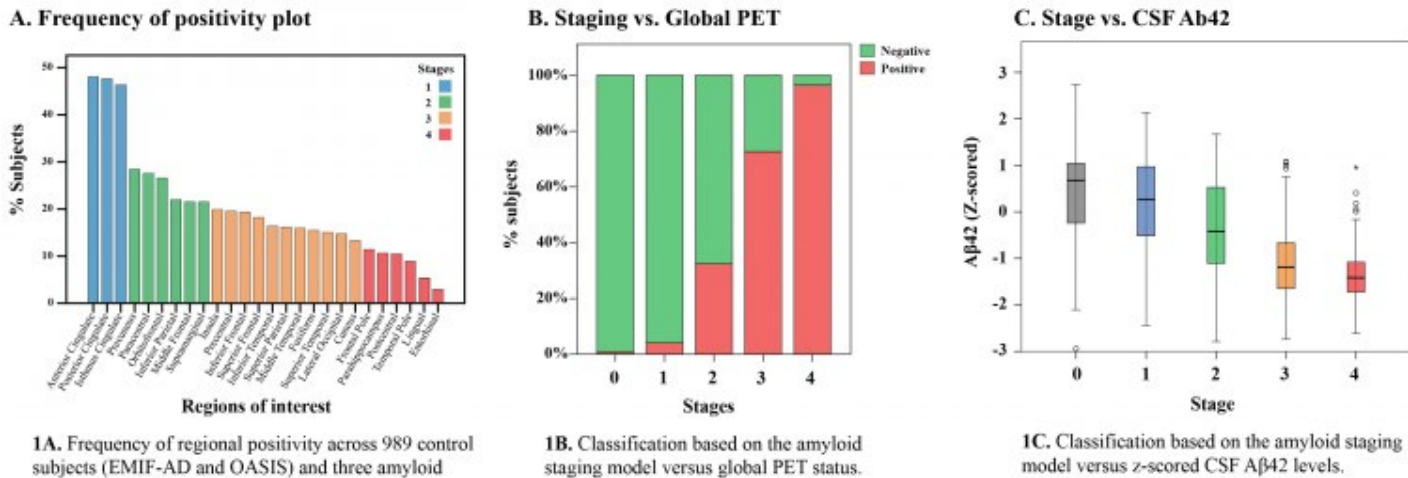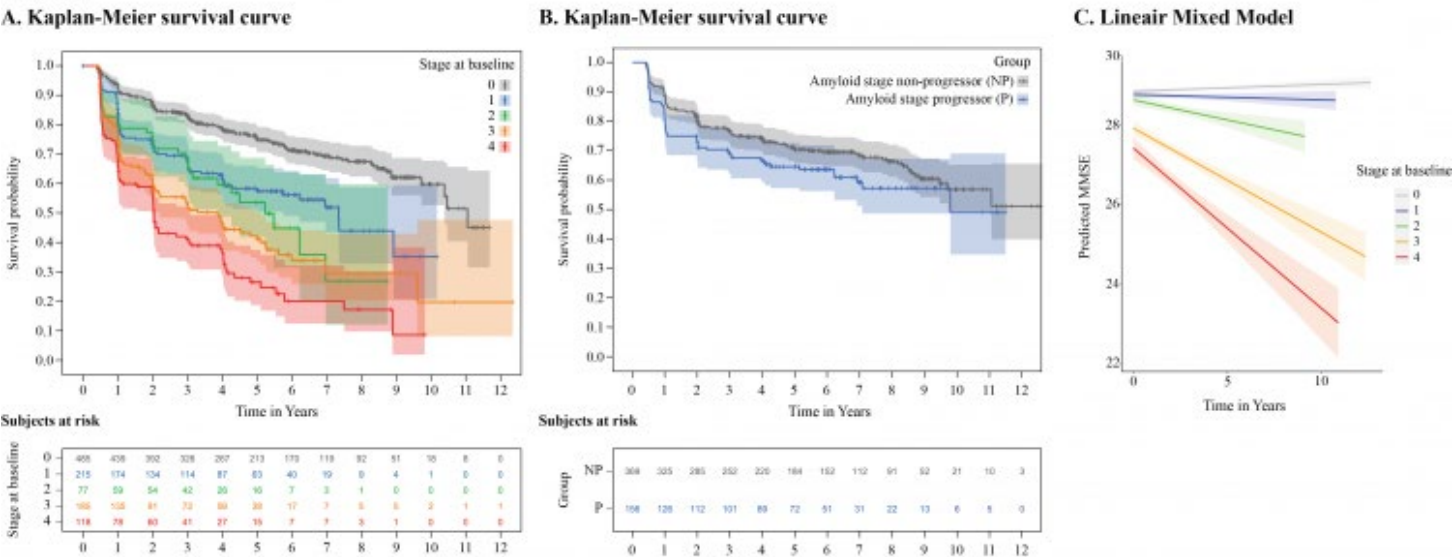

1A. Frequency of regional positivity across 989 control subjects (EMIF-AD and OASIS) and three amyloid tracers ([18F]flutemetamol, [18F]florbetapir, and [11C]PIB), used to construct the model. The colours represent the 4 different stages as defined by the k-means clustering analysis.

B. Staging vs. Global PET

1B. Classification based on the amyloid staging model versus global PET status.

C. Stage vs. CSF Ab42

1C. Classification based on the amyloid staging model versus z-scored CSF Aβ42 levels.

Figure 2.

A. Kaplan-Meier survival curve

B. Kaplan-Meier survival curve

C. Lineair Mixed Model

2A/B. Kaplan-Meier survival plots, in which subjects with a diagnosis of dementia and a MMSE of ≤ 27 at baseline were excluded. The 'event' was reaching a MMSE score of ≤ 27. For **B** only subjects with a baseline stage < 3 were included, where those classified in a higher stage at follow-up PET were considered 'amyloid progressors', and those who remained stable considered 'amyloid non-progressors'.

Keywords: *Amyloid PET, regional, staging, multi-cohort, prevention*

P138: PET analysis of verubecestat effect on amyloid load in mild-to-moderate Alzheimer's disease patients (EPOCH trial)

Cyrille Sur[1], Katarzyna Adamczuk[2], Mehul Sampat[2], James Kost[1], David Scott[2], Joyce Suhy[2], Michael Egan[1]

[1]*Merck & Co., inc., West Point, PA, US*
[2]*Bioclinica, Newark, CA, US*

A recent trial in mild-to-moderate AD patients with BACE inhibitor verubecestat failed to improve cognition. However, verubecestat showed a small reduction of cortical amyloid load at week 78. As verubecestat treated patients exhibited a modest increase in brain volume loss, we investigate the relationship between amyloid loss and MRI volume reduction and the potential impact of partial volume correction (PVC) on amyloid PET signal. Participants between ≥ 55 and ≤ 85 years of age with probable AD and an MMSE score ≥ 15 and ≤ 26 were enrolled. A subgroup of subjects received a Vizamyl scan at baseline and a follow-up scan at week 78. Amyloid PET images were centrally collected, quality controlled, and analyzed at Bioclinica. The 3D-T1 images were segmented and parcellated into anatomical VOIs using masks generated by FreeSurfer (5.3.). PVC was performed according to the Meltzer (MZ) and the SGTM (symmetric geometric transfer matrix) approaches. At baseline, non-PVC mean (SD) Vizamyl composite cortical SUVR were similar in placebo (0.88+/-0.11; n=14), verubecestat 12 mg (0.89+/-0.10; n=20) and 40 mg (0.87+/-0.11; n=10) groups. At week 78 a significant effect of verubescestat was found with a difference in least square mean of -0.03 (p=0.0066) and -0.04 (p<0.0001) for 12 and 40 mg dose, respectively. A strong correlation was found between no PVC and MZ PVC (r2:0.94) or SGTM PVC (r2:0.92) SUVR values. PVC of composite cortical SUVR values with MZ or SGTM methods did not change the pattern of verubecestat effect on amyloid load at week 78. Regression analysis between hippocampus volume and amyloid SUVR change at week 78 did not reveal a meaningful correlation. Treatment with verubecestat for 78 weeks resulted in a small reduction in brain amyloid load. This effect was dose dependent, resistant to partial volume correction and not related to change in brain structure volume.

Keywords: *verubecestat, Vizamyl, PET, BACE, clinical*

P139: Effect of verubecestat on amyloid load in prodromal Alzheimer's disease patients: Results from the PhIII APECS trial

Cyrille Sur[1], James Kost[1], Katarzyna Adamczuk[2], David Scott[2], Joyce Suhy[2], Michael Egan[1]

[1]*Merck & Co., inc., West Point, PA, US*
[2]*Bioclinica, Newark, CA, US*

In a recent Phase-3 trial BACE inhibitor verubecestat was associated with poorer clinical outcomes compared with placebo in prodromal AD subjects. Here we report on the effect of 104 weeks of verubecestat treatment on cortical amyloid load and the relationship between amyloid load status and clinical outcomes.

Participants 50-80 years of age with prodromal AD were randomized in a double-blind, 24-month, placebo-controlled trial of verubecestat (12mg and 40mg). A subgroup of subjects received a baseline and week 104 Vizamyl scan. Amyloid PET images were centrally collected and quality controlled and analyzed at Bioclinica. Composite SUVR was computed using subcortical white matter as reference region.

At baseline, composite cortical SUVR were similar in placebo (0.85+/-0.06; n=65), verubecestat 12 mg (0.86+/-0.07; n=63) and 40 mg (0.87+/-0.07; n=59) groups. At week 104, a reduction (mean, 95% CI) in PET cortical amyloid load SUVR was observed in subjects receiving 12 mg (-0.03 (-0.04,-0.03)) and 40 mg (-0.04, (-0.05,-0.04)) of verubecestat, respectively. Compared to placebo, verubescestat significantly reduced PET cortical amyloid load SUVR with a difference in least-square mean of -0.05 (p<0.0001) and -0.06 (p<0.0001) for 12 and 40 mg dose, respectively. Subgroup analysis suggests that verubecestat effect at week 104 was independent of baseline amyloid load. Regression analysis indicated that verubecestat effect on ADAS-Cog13 at week 104 was not meaningfully correlated with reduction in PET cortical amyloid load SUVR. Finally, patient baseline amyloid load did not interact with verubecestat effect on CDR-SB at week 104.

In prodromal AD patients, treatment with BACE inhibitor verubecestat for 104 weeks resulted in a small, robust reduction in brain amyloid load. This effect was dose dependent but not correlated to baseline amyloid load. Verubecestat poorer cognitive outcomes in prodromal AD patients were not related to baseline cortical amyloid or week 104 drug-dependent changes in amyloid load.

Keywords: *verubecestat, Vizamyl, PET, BACE, clinical*

P140: AV1451 retention is associated with hippocampal volume and memory declines in cognitively normal older adults

Jacob Ziontz[1], Murat Bilgel[1], Andrea Shafer[1], Danielle June[1], Dean Wong[2], Susan Resnick[1]

[1]Laboratory of Behavioral Neuroscience, National Institute on Aging, Baltimore, MD, US
[2]Department of Radiology and Radiological Science, Johns Hopkins University School of Medicine, Baltimore, MD, US

Introduction: The relationship between tau and longitudinal changes in hippocampal volume and memory independent of amyloid status and brain atrophy has not been fully characterized in cognitively normal individuals.

Methods: We analyzed cross-sectional AV1451 PET data of 51 cognitively normal individuals (mean age 77.8, SD 9.2) from the Baltimore Longitudinal Study of Aging in relation to retrospective change in hippocampal volume (n=248 observations) and memory performance (n=361 observations). AV1451 SUVR was computed within Braak tau staging regions, and retrospective changes in hippocampal volume and memory performance (CVLT long-delay free recall) were assessed using linear mixed effects models with age at and time from AV1451 scan, sex, years of education, amyloid positivity, amyloid*time, AV1451 SUVR, and AV1451 SUVR*time as independent variables. Additionally, we controlled for hippocampal volume at AV1451 visit and its interaction with time in examining changes in memory to determine if cross-sectional differences in hippocampal volume accounted for the relationship between AV1451 SUVR and retrospective memory change.

Results: Adjusting for amyloid positivity, greater entorhinal cortex AV1451 SUVR was associated with a trend to steeper decline in hippocampal volume (β=-58.43, p=0.063). Adjusting for both amyloid positivity and hippocampal volume, higher entorhinal AV1451 SUVR was also associated with steeper decline in CVLT long-delay free recall (β=-0.086, p=0.048, Figure 1). No statistically significant associations between hippocampal volume or memory decline and AV1451 SUVR in other Braak regions were observed.

Discussion: We found that AV1451 retention in the entorhinal cortex, independent of amyloid status, was associated with steeper decline in hippocampal volume, and that steeper memory decline was associated with entorhinal AV1451 retention independent of both amyloid status and brain atrophy. Early tau burden may be useful in predicting brain volume and memory changes even in cognitively normal individuals.
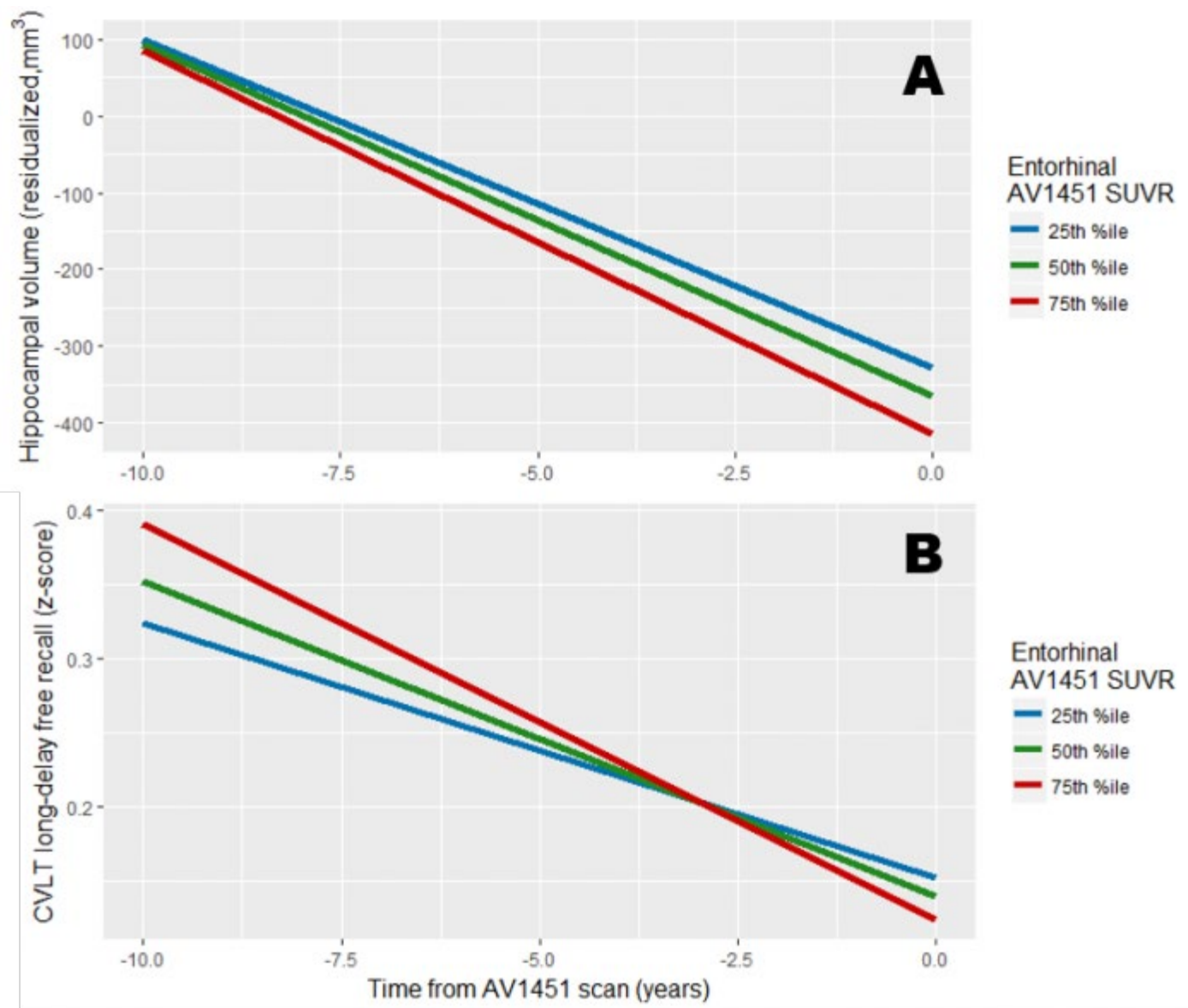
Figure 1. Population trajectory of (A) hippocampal volume and (B) CVLT long-delay free recall determined using linear mixed effects models with age at and time from AV1451 scan, sex, years of education, amyloid positivity, amyloid*time, entorhinal AV1451 SUVR, and entorhinal AV1451 SUVR*time as independent variables. Hippocampal volume at time of AV1451 scan, calculated as difference from expected volume at a given intracranial volume, and hippocampal volume*time are included as covariates in the association with memory. Predicted change is visualized for the population average with entorhinal cortex AV1451 SUVR in the 25th, 50th, and 75th percentile.

Keywords: *AV1451, tau, memory, brain atrophy, PET*

P141: [11C]PIB PET is associated with the brain biopsy amyloid β load and CSF amyloid β levels in subjects with normal pressure hydrocephalus

Juha Rinne[1], Timo Suotunen[1], Jaana Rummukainen[2], Sanna-Kaisa Herukka[3], Ossi Nerg[3], Anne Koivisto[3], Tuomas Rauramaa[2], Kjell Nagren[4], Mikko Hiltunen[5], Irina Alzfuzoff[6], Jaakko Rinne[1], Juha Jääskeläinen[3], Hilkka Soininen[9], Ville Leinonen[3]

[1]*Turku PET Centre, University of Turku, Turku, Finland*
[2]*Department of Clinical Pathology, Kuopio University Hospital, Kuopio, Finland*
[3]*Neurology of NeuroCenter, Kuopio University Hospital, Kuopio, Finland*
[4]*Department of Nuclear Medicine, PET and Cyclotron Unit, Odense University Hospital, Odense, Denmark*
[5]*Institute of Biomedicine, University of Eastern Finland, Kuopio, Finland*
[6]*Department of Immunology, Genetics and Pathology, Uppsala University, Uppsala, Sweden*
[7]*Clinical Neurosciences, Department of Neurosurgery, Turku University Hospital, Turku, Finland*
[8]*Institute of Clinical Medicine, Neurosurgery, University of Eastern Finland, Kuopio, Finland*
[9]*Institute of Clinical Medicine, Neurology, University of Eastern Finland, Kuopio, Finland*

Background: Idiopathic normal pressure hydrocephalus (iNPH) is frequently associated with concomitant Aβ pathology.

Objective: To compare [^{11}C]PIB PET in patients with iNPH to Aβ and hyperphosphorylated-tau (HPτ) in the right frontal cortical biopsy, CSF Aβ, the response to a CSF shunt, and the final clinical diagnosis of AD.

Methods: Twenty one patients from Kuopio NPH Registry (www.uef.fi/nph) with intraventricular pressure monitoring, immunostaining for Aβ and HPτ in the right frontal cortical biopsies, and MMSE and CDR underwent [^{11}C]PIB PET. Aβ, total tau, and $P\tau_{181}$ were measured by ELISA from the ventricular (n=15) and the lumbar (n=9) CSF.

Results: [^{11}C]PIB uptake in the right frontal cortex (ρ=0.60, p<0.01, Figure 1) and the combined neocortical [^{11}C]PIB uptake score (ρ=0.61, p<0.01) were associated with a higher Aβ load in the right frontal cortical biopsy. Excluding one (1/15) outlier, [^{11}C]PIB uptake was also associated with the ventricular CSF Aβ (ρ=- 0.58, p=0.03, Figure 2). Higher MMSE values were associated with lower lumbar CSF tau-levels (r = - 0.77, p = 0.015) and a similar trend was seen for phospho-tau (r = - 0.61, p = 0.081). No significant association was seen between the MMSE and the ventricular Aβ-, tau- or phospho-tau levels or with the combined neocortical [11C]PIB uptake score. Response to the shunt was seen in 13 out of the 15 shunted patients. AD was diagnosed in 8 patients during a median follow-up of 6 years (mean 7.3±2.4 years). Long-term outcome of the shunt operation was worse in patients with concomitant AD pathology.

Conclusions: The findings suggest that [^{11}C]PIB PET can reliably detect simultaneous amyloid pathology among iNPH patients. Further studies will show whether amyloid PET imaging can predict the clinical response to shunt operation. The presence of Aβ pathology in patients with iNPH might also warrant treatment with the current AD drugs.
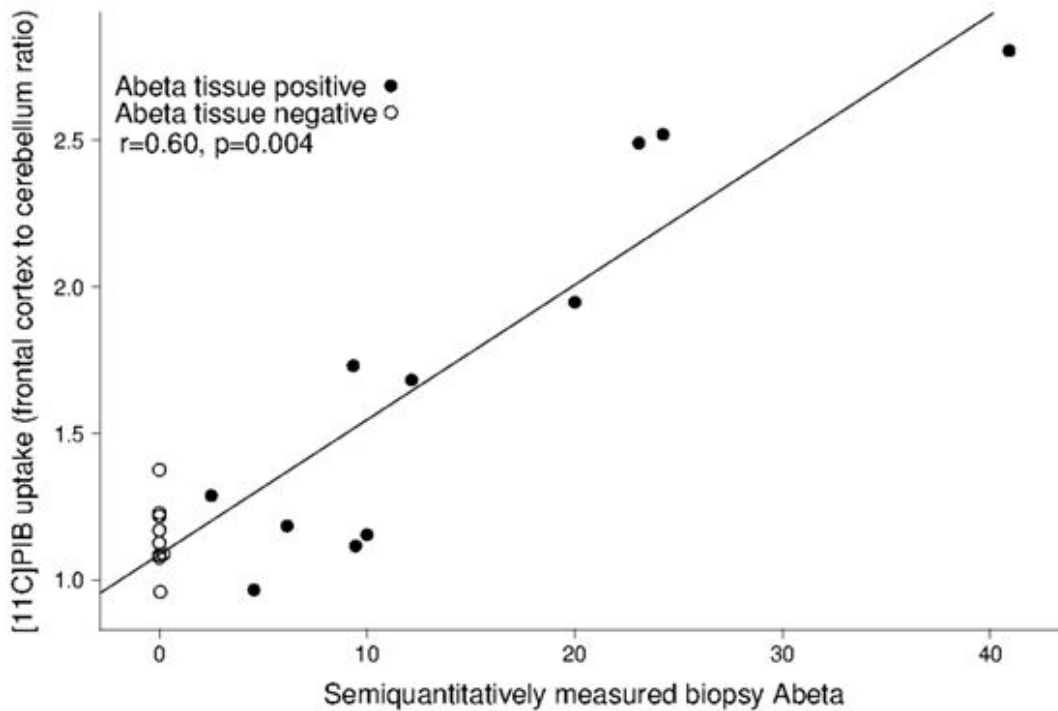
Figure 1: Scatterplot of the tissue Aβ (the number of the plaques divided by the area of the gray matter (mm^2)) and [^{11}C]PIB uptake in the right frontal cortex expressed as the frontal cortex to the cerebellar cortex ratio from 60 to 90 min
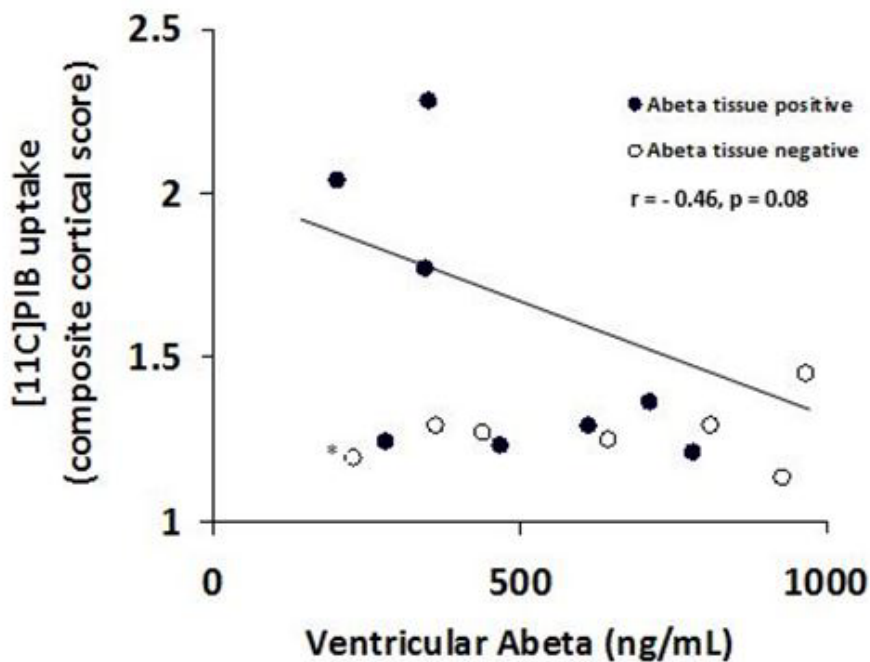

Figure 2: Scatterplot of the ventricular CSF Aβ1-42 (pg/mL) level and the composite neocortical [^{11}C]PIB uptake score. An outlier with a negative tissue biopsy for beta-amyloid and a normal [^{11}C]PIB uptake, but low ventricular CSF beta-amyloid concentration is marked with an asterix (*). Without this outlier the correlation between ventricular Aβ1-42 and composite neocortical [^{11}C]PIB uptake score was r = -0.58, p-value = 0.03.

Keywords: *Normal pressure hydrocephalus, NPH, Alzheimer, amyloid, tau*

P142: The BIN1 rs744373 SNP is associated with increased tau-PET levels and worse memory independent of amyloid

Nicolai Franzmeier[1], Julia Neitzel[1], Anna Rubinski[1], Michael Ewers[1]

[1]*Institute for Stroke and Dementia Research, Klinikum der Universität München, Ludwig-Maximilians-Universität LMU, Munich, Germany*

Background: The single nucleotide polymorphism (SNP) rs744373 in the bridging integrator-1 gene (**BIN1**) is after ApoE4 one of the strongest genetic risk factors of Alzheimer's disease (AD). BIN1 expression is altered in AD, where in-vitro findings suggest that BIN1 disturbances may contribute to the propagation of tau pathology via endocytosis-mediated tau transmission. However, whether **BIN1**-rs744373 is associated with higher tau pathology is unknown. Here, we tested for the first time whether carriage of the **BIN1**-rs744373 risk-allele G was associated with increased PET-assessed fibrillary tau, and for exploratory reasons, PET-assessed beta-amyloid in non-demented elderly subjects.

Methods: We included AV1451 tau-PET and AV45 amyloid-PET data from 89 cognitively normal and mild cognitively impaired subjects from the Alzheimer's Disease Neuroimaging Initiative. The **BIN1**-rs744373 genotype was extracted from GWAS data. Tau- and amyloid-PET uptake were each extracted globally and for established regional staging ROIs (Figure 1). Via ANCOVA, we tested whether **BIN1**-rs744373 carriage is associated with PET values, controlled for age, gender, education, diagnosis and ApoE4-status. In exploratory analyses, we assessed whether any association between **BIN1**-rs744373 and a memory composite score is mediated by altered global tau PET levels.

Results: We found that **BIN1**-rs744373 risk-allele carriers showed elevation of global and regional tau PET levels for Braak stages 2-6 when compared to non-carriers ($p<0.05$), with effect sized between $d=0.4$–0.6 (Fig. 2A). In contrast, the **BIN1**-rs744373 SNP had no effect on AV45 PET-assessed amyloid (Fig. 2B). The associations between **BIN1**-rs744373 and elevated tau levels were independent of amyloid load and clinical status. Exploratory analysis showed that the **BIN1**-rs744373 risk-allele was associated with worse memory performance, mediated by increased global tau levels (Fig. 3).

Conclusion: Together, our findings show that **BIN1**-rs744373 is selectively associated with elevated tau but not amyloid pathology, which may underlie the **BIN1** SNP associated increase in the risk for AD dementia.
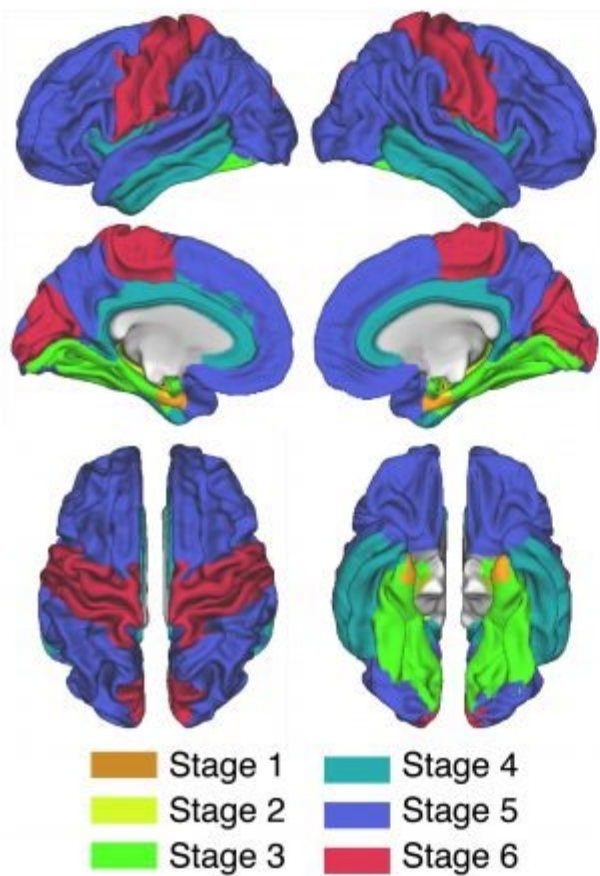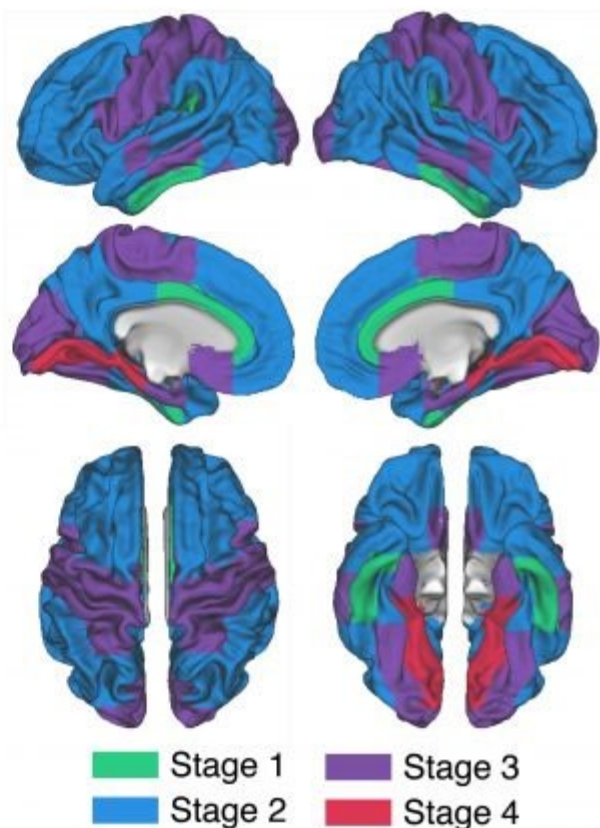
Figure 1: Spatial mapping of braak- and amyloid stage specific ROIs that were used to determine regional AV1451 tau- and AV45 amyloid-PET uptake.
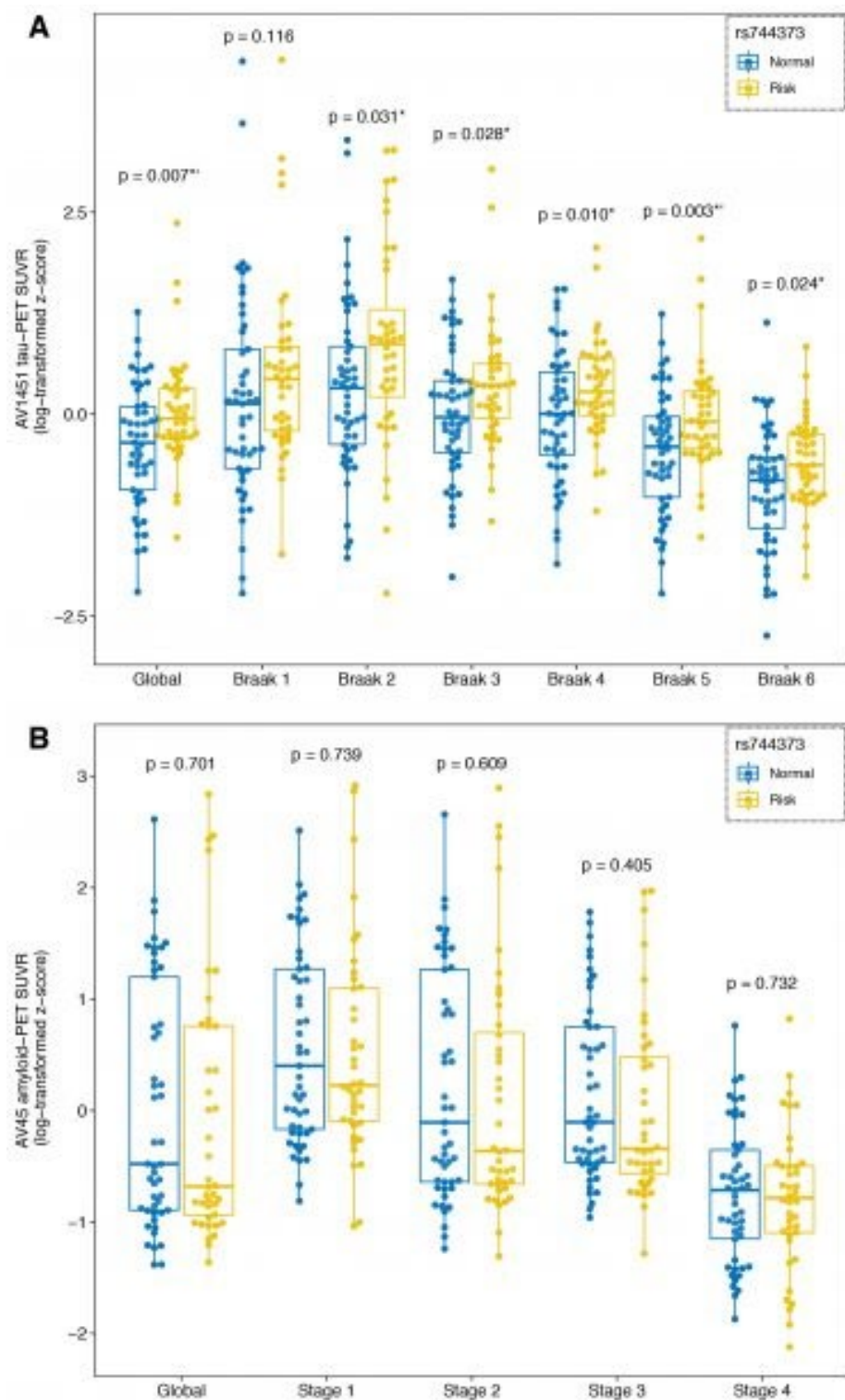
Figure 2: (A) Boxplot showing the differences in global or regional AV1451 tau-PET SUVRs between BIN1 rs744373 risk allele vs. normal allele carriers. P-values are based on ANCOVA models controlled for age, gender, education, diagnosis and memory performance (i.e. ADNI-MEM). (B) Differences in global or regional AV45 amyloid-PET uptake between BIN1 rs744373 risk allele vs. normal allele carriers. P-values are again derived from ANCOVA models controlled for age, gender, education, diagnosis, ApoE ε4 carrier status and grey matter volume of the respective ROI.
* = significant at p<0.05 (uncorrected);
' = significant after Bonferroni correction

390
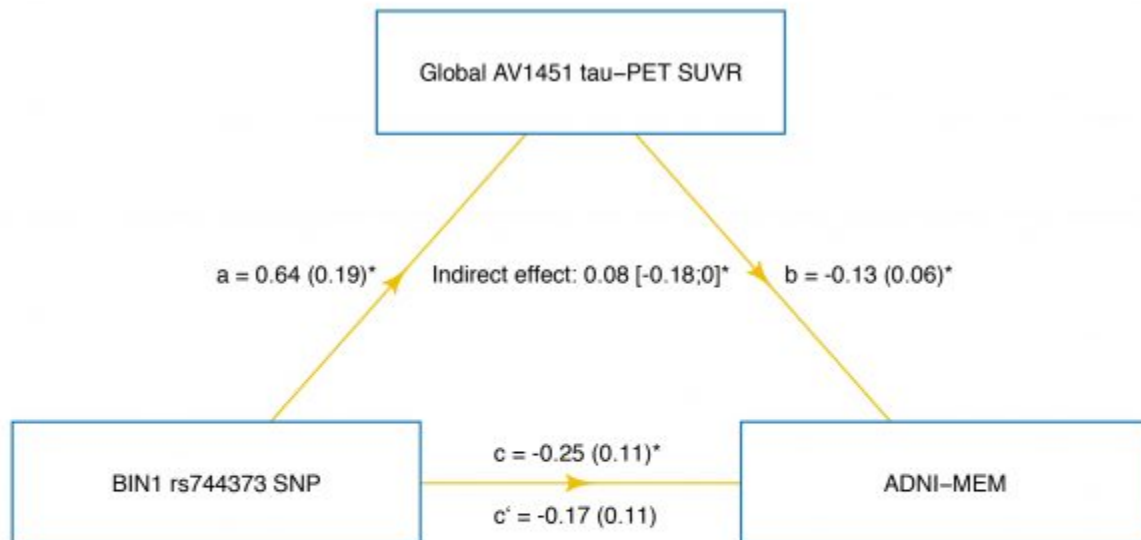
Figure 3: Path diagram of the mediation model, showing that associations between BIN1 rs744373 risk-allele carriage and worse memory are mediated via Global AV1451 tau-PET uptake. Path-weights are displayed as beta values with standard errors in brackets. All paths are controlled for age, gender, education, diagnosis, global AV45 amyloid-PET uptake and ApoE ε4 carrier status. Asterisks indicate p-values below 0.05. Significance of the indirect effect was determined using bootstrapping with 10 000 iterations.

P143: Optimal scanning time for the novel tau PET Tracer 18F-APN-1607

Chin-Chang Huang[1], Ing-Tsung Hsiao[2,3], Kun-Ju Lin[2,3], Ciou-Fang Lian[2,3], Jung-Lung Hsu[1], Kuo-Lun Huang[1]

[1]*Department of Neurology, Chang Gung Memorial Hospital, Taoyuan, Taiwan*
[2]*Medical Imaging & Radiological Sciences and Healthy Aging Research Center, Chang Gung University, Taoyuan, Taiwan*
[3]*Molecular Imaging Center and Nuclear Medicine, Chang Gung Memorial Hospital, Taoyan, Taiwan*

Introduction: ^{18}F-APN-1607 (previously ^{18}F-PMPBB3) is a novel PET tracer being developed to image tau aggregates in Alzheimer's disease (AD) and non-AD tauopathies. This study aimed to identify the optimal scanning time for obtaining summed ^{18}F-APN-1607 images in AD patients and healthy cognitively normal (CN) adults.

Methods: A total of 20 subjects (8 AD and 12 CN) underwent dynamic ^{18}F-APN-1607 scanning. MRI was performed to enable image registration. Serial PET images were acquired for 150 min. The dynamic images were motion corrected and rearranged into various sets of 10-min scans for further analysis. Each image was spatially normalized to MNI space. Volumes of interest (VOIs) for regions reflecting Braak stages I/II, III/IV and V/VI, as well as various cortical and subcortical structures were delineated from individual MRI scans. SUVRs for VOIs were computed using cerebellar cortex as reference. Distribution volume ratios (DVRs) were computed from Logan graphical analysis using cerebellar cortex as the input. SUVR performance was evaluated based on the correlation of SUVR to DVR, stability, feasibility and Cohen effect size.

Results: Time activity curves and DVR results showed higher ^{18}F-APN-1607 uptakefor AD (mean DVR = [1.080~1.477]) as compared to CN (mean DVR = [0.824~ 0.976]). At later time windows, consistently higher correlations of SUVRs to DVR were observed for each VOI and reached maximal values at around 100 min. The group mean SUVR differences between AD and CN increased and reached relatively stable values after 90 min. The effect sizes for all VOIs increased and reached peak values at around 50-70min; they decreased steadily thereafter.

Conclusion: The optimal scanning time for ^{18}F-APN-1607 is 90-110 minutes post-injection based on higher correlation of SUVR to DVR, differentiation between AD and CN, stability and feasibility.

Keywords: *Tau PET imaging, 18F-APN-1607, optimal scanning time, Alzheimer's disease*

P144: Associations between behavioral factors and Alzheimer's pathology: Findings from cognitively normal older adults at risk of AD and presymptomatic ADAD mutation carriers

Alexa Pichet Binette[1,3], Julie Gonneaud[2,3], Hazal Ozlen[3], Christophe Bedetti[3], John Morris[4,6], Randall Bateman[4,6], Tammie Benzinger[4,5], Judes Poirier[2,3], John Breitner[2,3], Sylvia Villeneuve[2,3], PREVENT-AD Research Group[3], DIAN Study Group[4]

[1]*Integrated Program in Neuroscience, McGill University, Montreal, QC, Canada*
[2]*Department of Psychiatry, McGill University, Montreal, QC, Canada*
[3]*Douglas Mental Health University Institute, StoP-AD Centre, Montreal, QC, Canada*
[4]*Knight Alzheimer's Disease Research Center, Washington University School of Medicine, St. Louis, MO, US*
[5]*Department of Radiology, Washington University School of Medicine, St. Louis, MO, US*
[6]*Department of Neurology, Washington University School of Medicine, St. Louis, MO, US*

Objective: To assess whether combinations of behavioral factors are related to β-amyloid (Aβ) and **tau** pathology in older adults with a family history of Alzheimer's disease (AD) dementia and to Aβ in autosomal dominant AD (ADAD) mutation carriers.

Methods: We included 111 cognitively normal older adults from the PREVENT-AD study (age=67±5) who had Aβ ($[^{18}F]$NAV4694) and **tau** ($[^{18}F]$AV1451) PET scans and 117 presymptomatic mutation carriers from the DIAN study (age=35±9) who had an Aβ ($[^{11}C]$PIB) PET scan. SUVRs were extracted from FreeSurfer Desikan regions. Personality traits, neuropsychiatric factors and cognitive lifestyle were assessed, using different questionnaires in PREVENT-AD and DIAN (Table 1). Partial least squares correlations with permutation tests were applied to assess which combinations of behavioral factors (derived as latent variables), if any, related to Aβ and **tau** deposition in PREVENT-AD and to Aβ in DIAN.

Results: One latent variable related behavioral factors with Aβ (p=0.03) and **tau** (p=0.03) in PREVENT-AD, and with Aβ (p<0.01) in DIAN. In PREVENT-AD, widespread Aβ was associated to a combination of higher neuroticism, apathy, lower education and extraversion (Fig.1A), while a combination of higher neuroticism, social isolation, lower cognitive activity and extraversion was associated with higher **tau** predominantly in temporal regions (Fig.2). In DIAN, widespread Aβ was associated to a combination of higher neuropsychiatric factor and lower years of education (Fig.1B).

Conclusions: Our multivariate approach revealed that both in individuals at risk of sporadic AD and individuals in the presymptomatic phase of ADAD, combinations of different behavioral factors are associated with AD pathology. While personality traits and cognitive lifestyle seem to be more related to pathology in preclinical sporadic AD, only cognitive lifestyle and neuropsychiatric factor seem to influence Aβ in the preclinical phase of ADAD. Longitudinal evaluations will precise whether such factors are drivers, consequences of accumulating AD pathology, or both.

Table 1. Behavioral factors included in each cohort

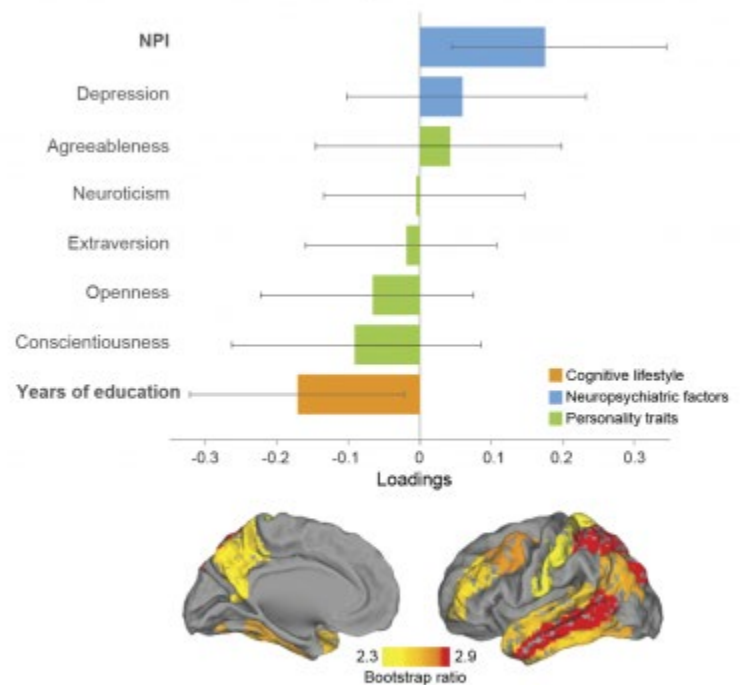|	PREVENT-AD	DIAN
Personality traits	**Big5 inventory** *(John et al., 1991)* - Neuroticism - Extraversion - Agreeableness - Conscientiousness - Openness	**NEO-IPIP** *(Goldberg, 1999)* - Neuroticism - Extraversion - Agreeableness - Conscientiousness - Openness
Neuropsychiatric factors	**Geriatric depression scale** *(Yesavage et al., 1983)* **Geriatric anxiety inventory** *(Pachana et al., 2007)* **Stress subscale** *(Lovibond & Lovibond, 1995)* **Apathy Evaluation Scale** *(Martin & Biedrzycki, 1991)*	**Geriatric depression scale** *(Yesavage et al., 1983)* **Neuropsychiatric Inventory Questionnaire (NPI-Q)** *(Cummings et al, 1994)*
Cognitive lifestyle	**Years of education** **Lifetime Cognitive activity** *(Wilson et al., 2002)* **Social isolation** *(Donald & Ware, 1984)*	**Years of education**

Figure 1

A. PREVENT-AD - Behavioral factors x Aβ
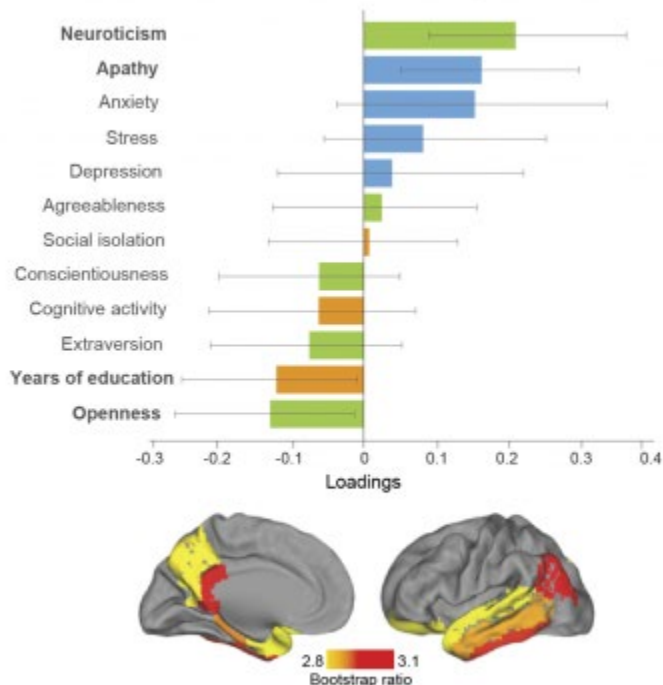
B. DIAN - Behavioral factors x Aβ

Bar graph represents the loading of each behavioral factor on the latent variable related to Aβ accumulation (in older adults from PREVENT-AD in **1A** and in DIAN mutation carriers in **1B**). Confidence intervals are derived from bootstrap resampling. Top ten regions showing highest Aβ burden as a function of the combination of behavioral factors are projected on the brains.
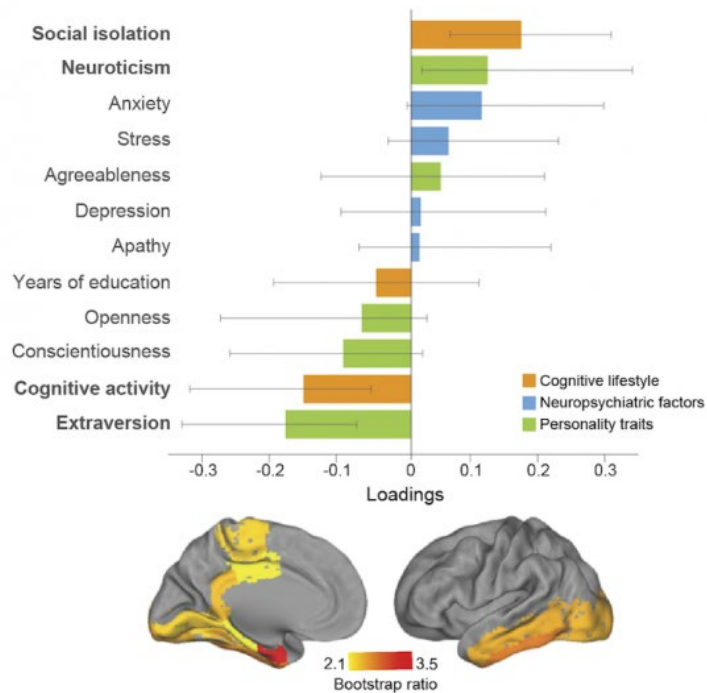
Figure 2

PREVENT-AD - Behavioral factors x tau

Bar graph represents the loading of each behavioral factor on the latent variable related to tau accumulation in older adults from PREVENT-AD. Confidence intervals are derived from bootstrap resampling. Top ten regions showing highest tau burden as a function of the combination of behavioral factors are projected on the brains.

P145: Early localized network dysfunction in APOE ε4 carriers without biomarker evidence of Alzheimer's disease

Omar Butt[1], Jeremy Strain[1], Julie Wisch[1], Suzanne Schindler[1], Anne Fagan[1], Carlos Curchaga[1], Tammie Benzinger[1], Beau Ances[1]

[1]*Washington University in Saint Louis, Saint Louis, MO, US*

Background: **APOE** ε4 has been linked to accelerated amyloid deposition and tau-tangle formation. Even at subthreshold amyloid/tau levels, the resulting microcellular changes likely lead to synaptic dysfunction with subsequent network disruptions. The arrangement of these disruptions in pre-clinical AD remains enigmatic.

Methods: Using cross-sectional analyses, we examined resting-state scans from 93 cognitively-normal adults (CDR 0) without biomarker evidence of AD (38M/55F, age 77.9 ± 7.41; n = 80 non-carriers, 13 carriers) from the Knight Alzheimer's Disease Research Center using defined criteria (Hansson et al 2018). Resting state data was aggregated into canonical cortical networks based on previously defined criteria (Power et al 2011), with particular focus on the default-mode, memory, and salience (i.e. DMS) networks. The resulting 298x298 connectivity matrix was then masked to only examine intra-hemispheric and inter-hemispheric connections between carriers/non-carriers.

Results: Qualitative differences observed in the group difference matrix (Fig. A) were quantified by averaging, with only the DMS networks revealing significant group differences between, not within, that network cluster ([0.0014 v -0.266]; p = 0.0296, Fig. B). Observed differences were primarily due to a significant weakening of inter-hemispheric relative to intra-hemispheric connections (Fig. C, Fig. D). Using the amyloid, tau, neurodegeneration criteria (Jack et al, 2013,2016) participants were then categorized per A/T/N classification guidelines. Despite the observed network changes, all subjects were noted to be subthreshold across all major biomarkers, with trends toward significant group difference observed in CSF Ab42 only ([1539 v 1358]; p = 0.0625, Fig. E).

Conclusions: Early network changes in key AD-affected networks is driven by inter-hemispheric connections prior to reaching biomarker threshold. These disruptions may be related to subthreshold biomarker changes, in particular CSF Ab42. Our results would support the integration of the **APOE** ε4 allele genetic testing into the A/T/N classification criteria for AD.

Figures A-E

P146: Association between retinal thickness and brain β-amyloid accumulation in individuals with Subjective Cognitive Decline: data from the FACEHBI study

Marta Marquié[1], Gemma Monté-Rubio[1], Octavio Rodríguez-Gómez[1,2], Ángela Sanabria[1], Miguel Castilla-Martí[3,4], Joan Martínez[1], Montserrat Alegret[1], Alba Pérez-Cordón[1], Francisco Lomeña[5], Javier Pavia[5], Rosella Gismondi[6], Santi Bullich[6], Assumpta Vivas-Larruy[7], Miguel Ángel Tejero[7], Marta Gómez-Chiari[7], Adelina Orellana[1], Sergi Valero[1], Agustín Ruiz[1,2], Lluis Tárraga[1], Mercè Boada[1,2]

[1]*Research Center and Memory Clinic, Fundació ACE Institut Català de Neurociències Aplicades - Universitat Internacional de Catalunya (UIC), Barcelona, Spain*
[2]*Centro de Investigación Biomédica en Red sobre Enfermedades Neurodegenerativas (CIBERNED), Instituto de Salud Carlos III, Madrid, Spain*
[3]*Clínica Oftalmológica Dr. Castilla, Barcelona, Spain*
[4]*Department of Ophthalmology, Hospital del Mar and Hospital de l'Esperança - Parc de Salut Mar, Barcelona, Spain*
[5]*Hospital Clínic de Barcelona, Barcelona, Spain*
[6]*Life Molecular Imaging GmbH, Berlin, Germany*
[7]*Clínica Corachan, Barcelona, Spain*

Background: Optical coherence tomography (OCT) is a non-invasive tool for the quantification of retinal structural changes, and AD patients exhibit thinning of several retinal layers compared to healthy controls. Subjective Cognitive Decline (SCD) has been proposed as risk factor for progression to AD, but there is little data about the role of OCT in preclinical AD. We explored whether retinal changes are detectable in SCD and their association with brain amyloid deposition.

Methods: 200 SCD participants of Fundació ACE Healthy Brain Initiative (FACEHBI) aged 49 and over underwent 3D-OCT Maestro®, brain MRI and PET-Florbetaben at baseline (v0). MRI and PET-FBB were repeated after 2-y (v2). OCT scan measurements from 155 AD patients were added for comparison. Global standardized uptake value ratio (SUVR)=1.35 was used as threshold for amyloid positivity (Aβ+). We compared peripapillary retinal nerve fiber layer (RNFL) and macular (fovea, inner and outer regions) thickness across groups and its association with global SUVR.

Results: AD patients showed significant thinning of the macula compared to all SCD individuals (n=150), while no group differences in RNFL were observed. At v0, SCD_Aβ+ (n=16) and SCD_Aβ- (n=134) groups presented similar retinal measurements. At v2 the SCD_Aβ+ group (n=18) exhibited thicker fovea and inner macula compared to the SCD_Aβ- group (n=104), while no differences were detected in RNFL or outer macula. Weak but significant correlations between global SUVR and macular thickness were present at v0 and v2.

Discussion: In SCD individuals, increased thickness of the fovea and inner macula predicted future Aβ brain deposition, while thinning of these retinal regions was evident in AD patients. These preliminary results suggest that inflammation of macular regions occurs very early in the course of AD and precedes retinal atrophy that emerges as dementia progresses. OCT may be a useful tool to identify preclinical AD among SCD individuals.

Keywords: *Optical Coherence Tomography, retina, Subjective Cognitive Decline, Florbetaben, amyloid*

P147: Image features and clinical associations of the novel tau PET tracer 18F-APN-1607 in Alzheimer's disease

Jung-Lung Hsu[1], Kun-Ju Lin[2,3], Ing-Tsung Hsiao[2,3], Ciou-Fang Lian[2,3], Chin-Chang Huang[1], Kuo-Lun Huang[1], Tzu-Chen Yen[2,3]

[1]*Department of Neurology, Chang Gung Memorial Hospital Linkou Medical Center and College of Medicine, Chang-Gung University, Taoyuan, Taiwan*
[2]*Department of Nuclear Medicine and Molecular Imaging Center, Linkou Chang Gung Memorial Hospital, Taoyuan, Taiwan*
[3]*Department of Medical Imaging and Radiological Sciences and Healthy Aging Research Center, Chang Gung University, Taoyuan, Taiwan*

Background: Aggregated tau is a major neuropathological feature of Alzheimer's disease (AD) and non-AD tauopathies. In the current study, the novel tau PET tracer ^{18}F-APN-1607 (previously ^{18}F-PM-PBB3) was explored in AD and controls.

Methods: Altogether, 21 participants (9 AD dementia patients and 12 controls) were studied. Demographic, clinical, and apolipoprotein E ε4 (APOE4) carrier status data were collected, and amyloid PET (Florbetapir) and structural brain MRI were performed for all participants. Amyloid status was assessed visually. For tau PET ^{18}F-APN-1607 (mean dosage: 378.2 ± 11.2 MBq) was injected and participants were imaged from 80-100 minutes post-injection on a Siemens Biograph mCT PET/CT scanner. Attenuation correction was performed for both amyloid and tau PET. Imaging preprocesses including motion correction, spatial coregistration/normalization and smoothing were performed by PNEURO (PMOD). SUVrs were calculated for select brain regions using cerebellar gray matter as reference. Nonparametric Wilcoxon analysis was used to assess group differences. Tau uptake data were considered numerically and by amyloid and APOE4 carrier status.

Results: AD patients were significantly older than controls and had significantly lower MMSE and higher ADAS-cog scores. ^{18}F-APN-1607 SUVrs in the frontal, parietal, temporal, occipital lobes and the precuneus, anterior and posterior cingulate were significantly higher in patients with AD than controls ($p < 0.01$), but the hippocampal SUVr did not differ. Florbetapir SUVrs in the same regions were also significantly higher in AD patients than controls ($p < 0.01$); all AD patients were amyloid positive. Age and gender did not affect regional ^{18}F-APN-1607 and Florbetapir SUVrs by regression analysis and Wilcoxon tests. MMSE, ADAS-cog and CDR-SB scores were significantly correlated with many regional ^{18}F-APN-1607 and Florbetapir SUVrs ($p < 0.01$) by regression analysis.

Conclusion: ^{18}F-APN-1607 tau PET differentiated AD patients from controls and regional tau signal intensity was significantly associated with cognitive scores and dementia severity.

Keywords: *18F-APN-1607, tau, AD, PET,*

P148: Safety, biodistribution and radiation dosimetry for the tau PET Tracer 18F-APN-1607 in healthy human subjects

Kun-Ju Lin[1,2], Ing-Tsung Hsiao[1,2], Ciou-Fang Lian[1,2], Chin-Chang Huang[3], Jung-Lung Hsu[3], Kuo-Lun Huang[3], Tzu-Chen Yen[1]

[1]*Department of Nuclear Medicine and Molecular Imaging Center, Linkou Chang Gung Memorial Hospital, Taoyuan, Taiwan*
[2]*Department of Medical Imaging and Radiological Sciences and Healthy Aging Research Center, Chang Gung University, Taoyuan, Taiwan*
[3]*Department of Neurology, Chang Gung Memorial Hospital Linkou Medical Center and College of Medicine, Chang-Gung University, Taoyuan, Taiwan*

Background: ^{18}F-APN-1607 (previously ^{18}F-PM-PBB3) is a novel radiotracer that demonstrates high binding selectivity and affinity for aggregated tau and does not exhibit off-target binding in the living brain as seen for some other tau tracers. The present study aimed to assess estimate the radiation dose of ^{18}F-APN-1607 in humans and to compare the clinical radiation dosimetry results to estimations published previously using preclinical data.

Methods: Serial whole-body PET/CT imaging was performed for 240 min on 12 healthy adult volunteers after injecting ^{18}F-APN-1607 (mean administered activity, 379.0 ± 7.0 MBq; range, 365.9-389.6 MBq). Safety/tolerability were assessed. The bladder and gallbladder were delineated on PET images, and other organs were delineated on CT images. Voided urine activity was recorded. The decay-corrected and normalized ^{18}F-APN-1607 activity of 15 source-organ regions as a function of time was entered into OLINDA/EXM software to calculate the effective dose for each subject following the medical internal radiation dosimetry schema.

Results: ^{18}F-APN-1607 was safe and well tolerated. The highest mean initial uptake at 10 min after injection was in the liver ($29.4\% \pm 5.2\%$), intestine ($8.4\% \pm 2.0\%$), lung ($4.4\% \pm 2.8\%$), and kidney ($3.3\% \pm 1.1\%$). The highest mean absorbed radiation dose was in the upper large intestine (182.1 ± 56.8 μGy/MBq), small intestine (168.2 ± 32.3 μGy/MBq), gallbladder wall (109.0 ± 60.8 μGy/MBq), and liver (79.9 ± 25.8 μGy/MBq). The resultant whole-body effective dose was 34.5 ± 3.4 μSv/MBq.

Conclusion: Injection of 370 MBq of ^{18}F-APN-1607 would lead to an estimated effective dose of 12.8 mSv; hence, ^{18}F-APN-1607 has a radiation burden similar to that of other commonly used PET tracers. Our findings in humans were consistent with recently published estimates extrapolated from dosimetry data in mice.

Keywords: *18F-APN-1607, Alzheimer's disease, radiation dosimetry, tau, whole body biodistribution*

P149: Longitudinal associations between Aβ and glucose metabolism in a normal elderly population

Dana Tudorascu[1], Zheming Yu[2], Stewart Anderson[3], Beth Snitz[4], Davneet Minhas[2], Charles Laymon[2], Brian Lopresti[2], Chester Mathis[2], Howard Aizenstein[5], William Klunk[5], <u>Ann Cohen</u>[5]

[1]*University of Pittsburgh School of Medicine, Department of Medicine, Pittsburgh, PA, US*
[2]*University of Pittsburgh School of Medicine Department of Radiology, Pittsburgh, PA, US*
[3]*Univeristy of Pittsburgh Graduate School of Public Health, Department of Biostatistics, Pittsburgh, PA, US*
[4]*University of Pittsburgh School of Medicine Department of Neurology, Pittsburgh, PA, US*
[5]*University of Pittsburgh School of Medicine Department of Psychiatry, Pittsburgh, PA, US*

Inverse correlations between Aβand cerebral metabolism in Alzheimer's disease suggests local Ab-induces metabolic insults. In MCI, we have previously observed no significant negative correlations between PiB and FDG, but found frequent positive correlations without elevations in metabolism, particularly in frontal brain regions. These findings suggest that in MCI, higher basal metabolism (i.e., brain reserve) could be increasing the level of Abnecessary for cognitive impairment. The objective of the present study was to explore associations between change in Ab and glucose metabolism over time in cognitively normal elderly (CN).

Ninety-eight CN received [^{11}C]PiB and [^{18}F]FDG PET, longitudinally, 24 months apart. To assess associations between trajectories of Aβand metabolism, linear mixed effects models were used. The model was fit for each ROI separately with fixed effects of time, glucose metabolism (time dependent predictor of interest), age (time dependent covariate), APOE, education and random intercept and slope accounting for within-subject correlation.

Statistically significant positive associations ($p<0.05$) were observed globally ($\beta=0.45$, (0.15,0.77) and locally in Anterior Cingulate ($\beta=0.76$, (0.37, 1.16)), Superior Frontal ($\beta=0.52$, (0.26, 0.79)), INS (0.45, (0.05, 0.84)) Lateral Temporal ($\beta=0.37$, (0.04, 0.69)), Parietal ($\beta=0.40$, (0.12, 0.69)), and OrbitoFrontal ($\beta=0.50$, (0.08, 0.91)) cortices. We observed significant distant associations across PiB and FDG ROIs: PiB Anterior Cingulate and OrbitoFrontal FDG ($\beta=0.64$, (0.17, 1.11)), Superior Frontal PiB with Insula FDG ($\beta=0.58$, (0.16, 1.00)), with Lateral Temporal FDG ($\beta=0.46$, (0.06, 0.86)), and with Parietal FDG ($\beta=0.44$, (0.12, 0.76)),Parietal PiB with Superior FrontalFDG ($\beta=0.44$, (0.20, 0.68)), with Lateral Temporal FDG ($\beta=0.37$, (0.01, 0.73)), and with OrbitoFrontal FDG ($\beta=0.40$, (0.13, 0.68)).

These data suggest that in CN glucose metabolism is increasing in concert with increasing Abpathology. These data suggest that a reactive hypermetabolism occurs in CN as Ab-load increases in the brain.

Keywords: *PiB, FDG, cognitive reserve*

P150: Associations between Aβ, tau, and cerebrovascular reactivity in a non-demented elderly population

Ann Cohen[1], Theodore Huppert[1], Dana Tudorascu[1], Beth Snitz[1], Charles Laymon[1], Brian Lopresti[1], Chester Mathis[1], Neelesh Nadkarni[1], Oscar Lopez[1], Howard Aizenstein[1], William Klunk[1], Steven Reis[1]

[1]*University of Pittsburgh School of Medicine, Pittsburgh, PA, US*

Several studies have suggested that cerebrovascular reactivity (CVR) in response to hypercapnia is reduced in Alzheimer's disease (AD). However, little is known about the relationship of CVR to AD neuropathology including Aβand tau. The objective of the present study was to explore associations between Ab, tau and CVR cross-sectionally in a group of non-demented elderly (NDE).

Twenty-six NDE (age=73.6±2.9 years; education=15.7±2.5 years; 42% African American; 95% female) received [^{11}C]PiB and [^{18}F]AV-1451 PET, and ASL MRI with and without hypercapnia (using 5% carbon dioxide). SUVR images were generated from PET data (50-70 minute [^{11}C]PiB; 80-100 minute [^{18}F]AV-1451) using cerebellar gray matter as the reference region. ASL data were normalized to the cortical white matter flow in the baseline air condition. To assess associations between Ab, tau and CVR, global PiB or summary AV-1451 (Mishra et al., 2017) SUVR were used as predictors of interest in a regression with ASL measures with and without CVR for each region of interest as the outcome.

No statistically significant associations were observed between PiB and either baseline ASL or ASL during hypercapnia. However, there was a significant positive association between global PiB and summary AV-1451 SUVR ($p<0.001$). Significant positive associations ($p<0.05$) were observed between baseline ASL and AV-1451 in anterior cingulate, precuneus and superior temporal cortex. Widespread significant positive associations ($p<0.005$) between ASL during hypercapnia and AV-1451 in anterior cingulate, superior frontal, orbitofrontal, insula, lateral temporal, parietal, precuneus and posterior cingulate cortices.

In this NDE population there are positive associations between tau pathology and brain blood flow that become more widespread and apparent during a CVR challenge. These data suggest that a reactive response in brain blood flow occurs as tau pathology emerges in the brain.

P151: Comparing amyloid PET tracers and interpretation strategies: A multicenter study

Gérard Bischof[1], Peter Bartenstein[2], Henryk Barthel[3], Bart van Berckel[4], Vincent Doré[5], Thilo van Eimeren[1,6,7], Norman Forster[8], Jochen Hammes[1], Andriaan Lammertsma[4], Satoshi Minoshima[8], Chris Rowe[5], Osama Sabri[3], John Seibyl[9], Koen van Laere[10], Rik Vandenberghe[11], Victor Villemagne[5], Igor Yakushev[12], Alexander Drzezga[12]

[1]*Multimodal Neuroimaging Group, Department of Nuclear Medicine, University Hospital Cologne, Cologne, DE*
[2]*Department of Nuclear Medicine, LMU Munich, Munich, Germany*
[3]*Univeristy Hospital of Leipzig, Department of Nuclear Medicine, Leipzig, Germany*
[4]*VU University Medical Center Amsterdam, Radiology and Nuclear Medicine, Amsterdam, The Netherlands*
[5]*The University of Melbourne, Melbourne, Australia*
[6]*Department of Neurology, University Hospital Cologne, Cologne, Germany*
[7]*German Center for Neurodegeneratives Diseases (DZNE), Bonn, Germany*
[8]*Department of Radiology and Imaging Sciences, University of Utah, Salt Lake City, UT, US*
[9]*Institute for Neurodegenerative Disorders, New Haven, Connecticut, USA, New Haven, CT, US*
[10]*Memory Clinic, University Hospital Leuven, Leuven, Belgium*
[11]*Department of Neurosciences, KU Leuven, Leuven, Belgium*
[12]*Department of Nuclear Medicine, Technical University of Munich, Munich, Germany*

Three Fluorine 18-labelled tracers are currently commercially available to measure cerebral amyloid pathology and assist in the diagnosis of possible Alzheimer's Disease (AD); Florbetapir, Flutemetamol and Florbetaben. FDA-/EMA approved visual rating guidelines to render a scan as positive or negative differ considerably including color scale, intensity-scaling, definitions of a region and spatial and signal thresholds to determine positivity. Standardization of visual reading would be highly desirable to ensure that diagnostic classification, patient selection and therapeutic decisions are comparable, independently of the tracer. Here, we examined the comparability of different visual interpretation protocols on the three different commercially available amyloid tracers. In a multicentric approach, a total of 18 PET-Scans were compiled for this study (6 scans for each of the three tracers, matched for diagnostic categories). Each scan was pre-categorized with tracer-specific thresholds into amyloid positive or negative and submitted to an in-house-created online rating tool. On this platform, every single scan was presented for reading according to each of the three visual ratings schemes to a team of certified expert readers from Australia, Europe and the US. We analyzed interrater reliability and further assessed which visual rating schemes produces the highest reliability across tracers. Finally, we compared the correspondence of each response with the binary pre-classification based on a quantitative threshold. We observed that overall reading consistency was relatively high for all visual ratings scales. When comparing the visual reads with the standard of truth (SUVR estimates) similar accuracy rates were achieved across tracers. Variability in reading consistency among experts was most pronounced for Flutemetamol and Florbetapir visual ratings scales. Our preliminary data suggests that for visual assessment with regard to non-quantitative evaluation, may be sufficient to ensure relatively good levels of standardization. Unification of visual rating guidelines however may eliminate the existing variability across visual rating schemes.

Keywords: *Amyloid, PET, Visual Interpretation Strategies, Alzheimer's Disease, CAPTAIN's*

P152: Amyloid and memory impairment have additive effects on microglial activation but not tau pathology

William Charles Kreisl[1], Sha Tao[1], James Zou[1], Aubrey S. Johnson[1], Zeljko Tomljanovic[1], Qolamreza Razlighi[1], Adam M. Brickman[1], Seonjoo Lee[1], Yaakov S. Stern[1]

[1]*Columbia University Irving Medical Center, New York, NY, US*

Background: We sought to determine if amyloid accumulation and memory impairment have independent effects on microglial activation and tau pathology.

Methods: Fifty-seven older adults were stratified by amyloid status (positive or negative) and cognitive status (amnestic patient or normal control) based on ^{18}F-florbetaben PET, history, and neuropsychological testing. Participants had ^{11}C-PBR28 PET to measure microglial activation. A subset (n=44) had ^{18}F-MK6240 PET to measure tau pathology. Multivariate and univariate analyses of covariance were performed to test for effects of amyloid and cognitive status on either ^{11}C-PBR28 or ^{18}F-MK6240 binding, controlling for age (and **TSPO** genotype for ^{11}C-PBR28 binding).

Results: Twenty-three amyloid-positive patients, 7 amyloid-positive controls, 10 amyloid-negative patients, and 17 amyloid-negative controls had ^{11}C-PBR28 imaging. Of these, 14 amyloid-positive patients, 7 amyloid-positive controls, 9 amyloid-negative patients, and 14 amyloid-negative controls had ^{18}F-MK6240 imaging. Amyloid and cognitive status both had effects on ^{11}C-PBR28 binding ($p < 0.008$), with no interaction between these two factors ($p = 0.672$). In neocortical regions and medial temporal cortex these effects were additive, such that amyloid-positive patients had greater ^{11}C-PBR28 binding than amyloid-negative controls, with amyloid-positive controls and amyloid-negative patients having intermediate binding (Fig 1). In contrast, while amyloid and cognitive status both had effects on ^{18}F-MK6240 binding ($p < 0.02$), we found a significant interaction between these two factors ($p = 0.025$). In neocortical regions and medial temporal cortex, we found increased ^{18}F-MK6240 binding in amyloid-positive patients only ($p < 0.05$).

Conclusion: In the absence of cognitive symptoms, amyloid is associated with microglial activation but not tau pathology. These results are consistent with a temporal order of AD pathophysiology with early amyloid accumulation and microglial activation, followed by concurrence of tau pathology and memory impairment. The additive effect of amyloid and memory impairment on ^{11}C-PBR28 binding suggests microglial activation increases throughout the AD process.
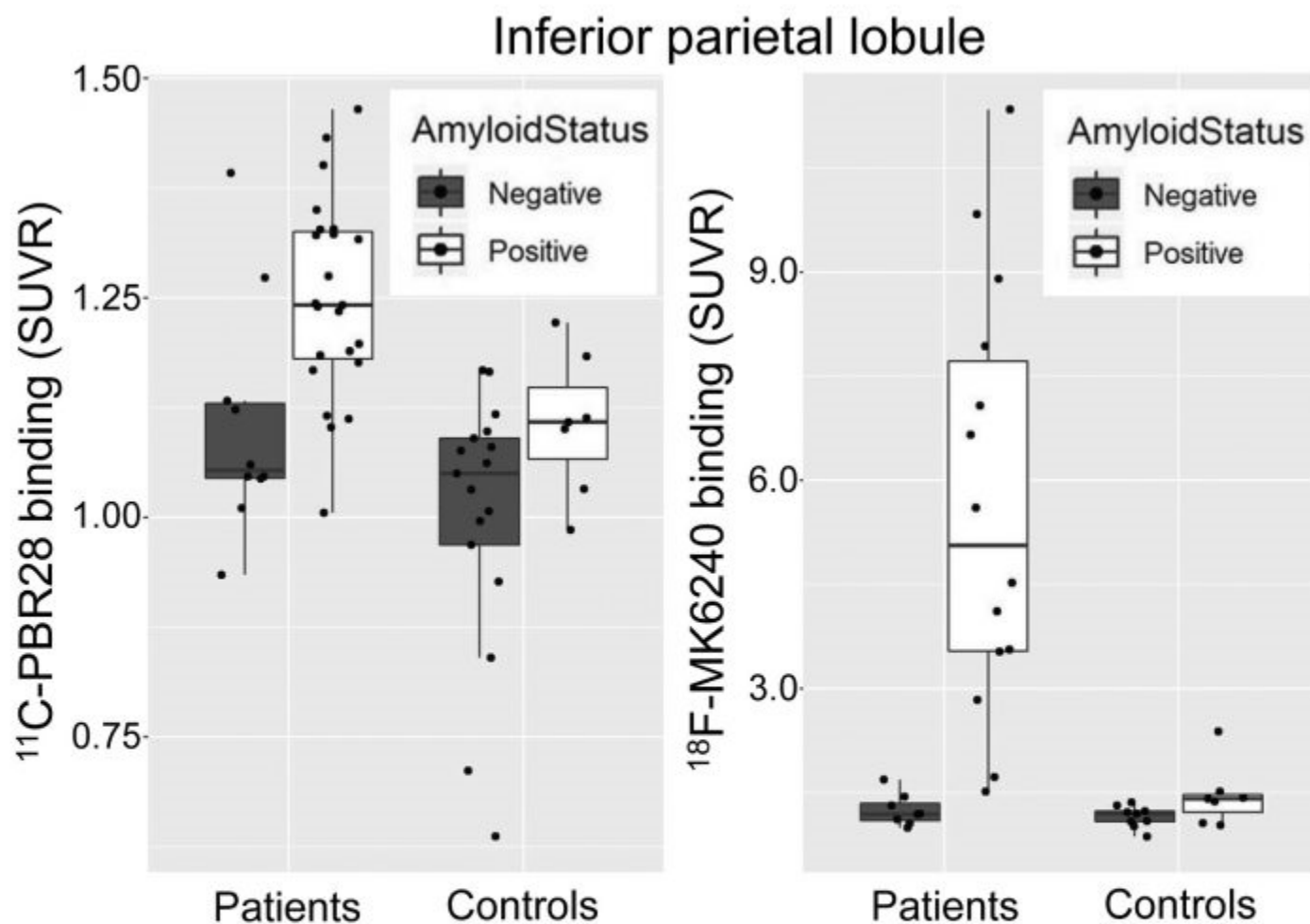
Inferior parietal lobule

Fig. 1. Jitter plots showing ^{11}C-PBR28 (left) and ^{18}F-MK6240 (right) binding in inferior parietal lobule, in participants stratified by amyloid and cognitive status. For ^{11}C-PBR28, amyloid-positive patients had greater binding than amyloid-negative controls, with amyloid-positive controls and amyloid-negative patients having intermediate amounts of binding. However, for ^{18}F-MK6240, greater binding is seen in amyloid-positive patients only.

P153: A preliminary analysis of the association between cerebral blood flow and amyloid and tau PET binding in older adults

Daniel Albrecht[1], A. Lisette Isenberg[1], Joy Stradford[1], Teresa Monreal[1], Kay Jann[1], Judy Pa[1]

[1]Department of Neurology, Mark and Mary Stevens Neuroimaging and Informatics Institute, University of Southern California (USC), Los Angeles, CA, US
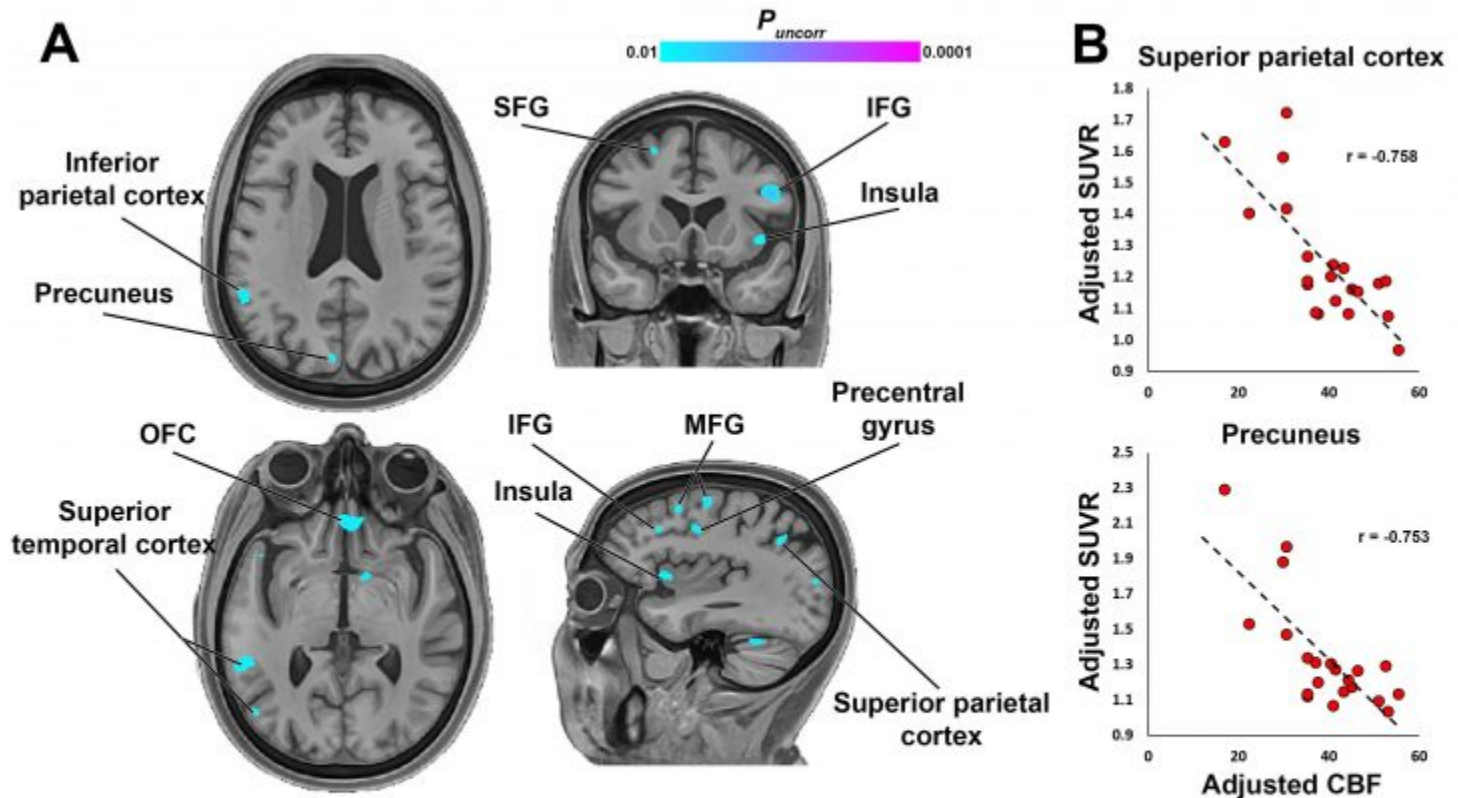

Figure 1. [^{18}F]Florbetaben signal is negatively associated with CBF.
A. Results from a voxelwise regression between [^{18}F]Florbetaben SUVR and global gray matter CBF across the entire sample (n = 21). Clusters shown in cool colorscale depict significant negative relationships. All clusters survived significance at $p < 0.005$, but results are thresholded at $p < 0.01$ for display purposes.
B. For visualization purposes, average SUVR and CBF from representative clusters in panel A are plotted, adjusted for age.
SFG/MFG/IFG: superior/middle/inferior frontal gyrus; OFC: orbitofrontal cortex

Recent studies reported associations between increased amyloid deposition and decreased cerebral blood flow (CBF), throughout the progression of Alzheimer's disease (AD). However, the relationship between CBF and protein binding has not been assessed for tau PET tracers, or with other amyloid PET tracers.

Therefore, we assessed the presence of these relationships in 21 participants (67.3±6.9 years, MMSE: 28.9±1.0) with [^{18}F]florbetaben, [^{18}F]AV-1451, structural T1, and pseudo-continuous arterial spin labeling (pCASL) scans acquired 4.29±7.2 days apart. Subjects were stratified into low-high groups based on median splits of [^{18}F]florbetaben and [^{18}F]AV-1451 composite SUVR. Relationships between SUVR and global gray matter (GM) CBF were assessed on a voxel-wise basis in the whole sample (n=21) and within low-high groups, covarying for age. Significance was set at $p < 0.01$, uncorrected, due to the exploratory nature of the study.

Across all subjects, we observed negative correlations between: 1) [18F]florbetaben SUVR and CBF in cortical regions known to have amyloid deposition (Figure 1) and 2) [18F]AV-1451 SUVR and CBF in regions known to exhibit early tau deposition (Figure 2). In the low-high median split analysis, patterns of SUVR-CBF correlations appeared to follow the presumed timecourse of amyloid or tau protein deposition (Figure 3). For example, in the low-amyloid group, the ACC and precuneus demonstrated negative SUVR-CBF correlations, whereas in the high-amyloid group negative correlations were restricted to lateral cortical regions (e.g. temporal/parietal lobes). Few SUVR-CBF correlations were observed in the low-tau group, but in the high-tau group several regions showed negative correlations, including inferior temporal cortex and orbitofrontal cortex.

Results from this preliminary analysis support previous evidence of negative relationships between amyloid binding and CBF for the [18F]florbetaben amyloid tracer, and extend these findings to a clinically meaningful pattern of tau binding. Future, longitudinal studies are needed to explore the temporal relationship between AD-related protein binding and CBF.
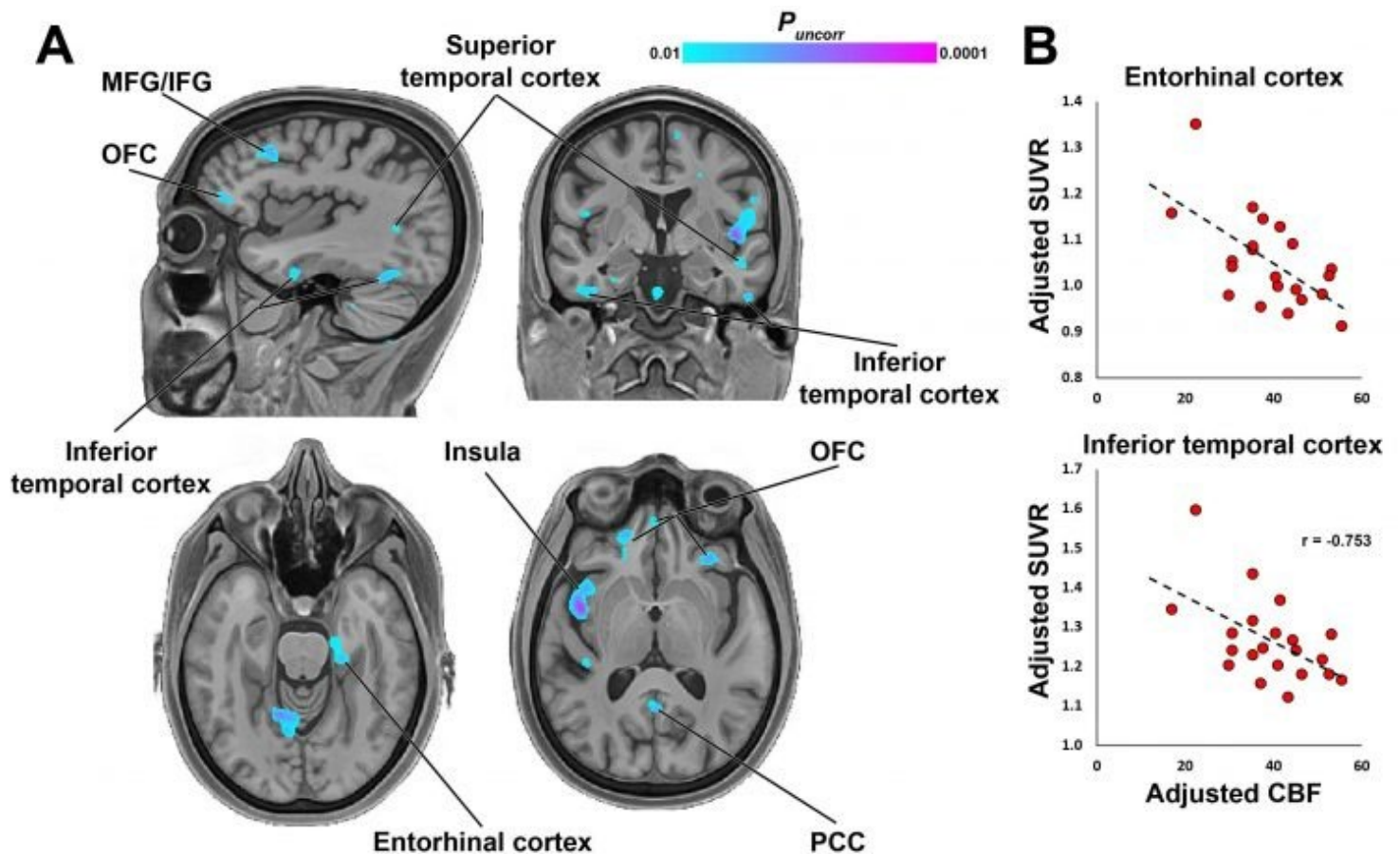

Figure 2. [18F]AV-1451 signal is negatively associated with CBF.
A. Results from a voxelwise regression between [18F]AV-1451 SUVR and global gray matter CBF across the entire sample (n = 21). Clusters shown in cool colorscale depict significant negative relationships. All clusters survived significance at $p < 0.005$, but results are thresholded at $p < 0.01$ for display purposes.
B. For visualization purposes, average SUVR and CBF from representative clusters in panel A are plotted, adjusted for age.
MFG/IFG: middle/inferior frontal gyrus; OFC: orbitofrontal cortex; PCC: posterior cingulate cortex
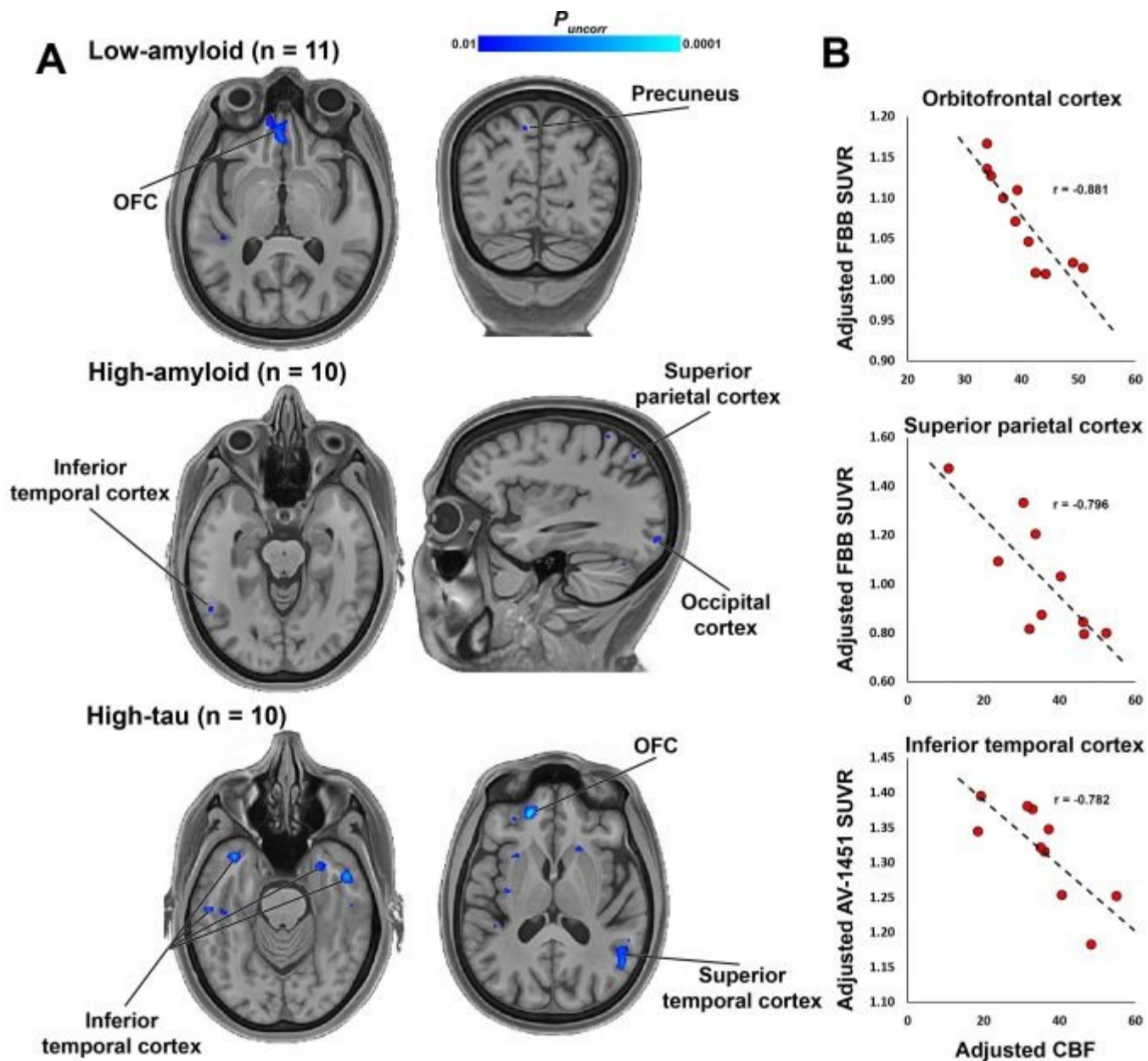
Figure 3. Low-high median splits of [18F]Florbetaben and [18F]AV-1451 SUVR and correlations with CBF
A. Results from voxelwise regression between CBF and SUVR in subjects with high [18F]Florbetaben SUVR (top row), low [18F]Florbetaben SUVR (middle row), and high [18F]AV-1451 SUVR (bottom row).
Clusters shown in blue colorscale depict significant negative relationships.
B. For visualization purposes, average SUVR and CBF from representative clusters in panel A are plotted, adjusted for age.
OFC: orbitofrontal cortex

P154: Random forests of amyloid PET may pinpoint key brain regions predictive of MoCA score

Katherine Zukotynski[14], Vincent Gaudet[2], Phillip Kuo[3], Sabrina Adamo[4], Maged Goubran[4], Christopher Scott[4], Christian Bocti[5], Michael Borrie[6], Howard Chertkow[7], Richard Frayne[8], Robin Hsiung[9], Robert Jr. Laforce[10], Michael Noseworthy[1], Frank Prato[6], Jim Sahlas[1], Eric Smith[11], Vesna Sossi[9], Alex Thiel[7], Jean-Paul Soucy[12], Jean-Claude Tardif[13], <u>Sandra Black</u>[4]

[1]*McMaster University, Hamilton, ON, Canada*
[2]*University of Waterloo, Waterloo, ON, Canada*
[3]*University of Arizona, Tucson, AZ, US*
[4]*Sunnybrook Research Institute, Toronto, ON, Canada*
[5]*Université de Sherbrooke, Sherbrooke, QC, Canada*
[6]*Western University, London, ON, Canada*
[7]*Jewish General Hospital, Montreal, QC, Canada*
[8]*University of Calgary, Calgary, AB, CA*
[9]*University of British Columbia, Vancouver, BC, Canada*
[10]*Université Laval, Québec, QC, Canada*
[11]*Hotchkiss Brain Institute, Calgary, AB, CA*
[12]*Montreal Neurological Institute, Montreal, QC, Canada*
[13]*Montreal Heart Institute, Montreal, QC, Canada*
[14]*University of Toronto, Toronto, ON, Canada*

Objectives: To evaluate if random forests (RF) using amyloid PET quantitative data can identify brain regions correlating with Montreal Cognitive Assessment (MoCA) scores.

Methods: Fifty-five participants with mild cognitive impairment (MCI), early Alzheimer's disease (AD) or transient ischemic events (Mini Mental Status Examination score>20) and severe periventricular hyperintensities (Fazekas score=3) were recruited from memory (37) and stroke (18) clinics. Each participant had an (18)F-florbetapir PET (clinical read: 22 positive, 33 negative for amyloid deposition) processed using a MINC toolkit with SUVRs calculated for 59 regions of interest (ROIs) normalized to cerebellar grey matter. MoCA scores for each participant were categorized as: normal ($\geq$26; 18 cases) or impaired (<26; 37 cases). SUVRs (not clinical reads) and MoCA categories were used to train an RF classifier with the objective of determining key ROIs for predicting MoCA score.

Results: A 100,000-tree RF (12 cases and 12 features per tree) was trained with 55 cases. The most frequent root node feature (number of trees, mean SUVR for decision, standard deviation) was: 1) right posterior cingulate (5147, 1.35, 0.19), 2) right precuneus (3901, 1.19, 0.15), 3) left posterior cingulate (3792, 1.27, 0.21), 4) left precuneus (3577, 1.21, 0.20), and 5) right anterior cingulate gyrus (3208, 1.24, 0.18). A 100,000-tree RF (10 cases, 12 features per tree) was constructed using 37 cases from memory clinics (8 normal, 29 impaired). The most frequent root node feature was: 1) right posterior cingulate (5022, 1.36, 0.16), 2) left posterior cingulate (4690, 1.26, 0.20), 3) left precuneus (4345, 1.07, 0.12), 4) left middle orbitofrontal gyrus (3748, 1.27, 0.14), and 5) right middle orbitofrontal gyrus (3745, 1.30, 0.13).

Conclusions: RFs using amyloid PET quantitation may identify key brain regions predictive of MoCA score. More data is needed to demonstrate classification accuracy.

Keywords: *Dementia, amyloid PET, machine learning, random forests, MoCA*

P155: Comparison of objective and self-reported sleep, tau, and Aβ in healthy older adults

Joseph Winer[1], Laura Fenton[2], Theresa Harrison[2], Anne Maass[2,3], Suzanne Baker[4], William Jagust[2,4]

[1]*Department of Psychology, University of California, Berkeley, Berkeley, CA, US*
[2]*Helen Wills Neuroscience Institute, University of California, Berkeley, Berkeley, CA, US*
[3]*German Center for Neurodegenerative Diseases, Magdeburg, Germany*
[4]*Molecular Biophysics and Integrated Bioimaging, Lawrence Berkeley National Lab, Berkeley, CA, US*

Background: Converging evidence supports a bi-directional relationship between sleep disruption and the progression of Alzheimer's disease (AD). β-amyloid (Aβ) burden has been linked to worse objective and self-reported sleep quality in healthy older adults. It is unknown whether tau pathology contributes to these associations.

Methods: We compared objective and self-reported measures of sleep quality to 18F-FTP and 11C-PIB retention in healthy older adults (N=31, age 78.7 ± 7.4). Objective sleep was assessed using 7 nights of at-home wristwatch actigraphy, with analyses focusing on both averages (duration, midpoint, efficiency, fragmentation) and variability (duration, midpoint) across the recording period. Subjective sleep was assessed using the Pittsburgh Sleep Quality Index. 18F-FTP SUVRs (80-100 min, inferior cerebellar gray reference) were calculated for each subject in a composite ROI of temporal cortical regions. A global cortical 11C-PIB DVR (0-90 min, cerebellar gray reference) was also calculated. All analyses were adjusted for age and gender.

Results: Greater cortical 11C-PIB DVR predicted shorter average sleep duration (Figure 1A; r=-0.49, p=0.01), which remained significant when adjusting for 18F-FTP SUVR. However, self-reported sleep duration was not related to 11C-PIB DVR, and greater 11C-PIB DVR predicted overestimation of sleep duration (Figure 1B; r=0.40, p=0.03). Subjects with greater 11C-PIB DVR also tended to have more variable sleep timing and sleep duration, but these associations were not significant. Sleep quality measures of efficiency and fragmentation were not associated with 11C-PIB DVR. 18F-FTP SUVR was not associated with any objective or subjective sleep metrics.

Conclusions: These preliminary findings confirm an association between Aβ burden and objective sleep disruption. This association was independent of tau burden. Aβ was also associated with overestimated sleep duration, suggesting that self-reported sleep may be inaccurate in the context of Aβ deposition.
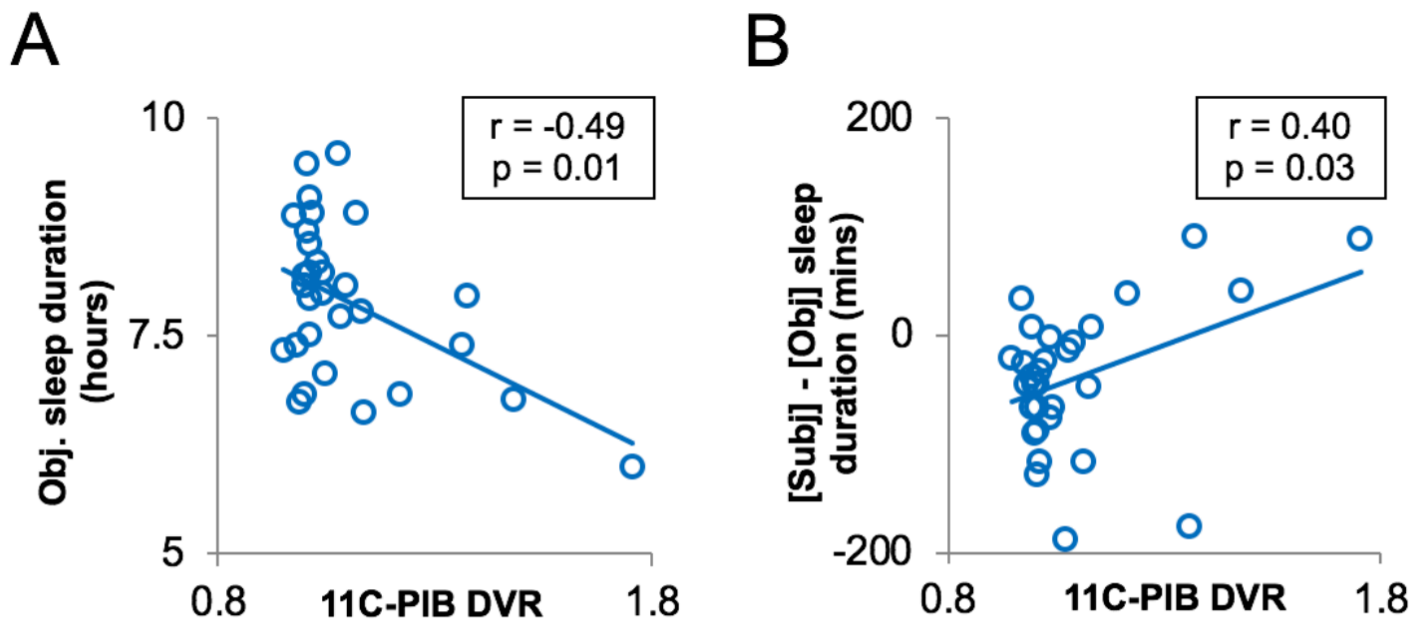
Fig. 1. A) Greater cortical ^{11}C-PIB DVR predicts shorter average sleep duration measured by a week of wristwatch actigraphy recording. B) Greater ^{11}C-PIB DVR predicts overestimation of sleep duration, calculated as self-reported sleep duration minus the actigraphy-measured average sleep duration. Most subjects tend to underestimate their sleep duration.

Keywords: *sleep, amyloid, tau, aging*

P156: Relation of cardiovascular risk factors to markers of pathology and memory in autosomal-dominant Alzheimer's disease

Jairo Martínez[1], Edmarie Guzmán-Vélez[1], Enmanuelle Padilla-Delgado[1], Clara Vila-Castelar[1], Joshua Fuller[1,2], Arabiye Artola[1], Reisa Sperling[1,3], Yakeel T Quiroz[1,4]

[1]1Massachusetts General Hospital, Boston, MA, US
[2]Boston University, Boston, MA, US
[3]Brigham and Women's Hospital, Boston, MA, US
[4]Universidad de Antioquia, Medellin, CO

Background: Cardiovascular risk factors have been suggested to predict cognitive decline and onset of Alzheimer's disease (AD). However, it is uncertain if cardiovascular risk factors relate to cognitive functioning and AD pathology (e.g. amyloid and tau) in individuals with autosomal-dominant AD (ADAD), who will develop dementia in their forties. We sought to test the hypothesis that greater cardiovascular risk, as measured by the Framingham Heart Study general cardiovascular disease risk score (FHS-CVD), is associated with worse memory and greater AD pathology in the world's largest kindred with ADAD.

Methods: 16 Presenilin-1 (PSEN-1) E280A mutation carriers (14 asymptomatic and 2 symptomatic), and 21 family member non-carriers ages 28 to 45 participated in the study. The FHS-CVD was calculated for each participant. They underwent amyloid (Pittsburgh Compound B) and tau (FTP) PET imaging, MRI, and completed the CERAD word list recall test. Spearman's rho correlations were used to examine relationships between FHS-CVD, AD pathology, and memory.

Results: There were no significant differences between mutation carriers and non-carriers in the FHS-CVD scores ($p=.220$). In carriers, there were no significant correlations between FHS-CVD and cortical amyloid ($p=.165$) or tau pathology in the entorhinal cortex ($p=.778$). However, carriers with higher FHS-CVD scores had greater tau pathology in the inferior temporal lobe ($r=.605$, $p=.013$), and worse episodic memory ($r=-.682$, $p=.004$).

Conclusion: Preliminary findings suggest that cardiovascular risk factors are associated with worse episodic memory and regional tau pathology accumulation in a group of non-demented individuals with ADAD. A larger sample is needed to better understand the association between cardiovascular risk factors, AD pathology, and cognitive functioning in individuals at high risk for AD.

Keywords: *cardiovascular risk, early-onset Alzheimer's disease, tau pathology, amyloid pathology, PET imaging*

P157: Beta-amyloid accumulation in non-demented elderly individuals correlates with baseline beta-amyloid load, ApoE genotype and age

Anton Gietl[1], Valerie Treyer[1,4], Andreas Buchmann[1], Rafael Meyer[1,5], Antje Saake[1], Esmeralda Gruber[1], Linjing Mu[4], Paul Unschuld[1,3], Alfred Buck[4], Roger Nitsch[1,2], Christoph Hock[1,2]

[1]*Institute for Regenerative Medicine (IREM), University of Zurich, Schlieren, Switzerland*
[2]*Neurimmune, Schlieren-Zurich, Schlieren, Switzerland*
[3]*Hospital for Psychogeriatric Medicine, University of Zurich, Zurich, Switzerland*
[4]*Department of Nuclear Medicine, University Hospital of Zurich, Zurich, Switzerland*
[5]*Psychiatric Services Aargau, Brugg, Switzerland*

Age and ApoE genotype are established predictors for beta-amyloid load when measured cross-sectional, but the contribution to longitudinal beta-amyloid accumulation has been debated. Clarification of this contribution would be of relevance for the development of anti-amyloid therapies and strategies aiming at modifying the effect of ApoE4 on beta-amyloid deposition.

60 elderly cognitively unimpaired subjects with a mean age of 68.3 years (range 56-80, sd: 5.7) were followed over a time period of about three years and assessed with two beta-amyloid PET-scans using 11-C-Pittsburgh compound B at baseline and at the end of the observation period. PET data was analyzed with brain parcellation method using PMOD and 3D baseline MRI. Beta-amyloid accumulation was defined as a change from baseline greater than zero.

44 subjects (13 E4 carrier and 30 E4 non carrier) were identified as beta-amyloid accumulators, while beta-amyloid remained unchanged in 16 subjects. In accumulators, beta-amyloid accumulation (SUVR change per year) was associated with higher baseline levels of amyloid-load (rho: 0.48; p=0.001) and higher age at baseline (rho: 0.36, p=0.015). When grouped according to ApoE genotype, those with an epsilon4 allele (E4 carrier) showed higher baseline beta-amyloid load, as well as higher beta-amyloid accumulation over time (Median SUVR change per year: 0.03/IQR 0.05) as compared to subjects without an epsilon4 allele (Median SUVR change per year: 0.01/IQR 0.02; Mann Whitney U: 279 p=0.026). Baseline levels of beta-amyloid or beta-amyloid accumulation did not show a significant correlation with cognitive deficits at baseline or change in cognitive performance over time.

Consistent with previous reports, in a cognitively intact and clinically healthy elderly population, ApoE4 genotype and age constitute drivers of beta-amyloid load. Furthermore, our findings support the view that ApoE contributes to beta-amyloid accumulation in preclinical AD populations. This may have implications for the timing of anti-amyloid and anti-E4 therapeutic strategies.

Keywords: *ApoE, beta-amyloid, PET, accumulation, cognitive*

P158: Identification of rapid amyloid accumulators: A longitudinal PET amyloid study

Ivan Koychev[1], Nemanja Vaci[1], Murat Bilgel[2], Yang An[2], Marilyn Albert[3], Susan Resnick[2]

[1]*Department of Psychiatry, University of Oxford, Oxford, UK*
[2]*Laboratory of Behavioral Neuroscience, Intramural Research Program, National Institute on Aging, Baltimore, MD, US*
[3]*Department of Neurology, Johns Hopkins School of Medicine, Baltimore, MD, US*

Introduction: Evidence that any accumulating amyloid associates with worsening cognition, cortical atrophy and tau deposition argues for interventional trials in AD focusing on cases with emerging rather than widespread amyloid. We investigated the existence and potential for prediction of distinct latent classes of rapid accumulation as well as time points of significant increase in amyloid burden.

Methods: Cortical distribution volume ratio (cDVR) was derived from 190 Baltimore Longitudinal Study of Aging participants (mean age 79±8, mean MMSE 28±2) using ^{11}C-Pittsburgh compound-B imaging (mean scans 3, range 1-9).

Mixed effects modelling together with logistic regression was used to investigate existence of latent classes based on amyloid age-related longitudinal trajectorys and their predictors (sex, race, education, APOE4 status, MMSE and structural MRI). Generalised additive modelling characterised the non-linear age-related trajectories of cDVR and the effects of APOE4.

Results: The latent class analysis revealed two distinct age-related amyloid accumulation classes. The accumulators had a significantly higher intercept and steeper slope relative to the non-accumulators. Class membership was predicted by APOE4 (OR = 3.24 (1.44 – 7.31) p <.01) and volume-corrected grey matter (β = -0.016, p< .01), with a trend for increased risk for males (OR = 2.52 (0.90 – 7.03) p = .07). Area under the Receiver Operating Characteristic (ROC) curve was 0.72. Modelling of non-linear age-related trajectories of cDVR revealed a significant increase in rate of accumulation starting at mean age of 68 which was influenced by APOE4 carrier status (60 for carriers, 69 for non-carriers).

Conclusions: The results demonstrate the existence of amyloid accumulators and non-accumulators as well as time points of significant acceleration in accumulation rate. The predictive value of the models was modest which highlights the importance of enriching them through biomarkers that may be more relevant to the earliest stages of the disease.

Keywords: *Alzheimer's disease, amyloid accumulators, prediction models*

P159: Age-of-onset dependent associations between [18F]Flortaucipir PET and cognitive impairment in Alzheimer's disease

Denise Visser[1], Emma Wolters[1,2], Sander Verfaillie[1], Rik Ossenkoppele[2,3], Tessa Timmers[1,2], Hayel Tuncel[1], Sandeep Golla[1], Ronald Boellaard[1], Bert Windhorst[1], Philip Scheltens[2], Wiesje van der Flier[2,4], Bart van Berckel[1]

[1]Department of Radiology & Nuclear Medicine, Amsterdam Neuroscience, Vrije Universiteit Amsterdam, Amsterdam UMC, Amsterdam, The Netherlands
[2]Alzheimer Center Amsterdam, Department of Neurology, Amsterdam Neuroscience, Vrije Universiteit Amsterdam, Amsterdam UMC, Amsterdam, The Netherlands
[3]Clinical Memory Research Unit, Lund University, Lund, Sweden
[4]Department of Epidemiology and Biostatistics, Vrije Universiteit Amsterdam, Amsterdam UMC, Amsterdam, The Netherlands

Background: Early-onset (EO-) Alzheimer's disease (AD) patients show more and topographically different accumulation of tau pathology compared with late-onset (LO-) AD patients. Tau pathology is tightly coupled to cognitive impairment. The aim of this study was to investigate whether associations between **in vivo** tau pathology and severity of cognitive impairment were different in EO- and LOAD.

Methods: We included 65 amyloid positive patients with mild cognitive impairment (n=9) or AD dementia (n=56), divided into EOAD (age <65 years) and LOAD (age ≥65 years)[Table 1]. All underwent a 130-minutes dynamic [^{18}F]Flortaucipir PET scan. Parametric images were generated using receptor parametric mapping (RPM; reference region cerebellar grey matter) to extract binding potential (BP$_{ND}$) in five Hammers-atlas based cortical regions-of-interest (ROI's; medial temporal, lateral temporal, parietal, occipital and frontal). Partial volume correction was applied using the Hypr-IDM-Hypr method. Standardized neuropsychological assessment covered four domains (memory, executive functioning, language, and attention). Linear regression analyses were performed between regional [^{18}F]Flortaucipir BP$_{ND}$ and cognition (Z-transformed), adjusted for age, sex, education and an additional interaction term for age-of-onset (binary). Results were FDR-corrected.

Results: Overall, worse memory performance was associated with higher medial temporal [^{18}F]Flortaucipir BP$_{ND}$[Table 2]. Worse executive function and attention scores were associated with higher lateral temporal, parietal, frontal and occipital [^{18}F]Flortaucipir BP$_{ND}$, except for attention and occipital [^{18}F]Flortaucipir BP$_{ND}$. Worse language performance was associated with higher [^{18}F]Flortaucipir BP$_{ND}$ in all ROI's. Regarding age-of-onset effects, we only found an interaction for attention in the lateral temporal (p=.035) and parietal (p=.030) regions. Stratified analyses revealed that [^{18}F]Flortaucipir BP$_{ND}$ more strongly associated with worse attention in EOAD compared with LOAD[Figure 1].

Conclusion: The association between **in vivo** tau pathology and severity of cognitive impairment differed only between EOAD and LOAD for the attention domain. Particularly, higher parietal tau burden was more strongly associated with attention impairment in EOAD.

Table 1. Overview of demographics, neuropsychology and [^{18}F]Flortaucipir PET

	EOAD (n=26)	LOAD (n=39)
Age	60 (4)***	71 (5)
Sex (female/male)	15/11	17/22
Education	6 [3-7]	5 [3-7]
MMSE	22 (5)	23 (4)
Neuropsychology (domain scores)		
Memory[a]	.13 (.84)	-.12 (.81)
Executive Function[b]	-.14 (.74)	.02 (.86)
Language[c]	-.05 (1.14)	-.07 (.67)
Attention[d]	-.30 (1.03)	.13 (.59)
[^{18}F]Flortaucipir BP$_{ND}$		
Medial Temporal	.346 (.162)	.361 (.217)
Lateral Temporal	.767 (.338)	.599 (.404)
Parietal	1.278 (.556)***	.555 (.387)
Occipital	.975 (.599)***	.473 (.287)
Frontal	.417 (.261)***	.150 (.217)

Mean (SD) are reported for all variables, except for sex (n$_{female}$/n$_{male}$) and education (median [minimum-maximum]). Domain scores were created by averaging Z-transformed test-scores of the following tests: [a]Immediate Recall of the Dutch version of the RAVLT, Delayed Recall of the Dutch version of the RAVLT, Visual Association Test-A; [b]Stroop III Color Word, Phonemic Verbal Fluency (D-A-T), Digit Span Backwards; [c]Category Fluency-Animals, Visual Association Test-Naming; [d]Trail Making Test-A, Stroop I word reading, Stroop II Color naming and Digit Span Forward. Parametric [^{18}F]Flortaucipir images were partial volume corrected using the Hypr-IDM-Hypr method. BP$_{ND}$ = non-displaceable binding potential. *p<0.05, **p<0.01, ***p<0.001

Table 2. Associations between [^{18}F]Flortaucipir and cognition

	Memory	Executive Function	Language	Attention
Medial Temporal				
β	-.394*	-.218	-.340*	-.002
β interaction				
Lateral Temporal				
β	-.202	-.309*	-.470*	-.281
β interaction				**-.448***
Parietal				
β	-.169	-.440*	-.418*	-.687*
β interaction				**-.535***
Occipital				
β	-.246	-.263	-.444*	-.461*
β interaction				
Frontal				
β	-.137	-.354*	-.390*	-.482*
β interaction				

Linear regression analyses were performed, adjusting for age, sex and education. Standardized β (stdβ) are reported. Additional analyses were performed including an interaction of [^{18}F]Flortaucipir and age-of-onset (binary). Only stdβ of significant interactions are reported. *p<0.05$_{FDR}$
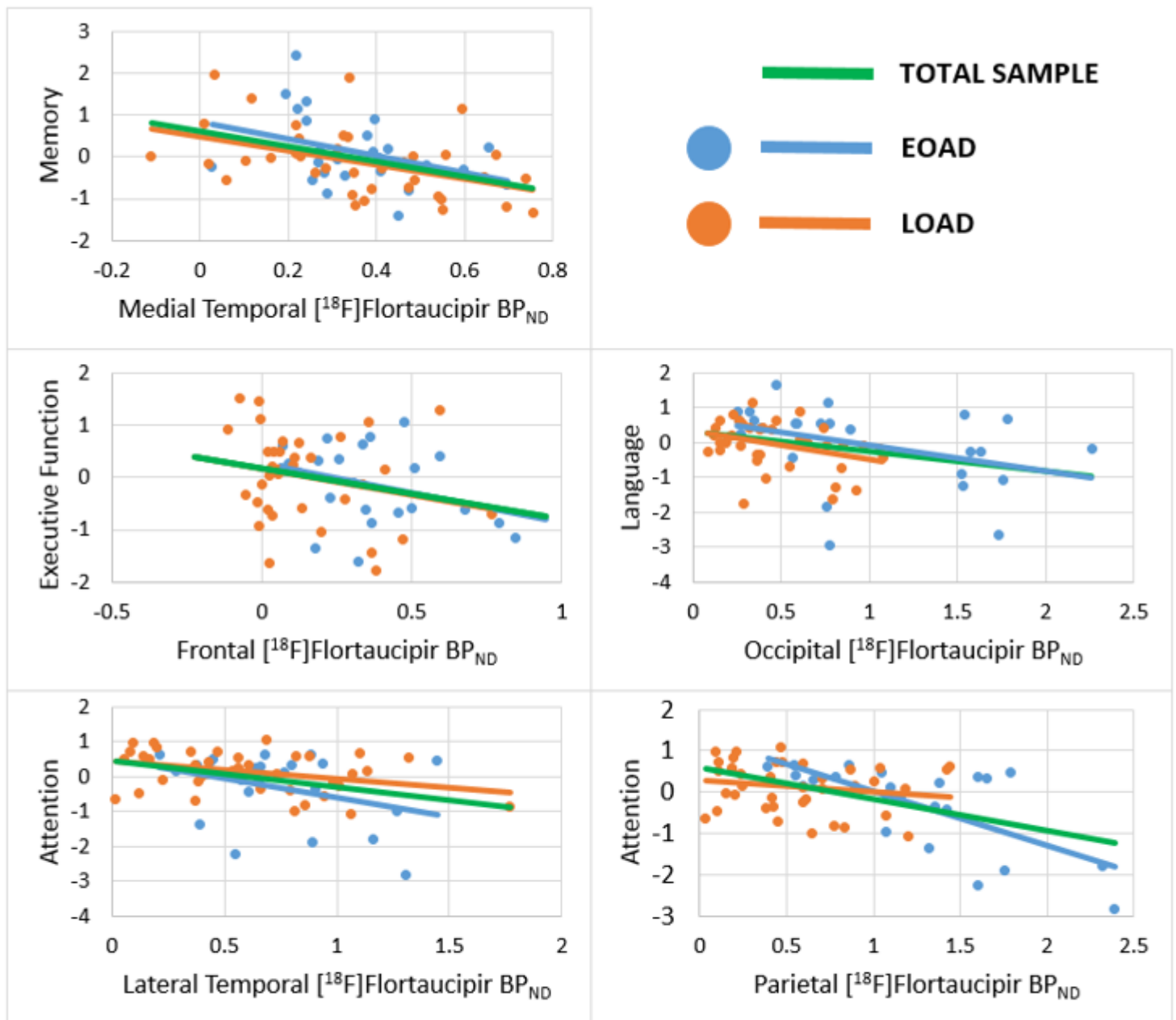
Figure 1. Associations between [18F]Flortaucipir BP$_{ND}$ and cognition. Cognition scores were Z-transformed and domain scores were created. Parametric [18F]Flortaucipir images were partial volume corrected using the Hypr-IDM-Hypr method. EOAD = early-onset Alzheimer's disease, LOAD = late-onset Alzheimer's disease, BP$_{ND}$ = non-displaceable binding potential.

Keywords: *Tau, Positron emission tomography (PET), cognition, age-of-onset*

P160: Derivation of amyloid PET centiloid cut-offs using core AD CSF biomarkers including the whole Alzheimer's continuum: a joint analysis in ALFA and ADNI

Gemma Salvadó[1], Anna Brugulat-Serrat[1], Carles Falcon[1], Javier Pavia[2,3], Aida Niñerola[2], Andrés Perissinotti[2], Francisco Lomeña[2], Henrik Zetterberg[4,5,6,7], Kaj Blennow[4,5], José Luis Molinuevo[1], Juan Domingo Gispert[1,3], for the ADNI, TRIBEKA Consortium and ALFA study[8]

[1]*Barcelonaβeta Brain Research Center, Pasqual Maragall Foundation, Barcelona, Spain*
[2]*Nuclear Medicine Department, Hospital Clínic, Barcelona; Instititut d'Investigacions Biomèdiques August Pi i Sunyer, Barcelona, Spain*
[3]*CIBER de Bioengeniería, Biomateriales y Nanomedicina, Barcelona, Spain*
[4]*Clinical Neurochemistry Laboratory, Sahlgrenska University Hospital, Mölndal, Sweden*
[5]*Department of Psychiatry and Neurochemistry, Institute of Neuroscience and Physiology, Sahlgrenska Academy at University of Gothenburg, Sahlgrenska University Hospital, Mölndal, Sweden*
[6]*Department of Neurodegenerative Disease, UCL Institute of Neurology, Queen Square, London, UK*
[7]*UK Dementia Research Institute, London, UK*
[8]*Alzheimer's Disease Neuroimaging Inititative, TRIBEKA Consortium, ALFA study, Barcelona, Spain*

Background: Recent studies suggest that lowering of CSF levels of $A\beta_{1-42}$ may be an earlier marker of brain amyloidosis than a positive amyloid PET scan. Centiloids[1] can be useful to harmonize amyloid PET cut-offs across tracers and quantification methods. Our aim is to derive centiloid cut-offs using core Alzheimer's disease (AD) CSF biomarkers as the reference standard for amyloid positivity, as these can be more sensitive to early amyloid accumulation than visual reading.

Methods: We used 205 scans of cognitively normal (CN) participants from the ALFA cohort[2] and 311 PET scans including CN, patients with mild cognitive impairment and AD dementia from ADNI covering the full Alzheimer's **continuum**. All these participants had core AD CSF biomarkers ($A\beta_{1-42}$ and pTau) analysed using fully automated assays on the Elecsys platform.

PET scans were quantified using the centiloid scale[1]. To derive individual centiloid cut-offs, we performed ROC analysis against CSF dichotomized values (with previously reported cut-offs[3]). Optimal cut-offs were also determined as those with the highest Youden's index (YI) or overall percent agreement (OPA). Positive and negative percent agreement (PPA, NPA) were also computed, as well as positive and negative predictive value (PPV, NPV).

Results: Figure 1 shows the scatterplots of centiloid PET vs CSF biomarker values, split by clinical-cohort. Cut-offs against $A\beta_{1-42}$ and pTau/$A\beta_{1-42}$ are shown in Figures 2-3. The lowest PET cut-off was 10 Centiloids against $A\beta_{1-42}$ (AUC:0.87[0.84-0.90], YI:0.67[0.60-0.73], OPA:0.84[0.80-0.87]). The cut-off for pTau/$A\beta_{1-42}$ was 27 centiloids (AUC:0.97[0.96-0.99], YI:0.89[0.85-0.93], OPA:0.95[0.92-0.96]).

Conclusions: We found two thresholds could be used to determine informative inflection points across the disease **continuum**. The first, more conservative cut-off, derived using the pTau/$A\beta_{1-42}$ ratio, was 27 centiloids, whilst a lower cut-off (10 centiloids) was identified using CSF $A\beta_{1-42}$ alone. These cut-offs are in line with recent neuropathological analyses[4].

References:

[1]Klunk, 2015

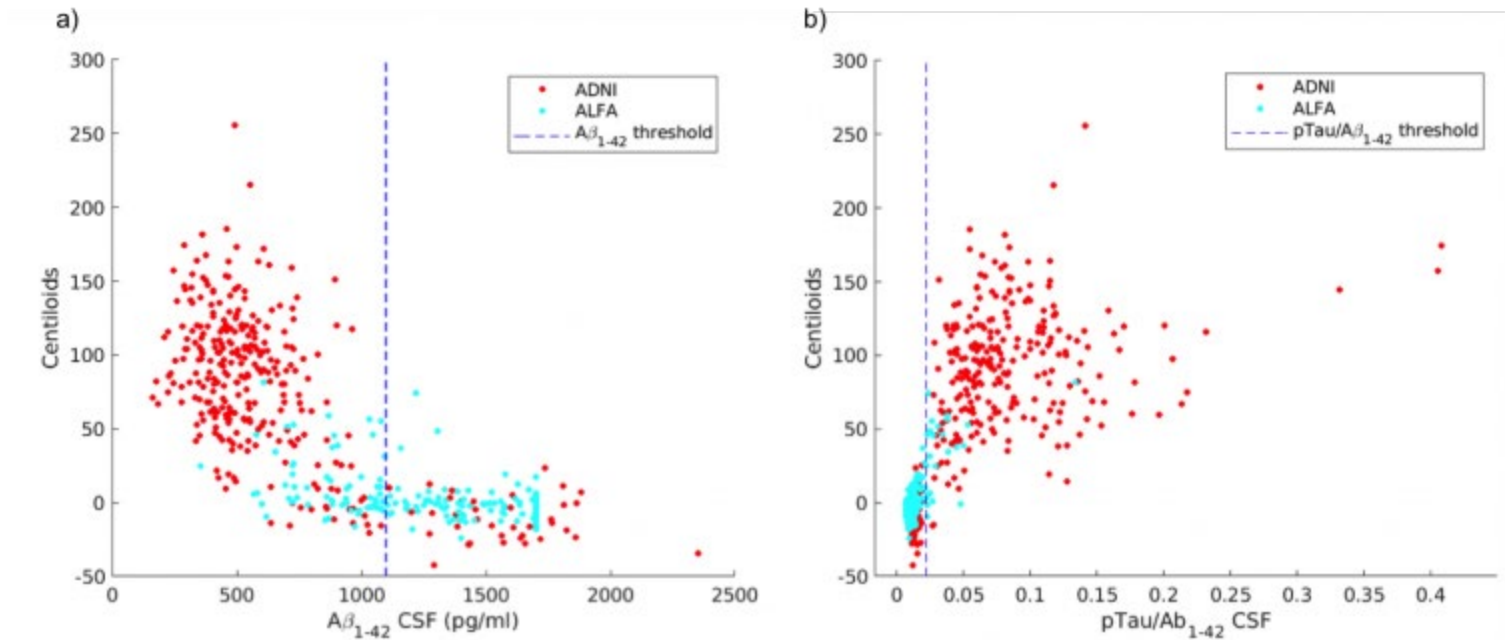[2]Molinuevo, 2016

[3]Schindler, 2018

[4]La Joie, 2018

Figure 1: Relationship between Centiloid PET quantification and CSF biomarkers. We show Centiloids against $A\beta_{1-42}$ (a), and against pTau/$A\beta_{1-42}$ ratio (b). The colour of the points indicate the database provenance (red: ADNI, cian: ALFA). Vertical lines indicate the thresholds for CSF biomarkers ($A\beta_{1-42}$: 1098 pg/ml, pTau/$A\beta_{1-42}$: 0.022).
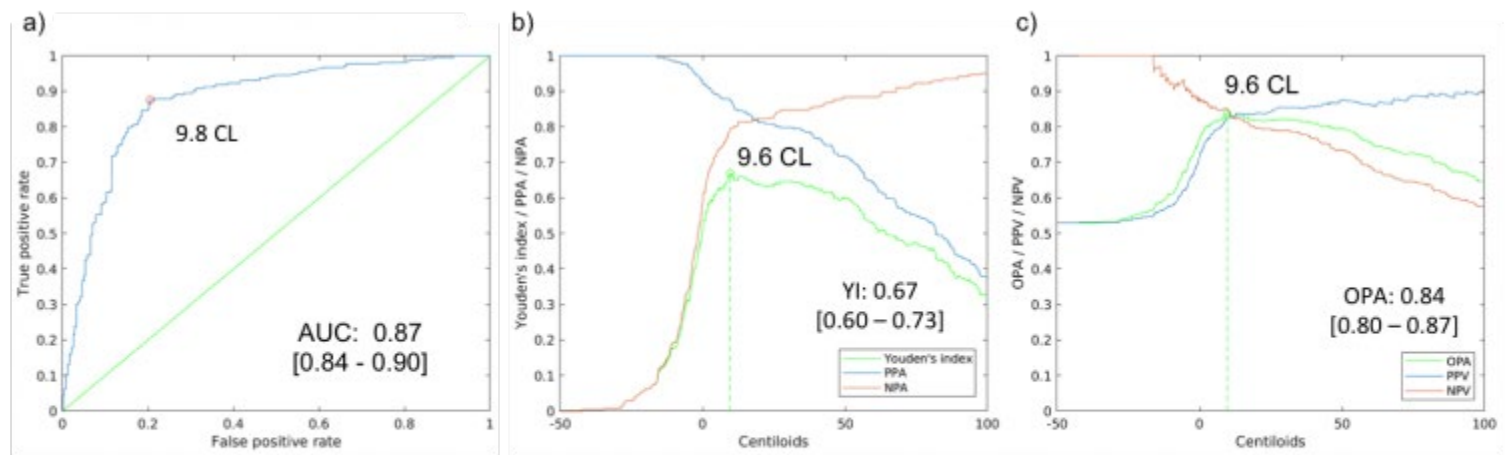

Figure 2: Centiloids cut-off derivation against $A\beta_{1-42}$ measured in CSF. Subfigures show ROC analysis (a), Younden's index , PPA and NPA (b) and OPA, PPV and NPV (c). All numbers between brackets indicate the 95%CI.
Abbreviations: CL, centiloid; CSF, cerebrospinal fluid; ROC, receiver operating curve; PPA, positive percent agreement ("sensitivity"); NPA, negative percent agreement ("specificity"); OPA, overall percent agreement ("accuracy"); PPV, positive predictive value; NPV, negative predictive value; 95%CI, 95% confidence intervall.
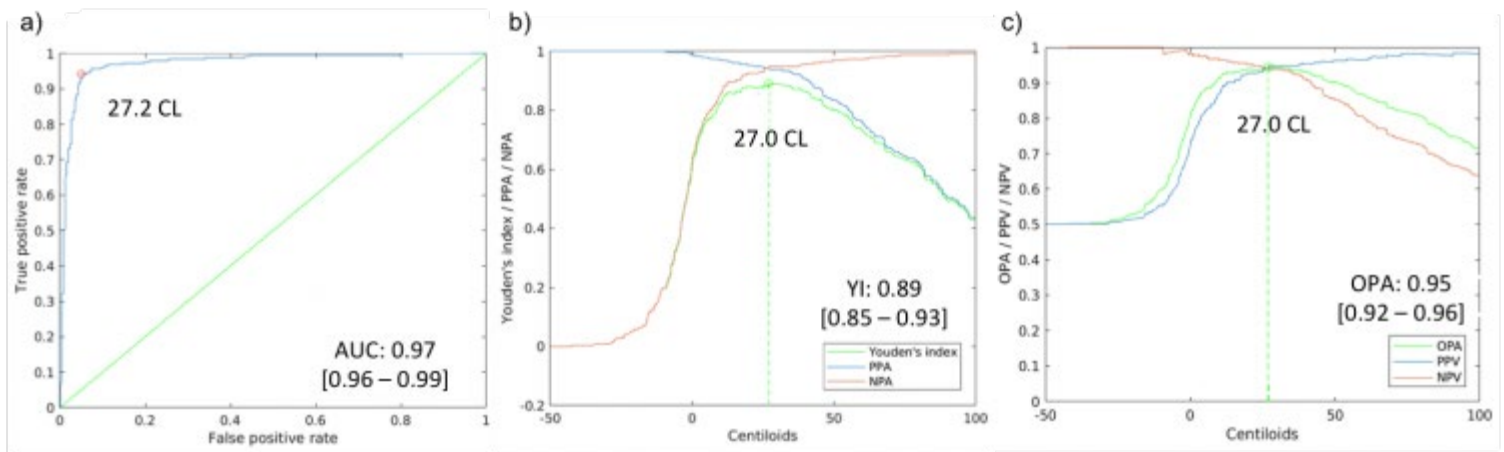
Figure 3: Centiloids cut-off derivation against pTau/Aβ_{1-42} measured in CSF. Subfigures show ROC analysis (a), Younden's index , PPA and NPA (b) and OPA, PPV and NPV (c). All numbers between brackets indicate the 95%CI.
Abbreviations: CL, centiloid; CSF, cerebrospinal fluid; ROC, receiver operating curve; YI, Youden's index; PPA, positive percent agreement ("sensitivity"); NPA, negative percent agreement ("specificity"); OPA, overall percent agreement ("accuracy"); PPV, positive predictive value; NPV, negative predictive value; 95%CI, 95% confidence intervall.

P161: SSRI reduces CSF Ab42 in healthy older adults and transgenic mice: dose, duration and baseline amyloid effects

Yvette Sheline[1], Joy Snider[2], Jin-Moo Lee[2], Kristin Linn[3], Anne Fagan[2], Ping Yan[2], Irem Aselcioglu[1], Teresa Waligorska[4], Magda Korecka[4], John Morris[2], Leslie Shaw[4], John Cirrito[2]

[1]*Departments of Psychiatry, Neurology, Radiology, University of Pennsylvania, Philadelphia, PA, US*
[2]*Department of Neurology, Washington University, St Louis, MO, US*
[3]*Department of Biostatistics, Epidemiology, Bioinformatics, University of Pennsylvania, Philadelphia, PA, US*
[4]*Department of Pathology, University of Pennsylvania, Philadelphia, PA, US*

Rationale: Serotonin signaling suppresses amyloid-b (Ab) in animal models of Alzheimer's disease (AD) and young healthy humans.

Objectives: Mouse experiments used transgenic mice (APP/PS1) in microdialysis, chronic dosing and 2-photon microscopy studies to assess effects of the SSRIs citalopram (CIT) and escitalopram (ESC) on: 1) interstitial fluid (ISF) amyloid levels; 2) plaque accumulation and 3) individual plaque growth using 2-photon microscopy. Elderly humans (n =114) were randomized to either: placebo; 20 mg ESC x 2 weeks; 20 mg ESC x 8 weeks or 30 mg ESC x 8 weeks.

Findings: In rodent studies, ESC reduced ISF Ab by $25.6 \pm 6.1\%$. Hippocampal plaque load was reduced by $28.7 \pm 0.05\%$ ($p<0.05$) and $34.4 \pm 0.05\%$ ($p<0.01$) for chronic administration of ESC 2.5 mg/day and 5 mg/day, respectively but not by vehicle. ESC at 5mg/kg but not 2.5 mg/kg arrested individual plaque growth. Humans exhibited an overall 9.5% difference in reduction between ESC treated and placebo groups ($p < 0.001$); baseline amyloid positive status was associated with less percent reduction in $A\beta_{42}$ ($p = 0.006$).

Conclusions: Chronic doses of ESC decreased the level of CSF $A\beta_{42}$ in cognitively normal elderly, the target group for AD prevention and in AD mouse models.

The relatively modest reduction in CSF $A\beta$ shown in the current study makes it unlikely that the currently available SSRIs would be developed for this purpose, although if a greater reduction could be demonstrated for the higher 30 mg dose the feasibility might be higher. In previous studies we demonstrated that the SSRI mechanism of action operated through ERK via binding to the 5-HT4, 5-HT6 and 5HT7 receptors. This offers the opportunity for developing drugs with higher affinity for these receptors as agents for reducing CSF $A\beta$ and plaque accumulation and could lead to new therapeutic preventive strategies.

Keywords: *CSF Aβ42, SSRI, prevention, lumbar puncture*

P162: Determination of the optimal scanning time point for the assessment of tau deposition in Alzheimer's disease using [18F]PI-2620 PET

Santiago Bullich[1], Andre Mueller[1], Olivier Barret[2], Mathias Berndt[1], Jennifer Madonia[2], John Seibyl[2], Ken Marek[2], Andrew Stephens[1]

[1]*Life Molecular Imaging, Berlin, Germany*
[2]*Invicro LLC, New Haven, CT, US*

Background: Tau deposition is a key pathologic feature of AD. ^{18}F-PI-2620 is a novel tau PET-tracer with a high affinity for pathological tau. The ability of PI-2620 to measure the spatial distribution of tau pathology in AD was demonstrated previously. The objective of this study was to determine the optimal scanning time for the assessment of tau-deposition in AD using ^{18}F-PI-2620.

Methods: Three NDC and 3 AD subjects underwent two dynamic PET scans up to 180min p.i. including arterial sampling and metabolite correction. Regions-of-interest were delineated in the mesial-temporal (Me), temporoparietal (Te) and the rest of the neo-cortex (R) following the MeTeR methodology. DVR was estimated using full tracer kinetics. SUVR were determined at different time points after injection using Cerebellar cortex as reference region. SUVR, effect size, test-retest variability and correlation between BP_{ND} and SUVR were evaluated over time.

Results: Strong correlation was found between BP_{ND} and SUVR-1 after 30min p.i. ($R^2 > 0.90$) (($BP_{ND} = 1.10 \cdot SUVR + 0.05$, $R2 = 0.98$ at 30-60min; $BP_{ND} = 1.22 \cdot SUVR + 0.05$, $R2 = 0.97$ at 45-75min; $BP_{ND} = 1.31 \cdot SUVR + 0.03$, $R2 = 0.96$ at 60-90min). Pseudo-equilibrium was reached around 40min in regions with moderate uptake. In cortical regions with high uptake, pseudo-equilibrium was not achieved and SUVR steadily increased during the whole scan. Average effect-size (Cohen's d) was 3.82 (30-60min), 3.80 (45-75min), 3.75 (60-90min), 3.13 (120-150min). The average test-retest variability across different regions was similar at 30-60min (4.75%), 45-75min (4.87%) and 60-90min (4.60%) and increased at later time points (6.32% at 120-150min).

Conclusion: Performance of ^{18}F-PI-2620 PET scans in different imaging windows between 30 and 90min p.i. were similar in AD similar. Outside of the 30 to 90min p.i. imaging window quantification accuracy, effect size, test-retest variability was impaired. ^{18}F-PI-2620 PET scans acquired at 45-75min p.i. provides excellent quantification accuracy, effect size, test-retest variability and visual assessment and is the proposed imaging time point for AD.

Keywords: *PET, tau, PI-2620, Test-retest, scanning time*

P163: Prediction of brain age using resting-state functional connectivity suggests accelerated aging in the preclinical phase of autosomal dominant Alzheimer's disease, irrespectively of amyloid pathology

Julie Gonneaud[1], Etienne Vachon-Presseau[1,2], Alexis Baria[1], Alexa Pichet Binette[1], Tammie Benzinger[3], John Morris[3], Randall Bateman[3], John Breitner[1], Judes Poirier[1], Sylvia Villeneuve[1], The DIAN Study Group[3], PREVENT-AD Research Group[1]

[1]*Douglas Mental Health Institute, McGill University, Montreal, QC, Canada*
[2]*Northwestern University, Chicago, IL, US*
[3]*Knight Alzheimer's Disease Research Center, Washington University School of Medicine, Saint Louis, MO, US*

Objective: To assess functional brain aging in the preclinical phase of autosomal dominant Alzheimer's disease (ADAD) and individuals at risk of sporadic AD (sAD), and its relationship with amyloid (Aβ) pathology.

Methods: Cognitively normal participants from 18 to 94 years old from the DIAN, PREVENT-AD, CamCAN, ADNI, and ICBM cohorts were included (Table). We used graph metrics from resting state fMRI (rsfMRI) to generate a neural net model predicting age (training set n=773; validation set n= 47). Age was then predicted in DIAN and PREVENT-AD (test set; n=158 and n=357, respectively) to assess the effect of AD genetic determinant/risk (ADAD mutation in DIAN and **APOE**4 in PREVENT-AD) on the discrepancy between functional brain aging and actual age. The effect of Aβ burden on brain prediction was assessed additionally in individuals with Aβ-PET.

Results: Age can be predicted from functional topological properties constructed from rsfMRI in a large number of participants selected across multi-site cohorts (Figure1). Importantly, our model estimated that cognitively normal DIAN mutation carriers were in average older than their actual age, and this discrepancy between the estimated and actual age was greater than in non-carriers (Figure2A). Aβ status (or load) however had no impact on the discrepancy between predicted and actual age (Figure2A). In the PREVENT-AD, neither **APOE**4 or Aβ burden was related to an over estimation of age (Figure2B).

Conclusions: Using rsfMRI graph metrics, we have developed a model that can predict brain age across the lifespan. Applying this model to predict brain aging in the context of preclinical AD suggest that the presymptomatic phase of ADAD may be characterized by accelerated functional brain aging. This phenomenon is independent from, and might therefore precede, Aβ accumulation.

Table. Data sets (sample size [age range in years])

Cohorts	Training set	Validation set	Test set
DIAN mut. noncarriers	105 [19-69 yo]	-	30 [18-61 yo]
DIAN mutation carriers	-	-	128 [20-58 yo]
PREVENT-AD	36 [55-78 yo]	-	257 [55-84 yo]
CamCAN	602 [18-87 yo]	-	100 [18-88 yo]
ADNI	30 [65-90 yo]	-	15 [66-94 yo]
ICBM	-	47 [19-79 yo]	-
Total sample	**773** [18-90 yo]	**47** [19-79 yo]	**530** [18-94 yo]

Model was built on the training set and optimized based on its generalizability in the validation set. Finally, model's predictions (difference between actual age and age predicted from brain function) were analyzed in the test set.
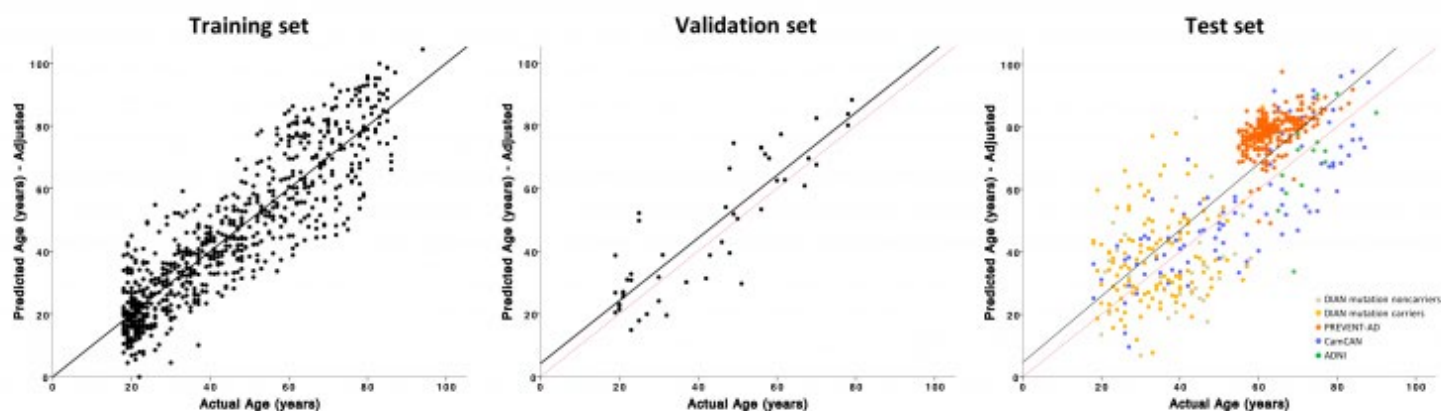
Figure1. Brain Age model performance across data sets. Correlations between actual age (x-axis) and age predicted by the neural network (y-axis) are represented across the different sets. Black lines represent the correlation between predicted and actual age while red lines correspond to the optimal fit (from the training set).
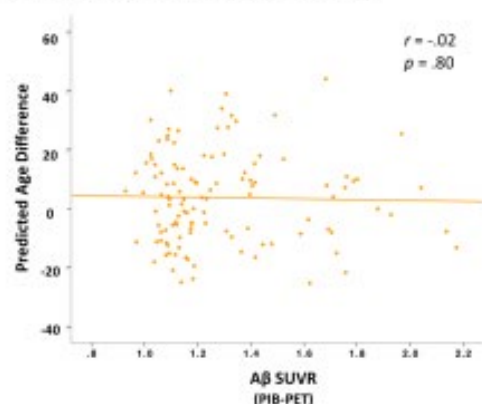
A. DIAN

1. Influence of genetic mutation
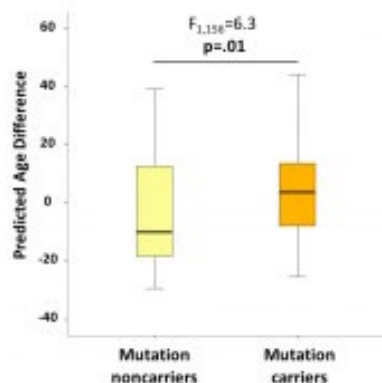
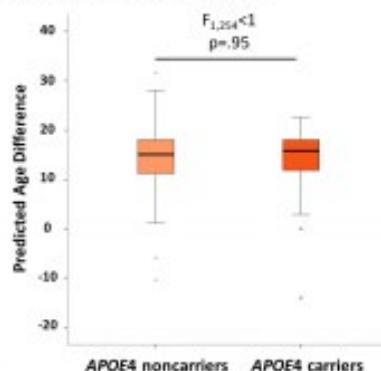**2. Influence of beta-amyloid (Aβ) status**
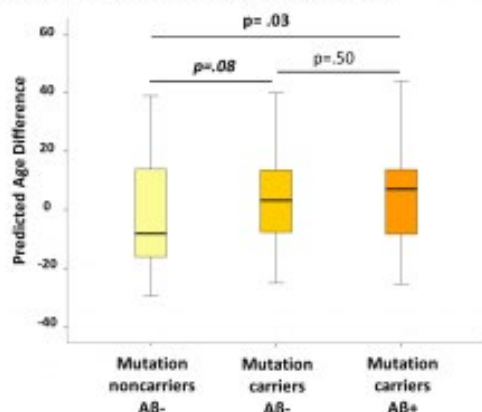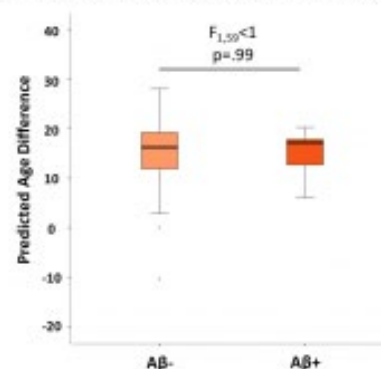
3. Influence of beta-amyloid (Aβ) load

B. PREVENT-AD

1. Influence of genetic risk

2. Influence of beta-amyloid (Aβ) status
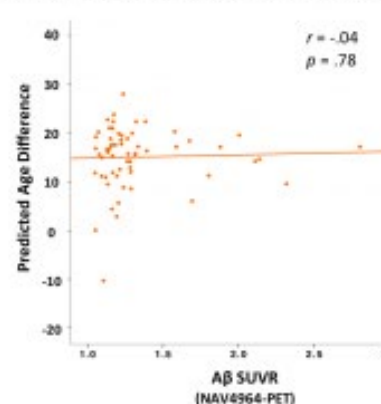
3. Influence of beta-amyloid (Aβ) load

Figure 2. Difference between the age predicted from brain function and actual age in DIAN (A) and PREVENT-AD (B). Brain age is overestimated in autosomal dominant mutation carriers compared to noncarriers (A.1.) but this overestimation in mutation carriers is not associated with beta-amyloid (Aβ) status (A.2) or load (A.3). In individuals at risk of sporadic Alzheimer's disease, brain age is overestimated irrespectively of APOE4 genotype (B.1.) and Aβ status (B.2) or load (B.3).

P164: Vascular risk factors and multimodal neuroimaging biomarkers: Preliminary analyses from a biracial older adult cohort

Samuel Lockhart[1], Suzanne Craft[1], Bonnie Sachs[1,2,3], Stephen Rapp[4], Youngkyoo Jung[5,6], Christopher Whitlow[5,6,7], Kathleen Hayden[3], Timothy Hughes[1,8]

[1]*Department of Internal Medicine, Wake Forest School of Medicine, Winston-Salem, NC, US*
[2]*Department of Neurology, Wake Forest School of Medicine, Winston-Salem, NC, US*
[3]*Department of Social Sciences and Health Policy, Wake Forest School of Medicine, Winston-Salem, NC, US*
[4]*Department of Psychiatry and Behavioral Medicine, Wake Forest School of Medicine, Winston-Salem, NC, US*
[5]*Department of Radiology, Wake Forest School of Medicine, Winston-Salem, NC, US*
[6]*Department of Biomedical Engineering, Wake Forest School of Medicine, Winston-Salem, NC, US*
[7]*Department of Biostatistical Sciences, Wake Forest School of Medicine, Winston-Salem, NC, US*
[8]*Department of Epidemiology and Prevention, Wake Forest School of Medicine, Winston-Salem, NC, US*

Objective: To examine antecedent vascular risk factors (VRFs) and neuroimaging measures (Aβ-PET, T1/FLAIR MRI) in a biracial (African-American [AA] and Caucasian) longitudinal cohort.

Methods: 90 participants from the Wake Forest ADRC Multi-Ethnic Study of Atherosclerosis (MESA) Core underwent baseline (2000-02) VRF assessment, and brain MRI and PET (2016-18). Baseline VRF scores included: Cardiovascular risk factors, aging and dementia (CAIDE) score; Framingham global risk score (FRS); an atherosclerotic cardiovascular disease risk estimate (ASCVD); and systolic blood pressure (SBP). Global PiB SUVR (40-70 min, cerebellar grey reference) was averaged from a cortical region of interest (ROI), with a 1.21 SUVR threshold demarcating Aβ- and Aβ+ groups. Cortical thickness was estimated from T1 using FreeSurfer in an AD-signature meta-ROI. Log-normalized global WMH volume was calculated from FLAIR corrected by head size.

Results: We did not observe significant ethnic differences in imaging measures of Aβ, cortical thickness, or WMH volume (Table). Ethnicity was not a significant predictor of brain Aβ, controlling for age, **APOE-ε4**, sex, education, and cortical thickness (**p**=.23). We found baseline VRF differences between ethnic groups, such that AA exhibited significantly greater ASCVD, SBP, and FRS (marginal) than Caucasians. Associations of Aβ with WMH and cortical thickness were strongest among Aβ+ participants, regardless of race (Figure 1; WMH **r**=.40, **p**=.039; cortical thickness **r**=-.38, **p**=.053). Further, we observed significant associations of elevations in VRFs with reduced cortical thickness and greater WMH (Figure 2), but not Aβ.

Conclusions: In contrast with recent studies showing Aβ-PET ethnic differences, our early single-site results suggest that AA are not more likely to be Aβ+ than Caucasians when additional confounders are addressed. Elevations in baseline VRFs are associated with increased WMH and reduced cortical thickness, but not elevated brain Aβ, in a bi-racial older adult sample. Ongoing analyses will examine ethnic differences in VRFs, imaging markers, and cognition.

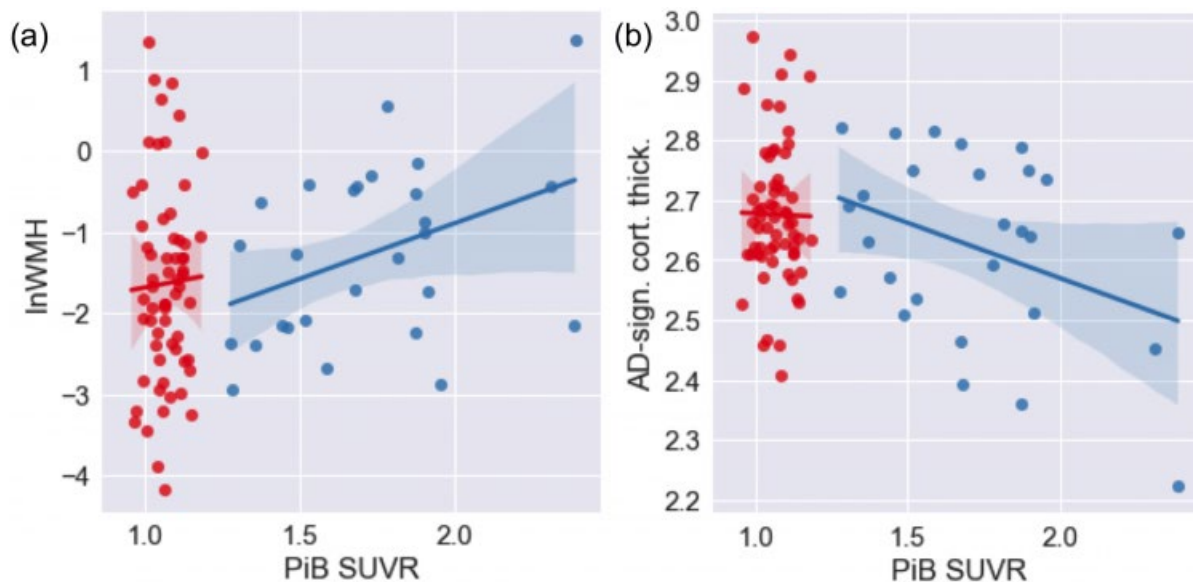| Table. MESA measures by ethnic group			
	Caucasian	AA	*p*
n	49	41	ns
Age, M (SD)	71.8 (5.8)	72.3 (8.0)	ns
CN, n (%)	39 (80%)	31 (76%)	ns
APOE-ε4 -/+/missing	31/15/3	24/15/2	ns
PiB SUVR, M (SD)	1.30 (.38)	1.21 (.30)	ns
PiB+, n (%)	16 (33%)	11 (27%)	ns
Cort. thick., mm, M (SD)	2.68 (.13)	2.63 (.13)	0.088
% WMH vol., median	0.18	0.21	ns
% ASCVD, M (SD)	5.1 (4.0)	9.3 (7.0)	<.001*
SBP, M (SD)	120.6 (17)	136.9 (24)	<.001*
FRS, M (SD)	9.58 (6.4)	12.6 (8.2)	0.056
CAIDE, M (SD)	6.47 (2.0)	6.63 (2.1)	ns

Figure 1. (a) PiB SUVR (x) vs. log-norm. WMH volume (y). (b) PiB SUVR (x) vs. AD-signature cortical thickness (y). PiB- subjects in red; PiB+ in blue.
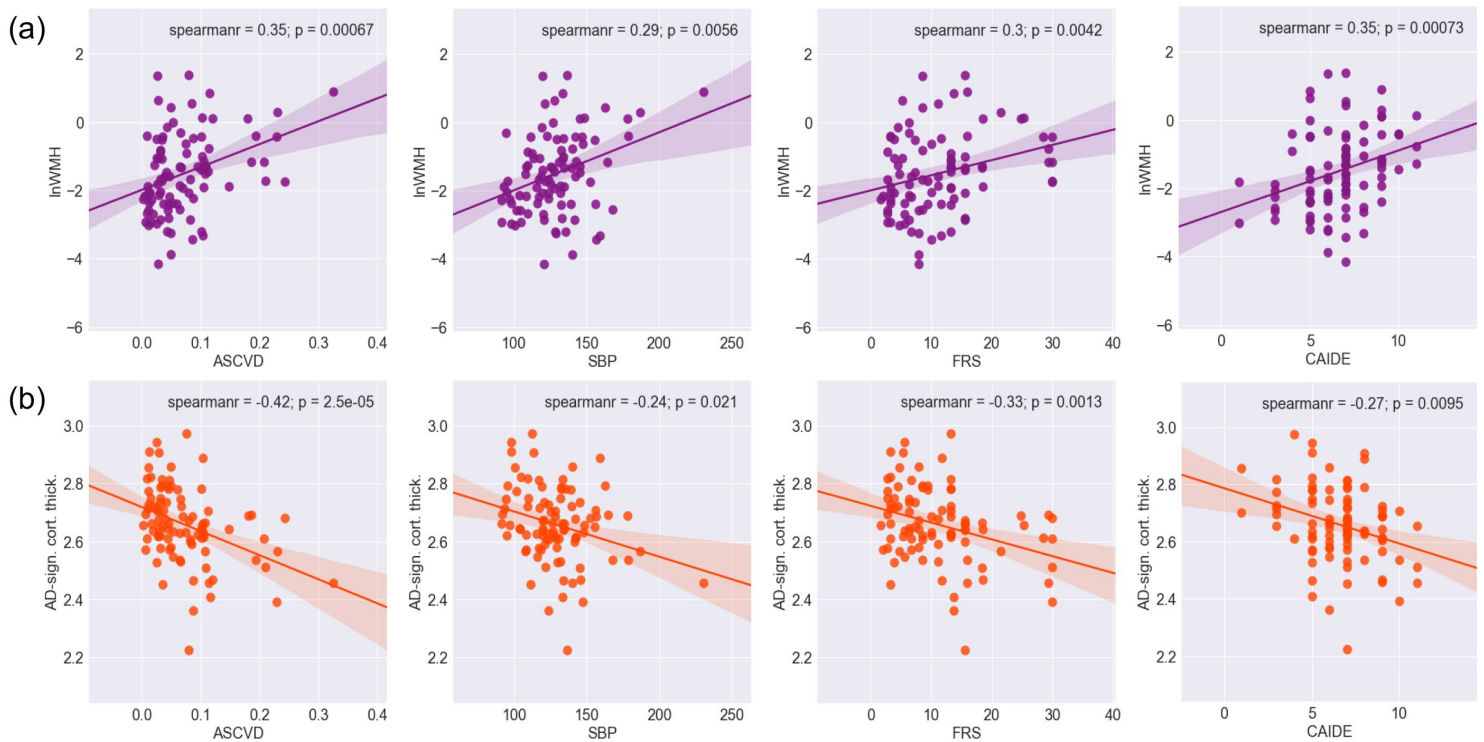
Figure 2. (a) VRFs (x) vs. log-norm. WMH volume (y). (b) VRFs (x) vs. AD-signature cortical thickness (y).

P165: Chronic low-grade inflammation associates with lower TSPO binding in elderly individuals without dementia

Laura Ekblad[1], Sini Toppala[1,2], Jouni Tuisku[1], Semi Helin[1], Päivi Marjamäki[1], Hanna Laine[2,3], Antti Jula[5], Matti Viitanen[2,4], Juha Rinne[1,6]

[1]*Turku PET Centre, University of Turku, Turku, Finland*
[2]*Turku City Hospital, Department of Geriatrics, University of Turku, Turku, Finland*
[3]*Department of Medicine, Turku University Hospital, Turku, Finland*
[4]*Clinical Geriatrics, Karolinska Institute, Karolinska University Hospital, Huddinge, Sweden*
[5]*National Institute for Health and Welfare, Turku, Finland*
[6]*Division of Clinical Neurosciences, Turku University Hospital, Turku, Finland*

Background: Obesity and insulin resistance associate with chronic low-grade inflammation, and with an increased risk for Alzheimer's disease. We evaluated if metabolic risk factors are associated with TSPO binding, a marker of neuroinflammation, in elderly individuals without dementia.

Methods: We examined 60 elderly volunteers with [11C]PIB-PET in 2014–2016. The participants were recruited according to their midlife insulin resistance (HOMA-IR) and their APOE genotype. 30 individuals had elevated HOMA-IR (IR+ group), and 30 controls had normal HOMA-IR values in 2000 (IR- group). Both groups contained 15 APOEε4 carriers. High (HAB) and mixed affinity binders (MAB) for TSPO (n=55) underwent [11C]PBR28 imaging. Participants who had arterial blood sampling (n=44) were included in the Logan analyses. Distribution volumes of the MAB and HAB groups were standardized to the mean of each group to obtain comparable z-scores.

Results: 33.3% of the IR- group and 56.5% of the IR+ group were amyloid positive (PIB SUVR >1.5). Unexpectedly, the IR+ group had lower [11C]PBR28 binding in the medial temporal cortex (p=0.039) and in the striatum (p=0.031) than the IR- group. Higher logarithmic HOMA-IR and high sensitivity CRP (hs-CRP) at time of PET scans correlated negatively with [11C]PBR28 binding in both gray (Figure 1.) and white matter. Higher hs-CRP independently predicted lower PBR28 gray (p=0.02) and white matter z-scores (p=0.03) in linear regression models after adjustments for age, sex, APOEε4, HOMA-IR, BMI and serum total cholesterol. No interactions were found between PIB status and hs-CRP on the association with [11C]PBR28 z-scores.

Conclusions: Higher hs-CRP, a marker of low-grade inflammation, predicts lower TSPO binding in amyloid positive and negative elderly individuals without dementia. Preclinical studies suggest that TSPO expression is decreased in human macrophages after an inflammatory stimulus. Our results suggest that systemic low-grade inflammation could influence TSPO binding in the brain.

Table 1_Characteristics in the total study population and according to midlife insulin resistance (IR) group.

	all	IR-	IR+	p-value
n	44	21	23	
female n/%	26 (59.0)	13 /61.9	13 /56.5	0.72
age	70.1 (3.1)	69.8 (3.6)	70.4 (2.8)	0.55
PIB positive n / %	20 /45.4	7 / 33.3	13 / 56.5	0.12
APOEε4 carrier n / %	22 / 50.0	10 /47.6	12 / 52.2	0.76
MAB n / %	20 / 45.5	11 / 52.4	9 / 39.1	0.38
HAB n / %	24 / 54.5	10 / 47.6	14 / 60.9	0.38
educational level (n)				0.03
primary school	15	3	12	
middle or comprehensive school	14	7	7	
high school	6	4	2	
college or university	9	7	2	
CERAD total score	90 (83–95)	93 (87–95)	87 (80–91)	0.02
BMI	26.5 (3.8)	24.6 (2.7)	28.3 (3.7)	0.0005
HOMA-IR	2.2 (1.4–3.5)	1.6 (1.0–2.4)	3.2 (2.1–5.4)	0.0002
hs-CRP	1.1 (0.6–2.6)	0.8 (0.6–2.3)	1.3 (0.8–2.8)	0.15
serum total cholesterol	5.1 (0.8)	5.2 (0.9)	5.0 (0.8)	0.46

The results are shown as mean (SD) for normally distributed variables or as median (interquartile range) for variables with a skewed distribution. *P*-values for a difference between IR- and IR+ groups, assessed with Student's *t*-test (normally distributed variables), Wilcoxon test (skewed variables) or χ^2 test (categorical variables).

Figure 1_Correlations between metabolic variables and PBR28 gray matter cortex z-score in PIB negative and positive individuals. r=Pearson's correlation coefficient.
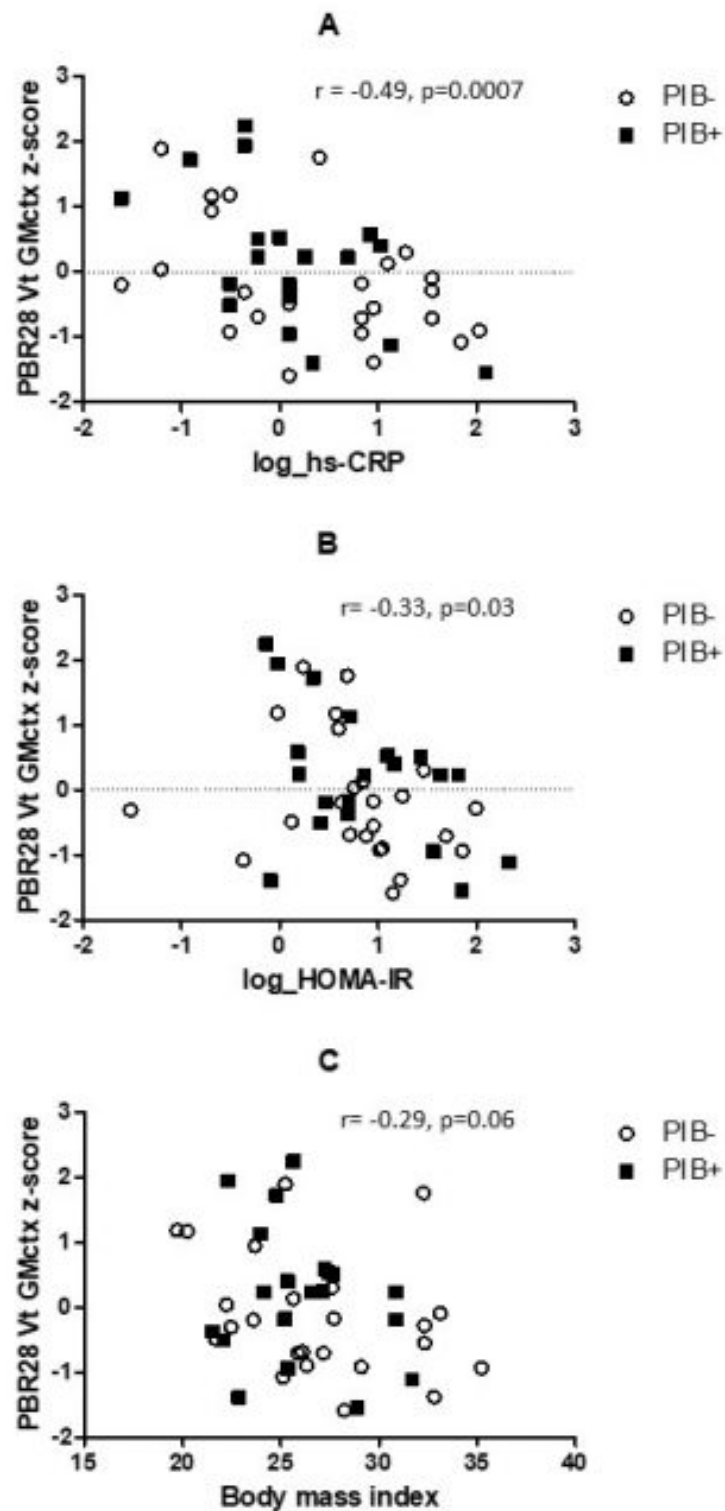
P166: Cognitive trajectory of subcortical vascular cognitive impairment

Hee Jin Kim[1,2], Sook-young Woo[7], Hyemin Jang[1,2], Su Hyun Cho[1,2], Seung Ju Kim[1,2], Kyung-Han Lee[3], Sung Tae Kim[4], Jae Seung Kim[5], Jae Hong Lee[6], Seonwoo Kim[7], Sang Won Seo[1,2]

[1]Departments of Neurology, Samsung Medical Center, Sungkyunkwan University School of Medicine, Seoul, Korea
[2]Neuroscience Center, Samsung Medical Center, Seoul, Korea
[3]Departments of Nuclear Medicine, Samsung Medical Center, Sungkyunkwan University School of Medicine, Seoul, Korea
[4]Departments of Radiology, Samsung Medical Center, Sungkyunkwan University School of Medicine, Seoul, Korea
[5]Department of Nuclear Medicine, Asan Medical Center, University of Ulsan College of Medicine, Seoul, Korea
[6]Department of Neurology, Asan Medical Center, University of Ulsan College of Medicine, Seoul, Korea
[7]Statistics and Data Center, Samsung Medical Center, Seoul, Korea

Objective: Cognitive trajectory of subcortical vascular cognitive impairment (SVCI) patients is not well known. We aimed to identify long-term cognitive trajectory of SVCI patients.

Methods: We recruited 217 SVCI (136 subcortical vascular mild cognitive impairment (svMCI) and 81 subcortical vascular dementia (SVaD)) patients between 2007 and 2016 at Samsung Medical Center in Seoul, Korea. Patients underwent amyloid PET and brain MRI at baseline and were annually evaluated with neuropsychological tests. The mean follow-up duration was 5.3 years. To estimate the long cognitive trajectory of SVCI patients, we linked the clinical dementia rating sum of boxes (CDR-SOB) score trajectories of svMCI and SVaD patients by using accelerated longitudinal model.

Results: Our accelerated longitudinal model showed that it would take approximately 10.2 years for an svMCI patient to reach the SVaD stage. In the case of amyloid-beta positive svMCI, we estimated that it would take approximately 7.0 years to reach SVaD stage.

Conclusion: We estimate that it takes 10.2 years for a svMCI patient to reach the SVaD stage and which shortens by 7.0 years when amyloid is combined.
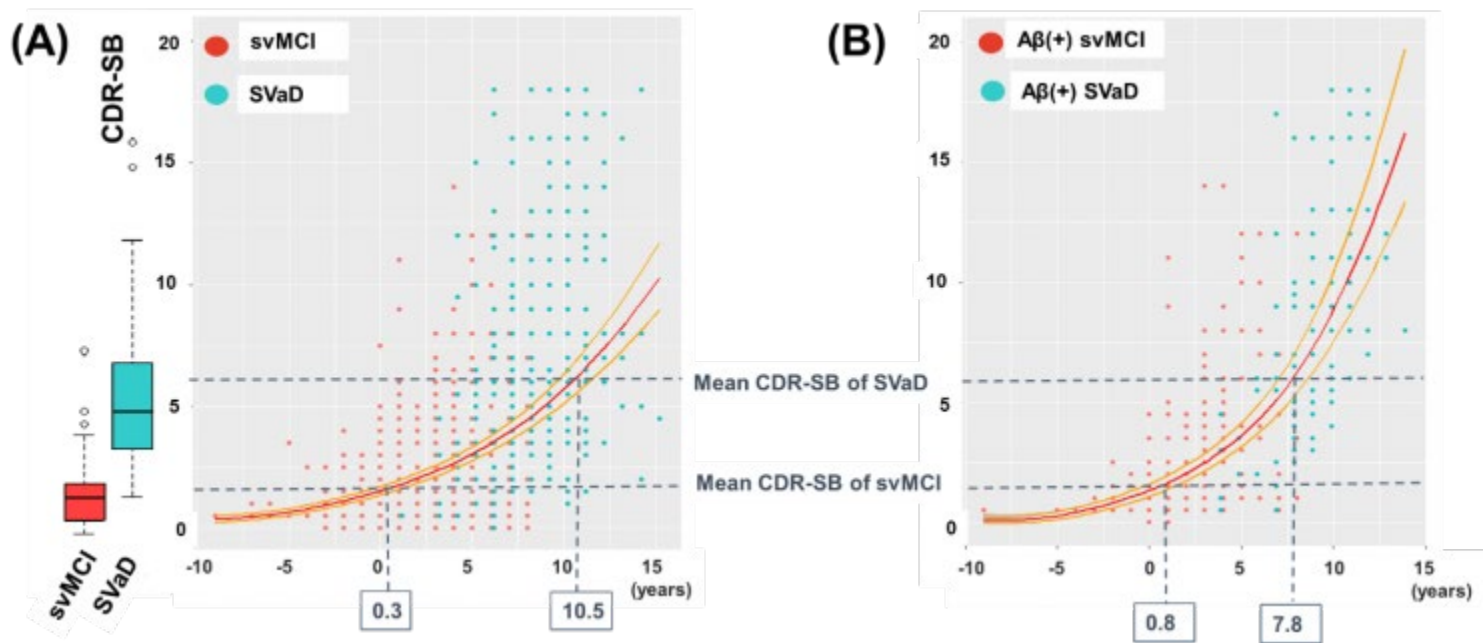
Figure 1. Cognitive trajectory of SVCI patients (A) and amyloid positive SVCI patients (B)

P167: F18-PI2620 Tau PET in three memory clinic patients with uncertain CSF biomarker profiles

Alexander Frolov[1], Sharon Sha[1], Carolyn A. Fredericks[1], Ayesha Nadiadwala[1], Carmen Azevedo[1], Jacob N. Hall[1], Tyler Toueg[1], Jessa B. Castillo[1], Gayle K. Deutsch[1], Michael D. Greicius[1], Guido A. Davidzon[1], Greg Zaharchuk[1], Frederick T. Chin[1], Elizabeth C. Mormino[1]

[1]*Stanford Univeristy, Palo Alto, CA, US*

Cerebrospinal spinal fluid (CSF) amyloid and tau levels are useful biomarkers in Alzheimer's disease (AD), and are increasingly being used in research, clinical diagnosis, and clinical trial enrollment. However, indeterminate results can occur when amyloid (AB42) and phosphorylated tau (pTau) levels are discordant or when either measure is borderline. Recently, tau PET scans have emerged as useful tools for **in vivo** visualization of the distribution of tau pathology, and may complement CSF biomarkers. We sought to explore the spatial uptake pattern of tau PET in our memory clinic patients with cognitive symptoms and indeterminate CSF amyloid/tau profiles using a novel tau PET ligand, F18-PI2620, and to determine the extent to which the anatomic distribution of tau signal would correlate with the patients' clinical symptoms. Patients were recruited based on indeterminate CSF profiles (assay cutoffs of AB42<500 and pTau>68 pg/mL were considered positive): Case A was a 60 year old man with a clinical diagnosis of AD and CSF taken in the subacute period of a lacunar left corona radiata stroke (CSF AB42=560.1; pTau=242.3); Case B was a 70 year old woman with a clinical diagnosis of AD and a discordant CSF profile (CSF AB42=329.55; pTau=48.65); Case C was a 58 year old woman with a clinical diagnosis of MCI and a borderline CSF profile (CSF AB42=523.75; pTau=63.85). In all cases, there was evidence of robust cortical tau deposition that was aligned with clinical symptoms (Figure 1). This data demonstrates that tau PET can complement CSF biomarkers in indeterminate cases, that tau PET signal distribution aligns with clinical symptoms, and that atypical presentations of AD may decrease the correspondence between CSF pTau and elevated tau PET signal. This suggests the need for further research to more precisely delineate the relationships between CSF AD biomarkers, tau PET signal, and clinical symptoms.
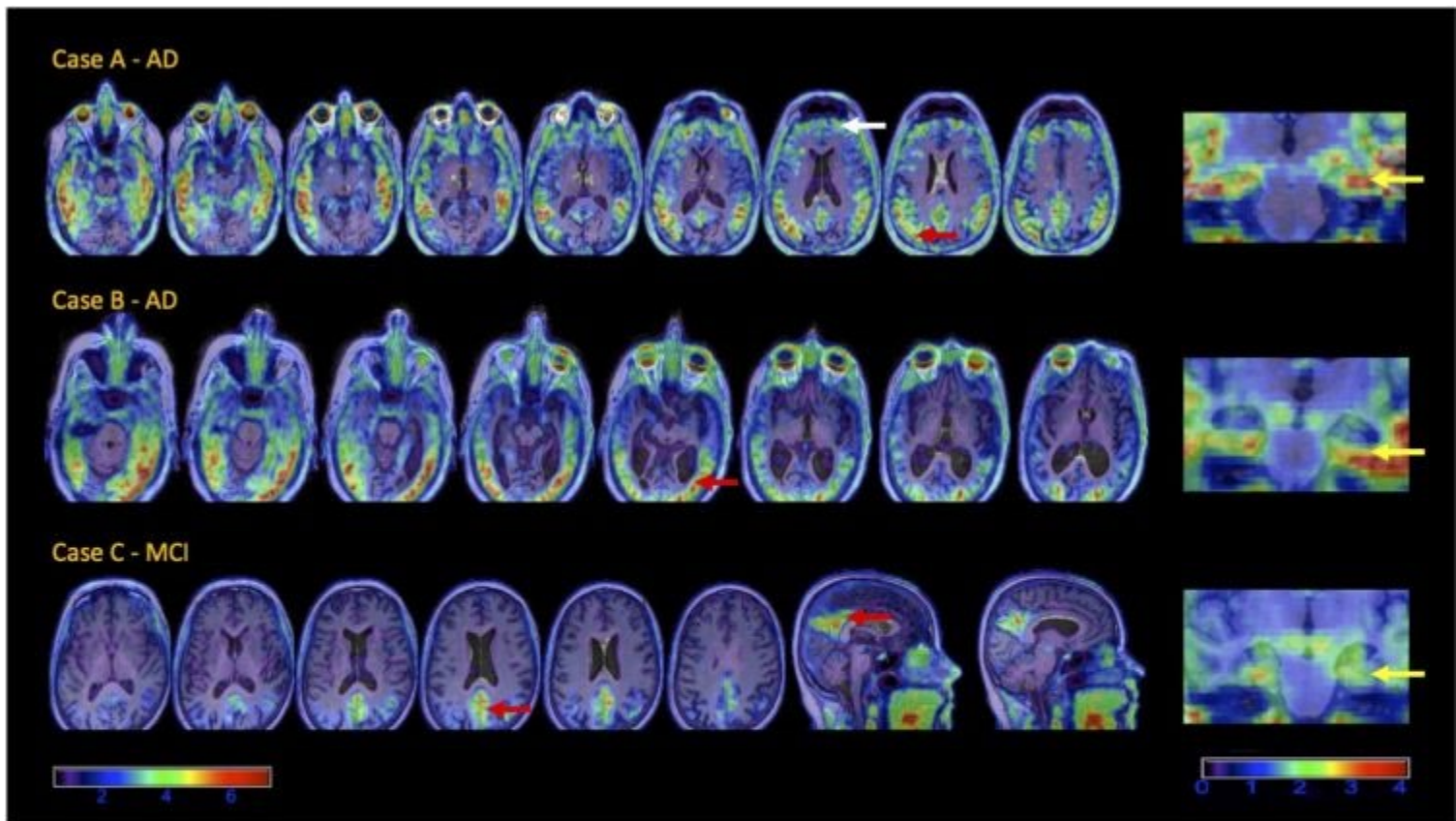
Figure 1. Representative tau PET slices for the three indeterminate cases using the F18-PI2620 Tau PET. Images are SUVRs, normalized by the inferior cerebellum. The scale for the axial and sagittal slices to the left ranges from SUVR values between 0-7, while the scale for the cropped coronal slices to the right ranges from 0-4. The early and predominant symptoms for the cases were as follows: Case A – dysexecutive, visuospatial; Case B – visuospatial, psychiatric; Case C – amnestic, visuospatial, dysexecutive. Tau tracer uptake generally aligned with clinical symptoms: the white arrow shows frontal involvement in Case A, in whom dysexecutive symptoms were prominent. Red arrows show prominent parieto-occipital involvement in all three cases, and visuospatial symptoms were prominent in all. In Case C, tracer uptake was generally more focal (red arrow), and significant frontal involvement was lacking despite dysexecutive symptoms, which could relate to this patient's relatively milder symptoms (MCI rather than AD). Yellow arrows indicate that the medial temporal lobe was involved in all three cases, though similarly there was less avid uptake in Case C as compared to Cases A and B.

Keywords: *Tau, Amyloid, PET, CSF, differential diagnosis*

P168: Differential associations of cortisol plasma level with glucose metabolism, hippocampal atrophy, and amyloid deposition across Alzheimer's disease stages

Hwamee Oh[1], Hoi-Chung Leung[1], Turhan Canli[1], Mark Slifstein[2]

[1]Department of Psychology, State University of New York at Stony Brook, Stony Brook, NY, US
[2]Department of Psychiatry, Stony Brook University Health Sciences Center School of Medicine, State University of New York at Stony Brook, Stony Brook, NY, US

Background: A predisposition to stress or expression of chronic stress-related symptoms has been considered as a risk factor for Alzheimer's disease (AD). To elucidate a neural mechanism underlying the risk of AD, we examined the relationship between glucocorticoids, glucose metabolism, hippocampal volume, and amyloid deposition across Alzheimer's disease stages.

Methods: We assessed cortisol plasma level (cortisol), FDG counts in AD signature cortical regions, adjusted hippocampal volume, and mean cortical PIB counts normalized to cerebellum reference regions in 58 cognitively normal older adults (CNs), 396 participants with mild cognitive impairment (MCIs) and 112 AD patients in the Alzheimer's Disease Neuroimaging Initiative. Multiple regression models were applied to assess the relationships between these measures across all groups, followed by within-group analyses. For psychological measures, geriatric depression scale total scores were assessed in relation to cortisol.

Results: Higher cortisol was associated with AD stages as well as adjusted hippocampal volume across all groups, which replicates previous findings. Higher cortisol was associated with lower glucose metabolism in AD signature regions across all groups. Among CNs, however, the association of cortisol with glucose metabolism in AD signature regions was positive, while being negative in MCIs and AD patients. Differential associations between cortisol and adjusted hippocampal volume by group were also found showing that a negative relationship of cortisol with hippocampal volume was present only within MCI participants. Neither amyloid burden nor geriatric depression scale total scores were related to cortisol in any group.

Conclusions: A positive relationship between cortisol and glucose metabolic rates in cognitively normal older adults may indicate a role of individuals' susceptibility to stress in neuronal hyperexcitability in the early stage of AD and confer risk for neurodegeneration and the development of AD. Longitudinal evaluations are warranted to address the directionality between these measures and amyloid pathology.

Keywords: *Stress, risk factor, glucose metabolism, hippocampal atrophy, amyloid deposition*

P169: Cerebral small vessel disease is associated with medial temporal lobe hyperconnectivity in pre-clinical AD

<u>Minjie Wu</u>[1], Dana Tudorascu[2], Chester Mathis[3], Brian Lopresti[3], Ann Cohen[1], Beth Snitz[4], William Klunk[1], Howard Aizenstein[1,5]

[1]*Department of Psychiatry, University of Pittsburgh, Pittsburgh, PA, US*
[2]*Departments of Medicine and Biostatistics, University of Pittsburgh, Pittsburgh, PA, US*
[3]*Department of Radiology, University of Pittsburgh, Pittsburgh, PA, US*
[4]*Department of Neurology, University of Pittsburgh, Pittsburgh, PA, US*
[5]*Department of Bioengineering, University of Pittsburgh, Pittsburgh, PA, US*

Introduction: Growing evidence suggests cerebral small vessel disease (CSVD) may contribute to and accelerate the development and progression of Alzheimer's disease (AD) and dementia. CSVD may be a modifiable risk factor that can be targeted to delay the progression of AD, and White matter hyperintensities (WMHs) are one of main imaging markers of CSVD. In this study, we investigated how brain amyloid (Aβ) and WMH burden interact in their effect on the functional integrity of the memory network.

Methods: Sixty-one cognitively normal older adults (age: 75.8 ± 6.4 years) were included. Global amyloid load (SUVR) was measured using PiB PET imaging. WMH volume was automatically assessed using a T2-weighted FLAIR MR image, and using WMH median split participants were divided into two groups: High WMHs and Low WMHs. Hippocampal functional connectivity was evaluated using generalized psychophysiological interaction analysis while participants were performing a face-name associative memory fMRI task.

Results: Compared to those with Low WMH burden, older adults with High WMH burden had different patterns of hippocampal connectivity with increased amyloid burden (Fig. 1). Specifically, in older adults with High WMHs, greater amyloid burden was associated with greater hippocampal local connectivity (e.g., hippocampal-parahippocampal connectivity), whereas in those with low WMHs, greater amyloid burden was associated with greater hippocampal distal connectivity (i.e., hippocampal-prefrontal connectivity) (**p's**<0.05). The effects were significant for both left and right hippocampal connectivity.

Conclusion: We found that among individuals with pre-clinical AD, those with High WMHs showed a more localized pattern of hippocampal hyperconnectivity and distal hypoconnectivity. White matter disruption may lead to a more localized pattern of activity. This regional medial temporal lobe hyperconnectivity may exacerbate the neurodegenerative cascade through excitotoxicity.
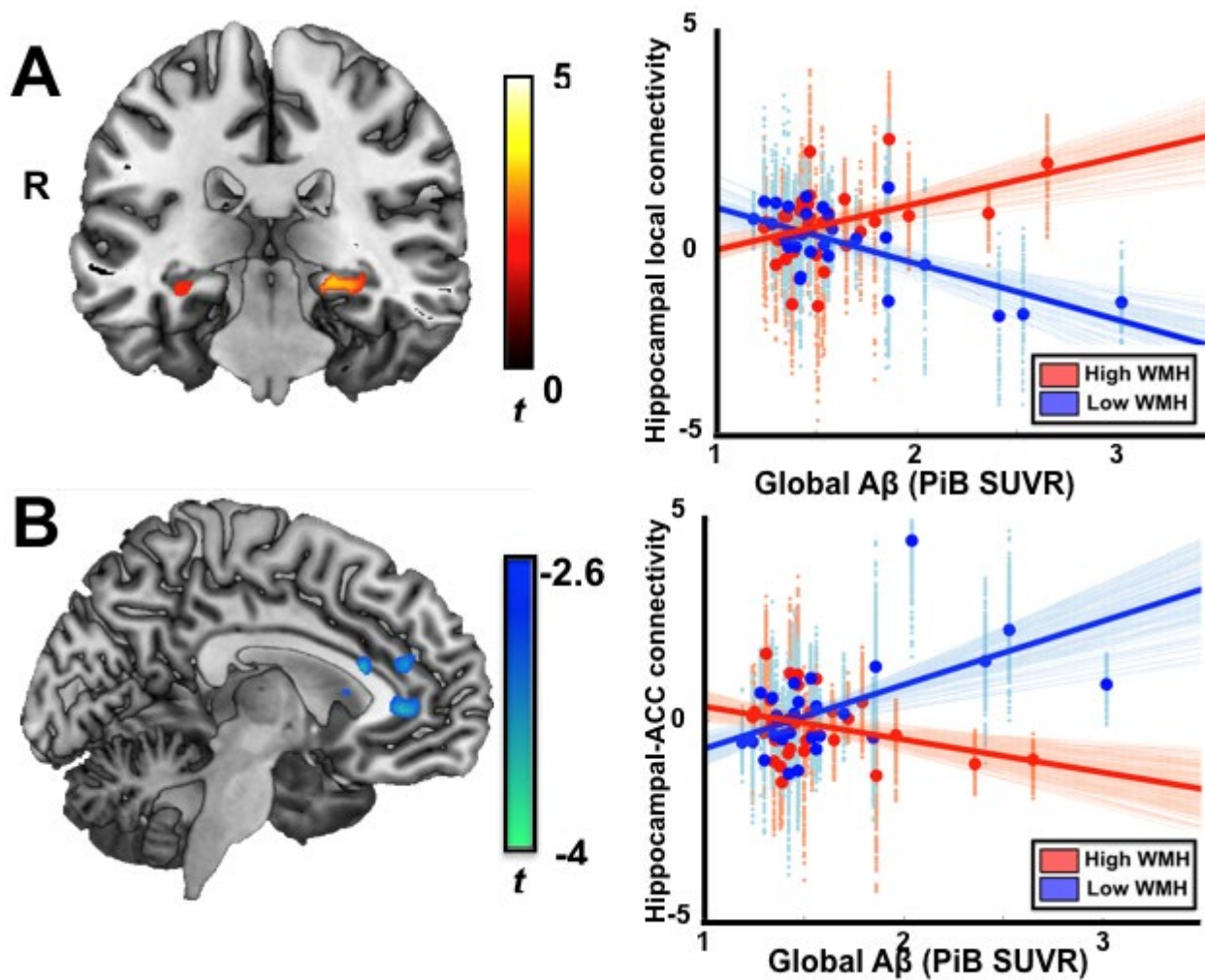
Fig. 1. With increased brain amyloid, individuals with High WMHs showed A. hippocampal local hyperconnectivity, and B. hippocampal-frontal hypoconnectivity, compared to those with Low WMHs (**p**<0.05).

P170: Modeling PiB PET trajectory groups identifies a subgroup with PiB beta-amyloid accumulation near age 50 and predicts MK-6240 SUVR

Rebecca Koscik[1], Tobey Betthauser[1], Erin Jonaitis[1], Lindsay Clark[1], Samantha Allison[1], Kimberly Mueller[1], Bruce Hermann[1], Jennifer Poetter[1], Leah Sanson[1], Heather Shouel[1], Nathaniel Chin[1], Bradley Christian[1], Sterling Johnson[1]

[1]*University of Wisconsin-Madison School of Medicine and Public Health, Madison, WI, US*

Objective: The timing of detectable beta-amyloid plaque and neurofibrillary tangle (NFT) accumulation is unknown. This study identified PiB PET-based beta-amyloid trajectory groups in late middle-aged persons, estimated PiB(+) age, and related these to MK-6240 SUVR.Method: Participants from the Wisconsin Registry for Alzheimer's Prevention (WRAP) who had completed ≥two [C-11]PiB PET scans were included in pattern mixture modeling to identify age-based PiB trajectory groups (n=167; modeling mean PiB DVR in 8 cortical regions ("global PiB", cerebellum GM reference, Logan graphical analysis). PiB trajectory group residuals were used to assign group among those with one PiB Scan (n=61). Individualized estimated PiB(+) ages ("≃PiB(+) age", global PiB≥1.2) were calculated, weighting by PiB trajectory group membership probabilities. MK-6240 SUVR (70-90min, inferior cerebellum GM reference) was compared across PiB trajectory groups in a subset with both PET tracers (n=130); ≃PiB(+) age was investigated as a predictor of MK-6240 SUVR (entorhinal cortex, hippocampus, inferior temporal gyrus, amygdala).

Results: Four PiB trajectory groups were identified: the largest (72%) having no predicted PiB accumulation and three with differing ≃PiB(+) ages and accumulation rates (Figure1, Table1). Groups with younger ≃PiB(+) ages had more **APOE-ε4** carriers and worse cognitive status (Table1). ≃PiB(+) age differed across last cognitive status (unimpaired-stable, mean(sd)=80.3(0.8) years; unimpaired-declining, mean(sd)=75.9(2.0); and MCI, mean(sd)=67.4(3.2); p-value=0.0001). MK-6240 SUVR differed between PiB trajectory groups and began increasing after ≃PiB(+) age (Table1; Figure2). The difference between ≃PiB(+) age and MK-6240 scan age was 10.4 years earlier in individuals with elevated hippocampal MK-6240 SUVR (p=.002, 95% CI=4.1-16.7).

Conclusions: Beta-amyloid accumulation potentially begins in the early 50's, particularly among **APOE-ε4** carriers. Years since ≃PiB(+) age predicted MK-6240 SUVR in Braak-associated regions and suggested that PET-measureable amyloid plaques precede measurable NFTs by ≥4 years. PiB trajectory models may allow earlier identification of persons at-risk of developing further AD pathophysiology or AD-dementia.

Table 1: Sample Characteristics and MK-6240 SUVR by PiB Trajectory Group

| | Overall | PiB Trajectory Group | | | | |
| | | 1 | 2 | 3 | 4 | |
		(Stable low)	(Slow, later increase)	(Mid speed and age increase)	(Early, fastest increase)	p-value[**]
All with at least 1 [C-11]PiB Scan	n=228	165(72.4%)	27(11.8%)	18(7.9%)	18(7.9%)	NA
Group estimated age (years) at which PiB=1.2*, mean(sd)	79.2(10.8)	84.7(1.8)	76.5(4.4)	60.9(1.3)	50.9(0.85)	<.0001
Age at baseline PiB, mean(sd)	61.5(6.3)	60.9(6.3)	65.2(5.9)	61.5(7.0)	62.2(5.4)	0.012
WRAT3 Readstn, mean(sd)	107.0(9.2)	106.6(9.7)	109.7(6.1)	105.8(9.5)	107.7(7.8)	0.39
Education of BA/BS or more, n(%)	156(68.4%)	105(63.6%)	23(85.2%)	13(72.2%)	15(83.3%)	0.07
Female, n(%)	156(68.4%)	115(69.7%)	18(66.7%)	9(50.0%)	14(77.8%)	0.31
APOE-ε4 carrier, n(% of 227)	94(41.1%)	53(32.2%)	16(59.3%)	12(70.6%)	13(72.2%)	<0.0001
White/Non-Hispanic Caucasian, n(%)	213(93.4%)	152(92.7%)	27(100%)	17(94.4%)	16(88.9%)	0.39
Cognitive status at most recent assessment**, n(% of 225)						0.003
Cognitively Unimpaired - Stable	186(82.7%)	142(87.1%)	21(80.8%)	12(66.7%)	11(61.1%)	
Cognitively Unimpaired - Declining	28(12.4%)	18(11.0%)	2(7.7%)	4(22.2%)	4(22.2%)	
MCI	11(4.9%)	3(1.8%)	3(11.5%)	2(11.1%)	3(16.7%)	
Subset with [F-18]MK-6240 PET						
PiB-trajectory group, n(%)	n=130	88(67.7)	18(13.9)	11(8.5)	13(10.0)	NA
Age at MK-6240 PET, mean(sd)	67.7(5.8)	67.0(6.2)	69.1(4.9)	70.1(5.6)	68.5(3.4)	0.22
Estimated years since global PiB=1.2 (at time of MK-6240 scan), mean(sd)	-10.6(13.8)	-17.9(6.1)	-7.3(7.5)	9.7(5.6)	17.6(3.7)	<.0001
MK-6240(+) Hippocampus*, n(%)	22(16.9%)	6(6.8)	2(11.1)	5(45.5)	9(69.2)	<.0001
MK-6240 ROI SUVR's, mean(sd)						
Entorhinal Cortex	1.09(0.30)	1.01(0.138)	1.04(0.19)	1.25(0.37)	1.58(0.56)	<.0001
Hippocampus	0.94(0.22)	0.88(0.12)	0.87(0.13)	1.05(0.22)	1.30(0.40)	<.0001
Inferior Temporal Gyrus	1.17(0.34)	1.09(0.11)	1.13(0.10)	1.25(0.33)	1.67(0.86)	<.0001
Amygdala	0.89(0.29)	0.81(0.10)	0.83(0.12)	1.00(0.27)	1.46(0.55)	<.0001

*Based on weighted beta's from trajectory models including intercept (groups 1-4), linear (groups 2-4), and quadratic (groups 3-4) age effects, using each participant's probability of membership to weight the beta's from each group for each participant. Estimated ages of PiB+ were >85 were truncated to 85 years.

**Cognitive Statuses determined via multi-disciplinary consensus team review (blind to biomarker status): Cognitively Unimpaired-Declining indicates research category with deficits on one or more tests that are at least 1.5 standard deviations below expected relative to internal WRAP norms but deficits are not severe enough to meet criteria for Mild Cognitive Impairment.

[†]MK-6240 hippocampus positivity defined as hippocampus SUVR >1.06 (= 1.5 standard deviations above the mea

[**] p-values are from anova's (continuous variables) or Fisher's exact tests (categorical variables); post-omnibus pairwise group comparisons of MK-6240 SUVR showed consistent pattern across ROI's of PiB trajectory groups 3 and 4 differing from group 1 and each other. Group 2 MK-6240 SUVR differed from PiB trajectory group 4 in the hippocampus and ITG (see also left panel of Figure 2 for MK-6240 hippocampus SUVR by PiB trajectory group).

Figure1: Global PiB DVR vs Age, Group Trajectory Lines and Observed Values
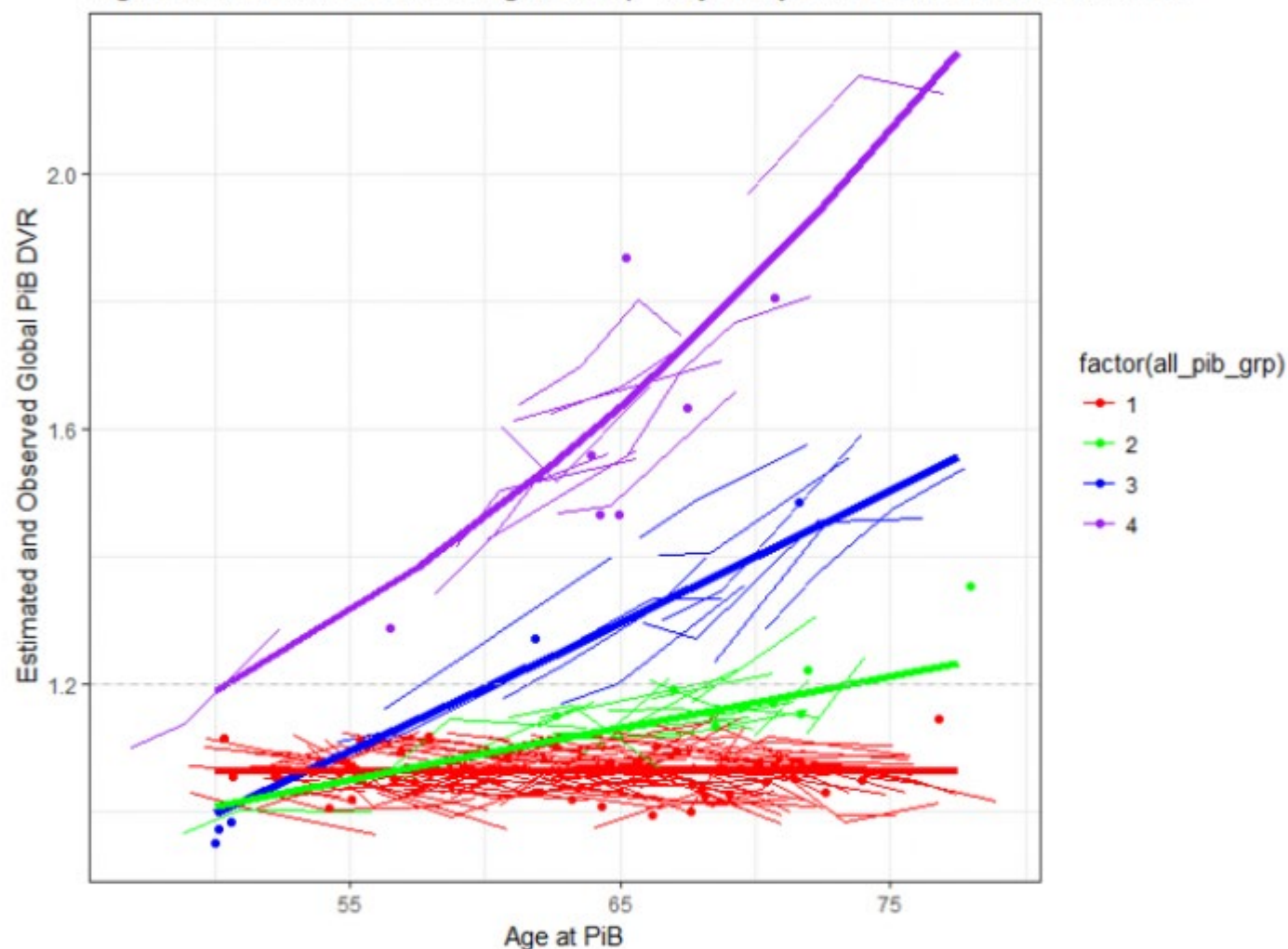
Figure1 legend: Age was centered at 65 years for PiB-trajectory modeling to allow consideration of polynomial age terms. Thick lines depict the predicted group trajectories across the ages 50-75. Group 1 (red), included only an intercept (global PiB DVR ~ 1.06, regardless of age). Group 2 (green) included a linear term (global PiB DVR ~ 1.13 + .008*age). Groups 3 and 4 (blue and purple, respectively), both included quadratic age terms (Group 3 global PiB DVR ~1.3 + 0.02*age + .00004*age*age; Group 4 global PiB DVR ~ 1.6 + .04*age + .0005*age*age). Thin lines depict observed individual longitudinal global PiB DVR values for individuals with 2-4 PiB scans (n=167) while dots depict PiB values for individuals having a single PiB scan (n=61). The horizontal dotted line at 1.2 indicates the threshold for PiB positivity.

Figure2: MK-6240 Hippocampus SUVR vs PiB Trajectory Groups (Left) and Years from Estimated PiB(+) Age to MK-6240 Scan Age (Right)
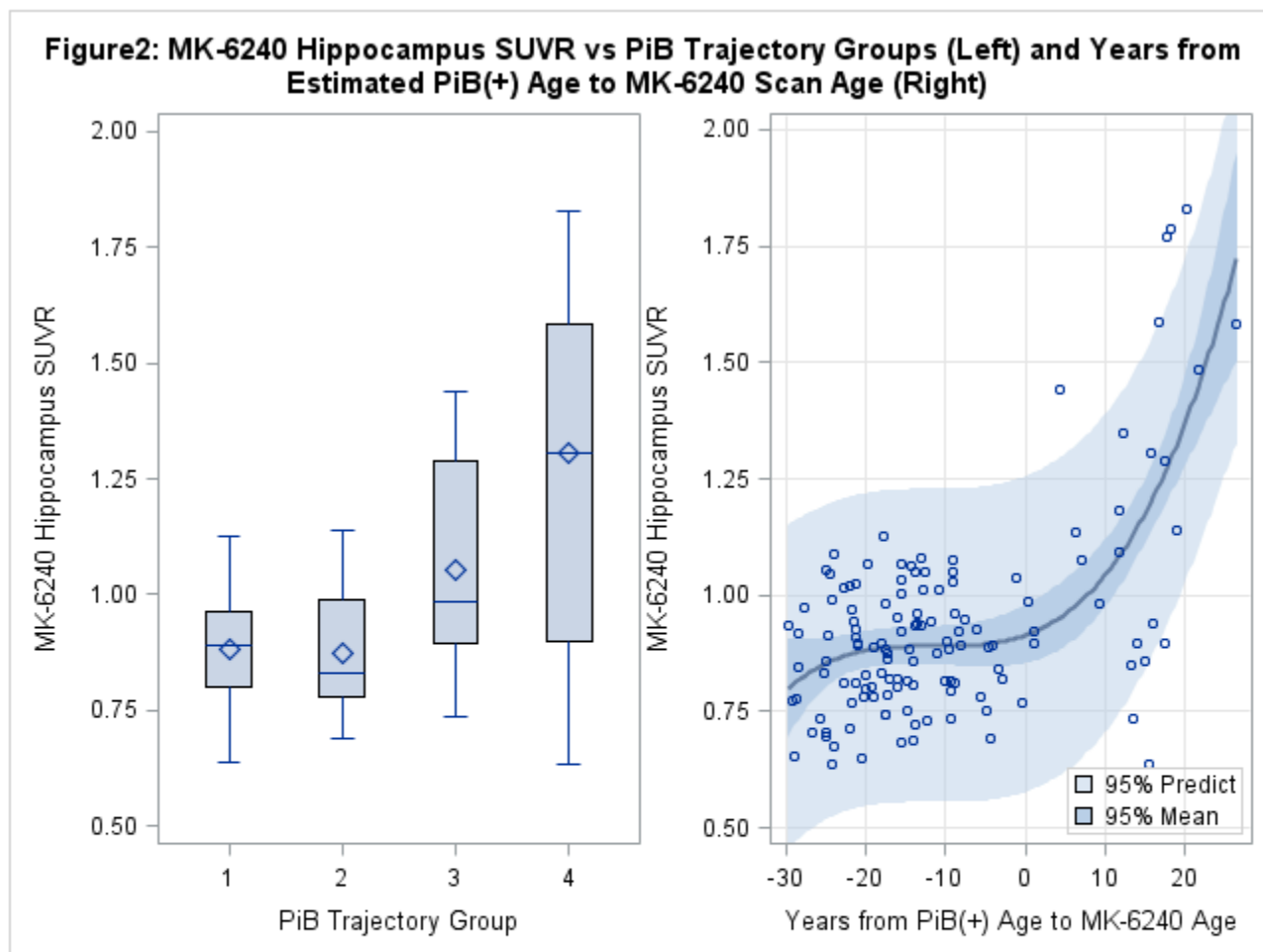
Figure2 legend: The left panel depicts boxplots of MK-6240 hippocampus SUVR values across each of the PiB trajectory groups (group 1=predicted non-PiB accumulators, groups 2-4=slowest/latest to fastest/earliest PiB accumulators. The right panel depicts the non-linear relationship between the difference in estimated PiB(+) age and the age at MK-6240 scan, and MK-6240 SUVR in the hippocampus (X-axis values <0 indicate MK-6240 scan age is less than the estimated PiB(+) age {for those in PiB group 1, estimated PiB+ age was truncated to 85}). Patterns of significance were similar for the three other regions examined: entorhinal cortex, inferior temporal gyrus, and amygdala.

Keywords: *beta-amyloid plaques, neurofibrillary tangles, pattern mixture modeling, PET imaging*

P171: Application of amyloid and tau classification system in subcortical vascular cognitive impairment patients

Hyemin Jang[1], Hee Jin Kim[1], Seongbeom Park[1], Yu Hyun Park[1], Yeongsim Choe[1], Hanna Cho[2], Chul Hyoung Lyoo[1], Jin San Lee[3], Yeshin Kim[4], Soo Hyun Cho[1], Seung Joo Kim[1], Jun Pyo Kim[1], Young Hee Jung[1], Young Hoon Ryu[2], Jae Young Choi[2], Seung Hwan Moon[1], Joon-Kyung Seong[5], Charles DeCarli[6], Michael W. Weiner[7], Samuel N. Lockhart[8], Duk L. Na[1], Sang Won Seo[1]

[1]*Department of Neurology, Samsung Medical Center, Seoul, KR*
[2]*Department of Neurology, Gangnam Severance Hospital, Seoul, KR*
[3]*Kyung Hee University Hospital, Seoul, KR*
[4]*Kangwon National University Hospital, Chuncheon, KR*
[5]*School of Biomedical Engineering, Korea University, Seoul, KR*
[6]*Department of Neurology and Center for Neuroscience, University of California, Davis, CA, US*
[7]*Center for Imaging of Neurodegenerative Diseases, University of California, San Francisco, CA, US*
[8]*Wake Forest School of Medicine, Winston-Salem, NC, US*

Introduction: Patients with subcortical vascular cognitive impairment (SVCI), which is characterized by extensive cerebral small vessel disease (CSVD), show distinct cognitive trajectories by Alzheimer's disease (AD) biomarker profiles. We applied "AT" classification system by focusing on specific AD biomarkers – Aβ (A), Tau (T) – and investigated its clinical significance in SVCI.

Methods: A total of 60 SVCI patients who underwent neuropsychological test, brain magnetic resonance imaging (MRI), florbetaben PET, and AV1451 PET scans were included. Retrospective neuropsychological test and MRI data were collected to investigate the longitudinal changes in these measures. Participants were classified as abnormal Aß (A+) when florbetaben PET was positive by visual assessment and abnormal tau (T+) when AV1451 PET showed that in-vivo Braak stage using the conditional inference tree method was $\geq$ III/IV. We compared cognitive decline and longitudinal change in hippocampal volume (HV) and cortical thickness between different AT groups using the linear mixed effects model.

Results: Among 60 patients, 33 patients (55%) were A-, 20 (74.1% of A+) were A+T-, and 7 (25.9% of A+) were A+T+. A+T- SVCI had a steeper decline in general cognition (MMSE, $p < 0.001$; CDR-SB, $p = 0.006$), language ($p < 0.001$), memory ($p = 0.025$), and frontal ($p = 0.047$) domains and a steeper decrease in HV than A-SVCI. A+T+ SVCI showed a steeper decline in general cognition (MMSE, $p < 0.001$; CDR-SB, $p < 0.001$), attention ($p < 0.001$), visuospatial ($p < 0.001$) and language ($p = 0.006$) domains and a significantly greater cortical thinning in all cortical regions than A+T- SVCI.

Discussion: Our findings showed that AT system successfully characterized SVCI patients. We, furthermore, suggested that a combination of biomarker abnormalities is useful for the research framework in clinically diagnosed non-AD patients including SVCI patients as well.
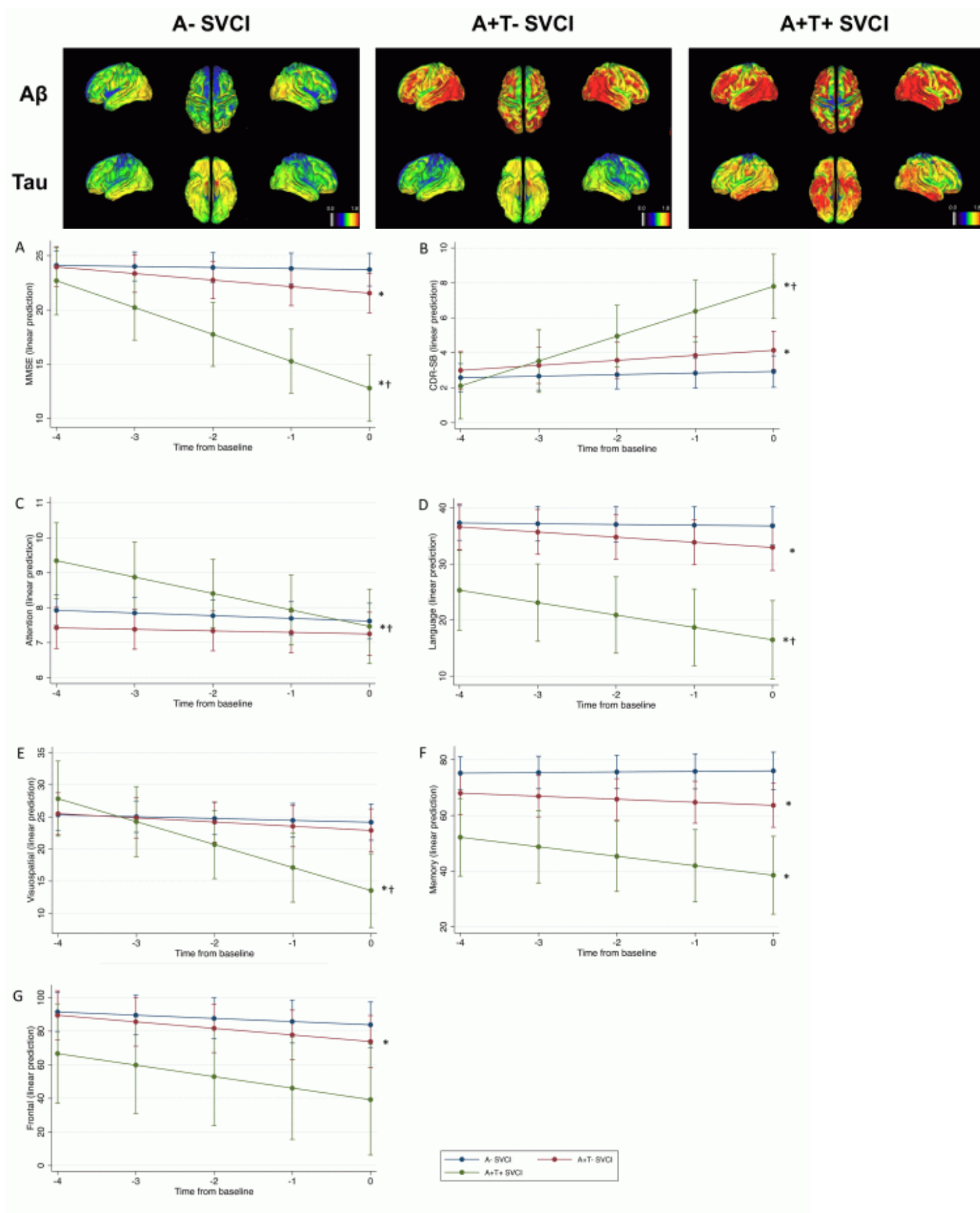
Friday, January 18, 2019 - 10:45 am - 12:00 pm

Podium Session

Session 7: Multi-modality: cognitively normal

CHAIRS: Tobey Betthauser, William Jagust

10:45 am - 12:00 pm	Session 7: Multi-modality: cognitively normal	CHAIRS: **William Jagust**, University of California, Berkeley, Berkeley, CA, US **Tobey Betthauser**, University of Wisconsin-Madison School of Medicine and Public Health, Madison, WI, US	Page
10:45	Protective effect of physical activity on prospective cognitive decline and longitudinal neurodegeneration in clinically normal older adults with elevated β-amyloid burden	**Jennifer Rabin**, Massachusetts General Hospital, Boston, MA, US	445
11:00	MRI measures of neurodegeneration and vascular injury, but not amyloid status predict cognitive decline in normal individuals followed for more than nine years	**Charles DeCarli**, University of California at Davis, Sacramento, CA, US	449
11:15	Fluorodeoxyglucose and Flortaucipir PET independently predict subsequent cognitive decline in clinically normal adults with elevated amyloid	**Bernard Hanseeuw**, Cliniques Universitaires Saint-Luc, Brussels, Belgium	451
11:30	MK-6240 and PIB PET are associated with retrospective cognitive trajectories in late-middle aged persons clinically unimpaired at baseline	**Sterling Johnson**, University of Wisconsin-Madison School of Medicine and Public Health, Madison, WI, US	455
11:45	Individual variations in sleep architecture are associated with tau PET, cognition, and functional network architecture: Preliminary findings from the Harvard Aging Brain Study	**Jasmeer Chhatwal**, Massachusetts General Hospital, Boston, MA, US	459
12:00 pm - 12:30 pm	Discussion		

Protective effect of physical activity on prospective cognitive decline and longitudinal neurodegeneration in clinically normal older adults with elevated β-amyloid burden

Jennifer Rabin[1], Hannah Klein[1], Dylan Kirn[1], Aaron Schultz[1], Olivia Hampton[1], Rachel Buckley[1,2,3], Edmarie Guzman-Velez[1], Yakeel Quiroz[1], Michael Properzi[1], Trey Hedden[1,4], Hyun-Sik Yang[1,5], Gad Marshall[1,5], Dorene Rentz[1,5], Keith Johnson[1,5], Reisa Sperling[1,5], Jasmeer Chhatwal[1]

[1]*Massachusetts General Hospital, Boston, MA, US*
[2]*The Florey Institute, The University of Melbourne, Victoria, Australia, Victoria, Australia*
[3]*Melbourne School of Psychological Science, University of Melbourne, Victoria, Australia*
[4]*Icahn School of Medicine at Mount Sinai, New York, NY, US*
[5]*Center for Alzheimer Research and Treatment, Department of Neurology, Brigham and Women's Hospital, Boston, MA, US*

Objective: To examine the protective effects of physical activity on prospective cognitive decline and longitudinal neurodegeneration in the setting of elevated β-amyloid (Aβ) burden.

Methods: We examined longitudinal imaging and cognitive data from 183 clinically normal participants in the Harvard Aging Brain Study (mean age=73.4±6.2 years). Baseline physical activity was quantified with a waistband-mounted pedometer. Baseline Aβ burden was measured with Pittsburgh Compound-B PET. Cognition was measured annually with the Preclinical Alzheimer Cognitive Composite (PACC; median follow-up=6.0±1.1 years). Neurodegeneration was assessed with longitudinal magnetic resonance imaging (2–4 scans per subject, median follow-up =4.5±1.3 years). Physical activity and Aβ were examined as interactive predictors of cognitive decline and total gray matter volume in separate linear mixed models, adjusting for age, sex, education, intracranial volume, **APOE** e4 status, and their interactions with time.

Results: We observed a significant interaction between physical activity and Aβ in relation to longitudinal PACC (t=3.79, p<0.001; Figure 1), such that in the context of elevated Aβ burden, those with greater physical activity at baseline showed less cognitive decline over time. This interaction remained significant after controlling for vascular risk factors using the Framingham Cardiovascular Disease Risk Score (FHS-CVD; t=3.75, p<0.001). We also observed a significant interaction between physical activity and Aβ on longitudinal gray matter volume, whereby greater physical activity was associated with a slower rate of neurodegeneration in individuals with elevated Aβ burden (t=3.17, p=0.002; Figure 2). This effect remained significant after adjusting for FHS-CVD. Follow-up regional analyses revealed that the interaction of physical activity with Aβ was associated with cortical thinning in medial and lateral temporal and medial parietal regions (Figure 3).

Conclusions: Physical activity may be protective against cognitive decline and neurodegeneration in older adults with elevated Aβ burden. These findings have implications for preventive health care and interventional studies in preclinical Alzheimer's disease.
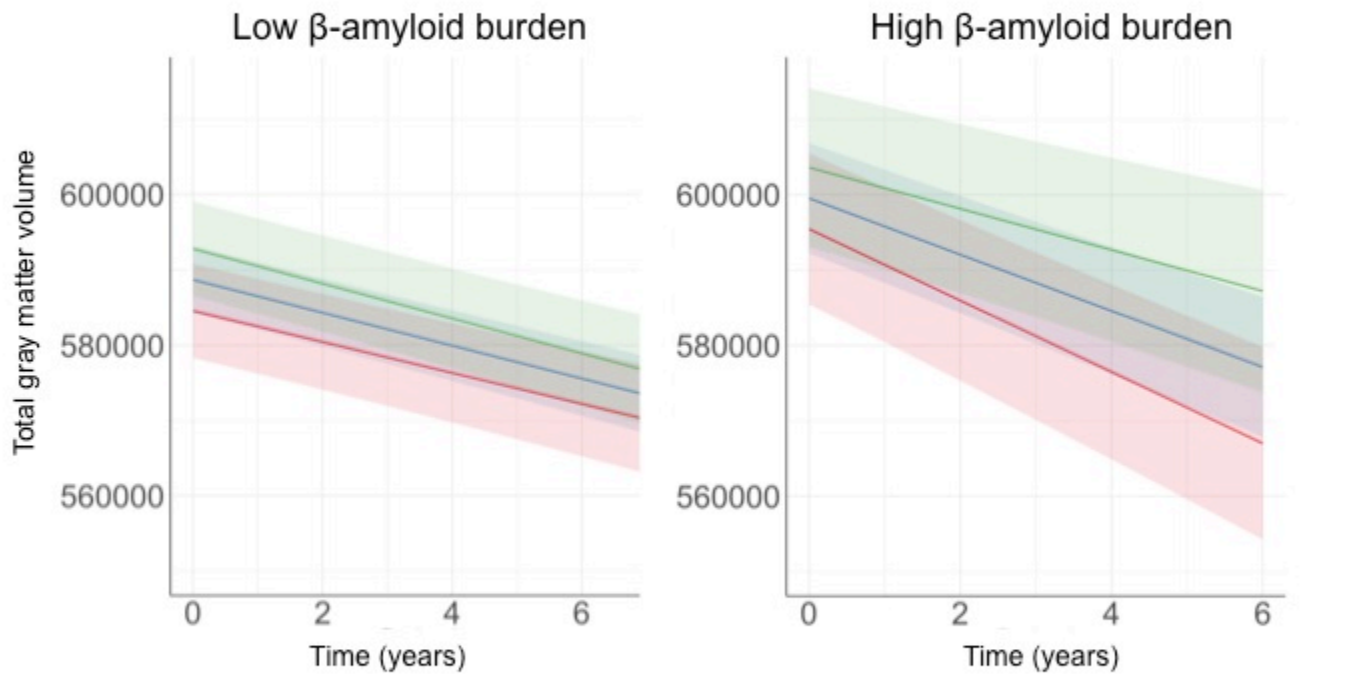
Figure 1.
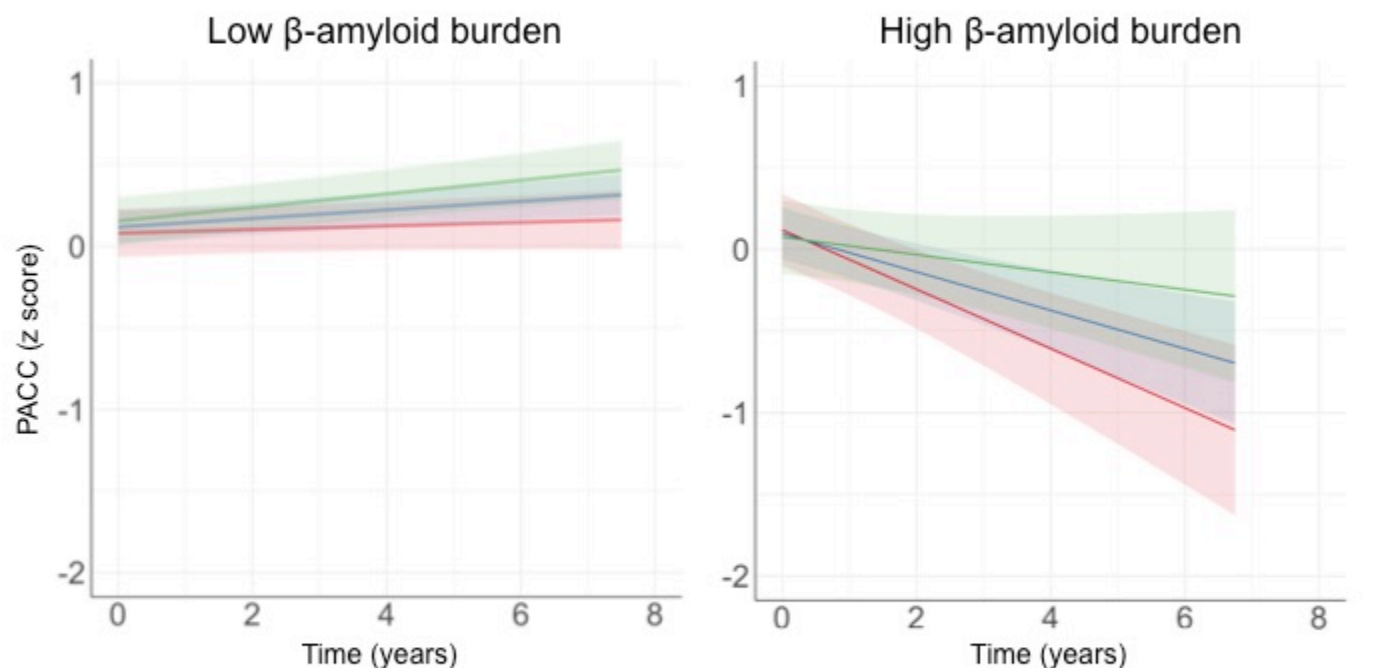
The plots depict the interaction of physical activity x Aβ x time on cognitive decline. For visualization purposes, the effect of physical activity on cognitive decline is plotted in low vs. high Aβ groups. In the context of elevated Aβ burden, those with greater physical activity at baseline showed less cognitive decline over time (t=3.79, p<0.001). Shaded regions represent the 95% confidence intervals.

Figure 2.

The plots depict the interaction of physical activity x Aβ x time on total gray matter volume. For visualization purposes, the effect of physical activity on gray matter volume is plotted in low vs. high Aβ groups. Greater physical activity was associated with a slower rate of neurodegeneration in individuals with elevated Aβ burden (t=3.17, p=0.002). Shaded regions represent the 95% confidence intervals.

Figure 3.
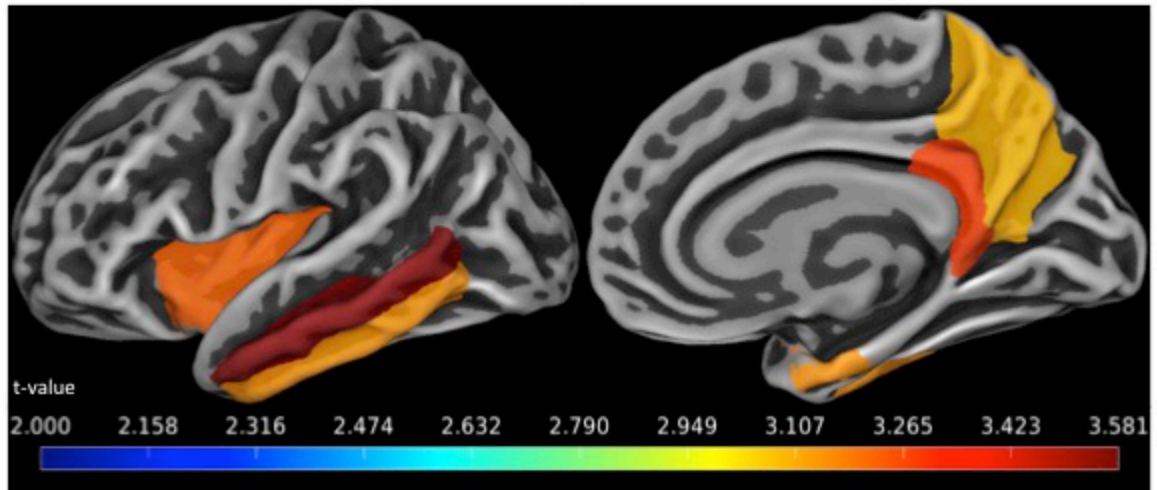
FreeSurfer-defined regions in which the interaction of physical activity and Aβ is associated with rates of cortical thinning. Regions were averaged across left and right hemispheres. In all regions shown, higher levels of physical activity in the setting of elevated Aβ were associated with slower rates of neurodegeneration. Color bars indicate the t-statistic for the association, controlling for age, sex, years of education, *APOE* ε4 status, and their interactions with time. Regions shown are p < 0.05 corrected for multiple comparisons (FWE).

MRI measures of neurodegeneration and vascular injury, but not amyloid status predict cognitive decline in normal individuals followed for more than nine years

Charles DeCarli[1], Evan Fetcher[1], Danielle Harvey[1], John Olichney[1], Sarah Farias[1], Pauline Maillard[1]

[1]*University of California at Davis, Sacramento, CA, US*

Background: Various studies show that white matter hyperintensities (WMH) predict transition from normal to clinically relevant cognitive impairment over 10 years, that excessive amyloid on PET imaging is associated decline in cognitive ability over a period of almost 4 years and an interaction between vascular risk and amyloid status among cognitively normal individuals followed for nearly 4 years. In this study, we report data from cognitively normal individuals having both MRI and amyloid PET imaging followed an average of nearly 10 years.

Methods: Subjects were recruited from the UC Davis ADC Diversity Study who were cognitively normal at baseline, time of PET and MRI imaging and received yearly cognitive assessment. Mixed model regression with random slope and intercept was calculated for memory and executive function over the entire period of observation.

Results: Table 1 summarizes baseline demographic, MRI and Cognitive measures. No significant differences were found due to amyloid status. Table 2 summarizes MRI predictors of cognitive decline adjusting for age, gender and education. WMH was significantly associated with slope and intercept of memory and intercept of executive performance. Hippocampal volume was significantly associated with slope of memory performance. Table 3 summarizes previously significant MRI measures as well as the addition of amyloid status. WMH was significantly associated with intercept and slope of memory performance whereas hippocampus was significantly associated with intercept with a trend for slope. WMH and Hippocampus were associated with intercept of executive function. Amyloid status did not influence cognition with the exception of a trend towards the slope of executive function over time.

Conclusion: In this study of a cognitively normal individuals followed nearly 10 years, vascular brain injury as measured by WMH volumes was found to have the most consistent impact on cognition followed by hippocampal measures, while amyloid status had only a weak effect.

Table 1. Baseline Measures

Measure	Amyloid Negative	Amyloid Positive
Age	73.7 + 6.7	75.0 + 6.2
Gender (%F)	57	32
Education	14.7 + 3.9	15.4 + 3.6
Gray Matter*	470.4 + 2.2	474.5 + 3.7
White Matter Hyperintensities (WMH)	6.8 + 1.0	9.5 + 1.7
Hippocampus	6.4 + 0.05	6.5 + 0.1
Lateral Ventricle	32.5 + 1.4	37.2 + 2.3
Memory	0.99 + 0.08	0.90 + 0.13
Executive	0.79 + 0.06	0.63 + 0.11

*MRI measures reported in cubic centimeters adjusted for age, gender and head size
*Cognitive measures reported in standard deviations adjusted for age, gender and educational achievement.

Table 2. Baseline MRI Predictors of Cognition

Measure	Memory	Executive
Time	-0.013 + 0.006*	-0.01 + 0.005*
Gray Matter	-0.002 + 0.003	-0.003 + 0.002
Gray Matter * time	-0.000 + 0.0002	0.0002 + 0.0002
WMH	-0.014 + 0.007^	-0.01 + 0.005^
WMH * time	-0.002 + 0.0005*	-0.0005 + 0.0005
Hippocampus	0.23 + 0.13	0.16 + 0.10
Hippocampus*time	0.006 + 0.01^	0.005 + 0.009
Lateral Ventricle	-0.002 + 0.006	-0.009 + 0.004
Lateral Ventricle * time	-0.0003 + 0.0004	-0.0004 + 0.0004

*p <0.01
^p >0.05 and <0.1

Table 3. MRI and PET Predictors of Cognition

Measure	Memory	Executive
Time	-0.02 + 0.007*	-0.017 + 0.005*
WMH	-0.014 + 0.007*	-0.01 + 0.005*
WMH * time	-0.0014 + 0.0005*	-0.0005 + 0.0004
Hippocampus	0.26 + 0.12*	0.22 + 0.09*
Hippocampus*time	0.01 + 0.01^	0.01 + 0.008
Amyloid Status (0)	0.05 + 0.8	0.09 + 0.06
Amyloid Status (0) *time	0.004 + 0.006	0.009 + 0.005^

*p <0.01
^p >0.05 and <0.1

Fluorodeoxyglucose and Flortaucipir PET independently predict subsequent cognitive decline in clinically normal adults with elevated amyloid

Danielle Mayblyum[1], Bernard Hanseeuw[1,2], Justin Sanchez[1], Samantha Katz[1], Kirsten Moody[1], Tobias Estime[1], Heidi Jacobs[1], Rachel Buckley[1,3], Jorge Sepulcre[1], Aaron Schultz[1], Alex Becker[1], Kathryn Papp[1,3], Dorene Rentz[1,3], Reisa Sperling[1,3], Keith Johnson[1]

[1]*Massachusetts General Hospital, Boston, MA, US*
[2]*Cliniques Universitaires Saint-Luc, Brussels, Belgium*
[3]*Brigham and Women Hospital, Boston, MA, US*

Background: Fluorodeoxyglucose (FDG), and more recently Flortaucipir (FTP) PET signals, have both been evaluated in individuals with preclinical Alzheimer's disease. We compared how these two tracers predicted subsequent cognitive decline in high-amyloid participants from the Harvard Aging Brain Study, in comparison with low-amyloid participants.

Methods: We analyzed data from 131 clinically normal adults with FDG, FTP, and PiB-PET acquired within a year, as well as prospective cognitive evaluations over a mean three-year follow-up (Table 1). PET data were scaled on cerebellar cortex and corrected for partial volume effects. We focused analyses on three pre-defined Freesurfer regions-of-interest: entorhinal cortex, inferior temporal, and isthmus cingulate. Cognition was assessed using the Preclinical Alzheimer's Cognitive Composite (PACC-5). We evaluated the association between PET and cognition using linear mixed-effect models with random intercepts and slopes. We evaluated how using FDG or FTP as inclusion criteria in addition to PiB would impact the power of prevention clinical trials. Analyses were adjusted for age, sex, and education.

Results: PiB predicted cognitive decline in interaction with FDG in entorhinal cortex and isthmus cingulate, and with FTP in entorhinal cortex and inferior temporal, such that both FDG and FTP predicted decline in the high-PiB, while neither were predictive in the low-PiB participants (Fig.1). When competing in the same model, FTP outperformed isthmus cingulate and inferior temporal FDG, but entorhinal FDG (p<0.001) predicted PACC decline after adjusting for entorhinal or inferior temporal FTP. Power analyses indicated that a preclinical AD trial would need to recruit fewer participants if entorhinal FDG was used as inclusion criteria in addition to PiB and/or FTP-PET (Fig.2).

Conclusion: In preclinical AD, isthmus cingulate hypometabolism predicts a tau-mediated cognitive decline. In contrast, entorhinal hypometabolism predicts cognitive decline that is partially independent of the tau-PET signal; and could therefore be used to enrich prevention trials.

Table 1. Subject demographic information

|	All	Low-PiB	High-PiB
N	131	90	41
Age	73.98 ± 8.29 (55.25-90.00)	72.54 ± 8.60 (55.25-90.00)	77.14 ± 6.65* (59.75-89.00)
E4+ N (%)	39 (29.77)	16 (17.78)	23 (56.10)**
Education	15.92 ± 2.97 (8.00-20.00)	15.98 ± 3.03 (8.00-20.00)	15.80 ± 2.86 (11.00-20.00)
Females N (%)	52 (39.69)	35 (38.89)	17 (41.46)
Prospective Cognitive Follow-up (years)	3.03 ± 1.43 (0.77-5.06)	2.96 ± 1.47 (0.77-5.01)	3.17 ± 1.32 (0.78-5.06)
Neocortical PiB DVR	1.42 ± 0.47 (1.03-2.89)	1.16 ± 0.06 (1.03-1.30)	2.00 ± 0.45** (1.30-2.89)
Entorhinal FDG SUVR	0.82 ± 0.12 (0.49-1.19)	0.82 ± 0.12 (0.49-1.09)	0.81 ± 0.13 (0.58-1.19)
Entorhinal FTP SUVR	1.39 ± 0.32 (0.84-2.51)	1.29 ± 0.23 (0.84-1.96)	1.61 ± 0.40** (1.03-2.51)
Inferior Temporal FDG SUVR	1.33 ± 0.12 (1.10-1.62)	1.34 ± 0.12 (1.11-1.62)	1.30 ± 0.13 (1.10-1.58)
Inferior Temporal FTP SUVR	1.46 ± 0.19 (1.02-2.06)	1.42 ± 0.14 (1.02-1.76)	1.56 ± 0.24** (1.19-2.06)
Isthmus Cingulate FDG SUVR	1.67 ± 0.21 (0.77-2.24)	1.67 ± 0.23 (0.77-2.18)	1.67 ± 0.19 (1.31-2.24)
Isthmus Cingulate FTP SUVR	1.25 ± 0.15 (0.79-1.62)	1.21 ± 0.13 (0.79-1.50)	1.33 ± 0.15** (1.12-1.62)

Legend: mean ± SD (min-max), *$p<0.05$, **$p<0.001$

Figure 1. Regional FDG and FTP-PET predictive of cognitive decline in clinically normal adults
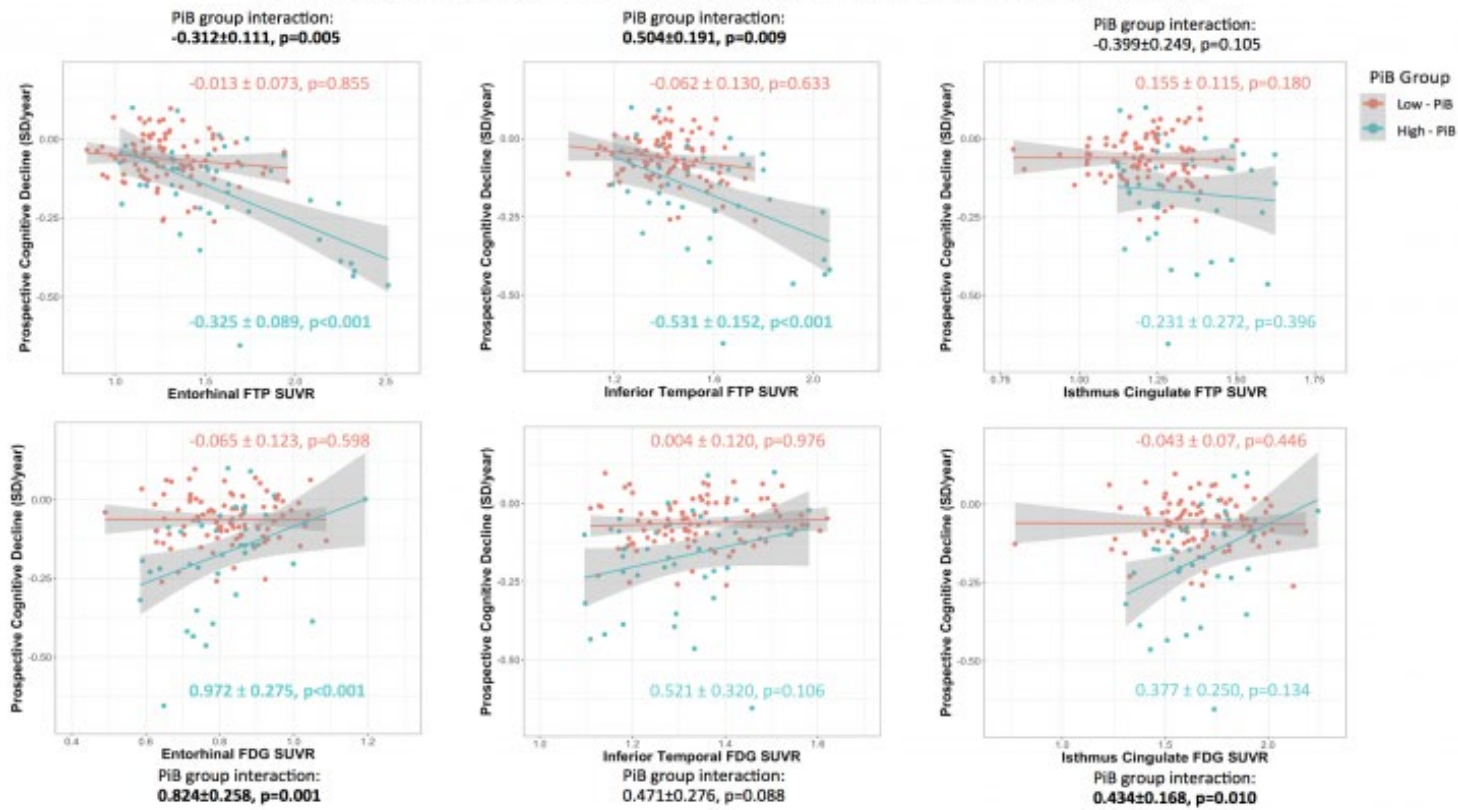
Legend: Cognitive decline was estimated using linear mixed-effect models predicting PACC-5 performance over time with a random intercept and slope per subject. Models were adjusted for age, sex, and education.

Figure 2. Power analyses
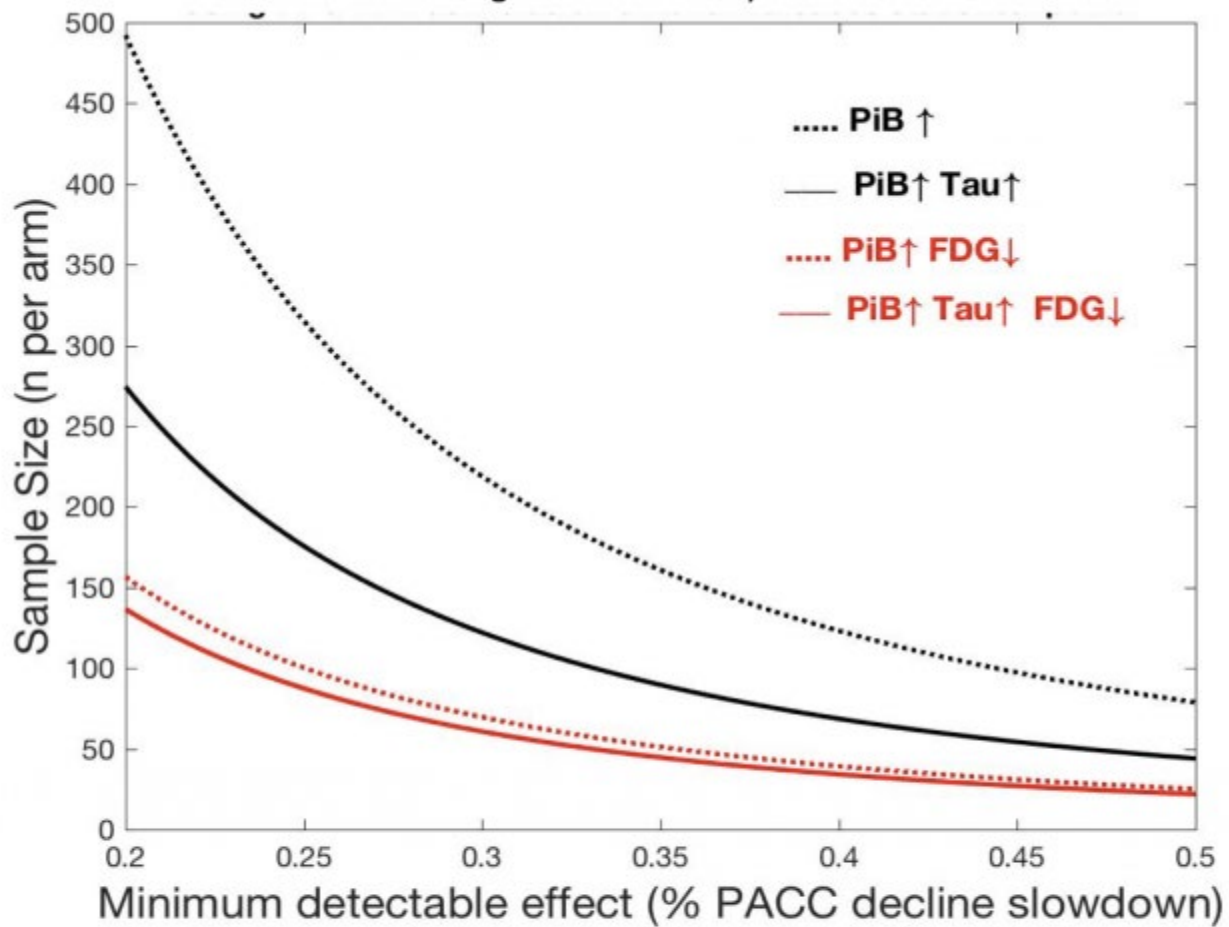
Legend: Number of high-amyloid clinically normal adults (Y-axis) that are needed to include per arm for detecting a given slope reduction on the Preclinical Alzheimer's Cognitive Composite (PACC-5, X-axis) with 80% power and alpha=0.05, in a four-year trial with annual cognitive assessments, using PiB-PET alone (black dotted line), PiB and FTP-PET (black plain line), PiB and FDG-PET (red dotted line) or PiB, FTP, and FDG-PET (red plain line) as inclusion criteria. FDG and FTP-PET were considered as low/high when the entorhinal signal was below/above the median value of the high-amyloid group.

Keywords: *fluorodeoxyglucose, flortaucipir, PiB, cognitive decline*

MK-6240 and PIB PET are associated with retrospective cognitive trajectories in late-middle aged persons clinically unimpaired at baseline

Tobey Betthauser[1], Erin Jonaitis[1], Rebecca Koscik[1], Samantha Allison[1], Alexander Converse[1], Dhanabalan Murali[1], Todd Barnhart[1], Charles Stone[1], Lindsay Clark[1], Bradley Christian[1], Sterling Johnson[1]

[1]*University of Wisconsin-Madison School of Medicine and Public Health, Madison, WI, US*

Objectives: This work investigated whether PET AD biomarkers for Aβ plaques and NFTs explain differences in longitudinal cognitive trajectories of individuals clinically unimpaired at their baseline assessment. Secondarily, associations between MK-6240, PiB and age were investigated.

Methods: Individuals (age at first composite=59±6 years) recruited from the Wisconsin Registry for Alzheimer's Disease Prevention (WRAP) underwent [F-18]MK-6240 and [C-11]PiB PET and T1-weighted MR imaging, and longitudinal cognitive assessment (Table1). A composite cognitive score (WRAP-PACC-3) was calculated for each assessment as the mean of Z-scored tests (RAVLT Total, WMS-R Logical Memory Delayed Recall, WAIS-R Digit Symbol). Individuals were grouped by biomarker status ascertained by PiB (global PiB DVR≥1.19; Logan, cerebellum GM) and MK-6240 (MK-6240 hippocampus SUVR>1.06 (mean+1.5SD of PiB(-) group; 0.88+0.18); inferior cerebellum GM, 70-90min) PET imaging. A linear mixed effects model (random person-level slopes and intercepts) tested the hypothesis that biomarker groups had different WRAP-PACC-3 trajectories (model, Figure1). Associations between MK-6240, PiB and age were investigated by voxelwise analysis of spatially normalized MK-6240 SUVR images.

Results: The age*group interaction indicated significantly different WRAP-PACC-3 trajectories amongst the four biomarker groups (Figure1). Tukey-adjusted post-hoc pairwise comparisons showed the PiB(+)/MK(+) group had a steeper age slope than all other groups, but other groups did not differ significantly. The ratio of model-estimated age effects on WRAP-PACC-3 indicated a 3.5-fold (1.8-8.2 95%CI) faster decline rate for the PiB(+)/MK(+) group compared to the PiB(-)/MK(-) group. MK-6240 SUVR was positively associated with global PiB DVR in regions associated with Braak NFT stages I-IV, but no association was observed with age (FWE=0.05, Figure2).

Conclusions: These results suggest concurrent NFT and Aβ pathophysiologies contribute to measurable cognitive decline prior to clinical impairment, consistent with the construct of preclinical AD, and that MK-6240-measured hippocampal NFTs may not be benign. MK-6240 appears to be an age-independent sensitive marker of AD NFT pathophysiology.

	PiB(-)/MK(-)	PiB(-)/MK(+)	PiB(+)/MK(-)	PiB(+)/MK(+)	Group Difference ANOVA/Fishers	Total
N	94	7	16	16	p=0.10	133
Age at *Baseline NP (yrs)	58 ± 6	60 ± 4	61 ± 5	62 ± 4	p=0.09	59 ± 6
Δt(baseline – last NP visit) (yrs)	7.5 ± 2.2	7.3 ± 0.5	7.3 ± 2.8	7.8 ± 2.1	p=0.92	67 ± 6
Number of NP Visits	4 ± 1	4 ± 0	4 ± 1	4 ± 1	p=0.99	4 ± 1
Δt(Last NP – MK PET) (yrs)	-1.0 ± 1.0	-1.7 ± 0.9	-1.1 ± 1.3	-0.8 ± 0.8	p=0.24	-1.0 ± 1.0
Δt(Last NP – PiB PET) (yrs)	-0.7 ± 1.4	-1.4 ± 1.1	-0.9 ± 1.1	-0.7 ± 0.82	p=0.53	-0.7 ± 1.3
Δt(First MCI Dx – MK PET) (yrs)	-0.9 (n=1)	-5.3 (n=1)	-4.7 (n=1)	-0.1 ± 0.1 (n=4)	NA	-1.9 ± 2.1 (n=7)
Demographic Comparisons						
% Female	70.2	57.1	43.8	81.3	p=0.10	67.7
% Non-Caucasian	7.4	0	6.3	0	P=0.61	6.0
% APOE-ε4 Carriers	†*28.7	*28.8	<u>56.3</u>	<u>87.5</u>	p<0.001	39.1
% Family History of Dementia	74.5	100	*50.0	<u>93.8</u>	p=0.01	75.2
WRAT-III Reading Score	107 ± 9	103 ± 3	109 ± 9	107 ± 8	p=0.50	107 ± 9
Longitudinal Neuropsychological Testing Comparisons						
% Baseline Clinical MCI	0	0	0	0	NA	0
% Last Clinical MCI	*1 (n=1)	14 (n=1)	6 (n=1)	<u>25 (n=4)</u>	p<0.001	5 (N=7)
Baseline CESD	7 ± 6	7 ± 8	4 ± 6	6 ± 6	p=0.36	6 ± 6
Last CESD	6 ± 7	2 ± 4	4 ± 4	7 ± 5	p=0.30	6 ± 7
Baseline WRAP-PACC-3	0.15 ± 0.70	-0.34 ± 0.78	0.22 ± 0.55	0.06 ± 0.58	p=0.27	0.12 ± 0.67
Last WRAP-PACC-3	*0.12 ± 0.70	-0.18 ± 0.80	*0.11 ± 0.86	<u>-0.76 ± 0.87</u>	p=0.0004	-0.002 ± 0.79
Baseline MMSE	29.4 ± 1	29.4 ± 0.8	29.7 ± 0.6	29.3 ± 0.9	p=0.57	29.4 ± 0.9
Last MMSE	*29.4 ± 0.8	29.4 ± 0.8	29.3 ± 1.2	<u>28.6 ± 1.5</u>	p=0.010	29.3 ± 1.0
Biomarker Comparisons						
Baseline Systolic BP	*126 ± 15	<u>109 ± 15</u>	121 ± 14	*130 ± 17	p=0.02	124 ± 15
Last Systolic BP	127 ± 14	117 ± 15	123 ± 17	132 ± 17	p=0.14	127 ± 15
MK-6240 Entorhinal Cortex SUVR at Last NP	*1.00 ± 0.14	*1.14 ± 0.10	*0.98 ± 0.15	<u>1.74 ± 0.39</u>	p<<0.001	1.10 ± 0.30
MK-6240 Hippocampus SUVR at Last NP	†*0.86 ± 0.11	<u>*1.08 ± 0.02</u>	†*0.85 ± 0.10	<u>†1.41 ± 0.25</u>	p<<0.001	0.94 ± 0.22
MK-6240 Inferior Temporal Gyrus SUVR at Last NP	*1.09 ± 0.12	*1.18 ± 0.08	*1.05 ± 0.10	<u>1.85 ± 0.82</u>	p<<0.001	1.18 ± 0.39
Global PiB DVR at Last NP	†*1.06 ± 0.05	†*1.09 ± 0.05	<u>*1.38 ± 0.18</u>	<u>†1.63 ± 0.21</u>	p<<0.001	1.17 ± 0.22

Table 1: Descriptive statistics and group comparisons for study variables, demographics, neuropsychological assessment scores, and biomarkers. Group differences were assessed by ANOVA and Fisher Exact tests for continuous and categorical variables, respectively, with post hoc pairwise comparisons. Groups with significantly different pairwise comparisons are indicated by the combination of text underlined in black and an asterisk or text underlined in red and a red dagger.

*Baseline corresponds to the first neuropsychological assessment where the WRAP-PACC-3 could be determined. In most cases this was their second neuropsychological assessment in the WRAP study.
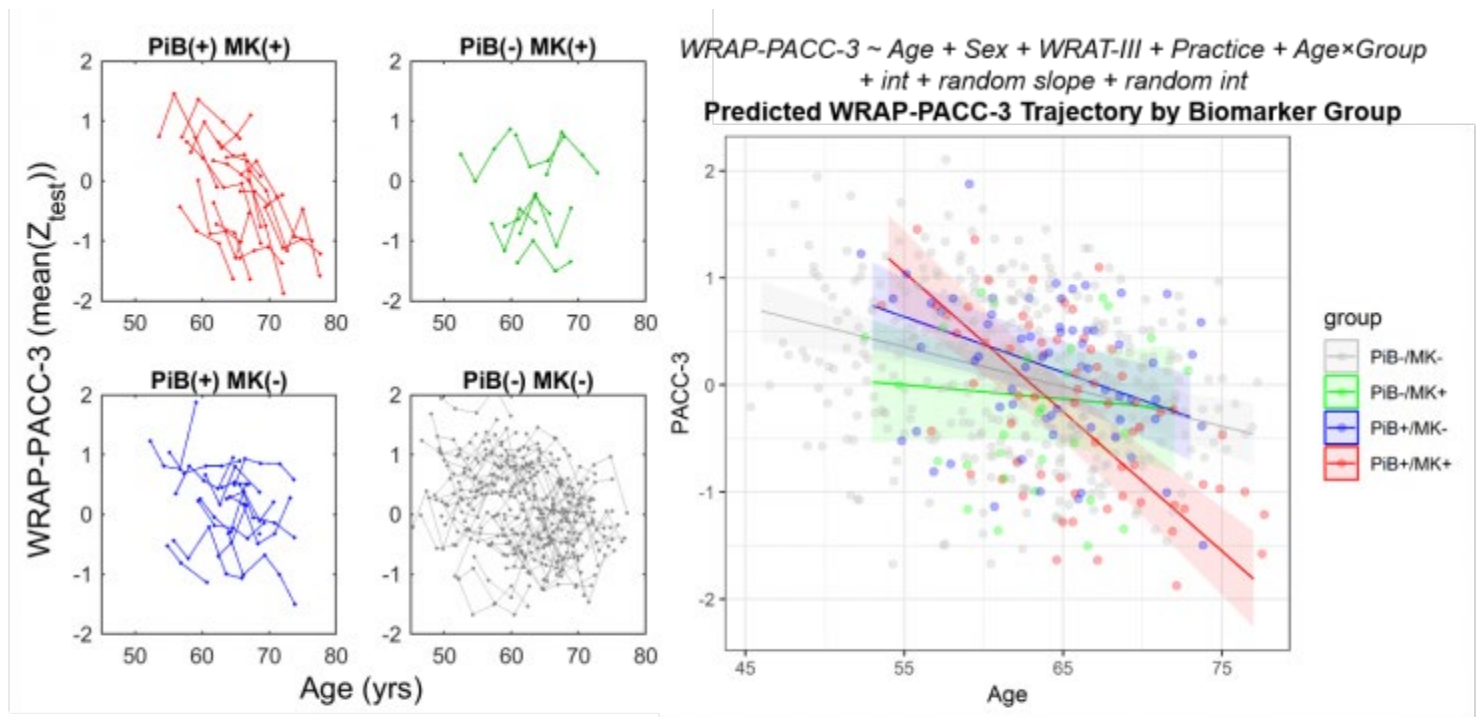
Figure 1: The four plots on the left show the longitudinal WRAP-PACC-3 performances of individuals in each of the four MK-6240/PiB positivity groups. The MK(+)/PiB(+) group indicated steeper decline in longitudinal WRAP-PACC-3 performance compared to other groups. This was confirmed in a linear mixed effects model showing a significant age x biomarker group interaction after adjusting for covariates (age, sex, WRAT-III reading score, and practice effects). The plot on the right shows the modeled simple-slopes for each biomarker group (solid lines) overlayed on the observed WRAP-PACC-3 scores. This model suggested that MK(+)/PiB(+) individuals had more negative cognitive trajectories than any other group. Neither the PiB(-)/MK(+) nor PiB(+)/MK(-) groups were significantly different from the PiB(-)/MK(-) group.
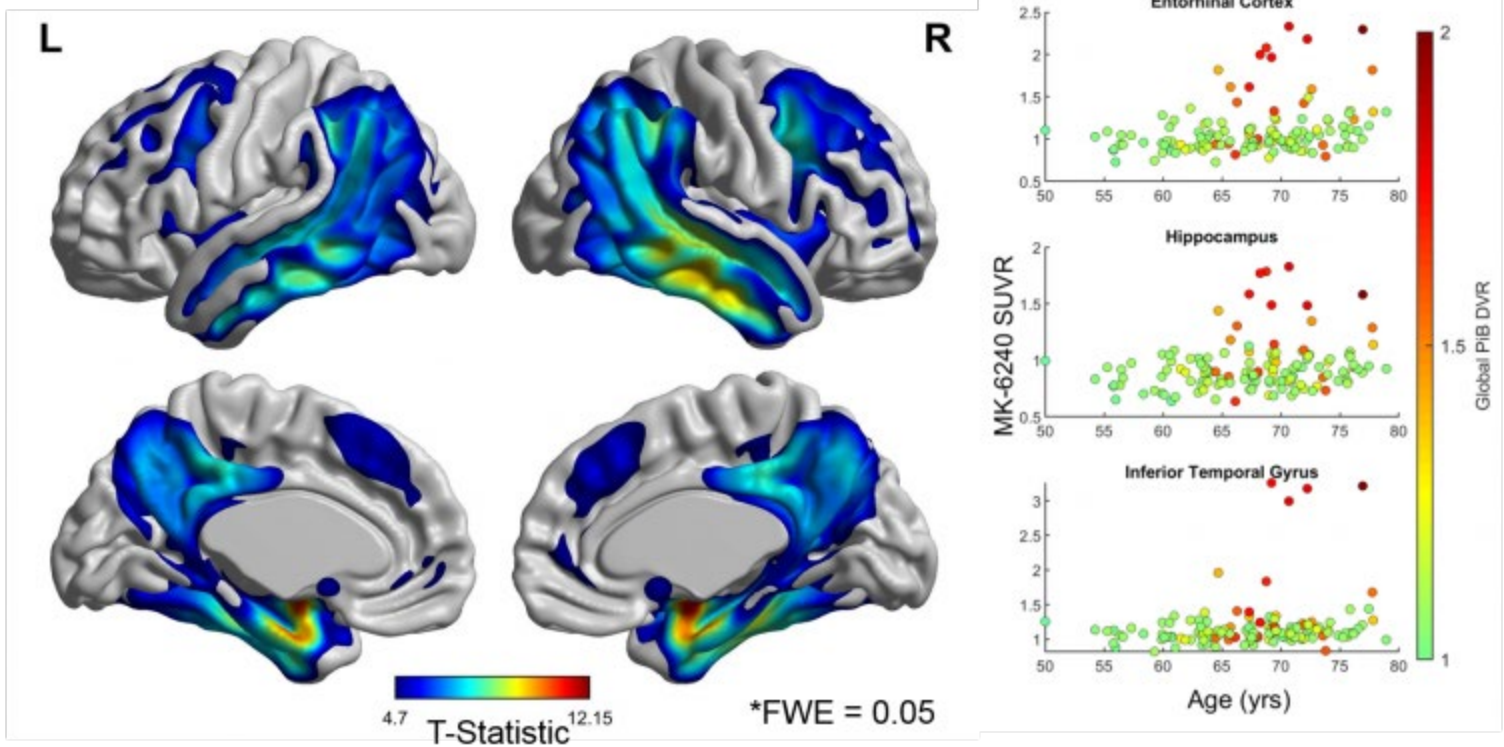
Figure 2: Voxelwise analysis (MK-6240 SUVR ~ Age + Global PiB DVR + int) indicated a significant positive association between MK-6240 SUVR and global PiB DVR, primarily in regions associated with Braak I-V staging (FWE = 0.05, left pane). Age was not a significant predictor of MK-6240 SUVR after familywise error correction. Regional plots of MK-6240 vs. age color coded by global PiB DVR (right pane) indicated persons did not generally have elevated MK-6240 SUVR in the absence of elevated PiB, but individuals that had elevated PiB DVRs did not necessarily have elevated MK-6240 SUVR.

Keywords: *longitudinal cognition, tau, beta-amyloid, MK-6240, PiB*

Individual variations in sleep architecture are associated with tau PET, cognition, and functional network architecture: Preliminary findings from the Harvard Aging Brain Study

Jasmeer Chhatwal[1,2,3], Ina Djonlagic[2,4], Aaron Schultz[1,2,3], Olivia Hampton[1], Dylan Kirn[1], Kathryn Papp[1,2,3], Dorene Rentz[1,2,3], Susan Redline[2,3], Keith Johnson[1,2,3], Reisa Sperling[1,2,3]

[1]*Massachusetts General Hospital, Department of Neurology, Boston, MA, US*
[2]*Harvard Medical School, Boston, MA, US*
[3]*Brigham and Women's Hospital, Boston, MA, US*
[4]*Beth Israel Deaconess Medical Center, Boston, MA, US*

Objective: Intriguing findings in animals and limited human studies suggest sleep may be critically important to tau and beta-amyloid production and clearance. However, it remains unclear how sleep may impact Alzheimer's disease biomarkers. We examined if individual variations in sleep architecture were associated with variations in regional tau PET (18F-flortaucipir; FTP), amyloid PET (11C-Pittsburgh Compound B; PiB), cognition, and resting-state network connectivity (rs-fcMRI) in a pilot sample of non-demented older adults.

Methods: At-home polysomnography (PSG), FTP and PiB PET, cognitive testing, and rs-fcMRI were assessed in 24 clinically-normal participants in the Harvard Aging Brain Study (HABS; mean age 74.1 ± 1.97 SE).

Results: Controlling for age and total sleep time, we observed that time in slow-wave (SWS; $p = 0.016$) and rapid-eye movement (REM; $p = 0.05$) sleep was inversely correlated with inferior temporal (ITC) tau, whereas time in Stage 1 (N1; $p = 0.006$) was positively correlated with ITC tau. Intriguingly, N1/SWS and REM were independently related to ITC tau. A positive correlation between N1 and PiB-PET was also observed ($p = 0.01$). Cognitive performance on the Preclinical Alzheimer's Cognitive Composite (PACC) was negatively associated with time in N1 ($p = 0.04$) and positively with REM sleep ($p = 0.001$), though correction for age attenuated these effects (N1: $p = 0.52$; REM: $p = 0.08$). Lastly, rs-fcMRI obtained the morning after PSG demonstrated that time in REM was positively associated with connectivity in two networks tied to memory performance (Default and Control; both $p < 0.01$, Fig. 3), correcting for age and total sleep time.

Conclusions: These preliminary results support the hypothesis that sleep disruption may drive or reflect tau accumulation, and that age-dependent cognitive changes may be related to changes in sleep. Lastly, modulation of network connectivity by REM sleep may provide a link between disrupted sleep and cognitive performance.
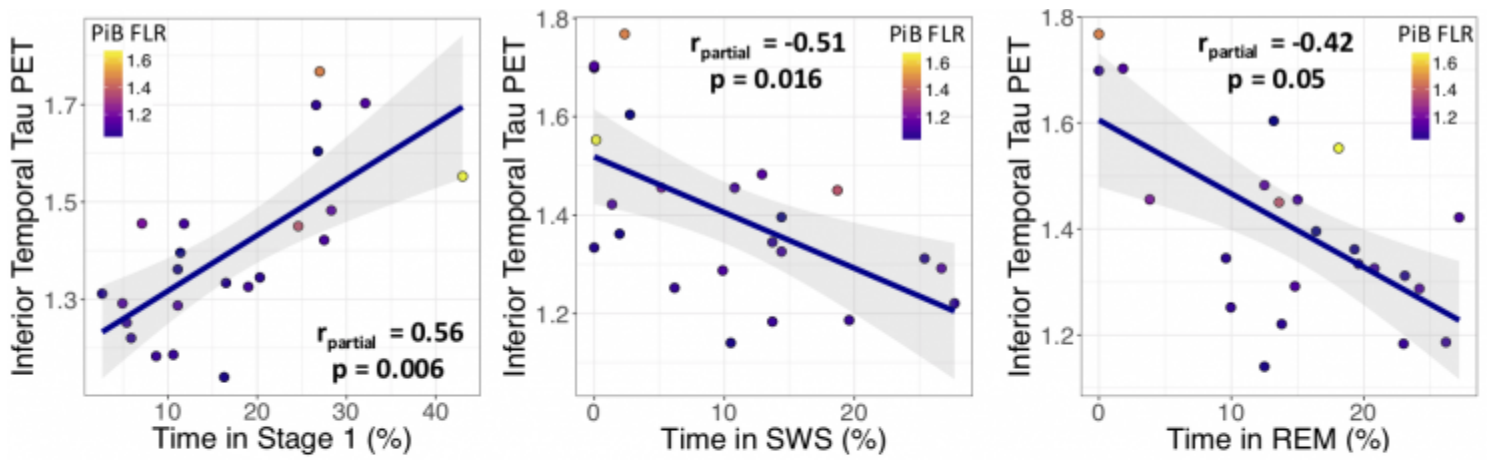
Figure 1: *Inferior temporal tau PET signal is associated with variations in sleep architecture.* Greater time in Stage 1 sleep (Left) was associated with greater 18F-FTP tau PET signal in the FS6-defined bilateral inferior temporal cortex (ITC) region (Left). Time in slow wave sleep (SWS; Middle) and rapid eye movement (REM: Right) sleep was inversely correlated with ITC tau PET signal. $R_{partial}$ values correspond to the relationship of sleep stage to partial volume corrected F18-FTP signal after correcting for age and total sleep time.
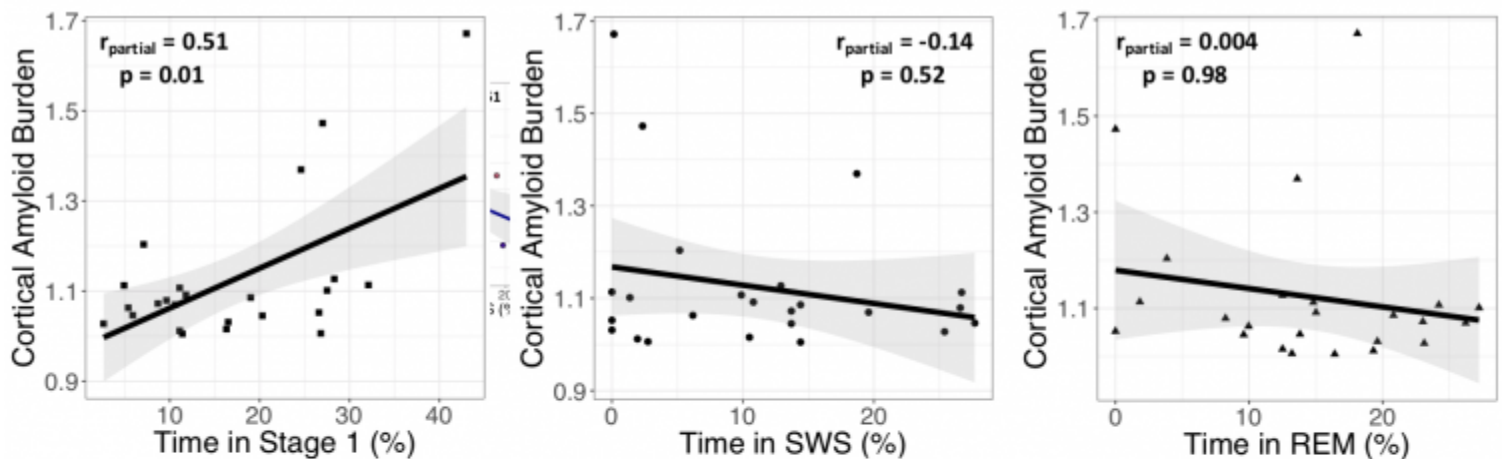
Figure 2: *Cortical amyloid burden is not clearly related to variations in sleep architecture.* Greater time in Stage 1 sleep (N1, Left) was significantly associated with greater cortical 11C-PiB (PiB SUVR FLR, partial volume corrected), but the limited number of high amyloid burden individuals in the sample limits the interpretation of this result (Left). Neither time in slow wave sleep (SWS; Middle) nor time in rapid eye movement (REM: Right) sleep were correlated with cortical amyloid burden. $R_{partial}$ values correspond to the relationship of sleep stage to partial volume corrected F18-FTP signal after correcting for age and total sleep time.

Slow Wave (mins)	REM Sleep (mins)	
0.16	0.52 **	Default
0	0.48 *	R Control
0.09	0.55 **	L Control
−0.22	−0.02	Dorsal Attention

Spearman's rho
* p < 0.05
** p < 0.01
n = 24

Figure 3: *Modulation of resting state network connectivity by night-before sleep.* Time in REM sleep was positively correlated with connectivity in 3 cortical networks previously associated with memory performance in HABS. Slow wave sleep time was not related to connectivity in any examined networks. Corrected for age and total sleep time.

Friday, January 18, 2019 - 12:30 pm - 01:00 pm

Keynote Lecture

Trojanowski, John

Tau strains and spreading in pure tauopathies and Alzheimer's disease

John Trojanowski

University of Pennsylvania, Philadelphia, PA, US

Intracellular inclusions of filamentous tau proteins are the hallmark lesions of several neurodegenerative tauopathies such as AD and related tauopathies. Growing evidence suggest that pathological tau spreads throughout the CNS through templated propagation of this tau pathology via neuroanatomical connectivity or through astrocytic and oligodendroglial pathways. Indeed, studies suggest that this spread might involve different self-propagating strains of pathological tau that could account for the diverse manifestations of AD and other neurodegenerative tauopathies as well as the emergence of glial and neuronal tau pathologies in disorders such as PSP and CBD. Recent studies have shown that tau aggregates may form distinct structural conformations, known as tau strains. Here, we developed a novel model to test the hypothesis that cell-to-cell transmission of different tau strains occurs in WT mice, and to investigate whether there are strain-specific differences in the pattern of tau transmission. By injecting pathological tau extracted from postmortem brains of AD (AD-tau), PSP-tau and CBD-tau patients into different brain regions of female WT mice, we demonstrated the induction and propagation of endogenous mouse tau aggregates. Specifically, we identified differences in tau strain potency between AD-tau, CBD-tau, and PSP-tau in WT mice. Moreover, differences in cell-type specificity of tau aggregate transmission were observed between tau strains such that only PSP-tau and CBD-tau strains induce astroglial and oligodendroglial tau inclusions, recapitulating the diversity of neuropathology in human tauopathies. Furthermore, we demonstrated the neuronal connectome, but not the tau strain, determines which brain regions develop tau pathology. Finally, CBD-tau and PSP-tau-injected mice showed spatiotemporal transmission of glial tau pathology, suggesting glial tau transmission contributes to the progression of tauopathies through an as yet unidentified glial connectome**.** Taken together, our data suggest that different tau strains determine seeding potency and cell-type specificity of tau aggregation that underlie the diversity of human tauopathies.

Friday, January 18, 2019 - 02:30 pm - 03:45 pm

Podium Session

Session 8: Multi-modality: patient populations

CHAIRS: Ann Cohen, Keith Johnson

02:30 pm – 03:45 pm	Session 8: Multi-modality: patient populations	CHAIRS: **Ann Cohen**, University of Pittsburgh, Pittsburgh, PA, US **Keith Johnson**, Massachusetts General Hospital, Boston, MA, US	Page
2:30	Tau imaging with [18F]Flortaucipir predicts the severity and the topography of subsequent cortical atrophy in patients with Alzheimer's disease	**Renaud La Joie**, University of California, San Francisco, San Francisco, CA, US	464
2:45	Epidemic spreading of tau through human functional brain connections	**Jacob Vogel**, Montreal Neurological Institute, McGill University, Montreal, QC, Canada	468
3:00	Spatial extent and topographical relationships between pathology accumulation and neurodegeneration in Alzheimer's disease	**Leonardo Iaccarino**, Memory and Aging Center, University of California San Francisco, San Francisco, CA, USA, San Francisco, CA, US	472
3:15	Functional connectivity associated with tau levels in aging, Alzheimer's, and small-vessel disease	**Nicolai Franzmeier**, Institute for Stroke and Dementia Research, Klinikum der Universität München, Ludwig-Maximilians-Universität LMU, Munich, Germany	475
3:30	Associations between longitudinal Aβ and cross-sectional tau in adults with Down syndrome	**Dana Tudorascu**, University of Pittsburgh, Pittsburgh, PA, US	480
03:45 pm - 04:15 pm	Discussion		

Tau imaging with [18F]Flortaucipir predicts the severity and the topography of subsequent cortical atrophy in patients with Alzheimer's disease

Renaud La Joie[1], Adrienne Visani[1], Suzanne Baker[3], Jesse Brown[1], Viktoriya Bourakova[1], Jungho Cha[1], Lauren Edwards[1], Mustafa Janabi[3], Zachary Miller[1], David Perry[1], Julie Pham[1], Kiran Chaudhary[1], Julio Rojas[1], Howard Rosen[1], William Seeley[1], Richard Tsai[1], Bruce Miller[1], William Jagust[2,3], Gil Rabinovici[1]

[1]University of California, San Francisco, San Francisco, CA, US
[2]University of California, Berkeley, Berkeley, CA, US
[3]Lawrence Berkeley National Laboratory, Berkeley, CA, US

Background: We aimed to assess whether β-amyloid (PIB) and tau (Florbetapir, FTP) PET could help predict longitudinal atrophy in patients with AD.

Methods: 32 PIB-positive cognitively impaired patients (44% dementia stage, 66% women, age=64 ± 9, MMSE=24 ± 4 at baseline) underwent baseline structural MRI and PET with both FTP and PIB, and a follow-up structural MRI (14.8 ± 3.1 months later). MRIs were preprocessed using SPM12's longitudinal registration pipeline to obtain longitudinal atrophy maps. PET SUVR were calculated using cerebellar GM (PIB) and inferior cerebellar GM (FTP) reference regions. Global cortical SUVR/atrophy values were extracted for each patient to compute groupwise correlations. Voxelwise correlations were calculated at the individual patient level to quantify the spatial similarity between baseline PET-SUVR and longitudinal atrophy maps.

Results: At the group level, longitudinal atrophy was maximal in the temporo-parietal cortex, strongly overlapping with areas of high baseline FTP-SUVR, while PIB-PET signal was more widespread (Figure 1). A strong association existed between greater atrophy rates and higher baseline FTP-SUVR ($r=0.67$, $p<0.001$) but not PIB-SUVR ($r=0.29$, $p=0.11$, Figure 2). Spatial correlation analyses revealed that, in all patients, longitudinal atrophy maps resembled baseline FTP maps (41% shared variance), while the correlation between PIB and atrophy was minimal (3% shared variance on average, $p<0.001$ compared to FTP). Older patients had lower atrophy rates, and that association was mediated by differences in baseline tau burden (older patients had lower baseline tau, see Figure 3a/b). The spatial similarity between baseline FTP and subsequent atrophy decreased with age (Figure 3c). All associations remained unchanged when controlling for baseline cortical thickness.

Conclusion: These data support disease models in which tau pathology is a major driver of regional neurodegeneration - especially in early onset patients, and highlight the relevance of tau-PET as a precision medicine tool to help predict individual patient's progression and design future clinical trials.
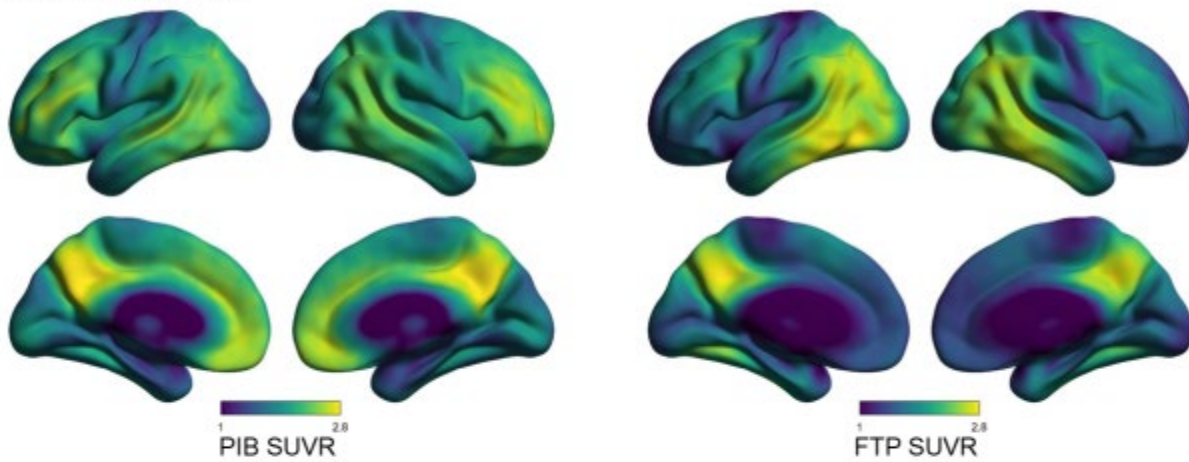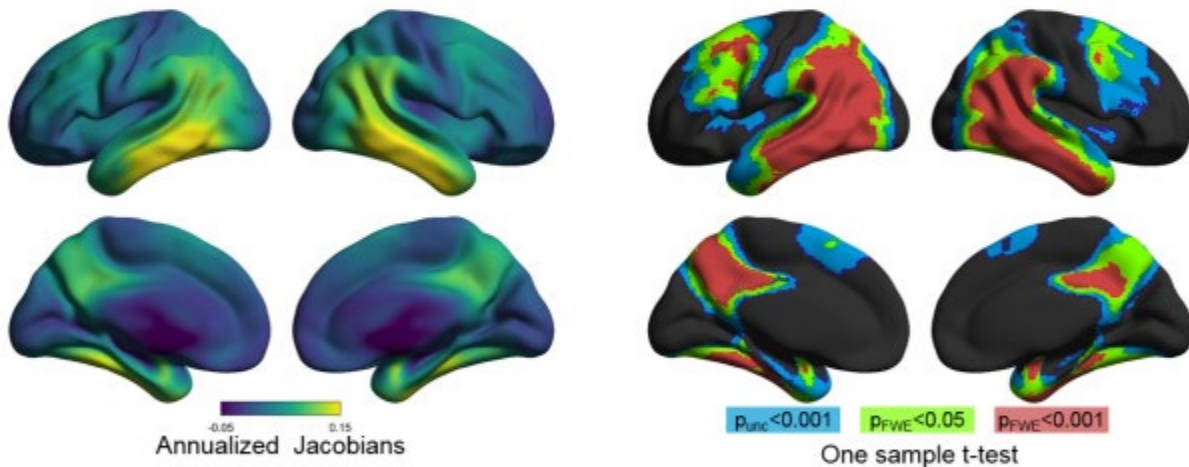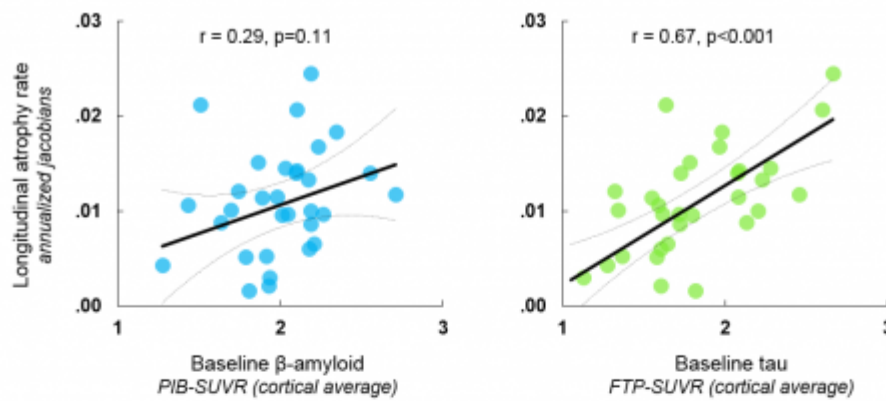
Figure 1

A. Average patterns of baseline PIB and FTP-PET in the group of 32 patients.
B. Pattern of longitudinal atrophy expressed as the group-average Jacobian map (left: higher Jacobian values indicate greater atrophy rates) or as the result of a one-sample t-test identifying voxels of significant atrophy (Jacobians > 0) at the group level (right); uncorrected and family wise error (FWE) corrected p values are provided.
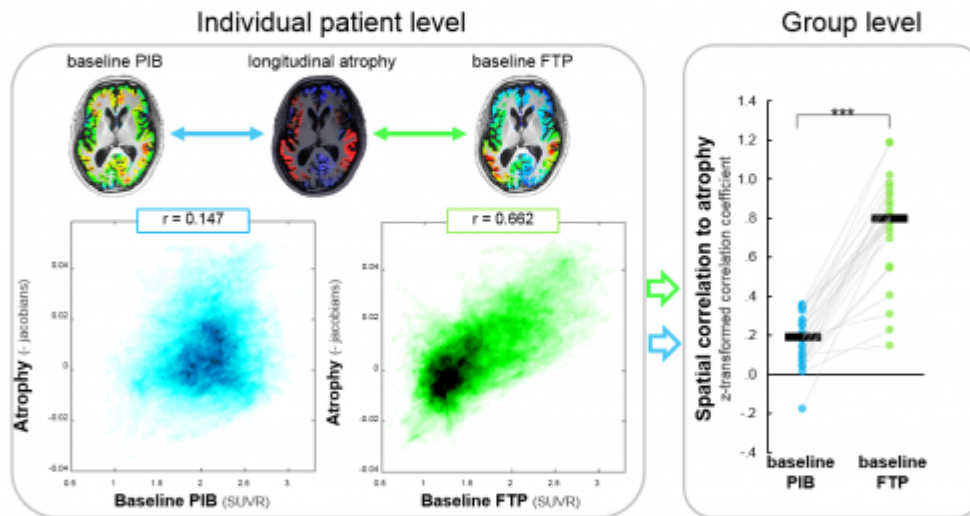
Figure 2

A. Bivariate correlations between baseline PET values (average cortical SUVR) and longitudinal atrophy rates (global cortical Jacobians) across patients.

B. Spatial correlation analyses. Analyses were conducted at the individual patient level to quantify the similarity between patterns of PET SUVR at baseline and maps of longitudinal atrophy. For each patient, correlations were assessed on all voxels of the cortex. Resulting correlation coefficients were z-transformed to be analyzed at the group level. Colored dots indicate z-transformed coefficients for each patient, and the black bars show the z(r) mean values: 0.183 (SE=0.046) for PIB; 0.780 (SE=0.046) for FTP. ***: p<0.001 (two-tailed paired t-test, t(31)=14.9).
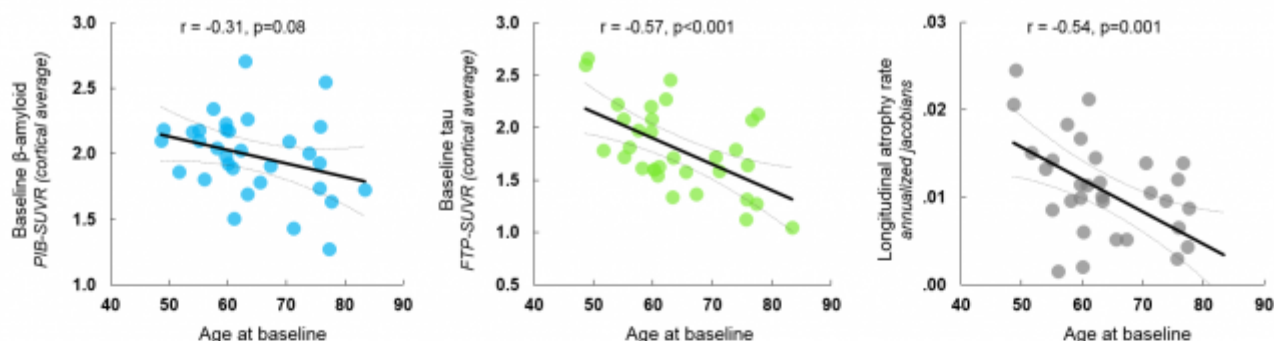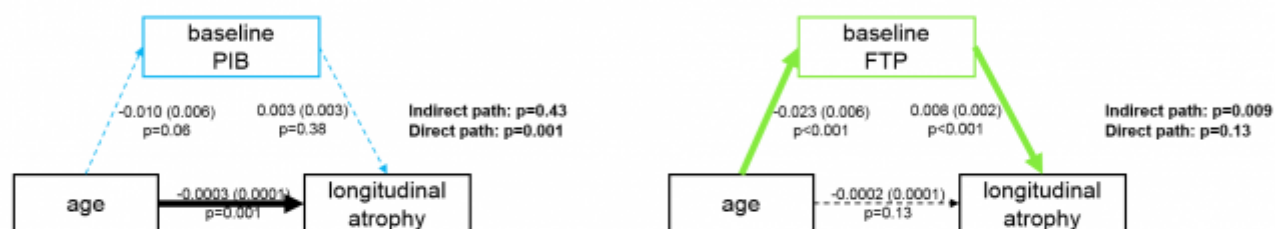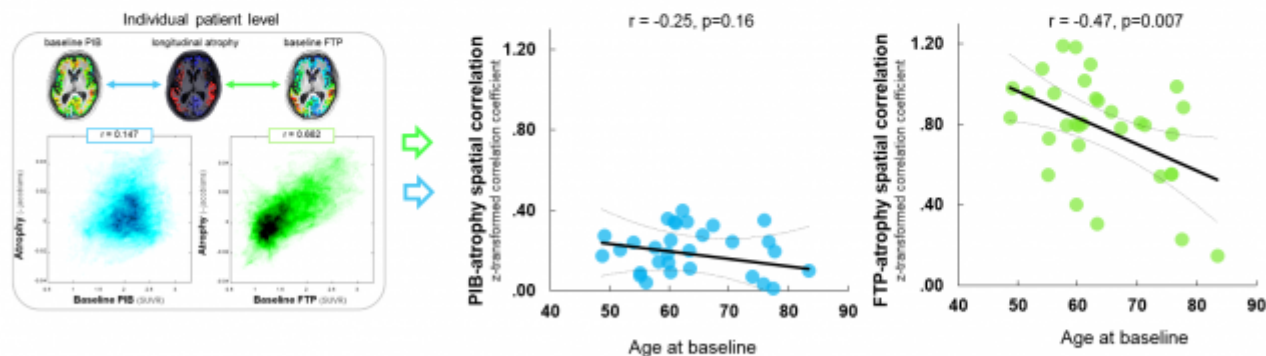
Figure 3. Associations between patient age and imaging findings.

A. Associations between age at baseline and i) baseline amyloid (global cortical PIB-SUVR, left), ii) baseline tau (global cortical FTP-SUVR, middle) and iii) longitudinal atrophy rates across patients. Younger patients had more abnormal findings across modalities although it was only a statistical trend for PIB.

B. Mediation analyses conducted based on variables from panel A. baseline cortical FTP significantly mediated the association between age and longitudinal atrophy, while PIB did not.

C. The spatial similarity between baseline tau and longitudinal atrophy maps (same as figure 2B) negatively correlated with age. The spatial correlation between baseline PIB and longitudinal atrophy was low regardless of patient age.

Epidemic spreading of tau through human functional brain connections

Jacob Vogel[1], Yasser Iturria-Medina[1], Olof Strandberg[2], Ruben Smith[2], Alan Evans[1], Oskar Hansson[2,3]

[1]*Montreal Neurological Institute, McGill University, Montreal, QC, Canada*
[2]*Clinical Memory Research Unit, Lund University, Lund, Sweden*
[3]*Memory Clinic, Skåne University Hospital, Lund, Sweden*

Animal studies have provided strong evidence for the propagation of neurofibrillary tau tangles through connected neurons. Here, we test the theory of tau spreading through communicating neurons in humans by placing a seed in the entorhinal cortex and allowing it to diffuse naturally through the human connectome, and comparing the predicted pattern of tau to observed regional tau load in living humans.

AV1451-PET scans from 175 cognitively intact individuals (69 amyloid-positive), 57 amyloid-positive individuals with mild cognitive impairment and 58 amyloid-positive individuals with suspected Alzheimer's dementia were aggregated from two multicenter studies and processed using a standard pipeline. Mean native-space AV1451 signal was extracted within 66 cortical ROIs from the Desikan-Killiany atlas, and these values were converted to tau-positive probabilities using regional mixture-modeling. A previously described Epidemic Spreading diffusion model (ESM) was fit to each individual's AV1451-PET data, where free parameters related to subject-specific age-at-onset, clearance rate and production rate were solved through simulation. The ESM was fit over resting-state functional connections extracted from 74 healthy young individuals; and separately over Euclidian distances between ROIs. Each model was fit specifying the bilateral entorhinal cortex as the epicenter of spread. ROI-level AV45 data was downloaded for ADNI subjects and converted to positivity-probabilities.

Threshold-free conversion of tau-PET data to tau-positivity probabilities resulted in a sparse and ordered distribution resembling previously described pathological spread and staging patterns (Figure 1). The ESM fitted over the functional connectome predicted 56% of the variance in whole-brain tau-PET pattern, whereas the Euclidian distance matrix explained only 22% (Figure 2A, 3). Furthermore, regions with higher amyloid tended to be underestimated by the model ($p < 0.001$; Figure 2B-D).

Whole-brain connectivity predicts regional tau-PET patterns far better than spatial diffusion, but fails to explain the entire picture. Among other factors, amyloid appears to interact with connectivity to influence tau spreading patterns.
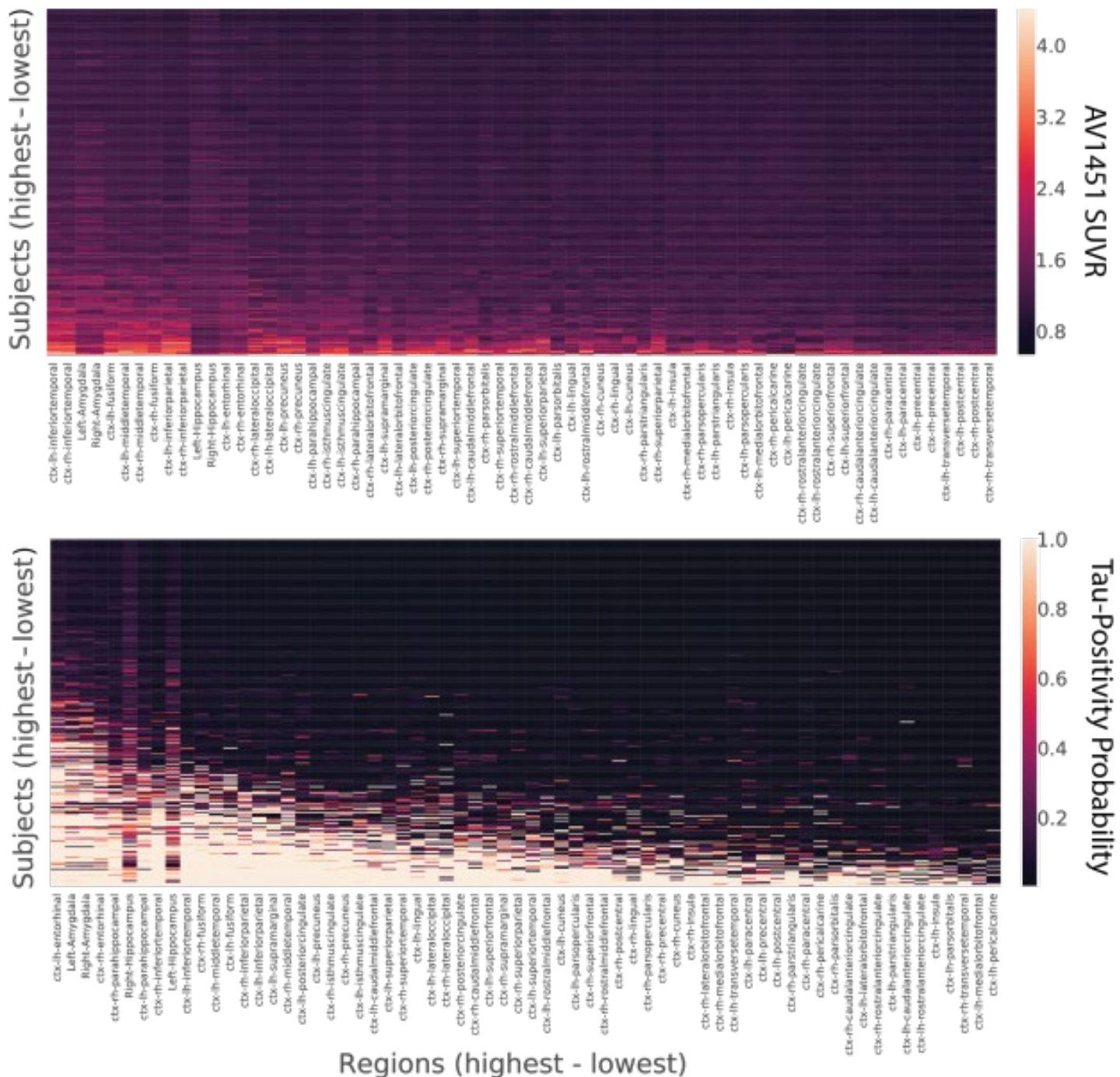
Figure 1: (Top) AV1451 SUVR values within each of the 66 ROIs (x-axis), for each of the 295 subjects (y-axis). Data is sorted to highlight a progression. (Bottom) The exact same data transformed using regional mixture modeling, and re-sorted based on the new values. Values represent the probability that a subject's SUVR falls on the rightmost of two guassian distributions within a given ROI. This transformation clearly improves both the sparsity of the data, as well as the ordering of the ROIs in the progression.
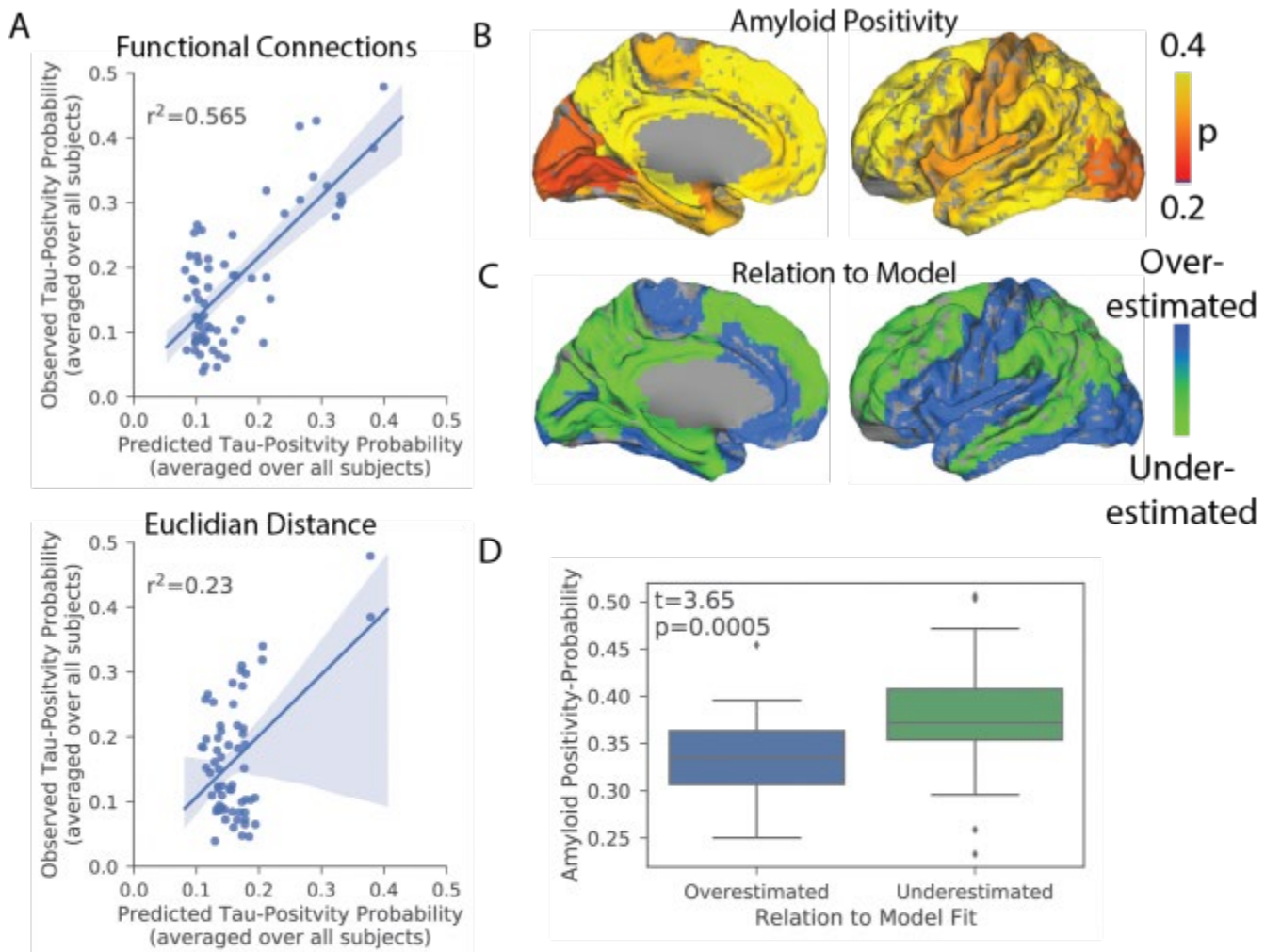
Figure 2: (A) Comparing the observed spatial pattern of tau with the pattern predicted by the ESM using a functional connectome (top) and euclidian distance matrix (bottom). Each dot represents the mean tau-positivity probability averaged over all subjects within a single ROI. (B) Average amyloid-positivity probability across all subjects for each ROI. (C) ROIs were classified as "Overestimated" (blue) or "Underestimated" (green) based on the sign of the residual, such that underestimated ROIs demonstrated more tau than predicted by the ESM. (D) Underestimated ROIs were more likely to demonstrate significant amyloid burden, suggesting amyloid may somehow impact either regional connectivity or tau propagation.
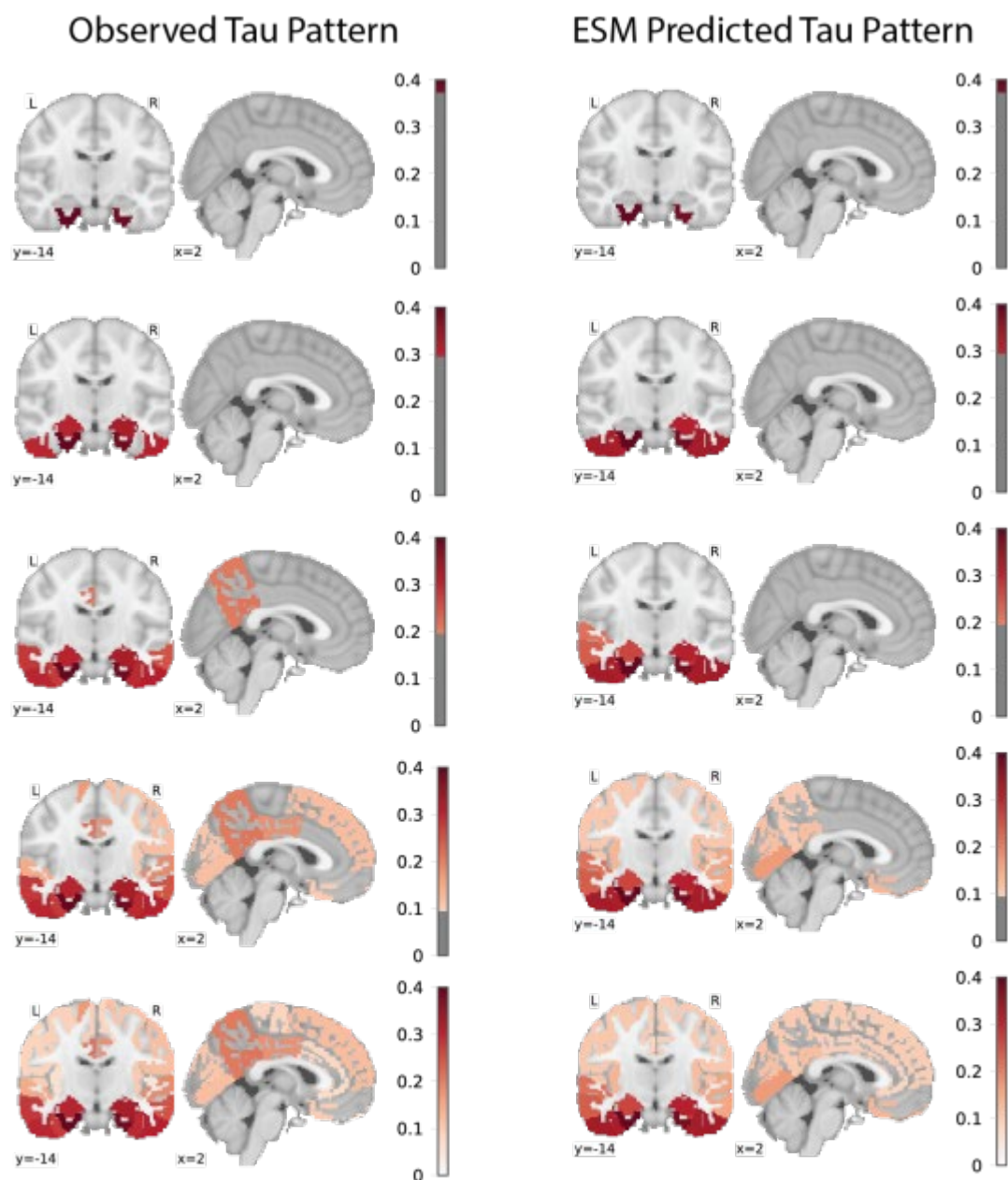
Figure 3: (Left) Average tau-positivity probability across all subjects for each ROI, thresholded at 0.38, 0.3, 0.2, 0.1 and 0. Regional values represent the probability that a subject in the dataset demonstrates positive AV1451 signal in this region. (Right) Regional tau-positivity probability predicted by the ESM.

Keywords: *Tau-PET, spread, connectivity, amyloid-PET, prediction*

Iaccarino, Leonardo

Spatial extent and topographical relationships between pathology accumulation and neurodegeneration in Alzheimer's disease

Leonardo Iaccarino[1], Daniel Schonhaut[1,2], Renaud La Joie[1,2], Rik Ossenkoppele[3], Alexandre Bejanin[1], Lauren Edwards[1], Gautam Tammewar[1], Julie Pham[1], Kiran Chaudhary[1], Mustafa Janabi[4], Suzanne Baker[4], Bruce Miller[1], William Jagust[2,4], Gil Rabinovici[1,2]

[1]*Memory and Aging Center, University of California San Francisco, San Francisco, CA, USA, San Francisco, CA, US*
[2]*Helen Wills Neuroscience Institute, University of California Berkeley, Berkeley, CA, USA, Berkeley, CA, US*
[3]*Department of Neurology & Alzheimer Center, Neuroscience Campus Amsterdam, VU University Medical Center, Amsterdam, the Netherlands, Amsterdam, The Netherlands*
[4]*Molecular Biophysics and Integrated Bioimaging Division, Lawrence Berkeley National Laboratory, Berkeley, CA, USA, Berkeley, CA, US*

Objective: To study the spatial extent and overlap of in vivo biomarkers of amyloid, tau deposition and neurodegeneration, investigating their relationships and variability within Alzheimer's Disease at both the group- and individual-levels.

Methods: Seventy-six amyloid-positive patients (age 64.9±9.6, N=39/76 Females, MMSE 21.79±5.72, CDR-sb 4.19±2.17) with a clinical diagnosis of AD or MCI due to AD and available ^{18}F-Flortaucipir (FTP), ^{11}C-PiB (PIB), ^{18}F-FDG (neurodegeneration/hypometabolism) PET and 3T MRI (neurodegeneration/atrophy) were included. W-score maps were created for each imaging-modality (thresholded W>1.65, p<0.05), adjusting for age, sex and Total Intracranial Volume (sMRI) based on amyloid-negative cognitively normal adults (PIB/FTP/MRI controls: N=46, age 71.3±19.2; FDG controls: N=40, age 73.8±15.8). FDG-PET and atrophy W-maps were combined into neurodegeneration maps (ND), with a voxel classified as ND+ when it was FDG+, MRI+, or both. Spatial extent was estimated as the proportion of **supra-**threshold voxels in the cortical gray matter for each imaging-modality or PIB±/FTP±/ND± combinations.

Results: Amyloid accumulation was the most diffuse (~90% of the GM involved, Figs. 1A-B), followed by tau (~71%) and neurodegeneration (~42%) (p<0.001 Friedman Test). At the individual patient level, the degree of spatial extent was PIB>FTP>ND in 75% of patients, followed by FTP>PIB>ND (15%) and PIB>ND>FTP (8%) (Fig. 2A). The inter-modality hierarchy of spatial extent was associated with age (p=0.004 Fisher Exact Test), with FTP>PIB>ND and PIB>ND>FTP being over-represented in youngest and oldest patients, respectively (Fig. 2B). Considering spatial overlap of imaging-modalities, at the group-level, the majority of supra-threshold voxels were PIB+/FTP+/ND+ (~34%), followed by PIB+/FTP+/ND- (~33%) and PIB+/FTP-/ND- (~19%), with other combinations showing small percentages (range 0-5%) (Fig. 3).

Discussion: Most patients showed the expected Amyloid>Tau>Neurodegeneration spatial hierarchy, but other variants exist. Signs of neurodegeneration almost always co-localize with combined amyloid-tau pathology, regardless of its severity, suggesting a synergistic neurotoxic effect and/or a shared regional vulnerability.
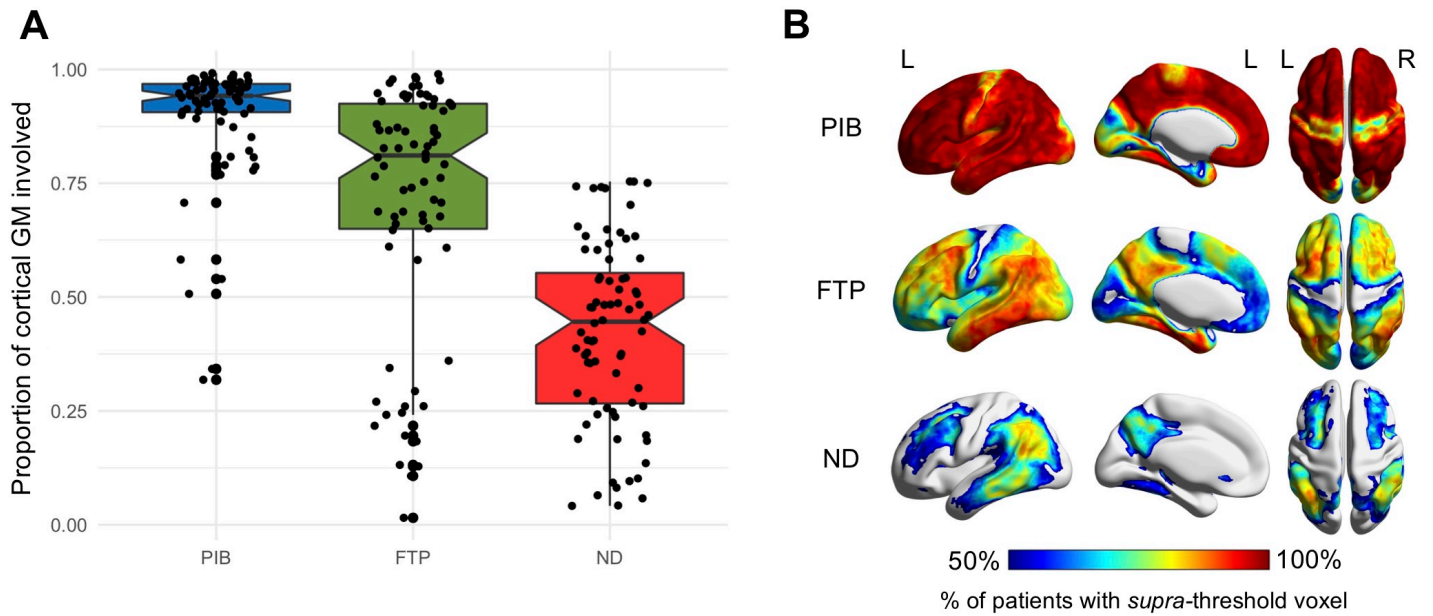
Figure 1: Spatial Extent and Voxel-wise frequency maps split by modality. **A)** Boxplots showing the distribution of spatial extent, in terms of proportion of cortical GM involved, for all the patients across modality. **B)** Three-dimensional surface renderings showing the percentage of patients with supra-threshold voxel values, split by modality. The minimum for the color scale was arbitrarily set to significant in at least half of the sample (>50%).
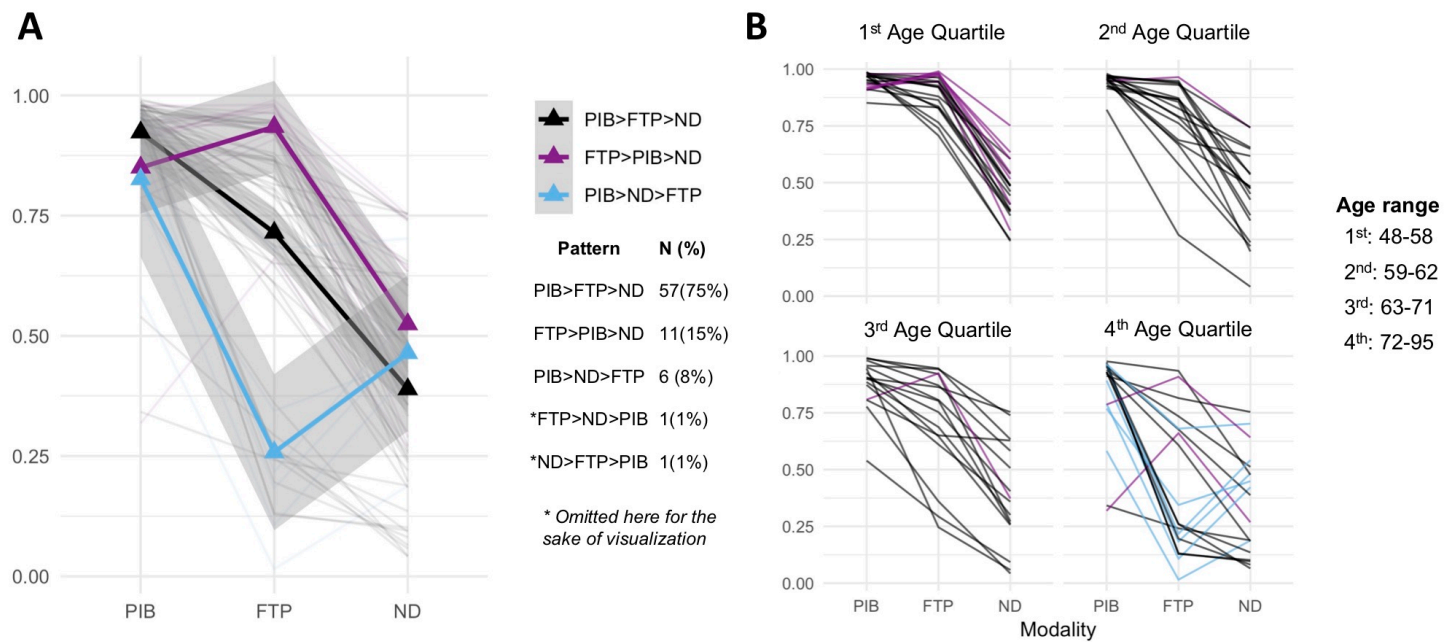

Figure 2: Multimodal degrees of biomarkers spatial extent. **A)** Spaghetti-plot showing average trend for the three most common spatial extent size inter-modality hierarchies. Triangles indicate the average values with the shaded area indicating confidence interval. The lines for FTP>ND>PIB and ND>FTP>PIB were omitted since they were shown by only 1 subject. **B)** Spaghetti-plots divided according to age quartiles. Age ranges in the different quartiles are indicated on the right.
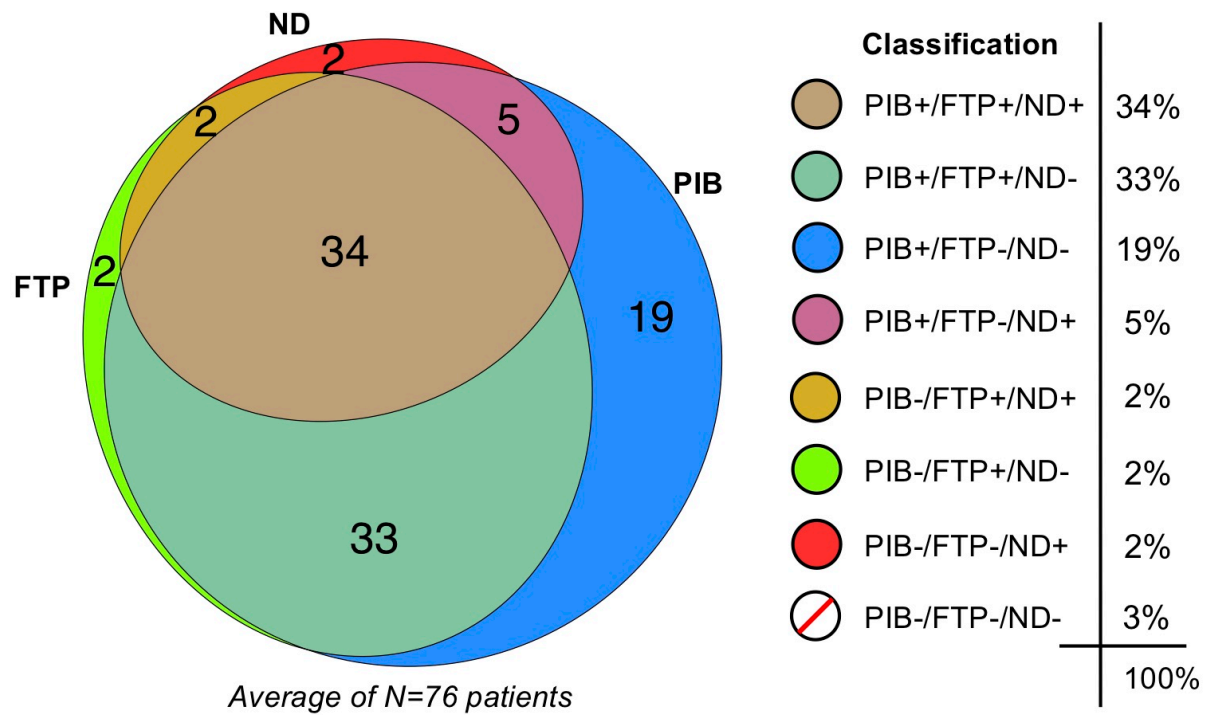
Figure 3: Group-level voxel-wise overlap of biomarker abnormalities. Venn Diagram showing the voxel-wise combinations of each imaging-modality biomarker positivity, using a PIB±/FTP±/ND± classification system. Data represent average at the whole-group level.

Functional connectivity associated with tau levels in aging, Alzheimer's, and small-vessel disease

Nicolai Franzmeier[1], Anna Rubinski[1], Julia Neitzel[1], Yeshin Kim[2,3,4], Alexander Damm[1], Duk Na[2,4], Hee Jin Kim[2,4], Chul Hyoung Lyoo[5], Hana Cho[5], Sofia Finsterwalder[1], Marco Duering[1], Sang Won Seo[2,4,7,8], Michael Ewers[1]

[1]*Institute for Stroke and Dementia Research, Klinikum der Universität München, Ludwig-Maximilians-Universität LMU, Munich, Germany*
[2]*Department of Neurology, Samsung Medical Center, Sungkyunkwan University School of Medicine, Seoul, Korea*
[3]*Department of Neurology, Kangwon National University Hospital, Kangwon National University College of Medicine, Chuncheon, Chuncheon, Korea*
[4]*Neuroscience Center, Samsung Medical Center, Seoul, Korea*
[5]*Department of Neurology, Gangnam Severance Hospital, Yonsei University College of Medicine, Seoul, Korea*
[6]*Department of Health Sciences and Technology, Samsung Advanced Institute of Health Sciences and Technology, Sungkyunkwan University, Seoul, Korea*
[7]*Department of Clinical Research Design and Evaluation, Samsung Advanced Institute of Health Sciences and Technology, Sungkyunkwan University, Seoul, Korea*
[8]*Center for Imaging of Neurodegenerative Diseases, University of California, San Francisco, San Francisco, CA, US*
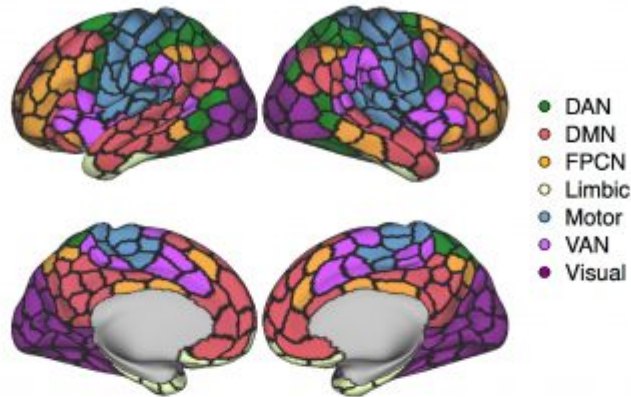
Background: Tau pathology is a core feature of AD but is also found enhanced in vascular cognitive impairment (VCI). Studies in AD and VCI showed a hierarchical tau-distribution, suggesting network-like tau-spreading across clinical conditions. **In-vitro** findings indicate that tau-spreading is enhanced by neural activity, raising the question whether functional brain architecture predicts tau patterns **in-vivo**. To address this, we assessed whether inter-regional resting-state fMRI connectivity is associated with AV1451 tau-PET covariance. Secondly, we tested whether connectivity of tau-hotspots, i.e. regions of earliest tau accumulation, predicts tau-levels in connected regions.

Methods: We included 55 cognitively normal amyloid-negative elderly (CN-Aβ-), 50 AD patients (i.e. amyloid-positive, preclinical to dementia), plus 36 patients with pure, amyloid-negative VCI. All subjects underwent AV1451 tau-PET and resting-state fMRI. Using a 400-ROI atlas (Fig. 1A), we computed for each group 400x400 whole-brain resting-state fMRI connectivity matrices (Fig. 2). To assess 400x400 spatial tau-covariance matrices (Fig 2), we extracted ROI-specific tau-PET-uptake and computed the across-subject correlations of tau-PET ROI-values (Fig. 1B). To assess the association between FC and tau, we computed the correlation between group-average connectivity and tau-covariance matrices. Second, we tested seed-based connectivity from tau-hotspots (regions with maximum tau-PET uptake) to the remaining 399 ROIs (targets) as a predictor of tau in target regions.

Results: Higher connectivity was associated with higher tau-covariance in corresponding ROIs in CN-Aβ-, AD and VCI (Fig. 3A-F). Higher connectivity of inferior-temporal tau-hotspots was predictive of tau-PET levels in functionally connected ROIs across all groups (Fig. 4A-C). Associations between connectivity and tau-covariance were independent of cognitive impairment, amyloid load or VCI severity.

Conclusions: Our findings suggest that higher inter-regional connectivity is associated with higher tau covariance, hence functional connectivity may contribute to the spreading pattern of tau. Amyloid and small-vessel disease burden may enhance overall tau levels, but do not determine spatial tau distribution.

A: 400 ROI Brain parcellation

- DAN
- DMN
- FPCN
- Limbic
- Motor
- VAN
- Visual

B: Tau covariance assessment

Tau-PET data

Subject 1

B1: Parcellate in 400 ROIs

B2: Vectorize ROI values

B3: Correlate all possible pairs of ROIs$_{i \, to \, j}$ across subjects to obtain 400x400 tau covariance matrix

| 1.2 | 1.5 | 1.9 | 0.9 | 1.1 | 1.5 | 1.7 | 2.1 | 1.8 | 1.4 | 1.0 | ... |

Subject 2

| 1.1 | 1.2 | 1.4 | 1.1 | 1.3 | 1.2 | 1.5 | 1.9 | 2.1 | 1.7 | 1.6 | ... |

Subject N

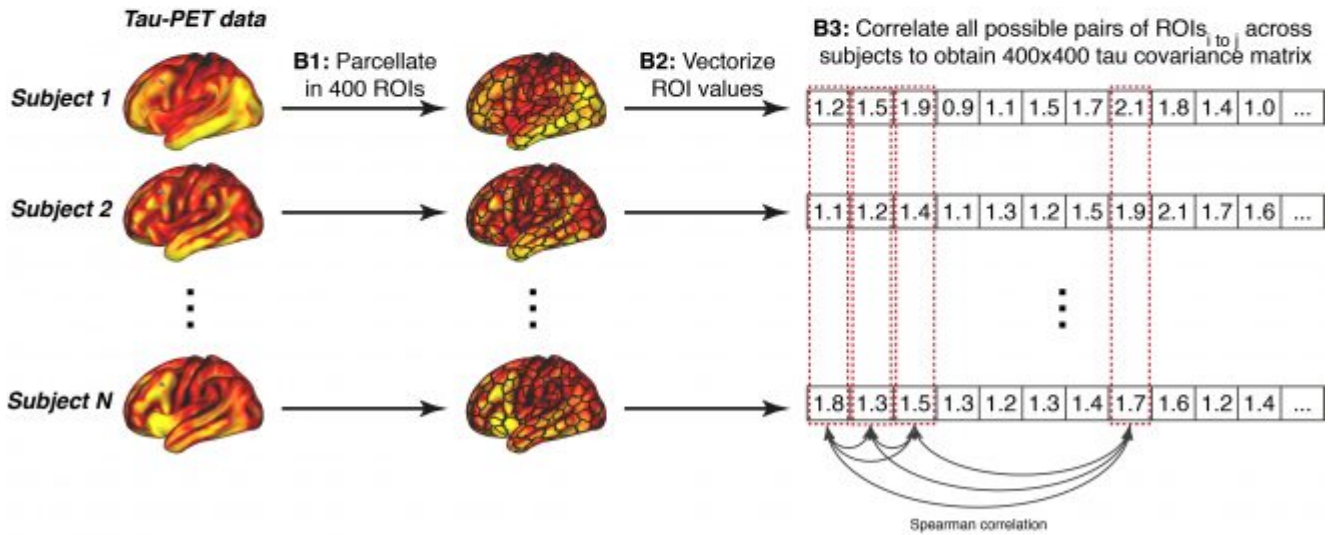| 1.8 | 1.3 | 1.5 | 1.3 | 1.2 | 1.3 | 1.4 | 1.7 | 1.6 | 1.2 | 1.4 | ... |

Spearman correlation

Figure 1: (A) Brain parcellation scheme(Schaefer et al., 2017) that was used for parcellating tau-PET and fMRI data. (B) Flow-Chart of the tau covariance analysis. (B1) Individual tau-PET scans are parcellated into 400 ROIs for each individual and (B2) mean ROI values are subsequently vectorized. Across subject tau values within a given ROI are correlated with all other ROIs using spearman-correlation (B3) to obtain a 400x400 tau covariance matrix. DAN=Dorsal Attention Network, DMN=Default-Mode Network, FPCN=Fronto-Parietal Control Network, VAN=Ventral Attention Network.

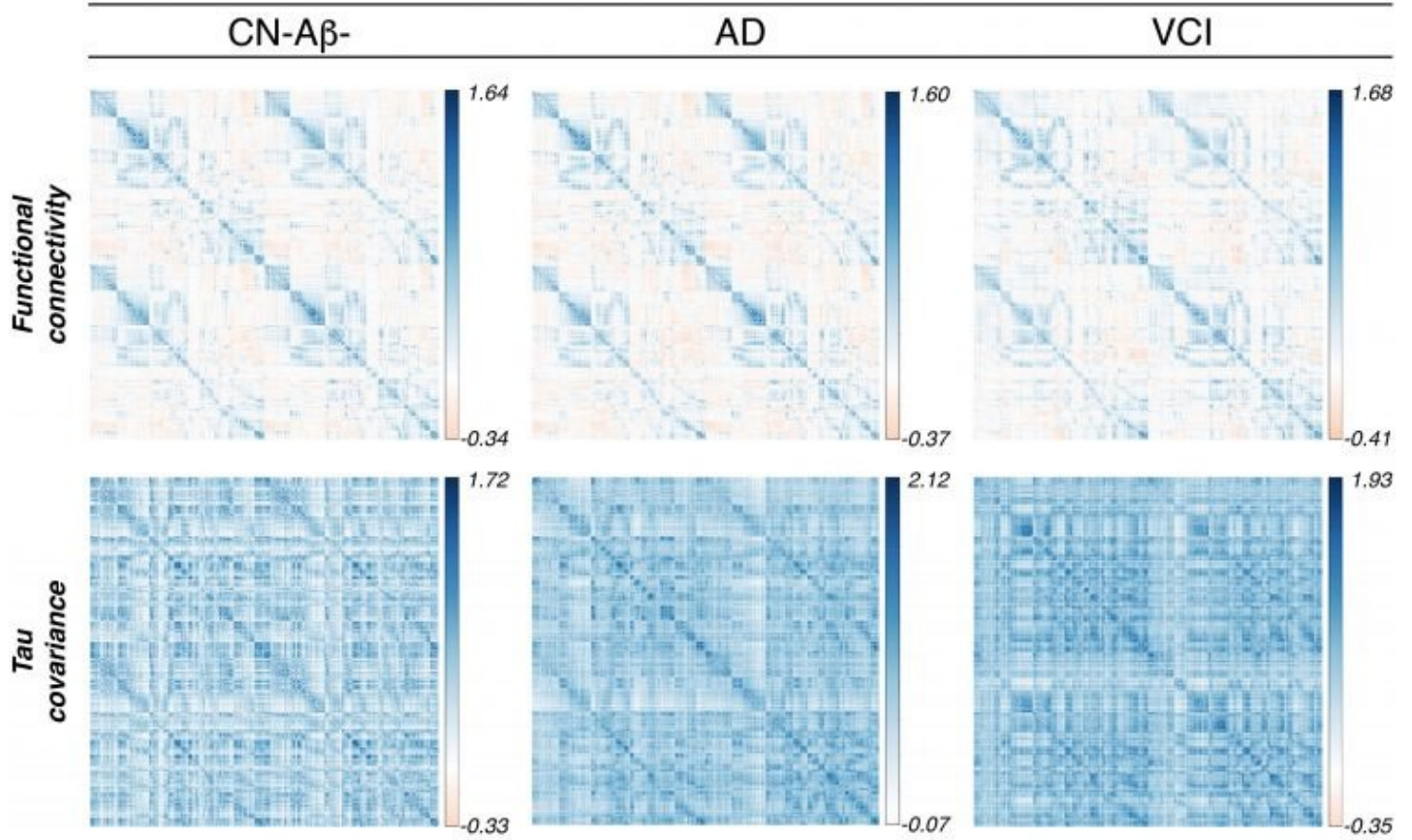# Group-mean functional connectivity and tau covariance

	CN-Aβ-	AD	VCI

Figure 2: Group mean functional connectivity and tau covariance matrices.

Functional connectivity associated with tau covariance

CN-Aβ-	AD	VCI

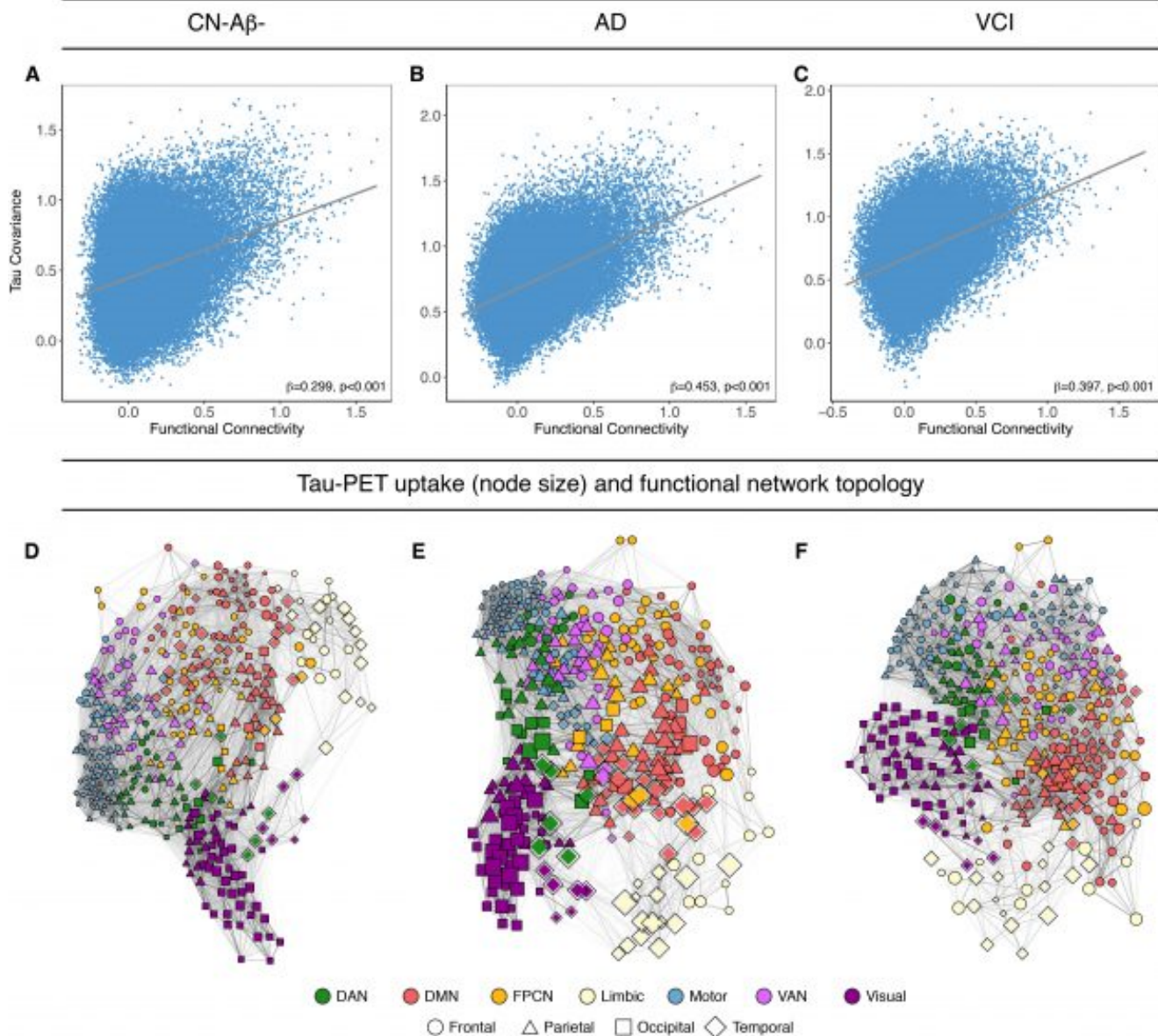## Tau-PET uptake (node size) and functional network topology

Figure 3: Scatterplots showing the associations between tau and FC for CN-Aβ- (A), AD (B) and VCI groups (C). Scatterplots are based on group-average data, significance for all analyses was determined using linear regression repeated on 1000 bootstrapped samples on which group-average FC and tau covariance were iteratively determined. (D-F) Force-directed graphs illustrating the association between functional network topology (node distance), tau-PET uptake (node size) and anatomical location (node symbol). Node proximity is defined based on the Fruchtermann-Reingold algorithm applied to group-average FC strength. DAN=Dorsal Attention Network, DMN=Default-Mode Network, FPCN=Fronto-Parietal Control Network, VAN=Ventral Attention Network

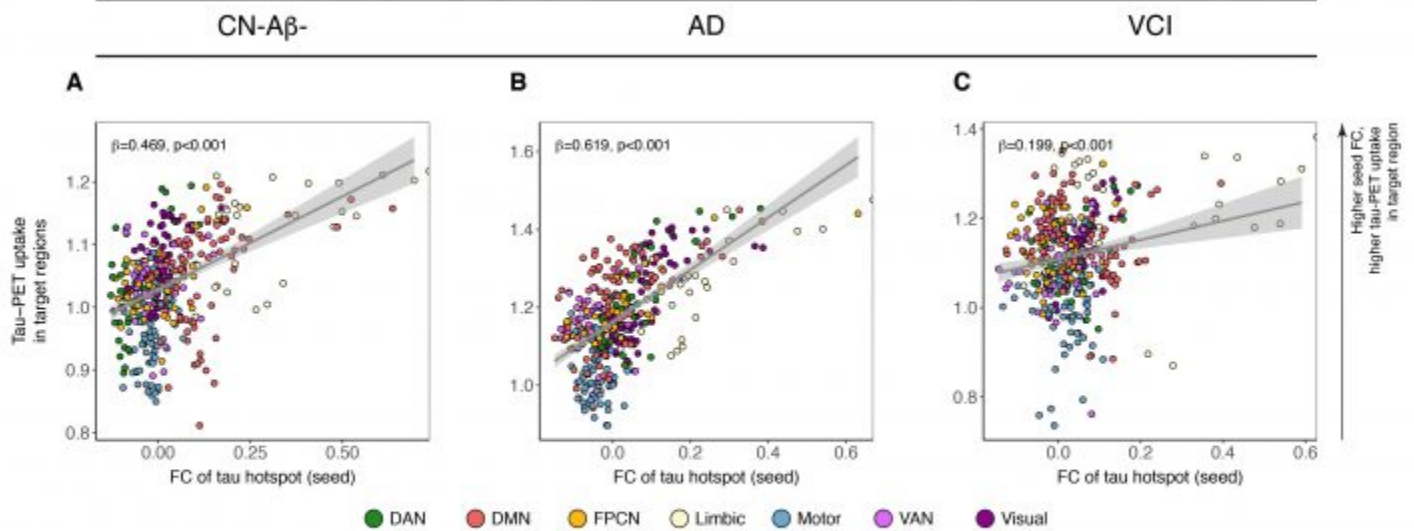## Functional connectivity associated with tau-PET uptake

Figure 4: (A-C) Relationship between seed FC of a tau-hotspot ROI (x-axis) and tau-PET uptake in the respective target regions (y-axis). Scatterplots are based on group-average FC or tau-PET uptake, significance for all analyses was determined using linear regression repeated on 1000 bootstrapped samples on which group-average FC and group-average tau-PET uptake were iteratively determined.

Associations between longitudinal Aβ and cross-sectional tau in adults with Down syndrome

Dana Tudorascu[1], Mattew Zammit[2], Karly Kody[2], Charles Laymon[1], Davneet Minhas[1], Paul Ellison[2], Shahid Zaman[3], Sterling Johnson[2], Chester Mathis[1], William Klunk[1], Ben Handen[1], Brad Christian[2], Ann Cohen[1]

[1]*University of Pittsburgh, Pittsburgh, PA, US*
[2]*University of Wisconsin, Madison, WI, US*
[3]*University of Cambridge, Cambridge, UK*

Table 1:

Region	Spearman's Correlation (95% CI)
Braak 1	0.03 (-0.25, 0.31)
Braak 2	0.13 (-0.15, 0.41)
Braak 3	0.15 (-0.14, 0.42)
Braak 4	0.20 (-0.09, 0.46)
Braak 5	**0.34 (0.06, 0.57)**
Braak 6	**0.32 (0.02, 0.55)**

Data is presented as Spearman's correlation estimates and 95% CI (SUVRs).
Significant associations are shown in bold.

Individual trajectories of Global PiB over time
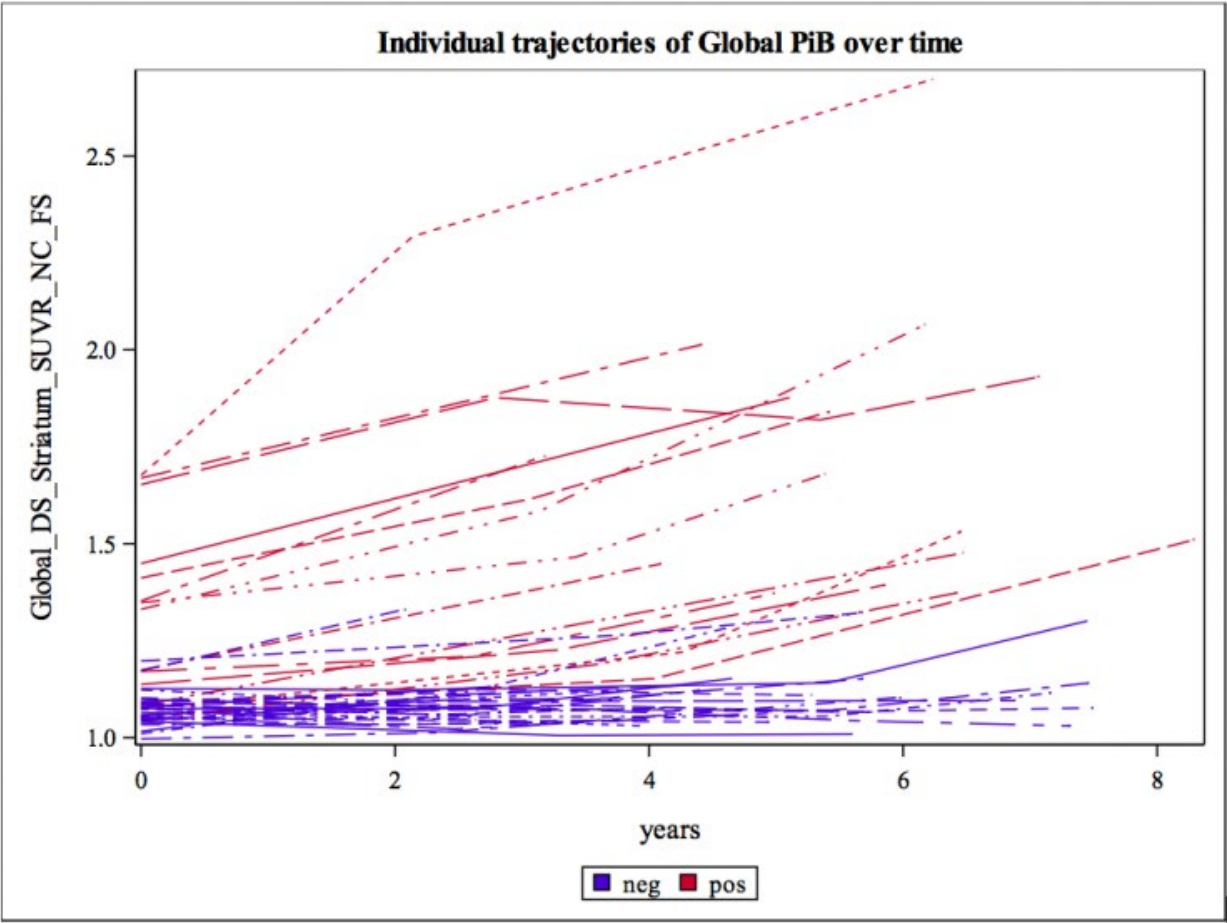
Introduction: Adults with Down syndrome (DS) are uniformly affected by AD pathology by their 30's and have a 70-80% chance of clinical dementia by their 60's. The present study used a non-parametric regression model to explore the associations between longitudinal rates of amyloid accumulation and the cross-sectional tau burden in adults with DS.

Methods: Forty-five participants (age=39.19±8.44) with multiple [11C]PiB scans over a period of 8 years and one [18F]AV-1451 scan were analyzed. FreeSurfer (v5.3.0) was used for the definition of ROIs. A two-stage analysis was performed: 1) a linear mixed model was applied to estimate the rates of change for global PiB over time and 2) the PiB estimated amyloid rates from the trajectories were used as predictors of interest in a non-parametric regression with AV-1451 for each Braak-associated (1-6) region as the outcome. Non-parametric regression was used for the second stage analysis due to presence of outlier observations in our AV-1451 data.

Results: Statistically significant associations were found between Braak regions at alpha=0.05 between PiB estimated amyloid trajectories and AV-1451 for Braak region 5 (r=0. 34, 95% CI (0.06, 0.57)) and Braak region 6 (r=0.32, 95% CI (0.02, 0.55)). All non-parametric correlations are presented in Table 1 along with the corresponding 95% CI. Figure 1 shows individual trajectory plots for PiB global SUVR over time by Aβ positivity that were used in our first stage model.

Discussion: For this DS population, we found that higher rates of accumulating amyloid pathology is associated with increased tau pathology in regions associated with higher Braak stages. As it can be seen from Table 1 the correlations are increasing from almost no correlation between PiB trajectories and AV-1451 SUVR for Braak region 1 to a 0.34 and 0.32 (medium effect size correlations) respectively for Braak 5 and Braak 6 regions.

Friday, January 18, 2019 - 05:05 pm - 06:20 pm

Podium Session

Session 9: Clinical Applications

CHAIRS: Gil Rabinovici, Pedro Rosa-Neto

05:05 pm - 06:20 pm	Session 9: Clinical Applications	CHAIRS: **Pedro Rosa-Neto**, McGill University, Montreal, QC, Canada **Gil Rabinovici**, University of California, San Francisco, CA, US	Page
5:05	Tau PET imaging with 18F-PI2620 in aging and neurodegenerative diseases	**Elizabeth Mormino**, Stanford University, Palo Alto, CA, US	483
5:20	In vivo distribution pattern of 18F-PM-PBB3 (18F-APN-1607) and its relationship with clinical features in diverse 4-repeat tauopathies	**Hitoshi Shimada**, National Institute of Radiological Sciences, National Institutes for Quantum and Radiological Science and Technology, Chiba, Japan	484
5:35	Tau imaging with 18F-MK6240 in Alzheimer's disease and in past traumatic brain injury	**Christopher Rowe**, Austin Health, Melbourne, Australia	485
5:50	[18F]-AV-1451 binding profile in early and late-onset Alzheimer's disease and suspected non-Alzheimer's pathophysiology	**Eddie Stage**, Indiana University School of Medicine, Indianapolis, IN, US	487
6:05	Towards a topographic imaging biomarker of TDP-43 pathology in amnestic dementia: patient stratification based on FDG-PET patterns in autopsy-confirmed cases	**Michel Grothe**, German Center for Neurodegenerative Diseases (DZNE) - Rostock, Germany	490
06:20 pm - 06:50 pm	Discussion		

Tau PET imaging with 18F-PI2620 in aging and neurodegenerative diseases

<u>Elizabeth Mormino</u>[1], Ayesha Nadiadwala[1], Carmen Azevedo[1], Wanjia Guo[1], Tyler Toueg[1], Jessa Castillo[1], Jacob Hall[1], Alexandra Trelle[1], Sharon Sha[1], Marc Harrison[1], Gayle Deutsch[1], Carolyn Fredericks[1], Michael Greicius[1], Guido Davidzon[1], Michelle James[1], Greg Zaharchuk[1], Anthony Wagner[1], Frederick Chin[1]

[1]*Stanford University, Palo Alto, CA, US*

Background: Measurement of the spatial distribution of Tau pathology is critical for early diagnosis and disease monitoring. We sought to investigate a novel Tau PET ligand, ^{18}F-PI2620, in aging and throughout the spectrum of Alzheimer's disease (AD).

Methods: Twenty-seven participants underwent Tau PET scanning with ^{18}F-PI2620 on a GE PET-MRI scanner: 15 older clinically normal (CN) individuals (age range=61-84), 3 Mild Cognitive Impairment (MCI, age range=68-77), and 5 AD dementia (age range=57-81), as well as 1 Amyloid-negative Dementia with Lewy Bodies patient (Age=61), 1 Semantic Variant Primary Progressive Aphasia (svPPA, Age=78), 1 Primary Progressive Palsy (PSP, Age=71), and 1 Corticobasal Syndrome (CBS, Age=76). Standardized uptake value ratios were computed 60-90 minutes post-injection and normalized to the inferior cerebellum, and compared across diagnostic categories. Regional group differences between CN and patients with MCI/AD were assessed with Wilcoxon signed-rank tests, whereas associations between continuous CSF measures (Aβ42 and pTau) with regional Tau within the CN group were assessed with Spearman's Rank correlation coefficients.

Results: The MCI/AD group showed elevated Tau in all regions compared to CN (p-values<0.05). Within the CN group, continuous levels of CSF Aβ42 were negatively associated with elevated Tau PET in medial temporal lobe regions (p-values<0.05). CSF pTau was not related to any regional Tau PET value. Qualitative examination across non-AD neurodegenerative disorders showed low uptake in Amyloid-negative DLB, PSP, and CBS, with focal uptake in the anterior temporal pole evident for svPPA.

Conclusions: Preliminary results suggest strong differences in cortical uptake of ^{18}F-PI2620 in patients along the AD trajectory compared to older CN. Amyloid-related differences among the CN group were detected in medial temporal lobe regions. This work suggests that ^{18}F-PI2620 detects Tau aggregation throughout the course of AD.

Keywords: Tau PET, normal aging, AD

In vivo distribution pattern of 18F-PM-PBB3 (18F-APN-1607) and its relationship with clinical features in diverse 4-repeat tauopathies

Hitoshi Shimada[1], Kenji Tagai[1], Manabu Kubota[1], Keisuke Takahata[1], Yuhei Takado[1], Hitoshi Shinotoh[1,2], Naoyoshi Yamamoto[1], Yasunori Sano[1], Chie Seki[1], Shigeki Hirano[1,3], Yasuyuki Kimura[1,4], Masanori Ichise[1], Maiko Ono[1], Paul Tempest[5], Ming-Kuei Jang[5], John Seibyl[6], Olivier Barret[6], David Alagille[6], Kenneth Mareck[6], Naruhiko Sahara[1], Kazunori Kawamura[1], Ming-Rong Zhang[1], Nobutaka Hattori[7], Satoshi Kuwabara[3], Tetsuya Suhara[1], Makoto Higuchi[1]

[1]*National Institute of Radiological Sciences, National Institutes for Quantum and Radiological Science and Technology, Chiba, Japan*
[2]*Neurology Clinic Chiba, Chiba, Japan*
[3]*Department of Neurology, Chiba University Graduate School of Medicine, Chiba, Japan*
[4]*National Center for Geriatrics and Gerontology, Obu, Japan*
[5]*APRINOIA Therapeutics Incorporated, Taipei, Taiwan*
[6]*Molecular Neuroimaging, A Division of inviCRO, New Haven, CT, US*
[7]*Department of Neurology, Juntendo University Graduate School of Medicine, Bunkyo, Japan*

Objectives: Our previous examinations demonstrated that PET with ^{18}F-PM-PBB3 (^{18}F-APN-1607) shows a characteristic distribution pattern in patients with 4-repeat tauopathies such as progressive supranuclear palsy (PSP) and corticobasal syndrome (CBS), which is distinct from that observed in Alzheimer's disease (AD). The present study aimed to investigate the association between ^{18}F-PM-PBB3 uptake and clinical features in patients with clinically diagnosed 4-repeat tauopathies.

Methods: 19 patients with 4-repeat tauopathies, including PSP with Richardson syndrome (PSP-RS), PSP with progressive gait freezing (PSP-PGF), PSP with predominant parkinsonism (PSP-P), PSP with predominant frontal presentation (PSP-F), PSP with ocular motor dysfunction (PSP-OM), PSP with predominant cerebellar ataxia (PSP-C), CBS-progressive non-fluent aphasia (CBS-PNFA), and biopsy-confirmed corticobasal degeneration (CBD) were recruited. Seven AD spectrum patients and 29 cognitively healthy controls (HCs) were also enrolled. All participants underwent PET scans with ^{18}F-PM-PBB3 and ^{11}C-PiB for estimating regional tau and Aβ deposition. Parametric ^{18}F-PM-PBB3- and ^{11}C-PiB- images were generated by voxel-based calculation of the standardized uptake value ratio (SUVR) to the cerebellar cortex.

Results: PiB-negative patients with 4-repeat tauopathies showed remarkable uptake of PM-PBB3 especially around subthalamic nucleus, basal ganglia, midbrain including nigra and red nucleus, and dentate nucleus. Compared with PSP-RS, patients with PSP-OM, PSP-PGF and CBS/CBD showed relatively milder PM-PBB3 uptake especially around the midbrain. In contrast, patients with 4-repeat tauopathies having verbal and/or behavioral symptoms also presented elevated PM-PBB3 uptake in some cortices as well as the above-mentioned regions. Patients with 4-repeat tauopathies were easily differentiated from AD spectrum patients as well as HCs both by visual assessment and quantitative comparison of SUVR values in certain brain regions.

Conclusions: Accumulations of PM-PBB3 may reflect characteristic distributions of tau pathologies in 4-repeat tauopathies, in conjunction with clinical manifestations. The present study provides further evidence for the potential utility of ^{18}F-PM-PBB3 PET in tracking 4-repeat tau pathologies.

Tau imaging with 18F-MK6240 in Alzheimer's disease and in past traumatic brain injury

Christopher Rowe[1], Vincent Dore[1,3], Amelia Hicks[4], Jennie Ponsford[4], Rachel Mulligan[1], Rodney Guzman[1], Regan Tyrell[1], Fiona Lamb[1], Pierrick Bourgeat[3], Tia Cummins[1], Jurgen Fripp[3], Victor Villemagne[1,2]

[1]*Department of Molecular Imaging & Therapy, Austin Health, Melbourne, Australia*
[2]*Florey Department, The University of Melbourne, Melbourne, Australia*
[3]*CSIRO e-Health Research Centre, Brisbane, Australia*
[4]*School of Psychological Sciences, Monash University, Melbourne, Australia*

Background: We evaluated ^{18}F-MK6240 to measure 3R4R tau aggregate burden in the brain in Alzheimer's disease (AD) and non-demented persons with past Traumatic Brain Injury (TBI).

Methods: We examined 128 participants: 70 healthy elderly controls (HC, 17 Ab+), 8 mild cognitive impairment (MCI, 4 Ab+), 10 Ab+AD, 4 other dementia (OD, 1 Ab+) and 36 TBI several decades earlier (5 Ab+) due to single (MVA+VET) or repetitive (Sports) injuries. Mesial temporal and temporoparietal tracer binding was assessed using SUVR at 90-110 min post injection with cerebellar cortex as reference region. Cut-offs were set at two standard deviations above the mean binding in Ab- HC.

Findings: AD and MCI images showed high target to background with no off-target binding and limbic, neocortical or mixed distribution patterns. Nine of 10 Ab+AD (90%), 2 of 4 Ab+MCI (50%), 4 of 17 Ab+HC (24%) had high temporoparietal cortex ^{18}F-MK6240 binding (Fig 1). All Ab+MCI and more Ab+HC had high mesial temporal binding (Fig 2). With the exception of one Ab- HC and one Ab+TBI, temporoparietal tracer retention in Ab- HC, TBI and OD was low. Compared to Ab- HC, significantly higher SUVR was observed in Ab+HC in mesial temporal (0.95 ± 0.17vs.1.27 ± 0.42, $p=0.0014$), but not in temporoparietal cortex (1.01 ± 0.14vs.1.17 ± 0.39, $p=0.32$). Significantly higher SUVR was observed in Ab+AD compared to Ab- HC in mesial temporal (2.12 ± 0.95 vs. 0.95 ± 0.17, $p<0.0001$, Cohen's d=1.7), and temporoparietal cortex 2.85 ± 1.81 vs. 1.01 ± 0.13, $p<0.0001$, Cohen's d=1.4).

Interpretation: ^{18}F-MK6240 PET discriminates well between AD and HC. In keeping with other recent biomarker studies, we found no evidence of increased AD pathology in persons with a remote history of traumatic brain injury.
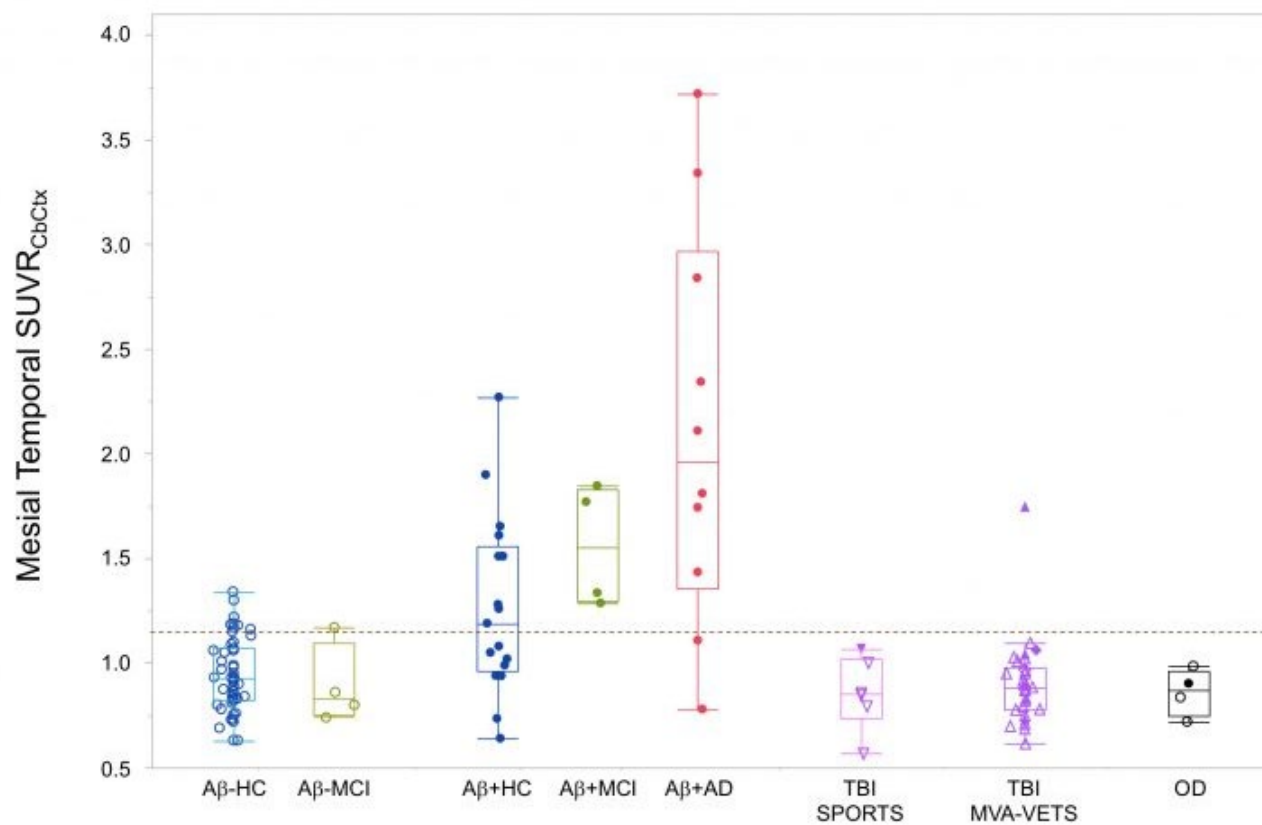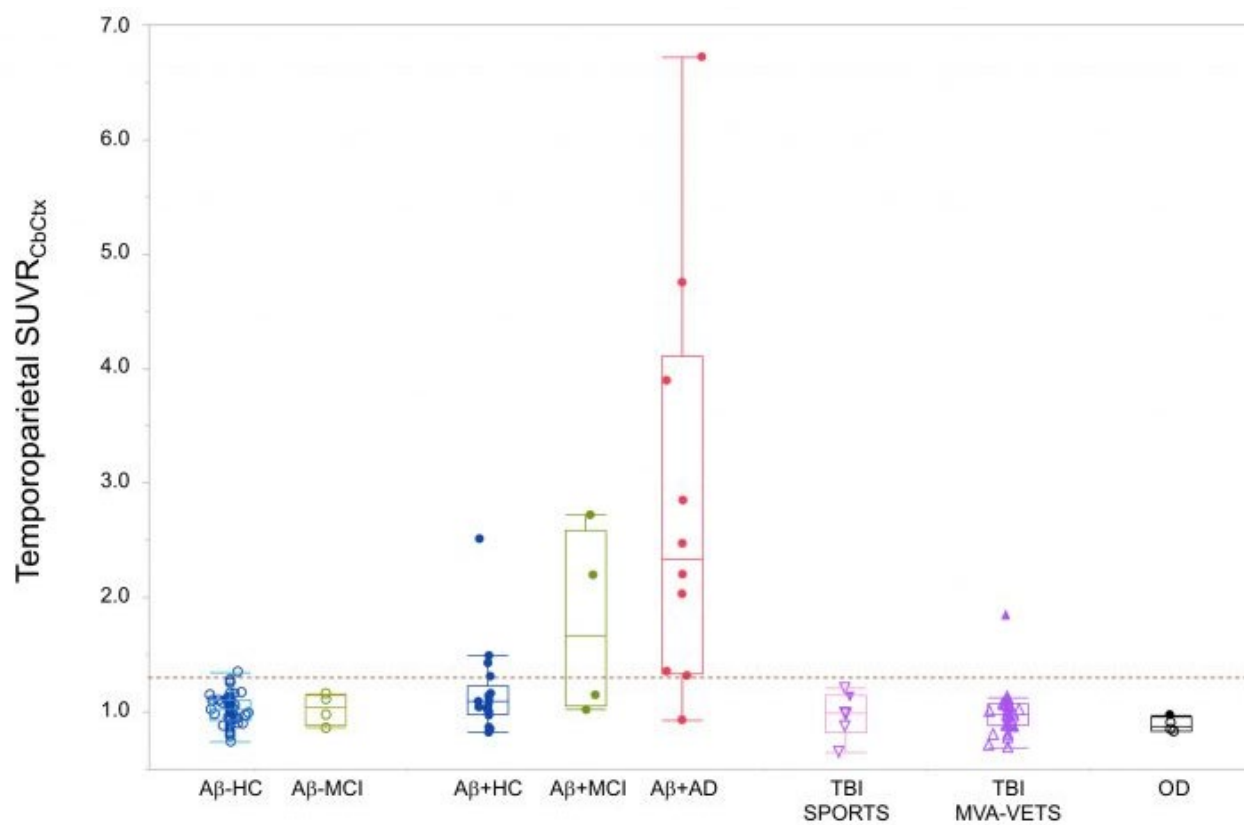
[18F]-AV-1451 binding profile in early and late-onset Alzheimer's disease and suspected non-Alzheimer's pathophysiology

Eddie Stage[1], Diana Svaldi[1], Meredith Phillips[1], Tugce Duran[1], Shannon Risacher[1], Andrew Saykin[1], Liana Apostolova[1]

[1]Indiana University School of Medicine, Indianapolis, IN, US

Objectives: Our objective was to compare [18F]-AV-1451 (Flortaucipir) scans on a voxel-wise basis in early-onset (EO) and late-onset (LO) cognitively impaired ADNI subjects, stratified by amyloid status, relative to cognitively normal controls (NC).

Methods: [18F]Flortaucipir scans from 187 amyloid-negative (Aβ-) NC, 14 Aβ+ EO (EOAD), 56 Aβ+ LO (LOAD), 44 Aβ- EO suspected non-Alzheimer's pathophysiology (EO-SNAP), and 42 Aβ- LO-SNAP subjects were downloaded and processed using standard techniques, with intensity normalization to the cerebellar crus to generate SUVR images. Aβ+ was defined as cortical [18F]-AV-45 SUVR$\geq$1.17 normalized to whole cerebellum. We generated statistical and effect-size maps of [18F]Flortaucipir SUVR between groups relative to NC using voxel-wise regression in SPM12 correcting for age, sex, and education.

Results: Demographic and amyloid burden comparisons can be seen in Table 1. Notably, diagnostic groups showed the expected significant difference in age and cognitive performance, as well as amyloid-PET SUVR ($p<0.001$). EOAD had the greatest tau burden, followed by LOAD and EO-SNAP (Figures 1 & 2). EOAD showed diffuse tau deposition throughout the cortex compared to NC. LOAD and EO-SNAP showed significantly more tau in the medial temporal, temporoparietal and posterior superior and middle frontal gyri than NC. LO-SNAP showed no significant clusters when compared to NC. β-coefficient maps (Figure 2) show the observed effect sizes for each comparison.

Conclusions: As expected, EOAD showed the greatest tau burden followed by LOAD. EO-SNAP showed medial temporal lobe uptake in the absence of significant amyloid burden indicating a trajectory for a non-AD neurodegenerative disorder.

Diagnostic Group (N)	NC (187)	EOAD (14)	LOAD (56)	EO-SNAP (44)	LO-SNAP (42)	p-value
Age, years mean (SD)	74.4 (7.4)	66.9 (6.4)	80.2 (5.6)	68.8 (4.9)	79.4 (5.7)	**<0.001**
Gender, Male %	57.2	50.0	35.7	38.6	38.1	**0.012**
Education, years mean (SD)	16.8 (2.4)	15.9 (2.2)	15.8 (2.7)	16.9 (2.6)	16.1 (3.0)	**0.029**
Global CDR, mean, (SD)	0.00 (0.00)	0.50 (0.00)	0.53 (0.11)	0.51 (0.08)	0.50 (0.00)	**<0.001**
MMSE, mean, (SD)	29.2 (1.0)	27.5 (2.4)	27.1 (2.4)	28.7 (1.3)	28.2 (1.8)	**<0.001**
SUVR, mean (SD)	1.03 (0.07)	1.43 (0.14)	1.42 (0.20)	1.02 (0.06)	0.98 (0.07)	**<0.001**

Table 1. Diagnostic group demographic table
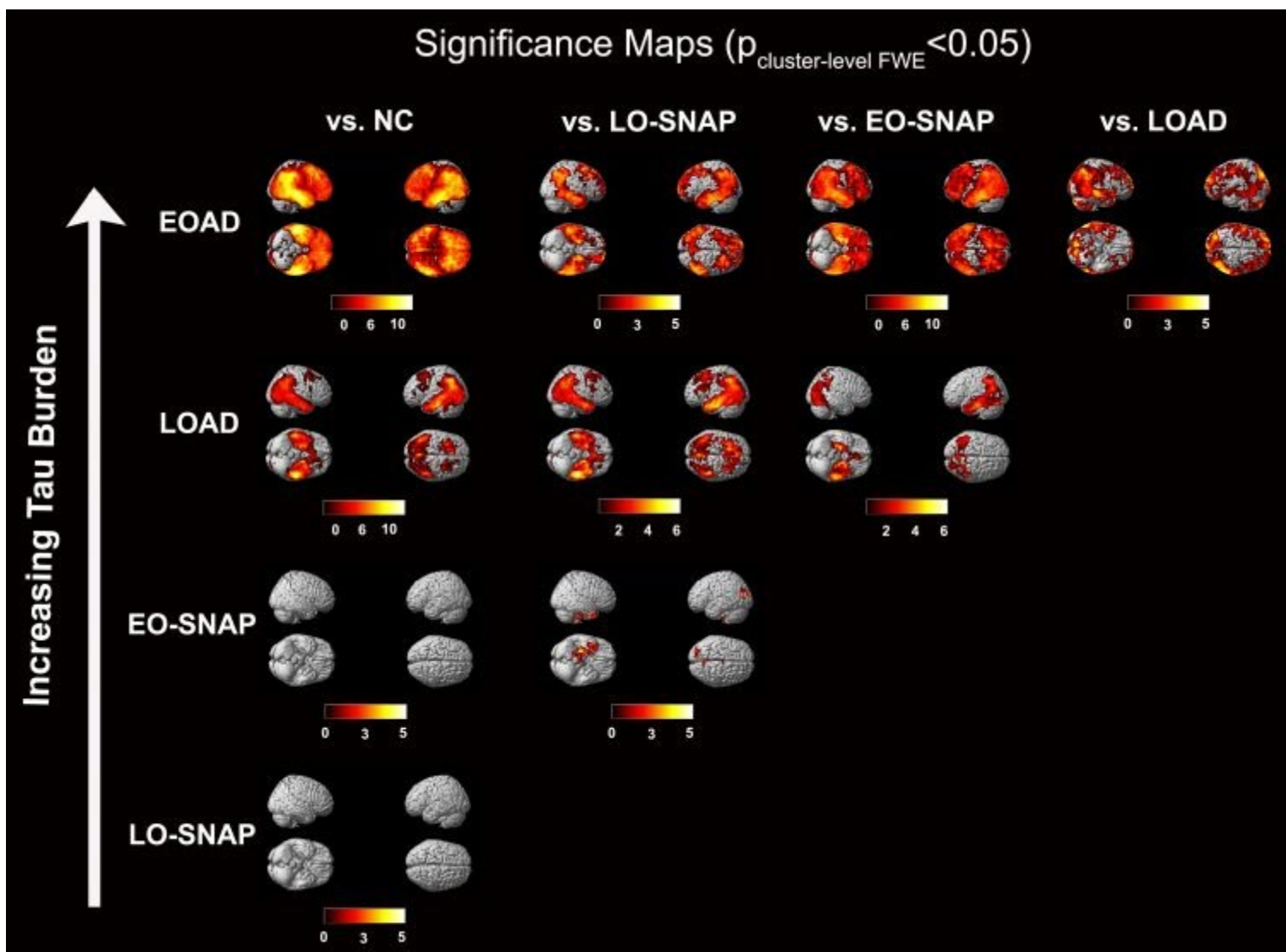
Figure 1. Statistical maps showing significant clusters of tau
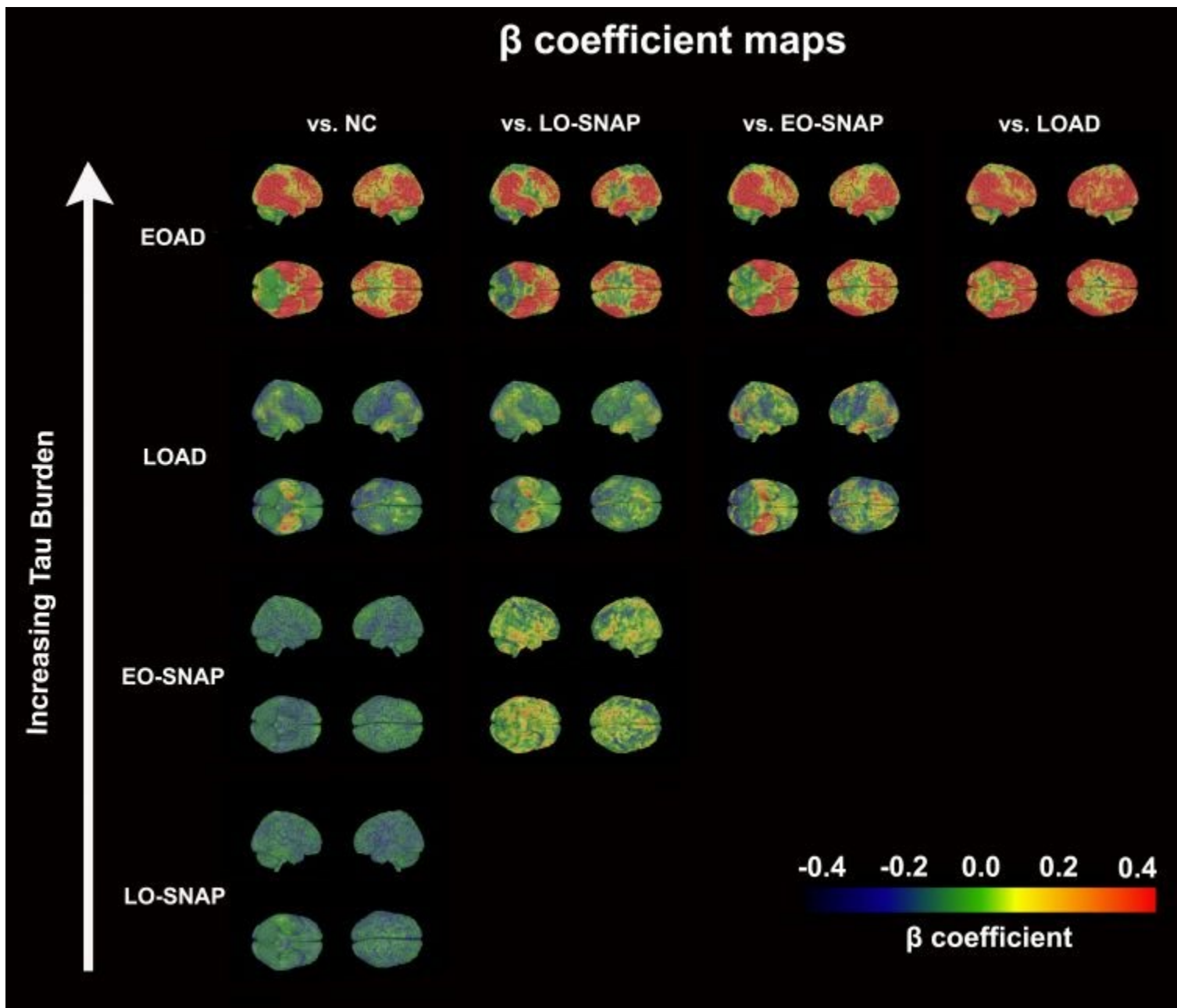
Figure 2. β-coefficient maps showing effect size of tau clusters

Towards a topographic imaging biomarker of TDP-43 pathology in amnestic dementia: patient stratification based on FDG-PET patterns in autopsy-confirmed cases

Michel Grothe[1], Catharina Lange[2], Kwangsik Nho[3], Andrew Saykin[3], Irina Jelistratova[1], Peter Nelson[4], Ralph Buchert[5], Stefan Teipel[1,6]

[1]*German Center for Neurodegenerative Diseases (DZNE) - Rostock, Germany*
[2]*Department of Nuclear Medicine, Charité – Universitätsmedizin Berlin, Berlin, Germany*
[3]*Department of Radiology and Imaging Sciences, Indiana University School of Medicine, Indianapolis, IN, US*
[4]*Sanders-Brown Center on Aging and Department of Pathology, University of Kentucky, Lexington, KY, US*
[5]*Department of Diagnostic and Interventional Radiology and Nuclear Medicine, University Medical Center Hamburg-Eppendorf, Hamburg, Germany*
[6]*Department of Psychosomatic Medicine, University of Rostock, Rostock, Germany*

Background: Limbic TDP-43 pathology is a frequent neuropathologic finding in advanced age that associates with hippocampal sclerosis (HS) and can result in amnestic deficits mimicking Alzheimer's disease (AD) dementia. Recent imaging-pathologic association studies suggest that TDP-43/HS is linked to a distinct neurodegeneration pattern that may be used to detect the condition in-vivo.

Methods: From the ADNI autopsy cohort we identified 41 patients with a clinical diagnosis of amnestic MCI or AD dementia at last clinical evaluation and availability of an FDG-PET scan. Six patients (15%) had limbic TDP-43 pathology but low AD pathology, two of whom also had HS. Seventeen patients showed typical AD pathology without co-morbid TDP-43/HS. "TDP-43-typical" and "AD-typical" hypometabolic patterns were estimated by contrasting FDG-PET data of the respective groups to normative data from healthy older controls (N=179). We then classified individual hypometabolic patterns of larger sets of AD dementia (N=251) and aMCI (N=403) patients according to the pathology-specific patterns using a spatial correlation approach, and tested for associations with clinical, molecular biomarker, and genetic features.

Results: Compared to AD-typical hypometabolism, the TDP-43-typical pattern showed more pronounced involvement of temporolimbic and frontal areas and less involvement of posterior temporo-parietal areas (Fig.1).
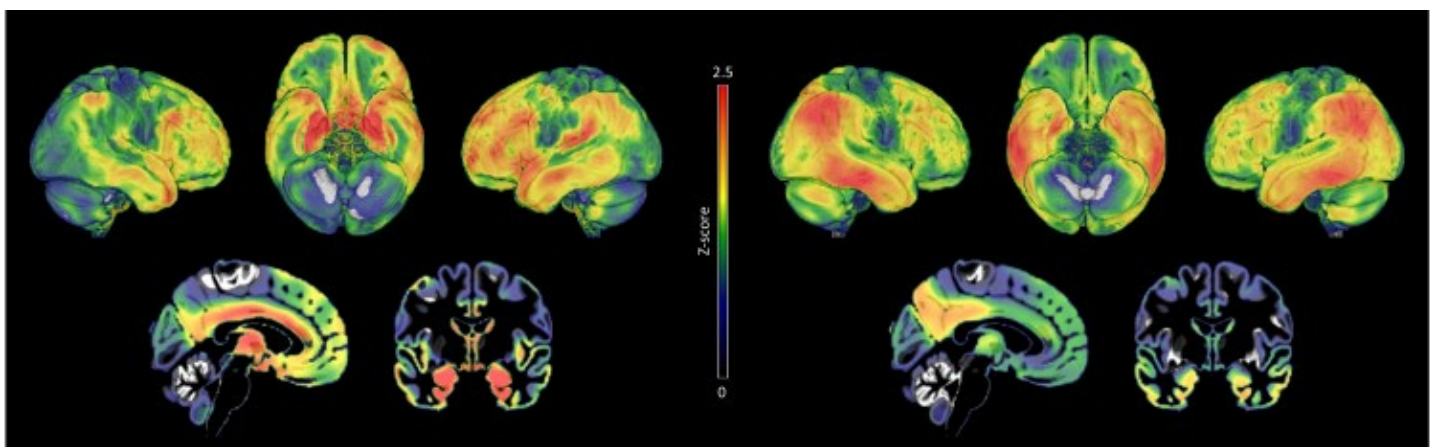
Fig. 1. Hypometabolic patterns of older amnestic patients whose neuropathological examination revealed underlying TDP-43/HS (left) or AD pathology (right). Warmer colors indicate stronger hypometabolism.

Clinically diagnosed AD dementia patients with a TDP-43-typical hypometabolic pattern (N=26, 10%) did not

differ significantly in global cognition or memory scores from other patients, but were less impaired in executive functions and showed less severe cognitive decline over follow-up (p<0.01). They were also significantly older, had lower levels of amyloid-β and tau biomarkers, lower APOE4 allele frequency, and higher frequency of the TMEM106B risk allele for TDP-43 pathology (all p<0.01). aMCI patients with TDP-43-typical hypometabolism showed similar disease characteristics.

Conclusions: A specific limbic-predominant topography of FDG-PET-measured hypometabolism identifies older amnestic patients whose clinical, genetic, and molecular biomarker features are consistent with an underlying TDP-43/HS pathology.

Keywords: TDP-43, Hippocampal Sclerosis, hypometabolism, Autopsy, imaging-pathologic association

The 13ᵗʰ Human Amyloid Imaging Conference is supported through educational grants and sponsorships from:

GOLD

Biogen

Lilly

For further information concerning Lilly grant funding visit www.lillygrantoffice.com

CERVEAU *technologies*

Silver

GE Healthcare

Avid Radiopharmaceuticals
A wholly owned subsidiary of Eli Lilly and Company

Invicro
A Konica Minolta Company

MERCK
INVENTING FOR LIFE

Bronze

abbvie

APRINOIA Therapeutics

Life Molecular Imaging

BIOCLINICA®
SEE MORE CLEARLY

www.worldeventsforum.com/hai or mobile app: https://my.yapp.us/HAICONF